Cell disorders in lysosomal storage diseases

Elise Roy

UNIVERSITÉ PARIS DESCARTES

PhD THESIS

A dissertation submitted in partial fulfillment
of the requirements for the degree of

DOCTOR of Health & Life Sciences

Specialized in Cellular and Molecular Biology

Doctoral School : GC2iD

CELL DISORDERS IN LYSOSOMAL STORAGE DISEASES

Defended on the 17th of February 2012

by Elise ROY

Chair	Pr Marc TARDIEU	Hôpital Bicêtre, France
Advisor	Dr Jean Michel HEARD	Institut Pasteur, France
Reviewers	Dr Bruno GOUD	Institut Curie, France
	Pr Maurizio SCARPA	University of Padova, Italy
Examiners	Pr Timothy COX	University of Cambridge, UK
	Dr Rosa RIOS	CABIMER, Spain

REMERCIEMENTS

Au terme de ce travail, je tiens à saluer toutes les personnes qui, de près ou de loin, ont contribué à la réalisation de ce projet.

Je remercie d'abord tout particulièrement **Jean Michel Heard** pour m'avoir permis de réaliser cette thèse et pour m'avoir donné l'opportunité de grandir professionnellement et de gagner une autonomie réelle. Je tiens à lui exprimer ma profonde reconnaissance pour m'avoir guidée et conseillée, et avoir su me laisser une large marge de liberté pour mener à bien ce travail, ainsi que pour m'avoir permis de présenter mes travaux à des congrès internationaux. J'espère avoir été digne de la confiance qu'il m'a accordée.
Mes remerciements vont également aux membres de mon jury de thèse pour toute l'attention qu'ils portent à ce travail. Je suis très reconnaissante à **Bruno Goud** et **Maurizio Scarpa** d'avoir accepté le rôle de rapporteur, et à **Tim Cox** et **Rosa Rios** d'avoir accepté d'être examinateurs de ma thèse. Je tiens à exprimer ma gratitude à **Marc Tardieu** qui me fait l'honneur de présider ce jury.

Un grand merci à tous les collègues qui m'ont apporté leur aide pratique, technique et scientifique, particulièrement à **Patricia Flamant** et **Françoise Thouron** pour la mise en place et l'exploitation du modèle cellulaire HeLa, et **Stéphanie Bigou** pour la microscopie électronique. L'aboutissement de ces recherches a également été encouragé par des discussions constructives avec **Sandrine Vitry**, **Julie Bruyère** et **Jérôme Ausseil**, que je remercie chaleureusement.
Je remercie aussi les thésards avec qui j'ai partagé un bureau pendant ces trois années, et auprès de qui j'ai trouvé une stimulation et une connivence motivantes : **Thomas, Julie** et **Diana**, ainsi que **Stéphane** pour sa bonne humeur permanente, sans oublier les autres **membres de l'unité Rétrovirus et Transfert Génétique**.

J'adresse toute mon amitié aux personnes incroyables rencontrées au **Children's Hospital de Philadelphie** avec qui j'ai fait route durant les presque trois années précédant le début de ma thèse. Un merci particulier à **Kathy High** et **Paris Margaritis** à qui j'adresse toute ma reconnaissance pour m'avoir donné la possibilité d'évoluer dans un cadre aussi stimulant, et pour m'avoir encouragée à me lancer dans l'aventure de la thèse. Cette expérience m'a laissé des souvenirs merveilleux.

Il m'est également impossible de ne pas penser aux personnes qui m'ont fait profiter de leurs connaissances et m'ont appris mon futur métier lors de différents stages en Suisse, Angleterre, Espagne et France.

Ces remerciements ne peuvent s'achever sans une pensée pour ma famille et mes amis que j'ai eus la chance d'avoir à mes côtés, qui m'ont soutenue tout au long de ces années de travail.

A mes **parents** tout d'abord, sans qui je ne serais pas là où j'en suis aujourd'hui. Merci pour l'éducation et l'amour que vous m'avez donnés, pour votre présence, et pour le soutien moral et matériel que vous n'avez jamais manqué de m'apporter. Je vous dédie ce travail en témoignage de mon infinie reconnaissance, avec tout mon amour.
A mes sœurs **Marielle** et **Nathalie**, mes « gamines », pour m'avoir toujours encouragée dans mes choix, et pour tous les bons moments passés ensemble qui sont gravés dans ma tête et dans mon cœur.
A mes beaux-frères **Lulu** et **Totof** pour leur bonne humeur.
A mes magnifiques neveux **Charlie** et **Léo**, pour tout le bonheur que vous m'apportez. Vous êtes encore tout petits, mais vous savez déjà ce que vous voulez, avec vos regards coquins, charmeurs ou roublards qui présagent des aventures hautes en couleur.
Je sais que mon absence a parfois été longue et j'espère pouvoir rattraper le retard accumulé.

Une spéciale dédicace aux **amis** funkys d'Orchamps qui m'ont suivie depuis l'école maternelle, et qui sont encore là après toutes ces années : Sri, Cees, Lolo, Paonnoum, Jup, Juf, Buibui, Alinou, Fred, Micka et Zézène. Merci à ma famille philadelphienne : Mettine, Federico, Junwei, Amiga et aux autres personnes qui m'ont apporté en plus de leur amitié, une richesse culturelle immense. Merci également aux filles de l'ESBS qui m'ont accompagnée de Strasbourg à Paris.

Enfin, une pensée émue pour tous ceux qui ne sont plus là aujourd'hui pour partager ce moment avec moi, mon pépère Nénèsse, mon Pa-pe, mon oncle Guy et ma tante Camille. Une énorme pensée va à Anthony. Tu me donnes la force de me battre, et me rappelle de ne pas oublier de profiter de la vie. Je ne t'oublie pas.

*Ce travail a été effectué grâce au soutien financier de **l'Association Française contre les Myopathies (AFM)**.*

ACKNOWLEDGEMENTS

This dissertation would not have become reality if it were not for the various people that directly and indirectly contributed to it.

In the first place I would like to record my gratitude to **Jean Michel Heard** who has supervised me throughout my thesis and who gave me the opportunity to grow professionally and gain increased independence. I sincerely acknowledge him for setting me free to follow my own lines, while guiding me with valuable comments and advice, and for giving me the opportunity to present my work at international meetings. Thank you for your confidence and trust on me.
My gratitude extends to my committee members **Bruno Goud** and **Maurizio Scarpa** for their commitment to reviewing this manuscript, and to **Tim Cox** and **Rosa Rios** for accepting the role of examiners. My sincere thanks go to **Marc Tardieu** who agreed to chair this committee.

I would also like to acknowledge all my colleagues for their technical and scientific help, particularly **Patricia Flamant** and **Françoise Thouron** for their hard work on the HeLa cell model, and **Stéphanie Bigou** for her help with electron microscopy. I am much indebted to **Sandrine Vitry**, **Julie Bruyère** and **Jérôme Ausseil** for their valuable advice in science discussion. Special thanks go to the other PhD students who shared my office during these three years **Thomas, Julie** and **Diana** for the nice interactions and complicity, to **Stéphane** for his constant good mood, and to all the other members of the **Rétrovirus et Transfert Génétique Unit**.

I would like to extend my special gratitude to all the incredible people that I met at the **Children's Hospital of Philadelphia** during the almost three years before starting this PhD adventure. Many thanks go in particular to **Kathy High** and **Paris Margaritis** for giving me the opportunity to work in such an enjoyable environment and for encouraging me to start a PhD. It has been a great gift to be a part of this group.
I would also like to thank the many people who have freely shared their knowledge and who taught me all about research during internships in Switzerland, England, Spain and France.

Last but not the least, I wish to thank my family and friends. Their love and affection has been the force which allowed me to reach this goal.

Most of all, a special thank you goes to my **parents**. I could not have come this far without their constant love, support and sacrifices. I would like to dedicate this thesis to them as a symbol of my gratitude, with all my love and affection.
Also many thanks to my sisters **Marielle** and **Nathalie**, my « gamines », for their continued encouragement and support. My head and my heart are filled with sweet memories of good times together.
Thank you to my brothers-in-law **Lulu** and **Totof** for their good mood.
A big kiss to my two adorable nephews **Charlie** and **Léo**, the best present of the past years.
I know my absence has been hard sometimes, and I hope I can make up for lost time.

Then, I especially want to mention those **friends** who have always been there from infant school: Sri, Cees, Lolo, Paonnoum, Jup, Juf, Buibui, Alinou, Fred, Micka and Zézène. Thank you to my Philly family: Mettine, Federico, Junwei, Amiga and the other persons who gave me their friendship and cultural perspectives which have enriched my life. Thank you also to the girls of the ESBS, who followed me from Strasbourg to Paris.

A final thought for those who are not here anymore to share this moment with me, my grandpa "Nénèsse"; my "Pa-pe", my uncle Guy and my aunt Camille. A particular thought goes to Anthony. You give me the strength to fight, and remind me that I should enjoy every moment of life. I do not forget you.

*Financial support for this work was gratefully received by the **Association Française contre les Myopathies (AFM)**.*

TABLE OF CONTENTS

ABBREVIATIONS

AAV	adeno-associated virus
AMPA	α-amino-3-hydroxy-5-methyl-4-isoxazolepropionic acid
AP	adaptor protein
ATP	adenosine triphosphate
BBB	blood-brain barrier
BMP	bone morphogenetic protein
BMT	bone marrow transplantation
CDK	cyclin-dependent kinase
CD-MPR	cation-dependent MPR
CGN	cis-Golgi network
CHO	chinese hamster ovary
CI-MPR	cation-independent MPR
CMA	chaperone-mediated autophagy
CNS	central nervous system
COP	coatamer protein
EB	embryoid body
ECM	extracellular matrix
EEA1	early endosome antigen 1
EET	enzyme enhancement therapy
EGF	epidermal growth factor
EGFR	epidermal growth factor receptor
ER	endoplasmic reticulum
ERGIC	ER-to-Golgi intermediate compartment
ERK	extracellular signal-regulated kinase
ESCRT	endosomal sorting complexes required for transport
ESCs	embryonic stem cells
FDA	food and drug administration
FGF	fibroblast growth factor
FGFR	FGF receptor
GAA	acid, alpha-glucosidase
GAG	glycosaminoglycan
GAP	GTPase activating proteins
GAP43	growth associated protein 43
GEF	guanine exchange factor
GGA	Golgi-associated, Gamma-adaptin ear-containing, ARF-binding protein
GlcA	glucuronic acid
GlcN	glucosamine
GPI	glycosyl-phosphatidyl-inositol
GSL	glycosphingolipid
GTP	guanosine triphosphate
HLA	human leukocyte antigen
HOPS	homotypic fusion and vacuole protein sorting
HS	heparan sulfate
HSC	heat shock protein
HSCc	hematopoietic stem cells

HSCT	hematopoietic stem cell transplantation
HSO	HS oligosaccharide
HSP	heat shock protein
IdoA	iduronic acid
IL	interleukin
ILVs	intraluminal vesicles
iMEF	irradiated mouse embryonic fibroblasts.
iPSc	induced pluripotent stem cells
LacCer	lactosylceramide
LAMP	lysosome-associated-membrane protein
LC3	microtubule-associated protein 1 light chain 3
LIMP	lysosomal integral membrane protein 2
LINCL	late infantile neuronal ceroid lipofuscinosis
LSD	lysosomal storage disease
M6P	mannose-6-phosphate
M6PR	M6P receptors
MAPK	mitogen-activated protein kinase
MHC	major histocompatibility complex
MPS	mucopolysaccharidosis
MRI	magnetic resonance imaging
mTOR	mammalian target of rapamycin
mTORC	mTOR complex
MVBs	multivesicular bodies
NAGLU	α-*N*-acetylglucosaminidase
NCL	neuronal ceroid lipofuscinosis
NPC	Niemann-Pick type C
NPCs	neural progenitor cells
NSCs	neural stem cells
PG	proteoglycans
ROS	reactive oxygen species
SCID	X-linked severe combined immune deficiency
scMAS	subunit c of mitochondrial ATP synthase
SERCA	sarcoplasmic/endoplasmic reticulum calcium-ATPase
SHH	sonic hedgehog
shRNA	small hairpin RNA
siRNA	small interference RNA
SNARE	soluble N- ethylmaleimide–sensitive factor attachment protein receptor
SRT	substrate reduction therapy
TGN	trans-Golgi network
TLR	toll-like receptor
TNFα	tumor necrosis factor α
UPR	unfolded protein response
VAMP	vesicle-associated membrane protein
VSV-G	vesicular stomatis virus membrane glycoprotein
VTI1B	vesicle transport through interaction with T-SNAREs homolog 1B
WNT	wingless
γ-TuRC	γ-Tubulin ring complex

INTRODUCTION

INTRODUCTION

1. THE LYSOSOME

1.1. Generalities

The lysosome, first described by De Duve et al. in 1955 is a cytoplasmic cellular organelle present in all nucleated eukaryotic cells. It is delimited by a single-layer lipid membrane and has an acidic internal pH of 4.5-5.0 that is maintained by an adenosine triphosphate (ATP)-dependent proton pump. Morphologically, it is a highly heterogeneous organelle. The lysosome size, shape, and number per cell are variable according to cell types. It may be spheric, ovoid, or occasionally tubular in shape, and may vary between 0.1 to 2 μm in size.

The primary cellular function of the lysosome is the degradation and recycling of several macromolecules, including nucleic acids, proteins, glycosaminoglycans (GAGs), oligosaccharides, sphingolipids, and other lipids. Whereas extracellular macromolecules are delivered toward the lysosome via phagocytosis or endocytosis, intracellular macromolecules are incorporated through autophagy.

Hydrolysis of these macromolecules is achieved by the action of soluble hydrolases present in the lumen of the lysosome that are active at the acidic pH of this organelle. 50-60 acid hydrolases (Journet et al., 2002) have been described to date, such as nucleases, proteases, glycosidases, sulfatases, phosphatases and lipases. Molecules degraded by the lysosome can leave this organelle either via diffusion, or with the aid of specialized transporters. This catabolic activity of the lysosome is of primary importance in maintaining the cell homeostasis. It provides building blocks of complex macromolecules for salvage and recycling pathways, allows protein turnover, downregulation of cell surface molecules and receptors, and inactivation of pathogenic organisms.

In addition to the soluble luminal hydrolases, the mammalian lysosome contains about 25 lysosomal membrane proteins, but additional membrane proteins are being revealed. Recent advances in proteomic analysis allowed the identification of about 215 integral membrane proteins, and 55 membrane-associated proteins (Bagshaw et al.,

2005). These membrane proteins mediate the essential functions of this organelle. They are involved in transport and sorting of substrates and digestion products, establishment of pH gradients, and maintenance of lysosomal structural integrity.

The most abundant lysosomal membrane proteins are the lysosome-associated-Membrane proteins 1 and 2 (LAMP1 and LAMP2), the lysosomal integral membrane protein 2 (LIMP2), and the tetraspanin CD63 (also referred to as LIMP1 or LAMP3). LAMPs and LIMPs together account for over 50% of the membrane proteins in a lysosome. LAMP1 and LAMP2 share a high amino acid sequence homology (37%). They are type I transmembrane proteins with a luminal N-terminal domain, one transmembrane domain, and a short C-terminal cytoplasmic tail that contains the signal sequence for their intracellular targeting following synthesis. Both proteins are heavily glycosylated with *N*-linked glycans and some *O*-linked glycans, glycosylation constituting about 60% of their total mass (~ 120 kDa). LIMP1 (53 kDa) and LIMP2 (74 kDa) are also major lysosomal membrane proteins, although they are less abundant than the LAMPs, and exhibit no homology to either LAMP1 or LAMP2. They are also highly glycosylated transmembrane proteins, carbohydrates representing about 35% and 20% of the molecular mass of LIMP1 and LIMP2, respectively. Whereas LIMP2 traverses the lysosomal membrane twice, LIMP1 spans it four times. Their N- and C-terminal domains are located in the cytoplasm.

The heavy glycosylation renders lysosomal membrane proteins resistant to degradation by lysosomal hydrolases (Fukuda, 1991). Their abundance is so high that they form a coat on the inner surface of the lysosomal membrane and serve as a protective barrier against lysosomal hydrolases, thus playing a critical role in the maintenance of the structural integrity and stability of the lysosome.

1.2. Routes to the lysosome

1.2.1. Biogenesis and transport of lysosomal proteins

Lysosome biogenesis is a result of the convergence of the endocytic and biosynthetic pathways of the cell. Lysosomal proteins are synthesized by ribosomes attached on the rough Endoplasmic Reticulum (ER) membrane in the form of a precursor containing a N-terminal signal sequence of 20-25 amino acids. This signal

sequence directs their translocation through the ER membrane. Once in the lumen of the ER, they lose the signal peptide through the action of a peptidase, and undergo *N*-glycosylation on asparagine residues within the sequence Asn-X-Ser/Thr. This *N*-glycosylation step consists in the addition of mannose-rich oligosaccharide chains containing three glucose (Glc), nine mannose (Man), and two *N*-acetylglucosamine (GlcNac) residues ($Glc_3Man_9GlcNac_2$). Lysosomal proteins are then transferred to the Golgi by vesicular transport. There are multiple pathways by which lysosomal proteins can reach the lysosome from the Golgi (Figure 1) (Braulke and Bonifacino, 2009).

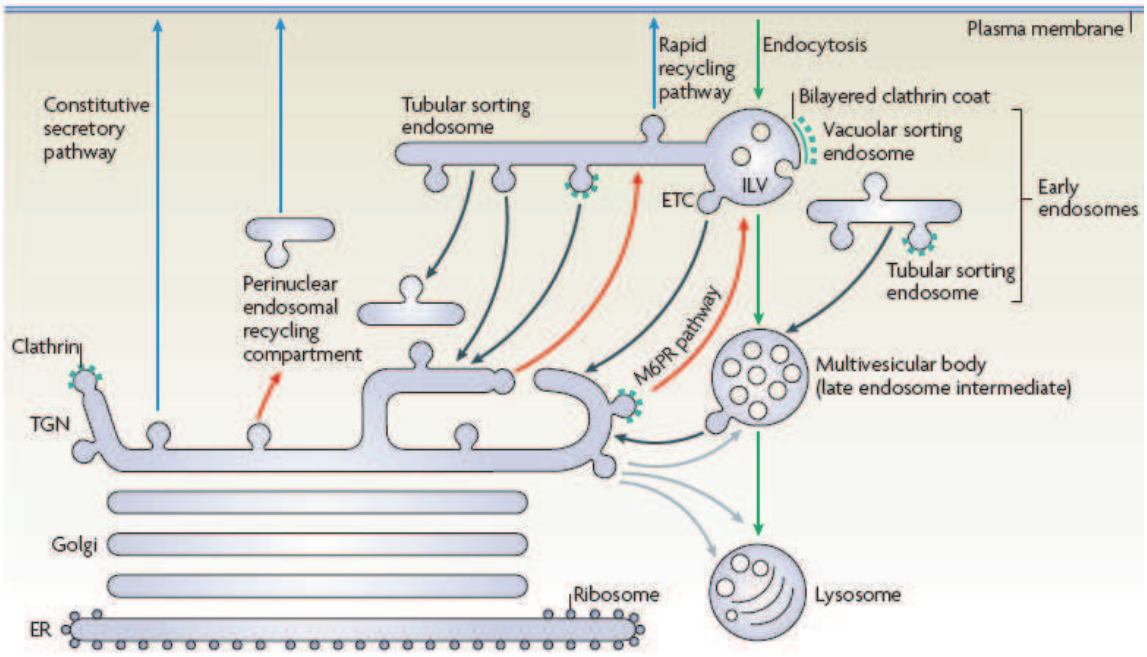

Figure 1: Lysosome biogenesis. The possible sites at which the biosynthetic and endocytic pathways can converge are shown. Green arrows: endocytic pathway. Blue arrows: indirect intracellular pathway. Red arrows: direct intracellular pathway. Grey arrows: alternative pathways. Black arrows: retrograde pathways.
From Saftig and Klumperman, 2009.

The best characterized pathway is the mannose-6-phosphate receptor-dependent transport of lysosomal hydrolases (Figure 2). Once in the cis-Golgi, lysosomal hydrolases acquire mannose-6-phosphate (M6P) residues on their oligosaccharide chains. This process requires the sequential action of two enzymes, a phosphotransferase, and a phosphodiesterase. First, an *N*-acetylglucosamine-1-phosphotransferase (phosphotransferase, EC 2.7.8.17) transfers *N*-acetylglucosamine-1-

phosphate from UDP-*N*-acetylglucosamine to C6 hydroxyl groups of mannoses, generating phosphodiester forms. Then, an *N*-acetylglucosamine-1-phosphodiester α *N*-acetylglucosaminidase (phosphodiesterase, EC 3.1.4.45) catalyzes the hydrolysis of the *N*-acetylglucosamine-1-phosphodiester, exposing M6P residues. It is the acquisition of the M6P marker that separates glycoproteins that are destined for the lysosome from secretory glycoproteins. Phosphorylated lysosomal hydrolases bind to M6P receptors (M6PR) located in the membranes of clathrin-coated vesicles budding from the trans-Golgi network (TGN). Two distinct M6PRs with molecular masses of 46 kDa (M6PR-46 or cation-dependent M6PR, CD-M6PR), and 300 kDa (M6PR-300 or cation-independent M6PR, CI-M6PR) exist (Ghosh et al., 2003). Both M6PRs are type I transmembrane glycoproteins. Distinct lysosomal hydrolases can exhibit different affinities for CD-M6PR and CI-M6PR.

The cytoplasmic tails of CD-M6PR and CI-M6PR contain specific motifs that mediate binding of the M6PR-enzyme complexes to the clathrin adaptor proteins AP-1 (adaptor protein-1) and GGA (Golgi-associated, Gamma-adaptin ear-containing, ARF-binding protein). These motifs are of different types: YXXØ (where Ø is a bulky hydrophobic residue) and [DE]XXXL[LI] for AP-1, and DXXLL for GGA. Interactions between the M6PR and the adaptor proteins lead to capture of the M6PR-enzyme complexes into clathrin-coated vesicles, which directly traffic from the TGN to endosomes and then to lysosomes. Following fusion with endosomes, lysosomal hydrolases are delivered into the endosomal lumen. The acidic pH of endosomes (pH ~5-6) triggers the dissociation of the lysosomal hydrolases from the M6PR, which allows the receptors to recycle back to the TGN. Thus, lysosomes are devoid of M6PR, which are only found in the TGN and endosomes, and at the plasma membrane. In fact, a fraction of the newly synthesized enzyme population escapes binding to M6PRs in the Golgi, and instead is transported to the plasma membrane, which also contains M6PRs. This fraction is secreted to the extracellular milieu, where it can bind M6PRs present on the plasma membrane of neighboring cells, and be subsequently endocytosed. This mechanism is called the secretion-recapture mechanism and concerns a variable fraction depending on the enzyme and cell type studied. In fibroblasts for instance, about 10% of beta-hexosaminidase is secreted before its delivery to lysosomes (Vladutiu and Rattazzi, 1979).

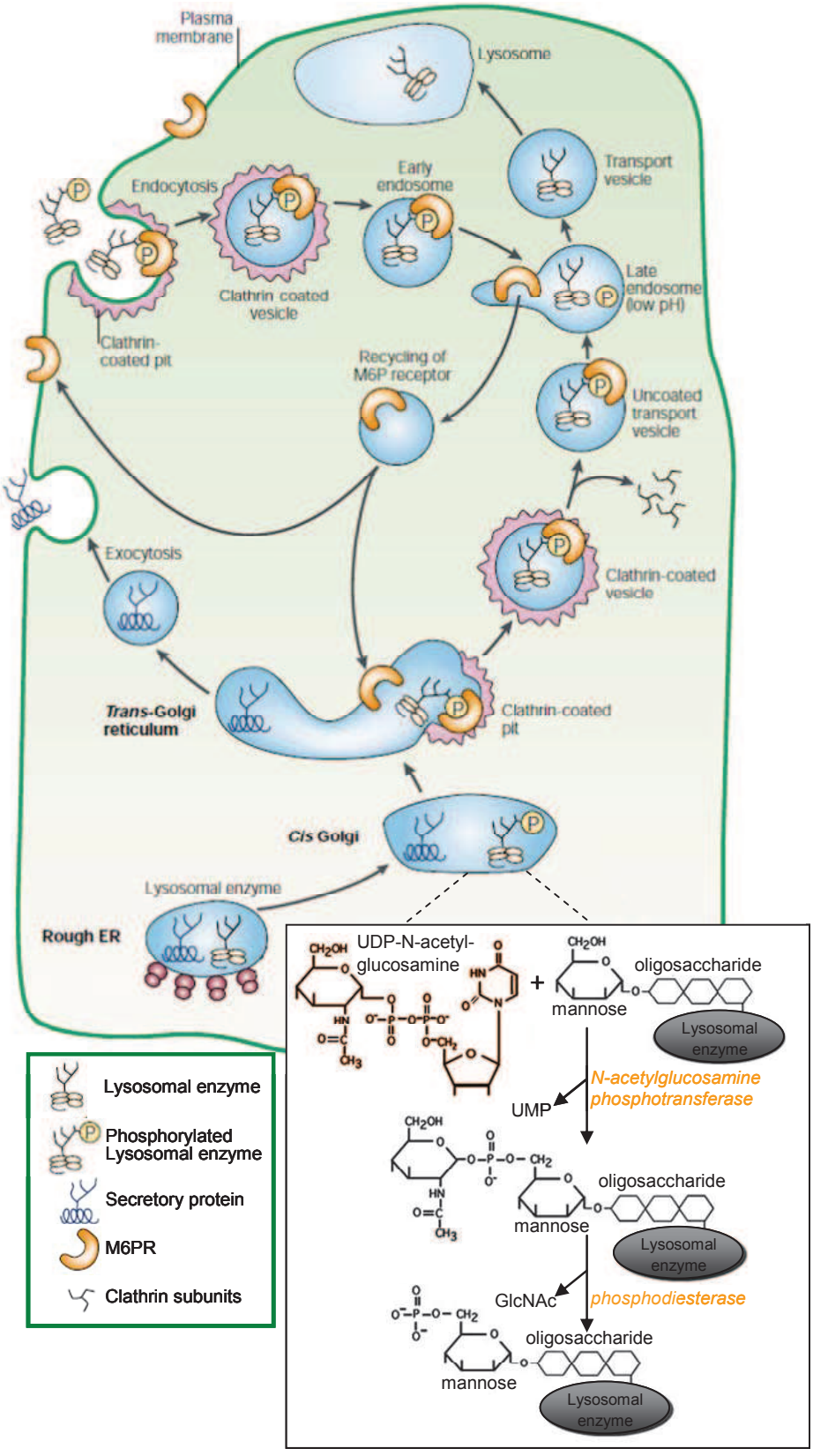

Figure 2: Lysosomal enzyme sorting by the M6PR system. *Adapted from Desnick and Schuchman, 2002.*

The requirement of the M6P marker for lysosome delivery only concerns lysosomal soluble hydrolases. Lysosomal membrane proteins, on the contrary, are not modified with M6P groups, and do not depend on the M6PR for sorting. Instead, they bear sorting signals in their cytosolic tail that mediate endosomal and lysosomal targeting (van Meel and Klumperman, 2008). Most targeting signals belong to the YXXΦ (e.g. for LAMP1, LAMP2 and LIMP1) or [DE]XXXL[LI] (e.g. for LIMP2) types. Lysosomal targeting of newly synthesized lysosomal membrane proteins occurs either by an indirect route or by a direct route. In the direct pathway, lysosomal membrane proteins are transported intracellularly from the TGN to the endo-lysosomal system. The indirect pathway involves transport from the TGN to the plasma membrane along the constitutive secretory pathway, followed by endocytosis and lysosome delivery. Newly synthetized LAMPs and LIMPs are transported mainly directly to the lysosome without appearing at the cell surface (Fukuda, 1991). Targeting signals equip lysosomal membrane proteins to use the AP-1–clathrin and GGA–clathrin dependent exits from the TGN. They can also be packed in distinct clathrin-coated vesicles bearing the AP-3 adaptor (Le Borgne et al., 1998).

Increasing evidence indicates the existence of multiple additional or alternative pathways for the transport of both lysosomal hydrolases and lysosomal membrane proteins, which may enter the endo-lysosomal system at different stages of maturation. For instance, the M6PR-dependent mechanism of lysosomal hydrolase transport from the TGN to the lysosome is not a rule. Studies in some cell types isolated from patients suffering Mucolipidosis type II, a disease in which soluble lysosomal hydrolases do not acquire M6P residues due to *N*-acetylglucosamine-1-phosphotransferase deficiency, showed that most lysosomal enzymes are still targeted correctly to the lysosome, indicating the existence of alternative M6PR-independent pathways to the lysosome (Owada and Neufeld, 1982). The same phenomenon was observed in mice deficient for both M6PRs (Dittmer et al., 1999). Such pathways are poorly characterized, with the exception of beta-glucocerebrosidase transport. The lysosomal membrane protein LIMP2 can act as a specific receptor for this lysosomal hydrolase (Reczek et al., 2007). LIMP2 binds beta-glucocerebrosidase at the ER step, guiding it all the way to the lysosome. Recently, sortilin has emerged has an alternative receptor capable of sorting lysosomal proteins directly from the Golgi to the lysosome. This direct lysosomal targeting concerns soluble lysosomal hydrolases such as some cathepsins or acid

sphingomyelinase and non-enzymatic cofactors such as sphingolipid activator proteins (Canuel et al., 2009; Ni and Morales, 2006). It thus appears that the site of entry of lysosomal proteins can be early or late endosomes, but also the lysosome directly.

1.2.2. The endocytic pathway to lysosomes

It is via the endocytic pathway that lysosomes receive proteins destined to lysosome biogenesis sorted from the TGN, as described above, as well as extracellular macromolecules for degradation (Luzio et al., 2009; Pryor and Luzio, 2009; van Meel and Klumperman, 2008). Extracellular substances may be cell surface receptors and their ligands, as well as lipids or proteoglycans. The degradative endocytic pathway starts at the plasma membrane, where uptake from the cell surface can occur in a clathrin-mediated or independent manner (Figure 3).

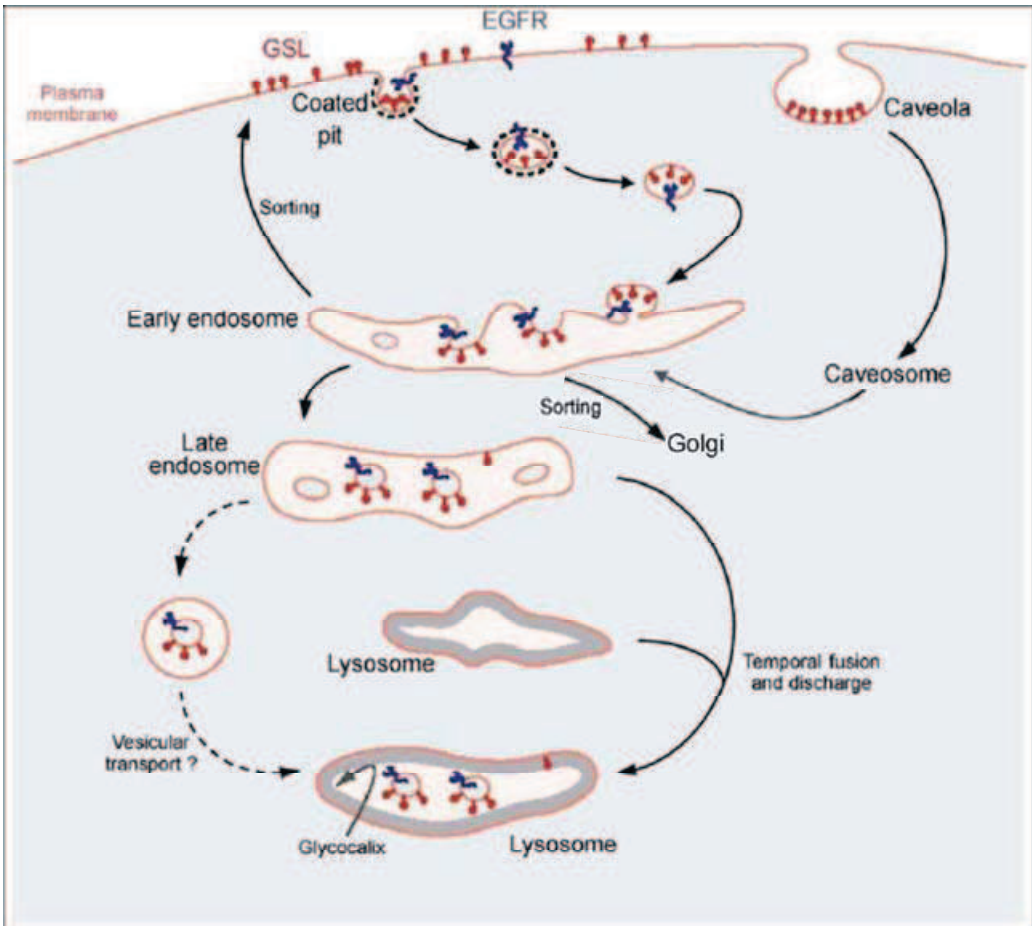

Figure 3: The endocytosis pathway. GSL: glycosphingolipids. EGFR: epidermal growth factor receptor. Glycocalix: protection offered by the carbohydrate part of LAMP and LIMP proteins. *Adapted from Schulze et al., 2009.*

In clathrin-mediated endocytosis, extracellular ligands and membrane components are taken up in vesicles coated with clathrin. The adaptor complex AP-2 is the main clathrin adaptor complex that functions at the cell surface. It is the adaptor complex that is first recruited to the plasma membrane, where it mediates the attachment of clathrin to membranes. Besides interaction with clathrin, AP-2 also provides binding sites for plasma membrane receptors. Indeed, the cytoplasmic domains of plasma membrane receptors contain tyrosine and di-leucine based motifs that are recognized by the adaptor complex. Some examples are the FDNPVY signal of the LDL receptor, the YTRF sequence of the transferrin receptor, or the LL signal of immune receptors expressed in leukocytes (Mellman, 1996).

Clathrin-independent endocytosis is supported by caveolae. Caveolae are flask-shaped invaginations of the plasma membrane that form lipid raft microdomains enriched in cholesterol and sphingolipid. They are associated with the dimeric protein caveolin that binds cholesterol, inserts as a loop into the inner leaflet of the plasma membrane and self-associates to form a striated coat on the surface of membrane invaginations.

After internalization, endocytosed macromolecules are incorporated into early endosomes. Here, they may recycle back to the plasma membrane or to internal sites in the cell, or continue to transit through the endosomal-lysosomal system for degradation. Macromolecules destined to degradation, as well as newly synthesized lysosomal proteins pass from early endosomes to late endosomes before delivery to lysosomes.

Distinction between early and late endosomes is based on their pH, early endosomes (pH ~6) being less acidic than late endosomes (pH ~5-6), and on expression of distinct biological markers. For example, early endosomes are marked by the presence of a small GTPase of the Rab family, Rab5, and its effector protein EEA1 (early endosome antigen 1). Late endosomes are marked by other small GTPases of the Rab family, Rab7 and Rab11. The formation of late endosomes from early endosomes requires the conversion from a Rab5-positive organelle into a Rab7-positive organelle. This process is regulated by the HOPS (homotypic fusion and vacuole protein sorting) complex, a guanine exchange factor (GEF) complex for Rab7 that also interacts with Rab5 (Rink et al., 2005).

Functional differences also characterize early and late endosomes. Early endosomes receive incoming endocytic cargo from the plasma membrane and the TGN, and play a

role in sorting of this cargo for recycling or for degradation. They are composed of a vacuolar part containing numerous intraluminal vesicles (ILVs), and of a tubular network. Generally, cargo destined for lysosomes is sorted into ILVs, whereas cargo to be recycled to the plasma membrane or to the TGN enters the tubular endosomal network.

Late endosomes no longer contain significant amounts of endocytosed recycling proteins, but instead have elevated levels of proteins that are destined for lysosomes, either newly synthesized lysosomal proteins, or proteins to be degraded. They contain more luminal vesicles than early endosomes, and are therefore often described as multivesicular bodies (MVBs). The best characterized signal for sorting of proteins into ILVs is ubiquitination, carried out by a cascade of enzymes called E1, E2 and E3. The ESCRT (endosomal sorting complexes required for transport) complexes are required for recognition and sorting of ubiquitylated cargo into the internal vesicles of MVBs.
The method of delivery of endocytosed macromolecules from endosomes to lysosomes is a matter of debate. Several theories have been proposed including maturation (of the endosome into a lysosome), vesicular transport (via vesicles carrying cargo from endosomes to lysosomes), kissing (transient contacts between endosomes and lysosomes, during which material is transferred between the organelles) and direct fusion (of the endosome to the lysosome to form a hybrid organelle). Recently, time-lapse confocal microscopy experiments have favored the kissing and direct fusion model (Bright et al., 2005).

Direct fusion of late endosomes with lysosomes involves three successive steps (Luzio et al., 2007): first, a tethering step, likely accomplished by the HOPS complex; second, the formation of a *trans*-SNARE (soluble N- ethylmaleimide–sensitive factor attachment protein receptor) complex that consists of Syntaxin-8, Syntaxin-7 and VTI1B (vesicle transport through interaction with T-SNAREs homolog 1B) on the late endosome membrane, and of VAMP7 (vesicle-associated membrane protein 7) on the opposing lysosomal membrane, bridging the two organelles; last, membrane fusion producing a hybrid organelle, from which the lysosome has to be re-formed via a maturation process.

In addition to clathrin-mediated endocytosis and clathrin-independent endocytosis, a mechanistically distinct form of endocytosis exists, phagocytosis. Phagocytosis represents a mechanism by which specialized cells such as macrophages, monocytes or

neutrophils engulf relatively large particles (>0.5 μm) including invading pathogens, apoptotic cells and other foreign particles. The phagocytic process starts with the binding of the particle to the cell surface mediated by receptors such as Fc receptors and complement receptors. Interaction between these receptors and particles results in signal transduction events mediated by Rho-family GTPases. Signaling cascades trigger the local remodeling of the actin cytoskeleton resulting in the formation of cell-surface extensions that engulf phagocytic particles, and lead to phagosome formation. The phagosome then undergoes a maturation process by fusion events with early and late endosomes as well as with lysosomes to form a hybrid-like organelle termed the phagolysosome. The fusion processes are regulated by proteins that are also involved in fusion processes in the endocytic pathway. For example, the fusion of phagosomes with early endosomes is stimulated by the small GTPase Rab5. During their transformation into phagolysosomes, phagosomes acquire markers of late endocytic organelles such as Rab7, LAMP1, and LAMP2 and lose markers of early endocytic organelles including Rab5. Phagolysosomes degrade the phagocytosed particle using proteases acquired by fusion with the endo/lysosomal compartment, and by the acquisition of ATPases involved in the acidification of the phagosome.

1.2.3. The autophagy pathway to lysosomes

The degradation of intracellular proteins is performed by two major mechanisms: the ubiquitin-proteasome system (UPS) and autophagy. Whereas the UPS degrades primarily short-lived proteins, autophagy is responsible for the degradation of several classes of long-lived (half-life > 5 hours) macromolecules and organelles. Under basal conditions, autophagy acts as a cytoplasmic quality control mechanism to eliminate altered macromolecules and damaged organelles. Under stress conditions (regarding the availability of nutrients, growth factors, and hormones, as well as oxidative and energetic stress signals or exposure to toxic compounds), autophagy is activated, providing material to support cell metabolism in challenging conditions, and allowing the removal of altered intracellular components including protein aggregates, oxidized lipids, damaged organelles, or even intracellular pathogens. Autophagy uses the lysosome to catabolize intracellular material. Three different types of autophagy have

been described in mammalian cells: macroautophagy, microautophagy, and chaperone-mediated autophagy (CMA).

Macroautophagy is the predominant form of autophagy. In macroautophagy, complete regions of the cytoplasm, including cytosolic proteins and entire organelles, are surrounded by a membrane and form an autophagosome.

The origin of autophagosome membranes is unclear. They may be derived from pre-existing organelle membranes, most likely from the ER membrane (maturation model), or they may be assembled at the site of autophagosome genesis from non-vesicular transport or de novo synthesis (assembly model) (Juhasz and Neufeld, 2006). The formation of autophagosomes requires autophagy related proteins (Atg proteins), identified in yeast and almost entirely conserved in eukaryotic cells (Klionsky, 2005; Suzuki and Ohsumi, 2007) (Figure 4). These proteins can be divided into four groups:

- The Atg1/ULK1 complex (Atg1 in yeast and ULK1 in mammals) and the mammalian target of rapamycin (mTOR) complex 1 (mTORC1) are involved in the initiation step of autophagosome formation (Pattingre et al., 2008). The protein kinase mTOR is part of the mTORC1 complex, and receives input signaling via the class I phosphoinositide 3-kinase signaling pathway, a key sensor of the extracellular environment. Under basal conditions, ULK1 is bound to mTORC1 and phosphorylated by mTOR, inhibiting macroautophagy initiation. Under stress conditions, the mTOR kinase activity is inhibited. This both suppresses cell growth to reduce energy demands, and dissociates the ULK1 complex from mTORC1, liberating it to trigger autophagosome biogenesis. ULK1 acts by recruiting downstream Atg proteins to the autophagosome formation site.
- Autophagosome nucleation requires a complex containing Atg6/Beclin1 (Atg6 in yeast and Beclin1 in mammals) that brings together the proteins and lipids giving rise to a pre-autophagosomal structure. This complex recruits a class III phosphatidylinositol 3-kinase to generate phosphatidylinositol 3-phosphate.
- Two ubiquitin-like proteins, Atg8 and Atg12 (called microtubule-associated protein 1 light chain 3, or LC3 in mammals), and two associated ubiquitin-like conjugation systems act in autophagosome formation and completion (Noda et al., 2009). The first pathway involves the covalent conjugation of Atg12 to Atg5 with the help of the ubiquitin-activating E1-like enzyme Atg7 and the E2-like

enzyme Atg10. A third protein, Atg16, links to the Atg12-Atg5 conjugate, forming a complex that participates in the nucleation step, and in the recruitment of the second pathway. The second pathway involves the conjugation of phosphatidylethanolamine (PE) to Atg8/LC3 by the sequential action of the protease Atg4, the E1-like enzyme Atg7, and the E2-like enzyme Atg3. Lipid conjugation converts Atg8/LC3 from a soluble form (named LC3-I) to an autophagosome membrane-associated form (named LC3-II). This second pathway is crucial for the expansion and completion steps (i.e. addition of membranes, and vesicle sealing to separate the cargo from contact with the cytosol).

- The mechanisms controlling the recycling pathway are poorly characterized, and include the Atg9 protein.

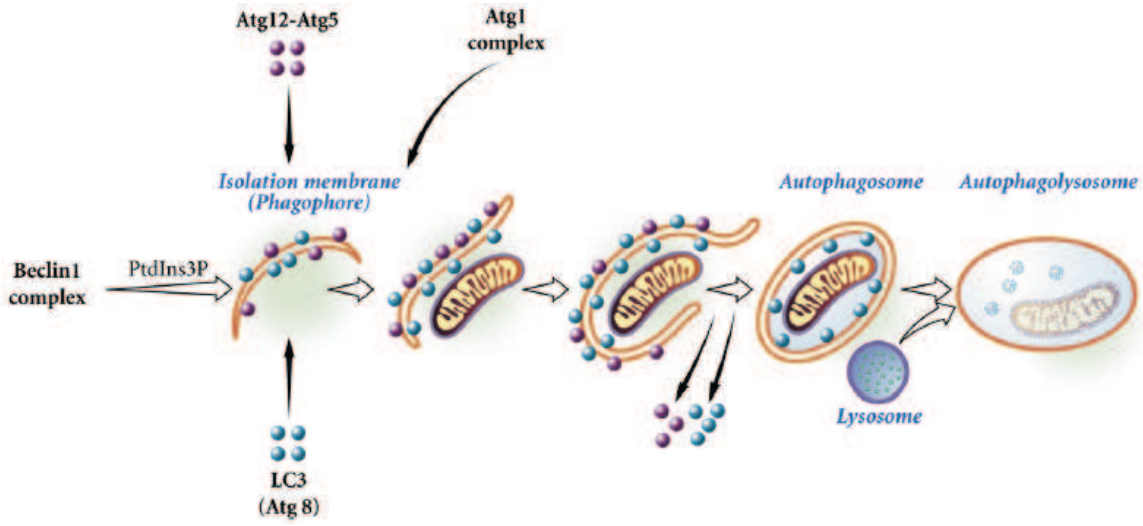

Figure 4: The autophagy pathway. *Adapted from Pattingre et al., 2008.*

After their formation as doubled-membrane vacuoles containing cytoplasmic material, autophagosomes undergo a stepwise maturation consisting in fusion events with late endosomal MVBs or lysosomes (Eskelinen, 2005). Autophagosomes that have fused with endosomes are called amphisomes, whereas autophagosomes or amphisomes that have fused with a lysosome are called autolysosomes. Maturation events require intact microtubules, and are regulated by proteins involved in docking and fusion of membrane compartments (i.e. the Rab GTPases Rab7 and Rab24, and the SNARE

protein VTI1B), by the SDK1 ATPase Associated with diverse cellular Activities (AAA ATPase) that is important for transport from endosomes to lysosomes, and by the proton pump v-ATPase that is essential to acidify the newly created autolysosome.
Because autophagosomes lack any enzymes, these maturation events are necessary for the acquisition of hydrolytic enzymes and vacuolar acidification required for degradation of cargo. The resulting macromolecules are then released back into the cytosol for re-use.

The first response to cellular stress is activation of macroautophagy. However, during prolonged cellular stress, the random degradation of intracellular component cannot be maintained, and CMA is up-regulated (Dice, 2007). CMA is a more selective form of autophagy, in which specific cytosolic molecules are targeted by molecular chaperones present in the cytosol and associated with the lysosomal membrane. Most substrate proteins for CMA contain a KFERQ-like peptide motif that is recognized by the cytosolic heat shock protein of 70 kDa (hsc70). Such sequences occur in approximately 30% of the cytosolic proteins. Hsc70 is part of a cytosolic molecular chaperone complex composed of multiple heat shock proteins. Amongst them, several proteins such as the heat shock protein of 40 kDa (hsp40) act as cochaperones that regulate hsc70 activity. Other proteins act as chaperones themselves. It is the case for the heat shock protein of 90 kDa (hsp90) that recognizes unfolded regions within proteins and prevents substrate protein aggregation. This molecular chaperone complex transports substrate proteins to the lysosomal membrane and unfolds them, a prerequisite to their translocation across the lysosomal membrane. Once at the lysosomal surface, the complex hsc70/cytosolic substrate binds to a lysosomal receptor, LAMP2a, an isoform of LAMP2 that arises by alternative splicing, and is directly pulled into the lysosome. The translocation process requires other chaperones present in the lysosomal lumen such as Hsc73. Substrate proteins are finally degraded in the lysosomal lumen.

A third autophagic pathway, microautophagy, has been described in yeast but has not yet been well characterized in eukaryotic cells (Uttenweiler and Mayer, 2008). In this type of autophagy, complete cytosolic regions are sequestered directly by the lysosome membrane through invaginations or tubulations that “pinch off” from the membrane into the lysosomal lumen where they are rapidly degraded. Like

macroautophagy, microautophagy is induced via the TOR signaling complex. In addition to TOR, microautophagy is controlled by a second regulatory complex, the EGO complex (composed of Ego1, Ego3 and the GTPase Gtr2). Macroautophagy seems to be a prerequisite for sustained microautophagy. Microautophagy is responsible for degradation of various cellular components, including the lysosomal membrane. Reducing the lysosomal size is crucial during macroautophagy, where an enormous influx of membrane arises from the fusion of autophagosomes with the lysosome. Microautophagy might hence be responsible for maintenance of organellar size and membrane composition rather than for cell survival under nutrient restriction.

1.3. The complexity of lysosomal functions

For decades, lysosomes have been illustrated as a simple waste disposal within the cell. There is now growing appreciation of the fact that lysosomes are not a 'dead-end' degradative organelle, but that they are part of a complex cell machinery, acting in concert with the endosomal and autophagosomal systems, and in coordination with the ubiquitin-proteasome system (Figure 5). In addition to its catalytic function, the lysosome is involved in a wide array of functions, including cell signaling, antigen presentation, immunity, plasma membrane repair, or initiation of apoptosis. Examples of such diversified lysosomal functions are listed below:

- The fusion of lysosomes with autophagosomes is the ultimate step of macroautophagy, a pathway that is involved in cell death and proliferation.
- Lysosomes are crucial for the maturation of phagosomes to phagolysosomes during phagocytosis, which is important for cellular pathogen defense.
- Lysosomes can fuse with the plasma membrane in response to an increase in the concentration of cytosolic Ca^{2+} that triggers lysosome exocytosis. Such lysosome exocytosis provides the extra membrane for plasma-membrane wound repair (Reddy et al., 2001; Rodriguez et al., 1997), and is also possibly involved in neurite outgrowth (Arantes and Andrews, 2006).
- Lysosomal damage seems to be an early event in the apoptotic signaling cascade prior to increase of the permeability of the mitochondrial membrane and release of apoptogenic factors. Lysosome-mediated apoptosis involves the lysosomal cathepsins. These proteolytic enzymes are able to cleave pro-apoptotic

molecules and caspases, acting as a mediator between lysosomes and mitochondria (Conus et al., 2008).

- Intracellular cholesterol homeostasis is controlled by lysosomal efflux through a lysosomal transporter, the Niemann-Pick, Type C1 protein (NPC1).
- The lysosomal membrane protein ceroid-lipofuscinosis, neuronal 3 (CLN3) might participate in synaptic vesicle transport/transmission (Jarvela et al., 1999).
- Lysosomal proteases are required for the generation of antigenic peptides from exogenous proteins, and are involved in trafficking and maturation of major histocompatibility complex (MHC) class II (Chapman, 1998; Driessen et al., 1999), thus playing a role in adaptive immunity.
- Lysosomal cathepsins have been described as important modulators of innate immune responses, by inducing apoptosis of inflammatory cells, by modulating the activity of certain cytokines playing an important role in inflammatory responses, and by inducing proteolytic cleavage of toll-like receptors (TLRs), which is a prerequisite for their signaling (Blomgran et al., 2007; Conus and Simon, 2010).

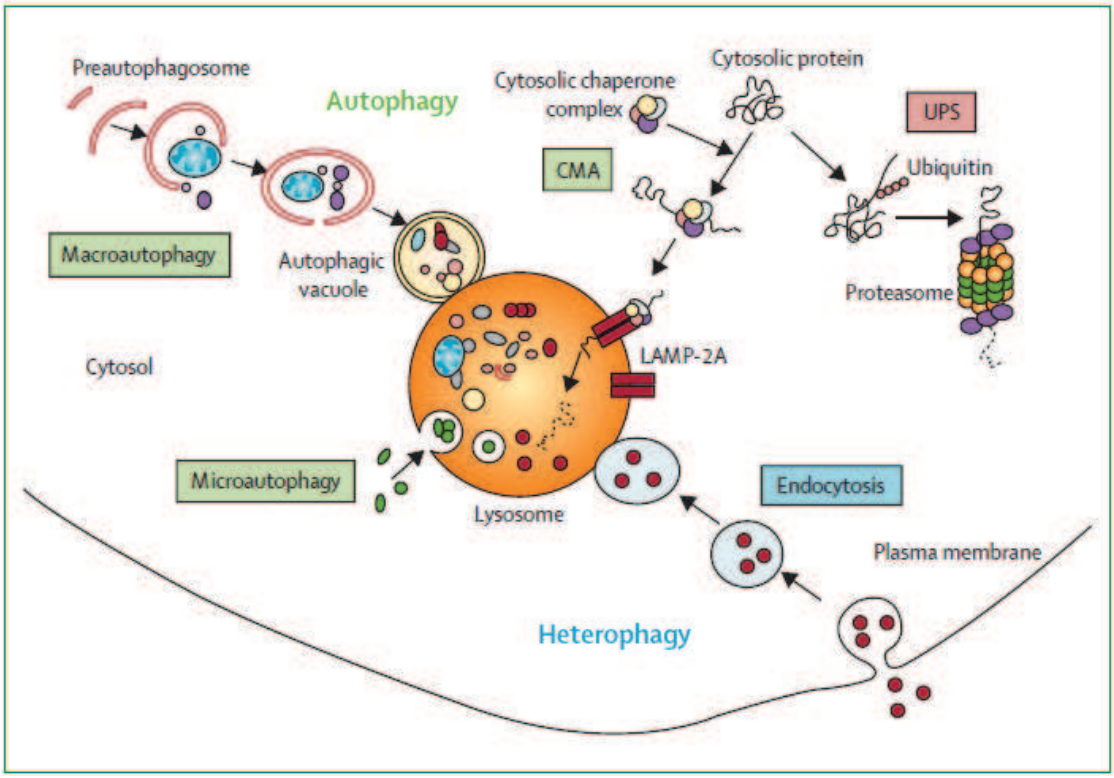

Figure 5: Degradative systems in mammalian cells. The endocytic and autophagy pathways converge to the lysosome. Another proteolytic system, the ubiquitin-proteasome system (UPS) degrades intracellular proteins equipped with an ubiquitin tag.
From Martinez-Vicente and Cuervo, 2007.

It is thus not surprising that lysosomal deregulation is associated with many diseases. In addition to Lysosomal Storage Diseases (detailed in section 2), there is increasing evidence that lysosomes and lysosomal activities may be involved in cancer (Fehrenbacher and Jaattela, 2005), autoimmune diseases (De Carvalho Bittencourt et al., 2005), arthritis (Salminen-Mankonen et al., 2007), atherosclerosis (Zschenker et al., 2006) or Alzeihmer's disease (Nixon and Cataldo, 2006).

It should be noted that lysosome-related organelles exist in a wide variety of cell-types and share compositional and physiological characteristics with conventional lysosomes. Depending on the cell-type they may either compose the entire pool of lysosomes or coexist with lysosomes. Some examples are melanosomes which function in melanin formation, storage and transfer; platelet dense granules which release ATP, ADP, serotonin and calcium for blood clotting; lamellar bodies of the lung epithelial type II cells which function in surfactant production; lytic granules of cytotoxic T lymphocytes and natural killer cells; Weibel-Palade bodies of endothelial cells and platelet alpha granules which function in platelet adhesion and blood clotting (Raposo et al., 2007).

2. LYSOSOMAL STORAGE DISORDERS

2.1. Generalities

Any disruption of lysosomal function can lead to Lysosomal Storage Diseases (LSDs). LSDs are inherited genetic diseases that are caused by mutations in genes that encode lysosomal hydrolases, lysosomal membrane proteins, as well as accessory proteins involved in the processing, trafficking, and targeting of lysosomal proteins (Platt and Walkley, 2004).

To date, mutations in more than 50 different proteins have been identified as causing LSDs, and this list is continuing growing. Amongst these mutations, the most common are mutations in genes encoding a lysosomal hydrolase.

Individually LSDs are rare, affecting between 1:50 000 and $1:4.10^6$ live births, Gaucher disease being the most frequent. However as a whole, this family of diseases has a prevalence of 1:5000 live births (Meikle et al., 1999) (Table 1) comparable with that seen for disorders such as cystic fibrosis, making them a considerable health burden.

As a consequence of lysosomal dysfunction, substrate degradation is impaired, leading to abnormal accumulation (or storage) of undegraded substrates. Storage material initially accumulates in endosomes and lysosomes, and eventually in other intracellular compartments and in the extracellular environment, compromising cellular functions.

2.2. Classification

LSDs are usually classified according to the nature of the primary stored material. Broad categories include mucopolysaccharidoses (MPSs), sphingolipidoses, mucolipidoses, glycoproteinoses, oligosaccharidoses, and glycogen storage diseases. In some cases, a deficiency in a single enzyme can cause the accumulation of multiple substrates. In multiple sulfatase deficiency for example, mutations in the *SUMF1* gene which encodes an enzyme responsible for the post-translational modification of all sulfatases, cause a profound reduction of sulfatase activities and result in the accumulation of sulfated lipids and GAGs.

Table 1: Prevalence of lysosomal storage diseases and mucopolysaccharidoses in the Netherlands and in Portugal.
Adapted from Poorthuis et al., 1999, and data from Genzyme.

a) Prevalence of lysosomal storage diseases.

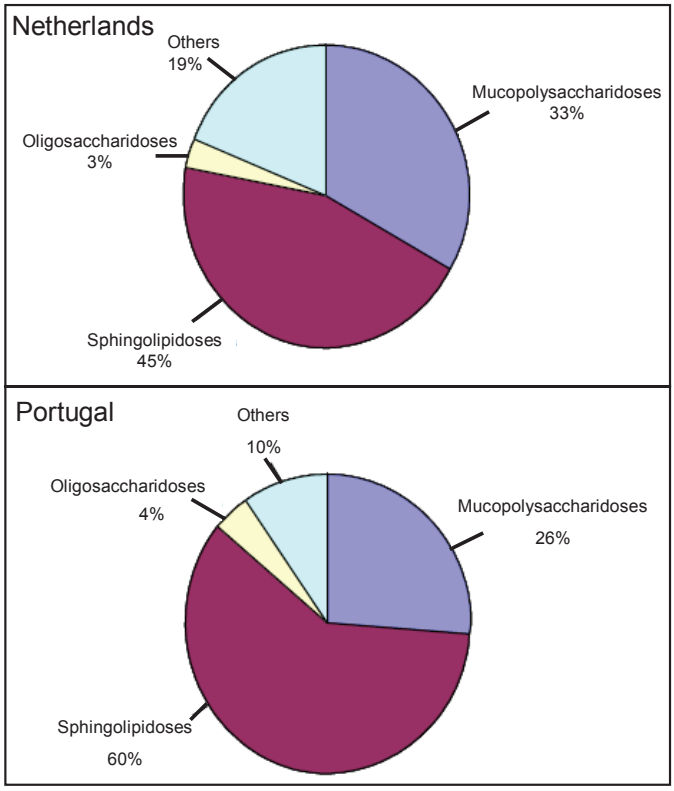

b) Prevalence of the different MPS types.

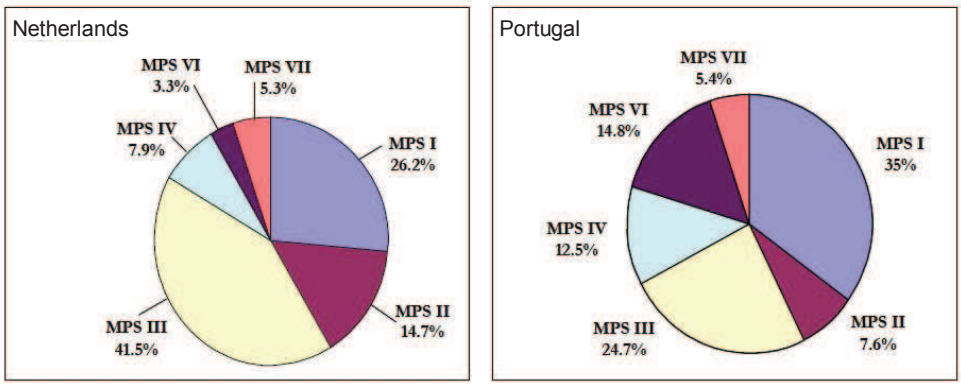

Alternatively to the storage material, LSDs may also be classified according to the type of protein deficiency. Although most defective proteins have a lysosomal location, some are enzymes located in the Golgi or in the ER. Defective proteins can be subdivided into:

- lysosomal hydrolases,
- transmembrane proteins, such as membrane transporters required for incorporation of substrates into the lysosome lumen, and release of degradation products out of the lysosome,
- co-factors or co-activators required for lysosomal enzyme function, for example the GM2 ganglioside activator protein whose defective function causes the AB variant of GM2 gangliosidosis,
- proteins protecting lysosomal enzymes. For instance, cathepsin A has a protective function for both beta-galactosidase and neuraminidase, preventing their intralysosomal proteolysis, and was shown to be deficient in patients with galactosialidosis, a combined deficiency of beta-galactosidase and neuraminidase,
- proteins involved in post-translational processing of lysosomal enzymes as it is the case in multiple sulfatase deficiency,
- enzymes involved in targeting mechanisms for protein localization to the lysosome such as one of the enzymes responsible for the acquisition of the M6P marker, *N*-acetylglucosamine-1-phosphotransferase, which is defective in mucolipidoses type II and III.
- proteins involved in intracellular trafficking. For example cells deficient in LAMP2 or mucolipin-1 display abnormal autophagy and endocytosis, respectively.

This kind of classification may be useful in cases where diseases have been erroneously characterized on the basis of the accumulating substrate before the enzyme defect was identified. For example, mucolipidoses II and III are now known to be caused by the defective targeting of lysosomal enzymes rather than a defect in lysosomal lipases. Similarly, three Niemann-Pick subclasses were initially classified as sphingolipidoses. Today, only Niemann-Pick type A and B have proven to result from mutations in enzymes involved in sphingolipid degradation. There is now evidence that Niemann-Pick type C (NPC), on the contrary, is caused by the defective activity of a

putative cholesterol transporter, the NPC1 protein, or by defects in the soluble lysosomal cholesterol binding NPC2 protein.

The type of protein deficiency and storage product associated with each disease are detailed in Table 2. Despite the distinctive types of storage material in different LSDs, they share many common biochemical, cellular and clinical features, as will be highlighted in the next sections.

Table 2: Classification of the main LSDs.

Disease	Protein deficiency	Chromosome location	Storage material
A. Deficiency of a lysosomal hydrolase or a co-activator			
Glycogen Storage Disease			
Pompe disease (Glycogen Storage Disease type II)	α-1,4-glucosidase or acid maltase	17q23	Glycogen
Sphingolipidoses			
Tay-Sachs (GM2 Gangliosidosis, B variant)	β-hexosaminidase A (α chain)	15q23-q24	GM2 ganglioside/asialo-GM2
Sandhoff (GM2 Gangliosidosis, O variant)	β-hexosaminidase A and B (β chain)	5q13	GM2 ganglioside/ asialo-GM2/globoside
GM2 Gangliosidosis, AB variant	GM2 activator	5q32-q33	GM2 ganglioside/asialo-GM2
GM1 Gangliosidosis, type I, II, III	β-galactosidase	3p21-pter	GM1 ganglioside/ galactosyloligosaccharides/KS
Gaucher disease	β-glucosidase/glucocerebrosidase or saposin C activator protein	1q21 10q21	Glucosylceramide
Niemann-Pick A and B	Sphingomyelinase	11p15.1-p15.4	Sphingomyelin
Krabbe	Galactocerebrosidase	14q31	Galactosylceramide/ galactosylsphingosine
Fabry	α-galactosidase A	Xq22	Globotriaosyl-digalactosylceramide
Metachromatic Leukodystrophy	Arylsulfatase A or saposin B activator protein	22q13-3 10q21	Sulfatides/GM1 ganglioside/ glycolipids
Farber	Ceramidase	8q22-21.2	Ceramide
Prosaposin deficiency	Prosaposin (precursor of saposins A, B, C, D)	10q22.1	Glucosylceramide/sulfatides/ ceramides
Lipidoses			
Wolman	Acid lipase	10q23.2-q23.3	Cholesterol esters
Glycoproteinoses			
α-mannosidosis	α-mannosidase	19q13.2-q12	α-mannosyl-oligosaccharides
β-mannosidosis	β-mannosidase	4q22-q25	β-mannosyl-oligosaccharides
Fucosidosis	α-fucosidase	1p24	Fucosyl-oligosaccharides/ fucosyl-glycolipids
Aspartylglucosaminuria	N-aspartyl β-glucosaminidase	4q32-q33	Aspartylglucosamine
Schindler and Kanzaki	α-N-acetyl-galactosaminidase or α-galactosidase B	22q13.1-q13.2	Oligosaccharides/GAGs/ glycosphingolipids
Sialidosis	α-neuraminidase	6p21.3	Sialyloligosaccharides
Mucopolysaccharidoses (MPS) (defective degradation of GAGs)			
MPS I (Hurler, Scheie, Huler:Scheie)	α-L-iduronidase	4p16.3	HS/DS
MPS II (Hunter)	Iduronate-2-sulfate sulfatase	Xq27-28	HS/DS
MPS IIIA (Sanfilippo A)	Heparan N-sulfatase	17q25.3	HS
MPS IIIB (Sanfilippo B)	α-N-acetyl-glucosaminidase	17q21.1	HS
MPS IIIC (Sanfilippo C)	Acetyl-CoA:α-glucosaminide acetyltransferase	8p11-8q11	HS
MPS IIID (Sanfilippo D)	N-acetylglucosamine-6-sulfatase	12q14	HS
MPS IV A (Morquio A)	Galactose-6-sulfatase	16q24.3	KS
MPS IV B (Morquio B)	β-galactosidase	3p21-pter	KS
MPS VI (Maroteaux-Lamy)	Galactosamine-4-sulfatase	5q13-q14	DS
MPS VII (Sly)	β-glucuronidase	7q21-q22	DS/HS/CS
Pycnodysostosis (defective degradation of polypeptides)			
Pycnodysostosis	Cathepsin K	1q21	Collagen fragments
Neuronal Ceroid Lipofuscinoses (NCL)			
NCL1	Palmitoyl-protein thioesterase (PPT)	1p32	saponins
NCL2	Tripeptidyl-peptidase (TPP)	11p15.5	scMAS

Disease	Protein deficiency	Chromosome location	Storage material
B. Deficiency of proteins protecting lysosomal enzymes			
Galactosialidosis	Cathepsin A	20q13.1	Sialyloligosaccharides/ Galactosyloligosaccharides
C. Deficiency of lysosomal membrane proteins and transporters			
Neuronal Ceroid Lipofuscinoses (NCL)			
NCL3	Battenin NCL3 transmembrane protein	16p12.1	scMAS
NCL5	Lysosomal glycoprotein (transmembrane or soluble protein)	13q22	scMAS
NCL6	NCL6 transmembrane protein	15q21-q23	scMAS
NCL7	NCL7 membrane protein	4q28	?
NCL8	NCL8 transmembrane protein	8p23	scMAS
Niemman-Pick type C			
Niemman-Pick, type C1	NPC-1 (membrane transporter)	18q11	Cholesterol/sphingolipids
Niemann-Pick, type C2	NPC-2 (soluble transporter)	14q24.3	Cholesterol/sphingolipids
Others			
Cystinosis	Cystin transporter (membrane transporter)	17p13	Cystin
Salla	Sialic acid transporter (membrane transporter)	6q14-15	Sialic acid
Cobalamin deficiency	Unkown cobalamin transporter	?	Cobalamin
D. Multiple deficiencies of lysosomal enzymes secondary to defective post-translational modification in the ER or the Golgi			
Multiple sulfatase deficiency			
Austin	Formylglycine Generating Enzyme	3p26	Sulfated lipids/GAGs
Deficiency of M6PR-dependent lysosomal targeting			
Mucolipidosis, type II (I-cell disease)	N-acetylglucosamine-1-phosphotransferase (α-β subunits)	16p	Oligosaccharides/ GAGs/lipids
Mucolipidosis, type III (pseudo-Hurler polydystrophy)	N-acetylglucosamine-1-phosphotransferase (γ subunits)	16p	Oligosaccharides/ GAGs/lipids
E. Deficiency of proteins involved in intracellular trafficking			
Mucolipidoses			
Mucolipidosis, type IV	Mucolipin-1	19p13.2-13.3	Defective endocytic pathway
Others			
Danon disease (Glycogen Storage Disease Type IIb)	LAMP2	Xq24-q25	Defective autophagy pathway

GAGs: glycosaminoglycans, KS: keratan sulfate, CS: chondroitin sulfate, HS: heparan sulfate, DS: dermatan sulfate, scMAS: subunit c of mitochondrial ATP synthase, LRO: lysosome-related organelles.

2.3. Molecular genetics

All LSDs result from mutation in a single gene and are inherited in an autosomal recessive fashion, with three exceptions. These exceptions are Fabry disease and Hunter disease (also called MPSII), which are X-linked recessive diseases, as well as Danon disease, which is inherited in an X-linked dominant manner (Wilcox, 2004). Certain populations have a higher incidence of a particular LSD compared with the general population, largely as a result of ancestral founder mutations. For instance, four LSDs, namely Gaucher, Tay-Sachs, Niemann-Pick type A, and mucolipidosis IV are 50 to 60 times more frequent in Ashkenazi Jewish descendents.

For most LSDs, numerous mutations can affect the same gene, including missense, nonsense and splice-site mutations, deletions, insertions, duplications and inversions. In Tay-Sachs disease for example, over 50 mutations affecting the alpha-subunit of beta-hexosaminidase have been detected. A large allelic heterogeneity also underlies MPSIII diseases with new mutations recently identified, bringing the number of causative mutations to about 100 (Heron et al., 2011).

Some mutations lead to the complete loss of enzyme activity, whereas others lead to reduced activity. Null alleles may be due to major alterations (deletions, insertions, duplications or inversions), but also to small alterations (frameshifts, nonsense mutations, splicing mutations). In the latter case, enzymes frequently fold incorrectly. As a consequence they are retained in the ER, degraded, and they do not reach the lysosome, resulting in the absence of functional residual activity. Residual enzyme activity is only observed in the case of mutations that do not completely abolish folding, processing and catalytic activity of the protein, including missense mutations and mutations affecting splicing but located outside of the consensus site. Remnant residual activity usually does not exceed 5%.

The severity of the phenotype is to some extent related to the residual enzyme activity. In general, the lower the residual activity, the earlier the age of onset and the more severe the disease. For example, Pompe disease is a glycogen storage disease due to a deficiency of the lysosomal enzyme acid, alpha-glucosidase (GAA). Based on the age at onset of clinical symptoms and on the clinical course of the disease, it is classified into three clinical phenotypes, infantile, juvenile and adult. Whereas patients with early onset, infantile Pompe disease have a complete GAA deficiency, resulting

from fully deleterious mutations, patients with late-onset show mutations associated with residual enzyme activity levels (Reuser et al., 1995). The same observations apply to Tay-Sachs disease, a clinical variant of the GM2-gangliosidosis caused by mutation in the gene encoding the alpha subunit of beta-hexosaminidase A. In most cases, enzyme activity is nearly completely absent in the early onset form of Tay-Sachs disease, and patients die within the first years of life. For instance, the mutations R178H (active site mutation that renders the enzyme unable to hydrolyze its physiological substrate) and R499H (mutated enzyme retained in the ER and degraded) are predictive of an early onset and rapidly progressive course (Maegawa et al., 2006; Ohno et al., 2008). In the adult form, symptoms are less severe and develop more slowly, due to the presence of at least one allele associated with residual enzyme activity, generally bearing the G269S mutation, only causing a small structural change on the surface of the protein without affecting the active site (Neudorfer et al., 2005).

However, only in some diseases, phenotypic variability can be explained by differing levels of residual activity. For most LSDs, no obvious genotype–phenotype correlation has been established, and patients with a similar genetic background, and sometimes with the same mutation, can present different clinical symptoms and progression, even amongst affected siblings in the same family including monozygotic twins (Amaral et al., 1994; d'Azzo et al., 1984; Lachmann et al., 2004a). This considerable phenotypic heterogeneity implies that predictions about disease severity, pathology and clinical course can rarely be made on the basis on mutational analysis only. It also suggests the influence of non-genetic factors like environmental factors, modifying genes (i.e. transcription factors), or epigenetic factors (Gieselmann, 2005). Despite our lack of knowledge, some indications corroborate the involvement of such factors:

- A patient study in Sandhoff disease (caused by mutations affecting the beta subunit of lysosomal beta-hexosaminidase A and B) indicates that differences in the splicing machinery between individuals or between different racial groups may influence the phenotypic expression of splice-site mutations (McInnes et al., 1992).
- In a mouse model of Krabbe disease (caused by deficiency of lysosomal galactosylceramidase), hormone administration improves the clinical,

biochemical and pathological features associated with the disease (Matsuda et al., 2001).

- Four transcription factors have been found to regulate the activity of the lysosomal hydrolase acid beta-glucosidase, also called glucocerebrosidase, the deficient enzyme in Gaucher disease (Moran et al., 1997).
- In Gaucher and Tay-Sachs diseases, the activities of glucoceribrosidase and hexosaminidase are modulated by specific activator proteins, the saposin protein and the GM2 activator, respectively. Investigations have suggested that activator proteins may be responsible for the clinical variability between individuals with identical genotypes (Levy et al., 1991; Meier et al., 1991).

2.4. Clinical manifestations

Because lysosomes are present in all eukaryotic cells (with the exception of erythrocytes), and because lysosomal substrates have key roles in many cellular functions, the effects of lysosomal impairment are widespread. Storage may affect the brain, viscera, bones and connective tissues. In many diseases, central nervous system (CNS) involvement is particularly prevalent with minimal peripheral involvement (for example in Sanfilippo disease), whereas in other diseases, the symptoms are restricted to peripheral tissues and organs (for example in Fabry disease).

The age of onset, severity of symptoms, organ systems affected, and CNS manifestations can vary markedly within a single disorder type or subtype. Many disorders may exist in three forms, infantile, juvenile and adult, as in Pompe, Tay-Sachs (seen above), Gaucher, Sandhoff, Metachromatic Leukodystrophy, and GM1 gangliosidosis. Usually, in the most severe, infantile forms, symptoms arise from brain pathology, while in milder adult forms disability results mainly from peripheral symptoms. Juvenile forms are intermediate between infantile and adult forms. In the case of Gaucher disease three major classes have been defined, depending on the absence or presence and severity of neurological involvement. Type I (historically called the adult form) is the non-neuronopathic form. It is the mildest form, affecting the liver, spleen, bones, and blood cells. Both type II and type III have neuronopathic involvement. Patients with type II Gaucher disease (acute infantile neuronopathic form)

exhibit early onset, whereas patients with type III (subacute juvenile neuronopathic) present later onset neurological symptoms.

Brain pathology involves two-thirds of all LSDs, with neurons being particularly vulnerable, which makes LSDs the most common cause of pediatric neurodegenerative disease. Here, clinical manifestations may involve mental retardation, progressive regression after a period of normal development, dementia, sensory loss including blindness or deafness, motor system dysfunction, seizures, brain atrophy, demyelination, sleep and behavioral disturbances. Affected individuals generally appear normal at birth but symptoms appear soon after birth. Neuropathology is progressive and ultimately leads to death at an early age.

Pathology in peripheral organs may result in organ enlargement such as hepatosplenomegaly or cardiomegaly, cardio-respiratory failure, gastrointestinal, vascular, or renal symptoms, growth restriction, dysostosis multiplex (bone changes), joint stiffness, skeletal deformation, facial dysmorphism ("coarse" facial phenotype), dermatological manifestations such as pigmentation defects and skin eruptions, immune deficiency, muscle atrophy and so forth.

In LSDs, there is a good correlation between the clinical and pathological picture on the one hand, and on the other hand the nature of the accumulating substrate, its physiological function and the cell types in which it accumulates. Affected tissues and organs are those which synthesize the substrate or acquire it by active mechanism such as phagocytosis, and in which the substrate turnover is physiologically high. For example, the enzyme *N*-acetyl-galactosamine-6-sulfate is critical in the lysosomal breakdown of keratan sulfate, primarily found in the skeletal system. A defect in this enzyme, as in MPS type IVA, causes abnormal storage of keratan sulfate in the skeletal system, thus resulting in severe skeletal problems. Individuals with defects related to myelin metabolism such as in Krabbe disease or Metachromatic Leukodystrophy will present with CNS pathology. Alternatively, glycogen-storage diseases such as Pompe disease are characterized by myopathy, which is expected on the basis of the important role that glycogen has in muscle.

In fact, this heterogeneity regarding affected organs or tissues is governed, at least in part, by complex enzyme kinetics. Each organ system or tissue has a threshold of enzymatic activity below which pathological changes occur. This threshold can differ in

different tissues, and at a cellular level it is dependent on substrate flux, cellular turnover, and metabolic demands.

2.5. Diagnosis

LSDs typically are not evident at birth, and they are commonly progressive in nature. Early diagnosis is critical for the efficacy of many available treatments. Diagnosis can prove difficult because of the marked heterogeneity in clinical expression within disorders, and due to the clinical similarities amongst many disorders. A delay between onset of symptoms and diagnosis is common. A pediatrician may be able to quickly identify problems in an infant with classic MPSI-H (Hurler syndrome) showing specific symptoms such as coarsening features and neurodegenerative decline. However, more attenuated forms of MPSI-S (Scheie syndrome) may go unnoticed for years, due to the subtle progressive nature of the disease and the absence of intellectual deterioration. Children with MPSIII commonly present with behavioural problems and are thereby often misdiagnosed with autism or attention deficit hyperactivity disorder (ADHD). Diagnosis test for MPSIII is generally considered later, after several other pathologies have been excluded. This points to the importance of informing clinicians and raise their awareness of the problems involved in diagnosing rare diseases.

In case of clinical suspicion, a battery of tests may be necessary to arrive at a definitive diagnosis. Diagnostic tools include screening tests on both blood and urine. Storage material can be excreted in urines, and detected by electrophoretic and chromatography methods, for example sialic acid or oligosaccharides in mucolipidoses, and GAGs in MPS. The most reliable method for definitive diagnosis is the demonstration of deficient enzyme activity. Usually performed on blood samples, specific enzyme assays use artificial fluorogenic, chromogenic, or radioactive substrates.

For some disorders involving defective transporters or activator proteins, more complicated diagnostic assays on cultured skin fibroblasts have to be performed. Cholesterol accumulation in NPC can be revealed by filipin staining on cultured skin fibroblasts. When an LSD is strongly suspected, but initial biochemical studies are normal, more invasive procedures may be indicated. They rely on a tissue biopsy that

will be studied at the ultrastructural level by electron microscopy to confirm the presence of lysosomal distensions typical of all LSDs. DNA analysis can also be performed, although it is not a method of choice because of the heterogeneity of mutations.

In addition, mass spectrometry techniques may be useful for diagnosis. Advances in such techniques have allowed to directly analyze the activity of lysosomal enzymes (Gerber et al., 2001; Li et al., 2004), to detect storage products, and to identify specific biomarkers, best illustrated by chitotriosidase, a biomarker that exhibits on average 1000 fold higher plasma levels in Gaucher patients (Aerts et al., 2005).

Prenatal diagnosis is only performed in the case of family history. It can be achieved on amniotic fluid and chorionic villus samples by a variety of techniques including enzyme activity assays, molecular testing, or ultrastructural examination.

Presymptomatic newborn screening is nowadays non systematic, the rationale being that there is no treatment available for most LSDs. Furthermore, such screening tests would also detect newborns affected by late-onset variants of LSDs which will manifest only decades later, raising ethical concerns.

Systematic newborn screening is however conceivable in the case of diseases for which early treatments exist and are beneficial, or which have a high prevalence in a certain population. This would ensure early management, which is especially important because once damages have occurred, they can not be reversed in most LSDs, and would also ensure follow-up for affected patients. Long-term follow-up informations would provide a registry of patients that would be useful to assess genotype-phenotype relationships and study the natural history of conditions, and would impact the quality of current therapies and favor the development of novel therapies. For these reasons, several newborn screening public health programs have been launched, involving three LSDs, Pompe and Fabry diseases in the Tawainese population, and Krabbe disease in the state of New York (Chien et al., 2008; Hwu et al., 2009; Lin et al., 2009; Spada et al., 2006). For routine newborn screening, assays are performed using dried blood spots on filter papers. Tandem mass spectrometry (MS/MS) has proven accurate, but requires expensive equipments and extensive sample preparation.

Newborn screening program for Krabbe disease yielded surprising outcomes (Duffner et al.; Duffner et al., 2009). First, important discrepancies were raised between

the expected incidence of Krabbe disease and the actual observed incidence. Second, it appeared that neither galactocerebrosidase activity nor genetic mutation allowed reliable phenotype prediction. After several years, the majority of children with low galactocerebrosidase activity and two genetic mutations and who were therefore expected to manifest the early infantile phenotype have remained clinically unaffected. Many low-risk infants have also been identified, but it remains unknown whether they will ever develop Krabbe disease.

Finally, premarital genetic testing programs exist and concern populations in which a relatively high incidence for a specific LSD has been found. Mutation analysis is the method of choice when a few mutations account for the majority of the disease alleles, e.g. in the case of established founder mutations. In other cases, biochemical assays to measure enzyme activity are preferred. The first prevention program for LSD was initiated in the early seventies for the detection of Tay-Sachs carriers in the Ashkenazi Jewish population, and resulted in a reduction of 90% in the birth of Tay-Sachs children in this population (Bach et al., 2007).

2.6. Therapies

There are limited treatments clinically available for LSDs. Symptomatic palliative therapies are readily available, but only very marginally improve the outcome of these diseases. The most classical therapeutic intervention consists of bone marrow transplantation (BMT). For some LSDs, enzyme replacement therapy (ERT) is in clinical use.

LSDs affecting the brain present formidable difficulties in term of treatment, since existing approaches are only poorly efficient regarding CNS manifestations. An important obstacle comes from the blood-brain barrier (BBB) that restricts entry of therapeutic molecules to the CNS. Promising strategies are evolving to allow CNS targeting, such as substrate reduction therapy (SRT), enzyme enhancement therapy (EET), stop-codon readthrough, cell-mediated therapy, or gene therapy, but are still experimental.

The concept of M6P-based secretion and recapture mechanism is of considerable importance when considering therapy. Strategies consisting in therapeutic enzyme

delivery take advantage of the cross-correction mechanism, meaning that there is no need to target every cell (see section 1.2.1).

2.6.1. Bone marrow transplantation

When human leukocyte antigen (HLA)-matched donors are found, allogeneic hematopoietic stem cell transplantation (HSCT), also termed BMT, may be an option. Wild-type transplanted cells are engrafted into the patient and release some amount of the required enzyme in their environment, which can be taken up by neighboring cells. A limited number of the transplanted cells is able to cross the BBB, and donor-derived macrophages and microglia can populate the brain and cross-correct enzyme-deficient cells such as neurons or glia. Practical considerations limit this approach: the availability of compatible donors, the significant transplant-related morbidity and mortality rate (graft-versus-host disease) ranging between 10% and 25% (Hoogerbrugge et al., 1995), and the low and delayed brain repopulation by transplanted microglia, limiting efficiency of enzyme delivery to the brain.

This procedure has been assessed in a number of LSDs. Since the first BMT in 1980, over 500 patients with an LSD have received HSCT. Based on clinical experience, HSCT has led to promising results in the following diseases: MPS type I (Hurler syndrome), MPS type VI (Marateaux-Lamy syndrome), MPS type VII (Sly syndrome), Krabbe disease, Metachromatic Leukodystrophy, alpha-fucosidosis, alpha-mannosidosis, Gaucher disease, and Niemann-Pick disease type B (Peters and Steward, 2003). For most other LSDs, there are either limited or discouraging data to recommend such treatments.

Most successful results come from Hurler disease and Krabbe disease. In patients with Hurler disease, a rapid decline in GAG excretion was observed following transplantation. If performed early in the disease course, before the age of 2 years, and prior to the manifestation of neurological disease, HSCT has the potential to stabilize and even improve cognitive and neurological functions. In peripheral organs, transplantation results in improvement of obstructive airway symptoms, reduction of liver and spleen volume and stabilization of heart function. However, it has no effect on the skeletal disease. In infants diagnosed with Krabbe disease, HSCT significantly increases life span and ameliorates neurological outcome when performed before

disease onset (Escolar et al., 2005). Benefits are however limited, as children still develop motor difficulty, as well as persistent cognitive deficits. When the patient is already symptomatic, HSCT does not significantly modify the course of the disease.

More recently, alternative stem cell sources such as umbilical cord blood stem cells have been used. Cord blood has advantages compared with bone marrow hematopoietic stem cells, namely improved engraftment rate and lower morbidity rate related to graft-versus-host disease (Rocha et al., 2001). Because of the lower risk of graft-versus-host disease, requirements for HLA identity between donor and recipient are less stringent. Generally, stem cells originating from umbilical cord blood are derived from unrelated donors and release more enzyme than bone marrow hematopoietic stem cells. Indeed, these latter cells are often derived from family-related donors who are heterozygote for the disease allele and deliver little enzyme amounts. Despite these advantages, experience with umbilical cord blood stem cells led to similar conclusions regarding clinical efficacy, with limited improvement. To obtain more satisfactory results, a solution would be to increase enzyme production levels by gene therapy (see 2.6.7).

2.6.2. Enzyme replacement therapy

ERT consists in injecting highly purified human lysosomal enzymes intravenously. This approach can therefore not be used to treat LSDs characterized by neuronal pathology, because intravenously administered enzymes do not cross the BBB. ERT is clinically available in a number of LSDs with no neurological involvement. Current treatment protocols consist in lifelong frequent infusions which can vary from weekly to monthly.

ERT first became clinically available in 1991 with Food and Drug Administration (FDA) approval for imiglucerase, a recombinant enzyme for the treatment of non-neuronopathic (type I) Gaucher disease. Macrophages are the main pathological cell type involved in this disease, caused by glucocerebrosidase deficiency, making them important therapeutic targets. Strategies aimed at targeting glucocerebrosidase to macrophages take advantage of the mannose receptors (MRs) present on the cell surface of these cells. As carbohydrate moieties of the native glucocerebrosidase (either isolated

from placenta or produced by recombinant DNA technology) do not bear terminal mannose residues, the enzyme has to be treated with exoglycosidases to remove some sugar residues, thus exposing terminal mannose residues on the carbohydrate chains. Because macrophages are easily targeted by ERT, this treatment gives remarkable results, reducing the visceral manifestations (hepatosplenomegaly), improving hematological parameters, ameliorating skeletal damage, and reducing episodes of pain crises (Barton et al., 1991; Grabowski et al., 1995). ERT is a life-transforming treatment in this disease, reversing many of the pathological consequences, and preventing further progression.

The success of ERT in Gaucher disease led to the development of licensed products for several other LSDs, including different MPSs, Fabry disease, and Pompe disease. In contrast to Gaucher disease, these LSDs affect cell types that lack the MR. A different receptor, the M6PR, is used to allow uptake of lysosomal enzymes. Eukaryotic expression systems have been developed that are able to carry out the appropriate post-translational modifications of the enzymes, primarily the generation of M6P residues. Chinese hamster ovary (CHO) cells in which the cDNA encoding the desired lysosomal enzyme is overexpressed are typically used. Most of the recombinant enzyme is secreted into the culture medium, from which it can be purified, e.g. by chromatography. Reported results are summarized here:

- For Fabry disease, ERT using recombinant alpha-galactosidase A has been clinically available since 2003. Improvement in pain and gastrointestinal symptoms has been reported (Banikazemi et al., 2007; Ramaswami et al., 2007).
- Laronidase was approved in 2003 for use in MPS I and has been demonstrated to be safe and effective in patients with the milder forms of the disease (Hurler-Scheie and Scheie phenotypes), with reported improvements in hepatosplenomegaly and respiratory disease and decrease in urinary GAG excretion (Wraith et al., 2004).
- Recombinant arylsulfatase B was approved for clinical use in MPS VI in 2005 and has been associated with improvements in hepatosplenomegaly, joint movement, cardiopulmonary function, and pain as well as reduced excretion of urinary GAGs (Harmatz et al., 2006).
- Alglucosidase alpha is FDA approved for use in infantile Pompe disease. It has shown success in reversing pathology in cardiac muscle and extending life

expectancy in infantile patients. However, skeletal muscle has proven to be a more challenging target for ERT (Kishnani et al., 2007).

- The latest recombinant human enzymes available clinically are galsulfatase and idursulfase for the treatment of MPS VI and the mild form of MPS II, respectively. These enzymes allow improvement in pulmonary disease and hepatosplenomegaly and decreased excretion of urinary GAGs (Giugliani et al., 2011; Muenzer et al., 2006).

Although all of these treatments have shown encouraging results, none has approached the effect of imiglucerase in Gaucher disease. In fact, the degree and extent of benefit vary considerably depending on the affected tissues and organs. This is because the level of enzyme correction is governed by receptor-mediated uptake mechanisms, which is variable according to cell types. Thus, macrophages or Kupffer cells of the liver are easily accessible to intravenously delivered enzyme. By contrast, enzyme uptake is particularly limited in the kidney in Fabry disease, bone in the MPSs or skeletal muscle in Pompe disease. The fact that many manifestations do not respond or respond poorly to ERT implies that there is continued disease progression despite therapy, and points out the need for very early intervention to limit organ damage.

Possible complications can arise from the development of circulating antibodies directed against the infused protein. Such immunological reactions can be particularly feared in the case of null mutations where the immune system is naive to the missing lysosomal enzyme, but less in cases associated with residual enzyme activity where a mutant enzyme is present. Reported rates of antibody formation in treated patients range from 15% for Gaucher disease to 97% and 100% for MPS VI and Pompe disease, respectively. Two major problems have been identified in association with antibody responses to ERT. First, hypersensitivity reactions may develop either during or immediately after enzyme infusion. Clinical signs of hypersensitivity reactions (e.g. urticaria, fever, and chills) can be managed with antihistamines and non-steroidal anti-inflammatory drugs and by slowing the infusion rate. Second, although clinical experience showed that ERT continues to be effective even in the presence of antibodies, studies in animal models revealed that antibody reactivity may substantially limit the therapeutic efficacy of ERT. More precisely, these studies provided evidence that antibodies may inhibit enzyme uptake and redirect the enzyme to other tissues, affecting enzyme distribution, or they may lead to enzyme inactivation and degradation,

affecting enzyme action (Brooks et al., 1997; Dickson et al., 2008). In some cases, patients who initially had an immune reaction develop immune tolerance to the infused protein, characterized by a progressive decline in antibody titers (Kakavanos et al., 2003). Overall, it is rare that a patient will have to discontinue therapy because of adverse infusion reactions.

The lack of efficacy of ERT in treating some manifestations of LSDs (in particular CNS manifestations), the need for regular intravenous infusions and its high cost (the estimated cost in the US is between $90,000 to $565,000, depending on the disease and patient size) provide a rationale for the development of alternative therapies such as SRT, EET, cell therapy or gene therapy.

2.6.3. Substrate reduction therapy

In SRT, the aim is to reduce the biosynthesis of the accumulating substrate of a deficient enzyme to prevent storage. A balance between the rate of synthesis and the impaired rate of catabolism of the substrate is thus created. This strategy employs inhibitory molecules to restrain biosynthesis of metabolites upstream of the deficient catabolic pathway that is affected in particular. Although lack of complete inhibitor specificity and long-term disruption of biosynthetic routes may cause side effects and parallel metabolic imbalances, this therapeutic strategy holds great potential. A considerable advantage of inhibitor drugs is that they offer simple oral medication. So far, this approach has been applied only to glycosphingolipid storage diseases.

One drug is already FDA approved for use, miglustat, an inhibitor of glucosylceramide synthase, an enzyme which catalyzes the first step in the synthesis of glucosylceramide-based glycosphingolipids. As glucosylceramide is the precursor of several glycosphingolipids, miglustat represents a potential treatment for a variety of LSDs including Gaucher disease, Fabry disease, GM1- or GM2-gangliosidoses (such as Sandhoff and Tay-Sachs diseases), and even NPC. In mouse models of these diseases, miglustat has been demonstrated to clear glycosphingolipid storage in peripheral tissues and in the brain and to delay symptom onset and increase life expectancy (Lachmann, 2006).

Miglustat was first clinically developed for non-neuronopathic Gaucher patients. Eligible patients are those for whom ERT is unsuitable. This drug has proven effective in treating the systemic manifestations of the disease such as hepatosplenomegaly or hematological problems (Pastores et al., 2005). Subsequently, a number of trials have been carried out in neurological storage disorders, the rationale being that miglustat is able to cross the BBB to some extent since it is a small molecule. SRT did not show any effect on the neurological aspects of patients with neuronopathic Gaucher disease or GM2-gangliosidosis (Maegawa et al., 2009; Schiffmann et al., 2008; Shapiro et al., 2009). However, it showed stabilization of disease progression in NPC disease (Patterson et al., 2007), and miglustat is now licensed for the treatment of this disease in the European Union, Canada, Switzerland, Brazil, Australia, Turkey and Israel.

Overall, the potential of SRT in the case of neuropathology is still unclear. Other SRT molecules with greater specificity and improved delivery to the brain are now being developed. Besides inhibitors of glycosphingolipid synthesis, genistein, an inhibitor of Heparan Sulfate (HS) synthesis is being evaluated in MPSs (Arfi et al., 2010; Friso et al., 2010; Malinowska et al., 2009).

2.6.4. Enzyme enhancement therapy

EET aims at stabilization and rescue of an existing mutant enzyme by using chaperone molecules. The use of drug chaperones may be beneficial in LSDs that are caused by genetic mutations that do not affect enzyme functionality but cause enzyme misfolding defects, often missense mutation or frame-shift deletions (see paragraph 2.3). Chaperones function by stabilizing misfolded mutant proteins, such that the stabilized conformation can move out of the ER, escape proteasomal degradation and be delivered to the lysosome where they can express their residual enzyme activity. Chaperones can be substrate analogues, active-site inhibitors, cofactors or effector molecules. Potential pharmacological chaperones may be already commercially available, having been licensed for other indications.

This type of therapy appears to be mutation dependent, as diseases caused by null mutations resulting in no gene product, as well as mutations impairing enzyme activity or catalytic site would not be expected to be aided by chaperone therapy. As in SRT,

EET uses low-molecular-weight molecules that can be taken orally, and can cross the BBB and should have a better biodistribution than recombinant enzyme.

Various chemical and pharmacological chaperones have been used in research settings. On cultured fibroblasts isolated from Gaucher, Fabry, Sandhoff or Tay-Sachs patients with a missense mutation, EET resulted in increased enzyme activity and reduction of the storage product (Sawkar et al., 2002; Tropak et al., 2004; Yam et al., 2005). To determine if this approach would be effective *in vivo*, a patient with Fabry disease who had severe heart complications was treated with galactose infusions three times a week. Chaperone-mediated enhancement of residual alpha-galactosidase A activity led to marked improvements in cardiac function (Frustaci et al., 2001). Subsequent clinical development has focused on the imino sugar 1-deoxygalactonojirimycin, which has shown good efficacy in a mouse model of Fabry disease and is now in phase II of clinical development (Khanna et al., 2010).

A few studies on mouse models of LSDs including GM1-gangliosidosis and Fabry disease have documented the potential of EET on brain pathology (Khanna et al., 2010; Matsuda et al., 2003).

2.6.5. Stop-codon readthrough

Many LSD patients have a premature stop-codon mutation, e.g. 76% in MPSI or 52% in neuronal ceroid lipofuscinosis (NCL) type 1. Generally, premature stop-codon mutations result in minimal to no residual enzyme activity and are associated with a severe clinical phenotype. Here, a potential treatment strategy consists in using drugs which are known to influence the fidelity of the stop-codon recognition process, enhance the extent of readthrough and allow production of a full-length functional protein (Brooks et al., 2006). The antibiotic gentamicin can bind to the ribosomal RNA (rRNA), induce misreading of the stop-codon as a sense codon, and allow recognition of the stop-codon by a transfer RNA (tRNA) charged with an amino acid corresponding to the misread codon sequence. For example, the stop codons UAA or UAG can be misread as CAA or UGG, respectively (single-base misreading) leading to the incorporation of Glutamine or Tryptophan amino acids into the polypeptide chain. In some cases, readthrough can generate proteins with a missense mutation, but these

mutant proteins will have residual enzyme activity and help improve the clinical phenotype.

Stop-codon readthrough represents a means to provide enzyme from the biosynthetic route and presents potential advantages over ERT. Because drugs that are used to influence stop-codon readthrough are low-molecular-weight drugs, they can offer widespread access to different cells, tissues and organs and improve pathology in sites that are not easily accessible by ERT. Importantly, they are possibly able to cross the BBB and treat brain pathology.

Gentamicin-induced stop-codon readthrough has been investigated as a treatment for MPSI. *In vitro* it has been shown to correct alpha-L-iduronidase defect, reduce accumulation of primary storage products, and reduce cell pathology (Keeling et al., 2001). However, human trials with gentamicin for other genetic diseases such as Duchenne muscular dystrophy have obtained doubtful results (Malik et al.). New classes of molecules with readthrough activity are being developed and evaluated.

2.6.6. Stem cell-based therapy

Stem cells are defined as cells that have the ability to self-renew continuously and differentiate into diverse specialized cell types. Mammalian pluripotent stem cells can be embryonic stem cells (ESCs) derived from the inner cell mass of blastocysts, but recent technologies have also allowed the reprogrammation of adult somatic cells into embryonic-like pluripotent stem cells (Park et al., 2008b; Takahashi et al., 2007b; Yu et al., 2007). The generation of these induced pluripotent stem cells (iPSc) alleviates ethical issues raised with the use of embryonic stem cells.

Besides pluripotent stem cells which can differentiate into nearly every cell type, tissue-specific multipotent stem cells can be isolated in developing or adult organisms. Multipotent cells possess the ability to differentiate into a closely related family of cells. Examples include hematopoietic stem cells (HSCs) that can become erythrocytes, leukocytes or platelets, as well as neural stem cells (NSCs) or neural progenitor cells (NPCs) that can differentiate into the three major CNS cell types, neurons, astrocytes, and oligodendrocytes.

Although cell therapies for LSDs using human pluripotent stem cells are far from being a reality, there have been some trials with NSCs and NPCs. Several properties make them attractive: they are capable of migrating widely, differentiate into various cell types, and engraft within the host brain without disrupting normal function. Transplanted cells can serve as a source of enzyme, but also through their propagation capacity, they can offer the potential to repair damaged brain cells (cell replacement).
Studies in mice used NSCs or NPCs isolated from donor mice, derived from immortalized cell lines, or from human origin. In some cases, cells were genetically modified *in vitro* with retroviruses to overexpress the desired enzyme before transplantation. To bypass the BBB, NSCs and NPCs were transplanted into the brain of diseased animal models of MPSVII, Sandhoff, Niemann Pick A and Metachromatic Leukodystrophy (Shihabuddin and Aubert, 2010). These studies provided demonstration of the therapeutic potential of such approaches. Broad distribution of enzymatic activity in brain of transplanted mice, and reduction of lysosomal storage were reported.

A technology was developed to purify Human Central Nervous System Stem Cells (HuCNS-SC) using monoclonal antibodies directed against a cell surface marker of human NSCs, and expand these cells in culture. Preclinical studies have shown cell engraftment, migration, and differentiation into the three major CNS cell types following transplantation into the brain of immunodeficient mice, with long-term survival, and no evidence of tumor formation or adverse effects. These successful preclinical studies led to the initiation of a human clinical trial to evaluate the safety and effectiveness of neural stem cell-mediated therapy in children with infantile, or late infantile NCL (ClinicalTrials.gov identifier: NCT00337636). The protocol used includes delivery by direct transplantation into multiple sites within the brain, and medication to suppress the immune system. The results from a Phase I clinical trial demonstrated that high doses of human NSCs were well tolerated.

2.6.7. Gene therapy

General aspects of gene therapy

Gene therapy using viral vectors has been under development for the last two decades, and offers real hope for treating inherited diseases. In animal models, three

types of viral vectors have been used frequently in gene replacement strategies: adenoviruses, retroviruses, and adeno-associated viruses (AAV). In gene therapy, the transduction ability of these vectors is used, but non-essential viral coding sequences including those required for viral replication are removed and replaced with a functional copy of the gene of interest. The promotor/enhancer complex contained into the expression cassette restricts transgene expression to a target tissue. In order to produce these replication deficient virus particles, packaging cell lines are required that express the genes that have been deleted in the recombinant viral vector.

Adenoviral particles were often used because they are easy to produce, and because they do not integrate into the host genome. However, experience with adenoviruses showed that they only provide transient transgene expression due to brisk host immune responses, and their use in a clinical trial for ornithine transcarbamylase deficiency resulted in the death of a patient from systemic inflammatory response (Raper et al., 2003).

Today, retroviruses and AAV are preferred to adenoviruses, and gene therapy trials are now coalescing around two strategies: *ex vivo* gene transfer into progenitor cells using retroviruses (in particular the lentivirus subclass), and AAV-based *in vivo* gene transfer. In the former strategy, progenitor cells such as HSCs and other stem cells are isolated from the patient, grown *in vitro*, and transduced with retroviruses that are particularly efficient at transducing proliferative cells. Genetically modified cells expressing the desired protein are subsequently re-injected to the patient. Retroviral vectors are capable of integrating their genome into the host genome, providing prolonged protein expression. *In vivo* gene therapy consists in direct infusion of the AAV vector to the patient. AAV vectors have tropism for slowly dividing or non-dividing cells (such as liver, brain, heart, muscle and retina), where transgene expression can persist for years without the need for vector re-administration.
Retroviruses and AAV have been broadly used in gene therapy approaches for a variety of inherited disorders. Despite exciting preclinical data, unexpected complications appeared in clinical studies, and should be considered to design future gene therapy trials for LSDs.

The integrative property of retroviruses raised major safety issues. Random integration of the therapeutic vector genome into the patient's genome, a process called as insertional mutagenesis, was first reported in a clinical study for the treatment of X-linked severe combined immune deficiency (SCID). The procedure was an *ex vivo*

transduction of $CD34^+$ hematopoietic cells using "first-generation" gamma-retroviral vectors. Four patients developed leukemia as a result of vector integration into the LIM domain-only 2 (LMO2) proto-oncogene (Hacein-Bey-Abina et al., 2008). Advances in vector design led to the production of retroviral or lentiviral vectors with self-inactivating long-terminal repeats (LTRs) likely to reduce the risk of insertional mutagenesis (Modlich et al., 2006; Montini et al., 2006).

AAV vectors are considered safe, since AAV genomes persist mainly as stable episomes, and integrated AAV genomes are only rarely detected. When integration takes place, deletions at the site of integration have been found (Nakai et al., 2003). In a long-term study assessing the genotoxicity of high dose AAV-mediated gene transfer in mice, no evidence was found that AAV vectors cause insertional activation of oncogenes and subsequent tumor formation (Li et al., 2011). The major hurdle for *in vivo* gene transfer using AAV vectors results from immune responses to either the vector or the transgene product. In clinical studies for hemophilia, lipoprotein lipase deficiency, or muscular dystrophies, immunotoxicity was associated with loss of therapeutic efficacy (Manno et al., 2006; Mendell et al., 2010; Stroes et al., 2008). Two strategies have been developed to avoid immune responses, first vector co-administration with an immunosuppressive regimen (Mingozzi et al., 2007), and second development of more efficient vectors (Nathwani et al., 2011). Vector improvements include more efficient expression cassette, the use of AAV serotypes showing a stronger tropism for the targeted tissue, and the use of a self-complementary vector.

A better knowledge of potential complications of gene therapy, and the establishment of strategies to bypass these complications have led to exciting results, and gene therapy is moving closer to clinical applications. Over the past three years, there has been increasing reports of successful clinical trials for human genetic diseases including congenital blindness, X-linked adrenoleukodystrophy (a metabolic, peroxisomal disorder), or haemophilia (Aiuti et al., 2009; Bainbridge et al., 2008; Cartier et al., 2009; Maguire et al., 2009; Maguire et al., 2008; Nathwani, 2010). The first licensing application for a gene therapy drug for lipoprotein lipase deficiency has now been filed (Amsterdam Molecular Therapeutics, 2010; Gaudet et al., 2010).

Gene therapy applications for LSDs

Although gene therapy is not yet a reality for LSDs, encouraging progress is being made. LSDs provide a good model for such therapy because they are monogenic

diseases, with a known defective gene, and because even small increases in enzyme levels (10-20%) can greatly improve clinical outcome.

AAV-mediated *in vivo* gene transfer mainly focuses on two target organs: the liver and the brain. Following liver-directed gene transfer, the liver produces large amounts of therapeutic enzyme that is secreted into the bloodstream and recaptured by other organs through the M6PRs. This strategy has the potential to provide peripheral correction of a number of LSDs, but not necessarily CNS correction because of the BBB obstacle. Long-term efficacy of this technique has already been achieved in small and large animal models of several LSDs with systemic involvement. For example, correction of biochemical and pathological abnormalities (e.g. bone deformities, cardiovascular, renal or sensory dysfunctions) were demonstrated in mouse models of Fabry disease, MPSVII, MPSI, MPSII or Gaucher disease, accompanied with an increased life expectancy (Cardone et al., 2006; Daly et al., 2001; Jung et al., 2001; McEachern et al., 2006; Watson et al., 2006).

Several strategies have been developed to allow gene delivery to the CNS. Widespread distribution to the brain depends on the secretion-recapture mechanism, but also on anterograde and retrograde axonal transport, allowing delivery of therapeutic enzymes over long distances. Recent development with AAV serotypes may represent future avenues to overcome the BBB. AAV serotype 9 is able to cross the BBB and therefore can be injected intravenously and efficiently target neurons and astrocytes (Cearley and Wolfe, 2007; Foust et al., 2009). Another strategy to overcome the BBB relies on AAV engineering techniques. AAV capsid modifications were used to redirect the AAV vector tropism to the vascular endothelium of the diseased brain. Gene transfer using this engineered AAV vector resulted in cross-correction of the underlying neurons and glia and phenotypic improvement in murine models of two LSDs: late infantile NCL, and MPS type VII (Chen et al., 2009).

None of these strategies aimed at targeting the CNS have progressed beyond the pre-clinical stage. Current delivery techniques consist in direct intracerebral administration of AAV vectors at multiple sites for widespread distribution, using stereotactic injection techniques. Despite representing a somewhat invasive procedure, very relevant therapeutic results associated with this practice have been obtained. In animal models of LSDs with CNS involvement such as MPSI, MPSIII, late infantile NCL, Tay-Sachs, or Niemann Pick type A, AAV injections to the brain resulted in

reduction of storage material, and improvements of CNS function including reduction of neuropathology, improvement in neuronal plasticity, preservation of motor functions, or recovery of behavioural functions (Cachon-Gonzalez et al., 2006; Cressant et al., 2004; Desmaris et al., 2004; Dodge et al., 2005; Ellinwood et al., 2011; Passini et al., 2006).

Up to date, several clinical trials using AAV delivery to the brain to treat neurodegenerative diseases including Parkinson's disease, Canavan disease, and one LSD, late infantile NCL, have demonstrated the safety of this approach in humans. Adult human patients with Parkinson's disease were treated with a single or multiple AAV vector deposits in the brain, depending on the trial. In the neurturin trial, a treatment based on the delivery of a neurotrophic factor that protects neurons from death, patients received 12 AAV vector deposits in the striatum bilaterally. Tolerance to surgery and vector deposit was excellent in the 56 patients enrolled in the phase II neurturin trial (Marks et al.), as well as in 40 patients enrolled in various phase I studies with different protocols. In the Canavan disease and late infantile NCL trials, children were enrolled. In a phase I Canavan disease trial, ten children have been treated using intracranial infusion of an AAV vector via six burr holes (one injection site per hole) into the brain parenchyma, with no adverse events (McPhee et al., 2006). Clinical study of gene transfer for late infantile NCL was conducted using a similar procedure. In ten children with the disease, the vector was delivered into the brain parenchyma, through six burr holes, with two injections per hole, resulting in a total of 12 injection points, all located in the cerebral cortex (Worgall et al., 2008). One subject in this study developed intractable seizures and died 49 days post-surgery. The reasons of these serious adverse effects could not be determined under the conditions of the experiment, that is, wether they were related to the progression of the disease, the surgical procedure, or the vector itself. In the other subjects, results suggested -but did not fully prove- slowing of disease progression. There are two noteworthy limitations of this study. First, the number of injection sites, the volume injected, and the concentration of the vector were restricted on the basis of safety constraints, and it is likely that wide distribution within the brain and sustained high protein levels could not be achieved. Second, severely affected children were enrolled, for whom therapeutic benefit is expected to be limited. Indeed, brain atrophy, which can typically not be reversed by gene therapy, progressively develops in late infantile NCL patients. This emphasizes the importance of treating the disease as early as possible, and carefully evaluating clinical severity in enrolled patients. Based on these considerations, a new Phase I/II study was recently

initiated by the same group (ClinicalTrials.gov identifier: NCT01161576). This study uses the same delivery technique and expression cassette, but the latter is packaged into the AAVrh10 serotype instead of the AAV2 capsid used in the previous trial.

Besides liver-directed and CNS-directed strategies, it has to be noted that a muscle-directed clinical trial for Pompe disease has been approved and is expected to start at the end of the year (ClinicalTrials.gov identifier: NCT00976352).

Based on the positive clinical experience with BMT in some LSDs, *ex vivo* gene therapy using retrovirus or lentivirus-modified HSCs is considered as an attractive alternative for the treatment of LSDs. Gene transfer strategies may have significant advantages compared with conventional allogeneic stem cell transplantation. Because autologous cells are used for gene therapy, there is no risk of allogeneic transplant-related complications and graft-versus-host disease. Furthermore, genetically modified cells may express higher levels of the therapeutic enzyme and become more effective than wild-type cells. The efficacy of this procedure regarding correction of pathologic findings throughout the CNS, as well as peripheral organs has been demonstrated in many experiments on LSD animals and exceeds that exerted by wild-type HSCT. In MPSI mice, this procedure resulted in complete correction of disease manifestations, including neurologic and skeletal disease, pathology of liver, spleen and kidney (Visigalli et al., 2010; Zheng et al., 2003). In the mouse model of Metachromatic Leukodystrophy, an italian group showed full reconstitution of enzyme activity in the hematopoietic system. The development of motor conduction impairment, learning and coordination deficits, and neuropathological abnormalities typical of the disease were prevented (Biffi et al., 2006; Biffi et al., 2004). This same group is now moving from bench to bedside and is currently recruiting patients to assess the safety and efficacy of a gene therapy trial combined with autologous transplant of corrected HSCs. *Ex vivo* gene therapy approaches are also being tested in human clinical trials for MPSII (ClinicalTrials.gov identifier: NCT00004454), Gaucher and Fabry diseases (ClinicalTrials.gov identifiers: NCT00001234 and NCT00004294). A small (n=3 patients) human clinical trial in Gaucher disease using transduction of peripheral blood or bone marrow CD34+ cells with a retroviral vector encoding the glucocerebrosidase gene did not show significant clinical improvement (Dunbar et al., 1998). The low level of corrected cells (<0.02%) was not associated with any increase in glucocerebrosidase

enzyme activity in any patient following infusion of transduced cells. Modifications of vector systems and transduction conditions, along with partial myeloablation to allow higher levels of engraftment, may be necessary to achieve beneficial levels of correction in patients with Gaucher disease.

Considerations for gene therapy and other therapies include the need for early therapeutic intervention, before irreversible changes have occurred in the CNS. Although we do not yet fully know the level of plasticity of the CNS, it seems likely based on data derived from ERT that some levels of disease progression will be irreversible (Brooks et al., 2002). Second, a challenge of conducting clinical trials for LSDs is that meaningful endpoints for clinical investigation have not been defined. Indeed, defining clinical endpoints is particularly difficult in settings where the patient population is small, where there is considerable interpatient variability, the natural history of the disease progression is poorly defined, biomarkers to monitor therapeutic efficacy have not been validated, and secondary cellular events involved in the pathophysiology are unclear. In parallel with therapeutic trials, continued efforts should be given to exploring cascades of pathobiological events acting at the cell level in these diseases. A better knowledge of basic disease mechanisms can only impact therapeutic management of LSDs. It will define new disease markers and allow assesment of treatment efficacy toward these markers. In addition, it will help define the best conditions for treatment, and may give rise to new treatment strategies.

3. THE CELL BIOLOGY OF LSDs

In LSDs, primary genetic and biochemical defects consist in the interruption of the clearance of macromolecules meant for lysosomal destruction, resulting in cellular accumulation of undegraded or partially degraded metabolites. Once material starts to accumulate, it builds up within lysosomes until the lysosomal burden of the cell reaches some maximal level. Storage material then starts to accumulate in extra-lysosomal sites, and may be excreted out of the cell.

The accumulation of primary storage products triggers complex pathological cascades. Downstream events are responsible for the accumulation of secondary storage products. Pathological consequences thus extend far beyond the primarily affected metabolic pathway.

Although primary events are well characterized in most LSDs, secondary biochemical and cellular pathways involved in the pathophysiology of LSDs are poorly defined (Futerman and van Meer, 2004; Jeyakumar et al., 2005). Despite different primary storage products in different LSDs, similar secondary storage products and similar cell defects may be observed across diseases. Must research is focused on delineating the biochemical and cellular pathways that cause disease pathology. Pathogenically relevant mechanisms are highlighted below.

3.1. Cell vacuolation

The pathological hallmark of LSDs is the intracellular accumulation of storage vesicles with characteristics of lysosomes. Observations in animal models show progressively increasing number and size of storage vesicles with age in affected tissues, which is evocative of a slow and irreversible process.

Storage vesicles have long been considered to be enlarged lysosomes engorged with storage material. Lysosome proliferation and swelling could be an attempt to cope with the accumulation of storage material. In reality, the situation is much more complex, and the exact identity and origin of these storage vesicles remain to be established. Significant stream of vesicular traffic coming into contact with lysosomes comes from the endocytic and autophagic pathways. Lysosome dysfunction may disrupt normal intracellular vesicle trafficking to or from lysosomes. One possibility is that late

endosomes and autophagosomes may accumulate because they are unable to fuse with the lysosome. A second possibility would be that late endosomes and amphisomes are able to fuse with the lysosome, producing hybrid vesicles. However, these hybrid vesicles loaded with material to be degraded would not be processed normally due to impaired capacity for lysosomal degradation. Defects in the endo-lysosomal or macro-autophagy pathways that might account for intracellular vesicle accumulation have been reported in several LSDs, and will be detailed later. These possibilities are reinforced by morphological features characterizing storage vesicles. These morphological features are sometimes reminiscent of MVBs or autophagic vacuoles. In addition, storage vesicles are large, polymorphic, poorly mobile, and contain highly heterogeneous materials. They might therefore be distinct from lysosomes which are usually small, highly dynamic, and contain homogeneous dense material.

Examination of storage vacuoles by electron microscopy consistently revealed cytoplasmic vacuoles having a high degree of heterogeneity according to the affected cell type, but also within the same cell. The content of these vacuoles ranges from clear amorphous material, granular material, internal debris, internal vesicles, membrane fragments, dense aggregates and multilamellar structures occasionally forming zebra bodies (Figure 6). Interestingly, different types of primary storage products can be associated with similar storage lesions. Indeed, similar vesicle features are observed in different diseases, for example the presence of zebra bodies is widespread amongst LSDs.

It should be emphasized here that cellular alterations in LSDs are not only caused by the primary storage material present in the lysosome, but rather by accumulation of various primary and secondary storage products at other intracellular and extracellular locations. The high heterogeneity in the ultrastructure of storage vacuoles is consistent with a differential or uneven distribution of individual storage materials. If cascades of events triggered in different diseases converge to common biochemical alterations and to the accumulation of common secondary storage products in different LSDs, it is then understandable that similar storage lesions are observed in different diseases.

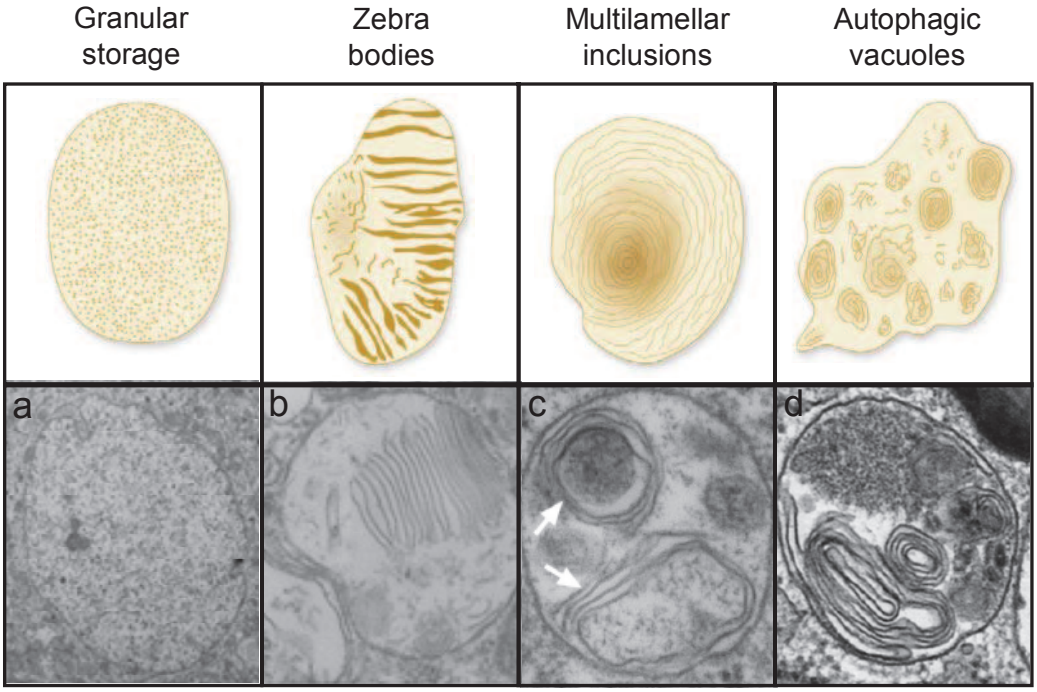

Figure 6: Morphology of storage vacuoles accumulating in LSDs. Schematic representation (top panel), and examples of electron micrographs (bottom panel) in MPSIIIB mouse brain sections (a-c), and in fibroblasts from mucolipidosis type IV patients (d). *Adapted from Parkinson-Lawrence et al., 2010 ; Vitry et al., 2010 ; Vergarajauregui et al., 2008.*

3.2. Accumulation of secondary metabolites

The identification of secondary metabolites in LSDs has often been the result of attempts to identify serum biomarkers that would be useful to follow disease progression and assess treatment efficacy. Some secondary metabolites are characteristic of a specific LSD, as chitotriosidase in Gaucher disease (as seen in section 2.5). A particular case comes from secondary accumulation of lipids, which is common to various LSDs. Secondarily accumulating lipids can belong to any of the major classes: sphingolipids, cholesterol and phospholipids (Walkley and Vanier, 2009).

Sphingolipids

The gangliosides GM2 and GM3 are the main sphingolipids accumulating in the brain of neurodegenerative LSDs comprising Niemann-Pick diseases, MPS, prosaposin deficiency, as well as some glycoproteinoses and NCL. The secondary accumulation of GM2 and GM3 gangliosides is believed to participate in neuropathology. Although

being often sequestered within the same neuron, GM2 and GM3 are not necessarily co-sequestered in the same vesicles. This suggests that these two gangliosides are sequentially processed in physically separate compartments within the endo-lysosomal system. Another hypothesis would be that they are being generated by independent cellular processes, e.g. by the synthetic *versus* degradative pathways.
A few studies have been performed on diseases with peripheral involvement. In the liver and spleen of Niemann-Pick diseases, sphingolipids amongst which GM2 and GM3 were also found to accumulate.

Cholesterol

Unesterified cholesterol accumulation has been reported in the liver and spleen of all three types of Niemann-Pick diseases. Whereas increase in cholesterol levels is attributable to the primary genetic defect in Niemann-Pick type C, it is clearly a secondary event in Niemann-Pick types A and B that are caused by defective sphingolipid hydrolysis. Conversely, accumulation of unesterified cholesterol in Niemann-Pick type C secondarily affects sphingolipid sorting and transport. In fact, cholesterol and sphingolipid levels, both components of lipid raft microdomains at the plasma membrane are inter-related in LSDs. Accumulation of one may lead to accumulation of the other.

In LSDs with CNS involvement, cholesterol accumulation can hardly be revealed in the brain, but it can easily be shown on individual neurons and glial cells by *in situ* filipin labelling, particularly in NPC, GM1 and GM2 gangliosidoses, alpha-mannosidosis, and several types of MPS. GM2 or GM3 gangliosides which are also accumulated in these diseases are present in independent populations of vesicles and show little co-localization with cholesterol.

Phospholipids

Different types of phospholipids are enriched in different LSDs. Interesting data come from a study performed in neurons from the mouse model of Gaucher disease. In these neurons, the levels of various phospholipids were elevated, which may account for the observed increase in neuritogenesis (Bodennec et al., 2002).

Consequences

Extra-lysosomal accumulation of lipid storage products can interfere with various cellular processes, and importantly, it could perturb plasma membrane lipid rafts. Lipid rafts are specialized patches of membrane where cholesterol and sphingolipids accumulate. They represent signaling platforms that link receptor-ligand interactions at the cell surface with intracellular signal transduction events, and are sometimes referred to as "glycosynapses". Lipid rafts are not restricted to the plasma membrane; they can also be transported in the endocytic pathway. It has been reported that cholesterol and sphingolipid excess results in impaired trafficking and accumulation of lipid rafts in the late endosomal compartment (Simons and Gruenberg, 2000 and discussed in the next paragraph). As certain proteins selectively reside in raft membranes, raft-associated proteins might become inappropriately sequestered, preventing them from trafficking to their normal sites of function. Mislocalization of raft proteins would have possible consequences on cell signaling. One note of caution is appropriate. Sphingolipids and cholesterol would be expected to reside in the same compartment in such context. However, as discussed above, they often appear in separate vesicle populations.

3.3. Alterations of intracellular trafficking

Since the fusion of lysosomes with late endosomes or autophagosomes is the terminal step of endocytosis and macroautophagy, respectively, a global lysosome malfunctioning can affect these pathways.

The best demonstration for malfunctioning of the endocytic pathway comes from experiments evaluating lipid trafficking in fibroblasts isolated from normal patients or LSD patients. When added exogenously, a short analogue of the sphingolipid lactosylceramide (LacCer) is transported to the Golgi in normal conditions. In fibroblasts obtained from some LSD patients (i.e. GM1 and GM2 gangliosidosis, prosaposin deficiency, metachromatic leukodystrophy, MPSIV, Fabry disease, Niemann-Pick disease, and Krabbe disease), it is misrouted and accumulates in late endosomes and lysosomes (Marks and Pagano, 2002). In the group of sphingolipid-storage diseases, the underlying mechanism involves the close correlation between sphingolipid and cholesterol levels that we just saw. Based on the observation that

Golgi targeting is restored upon cholesterol depletion, it has been postulated that altered intracellular distribution of cholesterol secondary to primary sphingolipid storage in turn leads to defective sphingolipid trafficking (Puri et al., 1999). Cholesterol homeostasis is itself linked to the activity of Rab proteins (Choudhury et al., 2002). Golgi targeting is dependent on several Rab proteins mediating vesicle trafficking along the endocytic pathway, implying that LacCer likely travels from late endosomes, and possibly from lysosomes to the Golgi. Overexpression of Rab proteins corrects the LacCer trafficking defect, and reduces cholesterol accumulation in LSD fibroblasts.

Another demonstration of defective endocytosis comes from experiments showing altered uptake of fluid-phase markers in NPC (Lachmann et al., 2004b).
Defective intracellular trafficking of proteins has also been reported in yeast models of LSDs. Depletion of the orthologue of the human protein responsible for juvenile NCL (Batten disease) in yeast led to mislocalization of the Golgi protein Yif1p to the vacuole, the yeast equivalent of the lysosome (Chattopadhyay et al., 2003). In a yeast model of mucolipidosis type IV, enhanced rate of uptake of fluid-phase markers and decreased degradation of endocytosed protein were seen (Fares and Greenwald, 2001).

Alteration of autophagy is also believed to contribute to LSD pathogenesis. Autophagy involvement has been observed in a number of LSDs including Danon disease, NCL, Pompe disease, Mucolipidosis, NPC, multiple sulfatase deficiency, MPS type IIIA or GM1-gangliosidosis (Ballabio and Gieselmann, 2009). Evidences of autophagy alterations include accumulation of autophagic vacuoles, autophagosome accumulation (LC3-II increase), enhanced autophagic degradation of long-lived proteins, or increased expression of Beclin-1, which is accumulated during autophagy induction. A block of autophagy (block of autophagosome-lysosome maturation) was recently suggested in multiple sulfatase deficiency and MPSIIIA. The presence of autophagosome accumulation can thus result either from autophagy overactivation, or a from a defective autophagosome maturation. A hypothesis that reconciles this apparent discrepancy between a block and an induction of autophagy is that lysosomal storage may affect fusion efficiency between autophagosomes and lysosomes, leading to a block of autophagy. Compensatory feedback mechanisms would in turn be activated, leading to activation of autophagy.

According to these data, it is not simply a dysfunction of the lysosome that is central to pathogenesis, but rather the entire endosomal/lysosomal system and autophagy that are compromised, impacting vesicle fusion and trafficking events.

3.4. Alterations of signaling pathways

There are different levels at which compounds accumulating in LSDs can affect signal transduction pathways (Ballabio and Gieselmann, 2009). First, storage compounds can function as ligands of receptors. Accumulation of extracellular storage compounds would lead to non-physiologic activation of these receptors. For example, GAGs accumulating in MPS can bind and activate the TLR4 receptor involved in the secretion of proinflammatory cytokines. Consistently, activation of TLR4 and its adaptor protein MyD88, leading to enhanced production of proinflammatory cytokines were reported in MPS animal models (Ausseil et al., 2008; Simonaro et al., 2008). Second, storage compounds can modify receptor responses. There is evidence that GAGs bind various growth factors, and that extracellular accumulation of GAGs in MPS causes impaired growth factor signaling. One of such growth factors is fibroblast growth factor (FGF)-2. Accumulation of extracellular HS, a subtype of GAGs, in MPS type I interferes with the binding of FGF-2 to its receptor and impairs signal transduction through this cascade (Pan et al., 2005). As FGF-2 acts in neuroprotection, impaired FGF-2 signaling pathway would be relevant to neurodegeneration occurring in this disease.

Finally, it is also the subcellular localization of receptors that can be affected in LSDs. Endocytosis of activated receptor complexes represents a mean to terminate signaling. Disturbed endosomal-lysosomal trafficking in LSDs can have consequences on delivery of receptors from the plasma membrane to the lysosome by endocytosis, as in NPC. In this disease, TLR4 receptors are upregulated in the endosomal fraction, associated with possible decreased lysosomal degradation, contributing to the inflammatory state in this disease (Suzuki et al., 2007). Means by which the endocytic process can regulate signaling mechanisms do not only involve internalization of receptor-ligand complexes or regulation of the composition of membranes (e.g. lipid rafts), endocytosis also plays an active role in signal propagation and amplification (Miaczynska et al., 2004).

3.5. Alterations of calcium homeostasis

Defective intracellular calcium homeostasis is one of the most common pathological features in LSDs. The major intracellular calcium store comes from the ER. Calcium is released from the ER to the cytosol via two types of calcium-release channels that reside in the ER membrane, the ryanodine receptor and the inositol 1,4,5-trisphosphate-gated calcium-release channel. The opposite mechanism, calcium uptake from the cytosol into the ER lumen occurs via the Sarcoplasmic/Endoplasmic Reticulum Calcium-ATPase (SERCA).

In Gaucher disease, increased calcium release from the ER occurs through the ryanodine receptor. The major sphingolipid that accumulates in this disease, glucosylceramide, directly modulates and overactivates this receptor (Vitner et al., 2010).

In Sandhoff and Niemann-Pick A diseases, elevated cytosolic calcium is due to a reduction in the rate of calcium uptake by SERCA. It has been shown in the case of Sandhoff disease that the storage compound GM2 ganglioside can modulate SERCA activity.

In GM1 gangliosidosis, calcium is depleted from the ER, due to GM1 interaction with the phosphorylated form of the inositol 1,4,5-trisphosphate-gated calcium-release channel (Sano et al., 2009).

Defective calcium homeostasis can also affect other organelles than the ER. While mitochondrial calcium homeostasis is altered in at least two LSDs, GM1 gangliosidosis and mucolipidosis type IV, defective lysosomal calcium homeostasis has been reported in NPC (Lloyd-Evans et al., 2008; Sano et al., 2009). Finally, in Batten disease, calcium homeostasis is altered by inhibition of a plasma-membrane voltage-gated calcium channel (Luiro et al., 2006).

Impaired calcium homeostasis can lead to ER stress, oxidative stress, and cell death. Whereas elevated cytosolic calcium results in activation of a mitochondria-mediated apoptotic pathway leading to caspase 9 activation, depletion of ER calcium stores induces ER stress and ER-mediated apoptosis through caspase 12 activation (Ginzburg et al., 2004). In addition, depletion of ER calcium stores interferes with proper folding of proteins in the ER lumen. As a consequence, cells enter a form of ER stress, the ‘unfolded protein response’ (UPR), which causes suppression of global protein synthesis, activation of stress gene expression, and induction of apoptosis. Activation of

UPR was shown in fibroblasts from a wide variety of both neurodegenerative and non-neurodegenerative LSDs (Wei et al., 2008), and was confirmed in the human infantile NCL brain, and using the GM1 gangliosidosis mouse model (Kim et al., 2006; Tessitore et al., 2004). However, mouse models of Gaucher disease and sialidosis showed no evidence for UPR activation (Farfel-Becker et al., 2009; Tessitore et al., 2004).

Defects in calcium homeostasis are of particular relevance for LSDs with CNS involvement. Calcium plays an important role in excitable cells such as neurons, where it induces immediate responses such as neurotransmitter release, as well as long-term responses via activation of cell signaling pathways. Dysregulation of calcium homeostasis may lead to neuronal dysfunction. In addition, high calcium concentrations may be toxic for neurons.

3.6. Oxidative stress and mitochondrial abnormalities

The imbalance between the production of reactive oxygen species (ROS) and antioxidant capacities of cells and organs leads to oxidative stress. ROS encompass a variety of chemical species, including superoxide ions, hydroxyl radicals, and hydrogen peroxide. Increased ROS levels result in oxidation of macromolecules such as nucleic acids, lipids and proteins, which alter their structure and function. In addition, increased ROS levels constitute a stress signal that activates specific redox-sensitive signaling pathways and may impact processes such as cell adhesion, immune responses or apoptosis (Droge, 2002). Oxidative stress has been highlighted in many neurodegenerative disorders including LSDs. In these diseases, oxidative stress may mediate neuronal damage and cell death. As lysosomes are very susceptible to oxidative stress, neuronal damage might be even more important in LSDs, due to the lysosomal overload. Oxidative stress phenomena have been reported in MPSI, MPSII, MPSIIIA, MPSIIIB, NPC, Gaucher disease, Fabry disease, or NCL (Arfi et al., 2011; Deganuto et al., 2007; Filippon et al., 2011; Fu et al., 2010; Heine et al., 2003; Reolon et al., 2009; Shen et al., 2008; Villani et al., 2009).

Mitochondria are potent generators of ROS; therefore, functional compromise of this organelle has a large impact on oxidative homeostasis. Mitochondrial abnormalities have been seen in several LSDs including MPSIIIB and several forms of NCL such as

late infantile NCL, as well as Batten disease. These abnormalities consist in altered enlarged mitochondria and/or accumulation of subunit c of mitochondrial ATP synthase (scMAS) (Ezaki et al., 1993; Hall et al., 1991; Ryazantsev et al., 2007). Since autophagy is the major route for destruction of damaged mitochondria, a defective autophagy pathway, as seen in a number of LSDs, may lead to accumulation of dysfunctional mitochondria, accompanied by increased oxidative stress.

3.7. Inflammation

Although the LSDs involve storage of self-components which should be immunologically silent, a common host response is the inappropriate activation of the innate immune system, inducing an atypical inflammatory response. Microglia and macrophages play a prominent role in this process. In type 1 Gaucher disease, acid-beta-glucosidase storage in macrophages leads to macrophage activation and release of cytokines and chemokines. In LSDs with CNS pathology, brain inflammation is common. In the brain, the inflammatory response is triggered by expansion and activation of resident microglia and astrocytes, and/or by influx of blood monocytes that, in turn, are activated. Activated astrocytes and microglia produce potentially neurotoxic chemokines and cytokines. Whereas the association of chronic neurodegeneration and inflammation is well established, the causative links between these events is debated. Numerous studies indicate that the inflammatory process may trigger acute neurodegeneration and/or dysmyelination, exacerbating pathogenesis. This implies that anti-inflammatory medications such as non-steroidal anti-inflammatory drugs, anti-cytokines, immunosuppressants or immunomodulators might be beneficial in some LSDs. In Sandhoff and Krabbe diseases and in NPC, anti-inflammatory therapy when administered alone or in combination with other therapeutic approaches was able to prolonge lifespan of affected mice (Jeyakumar et al., 2004; Luzi et al., 2009; Smith et al., 2009). In contrast, other studies suggest that microglial activation might be primed by the ongoing pathology, and that inhibition of microglia priming has no effect on the neurodegenerative course, like in MPSIIIB (Ausseil et al., 2008).

The exact mechanisms that lead to macrophages and microglia activation are unknown. Storage in these cells could induce mislocalization of key proteins to the lysosome, resulting in disrupted cell signaling. One trigger could be the clearance of

apoptotic neurons by phagocyting microglia. In normal conditions, the apoptotic process is anti-inflammatory in nature. In LSDs, clearance of apoptotic neurons, which are themselves accumulating storage products, could result in the development of a pro-inflammatory response.

3.8. CNS cell pathology

In the CNS, LSDs do not only impact neurons. Oligodendroglia –the myelin producing cells- can be affected, leading to myelinopathy. Astrocytes can be activated (astrocytosis), as well as microglia. Affected neurons contain storage vacuoles in the cell body and in dendrites, but not typically in axons. Storage is not acutely cytotoxic and does not lead to neuron death in the early stages of most types of LSDs. Neurons may rather survive for years, while exhibiting important morphological changes. Neuronal pathology is therefore chronic, in line with the progressive evolution of brain pathology in LSDs. Only by end stage disease, neuronal cell loss is observed, leading to brain atrophy. One exception is the family of neuronal ceroid lipofuscinoses in which neurons are subject to early death.

Morphological changes affecting neurons are termed ectopic dendritogenesis and axonal spheroids (Walkley, 1998) (Figure 7). Whereas the former change selectively impacts cortical pyramidal neurons, Purkinje cells are particularly vulnerable to the latter phenomenon. Ectopic dendritogenesis consists in the abnormal sprouting of new dendrites at the axon hillock. Axonal spheroids represent axon swellings and contain material with similar ultrastructure features across many types of LSDs, composed of collections of tubulovesicular profiles, mitochondria and dense and multivesicular-type bodies.

Another type of axon enlargement can be found: meganeurites. In contrast to axonal spheroids which are enlargements distal to the initial segment of the axon, meganeurites are enlargements proximal to this region. The morphology of meganeurites is disease specific as they contain typical storage bodies consistent with the defective lysosomal enzyme.

Defects in neuritogenesis are also frequently found. Reduced neurite outgrowth was described in primary cultures of neurons from animal models of LSDs including Sandhoff disease or NCL (Dunn et al., 1994; Pelled et al., 2003; Sango et al., 2005),

whereas neurite outgrowth was increased in the mouse models of Gaucher disease and MPSIIIB (Bodennec et al., 2002; Hocquemiller et al., 2010).

Neuronal changes represent an issue in terms of treatment since they seem to be irreversible. Once formed, ectopic dendrites and axonal spheroids remain after enzyme replacement and absence of the disease process, albeit neuronal vacuolation is normalized (Walkley et al., 1987).

Figure 7: Morphological alterations that neurons undergo in LSDs. Left: ectopic dendritogenesis. Right: axonal spheroid. *From Walkley, 1998.*

Although little is known about the link between lysosomal defects and changes in neuronal morphology, this certainly has profound consequences for neuron function. Disruption of the endosomal-lysosomal function and ganglioside storage in neurons can possibly explain the formation of axonal spheroids, the growth of ectopic dendrites and cell death.

A clear link has been established between GM2 ganglioside accumulation and ectopic dendritogenesis. A series of studies in fact established GM2 ganglioside as a metabolic product consistently elevated in the cerebral cortex of all LSDs characterized by ectopic dendritogenesis, with a correlation between the level of GM2 ganglioside and the extent of ectopic dendrite growth (Siegel and Walkley, 1994). In addition,

immunocytochemistry studies revealed GM2-positive vesicles localized in the cytoplasm of pyramidal neurons bearing ectopic dendrites (Walkley, 1995). The increase in GM2 is seen as a cause rather than a consequence of ectopic dendritogenesis. As mentioned earlier, GM2 accumulation can be responsible for alterations of calcium homeostasis and subsequent ER stress response resulting in apoptosis and neuron cell death.

Perturbation of the endosomal-lysosomal system in neurons may have a profound influence over signaling events at the synapses. For example, the density of the post-synaptic AMPA (α-amino-3-hydroxy-5-methyl-4-isoxazolepropionic acid) receptor is regulated in a highly dynamic manner by endocytosis. The depolarization of AMPA receptors is responsible for generating fast excitatory neurotransmission. Therefore, the endocytic process is positioned to have a critical influence on synaptic plasticity. It has been shown that overexpressing the GluR2 subunit of AMPA receptors in cultured neurons induces ectopic dendritogenesis (Passafaro et al., 2003). Compromise in AMPA receptor cycling secondary to compromise of the endosomal-lysosomal system is therefore a possible explanation for the formation of ectopic dendrites. Impaired growth factor signaling may also account for this phenomenon. It is known that growth factors, when applied on cortical neurons cultures, can cause exuberant growth of dendrites (McAllister, 2001).

Finally, storage bodies accumulating in the cell body of neurons might cause a block in retrograde transport of endocytic vesicles or other material from the axon to the cell body, inducing series of downstream consequences with prominent effects on neuronal morphology (Bellettato and Scarpa, 2010; Jeyakumar et al., 2005). The structural characteristics of heterogeneous materials accumulating in spheroids suggest that they may be the result of defects in retrograde transport. Indeed, accumulation of highly similar materials was reported when lesions were provoked in the distal axonal segments, or by interrupting retrograde transport using low temperature (Smith, 1980; Tsukita and Ishikawa, 1980). The cell type most susceptible to spheroid formation, Purkinje cells, is also highly susceptible to cell death. Cell death may be explained by a block of retrograde movements of growth factors or other elements essential for cell survival.

3.9. Link with other neurodegenerative diseases

Alteration of lysosomal function is well known to participate to the neurodegenerative process in adult-onset neurodegenerative diseases such as Alzheimer's or Parkinson's diseases. In these diseases, not only the neuronal lysosomal system is impaired, but also the two major cellular pathways converging on the lysosome, namely endocytosis and autophagy. As a matter of fact, the neurodegenerative phenotype is often associated with accumulation of lysosomes, autophagic vacuoles or enlarged endosomes (Nixon et al., 2008). Other secondary events like brain inflammation, oxidative stress, mitochondrial dysfunction, ER stress, or calcium dysregulation are common to paediatric and adult neurodegenerative diseases. Therefore, knowledge of the mechanism of action of LSDs may allow elucidation of features of adult disorders.

Analogies between neurodegenerative diseases affecting the elderly and neurodegeneration associated to LSDs are best illustrated in Alzheimer's disease. Alzeihmer's disease is characterized by deposits of beta-amyloid peptides and neurofibrillary tangles, composed of an abnormally phosphorylated form of the microtubule-associated protein Tau. A clear link has been established between these defects and lysosomal dysfunction, based on the following observations:

- Abundant active lysosomal hydrolases have been found surrounding amyloid plaques, implying that plaques may originate from lysosomal rupture (Cataldo et al., 1996).
- Amyloid-beta peptides can be produced through the endosomal-lysosomal system, under the action of lysosomal cathepsins (Bahr et al., 1994).
- Recent evidence has shown that dysfunction in the autophagic-lysosomal system impairs clearance of the protein Tau, and results in the formation of Tau insoluble aggregates in lysosomes (Hamano et al., 2008).
- The Alzheimer's disease brain is characterized by enlarged endosomes and by accumulation of autophagic vacuoles in degenerating neurons (Nixon et al., 2005).

It is therefore not surprising that tauopathy and accumulation of intracellular amyloid-beta peptides have been found in LSDs. Beta-amyloid aggregation has been reported in the brain of several LSDs including glycosphingolipid storage diseases or

MPSs (Boland et al., 2010; Ginsberg et al., 1999). This phenomenon can be explained by the accumulation of primary or secondary storage products in these diseases. Gangliosides that accumulate in GM2-gangliosidoses as a result of the primary genetic defect, but also in MPS due to secondary events, bind to amyloid beta-protein with high affinity (Ariga et al., 2001), and promote its aggregation (Yamamoto et al., 2005). On the other hand, sulfated GAGs, the primary storage product in MPS, stimulate Tau phosphorylation in Alzheimer's disease (Goedert et al., 1996). Consistently, increased lysozyme, which is known to induce the formation of hyperphosphorylated Tau, and increased hyperphosphorylated Tau itself have been reported in the mouse model of MPSIIIB (Ohmi et al., 2009).

4. MUCOPOLYSACCHARIDOSIS TYPE III

4.1. Generalities

Belonging to the group of LSDs, the MPSs form a family of inherited disorders caused by deficiencies of lysosomal enzymes required for the degradation of the various types of GAGs, namely heparan-, dermatan-, keratan- and chondroitin- sulfates. The classification of MPSs now recognizes ten different diseases associated with defects in the degradation of one or more GAGs: MPS types I, II, III (comprising four subtypes IIIA, IIIB, IIIC and IIID), IV (comprising two subtypes IVA and IVB), VI and VII (Neufeld and Muenzer, 2001).

The presence of HS seems to be linked to CNS involvement, whereas the presence of other GAGs is associated with peripheral defects. In fact, MPSI, MPSII and MPSIII which accumulate HS all suffer from neurological manifestations, while MPSVI and MPSIV, which hardly accumulate HS suffer "only" from peripheral but not CNS involvement.

MPSIII (also called Sanfilippo disease) may probably be defined as the most severe subgroup of MPS, as it is always characterized by a severe CNS involvement associated with attenuated expression of the disease in peripheral organs. The different subtypes of MPSIII result from the absence of one of four lysosomal enzymes that are required for the sequential degradation of HS [MPSIIIA: sulfamidase; MPSIIIB: α-*N*-acetylglucosaminidase (NAGLU); MPSIIIC: acetyl CoA:α-glucosaminide-*N*-acetyl transferase; MPSIIID: *N*-acetylglucosamine 6-sulfatase]. A deficiency in one of these enzymes is responsible for the accumulation of partially digested HS oligosaccharides (HSO) in lysosomes, which are also retrieved in endosomes and other cell compartments and released in the extracellular environmemnt. The four disease subtypes are clinically indistinguishable, although type A seems to have a more severe prognosis.

4.2. Molecular genetics, incidence and clinical manifestations

Mutations underlying MPSIII are highly heterogeneous. For example, over a hundred mutations are currently listed for MPSIIIB (Beesley et al., 2005; Heron et al.,

2011). Epidemiological studies in MPSIII did not allow the establishment of genotype-phenotype correlations, but showed that some mutant alleles may predominate in specific populations (Heron et al., 2011).

Although MPSIII is a rare disease, it is with Gaucher disease and metachromatic leukodystrophy one of the most prevalent LSD. Epidemiological studies of MPSIII in France, UK and Greece indicated an incidence of 0.68 per 100,000 live-births in France, with an estimation of 1.19 per 100,000 live-births in Europe (Heron et al., 2011). Sanflippo syndrome is heterogeneous regarding incidence of the different types in different countries. Whereas MPSIIIA predominates in northern Europe, MPSIIIB is the most prevalent in southern countries.

The median age at diagnosis is 4.5 years, with disease onset at 3.3 years. The appearance of symptoms can be divided into different phases (Cleary and Wraith, 1993). In the first phase, between the ages of 1 and 4 years, the clinical pattern consists in developmental delay, principally regarding language development. The second phase commonly begins around the age of 3 to 4 years, and is marked by attention deficit disorder, abnormal behavior, hyperactivity and aggressiveness. During this phase, sleep is often disturbed. A loss of previously acquired skills (developmental regression) leads to loss of autonomy. Independent walking and relational interactions are lost around the age of 10 years. Progressive neurological deterioration ultimately evolves toward seizures and profound mental retardation, with brain MRI showing white matter abnormalities and cortical atrophy (Zafeiriou et al., 2001). In the final stage, children encounter feeding difficulties due to an impaired swallowing mechanism. Mobility is severely impaired due to spasticity and joint stiffness. The median age of death is between 15 and 17 years, often due to respiratory complications.

Peripheral manifestations are usually mild and develop late in the disorder. They include coarse hair and facies and minimal skeletal disease (mild joint stiffness and mild dysostosis multiplex). Recurrent and sometimes severe diarrhea is frequently reported. Because somatic symptoms are mild, it often leads to a significant delay in diagnosis.

4.3. Treatment

No therapy is currently available for MPSIII: HSCT is not considered as a treatment option, and no ERT product is clinically available. Management consists of supportive

care and treatment of specific complications. For example, physical therapy consisting in motion exercises may help relieve joint stiffness. Oxygen supply, tracheotomy or tonsillectomy may improve obstructive airway disease.

There are several animal models of MPSIII available, helping investigations for developing therapies. The biochemical and pathologic features of these animal models are similar to those encountered in humans, but the clinical presentation may be milder. This paragraph will focus on the hope offered by gene therapy strategies, with particular emphasis on MPSIII type B for which a clinical trial is expected to start soon. In this disease, animal models include dogs and emu in which NAGLU mutations have occurred naturally, as well as a genetically engineered knockout mouse model (Aronovich et al., 2001; Ellinwood et al., 2003; Li et al., 1999).

Proof-of-concept of gene therapy has first been established in MPSIIIB mice (Cressant et al., 2004; Fu et al., 2002). Focal sources of NAGLU were created in the mouse brain through stereotaxic injections of AAV vectors. Two different AAV serotypes coding for human NAGLU have been tested: AAV2 and AAV5. These vectors were injected at a single site in the brains of 6-weeks old MPSIIIB mice. NAGLU was not only expressed at the site of injection. The enzyme was widely distributed in brain tissues. The extent of enzyme release beyond vector-positive regions was proportional to gene transfer and expression levels. The capture of NAGLU by microglia, astrocytes, and neurons was demonstrated by the disappearance of lysosomal storage lesions in areas devoid of vector genomes. In addition, NAGLU delivery induced a rapid reduction in GM2 and GM3 to normal levels and drastically reduced neuroinflammation in the entire brain. Finally, the aberrant behavior seen in MPSIIIB mice (hyperactivity and loss of fear), which recapitulates clinical symptoms in children, was corrected by treatment (Cressant et al., 2004).

In order to translate proof-of-concept of safety and efficacy from mouse models to human application, AAV-mediated gene therapy was explored in the brain of MPSIIIB dogs (Cressant et al., 2004). Animals received eight deposits of an AAV2.5-hNAGLU vector. Vector preparation included the use of a baculovirus vector for the introduction of the various components needed for AAV vector assembly in insect Sf9 cells. This method ensures high vector titers. Immunosuppression was mandatory to prevent immune response against the therapeutic enzyme. Without immunosuppression,

transduced cells are eliminated, impairing treatment efficacy, and neuroinflammation is triggered, raising serious safety concerns. In immunosuppressed dogs, vector was efficiently delivered throughout the brain and induced NAGLU production. Dosage of biochemical markers including GAGs, GM2 and GM3, and analysis of storage lesions on brain histological sections showed disease correction.

This preclinical study sets the basis for a phase I/II human trial aimed at assessing this treatment in Sanfilippo syndrome. Protocols for such trials will include the large-scale production of a clinical batch of AAV2.5-hNAGLU vector under good manufacturing practices (GMP). The surgical procedure, the immunosuppression regimen, or eligibility criteria have been specified. Patients with already advanced neuropathology will be excluded, as significant benefit would not be expected. Gene therapy should preferentially be performed at an early stage of disease development, and in the young brain, as the brain at this stage of development retains considerable plasticity. Clinical and biological markers used to determine safety endpoints will be specified.

Although gene therapy has proven effective in preventing accumulation of primary and secondary storage products, and in correcting storage lesions in the brain of animal models of MPSIIIB, one ignore to which extent this treatment will halt or revert the loss of neuronal plasticity, and be sufficient to ensure satisfactory cognitive development of affected children. This is due to a lack of knowledge regarding the pathogenic bases of the neurological disease. To address this question, it is necessary to identify cellular and molecular mechanisms responsible for the loss of neuronal plasticity. This knowledge will define new disease markers that will be useful to assess treatment efficacy. Recent studies in MPSIIIB mouse brains or in cultured MPSIIIB mouse neurons have identified cell defects related to neuritogenesis and cell markers showing modified expression including the growth cone protein GAP43 (growth associated protein 43), the mitochondrial protein scMAS, the synaptic component synaptophysin or inflammation markers, which were all corrected by gene transfer to the brain, or to cell culture (Ausseil et al., 2008; Hocquemiller et al., 2010; Vitry et al., 2009).

5. THE CELL BIOLOGY OF MPSIIIB

Specific cellular and molecular defects that have been highlighted as contributing to the neuronal pathology in MPSIIIB are detailed here. Most defects are in line with defects typically observed in LSDs, as discussed earlier in section 3. Some other defects have only been described in MPSIIIB so far, and have led to the introduction of new concepts regarding the pathophysiology of LSDs.

5.1. Storage products in MPSIIIB

In the MPSIIIB brain, HS accumulation is less prominent than would be expected from the genetic defect. Soluble HS is barely elevated in the brain of MPSIIIB mice, and only two-fold in the brain of human patients (Hadfield et al., 1980; Li et al., 1999). This suggests the existence of an alternative degradative pathway in the brain, likely using endo-heparanases to cleave HS into smaller fragments. In contrast, massive HS accumulation has been reported in somatic organs of MPSIIIB mice, primarily in liver and kidney, and to a lesser extent in lung, spleen, thymus and heart. In fact, whereas somatic organs primarily accumulate HS, MPSIIIB mouse neurons accumulate a number of secondary metabolites including the GM2 and GM3 gangliosides, cholesterol, ubiquitin, or scMAS. Ultrastructural studies indicate that GM2-, GM3- and scMAS-immunoreactive profiles appeared in vesicles containing membranous material reminiscent of zebra bodies, a hallmark of MPS diseases (McGlynn et al., 2004; Ryazantsev et al., 2007). GM3 showed partial colocalization with HS (McGlynn et al., 2004; Vitry et al., 2010). GM2 and GM3 gangliosides consistently sequestered in separate populations of vesicles. As seen in sphingolipid storage disorders, ganglioside accumulation in MPSIIIB was associated with elevated levels of free cholesterol. A strong regional correlation was observed between cholesterol and GM3 storage, but not between cholesterol and GM2 storage. Elevated scMAS levels were detected in the same areas as GAGs and unesterified cholesterol and in the same cells as ubiquitin and GM3. Interestingly, there was no strong association between the lysosomal marker LAMP1 and primary or secondary storage products in cortical sections or cultured cortical neurons from MPSIIIB mice. In LAMP1-positive storage vesicles, either only little colocalization or no colocalization were detected with HS, GM3, scMAS, or

ubiquitin (Vitry et al., 2010). These data are consistent with the notion that primary and/or secondary storage products mostly accumulate in structures distinct from LAMP1-positive storage vesicles.

5.2. Cellular basis for attenuated plasticity in the MPSIIIB brain

5.2.1. The FGF pathway

HS has a known role in FGF signaling on the cell surface. It interacts with FGF ligands, increasing the affinity of FGF for FGF receptors (FGFR). This results in the formation of a ternary complex, and subsequent activation of various signal transduction pathways. HS oligosaccharides (HSO) generated by heparanase digestion are biologically more active than the native HS-chain (Ma et al., 2006). They show more selective protein interactions and compete with native HS-chain for receptors binding. In MPSIIIB cells, HSO may be excreted in excessive amounts and trapped in the extracellular matrix (ECM) on the cell surface. Increased local concentration and increased reactivity of HSO in the FGFR environment may modify FGFR signaling pathways.

In the MPSIIIB mouse brain, expression of the FGF receptor FGFR-1, as well as its two ligands FGF-1 and FGF-2 was attenuated (Li et al., 2002). This presumably represents an adaptive response to elevated HSO levels in the ECM.

Key functions of FGF-2 are to regulate neurogenesis, as well as astrocytes proliferation and function. These functions were impaired in the MPSIIIB mouse brain, consistent with impaired FGF-2 expression. First, NSC showed a reduced capacity to proliferate. Second, an increase in the density of reactive astrocytes characterized by the glial fibrillary acidic protein marker (GFAP) was observed. These astrocytes however lacked responsiveness to acute injury. These deficits certainly lead to reduced neuronal health and attenuated plasticity.

5.2.2. Alterations of neuritogenesis

Neuritogenesis is a dynamic process combining neurite elongation, branching and

retraction. Neurite outgrowth results from alternate periods of extension and retraction. A balance between these two activities eventually ensures stabilization and maturation of the neuritic tree. In MPSIIIB mouse cortical neuron cultures, this balance was not achieved due to HSO accumulation (Hocquemiller et al., 2010). Defective retraction resulted in enhanced neurite length, increased branching and broader neuritic tree when neurite development was completed. This phenotype correlated with an increase of GAP43 expression levels over time, which was reported in MPSIIIB mouse cortical neuron cultures, and in MPSIIIB mouse brains (Ausseil et al., 2008; Hocquemiller et al., 2010; Li et al., 2002). GAP43 is the major protein of the growth cone, which controls neurite extension in response to external cues. GAP43 is a protein kinase C substrate. When dephosphorylated, it is found in areas of growth cone retraction. When phosphorylated, it can interact with several cytoskeletal proteins such as F-actin, stabilizing actin filaments and promoting neurite outgrowth (Caroni, 2001; Larsson, 2006). Increased GAP43 expression may account for extended neurite outgrowth in MPSIIIB, affecting cortical development and plasticity.

5.2.3. Synaptic pathology

Expression of synaptophysin, the most abundant protein of the synaptic vesicle membrane was diminished at a very early stage of the disease course in the MPSIIIB mouse cortex, as well as in cortical neuron cultures as a consequence of HSO accumulation (Vitry et al., 2009). This defect was due to modification of the synaptic vesicle components rather than a reduction of neuron or synapse numbers. The cause for reduced synaptophysin expression was an enhanced degradation by the proteasome. As synaptophysin presumably participates in exocytosis, in release of neurotransmitters, and in synaptic vesicle maturation, these data point to possible consequences on synaptic plasticity. Behavioural and cognitive defects observed at disease onset in MPSIIIB may partly arise from defects in synaptic functions.

5.3. Brain inflammation

In the MPSIIIB mouse model, it has been shown that the development of neuroinflammation may result from the stimulation of microglial cells by HSO accumulating in the extracellular environment (Ausseil et al., 2008). Microglia activation was mimicked by extracellular HSO purified from MPSIIIB patient urine, or by HSO produced by digestion of porcine HS with heparinase (a bacterial analog to the mammalian heparanase), but not by native HS chains. HSO-induced microglia activation was characterized by morphological changes, increased expression of the microglial marker CD11b, and by increased production of several cytokines and chemokines. It occurred through signals mediated by the cell surface innate immune response receptor TLR4 and its associated adaptor protein Myd88. Absence of brain inflammation in doubly mutant MPSIIIB TLR4-/- or MPSIIIB MyD88-/- young mice did not slow down the installation of neuropathology, supporting the view that neurodegeneration was primarily cell autonomous in MPSIIIB. However, neuroinflammation may still aggravate neuronal pathology in aging MPSIIIB mice.

5.4. Origin of intracellular vacuoles

Ultrastructural studies on MPSIIIB brain tissues and on cultured neurons have demonstrated extensive distended vesicles with abundant stored material. A comprehensive analysis of these vesicles revealed that they were abnormal lysosomes (Vitry et al., 2010) (Figure 8). The presented lysosomal features, namely they expressed the lysosomal membrane protein LAMP1 and the lysosomal hydrolase IDUA, and they were acidic, as shown by labelling with lysotracker. They differed from lysosomes by their large size and heterogeneous morphology. And finally, they did not receive material from the endosomal and autophagy pathways, which performed normally. In MPSIIIB cortical neuron cultures, markers like EEA1 (early endosome), M6PR (late endosomes and MVBs), or LC3 (autophagosomes) were not associated with LAMP1-positive vesicles. Endocytosis of tranferrin and dextran was normal and the dynamic exploration of autophagy did not show significant defect. These studies of autophagy included scoring of LC3 positive vesicles, estimation of the LC3I/LC3II ratio and the examination of long-lived protein turnover. However, involvement of the Golgi

apparatus in the formation of vesicular distension was suggested. Golgi stacks appeared abnormal and sometimes apposed or fused with distended vesicles. Enlarged vesicles expressed both markers of lysosomes (LAMP1) and of the pre-Golgi and cis-Golgi comparments, namely COPII and GM130, respectively. Finally, Golgi-localized GM130 staining was increased and extended in neurites of MPSIIIB mouse neurons. It has been proposed that alteration in the GM130-mediated control of vesicle trafficking in pre-Golgi and Golgi compartments may affect Golgi biogenesis and give rise to a dead-end storage compartment unable to interact and/or fuse with adjacent compartments. Material contained in the lumen of these vesicles could not be eliminated and progressively accumulate.

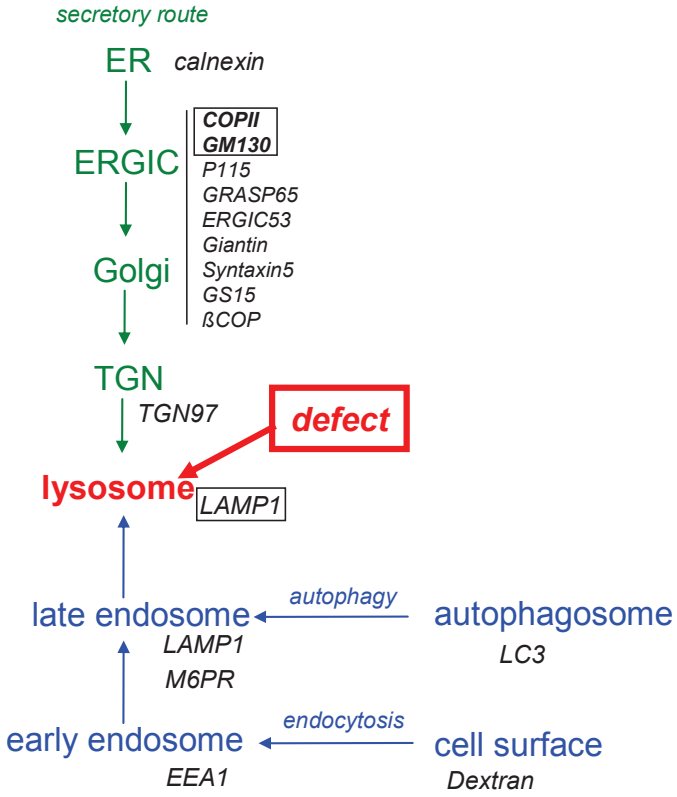

Figure 8: Formation of abnormal lysosomes in MPSIIIB mouse neurons. Schematic representation of the secretory (in green), autophagy, and endocytosis (in blue) pathways involved in lysosome (in red) biogenesis. Markers that have been investigated are indicated (in black). The boxes indicate markers found to be associated with storage vesicles in MPSIIIB mouse neurons.

The next section will concentrate on the description of the physiological functions of the Golgi apparatus and of the cis-Golgi protein GM130.

6. THE GOLGI APPARATUS

6.1. Structure

The Golgi apparatus is an organelle that is in close contact with the ER and has a perinuclear position. It is composed of disk-like membranes called cisternae. Golgi cisternae are arranged in a pile of ordered stacks of 3-8 cisternae. The Golgi stacks can be divided into three regions: cis-, medial-, and trans-Golgi. Newly synthesized proteins and lipids arrive from the ER at the cis side of a Golgi stack and then travel across the stack to the opposite trans-side where material exits for secretion. A potential advantage conferred by Golgi stacking is improved efficiency of trafficking through the Golgi, as there is little physical distance between cisternae.

A mammalian cell contains multiple Golgi stacks that are connected laterally by membrane tubules to form a Golgi ribbon. Homotypic tubular connections between equivalent cisternae can be formed. Tubules can also connect heterologous cisternae – for example a cis-cisterna in one region and a trans-cisterna in the next region. Such connections could facilitate the movement of molecules forwards and/or backwards through the Golgi to a significant extent.

In addition to stacks of cisternae, the Golgi is also composed of abundant vesicles, and of networks of branching tubules connected with the cis-most cisterna and the trans-most cisterna. These tubular networks are referred to as the cis-Golgi network (CGN) and the trans-Golgi network (TGN), respectively. Vesicles and tubules support transport of material within the Golgi, as well as transport to/from the Golgi. Most of intra-Golgi vesicles bear a COP (coatamer protein) coat and are about 50-60 nm diameter. Larger vesicles (80-90 nm diameter) emanate from the TGN and are covered with a clathrin coat that is thicker than the COP coats. The presence of clathrin-coated buds is a morphological hallmark of the TGN.

The Golgi apparatus is a highly dynamic and self-organizing organelle. It is able to rapidly change its shape, and to even disassemble and reassemble under a variety of physiological and pathological conditions. For example, the Golgi breaks down into small vesicles during mitosis. These vesicles partition between the two daughter cells, and are able to reassemble to produce a functional Golgi apparatus at the end of mitosis. The drug brefeldin A (BFA) causes the Golgi to fragment and fuse with the ER. Subsequent removal of the drug allows the Golgi to reappear.

The Golgi complex has two key functions. It houses the enzymes responsible for the processing of newly synthesized proteins and lipids, and serves as a site for the transport and sorting of these processed molecules to their final subcellular destinations.

6.2. A protein and lipid processing center

Proteins are synthesized by ribosomes present on the surface of the ER, and subsequently translocated in the ER lumen where *N*-glycosylation occurs on asparagine residues. Glycan chains introduced in the ER are homogeneous and relatively simple. It is in the Golgi apparatus that multiple processing reactions occur to produce more complex oligosaccharides and introduce structural diversification (see example of *N*-glycosylation, Figure 9). Although *N*-linked glycosylation on asparagine residues starts in the ER, further remodeling of *N*-linked glycan chains occurs in the Golgi. In contrast, *O*-linked glycosylation on serine or threonine residues is initiated in the Golgi. Not only proteins, but also lipids are substrates for *N*-linked and *O*-linked glycosylation and oligosaccharide-chain processing at the Golgi. The Golgi houses enzymes including glycosyltransferases and trimming enzymes which are able to respectively add and remove a variety of sugars at various stereospecific positions. Glycosyltransferases can be mannosidases, sialyltransferases, fucosyltransferases, galactosyltransferases or *N*-acetylglucosamine transferases. Examples of trimming enzymes include glucosidases or mannosidases. Apart from enzymes responsible for glycosylation, the Golgi contains enzymes required for other post-translational modifications of newly synthesized proteins and lipids (e.g. phosphorylation, methylation and sulfation). It also contains numerous pro-protein convertases (like furin) that cleave protein precursors into their mature forms.

Golgi enzymes are compartmentalized, so that processing of cargo proteins and lipids occurs sequentially during passage through the Golgi. In general, enzymes acting early in glycan biosynthetic pathways are concentrated in cis and medial compartments, whereas enzymes acting later tend to reside within the trans-Golgi compartment. The Golgi apparatus can therefore be viewed as an “assembly line” for the production of correctly glycosylated proteins and lipids. Post-Golgi compartments are enriched in

processed compounds while pre-Golgi membranes are enriched in precursor and immature forms.

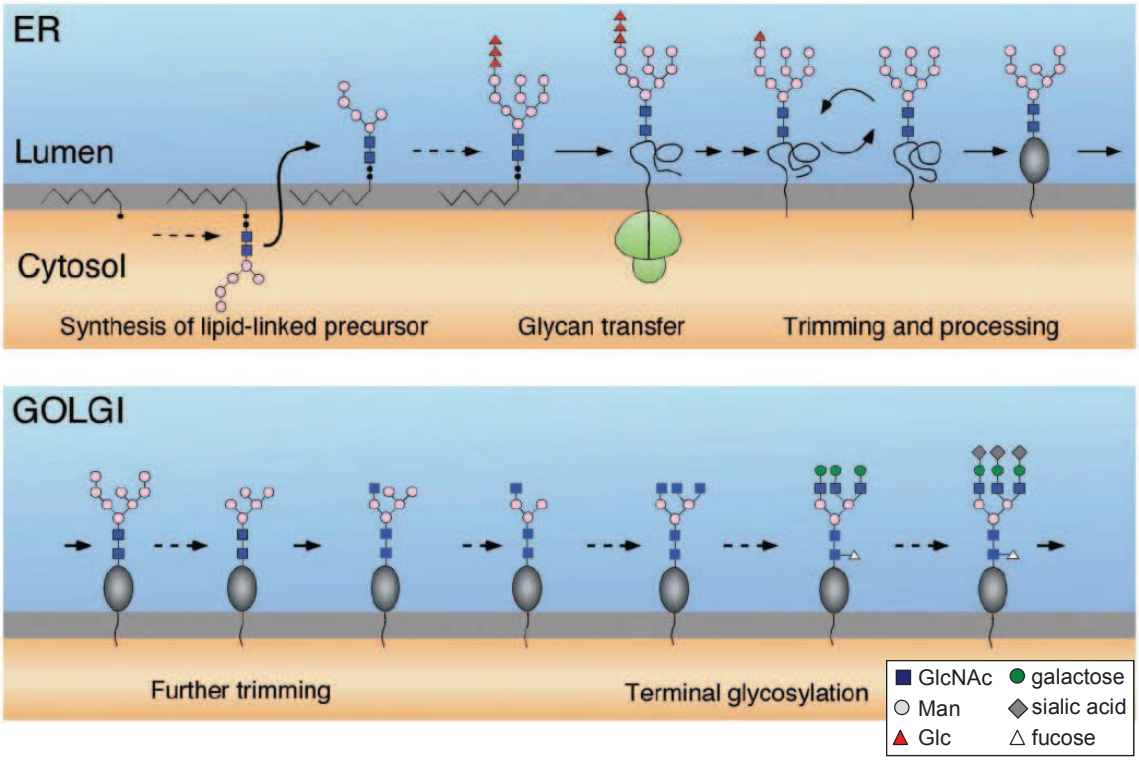

Figure 9: Golgi glycosylation machinery. Example of *N*-linked glycosylation is represented. In the ER, the glycan chain is initially introduced on asparagine residues as a high-mannose type tetradecasaccharide that consists of three glucose (Glc), nine mannose (Man), and two *N*-acetylglucosamine (GlcNAc) residues ($Glc_3Man_9GlcNAc_2$). Terminal glucose residues are trimmed sequentially by two glucosidases, leading to non-glucosylated Man_9-$GlcNAc_2$ saccharide chains. Once the glycoprotein has reached the Golgi complex, further mannose trimming occurs, and GlcNAc residues are added. Many pathways are possible for terminal glycosylation regarding the number of branches, and the number and identity of sugars added. Here, addition of terminal sialic acid, fucose and galactose residues are represented. *Adapted from Helenius and Aebi, 2001.*

In addition to the compartmentalization process, clusters of Golgi enzymes that direct the biosynthesis of specific glycan structures have been observed (de Graffenried and Bertozzi, 2004). For instance, two enzymes involved in *N*-linked glycan biosynthesis associate with one another, namely mannosidase II, and *N*-acetylglucosaminyltransferase I. Such associations have also been described in the case of enzymes involved in ganglioside biosynthesis (e.g. the two enzymes responsible for the sequential conversion of GM3 ganglioside to GM2 and GM1), or in the case of

enzymes involved in HS biosynthesis (e.g. the two enzymes produced from the *ext* genes responsible for elongation of HS chains).

6.3. A transport and sorting station

6.3.1. Transport to the Golgi

Newly synthesized secretory cargo proteins are packaged into COPII-coated vesicles at specialized ER exit sites lacking bound ribosomes. Subsequently, COPII vesicles can fuse directly with the cis-Golgi, they can fuse with each other or with the ER-to-Golgi intermediate compartment (ERGIC). On ERGIC membranes, a second type of coat assembles, the COPI coat. COPI-coated vesicles bud from the Golgi and from ERGIC elements to recycle components back to the ER. This retrograde movement of COPI vesicles is important, for instance, to recycle ER-resident proteins back to the ER after their processing in the Golgi. Strong evidence for the participation of COPI-vesicles in anterograde traffic between the ERGIC and the Golgi is lacking, although this possibility has to be considered. Instead, it has been shown that tubulo-vesicular membranes detach from the ERGIC and move toward the Golgi. When cargo are too large to be packed into COPII-coated vesicles, they can be directly included into protrusions of specialized ER domains forming large tubulo-vesicular structures. ER-derived, large containers can fuse with each other or with the pre-existing ERGIC, or they can move directly toward the Golgi without interaction with the ERGIC.

ER-derived, or ERGIC-derived tubulo-vesicular structures are called ER-to-Golgi carriers. They are transported to the Golgi along microtubules, a process that requires microtubule motor proteins (primarily dynein, together with its cofactor dynactin) to drive motility (Scales et al., 1997).

6.3.2. Cargo transport through the Golgi

There are two models explaining cargo movement through the Golgi. The vesicle transport model proposes that the Golgi cisternae are stable pre-existing structures through which the cargo molecules pass. In this model, also called the stable

compartment model, resident Golgi proteins are retained in the cisterna representing their final destination. Transport of cargo molecules is mediated by vesicles that bud from one cisterna and then fuse with the next one. The maturation model is more commonly admitted. This model assumes that new Golgi cisternae form de novo at the cis face, progressively mature through the stack, and ultimately peel off from the trans face. Secretory cargo proteins are thought to be carried forward by this process of cisternal progression. Meanwhile, cisternae maturation implies that cisternal components are recycled by a return flow from older to younger cisternae. This recycling is mediated by vesicles.

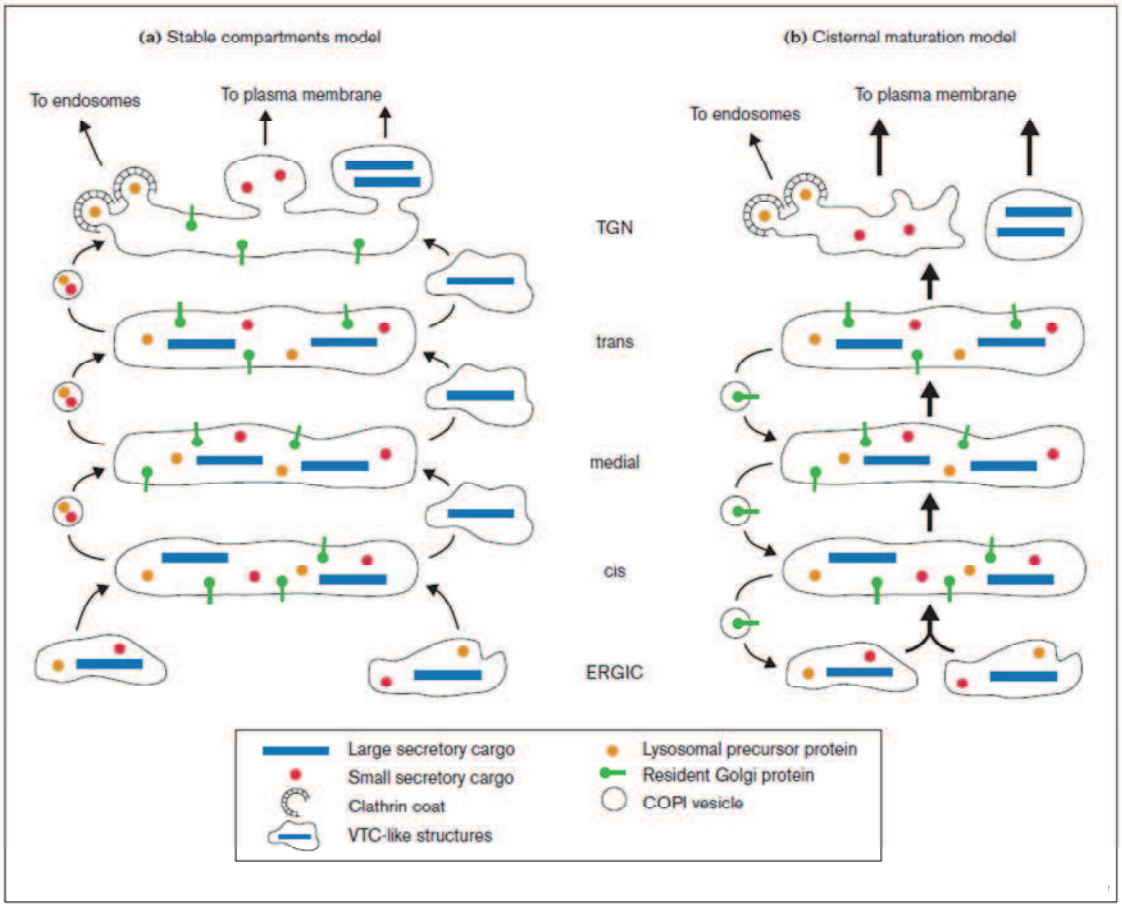

Figure 10: Models for cargo transport through the Golgi. (a) Anterograde transport of cargo molecules. Whereas small cargo transit through COPI vesicles, large cargo transit in vesicular-tubular membrane clusters (VTC)-like structures. (b) Retrograde transport of resident Golgi proteins via COPI vesicles. *From Glick, 2000.*

Both models are in line with the presence of numerous vesicles in the Golgi area. Many of these vesicles bear a COPI coat and are essential in intra-Golgi traffic. COPI vesicles may function in anterograde as well as retrograde transport through the stacks. The distinction between the two models centers on the content and directionality of

COPI-coated vesicles (Figure 10). In the stable compartment model, anterograde COPI vesicles carry the secretory cargo forward and exclude resident Golgi proteins. In the cisternal maturation model, retrograde COPI vesicles recycle Golgi proteins (including processing enzymes and structural components) to younger cisternae and exclude the secretory cargo. An important argument supporting this latter model is the demonstration that the secretory glycoprotein VSV-G (vesicular stomatis virus membrane glycoprotein) is excluded from COPI-coated vesicles. On the contrary, resident Golgi enzymes freely enter these vesicles (Pelham, 2001).

Scenario for Golgi formation also depends on which model is accepted. In the stable compartment model, tubulo-vesicular structures emanating from the ERGIC fuse with an already existing cis-Golgi. In the maturation transport model, ERGIC compartments contain all the necessary components to build a new Golgi cis-cisterna. ERGIC components fuse with each other to generate new Golgi cisternae.

More recently, a new model for intra-Golgi trafficking has been developed, called the rapid-partitioning model. The motivation for the development of this new model came from studies of the kinetics of cargo transport in living cells (Patterson et al., 2008). The classic cisternal maturation model predicts a lag before newly arrived cargo is exported from the Golgi. This prediction is based on the thesis that cargo molecules await arrival of enzymes for processing, which are delivered sequentially via retrograde trafficking, before they can exit from the Golgi. In addition, the cisternal maturation model predicts linear export kinetics, since it assumes that Golgi cisternae are formed at the cis face, move across the stacks, and peel off from the trans face at a constant rate. Recent studies of cargo kinetics demonstrated that, in contrast to the predictions of the cisternal maturation model, cargo molecules exited at an exponential rate proportional to their total Golgi abundance with no lag period (Patterson et al., 2008). Furthermore, upon arrival at the Golgi, cargo molecules quickly distributed throughout the system before differentially partitioning between two different membrane environments: processing domains enriched in processing enzymes and export domains from which transport intermediates bud from the Golgi. One proof of this idea came from cells treated with BFA. Whereas Golgi processing enzymes were redistributed into the ER upon BFA treatment, the cargo protein VSV-G only partially returned to the ER. A significant amount of VSV-G remained in the Golgi region and continued to be packaged into transport carriers directed toward the plasma membrane. Given these

results, a new model of intra-Golgi transport was constructed, that involves partitioning of cargo and Golgi enzymes within a two-phase membrane system.

The authors further included lipid trafficking pathways as an integral part of this model by showing that processing and export domains were characterized by specialized lipid environments that differentially retained resident and cargo proteins. It is well recognized that there is a cis-to-trans gradient of lipids through the Golgi, which mainly concerns glycerophospholipids and sphingolipids (Bretscher and Munro, 1993). This lipid gradient alone could explain the differential distribution of proteins within the stacks. Whereas domains enriched in glycerophospholipids preferentially retained Golgi processing enzymes, domains enriched in sphingolipids had a higher concentration of cargo molecules. A final key of this model relies on trafficking of cargo and processing enzymes in both directions through the Golgi. It has been proposed that rapid bidirectional trafficking throughout the Golgi system allows proteins to sample different lipid environments, and therefore promotes association with their optimal Golgi subdomain. For the first time, the rapid-partitioning model invokes lipid sorting as the driving force in intra-Golgi trafficking.

6.3.3. Sorting from the Golgi

Both the cis- and trans-faces of the Golgi apparatus are important sites for the sorting of proteins and lipids and delivery to specific subcellular destinations.
Sorting at the CGN participates in the recycling and transport of different molecules back to the ER. The majority of resident ER proteins contain the carboxy-terminal KDEL motif which is recognized by specific KDEL receptors present in the Golgi. These molecules are subsequently packaged into COPI-coated vesicles, supporting retrograde transport to the ER.

The TGN is a sorting station for cargo destined to apical and basolateral domains of the plasma membrane, or to the endo-lysosomal system. For each destination, distinct sorting signals are used (Figure 11). Different machineries recognize these signals, driving their incorporation into different post-Golgi routes. Sorting signals are contained in the cytoplasmic tail of cargo molecules, and sometimes in specific receptors for these molecules. As described in section 1.2.1, sorting signals directing transport to the endo-lysosomal system are either tyrosine-based (NPXY or YXXØ peptide motifs) or leucine-based ([DE]XXXL or DXXLL peptide motifs). These signals have also been

identified in some basolateral-directed proteins. The presence of common signals for these two destinations is not surprising, since the indirect route to the endo-lysosomal system involves an intermediate step at the basolateral plasma membrane. Another motif which participates in basolateral targeting is the di-leucine LL motif. This signal is also involved in endocytosis (see 1.2.2). Both basolateral and lysosomal proteins are sorted through interaction of sorting motifs with AP complexes. While basolateral transport is mediated by AP-1B, AP-3 and AP-4, endo-lysosomal transport is mediated by AP-1A, AP-3 and GGAs (Rodriguez-Boulan and Musch, 2005). AP-1, AP-2, AP-3 and GGAs have binding sites for clathrin, whereas AP-4 does not. Blocking AP-1, GGA, AP-3, and clathrin-budding machineries does not affect the secretion of constitutive cargo proteins, but it interferes with the regular trafficking of lysosomal proteins (Dell'Angelica et al., 1999; Hirst et al., 2000; Rehling et al., 1999).

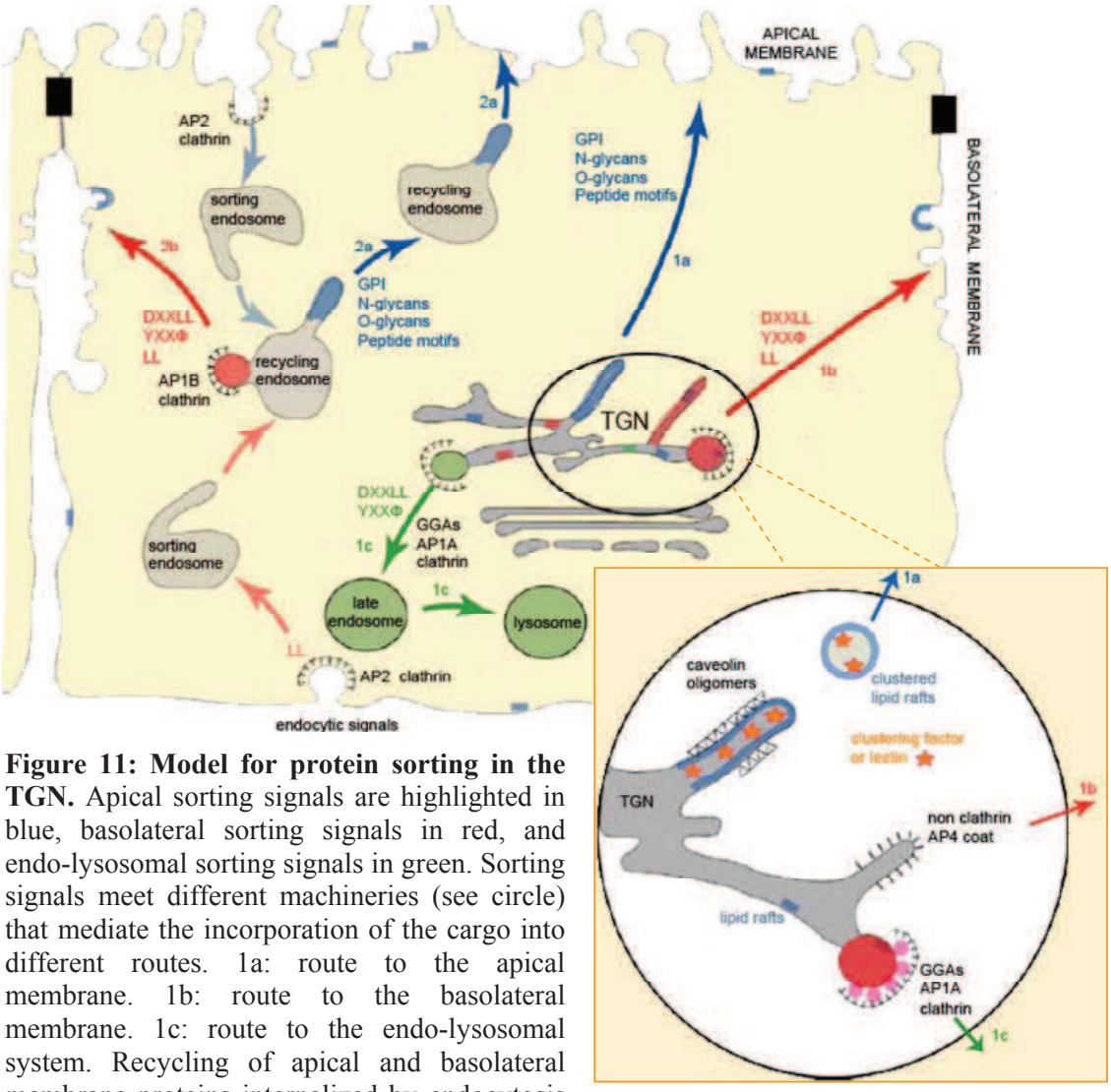

Figure 11: Model for protein sorting in the TGN. Apical sorting signals are highlighted in blue, basolateral sorting signals in red, and endo-lysosomal sorting signals in green. Sorting signals meet different machineries (see circle) that mediate the incorporation of the cargo into different routes. 1a: route to the apical membrane. 1b: route to the basolateral membrane. 1c: route to the endo-lysosomal system. Recycling of apical and basolateral membrane proteins internalized by endocytosis is also shown (routes 2a and 2b). *Adapted from Rodriguez-Boulan and Musch, 2005.*

Apical sorting signals comprise divergent moieties including lipids [glycosyl-phosphatidyl-inositol (GPI)], sugars (*N*-glycans, or *O*-glycans), or peptide motifs. These sorting signals can contribute to association with proteins driving transport to the apical plasma membrane, for example with microtubule motor proteins (Tai et al., 1999). *N*-linked and *O*-linked proteins and lipids can be recognized by lectin receptors such as galectin (Delacour et al., 2007). An unconventional mechanism for apical sorting is the association with lipid rafts. Many apical proteins have affinity for lipid microdomains assembled in the Golgi complex which are subsequently delivered to the apical membrane. Such association is mediated by the GPI anchor. Clustering of proteins associated with lipid rafts is the main mechanism for segregating apical raft-associated proteins from the basolateral proteins (Schuck and Simons, 2004).

The presence of different sorting machineries implies that cargo molecules are segregated physically into different TGN microdomains, depending on their final subcellular destination. It has been shown that the tubular network that characterizes the TGN does not only emanate from the last trans-Golgi cisterna (Ladinsky et al., 2002). Tubules can also emanate from the two adjacent trans-Golgi cisternae. However, only the trans-most cisterna and the tubules originating from it show clathrin-coated buds. Therefore, they primarily represent the exit site of molecules destined to the endo-lysosomal pathway. In contrast, secretory molecules presumably exit the preceding trans-cisternae via non-coated vesicles.

Shaping post-TGN carriers as vesicular and tubular structures requires membrane deformation and curvature, elongation of curved membranes into vesicular-tubular carriers, and fission. These mechanistic processes require cytoskeleton-based mechanical forces (Anitei and Hoflack, 2011; Hirschberg et al., 1998; Polishchuk et al., 2003). Actin-based motor proteins (myosins) and microtubule-based motor proteins (kinesins) provide tensile forces for elongation and fission of post-TGN carriers. Different kinesin (KIF) family members associate with different types of carriers. While KIF5B associates with all types of carriers, KIF1 and KIFC3 are associated with apical carriers, and KIF13A controls transport to the endo-lysosomal system. KIF13A interacts directly with AP-1. Its overexpression causes mislocalization of M6PR (Nakagawa et al., 2000).

6.3.4. Molecular mechanisms of vesicle transport

Cytosolic coat proteins are recruited and assembled on specific sites of the donor membrane by small GTP-binding proteins (ADP-ribosylation factor [ARF] for COPI and clathrin, Sar1p for COPII). The assembled coat deforms the membrane and eventually pinches off to produce a transport vesicle loaded with luminal and membrane embedded cargo molecules. The vesicle moves toward the acceptor compartment by diffusion or with the aid of a cytoskeletal track. The vesicle is then tethered on the target membrane, a process involving golgins (Figure 12). Tethering events are followed by disassembly of the vesicle coat and fusion with the target membrane. Vesicle fusion is mediated by SNARE proteins that are on both sides of the fusing membranes. A SNARE on the transport vesicle (v-SNARE) specifically recognizes and binds a SNARE on the target membrane (t-SNARE), forming a trans-SNARE complex. SNARE complex formation is responsible for bringing two apposed membranes in close proximity and promotes membrane fusion.

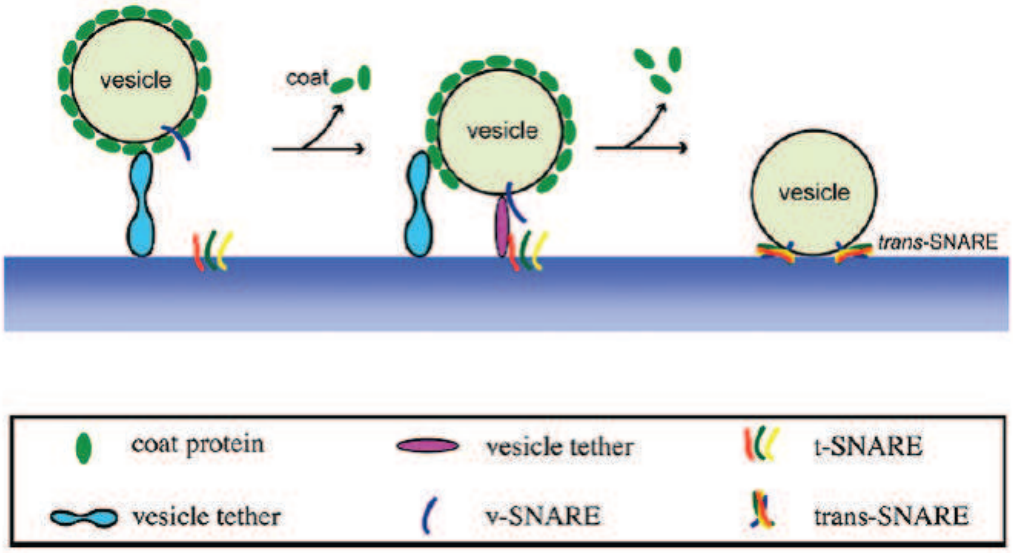

Figure 12: General principle of vesicle tethering and fusion to acceptor compartments. *FromCai et al., 2007.*

6.4. The Golgi matrix

Between and surrounding the cisternae a dense protein network is present, the Golgi matrix, that contains proteins providing a structural scaffold and allowing tethering

events. These proteins have been identified as members of the golgin and GRASP (Golgi reassembly and stacking protein) families.

Golgins are mainly coiled-coil proteins, and in some cases tail-anchored proteins associated with the cytoplasmic face of the Golgi membrane. Different golgins are located to distinct regions of the Golgi. For example, GM130 is preferentially localized to the cis-Golgi, whereas giantin and golgin97 are associated with the medial- and trans-side of the Golgi, respectively. This differential localization implies distinct roles for these proteins. Most golgins are regulated by interactions with small GTPases of the Rab family. Rab proteins may regulate golgin localization to Golgi membranes and induce conformational changes in the golgins, modulating their activity.

The coiled-coil nature of golgins implies that they have an extended rod-like conformation. This makes them ideal for linking or tethering membranes over a relatively large distance, allowing for the capture of both transport intermediates and Golgi elements (Figure 13). Tethering events are essential for the assembly and maintenance of the Golgi structure. Some golgins present at the Golgi rims are important for linking adjacent stacks forming the Golgi ribbon (Diao et al., 2003). In addition, cisternal stacking requires tethering of transport vesicles to Golgi cisternae, a process involving specific golgins (Shorter and Warren, 1999). Finally, some golgins play a role in linking the Golgi to the microtubule network, which is important for Golgi positioning in proximity to the centrosome (Rios et al., 2004; Rivero et al., 2009). Depleting these different types of golgins leads to Golgi fragmentation.

Tethering of transport vesicles such as retrograde and/or anterograde COPI vesicles or anterograde COPII vesicles to Golgi cisternae, as well as lateral tethering of Golgi elements to form a ribbon are followed by fusion events. In contrast, tethering of Golgi membranes during stacking of Golgi cisternae is not followed by fusion. Some golgins have been found to interact with SNARE proteins, directly coupling golgin-mediated tethering with SNARE-mediated fusion (Ganley et al., 2008; Shorter et al., 2002).

Besides golgins, the Golgi matrix also contains two GRASP proteins. GRASP65 is restricted to the cis-Golgi while GRASP55 is present in more medial cisternae. Their role is to regulate Golgi stacking. GRASP proteins oligomerize in trans to hold the adjacent Golgi membranes into stacks. Depletion of GRASP65 or GRASP55 led to reduction of the number of cisternae per stack (Sutterlin et al., 2005; Xiang and Wang, 2010), while expression of non-regulatable GRASP65 or GRASP655 mutants enhanced

Golgi stacking in interphase cells (Tang et al., 2010; Xiang and Wang, 2010). In addition, oligomerization of GRASP proteins between adjacent membranes mediates lateral fusion of the Golgi cisternae during Golgi ribbon formation. GRASP65 or GRASP55 depletion led to Golgi ribbon unlinking (Feinstein and Linstedt, 2008; Puthenveedu et al., 2006). The way by which GRASP proteins are able to regulate Golgi structure is through interactions with members of the golgin family. Whereas GRASP65 is able to bind GM130, GRASP55 interacts with golgin45.

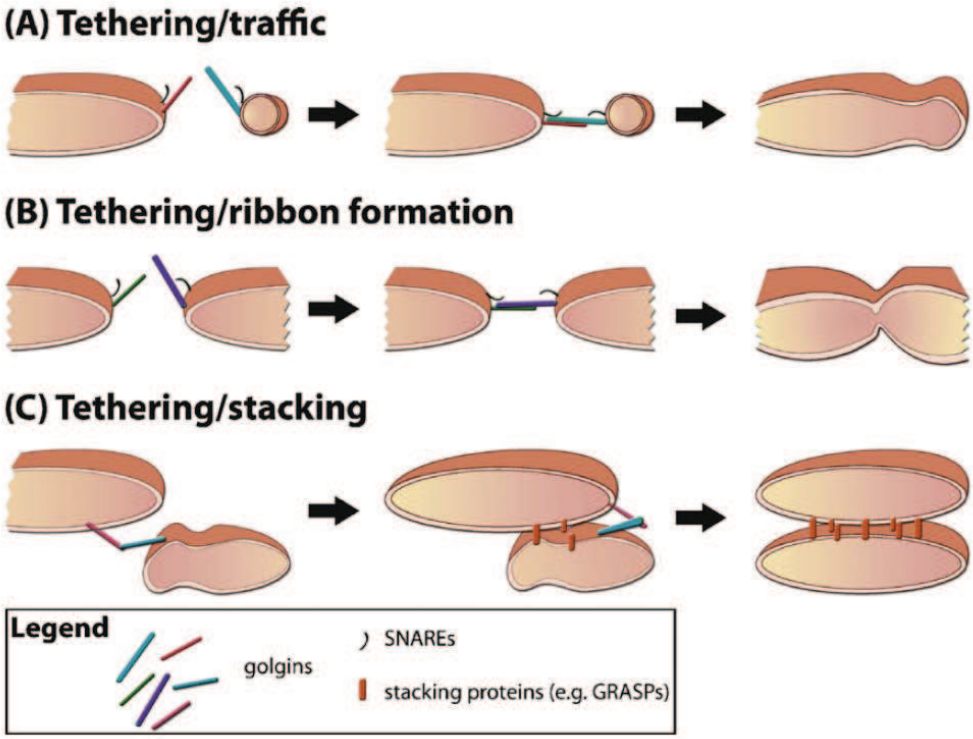

Figure 13: Golgi membrane tethering by golgins and GRASPs. Different membrane tethering events are supported by these proteins. (A) Tethering of transport vesicles to Golgi cisterna. (B) and (C) Tethering between two Golgi cisternae. The involvement of GRASPs in ribbon formation is not represented. *From Ramirez and Lowe, 2009.*

6.5. Golgi association with microtubules

A close relation exists between the Golgi and the microtubule cytoskeleton. In mammalian interphase cells, the Golgi ribbon is located next to the centrosome, which is composed of a pair of centrioles surrounded by a cloud of electron-dense material called the pericentriolar matrix. The pericentriolar γ-tubulin ring complexes (γ-TuRCs) interact with AKAP450 (A kinase anchoring protein), promoting microtubule

nucleation, with microtubule minus ends anchored at the centrosome, and plus ends extended toward the cell periphery (Takahashi et al., 2002). After drug-induced depolymerization of microtubules, the structure and the pericentrosomal positioning of the Golgi ribbon is lost. The Golgi stacks are disconnected from each other, dispersed in the cytoplasm, and redistributed to ER exit sites (Cole et al., 1996; Turner and Tartakoff, 1989). A similar phenotype is observed following inhibition of microtubule motor proteins, primarily dynein (Burkhardt, 1998; Corthesy-Theulaz et al., 1992; Palmer et al., 2009). One explanation for the Golgi scattering phenotype induced when dynein function is perturbed, or when microtubules are depolymerized, relies on their requirement for ER-to-Golgi traffic. Continued flow of material from the ER and concomitant inhibition of incorporation into Golgi stacks may result in Golgi fragmentation.

Although the centrosome is the major microtubule nucleation center, microtubules can also be nucleated by Golgi membranes according to a mechanism similar to that operating at the centrosome (Chabin-Brion et al., 2001) (Figure 14). Golgi-dependent microtubule nucleation requires the γ-TuRC complex, which may be recruited to the cis-Golgi through interactions with the Golgi proteins GMAP210 and AKAP450 (Rios et al., 2004; Rivero et al., 2009; Takahashi et al., 2002). AKAP450 is thus localized at both the Golgi and the centrosome (Takahashi et al., 1999; Witczak et al., 1999), and controls microtubule nucleation at both locations. AKAP450 is a huge protein which does not only anchor microtubules, but also a variety of enzymes to the Golgi and the centrosome. For example, it can anchor kinases, phosphatases and phosphodiesterases (Sillibourne et al., 2002; Takahashi et al., 1999; Tasken et al., 2001). It can also recruit cyclin E-cdk2, playing a role in centrosome duplication and cell cycle progression (Nishimura et al., 2005).

Golgi-nucleated microtubule seeds cannot give rise to microtubules unless they are associated with CLASP [CLIP (cytoplasmic linker protein)-associated proteins] (Efimov et al., 2007). CLASPs are recruited to the TGN; they coat microtubules nucleated at the cis-Golgi, promoting their stabilization and subsequent elongation toward the cell periphery. Microtubule seeds may either be formed at the cis-Golgi, dissociate, and bind the TGN or, consistent with the cisternal maturation model, they may stay associated with maturing cisternae until they become enriched in TGN proteins. Another possibility would be that short microtubules nucleated at the cis-Golgi

elongate within the Golgi ribbon until they reach the TGN where their plus ends are stabilized by GRASPs.

Golgi-derived microtubules are more extensively modified than those nucleated at the centrosome. Besides the acquisition of a CLASP coat, Golgi-derived microtubules become rapidly acetylated, which makes them more stable and resistant to nocodazole-induced depolymerization (Chabin-Brion et al., 2001). The organization of microtubules differs depending on whether they are nucleated at the Golgi or at the centrosome. In sharp contrast to radial centrosomal arrays, microtubules nucleated at the Golgi are preferentially oriented toward the leading edge of a migrating cell, resulting in an asymmetric network (Efimov et al., 2007).

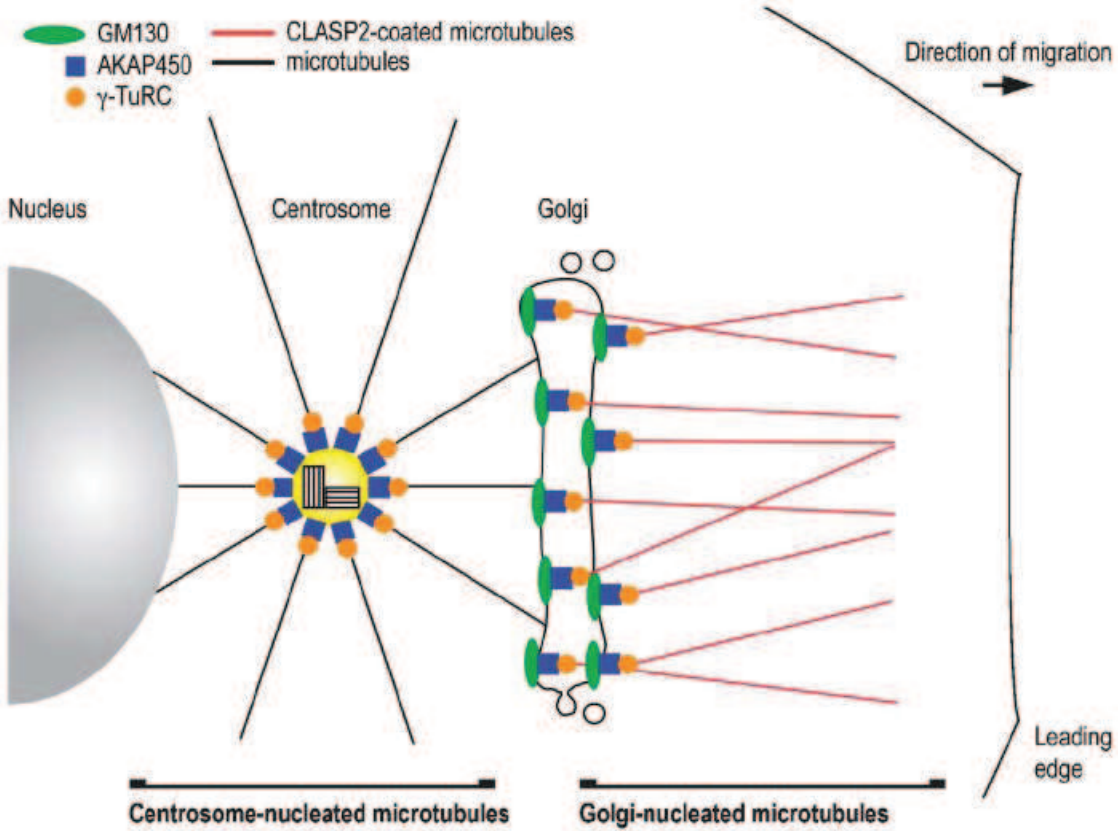

Figure 14: Comparison of centrosome-derived and Golgi-derived microtubules.
From Kodani and Sutterlin, 2009.

Besides the subset forming the asymmetric network, a second subset of Golgi-nucleated microtubules is critical for establishing continuity and proper morphology of the Golgi complex (Miller et al., 2009). This subset is arranged in a tangential fashion. Tangential microtubules act in a 'search and capture' manner to bring together

individual Golgi stacks. Lateral linking of Golgi mini-stacks by microtubules is followed by membrane fusion between adjacent stacks through a machinery involving GRASP proteins and probably SNARE complexes. In the absence of Golgi-derived microtubules, either when CLASP was depleted, or when AKAP450 was specifically dissociated from the Golgi without affecting the centrosomal fraction, Golgi fragments gathered in a circular array around the centrosome, but they failed to assemble and form a well-organized Golgi ribbon (Hurtado et al., 2011; Miller et al., 2009). As a consequence of disrupted functional continuity of the Golgi complex, Golgi enzyme mobility between stacks was decreased (Miller et al., 2009). The current model proposes that centrosome-derived and Golgi-derived microtubules act in concert for establishing proper organization of the Golgi complex. While Golgi-nucleated microtubules support Golgi ministacks clustering and assembly into a connected ribbon in the cell periphery, centrosomal microtubules drive transport of Golgi elements from the cell periphery to the cell center. Both steps depend on dynein (Burkhardt, 1998; Miller et al., 2009; Rivero et al., 2009).

6.6. Role in cell polarization and migration

The Golgi ribbon needs to be dynamic during cell polarization, which is a pre-requisite to cell migration. During polarization, both the centrosome and the Golgi undergo reorientation to face the leading edge of the cell. This process depends on GRASP65 phosphorylation by ERK (extracellular signal-regulated kinase) (Bisel et al., 2008). Expression of non-phosphorylatable forms of GRASP65 prevented Golgi and centrosome repositioning toward the leading edge and cell migration. Intriguingly, this block was overcome when Golgi membranes were artificially fragmented, indicating that Golgi membranes have to be remodeled to allow the coordinated reorientation of the centrosome and the Golgi. Even though the Golgi is dependent upon the centrosome for its positioning (see 6.5), the converse is also true. The mechanism by which GRASP65 phosphorylation induces Golgi remodeling during directed cell migration in interphase cells is similar to that brought into play during mitotic Golgi fragmentation (further detailed in section 7.4). ERK-driven GRASP65 phosphorylation causes loss of GRASP65 oligomerization, leading to Golgi cisternal unstacking.

Polarized cell motility is not only characterized by reorientation of the Golgi and centrosome toward the leading edge. Another hallmark of this process is the accumulation of Golgi-originated, post-translationally modified microtubules extending in the direction of the leading edge. The asymmetric microtubule network emanating from the Golgi apparatus provides tracks that support directional transport of Golgi-derived carriers to the cell front, a function that is essential for directional cell migration. In absence of Golgi-nucleated microtubules induced by CLASP depletion, polarized post-Golgi trafficking toward the leading edge was lost (Miller et al., 2009). Instead, cells showed randomized symmetric trafficking patterns. Directionality, but not efficiency of post-Golgi trafficking was affected. Random post-Golgi trafficking was accompanied with random migration. Abolishing microtubule formation at the Golgi through depletion of Golgi-localized AKAP450 but not centrosomal AKAP450, resulted in similar cell migration defects, although the Golgi and centrosome were able to reorient correctly (Rivero et al., 2009).

Finally, the pericentrosomal Golgi positioning is crucial for cell polarization and directional cell migration, further strengthening the importance of functional interactions between the Golgi and the centrosome. Cells lacking the golgin GMAP210 or golgin160 showed a fragmented and dispersed Golgi (Yadav et al., 2009). These cells were unable to form an asymmetric network of acetylated microtubules, they failed to secrete proteins in a directional manner and to efficiently re-orientate their centrosomes. Consistently, directed cell migration was lost. This study could not discriminate between the possibilities that loss of the Golgi ribbon integrity, or mislocalization of the Golgi, or both could affect cell polarization and directed cell migration. A recent study proposed that loss of the pericentrosomal position of the Golgi ribbon, rather than loss of Golgi ribbon integrity impacts directional cell polarization and migration (Hurtado et al., 2011). In this study, truncated AKAP450 fragments possessing Golgi binding capacities were overexpressed to specifically dissociate endogenous AKAP450 from the Golgi without affecting centrosomal AKAP450. Two different fragments were used, both inhibiting AKAP450-dependent Golgi nucleation capacities. The first fragment induced Golgi fragmentation without affecting its pericentrosomal positioning. This phenotype solely resulted from impaired microtubule nucleation at the Golgi. Expression of this fragment did not interfere with dynein recruitment to the Golgi, and Golgi elements could be translocated to the cell center, gathering in a circular array

around the centrosome. Overexpression of this fragment showed normal cell polarization and migration patterns, although delayed kinetics were observed. In contrast, the second fragment preserved integrity of the Golgi ribbon but induced separation of the Golgi ribbon from the centrosome. Contrary to the first fragment, this second fragment retained ability to bind microtubules, which presumably increased the chances of Golgi mini-stacks to encounter each other and assemble into an elongated ribbon. This truncated form of AKAP450 may interfere with dynein activity and inhibit transport of Golgi elements to the cell center. Overexpression of the second fragment prevented the cells from reorienting their centrosome and Golgi correctly, resulting in random migration patterns. This study is however controversial, since it implies that tangential linking of the Golgi stacks can be formed in the absence of Golgi-derived microtubules, and that centrosome-derived microtubules can compensate for this deficiency. In addition, it suggests that neither the Golgi morphology, nor Golgi-associated microtubule nucleation are critical for establishing polarized cell migration.

6.7. A signaling platform

A variety of signaling molecules are associated with Golgi membranes, including heterotrimeric G proteins, kinases such as Src family kinases (SFKs) or protein kinases A, C and D (PKA, PKC and PKD), molecules of the mitogen-activated protein kinase (MAPK) pathway such as Ras or ERK, and molecules of the Rho GTPases pathway such as Cdc42 (Mayinger, 2011; Wei and Seemann, 2009b; Wilson et al., 2011). These signaling transducers have diverse cellular roles. They are involved in the regulation of trafficking, cell polarization, cell motility and cell proliferation. They can also regulate the function of the Golgi. Therefore, the Golgi serves as an important signaling platform.

A center for integrating extracellular signals

The Golgi has been identified as a relay station for signaling networks initiated at the plasma membrane in response to extracellular stimuli. A growing body of evidence indicates that the Golgi may sense and integrate signals triggered at the plasma membrane, and thereby participate in the regulation of downstream events. Such

coordination between signaling events at the cell surface and at the Golgi is best illustrated by the Ras-induced signaling pathway.

Ras proteins are small GTPases that regulate cell proliferation, differentiation, and migration. In response to growth factors [e.g. epidermal growth factor (EGF) or FGF], extracellular receptors of the receptor tyrosine kinases family [e.g. EGF receptor (EGFR) or FGFR] dimerize, followed by autophosphorylation of tyrosine residues present in the cytoplasmic domain of the receptor molecule. The adaptor protein Grb2 binds to the phosphorylated tyrosine residues of activated receptors and recruits the GEF, SOS at the plasma membrane, activating Ras. However, Ras activation does not only occur at the plasma membrane. A significant portion of Ras is localized and activated at the Golgi apparatus in response to growth factor stimulation. At the Golgi, Ras is activated differently, through non-receptor protein tyrosine kinases of the Src family, which activates phospholipase Cγ1 (Bivona et al., 2003).

Ras activation kinetics differ between the Golgi and the plasma membrane. Activation of Ras at the plasma membrane is rapid and transient, whereas activation of Golgi-localized Ras is delayed but sustained (Chiu et al., 2002). The same second messenger, calcium, coordinates the shutdown of Ras activation at the plasma membrane, while activating Ras signaling at the Golgi.

Downstream effectors include the MAPK/ERK pathway. Ras activation stimulates ERK phosphorylation, with different ERK outpouts depending on the spatial membrane environment (Inder et al., 2008). Through this spatial regulation of Ras/ERK-mediated signaling events, different biological outcomes can be generated (Inder et al., 2008; Matallanas et al., 2006; Onken et al., 2006). In addition, the biological outcome depends on the amplitude and longevity of ERK signal. EGF is reported to invoke transient activation of ERK, resulting in cell proliferation of PC12 cells. FGF treatment induced sustained activation of this signaling pathway and resulted in differentiation of PC12 cells into a neuron-like phenotype (Kao et al., 2001; Wong et al., 2002; Yamada et al., 2004).

A well-described target for growth factor-induced ERK signaling on Golgi membranes is GRASP65. ERK activation leads to GRASP65 phosphorylation (Yoshimura et al., 2005), inducing remodeling of the Golgi architecture, and subsequent directed cell migration (Bisel et al., 2008).

Other signal transduction molecules regulated by extracellular cues have been localized on the Golgi, such as the small GTPase of the Rho family, Cdc42, as well as other components of the Rho GTPases signaling pathway (Donaldson and Lippincott-Schwartz, 2000; Larocca et al., 2004; Matas et al., 2004; Miura et al., 2002; Wu et al., 2000). This pathway regulates actin reorganization induced by a wide range of extracellular signals. Actin remodeling is essential in multiple cellular functions such as cell adhesion to the ECM and cell migration. Important receptors driving transduction of extracellular cues to the actin cytoskeleton are integrin receptors (Kim et al., 2011).

Integrins are heterodimeric transmembrane receptors composed of alpha and beta subunits. Eighteen alpha subunits and eight beta subunits can assemble into 24 different combinations. As integrin tails have no catalytic activity on their own, they must bind accessory molecules that mediate cell responses. An immediate consequence of integrin activation is their clustering and the formation of focal adhesions, attaching cells to the ECM. Focal adhesion proteins are rapidly phosphorylated and activated, in particular through a dual kinase complex formed by the focal adhesion kinase (FAK) and the Src kinase. Some proteins such as talin or vinculin subsequently interact with actin, linking integrins to the cytoskeleton. Other focal adhesion proteins such as FAK, paxillin or tensin act as actin modulators. Later, effects mediated by integrin clustering and activation of focal adhesion constituents lead to reorganization of the actin and microtubule cytoskeletons by recruiting and activating the Rho GTPases Rac, Cdc42 and RhoA, as well as Rho GTPase activating proteins (Rho-GAPs) and guanine exchange factors (Rho-GEFs). In migrating cells, Rac and Cdc42 activities predominate at the leading edge where they control actin polymerization, generating the protrusive force for the lamellipodium, followed by elongation of the microtubules that fill the protrusion. RhoA induces the contraction necessary for retracting the rear-end of a moving cell. Long-term consequences of integrin activation ultimately lead to cell proliferation and control of cell morphology.

Although there is no direct evidence that the Golgi can integrate signals from pathways activated by integrin receptors at the cell surface, the identification of the 14-3-3ζ protein at the Golgi apparatus supports this idea. Indeed, 14-3-3ζ is not only localized at the Golgi, but it has also been found associated with the cytoplasmic domains of specific integrin complexes (Bialkowska et al., 2003; Deakin et al., 2009; O'Toole et al., 2011). 14-3-3ζ acts as an adaptor protein and is required for integrin-induced activation of Rho GTPases and cytoskeletal reorganizations (Bialkowska et al.,

2003). It can therefore be hypothesized that 14-3-3ζ can also activate Golgi-localized Rho GTPases in response to integrin activation, with consequences on cell adhesion or cell migration.

A center for initiating intracellular signaling

In addition to sensing extracellular cues, the Golgi can also sense incoming traffic from the ER and respond by generating 'autochtonous' signaling cascades that exert a regulatory action on intra-Golgi trafficking. It has been well documented that ER chaperones arriving at the Golgi are recycled to the ER via a KDEL receptor/COPI-mediated mechanism, as mentioned in paragraph 6.3.3. It now appears that this chaperone-KDEL receptor binding is not just for retrieval but has an additional important function in 'activating' the KDEL receptor in response to an increased load of cargo arriving from the ER to the Golgi (Pulvirenti et al., 2008). Increased binding of ER chaperones to KDEL receptors initiates a signaling reaction characterized by activation of Golgi-localized SFKs and initiation of a phosphorylation cascade on the Golgi. In turn, this system up-regulates intra-Golgi trafficking and secretory capacity, and thereby maintains the dynamic equilibrium of the Golgi complex.

All the components of this chaperone–KDEL receptor-activated–SFK-phosphorylation cascade, from the initial signal to the final effectors, are intracellular. For the first time, this study defines the concept of 'inter-organelle signaling'.

A center for regulating cell division

Mitotic Golgi fragmentation requires several kinases including cyclin-dependent kinase 1 (cdk1), mitogen-activated protein kinase kinase 1 (MEK1), or polo-like kinase 1 (PLK1) (Persico et al., 2009; Wei and Seemann, 2009a). Some of the substrates of these kinases have been identified and include several golgins (i.e. GM130 and golgin84) and the GRASP proteins (Ramirez and Lowe, 2009). Golgi fragmentation is required for entry into mitosis. Its block results in cell cycle arrest, referred to as the 'Golgi mitotic checkpoint' (Sutterlin et al., 2002). Later, mitotic Golgi breakdown must be coordinated with other processes such as chromosome segregation or cytokinesis for successful cell division. Interestingly, evidence was obtained for a role for Golgi proteins in the orchestration of these different processes. In this respect, GRASP65 and GM130 have been shown to regulate spindle assembly, as their downregulation by siRNAs results in aberrant multipolar spindles (Kodani and Sutterlin, 2008; Sutterlin et

al., 2005), as will be further discussed in paragraph 7.4. Furthermore, mitotic disassembly of Golgi stacks correlates with the release of factors associated with Golgi membranes into the cytoplasm or their translocation into other intracellular locations. These factors become accessible to various binding partners and thereby they acquire new roles for the regulation of cell division. In support of this idea, several Golgi peripheral proteins have been found in various locations at different mitotic stages that regulate diverse aspects of cell division. For instance, COPI is recruited to the nuclear envelope at mitosis, where it promotes nuclear envelope breakdown (Liu et al., 2003). Clathrin, which participates in vesicle trafficking and cargo transport during interphase is targeted to the spindle during mitosis where it acts by anchoring microtubule fibers, thus stabilizing the mitotic spindle, and facilitating proper chromosome separation (Royle et al., 2005). A final example is Nir2, which localizes to the Golgi apparatus in interphase cells but is recruited to the cleavage furrow and midbody during cytokinesis. It has been shown that Nir2 phosphorylation by cdk1 during mitosis is an essential step for the completion of cytokinesis (Litvak et al., 2004).

Remodeling of the Golgi triggered by the activation of various kinases does not only regulate entry into mitosis and progression through mitosis, but it is also essential for the establishment of cell polarity preceding cell migration, as explained in paragraph 6.6.

7. THE MULTIPLE FUNCTIONS OF GM130

7.1. Characteristics

One of the most studied golgins is GM130. This golgin contains extensive regions of coiled-coil motifs (Figure 15). It is a peripheral membrane protein strongly attached to the cis-side of the Golgi and exposed to the cytoplasm. GM130 is anchored to Golgi membrane by its tight binding to GRASP65, which acts as a receptor for GM130 (Yoshimura et al., 2001). GRASP65 is itself attached to the Golgi apparatus via a lipid anchor (Barr et al., 1998). On the other hand, binding to GM130 is necessary for the targeting of GRASP65 to the Golgi membrane, suggesting that GM130 and GRASP65 cooperate and depend on each other for Golgi membrane binding (Bachert and Linstedt, 2010; Barr et al., 1998).

Other protein partners of GM130 include p115, syntaxin 5, the Rab1 GTPase, the GEF Tuba, AKAP450, or YSK1. These multiple interactions imply distinct roles for GM130.

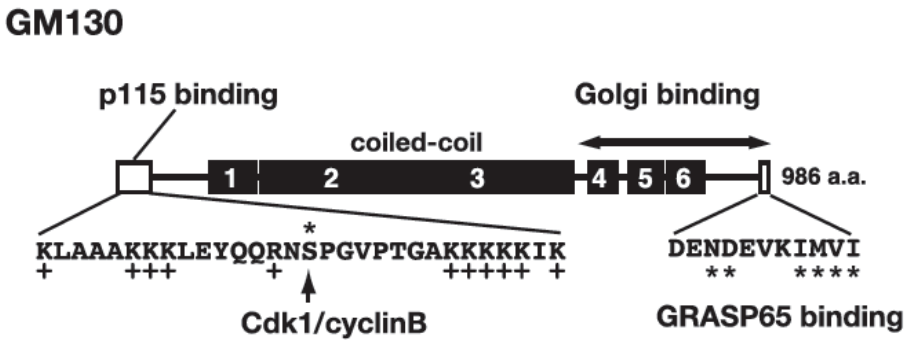

Figure 15: Mapping of GM130 protein domains. GM130 consists of six coiled-coil regions (black boxes). The Golgi binding domain is shown. The N-terminal 75 amino acids region contains positively-charged residues (indicated by '+') which bind p115. The C-terminal domain (position 976-986) contains hydrophobic residues (indicated by '*') which bind GRASP65. The serine residue phosphorylated by cdk1/cyclinB upon entry into mitosis is pointed. *From Nakamura, 2010.*
The domains interacting with Tuba and YSK1 are not represented and lie within the N-terminal first 690 amino-acids (Kodani et al., 2009), and the 75–271 region of GM130 (Preisinger et al., 2004), respectively. The domain interacting with AKAP450 is unknown.

7.2. Role in Golgi transport

GM130 and its binding protein p115 act as a tethering complex which participates in ER-to-Golgi transport and/or in intra-Golgi transport.

On the one hand, p115 is known to function in ER-to-Golgi transport. Addition of anti-p115 antibodies or depletion of p115 resulted in VSV-G arrest in the ERGIC compartment, before its delivery to the Golgi (Alvarez et al., 1999). p115 is localized to the ERGIC, which is the result of p115 recruitment by an activated Rab1 to COPII vesicles that subsequently form the ERGIC (Allan et al., 2000). p115 might participate in the tethering of COPII vesicles, as shown by experiments using the yeast homologue of p115 (Cao et al., 1998; Nakajima et al., 1991; Sapperstein et al., 1996). Furthermore, p115 might be involved in the docking of Golgi-derived COPI-coated retrieval vesicles with the ERGIC (Puthenveedu and Linstedt, 2001). The role for p115 at the ERGIC stage of transport seems to be independent of binding to GM130. However, it has been proposed that the activity of p115 in ER-to-Golgi transport is dependent upon GM130 binding at later stages, during translocation of ERGIC membranes to the cis-Golgi. Injection of antibodies competing for the binding of p115 to GM130 on the Golgi complex inhibited VSV-G traffic at the ER-to-Golgi step (Alvarez et al., 2001). This study supports a model where ER-to-Golgi transport requires the sequential action of ERGIC-associated p115 and Golgi-associated GM130. GM130 presumably acts as a receptor for p115 on the cis-Golgi, mediating transport of ERGIC-derived transport intermediates to the Golgi complex.

On the other hand, the association between GM130, p115 and giantin is crucial for COPI vesicle tethering to Golgi membranes and efficient transport of cargo through the Golgi apparatus (Seemann et al., 2000). p115 does not only interact with GM130, but also with giantin. GM130 is segregated from COPI vesicles and concentrated in cis-Golgi membranes. In contrast, giantin is enriched in COPI vesicles (Sonnichsen et al., 1998). Therefore, the ternary giantin–p115–GM130 complex is believed to tether COPI vesicles to the Golgi cisternae and facilitate vesicle fusion during inter-cisternal transport. Expression of a GM130 mutant lacking the p115 binding domain in interphase cells induced the accumulation of COPI-coated transport vesicles in the Golgi region (Seemann et al., 2000). In addition, it inhibited VSV-G transport to the plasma membrane, which was attributed to defective intra-Golgi transport. Although this model has been contradicted by the finding that GM130 and giantin compete to

bind the same p115 domain under certain in vitro conditions (Linstedt et al., 2000), other studies have shown that p115 is able to simultaneously bind giantin and GM130 under different conditions (Dirac-Svejstrup et al., 2000).

At the onset of mitosis, GM130 is phosphorylated on a serine residue by cdk1/cyclinB, which abolishes binding of p115 to GM130 (Lowe et al., 1998; Nakamura et al., 1997). Altough p115 can still bind giantin, it is no longer able to cross-link GM130. COPI vesicles accumulate as they are unable to tether and fuse to the Golgi cisternae. Continuous budding without fusion leads to the disassembly of the Golgi apparatus, and explains the observed fragmentation of the Golgi into clusters of vesicles during mitosis. This allows the mitotic Golgi clusters to be partitioned between the two daughter cells. At the end of mitosis, Golgi cisternae are regenerated and stacked. Cisternal stacking is preceded by a cisternal tethering reaction that involves p115, giantin and GM130 (Shorter and Warren, 1999). The actual stacking interactions are mediated by GRASP65 and GRASP55 (Tang et al., 2010).

Functional interaction between p115 and GM130 is not only important in the context of tethering, but also in the context of fusion.

On the one hand, both proteins are able to interact with activated Rab1. This latter is required for the targeting of p115 on COPII-coated vesicles budding from the ER, and it also controls the assembly and/or activity of GM130 on Golgi membranes (Moyer et al., 2001). These combined activities of activated Rab1 regulate docking and fusion of donor COPII vesicle transport intermediates to acceptor Golgi membranes. Interestingly, binding of Rab1 to GM130 is inhibited by binding of p115 to GM130 (Diao et al., 2008).

On the other hand, GM130 and p115 are able to interact with the t-SNARE syntaxin5. Binding of syntaxin5 to GM130 is also inhibited when p115 is bound to GM130 (Diao et al., 2008). The current model (Figure 16) is that GM130 binds syntaxin5 and Rab1 at the acceptor Golgi membrane, which keeps these proteins in close proximity to the tether. Upon p115 binding, a conformational change in GM130 triggers the dissociation of both Rab1 and syntaxin5. Simultaneously, p115 will adopt a new conformation allowing binding to Rab1 with a higher affinity on donor transport vesicles. This reaction results in the tethering of transport vesicles to Golgi membranes by the p115-GM130 complex. Syntaxin5 is most likely transferred from GM130 to

p115, facilitating formation of the SNARE complex between the donor vesicle and the acceptor membrane, followed by membrane fusion.

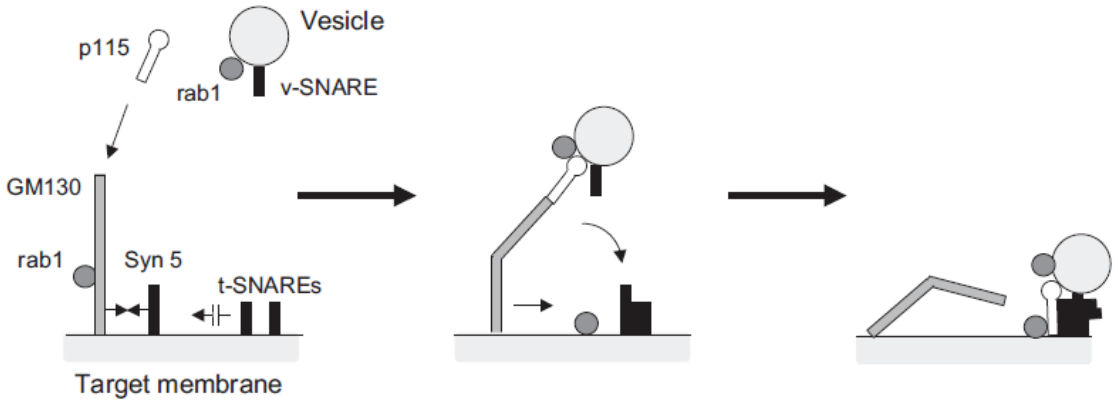

Figure 16: GM130 and p115 interactions with Rab1 and syntaxin5. Working model to describe how membrane tethering by GM130 and p115 are linked to SNARE assembly and fusion. *From Diao et al., 2008.*

7.3. Role in maintenance of the Golgi structure

Recent evidence suggests that GM130 is not only involved in heterotypic tethering of COPI-coated vesicles to the Golgi, or in the tethering of ERGIC membranes to the cis-Golgi, but also in homotypic tethering of ER-derived tubulo-vesicular transport carriers (Marra et al., 2007) and/or in homotypic tethering between neighboring cisternae (Puthenveedu et al., 2006). When these two tethering activities are lost, formation and maintenance of the Golgi structure is altered.

In the first study, GM130 was shown to control homotypic tethering and fusion of ER-to-Golgi carriers, a pre-requisite for their maturation into large membrane units and subsequent incorporation into the Golgi stacks. This is possible because ER-to-Golgi carriers can acquire GM130, which cycles between the cis-Golgi and the late ERGIC via membranous tubules connecting the two compartments (Marra et al., 2001). Following GM130 depletion, ER-to-Golgi carriers remained as distinct tubulo-vesicular entities and could not mature into flat, disk-like shaped cisternal membranes (Figure 17 A). This had an indirect effect on the Golgi structure. Reduced amounts of membrane delivered into the Golgi induced the shortening of the cisternae, and breakdown of the Golgi ribbon.

The second study showed that GM130, through interaction with GRASP65, is involved in lateral linking of the Golgi stacks to form an elongated ribbon. GM130-mediated ribbon formation was independent from p115. Depleting GM130 had a direct effect on the length of the Golgi stacks and induced a fragmentation of the Golgi similar to that observed in the first study. A model has been proposed in which GM130 is required for GRASP65 stabilization and targeting at the Golgi, whereas GRASP65, through its self-oligomerization properties, provokes lateral cisternal fusion reactions (Figure 17 C).

A third study may explain how GM130 can control Golgi organization. This study provided evidence that the ability of cis-Golgi membranes to nucleate microtubules requires GM130 (Rivero et al., 2009). GM130 binds AKAP450 and is required for the Golgi localization of AKAP450. In the absence of GM130, AKAP450 was displaced from the Golgi, and AKAP450-dependent microtubule nucleation occurred randomly throughout the cytoplasm. Consistently, GM130-depleted cells were unable to form stable, acetylated microtubules (Kodani and Sutterlin, 2008). Therefore, it can be assumed that GM130 indirectly controls tangential linking of Golgi mini-stacks by Golgi-derived microtubules and subsequent assembly of the Golgi ribbons (Figure 17 B). In addition to the effect of GM130 on AKAP450 network and microtubule assembly at the Golgi, the study by Rivero et al. also revealed an effect on the Golgi morphology. GM130 depletion induced Golgi fragmentation similar to that described in the above studies.

Although these three studies propose different mechanisms of action of GM130, they all converge to the same finding that depletion of GM130 does not appear to affect Golgi stacking, but continuity between individual stacks within the ribbon is lost.

These studies as well as other studies aimed at depleting other golgins or Golgi-nucleated microtubules point to the fact that neither Golgi ribbon integrity nor positioning are critical for global protein secretion. VSV-G trafficking from the ER to the cell surface appeared normal or only slightly delayed after GM130, GMAP210 or golgin160 depletion (Yadav et al., 2009), CLASP depletion (Miller et al., 2009), or depletion of the Golgi pool of AKAP450 (Hurtado et al., 2011). However, loss of the Golgi ribbon affected Golgi enzyme diffusion and equilibration, and optimal glycosylation of cargo (Marra et al., 2007; Miller et al., 2009; Puthenveedu et al., 2006).

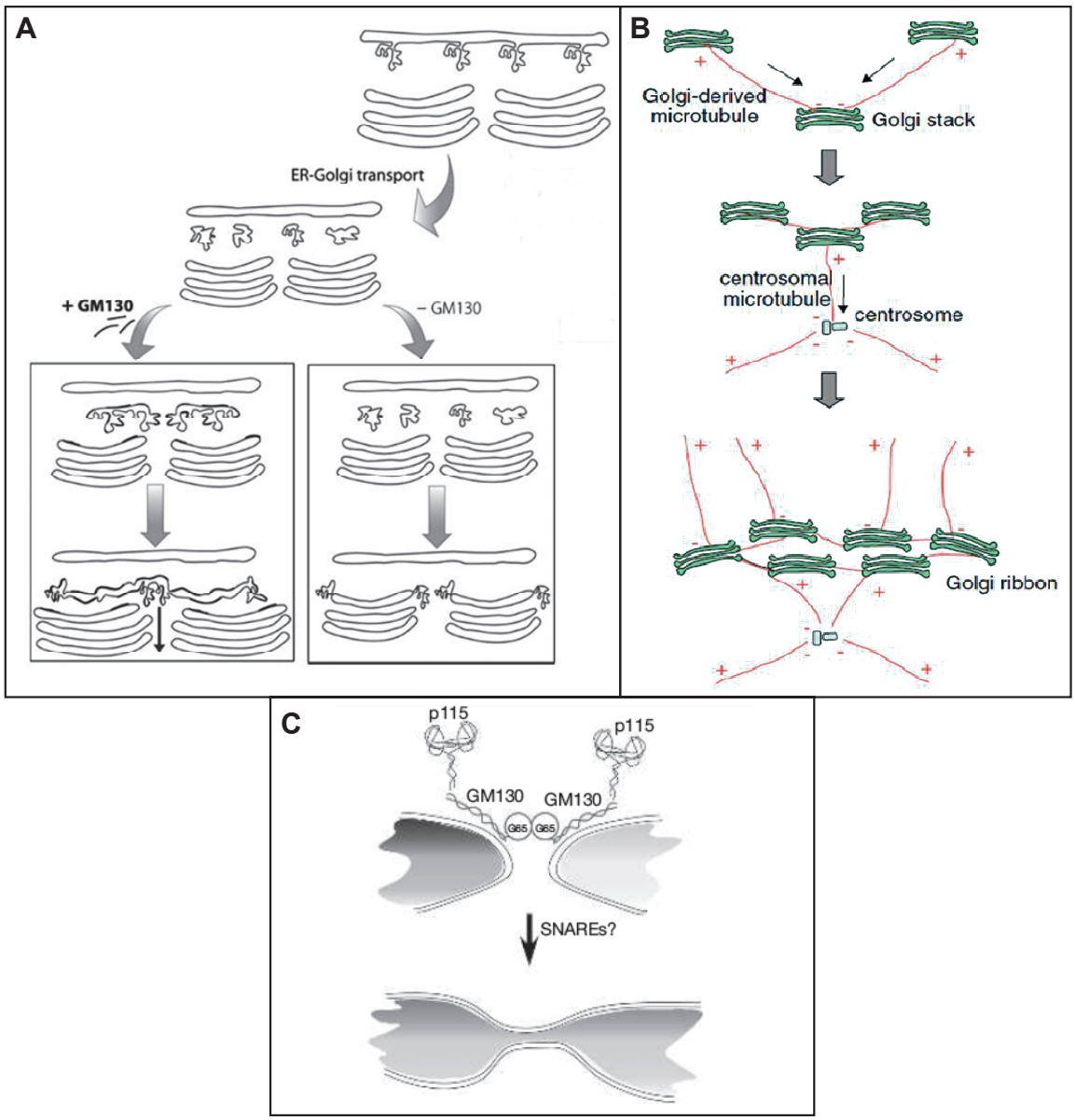

Figure 17: Models linking GM130 to formation and maintenance of the Golgi architecture.
(A) When ER-to-Golgi carriers acquire GM130 (left), they fuse with each other, generating disk-like membranes that are incorporated into the stacks, contributing to the formation of a new cisterna at the cis-face of the Golgi. In absence of GM130 (right), ER-to-Golgi carriers remain as distinct entities, causing the accumulation of tubulo-vesicular membranes, decrease of the cisternae length, and disconnection of the Golgi ribbon. *Adapted from Marra et al., 2007.*
(B) Microtubule-dependent Golgi ribbon assembly occurs in two phases. First, lateral cross-linking of Golgi stacks is driven by Golgi-derived microtubules. This phase is regulated by GM130-dependent Golgi-localized AKAP450. Second, the clustered stacks move along centrosomally nucleated microtubules, bringing them in the cell center. Golgi ribbon assembly precedes the establishment of tubular connections between the stacks, as seen in (C). *Adapted from Lowe, 2011.*
(C) Elongation and formation of a continuous Golgi ribbon is driven by GM130-localized, GRASP65 homo-oligomers at cisternal rims. Subsequent SNARE-mediated membrane fusion results in compartment equilibration. *From Puthenveedu et al., 2006.*

7.4. Role in cell cycle regulation

As mentioned elsewhere, Golgi fragmentation is required not only for inheritance but also for mitotic entrance itself, since its block results in the arrest of the cell cycle at the G2/M transition, which is called the 'Golgi mitotic checkpoint' (Sutterlin et al., 2002). In particular, mitotic Golgi disassembly is controlled by GM130 phosphorylation (see paragraph 7.2), and by GRASP65 phosphorylation. Whereas GRASP65 is phosphorylated by ERK during polarization (see paragraph 6.6), mitotic GRASP65 phosphorylation is mediated by cdk1/cyclinB. Phosphorylation inhibits GRASP65 oligomerization and promotes Golgi unlinking, thereby facilitating subsequent mitotic Golgi vesiculation (Wang et al., 2005; Wang et al., 2003b; Yoshimura et al., 2005).

It is therefore not surprising that inhibition of mitotic Golgi fragmentation via a functional block of GRASP65 or GM130 results in the arrest of the cell cycle. Inhibiting GRASP65 function either by expressing non-regulatable GRASP65 mutants or by injecting anti-GRASP65 antibodies arrested cells at the G2/M transition, which ultimately led to cell death (Sutterlin et al., 2002; Tang et al., 2010). In HeLa cells depleted for GRASP65, arrest in cell division was accompanied by the formation of multiple non-functional mitotic spindles (Sutterlin et al., 2005). Similarly, GM130 depletion caused aberrant multipolar spindle formation during mitosis in p53-negative cells, and cell cycle arrest at the G2/M transition in p53-positive cells (Kodani and Sutterlin, 2008).

In GM130-depleted cells, mitotic defects were preceded by centrosome defects during interphase. Although GM130 is not localized at the centrosome, it controls centrosome organization from the cis-Golgi membrane. GM130 depletion in different human cell lines resulted in centrosome multiplication and mislocalization in interphase cells (Kodani and Sutterlin, 2008). The supernumerary centrosomes were abnormal in term of composition, and defective with respect to microtubule organization and cell migration. Regulation of the centrosome organization and function by GM130 depends on GM130 interaction with the GEF Tuba (Kodani et al., 2009). This interaction promotes the activation of Cdc42, a small GTPase of the Rho family, by its GEF Tuba. The demonstration that the organization of the centrosome can be regulated by the Golgi protein GM130 shed light on the significance of the physical proximity between the Golgi and the centrosome.

7.5. Role in cell polarity and migration

Not only ERK, but also other kinases are recruited to the Golgi during cell migration. GM130 binds and activates the kinases YSK1 and MST4, and thereby contributes to signaling events at the Golgi apparatus (Preisinger et al., 2004). Upon activation, YSK1 phosphorylates its substrate 14-3-3ζ and potentially other downstream targets needed for normal cell migration and polarization. Interference with YSK1 function, either by using a dominant-negative mutant form of YSK1 unable to be activated by GM130, or by depleting YSK1, resulted in dispersal of the perinuclear Golgi ribbon into the cell periphery, failure to show polarization of the Golgi and the centrosome in the direction of migration, and disturbed cell migration. MST4 acts via an uncharacterized pathway by blocking cell migration.

The involvement of 14-3-3ζ is relevant with the role of the Golgi in intracellular signaling events. Indeed, 14-3-3ζ is an activator the Rho GTPases Rac1 and Cdc42 (Bialkowska et al. 2003), and it can also activate the Ras signaling pathway at the cell surface (Fantl et al., 1994; Freed et al., 1994). Since pools of Ras and Rho GTPases are known to be generated at the Golgi, it is possible that 14-3-3ζ can modulate these pathways at different subcellular locations including the plasma membrane and the Golgi.

GM130 and YSK1 have also been established as central players in neuronal polarization that is the formation of a single axon and multiple dendrites (Matsuki et al., 2010). GM130 and YSK1 are part of a neuronal polarization pathway involving the protein kinase LKB1. This pathway regulates axon initiation, which was lost when knocking down YSK1, LKB1 or GM130 in mouse or rat hippocampal neuronal cultures using small hairpin RNAs (shRNAs). In contrast, overexpressing YSK1 led to the formation of multiple axons. An opposing pathway based on Reelin and Dab1 signaling has been identified. Hippocampal neurons from dab1-/- mutant mice produced supernumerary axons.

Neuronal polarization is tightly linked to Golgi morphology. Reorientation of the Golgi and the adjoined centrosome is essential for establishment of the site of axon emergence (de Anda et al., 2005). Later, specialized Golgi outposts which populate

dendrites promote the elaboration of the dendritic tree (Horton et al., 2005; Ye et al., 2007). Consistently, the LKB1-YSK1-GM130 and Reelin-Dab1 pathways were reported as modulators of the Golgi morphology. Individually knocking down YSK1, LKB1 or GM130 resulted in Golgi fragmentation, whereas overexpressing YSK1 led to condensation of the Golgi into a smaller volume. In neurons of reelin-/- or dab1-/- mutant mice, the Golgi failed to extend normally into a dendritic process. In the same line, Reelin stimulation induced Golgi deployment into dendrites, which was suppressed by YSK1 overexpression. Therefore, the balance between the LKB1-YSK1-GM130 and the Reelin-Dab1 pathways regulate Golgi morphology and dispersion, axon specification, and dendrite growth.

Additional mechanisms can account for GM130-mediated control of cell polarization and migration. First, through its effect on centrosome organization, GM130 controls the network of centrosomally nucleated microtubules (Kodani and Sutterlin, 2008). In absence of GM130, aberrant centrosomes were unable to nucleate dynamic microtubules, or to reorient in response to a polarization stimulus. Second, GM130-dependent centrosome regulation involves the small GTPase Cdc42 (Kodani et al., 2009), a known regulator of cell polarization (Etienne-Manneville, 2006). Alternatively, GM130 may also control microtubule organization independently of its role in regulating centrosome function. GM130 may promote microtubule nucleation at the Golgi by recruiting the microtubule nucleation factor AKAP450 (Rivero et al., 2009). GM130-depleted cells were unable to form stable, acetylated microtubules, which are necessary for directional cell migration (Kodani and Sutterlin, 2008). Thus, GM130 may affect cell polarization and migration through effects on centrosome organization, Cdc42 activation, microtubule nucleation at the Golgi, and YSK1 activation.

The different functions of GM130 are summarized in Figure 18.

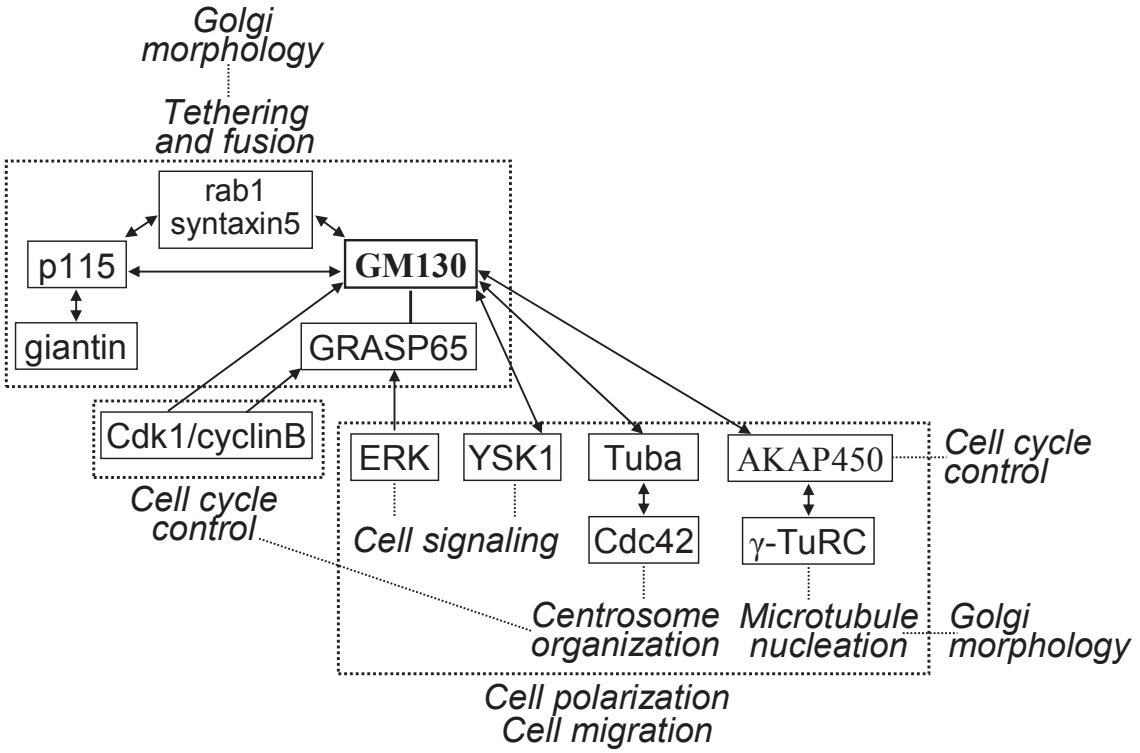

Figure 18: Proposed functions of GM130. GM130, together with p115, Rab1, syntaxin5, giantin and GRASP65 are involved in tethering and fusion events at the Golgi. GM130 participates in centrosome organization by an interaction with Tuba, which activates Cdc42, and in microtubule nucleation at the Golgi by an interaction with AKAP450, which recruits γ-TuRC. GM130 activities at the level of the centrosome, or microtubules, as well as GM130 interaction with YSK1 and GRASP65 control cell polarization and cell migration. Finally, GM130, together with GRASP65 are involved in cell cycle control. *Adapted from Nakamura, 2010.*

8. HS AND GANGLIOSIDE METABOLISM

Three classes of molecules synthesized in the Golgi apparatus are of high importance when considering MPSIIIB, namely lysosomal proteins, primary storage products of the HS family, and secondary storage products of the ganglioside family. The biosynthesis of lysosomal proteins has already been described elsewhere. This paragraph will concentrate on the biosynthesis of HS and gangliosides at the Golgi, as well as their degradation in the lysosome. The central role of these two organelles in the regulation of HS and ganglioside homeostasis will be pointed out. In addition, the physiological functions of HS and gangliosides will be highlighted.

Finally, mechanisms for deregulated HS and ganglioside metabolism in MPSIII and possible cellular consequences will be discussed. In the case of HS, lysosomal degradation is primarily impaired, although it can not be excluded that downstream mechanisms exist affecting HS biosynthesis as well. In the case of GM2 and GM3 gangliosides, it is not known whether mechanisms leading to accumulation primarily involve degradation into late endosomes/lysosomes (where GM1 → GM2 → GM3 conversion occurs), or synthesis and transport from the Golgi (where GM3 → GM2 → GM1 conversion occurs), or both.

8.1. HS

8.1.1. HS composition

HS is a member of the GAG family of macromolecules, which also includes chondroitin sulfate, dermatan sulfate, and keratan sulfate. All four groups are linear polysaccharides consisting of repeating disaccharide units composed of a hexuronic acid linked to a hexosamine. They differ in the type of carbohydrates they contain, in the geometry of the glycosidic linkage, and in the number and position of sulfate groups. In the case of HS, the hexuronic acid can be either glucuronic acid (GlcA), or its C5 epimer iduronic acid (IdoA). The hexosamine is a glucosamine (GlcN) (Figure 19). HS chains typically vary in length from 50 to 200 disaccharide units (molecular weight in the range of 25-100 kDa). Disaccharides can be modified on different positions. The hexuronic acid can be *O*-sulfated on the C2 position. *O*-sulfation can occur at the C6

position, and to some extent at the C3 position of the GlcN unit. The nitrogen at position 2 of glucosamine may be free (GlcN), *N*-sulfated ($GlcNSO_3$) or *N*-acetylated (GlcNAc). Based on substitution and epimerization patterns, HS could theoretically contain up to 48 distinct disaccharides, generating an enormous structural diversity of HS saccharide chains. Amongst these 48 potential disaccharide structures, only 23 naturally occurring structures have been identified so far (Esko and Selleck, 2002).

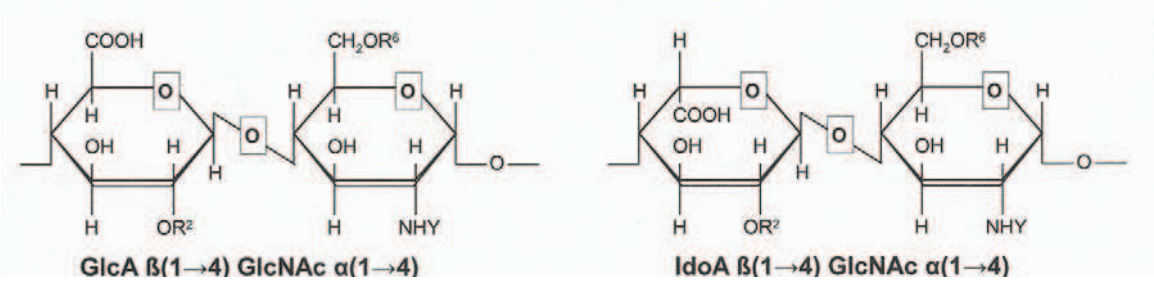

Figure 19: Structure of disaccharide units composing HS saccharide chains.
An hexosamine residue (GlcNAc) is associated with an uronic acid which can be a GlcA residue (left) or an IdoA residue (right). Substitutions can occur at different positions:
R^2: H or SO_3
R^6: H or SO_3
Y: H, SO_3 or Ac

Microdomains of different sulfation degree are apparent in HS chains, including highly sulfated sequences with contiguous *N*-sulfated disaccharides (so called NS domains), moderately sulfated domains with alternating *N*-sulfated and *N*-acetylated disaccharides (NA/NS domains), and low sulfated domains with stretches of *N*-acetylated disaccharides (NA domains). NS domains are associated with a large potential to interact with proteins. HS–protein interactions primarily depend on interactions between negatively charged sulfate and carboxyl groups in HS and positively charged amino acid residues in the protein (Salmivirta et al., 1996). The introduction of IdoA residues is another crucial modification for the protein-binding properties of HS chains. Sulfated domains are enriched in IdoA which has ring flexibility, conferring conformational versatility to the sugar chain.

8.1.2. HS biosynthesis

HS sugar chains are covalently linked to core proteins to form HS proteoglycans (HSPGs). The protein core can be a transmembrane protein (syndecan or fibroglycan), a membrane-bound protein anchored by GPI (glypican) or an excreted protein (agrin and perlecan). The biosynthesis of HS occurs mainly in the Golgi in a sequential manner (Figure 20). Membrane-bound Golgi enzymes utilize various monosaccharide building blocks after they have been activated to their UDP forms. A linkage tetrasaccharide is first added to the protein core composed of β-xylose, β1-4-galactose, β1-3-galactose, β1-3-GlcA. This first reaction is catalyzed by the successive action of a UDP-xylosyl transferase, a UDP-galactosyl transferase I, a UDP-galactosyl transferase II, and a UDP-GlcA transferase I. A GlcNAc residue is then added to the terminal GlcA residue of the linkage tetrasaccharide by a GlcNAc transferase I. The elongation of HS chains that is the consecutive addition of alternating GlcA and GlcNAc residues is mediated by the action of two enzymes, GlcA transferase II, and GlcNAc transferase II, respectively. These enzymes are the products of the *ext* genes, *ext*1 for the GlcNAc transferase and *ext*2 for the GlcA transferase. Whereas GlcA residues are added via a β(1→4) linkage, GlcNAc residues are added via an α(1→4) linkage. The initial product is a non-sulfated polymer composed of alternating sequences of GlcA and GlcNAc:

$[\text{GlcA } \beta(1\rightarrow4) \text{ GlcNAc } \alpha(1\rightarrow4)]_n$.

The HS chain is further modified in a specific and ordered manner. First, GlcNAc groups can be *N*-deacetylated and then *N*-sulfated, a process that is catalyzed by the enzyme GlcNAc *N*-deacetylase/*N*-sulfotransferase, giving rise to GlcN and $GlcNSO_3$. Then, GlcA groups along the chain can be epimerized into IdoA groups by the action of the enzyme C5-GlcA epimerase. This enzyme converts the carboxyl group on the C5 position of a glucuronic acid so that it is oriented below the hexose ring. Enzymes responsible for sulfation reactions act later in the HS biosynthetic cascade. A 2-*O*-GlcA/IdoA sulfotransferase catalyzes the addition of sulfate groups at C2 of GlcA and IdoA. Further sulfation on glucosamine residues can occur at the C6 and C3 residues by the enzymes 6-*O*-GlcN sulfotransferase and 3-*O*-GlcN sulfotransferase, respectively. In the Golgi, GlcA transferase and GlcNAc transferase (the products of *ext* genes) on the

one hand, and C5-GlcA epimerase and 2-*O*-GlcA/IdoA sulfotransferase on the other hand, associate with one another to form complexes.

Synthetized HSPGs are finally transported by exocytosis at the cell surface and in the ECM where they are ubiquitously expressed.

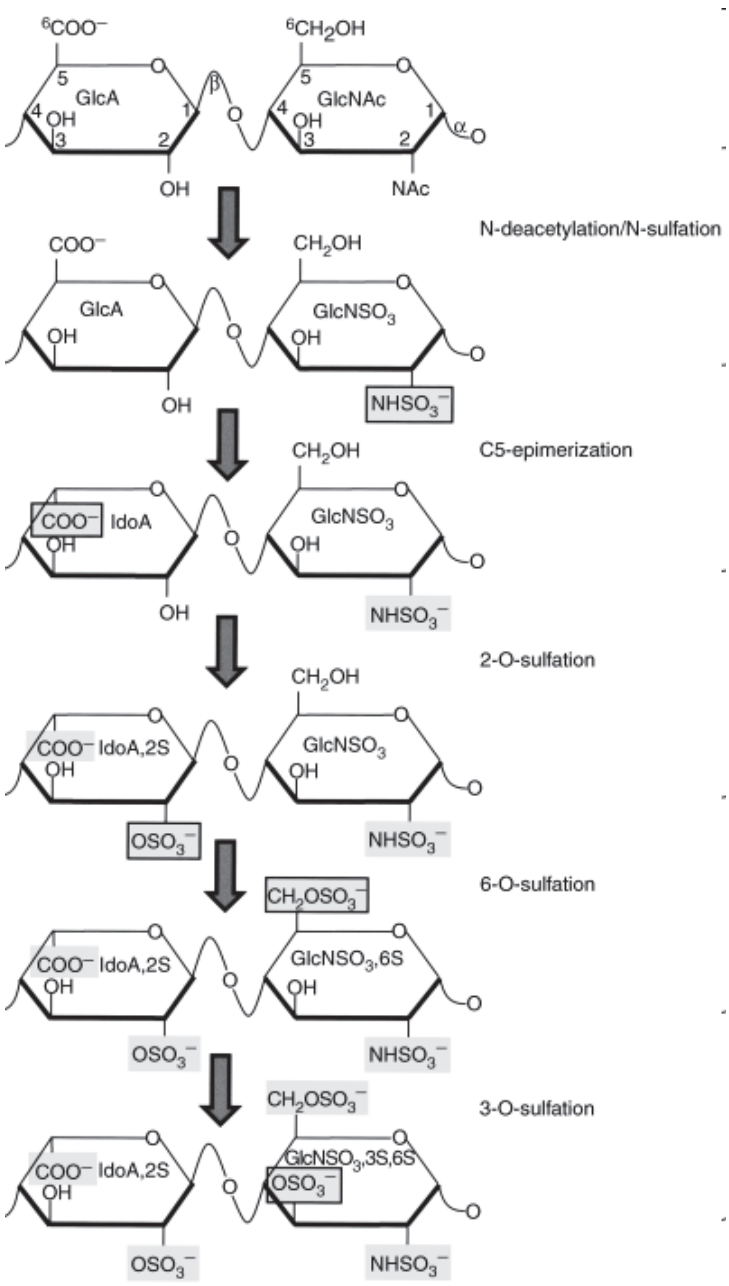

Figure 20: HS biosynthesis.
From Rops et al., 2004.

8.1.3. HS degradation

HSPGs at the cell surface or in the ECM are in a dynamic state. Cells can alter the HS structures they make in response to extracellular signals. HSPGs are constantly internalized, degraded and partially recycled to the cell surface. Their half-life is in the range of 3 to 8 hours (Stringer and Gallagher, 1997). Molecules are degraded in lysosomes after internalization by endocytosis. Endoglycanases (heparanases) present in early endosomes cleave saccharide chains internally, producing HSO. Resulting fragments have a length varying between 10 to 20 hexose units. The substrate specificity of heparanase has been unraveled recently (Peterson and Liu, 2010). Heparanase cleaves the linkage between a non-sulfated GlcA unit and a $GlcNSO_3$ unit carrying *O*-sulfation either at the C6 or the C3 position (Figure 21, first case). Alternatively, heparanase can cleave the linkage between a non-sulfated GlcA unit and a non-*O*-sulfated $GlcNSO_3$ unit when another *O*-sulfated $GlcNSO_3$ residue is present in proximity (Figure 21, second case). If this structure does not occur, the enzyme searches for a 2-*O*-sulfated GlcA residue located in proximity of the cleavage site (but not a 2-*O*-sulfated IdoA residue) (Figure 21, cases 3 and 4). A structure with repeating disaccharide units consisting of 2-*O*-sulfated IdoA and $GlcNSO_3$ residues inhibits the activity of heparanase (Figure 21, case 5).

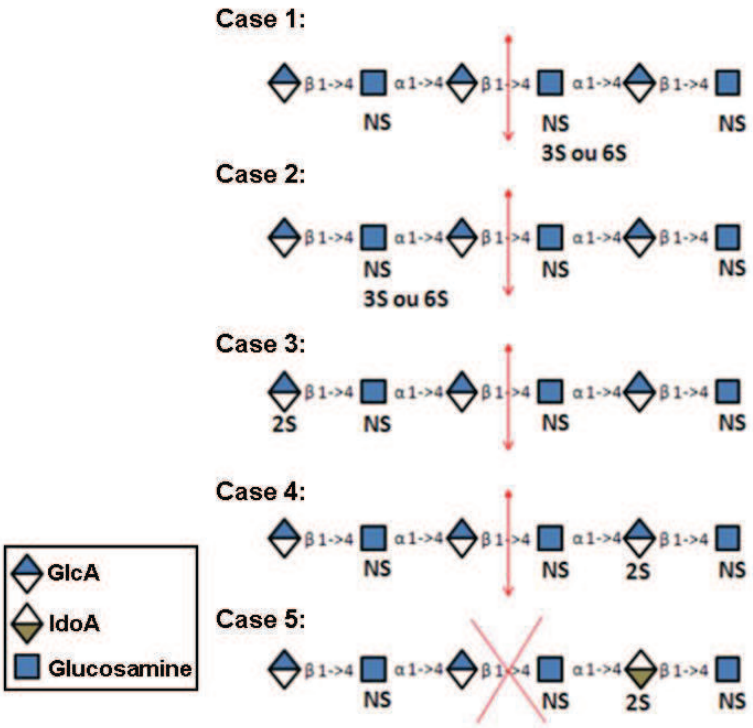

Figure 21: Heparanase substrate recognition sites.

HSO are further digested into monosaccharides in lysosomes through the sequential action of lysosomal exoglycanases at the non-reducing end of the chain. HS degradation is thus oriented from the non-reducing end toward the reducing end. Exoglycanases include three glycosidases, five sulfatases, and one acetyltransferase (Figure 22). A defect of each of the exoglycanases is responsible for a particular type of MPS.

More precisely, the three glycosidases (Figure 22, in blue) involved in the cleavage of terminal IdoA, GlcA and glucosamine residues are, in order, α-L-iduronidase, β-glucuronidase, and α-N-acetylglucosaminidase (NAGLU). Defects in these enzymes lead to MPSI, MPSVII, and MPSIIIB, respectively. NAGLU only catalyzes the removal of acetylated glucosamine residues (GlcNAc), a preliminary modification performed by the action of acetyl-CoA-N-acetyl transferase (Figure 22, in red), the enzyme deficient in MPSIIIC. The five sulfatases (Figure 22, in green) include iduronate-2-sulfatase required for the removal of sulfate groups at position 2 of IdoA (missing in MPSII); glucosamine-6-sulfatase specific for sulfate groups at position 6 of glucosamine residues (deficient in MPSIIID); sulfamidase responsible for eliminating sulfate groups linked to the nitrogen at position 2 of glucosamine residues (deficient in MPSIIIA); glucuronate-2-sulfatase and glucuronate-3-sulfatase required for the elimination of sulfate groups in GlcA (not associated with any known disease).

Monosaccharides building blocks resulting from lysosomal degradation are then recycled. HS proteoglycan digestion is very efficient in normal cells, such as proteoglycans or HSO are not detectable in intracellular organelles.

In each MPS disorder, it can be hypothesized that accumulating HSO possess a non-reducing end that is specific for the deficient enzyme. For instance, this non-reducing end would be GlcNAc in the case of MPSIIIB, or IdoA in the case of MPSI (Figure 23). In theory, minimal HSO sequences accumulating in MPSIIIB and MPSI are, respectively, [GlcNAc- uronic acid(S)] and [IdoA- hexosamineAc(S)].

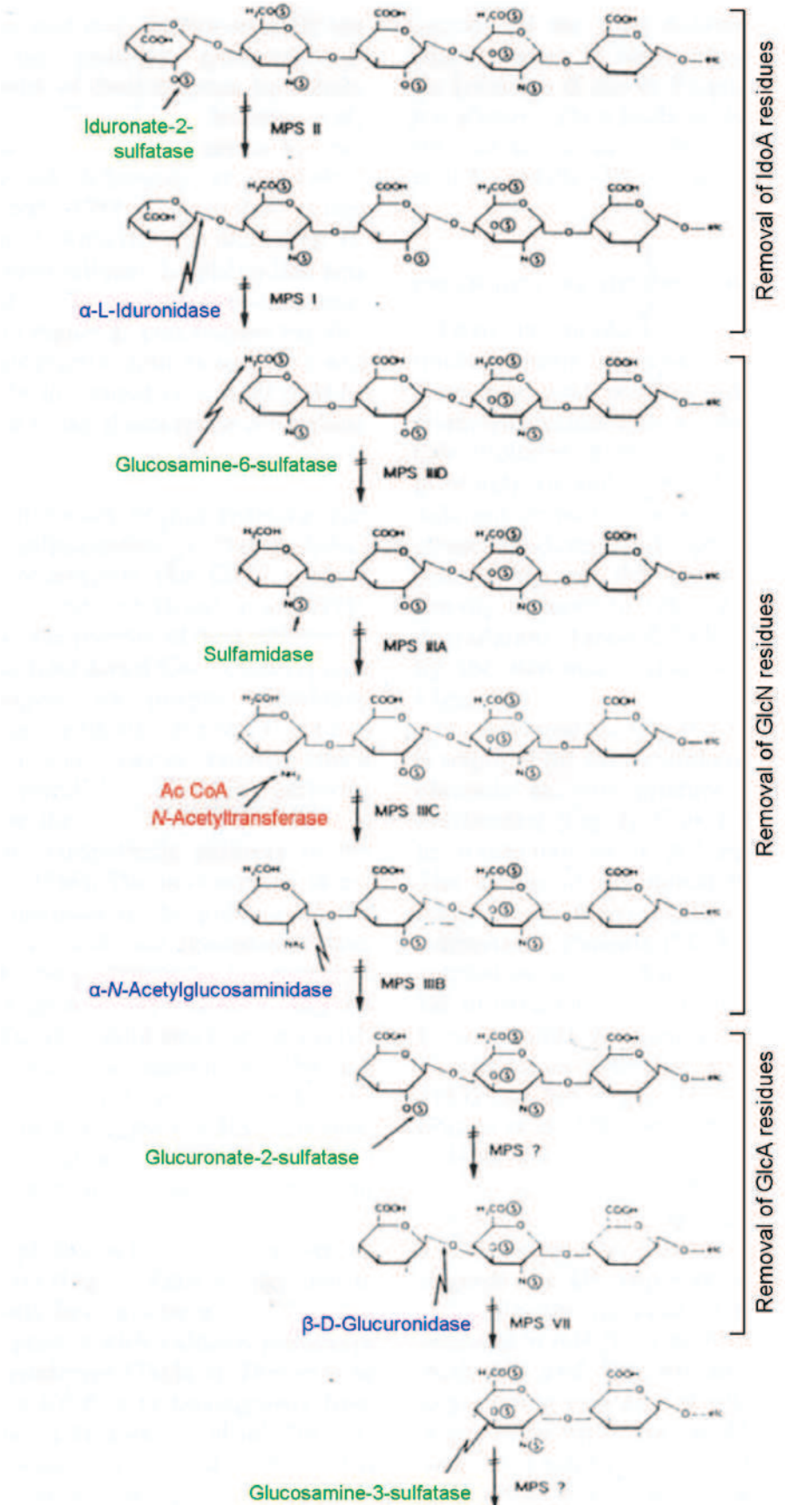

Figure 22: Stepwise degradation of HS in the lysosome. Three glycosidases (in blue), one acetyltransferase (in red) and five sulfatases (in green) are required. Diseases associated with deficiencies of each enzyme are indicated. *Adapted from Hopwood and Morris, 1990.*

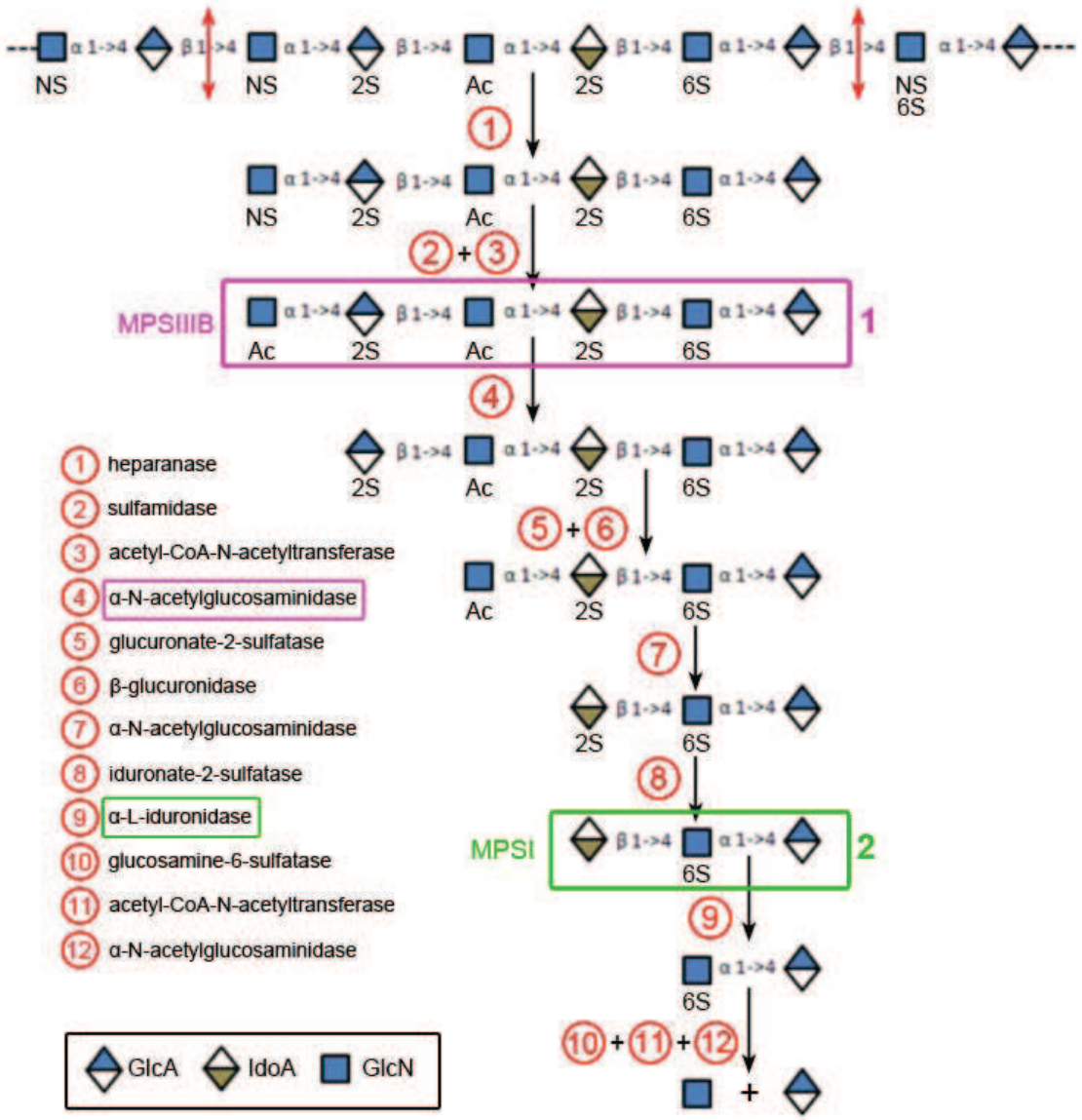

Figure 23: HSO species accumulating in MPS. An example of sequential degradation of a theoretical HS chain is represented. In this example, compound 1 (purple box) would represent one of the HSO species accumulating in MPSIIIB patients, whereas compound 2 (green box) would accumulate in MPSI patients.

8.1.4. The roles of HSPGs

HSPGs are major determinants of how the cells sense, integrate and respond to the cell environment. They mediate multiple biological activities as receptors or co-receptors for many protein ligands in the ECM (Esko and Selleck, 2002). Interactions with protein ligands are mediated via both protein-protein interactions and HS-protein

interactions. HSPGs primarily regulate interactions between adjacent cells and between cells and the ECM, and they control cell adhesion, proliferation and migration. Importantly, HSPGs cooperate with a major class of ECM receptors, integrins, to connect the ECM and the cytoskeleton (Lopes et al., 2006) (Figure 24).

Some examples of HS ligands involve cell surface enzymes, ECM constituents (e.g. fibrin, fibronectin, laminin, and various types of collagen), cell adhesion molecules (L-selectin, N-CAM), and soluble growth factors [EGF, FGF, insulin-like growth factor-2, platelet-derived growth factor, transforming growth factor β, vascular endothelial growth factor, hepatocyte growth factor]. In addition, HS chains possess the ability to bind to cytokines such as interleukin (IL)-5, IL-6, IL-8, IL-10, or tumor necrosis factor α (TNFα) (Whitelock and Iozzo, 2005), playing a role in cytokine action. HS play another role in inflammation by regulating the interaction between anti-thrombin III and Factor Xa, two components of the coagulation cascade. HS can also interact with lipases, for instance lipoprotein lipase, thus being important in lipid metabolism.

Genetic studies in Drosophila, Caenorhabditis elegans and in mice have revealed the essential role of HS in development. Mutations or knockouts of HS biosynthetic enzymes or HSPG core proteins have been shown to dramatically perturb signal transduction pathways involving morphogens including FGF, sonic hedgehog (shh), wingless (wnt), Notch, or bone morphogenetic protein (BMP).

HSPGs have important neurobiological functions. They play a role in the establishment and maintenance of neuronal connections and are therefore crucial for both CNS development and plasticity (Murrey and Hsieh-Wilson, 2008). Extracellular HS present in the cell environment modulate the binding of neurons to the substrate by modulating neuronal perception of environmental cues, interaction with the ECM and with cell adhesion molecules such as laminin or N-CAM. They regulate neural cell migration, the growth and guidance of axons, neuronal polarity and neurite outgrowth (Bovolenta and Fernaud-Espinosa, 2000). These effects are mediated by growth factors (e.g. FGFs), secreted morphogens (e.g. wnt or shh), repellents and attractants (e.g. Slit, netrin, or Semaphorins and Ephrins) (Hu 2001; Lin 2004).

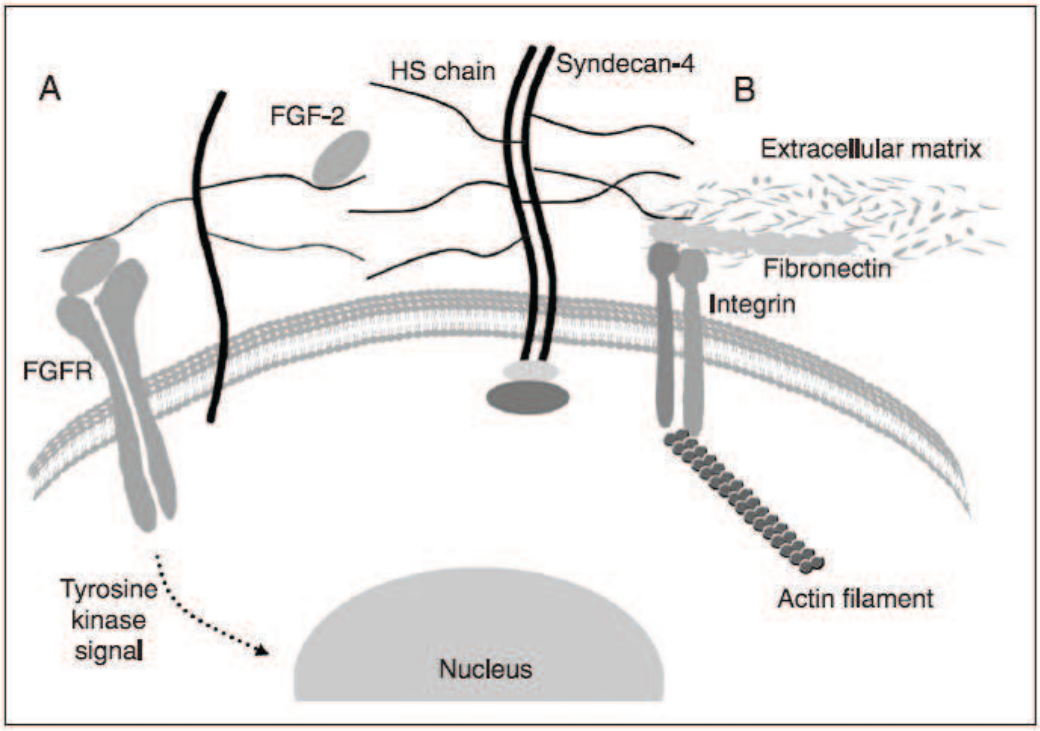

Figure 24: HSPGs-integrin cooperation. HSPGs modulate growth factor signaling (A) and participate in cell adhesion (B). (A) Formation of a ternary complex between HS, FGF and FGFR and subsequent signal transduction are represented. (B) Focal adhesion in which integrins and HSPGs cooperate to connect the ECM and the cytoskeleton is represented. *From Lopes et al., 2006.*

8.1.5. HS-protein interactions

HS-protein interactions do not depend on non-specific ionic interactions, but they are on the contrary regulated in a very specific manner. Specific structural motifs in HS are designed for selective interactions with certain proteins. The high degree of HS structural diversity, as described above, is thus of primary importance as it leads to the many binding of HS toward hundreds of proteins. Different sulfation patterns result from the variable distribution or activity of HS sulfotransferases, generating a 'saccharide code' conferring distinct profiles of ligand sensitivities to individual cells. Such 'codes' can be a specific pentasaccharide sequence containing a functionally essential 6-*O*-sulfated GlcNAc or $GlcNSO_3$ that mediates interaction with anti-thrombin III. In the case of lipoprotein lipase, the binding region within the HS chain is composed of five consecutive *N*- and 2,6-di-*O*-sulfated disaccharide repeats. Biochemical and structural studies have revealed the importance of 6-*O*-sulfation of HS for FGF signaling which appears to be required for interactions with FGF and FGFR (Nakato

and Kimata, 2002; Schlessinger et al., 2000). Whereas some proteins interact with short domains on HS chains, many proteins need longer sequences of HS. The different structures by which HS recognize so many distinct proteins are however only poorly characterized (Kreuger et al., 2006).

HS can act on proteins in different ways (Turnbull et al., 2001). They can influence protein conformation. For example, the specific pentasaccharide sequence in HS induces a conformational change in anti-thrombin III that accelerates its binding to coagulation Factor Xa 1000 folds. Another mechanism includes effects on protein-protein interactions. For example, longer HS sequences enhance juxtaposition between anti-thrombin III and thrombin, another actor of blood coagulation that also binds anti-thrombin III. HS chains can also serve as co-receptors for soluble growth factors such as FGF, increasing the affinity of FGF for its receptor FGFR. HS chains can also regulate protein localization at the cell surface, as it is the case for lipoprotein lipase. Finally, HS can protect proteins against degradation, regulate protein transport through basement membranes, and mediate protein internalization.

8.1.6. HSO species accumulating in MPS

In MPS, HSO are not only stored in lysosomes, but they can also accumulate outside these organelles and outside cells. Little is known about the nature of these fragments. Studies aiming at determining the structure of excreted HSO were performed in the urine of MPS patients, and revealed a complex mixture in term of length, carbohydrate composition, and sulfation pattern. HSO have first been analyzed by polyacrylamide gel electrophoresis, demonstrating a range of oligosaccharide structures from tetrasaccharides to structures with more than 20 disaccharide repeats (Byers et al., 1998), each type of MPS accumulating a distinct spectrum of GAGs. Mass spectrometry techniques have allowed the analysis of the composition and levels of sulfation of these HSO. In each MPS disorder, it was confirmed that the oligosaccharides that are elevated possess a non-reducing end that is specific for the deficient enzyme (Fuller et al., 2004). Only a minority of oligosaccharides showed non-reducing ends that were not reflective of the enzyme deficiency. Specific markers for each MPS have been identified (Table 3). For example a disaccharide [hexosamineSO_3- uronic acid] is accumulated in MPSIIIA (Fuller et al., 2004; King et al., 2006). MPSIIIB patients may be identified

using the tetrasaccharide [GlcNAc- uronic acid- hexosamineAc- uronic acid(S)]. MPSI patients have high levels of monosulfated di- and trisaccharides [IdoA- hexosamineAc(S)] and [IdoA- hexosamineAc- uronic acid(S)].

Disease	Theoretical minimal HSO sequence	HSO sequences detected in patient urines
MPSI	[IdoA- HNAc(S)]-	[IdoA- HNAc(S)] [IdoA- HNAc- UA(S)]
MPSIIIB	[GlcNAc- UA(S)]-	[GlcNAc- UA- HNAc- UA(S)]

Table 3: Disease-specific HSO biomarkers. Theoretical HSO sequences (see 8.1.3) and HSO sequences detected in patient urines are compared for MPSI and in MPSIIIB. UA: uronic acid. HNAc: N-acetyl-hexosamine.

Attempts have been made to draw a correlation between chemical structures of HSO and symptoms of patients suffering from various MPS types. Nuclear magnetic resonance analysis of urinary GAGs showed a possible correlation between the sulfation level and the severity of symptoms. Whereas MPS patients with CNS manifestations (i.e. MPSIIIA patients) excreted a highly sulfated variant of HS, patients with peripheral manifestations (i.e. MPSI and MPSII patients) excreted a different type of HS with lower sulfation (Hochuli et al., 2003). Another link has been proposed between the nature of chemical moieties at the non-reducing terminus and the presence or absence of behavioural symptoms in MPS (Wegrzyn et al., 2010). The presence of *N*-bounded or *O*-bounded acetyl or sulfate moieties in MPSIII or MPSII may lead to behavioural disturbances. In contrast, the absence of additional chemical moieties at the non-reducing terminus may result in no behavioural disturbance, like in MPSI or MPSVII.

It should be noted that analysis of urinary GAGs may not be reflective of the composition of GAGs accumulating in the CNS, as in the case of MPSIIIB for example. Indeed, as the most abundant disaccharide unit found in HS is GlcNAc-GlcA (representing 50% of HS disaccharide units), the probability that NAGLU will encounter its substrate site is high. NAGLU deficiency is thus expected to lead to the production of HSO fragments larger than the tetrasaccharide fragment found in urine. The nephron may preferentially filter and dialyse small HSO which accumulate in patient urine. In contrast, HSO accumulating in the CNS may have a highest structural

diversity. Therefore, GAG analysis on cerebrospinal fluid samples may be more appropriate regarding the status of HSO accumulating within brain tissues of affected patients.

8.2. Gangliosides

8.2.1. Ganglioside biosynthesis

Sphingolipids are a class of lipids which include sphingomyelin and glycosphingolipids (GSLs). Sphingolipid de novo biosynthesis starts in the ER with the formation of a common precursor, ceramide. Ceramide can either be processed to sphingomyelin via the addition of a phosphocholine headgroup or it can be glycosylated, producing GSLs. Glycosyltransferases acting in GSL biosynthesis can be galactosyltransferase (GalT) 3, giving rise to galactosylceramide (GalCer), and more often glucosyltransferase (GlcT), giving rise to glucosylceramide (GlcCer). GalCer-derived GSLs are only present in specialized cells; they represent the major lipids of the myelin sheath assembled around the axons of neurons by myelinating cells such as oligodendrocytes. In contrast, GlcCer is present in most eukaryotic cells. Whereas GalT3 is concentrated in the ER, GlcT is widely distributed between the ER and the cytosolic side of early Golgi membranes (Futerman and Pagano, 1991). Once produced and translocated into the lumen of the Golgi apparatus, the GalCer and GlcCer precursors can be further modified to complex GSLs by the stepwise addition of carbohydrate molecules. GSLs containing one or more sialic acid residues in the carbohydrate chain are referred to as gangliosides. A variety of gangliosides have been identified according to the number of sialic acids present and to their migration order in chromatography. Except for GM4, all gangliosides have LacCer as a precursor. LacCer is produced from GlcCer by the action of GalT1.

Biosynthesis of the first ganglioside, GM3, involves the addition of a sialic acid onto LacCer by a sialyltransferase (ST) 1 (Figure 25). GM3 can either be processed to the complex gangliosides of the “a” series including GM2, GM1 and GD1a, or it can be further sialosylated by the sequential action of ST2 and ST3, generating GD3 and GT3, respectively. GD3 and GT3 are the starting points for the “b” and “c” series of complex

gangliosides, respectively. At this branching point, the different enzymes compete for the utilization of a common pool of GM3 acceptors. It is the balance between the activities of the competing enzymes rather than the ordered spatial disposition of these enzymes along the Golgi cisternae that influences whether GM3 is used for the synthesis of “a”, “b” and “c” pathway gangliosides (Maxzud et al., 1995).

Along each series, elaboration of complex ganglioside structures from the simple gangliosides GM3, GD3, or GT3 is achieved by the sequential addition of *N*-acetylgalactosamine, galactose and sialic acid residues by non specific *N*-acetylgalactosaminyl-transferase (GalNAc-T), GalT2 and ST4 and ST5. A further series of GSLs ("o” series) can also originate from LacCer, independently from GM3 formation.

In the Golgi, an association has been observed amongst three enzymes involved in the biosynthesis of simple gangliosides, namely GalT1, ST1 and ST2. In addition, two enzymes that direct the biosynthesis of more complex gangliosides, namely GalNAcT and GalT2 associate through their N-terminal domains.

There is substantial evidence for a gradient distribution in the Golgi apparatus of the different glycosyltransferases involved in the ganglioside biosynthesis pathway, with earlier glycosylations prevailing in the cis- and medial-Golgi, and later glycosylations in the trans-Golgi and the TGN. The use of pharmacological agents that block intra-Golgi transport such as BFA has shed light on the localization of these enzymes. BFA treatment induces the TGN and trans-most Golgi cisternae to condense in a post-BFA compartment, while the proximal Golgi fuses with ER membranes. Studies with BFA indicated that the synthesis of LacCer and the simple gangliosides GM3, GD3, and GT3 occurs on the proximal site of the Golgi apparatus, probably in the cis-Golgi compartment. In contrast, synthesis of the complex gangliosides GM2, GM1 and GD1a is carried out in distal Golgi compartements (van Echten et al., 1990; Young et al., 1990). Further biochemical and immunocytochemical studies confirmed these findings, although they pointed out that the enzymes generating LacCer and the simple gangliosides GM3 and GD3 were not only present in proximal Golgi compartments, but their presence could spread along distal Golgi compartments (Allende et al., 2000; Maxzud et al., 1995).

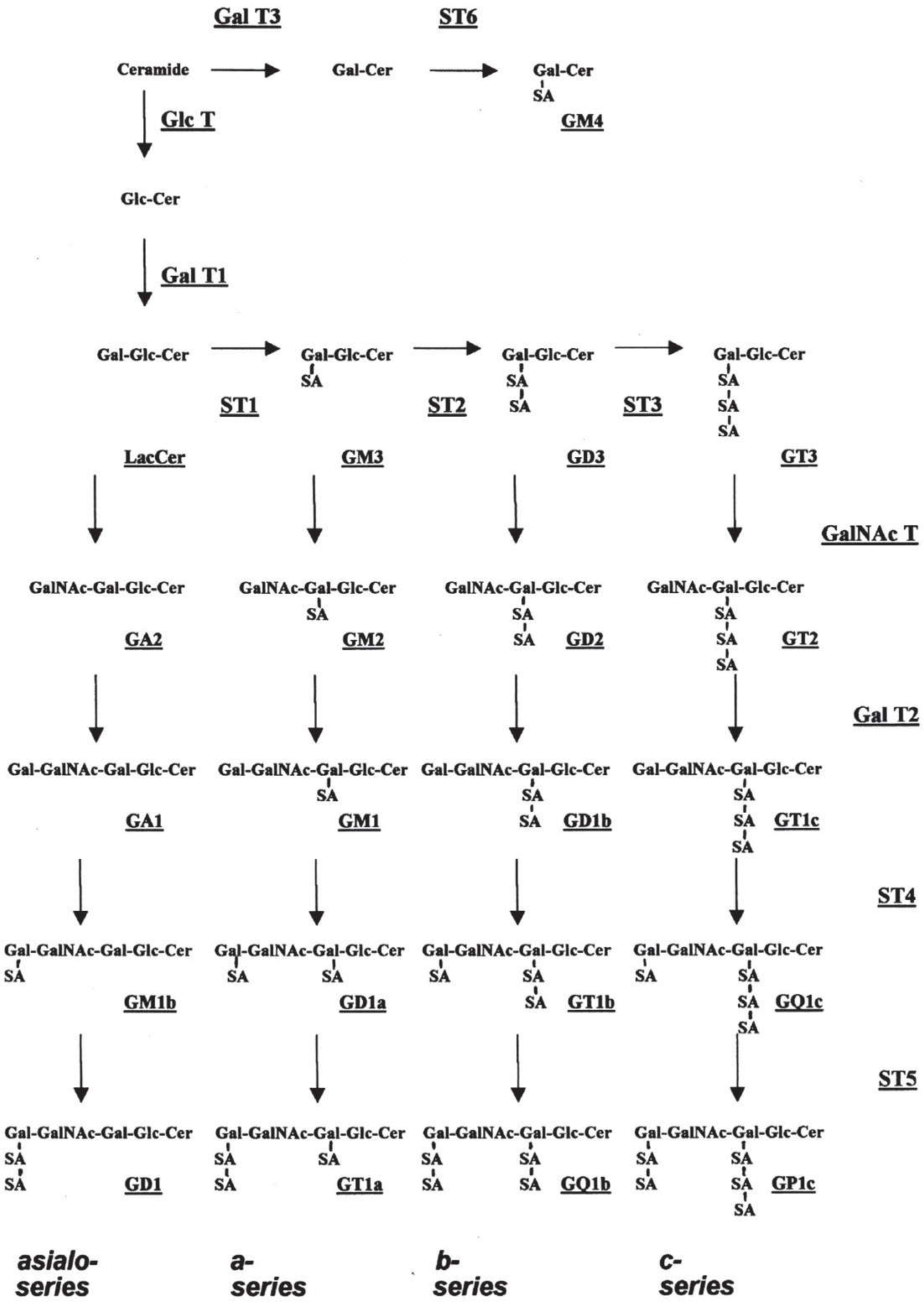

Figure 25: Ganglioside biosynthesis. *From Yu et al., 2004.*

8.2.2. Ganglioside transport and sorting

The main transport mechanism of GSLs is by vesicular transport along the exocytic and endocytic pathways. Matured GSLs synthesized de novo in the Golgi are transported to the cell surface along the exocytic pathway, where they become components of the plasma membrane. Inversely, they can be internalized from the cell surface by endocytosis. Following endocytosis, GSLs can follow different pathways. They can be directed to the late endosomal/lysosomal compartment, where they are degraded. They can transit through the Golgi where they are re-glycosylated before being delivered back to the plasma membrane. Alternatively, endocytosis can be followed by a direct return of unmodified GSLs to the plasma membrane (direct recycling), where they can undergo glycosylation or de-glycosylation by plasma membrane-bound enzymes. These processes of re-synthesis and remodeling maintain a dynamic composition of cell surface GSLs.

The mechanism for GSLs trafficking and sorting is based on their incorporation into lipid rafts formed at the Golgi, plasma membrane and endosomes (Degroote et al., 2004). As seen in paragraph 6.3.3, lipid rafts formed at the Golgi also sequester apical membrane proteins.

Lipid rafts undergo a tendency to bud into vesicles, facilitating their transport and they can incorporate proteins driving transport specificity. For instance, they can incorporate SNARE molecules, resulting in docking and fusion of exocytic vesicles to the plasma membrane. Sorting of GSLs internalized by endocytosis can be regulated at the plasma membrane and in early endosomes through caveolin and, as described in paragraph 3.3 some Rab proteins (Choudhury et al., 2002; Sharma et al., 2003).

8.2.3. Ganglioside degradation

GSLs incorporated into the limiting membrane of lysosomes are not degraded, because of the protection offered by LAMP and LIMP proteins from the attack by degrading enzymes. A distinct pool of membranes has to be present in the lysosomal compartment, which is accessible to degrading enzymes. Parts of the plasma membrane internalized by endocytosis reach the lysosome as small intra-lysosomal vesicles, acting as platforms for GSLs degradation.

The lipid composition of intra-lysosomal vesicles differs from that of the plasma membrane (Schulze et al., 2009). Cholesterol content is decreased in the internal membranes of the lysosome, whereas the concentration of ceramide and of the negatively charged lipid BMP [bis-(monoacylglycero)phosphate] is increased. In fact, cholesterol, which cannot be degraded in the lysosome, is transported out of inner lysosomal membranes by the NPC1/NPC2 system. This unique lipid composition is required for degradation of intra-lysosomal vesicles. Membranes poor in cholesterol and rich in ceramid are less rigid, which facilitates their degradation, whereas BMP acts as an activator of sphingolipid degradation.

GSLs degradation is also helped by the presence of lipid-binding proteins such as sphingolipid activator proteins (comprising the GM2 activator protein or saposins). Their role is to mediate the interaction between the membrane-bound lipid substrate and the water-soluble enzyme, or activate the enzyme directly.

Within the lysosome, ganglioside catabolism occurs by the stepwise action of specific sialidases and exoglycohydrolases, starting from the non-reducing terminal unit (Figure 26). The sequence of sugar removal from gangliosides is as follows (Tettamanti, 2004). Initially, a lysosomal sialidase 1 (also called neuraminidase 1) converts multi-sialogangliosides into mono-sialogangliosides GM1, GM2 or LacCer. From GM1, galactose is then removed to produce GM2, and from GM2 the *N*-acetyl-galactosamine residue is cleaved to form GM3, by the action of beta-galactosidase and beta-*N*-acetyl-hexosaminidase, respectively. In some cell types, sialic acid residues are effectively removed from GM1 and GM2 by a specific sialidase 2 (or neuraminidase 2) producing the corresponding derivatives of the asialo-series GA1 and GA2, which, through the sequential actions of beta-galactosidase and beta-*N*-acetyl-hexosaminidase, are converted to LacCer. LacCer is then degraded to ceramide by the action of beta-galactosidase and beta-glucosidase, respectively.

Some of the fragments resulting from lysosomal degradation (individual monosaccharides, long chain bases, fatty acids as well as intermediate by-products) can leave the lysosome and enter the cytosol where they are re-utilized in the salvage pathway. The salvage pathway represents a relevant event in ganglioside biosynthesis and turnover.

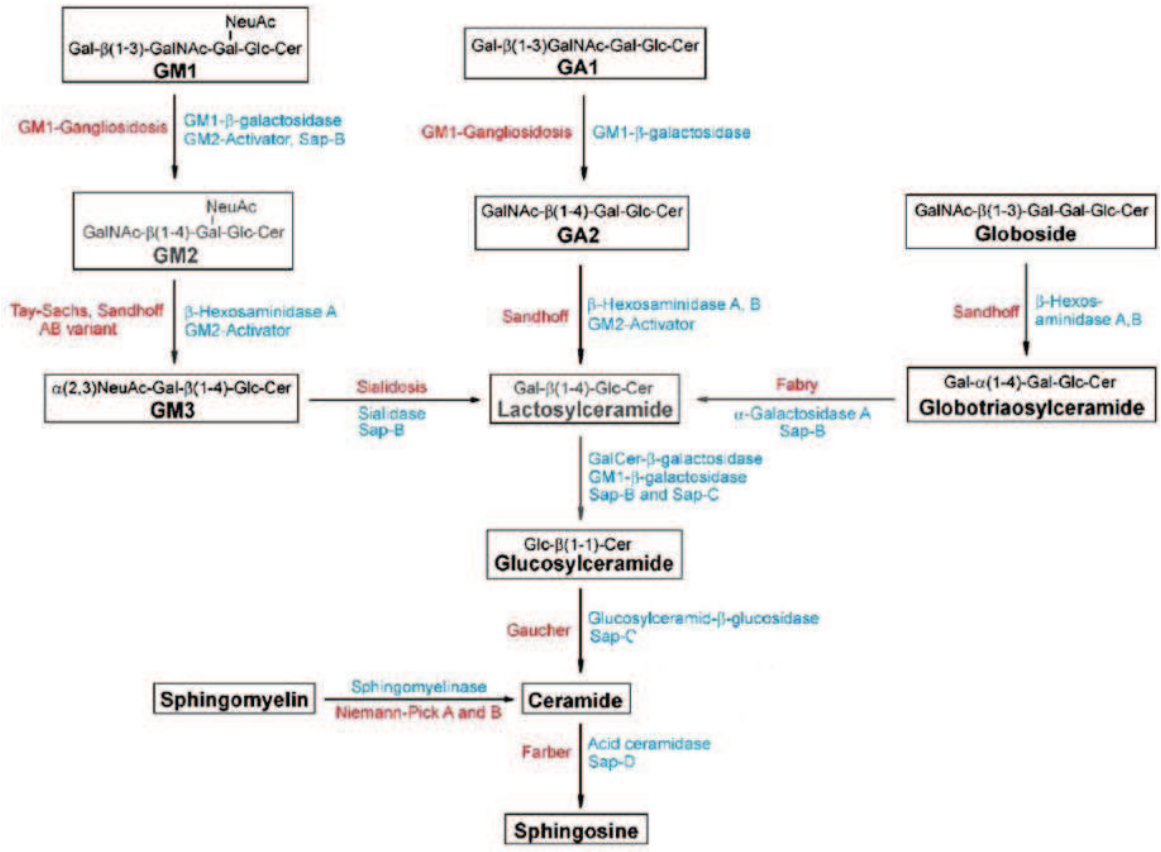

Figure 26: Stepwise degradation of GSLs in the lysosome. Enzymes and activator proteins involved (in blue), and enzyme-related diseases (in red) are indicated. Sap: saposin. *Adapted from Schulze et al., 2009.*

8.2.4. The roles of gangliosides

As mentioned in paragraph 3.2, membrane lipid rafts containing GSLs are specialized membrane platforms capable of transducing signaling events. At the plasma membrane, the hydrophobic ceramide moiety of GSLs acts as a membrane anchor, whereas the oligosaccharide chains are exposed toward the cell surface. GSL clusters at the cell surface can interact with pathogens, as well as with membrane-bound receptors and enzymes. These interactions control cell-pathogen interaction, cell-cell interaction and cell-matrix interaction. They can trigger intracellular signaling cascades, resulting in entry of the pathogen in the cell, adhesion, growth, motility, differentiation, migration or apoptosis. Furthermore, available evidence indicates that GSLs have functional roles essential during embryogenesis and brain development.

Whereas GSLs are ubiquitous components of the plasma membrane of all cells, the ganglioside subtype is particularly abundant in the brain and nervous tissues, where they constitute the major components of neuronal plasma membranes.

The major signaling system modulated by gangliosides present at membrane microdomains is the growth factor signaling by receptor tyrosine kinases. The ganglioside GM3 was initially found to down-regulate FGFR activation in response to FGF stimulation in fibroblast cells and in glial cells, resulting in defective cell proliferation or cell migration (Bremer and Hakomori, 1982; Meuillet et al., 1996). This concept was extended to the inhibitory effects of GM3 on EGFR. GM3 has been shown to directly interact with *N*-linked sugars on the extracellular domain of EGFR to inhibit its receptor tyrosine kinase activity (Kawashima et al., 2009; Miljan et al., 2002). In neuroblastoma cell lines, GM3 inhibited neurite outgrowth induced by platelet-derived growth factor receptors (PDGF) or insulin (Hynds et al., 1997).

The effect of gangliosides on cell proliferation and motility does not only rely on modulation of growth factor signaling. Gangliosides are also capable of modulating the function of various integrins, thereby influencing cell adhesion to the ECM. In fact, there is increasing evidence for a functional interaction ("cross-talk") of integrins with growth factor receptors. EGFR or FGFR can be activated by both direct ligand binding, but also by cross-talk with integrins. Such effect of cross-talk between integrins and EGFR or FGFR has been shown to be strongly influenced by GM3 within ganglioside-enriched microdomains (Toledo et al., 2005; Wang et al., 2003a).

Finally, the biological activity of cytokines has also been shown to be regulated by gangliosides, which can bind directly to cytokines such as interferon (IFN) or interleukins (ILs) (Besancon and Ankel, 1974; Chu and Sharom, 1990).

8.2.5. Ganglioside accumulation in MPS

The mechanism leading to ganglioside accumulation in MPS is largely unkown. Some hypotheses have been drawn, but evidence to support these hypotheses remains to be established. A first model is based on the observation that accumulating GAGs can inhibit the activity of a variety of lysosomal enzymes, some of which are required for ganglioside degradation (Avila and Convit, 1975; Kint et al., 1973). For instance, neuraminidase activity toward GM3 ganglioside is diminished in fibroblasts derived

from MPS patients, possibly due to GAG accumulation (Baumkotter and Cantz, 1983). However, it is not the sole explanation, as GM2 and GM3 gangliosides are also elevated in numerous other LSDs in which GAGs do not accumulate. Even more perplexing is the observation that GM2 and GM3 gangliosides are largely localized to separate populations of vesicles in several LSDs, suggesting that independent, or at least physically separate, mechanisms are responsible for their sequestration, as explained in paragraph 3.2. Other models based on more complex perturbations in GSL trafficking and/or homeostatic control mechanisms have been proposed. In addition to gangliosides, unesterified cholesterol also accumulates in MPSIII (McGlynn et al., 2004). This observation is consistent with data obtained in GSL storage disorders showing that GSL and cholesterol accumulation are inter-related (see 3.2). In this latter group of diseases, it has been shown that GSL and cholesterol-enriched membrane rafts were abnormally sequestered within late endosomes and lysosomes, due to sorting and transport defects (see 3.3). The same phenomenon might occur in MPS even though GSL storage is a secondary event. As regional correlation is common between the storage of GM3 and cholesterol in brains of mice with MPSIII diseases (McGlynn et al., 2004), it can be assumed that these two storage products sequester together in the late endosomal-lysosomal system and are the products of defective degradation. GM3 sequestration in the degradative compartment may result in a block in retrograde transport of simple GSL breakdown products from lysosomes to the Golgi, impacting the GSL synthetic pathway. Intense GM2 staining was often localized in vesicular compartments exhibiting neither GM3 nor filipin staining. Absence of co-localization between GM2 and GM3 implies that stored GM2 gangliosides are excluded from the degradative compartment, based on the assumption that all degradative enzymes required for the degradation of GSLs are spatially located within the same endosomal-lysosomal compartments. Elevated expression of GM2 gangliosides may therefore be derived of altered biosynthesis and transport from the Golgi rather than sequestration within the endosomal-lysosomal system. This model would explain how such distinct separate compartmentalization between GM3 and cholesterol on the one hand, and GM2 on the other hand, is achieved.

OBJECTIVES

OBJECTIVES

The MPSs represent a devastating group of LSDs. Advances in biochemistry and genetics over the past three decades have resulted in the identification of the key enzymes underlying these diseases, with subsequent isolation and characterization of the genes involved. Ultimately, these advances have led to the recent development of treatment strategies for some of the MPSs based on direct enzyme replacement. One of the major hurdles to be overcome for MPS subtypes with neurological consequences such as MPSIIIB is to target treatments based on enzyme delivery to the brain. This can possibly be achieved by gene replacement strategies, consisting in providing a functional copy of the defective gene product in the brain of affected patients. Clinical trials will evaluate such strategies in the near future. Experience gained by the development and evaluation of these treatments will be instructive for other rare genetic disorders, and for other neurodegenerative diseases. Although important benefits are expected, it is hard to predict the outcome regarding the correction of the brain plasticity, considering the complex molecular and cellular perturbations that underlie the MPS phenotypes. Coming to a better understanding of the pathophysiology of the MPSs has therefore become a necessity. Confrontation of basic knowledge of disease mechanisms with results of therapeutic gene therapy trials will give a unique opportunity for comprehensive understanding of the disease and definition of the best conditions for treatment. In particular, it will impact on decisions concerning patient eligibility criteria (age, clinical severity) and clinical trial endpoints (behaviour versus biological markers). In addition, pathophysiological studies may allow the identification of new potential targets for therapeutic intervention.

In MPSIIIB, studies of mechanisms acting in the human CNS have been limited to post-mortem biopsies, only providing indications about the final stage of the disease. Investigations have been facilitated by the creation of a murine model of MPSIIIB, which is available since 1999. Despite the existence of this model, the relationship between abnormal storage of partially degraded HS and neuronal dysfunction is still unclear. Primary MPSIIIB mouse neuron cultures are cumbersome to obtain and they present technical limitations. They offer limited susceptibility to DNA or siRNA transfection and they cannot be expanded to large amounts for biochemistry. In

addition, cells grown in these conditions are chronically deficient, and presumably upregulate compensatory mechanisms to survive. Therefore, their study not only reveals direct specific toxic effects of HSO accumulation, but also compensatory phenomena.

The objective of my PhD project was to decipher links between HSO accumulation, Golgi disorganization and GM130 dysfunction, which were previously observed in MPSIIIB primary mouse neurons. A goal was to describe how these perturbations account for cellular defects that are relevant to MPSIIIB pathophysiology. This work was facilitated by the creation of two original human cell models for MPSIIIB. First, a cell system was generated using the iPSc technology. Human skin fibroblasts of children with MPSIIIB were re-programmed into iPSc, and subsequentially differentiated to NSCs and neurons. Patient-specific iPSc were recently generated from patient fibroblasts to model human neurological diseases, including Parkinson disease, Huntington disease, Down Syndrome, or Amyotrophic Lateral Sclerosis (Dimos et al., 2008; Park et al., 2008a). The development of iPSc technology offers unique opportunities to study pathogenesis as it pertains to human neurons.

Second, we created a useful tool for biochemistry and cell biology investigations derived from the HeLa cell line. NAGLU, the deficient enzyme in MPSIIIB was specifically depleted in this immortalized cell line in an inducible manner. Acutely depleted HeLa cells represent a unique model to investigate pathological events induced by HSO toxicity at early time-point after enzyme depletion. They present many advantages, being well-suited for imaging, easily manipulable and having indefinite proliferation capacities. Such HeLa cell models have proven useful in studying the pathogenesis of mucolipidosis type IV (Miedel et al., 2008).

MATERIALS AND METHODS

MATERIALS AND METHODS

1. GENERATION OF IPSc FROM MPSIIIB HUMAN FIBROBLASTS

The establishment of a MPSIIIB disease model through patient-specific reprogramming involves two steps: first, generation of human iPSc from fibroblasts of MPSIIIB children, and second differentiation of the iPSc into neural progenitors and neurons (Figure 27).

To generate iPSc, the reprogramming transcription factors Oct4, Klf4, Sox2 [and in some cases c-Myc, which is dispensable for reprogramming (Nakagawa et al., 2008)] were expressed in patient fibroblasts by using gene transfer with retrovirus vectors (Park et al., 2008b). These factors are involved in self-renewal and pluripotency maintenance.

Once generated, iPSc clones were identified based upon morphological criteria, and submitted to different analyses aimed at verifying pluripotency. Expression of different pluripotency markers such as cytoplasmic alkaline phosphatase, stage-specific embryonic antigen (SSEA), tumor recognition antigen (TRA), or the endogenous nuclear transcription factors Oct4, Sox2, or Nanog was assayed by immunofluorescence or reverse transcription (RT)-PCR.

During iPSc generation, retroviruses integrate into the host genome, and are subsequently silenced after the induction of the pluripotent state and expression of the endogenous pluripotency genes. Persistence of transgene expression may render iPSc refractory to differentiation both in vitro and in vivo, and may lead to tumor formation following in vivo transplantation (Markoulaki et al., 2009; Takahashi and Yamanaka, 2006). Extinction of exogenously introduced Oct4, Klf4, Sox2 (and c-Myc) transgenes was verified by quantitative RT-PCR, using specific primers distinguishing them from endogenous genes.

Conversion of a differentiated state to a pluripotent state is accompanied by epigenetic changes comprising DNA methylation state and chromatin organization (Sridharan et al., 2009; Takahashi et al., 2007a). For instance, the transcription factor Oct4 is silenced through methylation in somatic cells, and demethylated upon reprogramming in iPSc. To determine the degree of reprogramming in iPSc clones, the degree of methylation of the Oct4 promoter was measured.

Continuous passaging of human iPSc can result in chromosomal abnormalities (Aasen et al., 2008). Genomic integrity was monitored by karyotype analysis.

The functional differentiation potential of isolated and propagated iPSc clones was further assessed both in vivo and in vitro. First, immunodeficient mice injected subcutaneously with iPSc formed teratoma six weeks post-injection. Histological examination was performed to determine whether teratoma comprised tissues representative of all three embryonic germ layers (ectoderm, mesoderm and endoderm) (Nakagawa et al., 2008; Park et al., 2008c; Takahashi et al., 2007b; Takahashi and Yamanaka, 2006). Second, the potential of iPSc to form embryoid bodies (EB) was assessed in vitro. To promote EB formation, iPSc were detached, transferred to suspension conditions and aggregated into clusters. The capacity of EBs to differentiate into the three germ layers was assessed following cell adhesion.

Once characterized and validated the iPSc cell lines were differentiated into a neuronal lineage. To promote neural differentiation and inhibit other germ layers, iPSc colonies were transferred to a neural medium supplemented with growth factors (FGF and EGF) and attachment was prevented, giving rise to proliferating neurospheres. Neurospheres were then dissociated and allowed to adhere to induce neural differentiation, resulting in neural progenitors and their differentiated mature neuronal progeny (Ebert et al., 2009).

To study MPSIIIB pathogenesis, phenotypes were characterized on iPSc, on neurospheres, and on neural progenitors and neurons derived from differentiation protocols.

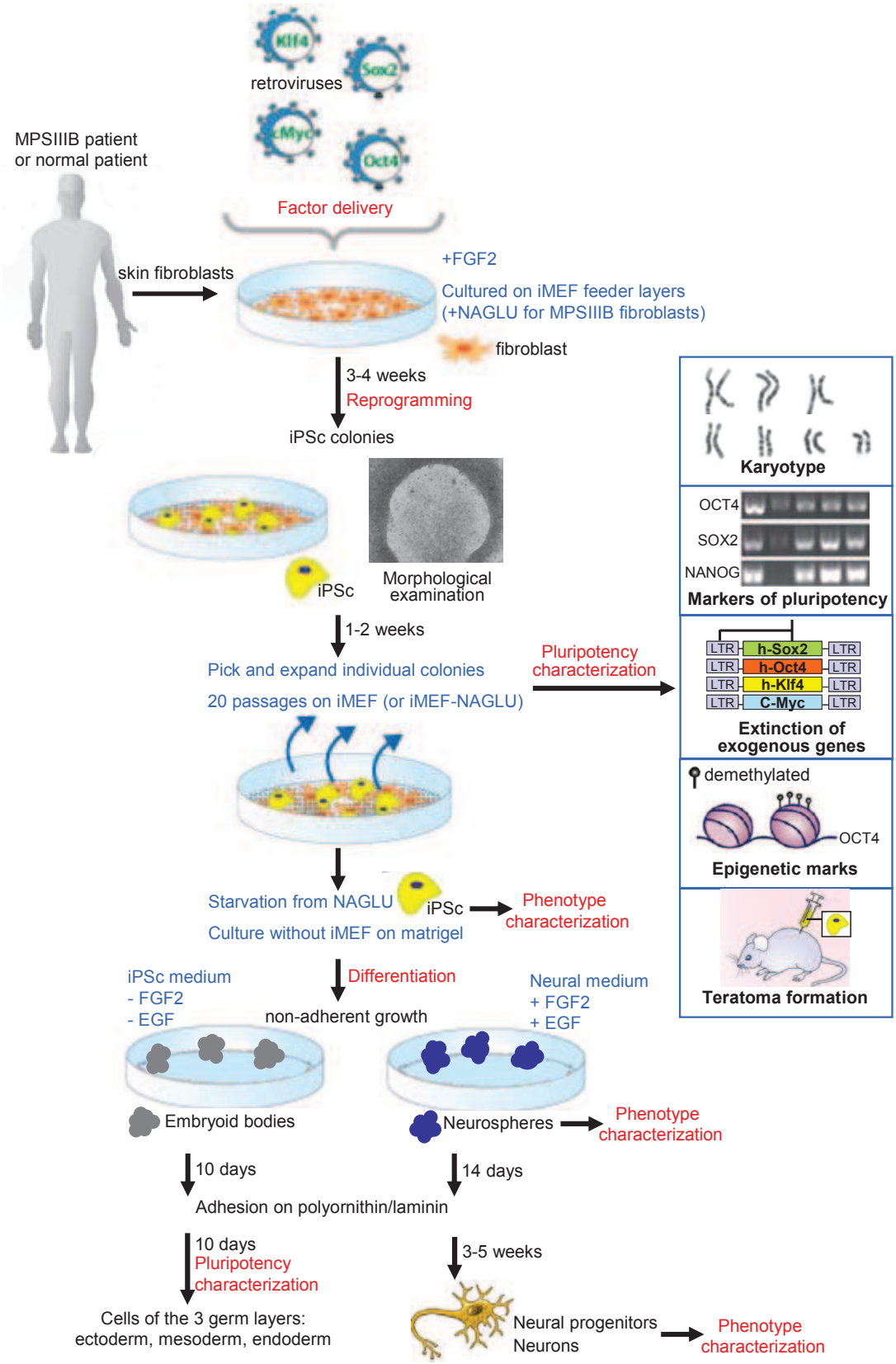

Figure 27: Generation and characterization of iPSc. iMEF: irradiated mouse embryonic fibroblasts.

2. GENERATION OF AN IMMORTALIZED CELL LINE MODEL

An immortalized HeLa cell line model was created, in which a specific small shRNA directed against NAGLU can be expressed in an inducible manner. A system based on regulatory elements from the tetracycline resistance operon of the *Escherichia coli* transposon Tn10 was used (Gossen and Bujard, 1992). Two different plasmids were introduced in HeLa cells (Figure 28). The first plasmid provides constitutive expression of a tetracycline repressor under control of the CMV promoter. The second plasmid encodes the NAGLU shRNA controlled by an inducible promoter comprising a human H1 promoter into which two copies of a tetracycline operator sequence ($TetO_2$) have been incorporated. In the absence of tetracycline, the tetracycline repressor forms a homodimer that binds with high affinity to each $TetO_2$ sequence and represses transcription of the NAGLU shRNA. The presence of tetracycline positively regulates the expression of the NAGLU shRNA. Tetracycline binds with high affinity to the tetracycline repressor homodimers, causing a conformational change in the repressor that triggers its dissociation from the operator, and allows induction of transcription of the NAGLU shRNA.

This system uses the native *Escherichia coli* repressor protein molecules, and is therefore different from the more commonly used Tet-On or Tet-Off systems which use a hybrid protein consisting of the tetracycline repressor fused to a transactivation domain.

Two different shRNAs were selected, based on preliminary tests aimed at assessing the efficacy of five different small interference RNAs (siRNAs) to inducing NAGLU depletion. Different cell clones expressing either of these two shRNAs were isolated. Phenotypic examination of tetracycline-induced, NAGLU-depleted cells was performed, compared to control cells of two kinds: non-depleted cells not treated with tetracycline from the same cell clones, and cell clones treated with tetracycline expressing a scrambled sequence corresponding to the selected shRNA sequences.

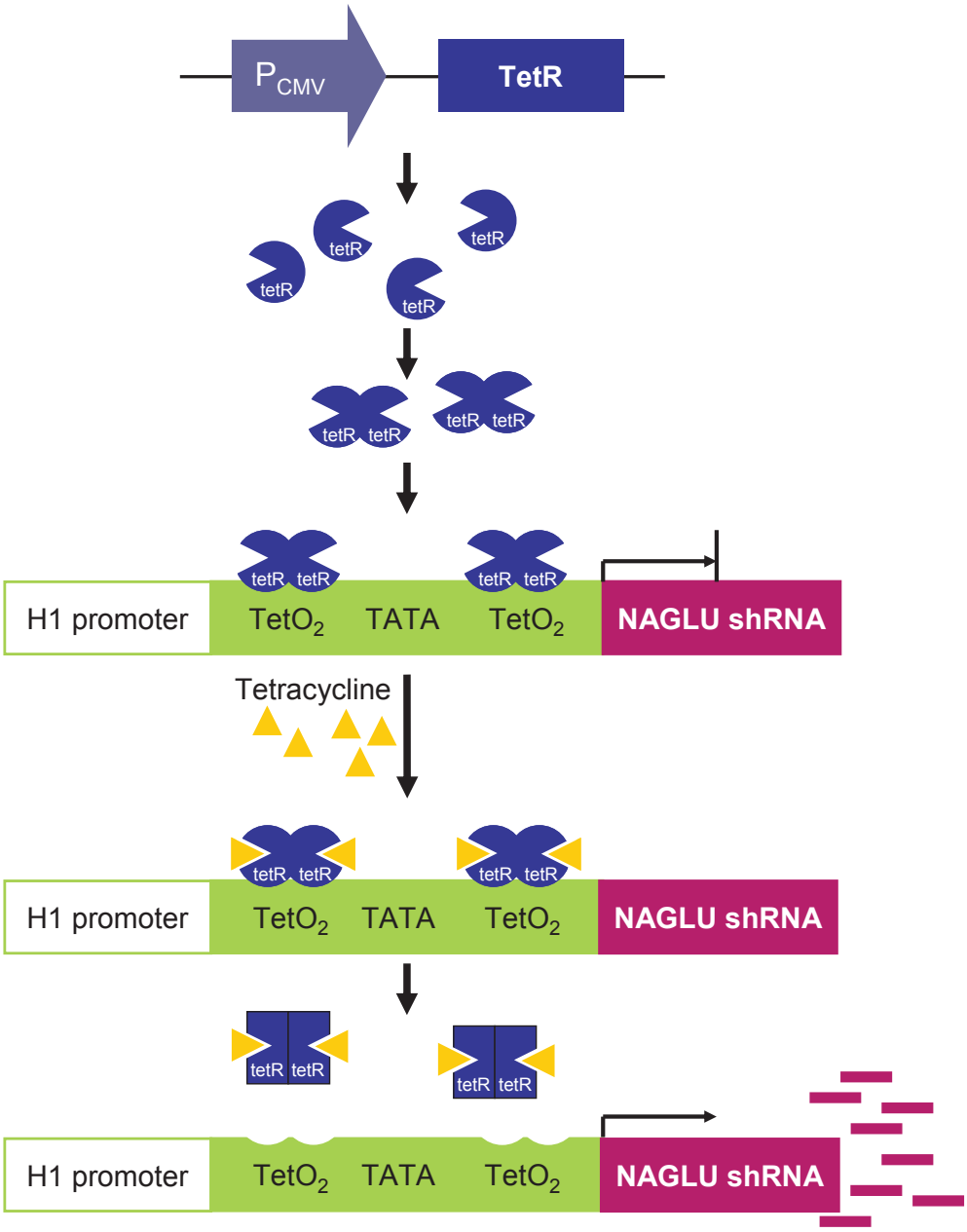

Figure 28: Mechanism of tetracycline-regulated expression of NAGLU shRNA.
TetR: tetracycline repressor. $TetO_2$: tetracycline operator.

RESULTS

RESULTS

ARTICLE 1

Modeling neuronal defects associated with a lysosomal disorder using patient-derived induced pluripotent stem cells

Human Molecular Genetics (2011) 20(18):3653-66

HMG Advance Access published June 30, 2011

Human Molecular Genetics, 2011 **1–14**
doi:10.1093/hmg/ddr285

Modeling neuronal defects associated with a lysosomal disorder using patient-derived induced pluripotent stem cells

Thomas Lemonnier[1,2], Stéphane Blanchard[1,2], Diana Toli[1,2], Elise Roy[1,2], Stéphanie Bigou[1,2], Roseline Froissart[3,4], Isabelle Rouvet[5], Sandrine Vitry[1,2], Jean Michel Heard[1,2] and Delphine Bohl[1,2,*]

[1]Institut Pasteur, Unité Rétrovirus et Transfert Génétique, 28 rue du Dr Roux, F-75015 Paris, France, [2]INSERM U622, F-75015 Paris, France, [3]Laboratoire des Maladies Héréditaires du Métabolisme, Centre de Biologie Est, Hospices Civils de Lyon, F-69677 Bron, France, [4]INSERM U820, Université Claude Bernard, F-69008 Lyon, France and [5]Centre de Biologie Cellulaire, GHE, Hospices Civils de Lyon, 59 Bd Pinel, 69500 Bron, France

Received April 22, 2011; Revised and Accepted June 14, 2011

By providing access to affected neurons, human induced pluripotent stem cells (iPSc) offer a unique opportunity to model human neurodegenerative diseases. We generated human iPSc from the skin fibroblasts of children with mucopolysaccharidosis type IIIB. In this fatal lysosomal storage disease, defective α-*N*-acetylglucosaminidase interrupts the degradation of heparan sulfate (HS) proteoglycans and induces cell disorders predominating in the central nervous system, causing relentless progression toward severe mental retardation. Partially digested proteoglycans, which affect fibroblast growth factor signaling, accumulated in patient cells. They impaired isolation of emerging iPSc unless exogenous supply of the missing enzyme cleared storage and restored cell proliferation. After several passages, patient iPSc starved of an exogenous enzyme continued to proliferate in the presence of fibroblast growth factor despite HS accumulation. Survival and neural differentiation of patient iPSc were comparable with unaffected controls. Whereas cell pathology was modest in floating neurosphere cultures, undifferentiated patient iPSc and their neuronal progeny expressed cell disorders consisting of storage vesicles and severe disorganization of Golgi ribbons associated with modified expression of the Golgi matrix protein GM130. Gene expression profiling in neural stem cells pointed to alterations of extracellular matrix constituents and cell–matrix interactions, whereas genes associated with lysosome or Golgi apparatus functions were downregulated. Taken together, these results suggest defective responses of patient undifferentiated stem cells and neurons to environmental cues, which possibly affect Golgi organization, cell migration and neuritogenesis. This could have potential consequences on post-natal neurological development, once HS proteoglycan accumulation becomes prominent in the affected child brain.

INTRODUCTION

Although neurodegenerative disorders are mostly prevalent in the elderly, they also occur early in life. In infants and children, inborn errors of metabolism, in particular lysosomal storage diseases (LSDs), represent the most frequent cause of neurodegeneration. LSDs result from inefficient recycling of macromolecule catabolites, which accumulate and cause a multitude of clinical symptoms, including progressive mental retardation.

Whereas primary genetic and biochemical disorders are well described in LSDs, the limitations of currently available study models hampered accurate exploration of downstream cascades of events. Investigations in mouse models or in

*To whom correspondence should be addressed at: Unité Rétrovirus et Transfert Génétique, INSERM U622, Département de Neuroscience, Institut Pasteur, 28 rue du Dr Roux, 75015 Paris, France. Tel: +33 145688412; Fax: +33 145688940; Email: delphine.bohl@pasteur.fr

patient cell cultures identified disorders consistent with cell autonomous dysfunctions. They affect endocytosis (1,2), macro-autophagy (3), calcium homeostasis (4,5), mitochondria (6), endoplasmic reticulum homeostasis (7,8), phospholipid synthesis (9,10), neurite outgrowth (5,11) and neural stem cell production, migration and differentiation (12). In the central nervous system (CNS), neural cell disorders are associated with neuroinflammation, which presumably aggravates neurodegeneration (13). However, the relevance of cell disorders to the neurological manifestations observed in children remains unclear.

Mucopolysaccharidosis IIIB (MPSIIIB, Sanfilippo syndrome type B) is an LSD caused by α-*N*-acetylglucosaminidase (NAGLU, EC 3.2.1.50) deficiency, a lysosomal hydrolase involved in heparan sulfate (HS) proteoglycan degradation. Severe neurological manifestations contrast with mild expression of the disease in peripheral organs. The onset of behavioral changes is at 3–5 years of age, followed by progressive mental retardation and premature death (14). Patient autopsy revealed storage lesions in the CNS, macrophages, liver and kidney epithelial cells, but not in other tissues (15–17). Similar pathology was observed in the mouse model of the disease (18,19). Predominance of pathology in the CNS emphasizes the importance of analyzing neural cells and neurons to elucidate pathophysiology. Intracellular vacuoles with characteristics of lysosomes in brain cells is the pathological hallmark of the disease. Studying these lesions in cortical neurons of the MPSIIIB mouse, we showed that they were associated with Golgi complex alterations and modified expression of the Golgi matrix protein GM130 (20), a tethering protein important for Golgi structure and dynamics (21). We did not observe disorders of endocytosis or macro-autophagy in these cells.

The re-programmation of human skin fibroblasts into induced pluripotent stem cells (iPSc) and their subsequent differentiation in neural progenitors and neurons provide access to human neurons, the cell type most relevant to clinical expression of MPSIIIB in children. Reprogramming of MPSIIIB patient fibroblasts was efficient. However, the proliferation of emerging iPSc was impaired unless the enzyme defect was complemented by an exogenous enzyme. Patient undifferentiated iPSc and neurons expressed cell disorders, which were not observed in parental skin fibroblasts and in floating neurospheres. These defects may affect neurological development in young children.

RESULTS

Complementation of enzymatic defect allows isolation of patient iPSc

Skin fibroblast primary cultures were established from two MPSIIIB patients for diagnosis purpose. Patient 1 was homozygous for a previously undescribed splice donor mutation in the *NAGLU* gene (c.531+1G>C). Patient 2 was homozygous for p.R482W mutation in exon 6 (22). NAGLU activity was below the detection threshold in cultured fibroblast extracts (0.04 ± 0.01 and 0.03 ± 0.02 μkat/kg, respectively, versus 1.23 ± 0.02 μkat/kg in controls).

Cultured fibroblasts were exposed to retroviral vectors encoding OCT4, SOX2, KLF4 (control and patient 2), or to these three vectors combined with a vector coding for c-MYC (control and patient 1). After exposure, fibroblasts were grown on a feeder layer of irradiated mouse embryonic fibroblasts (iMEF) in the presence of basic fibroblast growth factor (FGF2, 10 ng/ml). Emerging iPSc-like clones positive for alkaline phosphatase (AP) were visible after 3–4 weeks. Equivalent clone numbers were scored in control and MPSIIIB fibroblasts (~0.1% of plated fibroblasts with the four vectors, ~0.01% without c-MYC vector).

Control iPSc-like clones rapidly expanded (cloning efficiency 87.5%, $n = 24$). In contrast, patient iPSc-like clones poorly proliferated and were inefficiently cloned (cloning efficiency 2.5%, $n = 120$; Supplementary Material, Fig. S1). Since FGFs act in concert with HS proteoglycans to activate FGF receptors (23) and partially digested HS accumulates in MPSIIIB cells, we assumed that impaired proliferation of emerging patient iPSc resulted from altered FGF2 signaling caused by HS. We therefore isolated patient iPSc-like clones in the presence of exogenous NAGLU to clear HS (24). For that purpose, genetically engineered iMEF (NAGLU-iMEF) releasing NAGLU enzyme in culture supernatant were isolated. When grown on this feeder, patient iPSc-like clones rapidly expanded and were as efficiently cloned as control iPSc (cloning efficiency 83.3%, $n = 12$; Supplementary Material, Fig. S1).

Characterization of iPSc clones

iPSc clones from control (C1, C2, C3), patient 1 (P1.1, P1.2, P1.3) and patient 2 (P2.1, P2.2, P2.3) were propagated for at least 20 passages on iMEF (control), or NAGLU-iMEF (patients). They showed normal karyotypes at passages 15–20 (data not shown). Mutations in the *NAGLU* gene were retrieved in patient clones. Cells expressed markers of pluripotency (SSEA4, TRA1-60, NANOG, Fig. 1A). Quantitative PCR with reverse transcription (qRT-PCR) indicated efficient repression of exogenously introduced genes (Fig. 1B). Endogenous pluripotency-associated genes were re-activated (Fig. 1C). Whereas the OCT4 promoter was heavily methylated in parent fibroblasts, it was demethylated in iPSc clones, consistent with epigenetic reprogramming to pluripotency (Fig. 1D). Six weeks after transplantation in immunodeficient mice, all control or patient iPSc formed teratoma. Histological examination revealed tissues from the three embryonic germ layers (Fig. 1E). Thus, all control and patient iPSc clones were defined as human pluripotent iPSc.

Storage lesions are prominent in undifferentiated patient iPSc clones

Since exogenous NAGLU prevents expression of disease-related features, patient 1 and patient 2 iPSc clones were starved from the NAGLU enzyme after 15–20 passages. After transfer of patient iPSc clones to Matrigel^{TM}-coated wells in the presence of FGF2 (100 ng/ml) for 10 days, NAGLU catalytic activity was undetectable and cells were intensely stained with anti-HS antibodies (Fig. 2A).

Patient 1 and patient 2 undifferentiated iPSc clones accumulated vacuoles positive for the lysosome-associated membrane

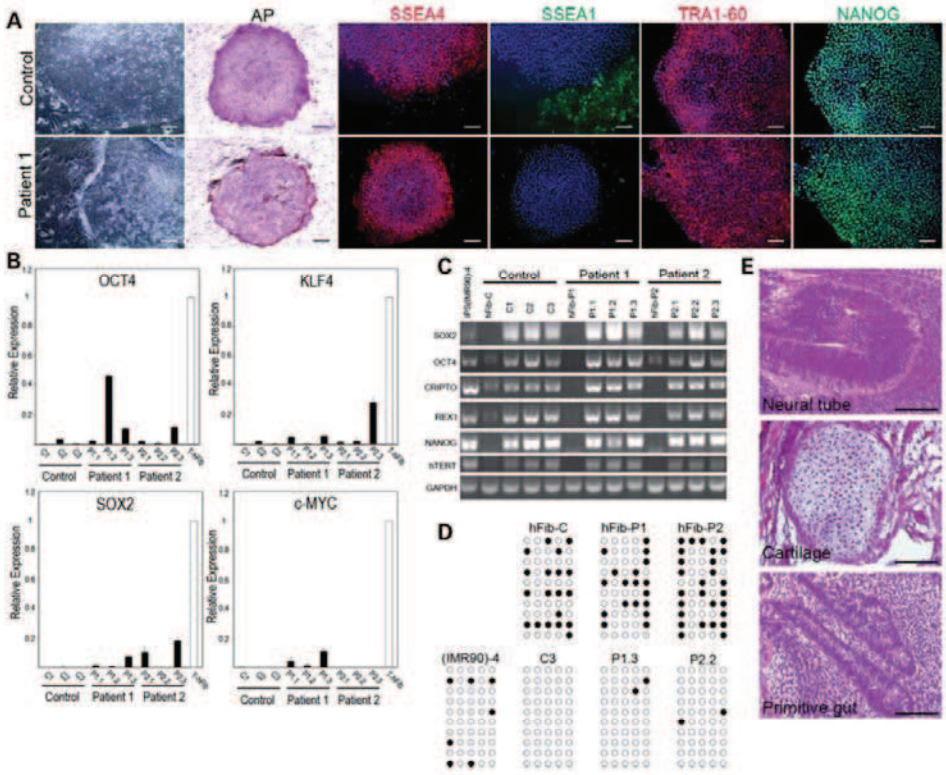

Figure 1. All control and patient iPSc clones exhibit human embryonic stem cell characteristics. (**A**) Representative images of iPSc clones emerging from control and patient fibroblasts growing on iMEF or NAGLU-iMEF feeder cells, respectively, are shown. Phase contrast views, AP staining, immunostaining for the pluripotency markers SSEA4, TRA-1-60 and NANOG and absence of staining for the differentiation factor SSEA1 are shown. Scale bars: 100 μm, except AP: 300 μm. (**B**) qRT-PCR shows that retroviral vector genomes coding for OCT4, KLF4, SOX2 and c-MYC mRNAs were silenced in iPSc clones (black bars), compared with parent human fibroblasts exposed to these vectors (T-hFib, white columns, value set to 1). Low persistent expression was detected in some clones, as reported by others (60). (**C**) RT-PCR shows that iPSc clones but not parent fibroblasts (hFib-C, hFib-P1, hFib-P2) expressed mRNAs coding for endogenous genes related to pluripotency. The iPS(IMR90)-4 cell clone was taken as a reference (56). GAPDH (glyceraldehyde-3-phosphate dehydrogenase) was an internal control for mRNA detection. (**D**) Bisulfite sequencing was used to detect methylation on cloned PCR products from DNA of iPSc clones (C3, P1.3, P2.2), parent fibroblasts (hFib-C, hFib-P1, hFib-P2) or the reference iPS(IMR90)-4 clone. Circles correspond to five methylation sites (columns) on the OCT4 gene promoter sequence (open, unmethylated; filled, methylated) (61). Ten PCR products (rows) from each cell line were analyzed. (**E**) All control and patient iPSc clones injected in Rag $\gamma C^{-/-}$ mouse skeletal muscle formed teratomas. Pictures show representative images of structures identified after 6 weeks including neural tissues (ectoderm), gut-like epithelial tissues (endoderm) and bone and cartilage (ectoderm). Hematoxylin and eosin staining, scale bar: 50 μm.

protein 1 (LAMP1) (Fig. 2B) and these vacuoles were highly distended ($1.50 \pm 0.17\ \mu m^2$ in patient iPSc, $n = 97$, versus $0.065 \pm 0.04\ \mu m^2$ in controls, $n = 88$, $P = 0.02$). Electron microscopy revealed large vesicles with heterogeneous contents (Fig. 2D). Western blot showed higher amounts of LAMP1 in patient than in control iPSc clones (Fig. 3A), whereas LAMP1 mRNA levels were equivalent (data not shown). Additional disorders consisted of Golgi alterations in both patients' iPSc clones with modified GM130 staining patterns (Fig. 2B) and co-staining of LAMP1-positive distended vesicles with anti-GM130 antibodies (Fig. 2C). Intense GM130 staining and expression in patient iPSc clones (Figs 2B and F and 3B) suggested increased Golgi size or GM130 reactivity outside Golgi. Moreover, Golgi structure was disorganized, consisting of fragmented ribbons, accumulating small vesicles and apposition of storage vesicles to Golgi cisterna rims (Fig. 2E). However, the vesicularization of Golgi stacks during mitosis was not affected in patients' iPSc (Supplementary Material, Fig S2A). Both patients showed similar defects. Taken together, these results showed that undifferentiated patient iPSc exhibited prominent cell pathology. In contrast, cell pathology was absent in parental patient skin fibroblasts despite HS accumulation (Fig. 2A). LAMP1 and GM130 expressions were comparable with control fibroblasts, and Golgi complexes showed similar morphology (Supplementary Material, Fig. S3).

Patient iPSc clones are pluripotent

iPSc differentiation can be examined *in vitro* by preventing cell adhesion, which results in the formation of embryoid bodies (EBs). After 10 days of non-adherent growth,

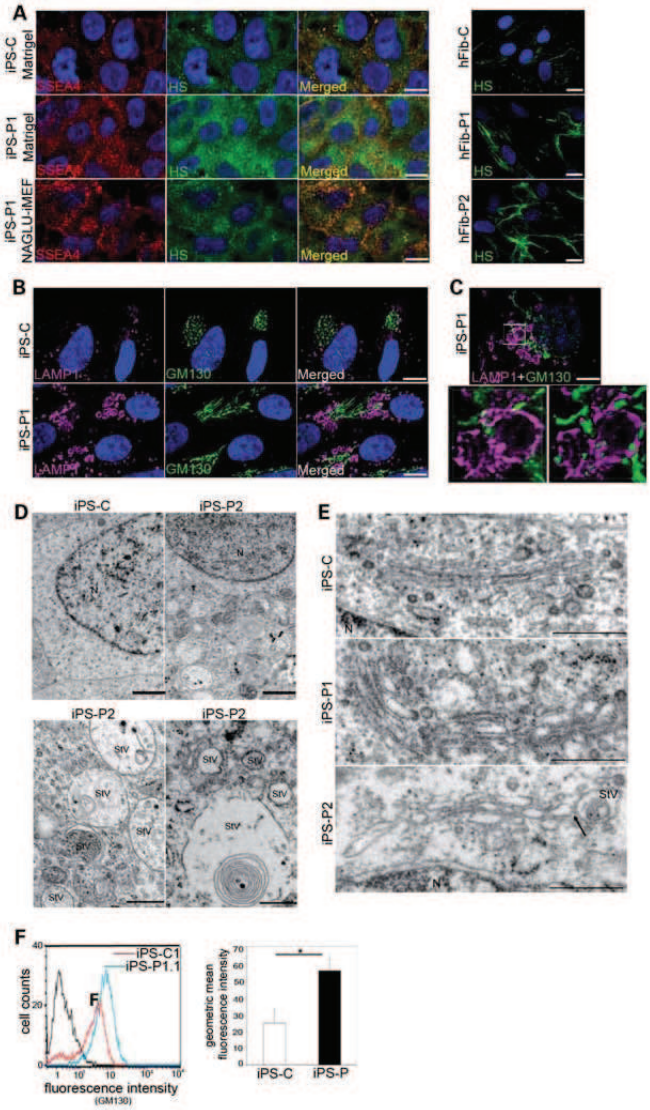

Figure 2. Undifferentiated patient iPSc express disease-related features. All control, patient 1 and patient 2 iPSc clones were cultured for 10 days on Matrigel™-coated wells. (**A**) (Left panels) Immunostaining reveals the accumulation of HS proteoglycans (in green) and expression of the pluripotency marker SSEA-4 (in red) in patient iPSc (iPS-P1 Matrigel), compared with control (iPS-C Matrigel), or with patient iPSc grown in the presence of exogenous NAGLU (iPS-P1 iMEF-NAGLU). Representative images of iPS clones are shown. Scale bar: 10 μm. (Right panels) Immunostaining shows HS proteoglycan accumulation (in green) in patient 1 (hFib-P1) and patient 2 (hFib-P2) fibroblasts compared with control (hFib-C). Scale bar: 20 μm. (**B C**) iPSc cultured on Matrigel™-coated wells were immunolabeled for LAMP1 (in purple) and GM130 (in green). (B) Confocal immunofluorescence shows distended LAMP1-positive vesicles and modified GM130 staining pattern in patient iPSc (iPS-P1), compared with control (iPS-C). Representative images are shown. Scale bar: 10 μm. (C) (Upper panel) High magnification confocal view of doubly stained cells. Scale bar: 5 μm. (Lower panels) Deconvoluted images without (left) or with (right) iso-surface treatment show contiguous staining for LAMP1 and GM130 in vesicle limiting membranes. (**D E**) iPSc cultured on Matrigel™-coated wells were processed for electron microscopy. (D) Low (top panels) or high (lower panels) magnification images show accumulation of enlarged intracellular vesicles with heterogeneous content in patient iPSc, but not in control iPSc. Representative images of one patient-2 iPSc clone (iPS-P2) and of one control clone (iPS-C) are shown. Similar observations were made in patient 1 iPSc clones. (E) Representative images of Golgi apparatus are shown. Normal cells (iPS-C) show Golgi ribbons with well-aligned and stacked cisternal membranes. In contrast, multiple short stacks are visible in iPS-P1, which are not linked to each other. In iPS-P2, cisternae are distended, interrupted and sometimes connected to storage vesicles (StV, arrow). N, nucleus. Scale bars: upper left panels: 1 μm; lower panels, right panels: 0.5 μm. (**F**) GM130 expression was quantified by flow cytometry in control (iPS-C) and patient (iPS-P) iPSc. After a 10-day culture period on Matrigel™-coated wells, dissociated iPSc were stained with an anti-GM130 antibody. An isotypic mAb was used as a negative control (black line). A representative flow cytometry diagram is shown. The bar chart on the right indicates mean ± SEM fluorescence intensity values from independent analyses of control ($n = 3$) or patient ($n = 4$) iPSc. $^*P < 0.05$ (Mann Whitney test).

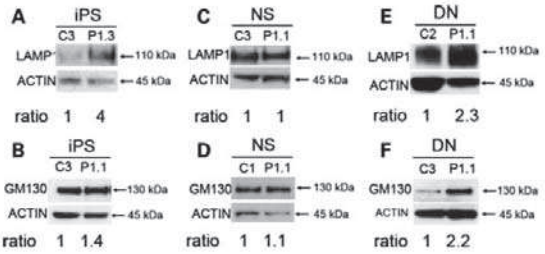

Figure 3. Western blot analysis of LAMP1 and GM130 protein content in patient iPSc, neurospheres and neurons. LAMP1 and GM130 were detected by western blot in protein extracts from (**A** and **B**) iPSc cultured on Matrigel for 10 days, (**C** and **D**) neurospheres cultured in suspension for 2 weeks and (**E** and **F**) cultures containing a mixture of precursors and differentiated neurons (DN) 17 days after adhesion of dissociated neurospheres. Control and patient cells show a 110 kDa LAMP1 signal and a 130 kDa GM130 signal. Actin signal was revealed to assess protein load on each lane. The ratio of specific signals to actin signals are indicated for each lane. Representative experiments are shown.

NAGLU activity was not detectable in patient 1 and patient 2 EB extracts (Supplementary Material, Fig. S4). The catalytic activity of other enzymes was also affected, as usually observed in LSDs (Supplementary Material, Fig. S4) (25). The formation and survival of EBs were nevertheless equally efficient for all control and patient iPSc clones. After adhesion for 10 days on polyornithine–laminin-coated cover slips, EBs derived from patients' clones accumulated enlarged intracellular LAMP1-positive vesicles (Fig. 4A). Despite both enzyme deficiency and cell pathology, iPSc differentiation was not impaired in this *in vitro* assay. All patient or control iPSc clones produced cells representing the three germ layers (Fig. 4B), including cells positive for MAP2 and nestin (ectoderm), α-smooth muscle actin (SMA) (mesoderm) and α-fetoprotein (AFP) (endoderm).

Neural stem cells derived from patient iPSc show modified gene expression profiles

All control, patient 1 and patient 2 iPSc clones give rise to proliferating floating neurospheres after removal from feeder layers and cultivation in the presence of FGF2 and epidermal growth factor (EGF). After 2 weeks of non-adherent growth, neurospheres expressed nestin, a marker of early neural progenitors (Fig. 5A). Patient 1 and patient 2 neurospheres accumulated glycosaminoglycan (GAG), including HS (Fig. 5B; Supplementary Material, S5). However, immunofluorescence (Fig. 5C), western blot (Fig. 3C and D) and flow cytometry analyses (Fig. 5D) did not show higher expression of LAMP1 or GM130 in patient than in control neural stem cells. Annexin assays indicated equivalent proportion of apoptotic cells in patient and control neural stem cells (Supplementary Material, Fig. S6). Electron microscopy examination of ultra-thin sections performed on neurosphere pellets revealed rare storage vacuoles, and although Golgi alterations were present, they were infrequent and milder than in undifferentiated iPSc (Fig. 5E).

With the aim to determine whether undegraded HS modify biological functions even in the absence of major visible cell pathology, we compared gene expression profiles between cells that did or did not accumulate HS. Total RNA was extracted from patient 2 parental fibroblasts before and after genetic correction of the enzyme defect, and from iPSc-derived neurosphere cultures (two controls, C1 and C3, and three patients, P1.1, P1.3, P2.3). Although only 50 mRNAs showed different levels in corrected and deficient fibroblasts (among 47 000 transcripts), NAGLU deficiency was associated with the modification of 3280 mRNAs (among 29 000 transcripts) in patient neural stem cells (microarray raw data available at http://www.ebi.ac.uk/arrayexpress/ E-MEXP-3033 and http://www.ncbi.nlm.nih.gov/geo/ GSE23075). Genes with modified expression overlapped between the two cell types (23 out of the 50 modified fibroblast transcripts, Supplementary Material, Table S1). They pointed to modifications of extracellular matrix (ECM) constituents (synthesis of HS chains, fibronectin, tenascin, thrombospondin, elastin, collagens III and XI, nidogen and laminin gamma, proteases and proteases inhibitor involved in matrix turnover), molecules involved in cell–matrix interactions (integrins, FGFs, FGF receptors, semaphorins, ephrin, ephrin receptor, Slit), cell adhesion (calpain, protein kinase Cβ, PDK1, phosphatidylinositol 3 kinase, tensin, parvin, RhoGTPases activating proteins, guanine exchange factors and Cdc42 effectors) and pathways transducing extra-cellular signals (PAK1, mitogen-activated kinases, c-fos, c-jun, phospholipase A2). Several constituents of the TGFβ and wnt signaling pathways were also modified. Predicted functional consequences focus on cell communication (P-value 8×10^{-6}), adhesion (3×10^{-4}), division (9×10^{-4}), motility (9×10^{-3}) and axon guidance (2×10^{-2}). Additional modifications detected in neural stem cells concerned developmental processes (4×10^{-21}), especially mesoderm (1×10^{-14}) and ectoderm (8×10^{-10}) development, neurogenesis (2×10^{-10}) or angiogenesis (9×10^{-7}).

Expression levels of genes encoding proteins associated with lysosomes or the Golgi were modified in patients' neural stem cells but not in patients' fibroblasts (Supplementary Material, Table S2). With the exception of DRAM (damage-regulated autophagy modulator, P-value 2×10^{-3}) and CD1d (10^{-2}), all genes encoding proteins associated with lysosomes (26) were downregulated in patient cells, including lysosomal hydrolases, proton pumps, transmembrane transporters and other lysosomal membrane proteins. With the exception of GOLM1 (Golgi membrane protein 1, P-value 2×10^{-3}), genes associated with Golgi morphology, localization and trafficking were downregulated.

Patient neurons show severe storage lesions and Golgi complex alterations

We next examined neural cell defects after adhesion of patient floating neurospheres. The differentiation of cells growing as floating neurospheres was induced by dissociation and adhesion on polyornithine–laminin-coated cover slips. Control and patient cultures contained equivalent proportions of β3-tubulin-positive differentiated neurons ($40.6 \pm 7.6\%$, $n = 328$, and $38 \pm 7.3\%$, $n = 339$, after 3 weeks, respectively, Fig. 6A), equivalent proportions of GABAergic neurons ($15.6 \pm 4.2\%$, $n = 275$, and $12.3 \pm 2.4\%$, $n = 224$, of the MAP2-positive neuron population after 5 weeks, respectively,

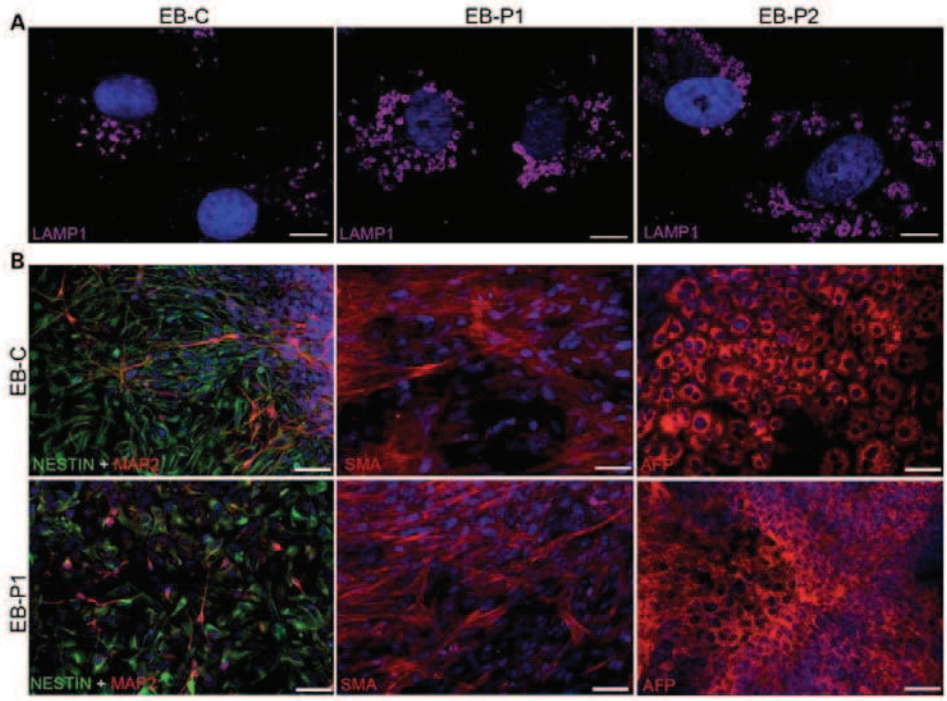

Figure 4. Patient iPSc are pluripotent. EBs were grown for 10 days in suspension culture in the absence of NAGLU supply and transferred to polyornithine–laminin-coated cover slips for 10 more days before immunolabeling. (**A**) Patient 1 (EB-P1) and patient 2 (EB-P2) EBs overexpress LAMP1 (in purple), compared with control EBs (EB-C). Representative images are shown. Scale bar: 10 μm. (**B**) Control (EB-C), patient 1 (EB-P1) and patient 2 (data not shown) EBs derived from all iPSc clones give rise to ectoderm (MAP2 in red and nestin in green), mesoderm (SMA, in red) and endoderm (AFP, in red). Representative images are shown. Scale bars: 50 μm.

Fig. 6B), equivalent ratios between GABAergic and glutamatergic neurons. Synaptophysin puncta outlining MAP2-positive neurons suggested efficient neuronal maturation (Fig. 6B). GFAP-positive cells represented $<0.1\%$ of differentiated cells. Cells positive for the oligodendrocytic markers O4 or NG2 were not observed. We did not observe differences in the kinetics, efficiency and differentiation pattern of patient 1 and patient 2 neurospheres compared with control cells (Fig. 6C). Annexin assays did not reveal difference in the proportions of apoptotic patient or control cells (Supplementary Material, Fig. S6).

Patient 1 and patient 2 cells examined after 5 weeks in differentiating conditions consisted of a mixture of neural precursors and differentiated neurons (Fig. 6A). Both patient neurons contained abundant distended LAMP1-positive vacuoles (Fig. 7A). Vacuole ultra-structure morphologies (Fig. 6D; Supplementary Material, S7) were reminiscent of those seen in undifferentiated patient iPSc (Fig. 2D). These storage vesicles were positive for LAMP1 and for the ganglioside GM3. The secondary accumulation if this glycosphingolipid is typical of MPSIII (Supplementary Material, Fig. S8). Western blot and staining showed increased LAMP1 and GM130 signals, compared with controls (Figs 3E and F and 7B). LAMP1-distended vesicles were co-stained with GM130 (Fig. 7C), and GM130 staining was more intense and broader with frequent extensions in neurites (Fig. 7D). Patient cells with neuronal morphology contained numerous abnormal Golgi complexes (Fig. 7E). Golgi complexes with disorganized morphology (51.2% in patients and 6.2% in controls) typically consisted of multiple short stacks that were not linked and often not aligned with respect to each other, associated with the accumulation of small vesicles. Storage vacuoles were frequently apposed at, or even connected to, the rims of fragmented ribbons. However, dysmorphic Golgi complexes collapsed in response to brefeldin A as efficiently as Golgi complexes in control cells, suggesting efficient vesicular trafficking in pre-Golgi compartments (Supplementary Material, Fig. S2B). These observations indicated prominent cell pathology in MPSIIIB human neurons.

DISCUSSION

We demonstrate that iPSc can be generated from the fibroblasts of children with MPSIIIB, a fatal LSD with major CNS involvement. NAGLU deficiency affected the proliferation of emerging iPSc clones, necessitating compensation of the genetic defect through enzyme replacement for efficient isolation. In contrast with parental patient fibroblasts, isolated iPSc rapidly exhibited prominent cell pathology once exogenous enzyme supply was halted. Disease expression did not

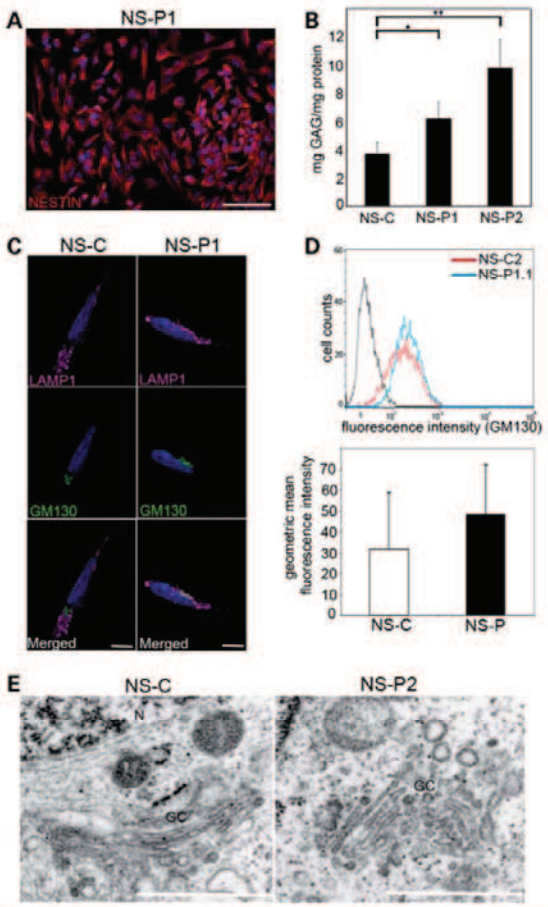

Figure 5. Neural precursors derived from patient iPSc clones have a mild phenotype. Neurosphere (NS) suspension cultures derived from each control (NS-C) and each patient iPSc clone (NS-P1 and NS-P2) were grown in the presence of FGF2, EGF and heparin and in the absence of exogenous NAGLU supply for 2 weeks. (**A**) Control and patient neurospheres were dissociated into single-cell suspension and plated on polyornithine–laminin-coated cover slips. Cells express nestin (in red) 1 day after adhesion. A representative image of one differentiated patient 1 clone is shown. Scale bar: 100 μm. (**B**) Sulfated proteoglycans were measured in crude extracts of floating neurospheres. NS-C value is the mean from determinations in neurospheres derived from control iPSc clones ($n = 5$). NS-P1 and NS-P2 values are means of independent determinations in neurospheres derived from patient 1 ($n = 6$) or patient 2 ($n = 6$) iPSc clones. Means are ± SEM. $^{*}P < 0.05$, $^{**}P < 0.01$ (Mann–Whitney test). (**C**) One day after adhesion, neural cells were immunolabeled for LAMP1 (in purple) and GM130 (in green). Apotome views show similar LAMP1 and GM130 signals in control and patient 1 neural cells. Similar observations were made in patient 2 cells. Scale bars: 10 μm. (**D**) GM130 expression was quantified by flow cytometry in control (NS-C) and patient (NS-P) cells. Neurospheres dissociated into single-cell suspensions were stained with an anti-GM130 antibody. One representative flow cytometry diagram is shown and the bar chart indicates mean ± SEM of independent determinations in control ($n = 4$) and patient ($n = 5$) neural cells. Difference is not significant (Mann–Whitney test). (**E**) Control (NS-C), patient 1 and patient 2 neurosphere pellets were processed for electron microscopy. High magnification images show representative images of Golgi complexes (GC). In few patient 2 cells (NS-P2), cisternae are interrupted and not well-aligned. Similar observations were made in patient 1 cells. N, nucleus. Scale bars: 0.5 μm.

impair iPSc survival and differentiation, allowing efficient isolation of affected neural stem cells and differentiated neurons. Whereas cell pathology was modest in floating neurosphere cultures, gene expression profiling revealed changes affecting multiple pathways, consistent with alterations of cell interactions with the environment. Neural stem cell adhesion and differentiation were accompanied by the installation of severe cell pathology consisting of intracellular vacuoles and severe disorganization of Golgi complex structure. The examination of patients' pluripotent stem cells and their neural and neuronal progenies revealed for the first time the existence of Golgi defects in a lysosomal disorder.

Patient iPSc required compensation of or adaptation to enzyme deficiency for proliferation. Fibroblast reprogrammation led to the emergence of iPSc clones with equal frequencies in patient and control fibroblasts. However, whereas clones emerging from normal fibroblasts rapidly proliferated in the presence of FGF2, emerging patient iPSc did not, suggesting inefficient response to this factor. This phenotype was reversed when feeder cells supplied the missing lysosomal enzyme. Enzyme replacement is currently a routine treatment for several MPSs (27). The exogenous enzyme clears GAGs, including HS, which accumulate as a consequence of the enzyme defect. HS proteoglycans act in concert with FGFs to transduce cell proliferation signals (23). In MPSs, the accumulation of partially degraded HS affects FGF2 signaling (28), as shown by impaired proliferation and survival of multipotent hematopoietic progenitors in MPSI mice (29), or inefficient FGF2-dependent neurogenesis and reduced FGF1, FGF2 and FGF1 receptor mRNA expression in MPSIIIB mice (12). Reversion of the proliferation defect of MPSIIIB patient iPSc after exogenous enzyme supply suggested that impaired FGF signaling was due to the accumulation of partially degraded HS. Impaired FGF signaling affects major biological functions in pluripotent stem cells, including self-renewal, proliferation, survival, differentiation and adhesion (30).

Enzyme replacement is sufficient to prevent pathology in mucopolysaccharidoses, indicating that partially degraded proteoglycans induce disorders. Once patient iPSc had been established in the presence of NAGLU exogenous enzyme, they could be starved from this supply. Enzyme-starved iPSc, as well as their progenies, rapidly accumulated HS proteoglycans. They nevertheless survived and efficiently proliferated, suggesting that efficient response to FGF2, and possibly to other undefined growth-survival factors, was now achieved despite HS accumulation. This observation is important as it indicates that modified biological functions identified in chronically deficient MPSIIIB cells may result from adaptive processes turned on to survive HS proteoglycan degradation defect.

Post-mortem studies of affected patient tissues (15,17) as well as pathology studies in MPSIIIB mice (18,19) showed predominant storage lesions in brain cells. These observations are consistent with the clinical expression of the disease, which predominates in the CNS. They are also consistent with mild or absent disease-related phenotype in patient skin fibroblasts, despite significant HS accumulation. Examination of human iPS-derived neurons, the cell type most relevant to clinical manifestation, therefore appears the best approach to investigate human MPSIIIB cell pathology. We show that

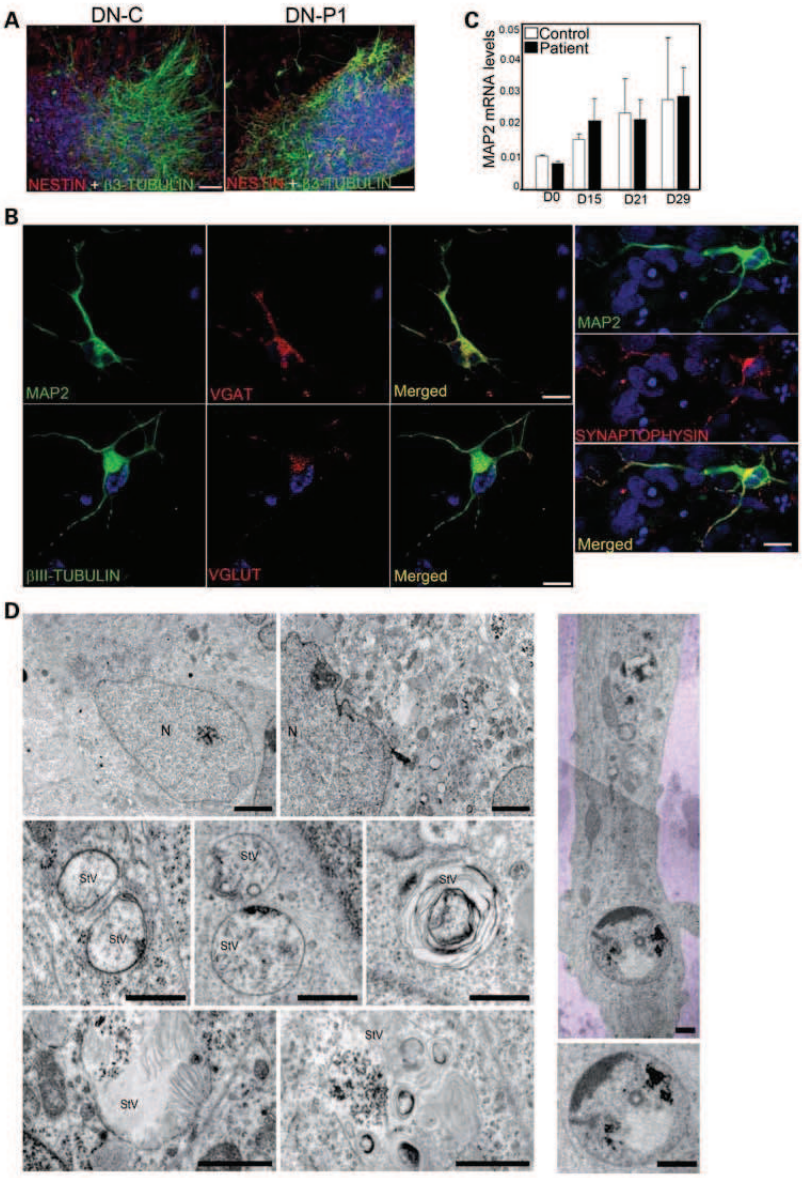

Figure 6. Storage vesicles accumulate in patient differentiated neurons. Cultures of control or patient neurons were obtained from dissociated neurospheres and plated on polyornithine laminin-coated cover slips. (**A**) Differentiated neurons positive for βIII-tubulin (in green) and neural precursors positive for nestin (in red) were observed after 3 weeks in control (DN-C), patient 1 (DN-P1) and patient 2 (not shown) cells. Representative images are shown. All control and patient iPSc clones differentiated with the same efficiencies. Scale bar: 100 μm. (**B**) (Left panels) MAP2-positive or βIII-tubulin-positive neurons (in green) expressing the GABA transporter VGAT (in red) or the glutamatergic transporter VGLUT (in red) were observed after 5 weeks in all neurosphere cultures. (Right panels) iPSc-derived MAP2-positive neurons (in green) express the mature neuronal marker synaptophysin (in red). Scale bar: 10 μm. (**C**) Equivalent amounts of MAP2 mRNAs were detected by qRT-PCR using amplification of ARPO mRNAs as a reference at days 0 (D0), 15 (D15), 21 (D21) and 29 (D29) after plating, indicating comparable differentiation kinetics for control and patient neurons. Data are means ± SEM ($n = 3$). (**D**) Cultures were processed for ultra-structural analysis 5 weeks after adhesion. Low magnification views (left panels, upper row) showed multiple intracellular vesicles in patient 1 (left) but not in control (right) cells with neuronal morphologies. Scale bars: 2 μm. High magnifications (left panels, medium and bottom rows) revealed intraluminal electro-dense fibrillar (medium left), granular (medium middle) or multilamellar (medium right, bottom) materials in patient 1 and patient 2 cells. (Two right panels) A distended vesicle (lower panel) in a long cell process (upper panel) that can be identified as a neuronal prolongation is shown. N, nucleus; StV, storage vesicle. Scale bars: 0.5 μm. See also Supplementary Material, Figure S7, showing a low magnification composite view of the same long process.

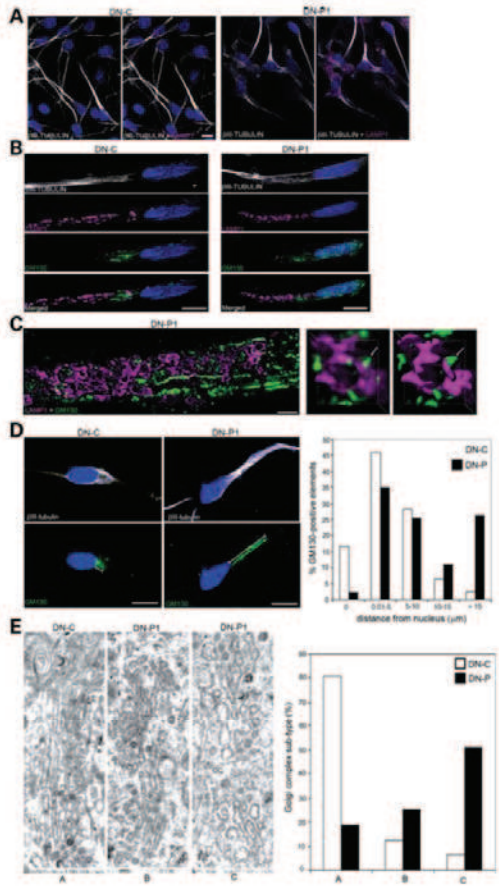

Figure 7. Golgi complex alterations in patient neurons. Control, patient 1 and patient 2 neurons derived from each iPSc clone were examined after 5 weeks of adherent culture. Cells were immunolabeled for βIII-tubulin (in white), LAMP1 (in purple) and GM130 (in green). (**A**) Low magnification confocal views show β3-tubulin-positive neurons (in white) accumulating LAMP1 (in purple)-distended vesicles. Scale bars: 10 μm. (**B**) High magnification of confocal views show more abundant distended LAMP1 vesicles and altered GM130 staining pattern in patient1 and patient 2 neurons compared with control (DN-C). Representative images of patient 1 neurons (DN-P1) are shown. Scale bars: 10 μm. (**C**) High magnification confocal view of a doubly stained neuron. Deconvoluted images without (left) or with (right) iso-surface treatment show contiguous staining for LAMP1 and GM130 in vesicle-limiting membranes (arrow). Scale bars: 2 μm. (**D**) The localization of GM130 signal with respect to the nucleus was analyzed in control and patient neurons. Left pictures are examples of low magnification Apotome views of neurons doubly stained for βIII-tubulin and GM130. Scale bar: 10 μm. The diagram in the right panel indicates the numbers of GM130-positive elements according to their distance from the nucleus in control ($n = 78$) and patient neurons ($n = 91$). Data show a broader dispersion of GM130 signals in patient than in control neurons. Neurons were randomly chosen for scoring (three independent experiments). (**E**) Golgi complex morphology was analyzed using electron microscopy in cells with a neuronal morphology. A typical Golgi complex in a control cell is shown on the left. Partially (middle picture) or fully (right picture) fragmented Golgi complexes in patients' cells are shown. Similar observations were made in patient 2. GC, Golgi complex; N, nucleus; StV, storage vesicle. Scale bar: 0.5 μm. The bar diagram on the right indicates the proportion of Golgi complex with normal (A), partially fragmented (B) or totally fragmented (C) morphology scored in control ($n = 32$) and patient ($n = 80$) randomly chosen cells.

patient iPSc provided suitable models for this purpose, exhibiting disorders that were not apparent in parental fibroblasts. The neuronal progeny of these cells also expressed disorders, suggesting that similar pathological processes affected pluripotent stem cells and neurons. These results are remarkable as there are currently very few neuronal disorders in which disease-related phenotype was documented in patient iPSc and/or their progeny (31–34).

Cell disorders in patient iPSc and neurons consist of intracellular storage vesicles, the hallmark of cell alterations in MPSIIIB. Vacuoles were associated and frequently apposed to major alterations of Golgi structure. Golgi complexes consisted of multiple short stacks that were not linked and often not aligned with respect to each other. Golgi defects were not associated with altered cell survival or differentiation. They were compatible with efficient vesicularization during mitosis or Golgi collapse in response to brefeldin A. Previous studies indicated that Golgi alterations induced by the depletion of GM130, a Golgi matrix protein necessary for proper cisternae stacking, do not affect transport kinetics in the secretory pathway (35). They may nevertheless be associated with defective glycoprotein sialylation (36) of glycosphingolipid synthesis (37). The secondary accumulation of GM3 gangliosides, which is associated with several MPS (10), might be related to Golgi structural alterations.

The Golgi phenotype is highly reminiscent of cells acutely depleted of GM130 using siRNAs (35,36). Thus, cell pathology combined GM130 overexpression with features consistent with GM130 loss-of-function, suggesting that GM130 was at least partly not functional in patient iPSc and neurons. Since partner proteins of GM130 that are needed to perform biological functions, like GRAPS65 or p115, were not detected in GM130-positive storage vesicles analyzed in mouse neurons (20), our hypothesis was that GM130 is stuck in a position that impairs appropriate interaction with its partners. GM130 functions are not limited to the formation of tethering complexes necessary for incorporation of pre-Golgi carriers into stacks, which ensures the maintenance of Golgi architecture (35,36). They also comprise control of microtubule nucleation at the Golgi surface (38) and Cdc42-mediated determination of cell polarity through interaction with the Cdc42 guanine exchange factor Tuba (39,40). Partial loss of GM130 function in human patient iPSc and neurons could therefore affect stem cell polarity, migration and motility and subsequently neurogenesis and neuritogenesis.

How are alterations observed in patient iPSc and their progeny related to HS accumulation? Although cell pathology was mild or absent in patient floating neurospheres or in parental fibroblasts, gene expression profiles revealed modified expression patterns relative to control cells in which HS did not accumulate. Most of the genes encoding constituents of the ECM were affected. Downregulation of HS2ST, HS6ST, HS3ST, the three enzymes responsible for the density and type of sulfation within HS saccharidic chains, suggested modified profiles of ligand sensitivities (41,42). Molecules involved in cell–matrix interactions were also modified, as well as downstream intracellular effectors associated with the mitogen-activated pathways, or the wnt and TGFβ pathways. These results are evocative of functional alterations of cell–matrix interactions.

HS proteoglycans are major determinants of how the cells sense environmental cues bound to ECM. As co-receptors for cell adhesion, cell proliferation and fate determination molecules and other extracellular signals, they collaborate with 'primary' receptors to control signaling. HS proteoglycans are endocytosed and fragmented into oligosaccharides by heparanases in early endosomes. In the absence of further degradation in lysosomes, as in NAGLU-deficient cells, oligosaccharides accumulate in intracellular compartments and are released in the environment, where they bind ECM proteins and modify the bioavailability of multiple signaling molecules. Changes in cell–matrix interactions resulting from this modified environment likely affect cell identification and responses to environmental cues important for adhesion, migration, process extension, polarization and fate specification (43–45). Modified control of the extra-cellular signal-regulated pathway, which is activated by FGFs and controls Golgi remodeling through the phosphorylation of GRASP65, might account for the observed disorganization of Golgi architecture (46). Interestingly, mild expression of this phenotype in floating neurospheres may result from less stringent dependence of non-adherent cells on matrix-bound cues, compared with adherent iPSc or differentiating neural cells. Similarly, matrix-bound cues important for iPSc and neural cells may be largely irrelevant for fibroblasts.

Previous gene expression profiling studies in MPSIIIB mouse tissues showed upregulation of genes related to lysosomal functions and inflammation (47–49). We were surprised that genes coding for lysosomal proteins, or proteins carrying mannose-6-phosphate residues (26), were either unchanged in fibroblasts accumulating HS or downregulated in patient neural stem cells. These observations do not support the hypothesis that deficient lysosomal functions induced lysosomes proliferation (50). In contrast, changes in the expression of genes related to Golgi functions in patient neural stem cells were consistent with the observed modifications of Golgi architecture.

Is MPSIIIB a developmental disease? Whereas cell defects identified in patient iPSc could impinge on their differentiation capacity, assays performed in several paradigms indicated that they behave like control iPSc, giving rise to differentiated cell progeny with similar efficiency, kinetics and pattern. These results appear consistent with the absence of clinical manifestations of the disease during fetal life and at birth in affected children (51,52) and animal models (19,53). However, these observations are not sufficient to conclude that stem cells behave normally in MPSIIIB. Indeed, the teratoma formation assay, which showed normal patient iPSc differentiation, was performed in recipient mice that are able to complement the enzymatic defect of patient iPSc. In affected humans, the CNS is presumably protected against HS proteoglycan toxicity until birth through the delivery of a maternal enzyme across the blood–brain barrier, as suggested by blood–brain barrier permeability to mannose-6-phosphate bearing molecules until birth in mice (54). Although EB formation and neural stem cell differentiation paradigms showed apparently normal behavior of patient iPSc in the absence of enzyme complementation, the accuracy of these *in vitro* assays is clearly not sufficient to detect subtle deviations from normal differentiation pattern, as they may occur *in vivo*. Considering the central role of matrix–cell interactions, cell migration, neurogenesis and neuritogenesis in post-natal CNS development, developmental damage may occur in MPSIIIB children. This possibility has major implications with regard to treatments aimed at restoring normal brain plasticity and cognition in affected children. Very early in life, reduction of HS burden is presumably the best situation for clinical success.

MATERIALS AND METHODS

iPSc generation and differentiation

Skin fibroblast cultures from two MPSIIIB patients and one non-affected volunteer were obtained from the Centre de Ressources Biologiques in Lyon (France) after approval by the competent authorities. A statement of biological samples was made according to French laws formulated by the Ministère de la Recherche et au Comité de Protection des Personnes Ile de France (reference DC-2009-1067). Fibroblasts were grown in DMEM Glutamax (Invitrogen) supplemented with 10% fetal bovin serum (FBS) (Sigma). iPSc clones were generated as previously described (55). Retrovirus plasmids carrying human cDNA coding for OCT4, SOX2, KLF4 and c-MYC were used (Addgene plasmids 17217, 17218, 17219, 17220). After VSV-G-pseudotyped retrovirus vector production, 5×10^4 cells for MPSIIIB fibroblasts and 10^5 cells for control fibroblasts were transduced twice with the retrovirus vectors in the presence of sulfate protamine (5 mg/ml, Sigma). Clones with well-defined hES-like morphology were observed 3 weeks after gene transfer. They were selected and manually picked 1 or 2 weeks later. iPSc clones were maintained on iMEF feeder layers in the following medium (iPSc medium): DMEM/F12 (Invitrogen) containing 20% KnockOut Serum Replacement (Invitrogen), 10 ng/ml of FGF2 (Miltenyi Biotech, Paris, France), 100 μM nonessential amino acids (Invitrogen) and 100 μM 2-mercaptoethanol (Invitrogen). Cultures were passaged every 5–10 days either manually or enzymatically with collagenase type IV (1 mg/ml) (Invitrogen). MPSIIIB iPSc clones were isolated and cultured on iMEF transduced with a lentivirus vector encoding human NAGLU (NAGLU-iMEF) (11). NAGLU activities in cell supernatants were increased 4.3-fold in transduced cells. To culture iPSc clones without iMEF, iPSc clones were transferred onto Matrigel™-coated wells (BD Biosciences) in mTeSR™1 medium (Stem Cell Technologies). iPSc clones were passaged either manually or enzymatically with dispase (2 mg/ml, Invitrogen). The iPS(IMR90)-4 cell clone (56) (WiCell Research Institute Madison, WA, USA) was also cultured on Matrigel™-coated wells in mTeSR™1 medium. For EB differentiation, iPSc clones were collected as small clusters after collagenase treatment. Clusters were resuspended in iPSc medium without FGF2. Ten days later, EBs were plated on polyornithine (20 μg/ml) and laminin (10 μg/ml)-coated cover slips and incubated for 8 additional days. For neural differentiation, neurospheres were generated as previously described (31). To induce neural differentiation, neurospheres were dissociated into single-cell suspension with Accumax (PAA Laboratories, Linz, Austria) and 2×10^5 cells were plated onto polyornithine–laminin-coated cover slips in DMEM/F12 supplemented with 2% B27 (Invitrogen). To quantify plating efficiencies, cells were fixed with 4%

paraformaldehyde (PFA) and stained with DAPI. At least 200 nuclei were counted per cell type ($n = 3$ experiments). Equivalent plating efficiencies were calculated between control and patient cells.

Immunocytochemistry and AP staining

AP staining was performed using the Leukocyte Alkaline Phosphatase Kit (Sigma). For immunocytochemistry, cells were fixed in 4% PFA for 20 min at room temperature. After washing with phosphate buffered saline (PBS, Invitrogen), cells were treated with PBS containing 2% normal goat serum (Invitrogen), 1% bovine serum albumin (Sigma) and saponin (0.01%, Sigma) or Triton X-100 (0.1%, Sigma) for 1 h at room temperature. Primary antibodies included mouse monoclonal anti-AFP (IgG2a, 1:200, Chemicon), anti-α-SMA (IgG2a, 1:200, Chemicon), anti-βIII-tubulin (IgG2a, 1:500, Eurogentec, Berkeley, CA, USA), anti-HS (IgM, 1:200, clone HepSS-1 kindly provided by Seikagaku Biobusiness Corporation, Tokyo, Japan), anti-GM3 (IgM, 1:100, kindly provided by Seikagaku Biobusiness Corporation), anti-LAMP1 (IgG1, 1:200, SouthernBiotech), anti-MAP2 (IgG1, 1:500, Chemicon), anti-O4 (IgM, 1:200, Stem Cell Technology), anti-SSEA4 (IgG3, 1:100, Chemicon), anti-SSEA1 (IgM, 1:100, Chemicon), anti-TRA1-60 (IgM, 1:100, Chemicon), anti-VGAT (IgG3, 1:400, Synaptic System, Göttingen, Germany), rabbit anti-GM130 (1:5000, Sigma), rabbit anti-NANOG (1:100, Abcam, Cambridge, UK), rabbit anti-nestin (1:400, Chemicon), rabbit anti-VGLUT (1:1000, Synaptic System), rabbit anti-synaptophysin (1:200, Synaptic System), rabbit anti-giantin (1:500, Covance, Princetown, NJ, USA), rabbit anti-NG2 (1:700, Chemicon). Secondary antibodies used were Alexa488 goat anti-mouse IgG1 (1:2000, Invitrogen), Alexa555 goat anti-mouse IgG1 (1:2000, Invitrogen), Alexa488 goat anti-mouse IgG2a (1:500, Invitrogen), Cy3 goat anti-mouse IgG3 (1:200, Jackson ImmunoResearch), rhodamine goat anti-mouse IgM (1:200, Millipore), FITC goat anti-mouse IgM (1:100, Jackson ImmunoResearch), biotin goat anti-mouse IgG1 (1:500, Jackson ImmunoResearch), Alexa488 goat anti-rabbit (1:1000, Invitrogen), Alexa555 goat anti-rabbit (1:1000, Invitrogen), Alexa647 streptavidin (1:500, Molecular Probes). Nucleus were stained with 1 mg/ml Hoechst H33342 (Invitrogen) and slides were mounted with Fluoromount G (Southern Biotech). Images were acquired either with an Axioplan 2 imaging optic microscope equipped with Apotome and AxioCam TR camera controlled by the AxioVision software (Zeiss, LE Pecq, France), or with an SP5 confocal system (Leica, Reuil-Malmaison, France). Confocal images were deconvoluted with the Huygens software (Svi, Hilversum, The Netherlands). Deconvoluted 3D images were constructed with the Imaris x64 software (Bitplan, Zurich, Switzerland).

Western blotting

Cells were homogenized in lysis buffer [0.1% SDS, 1% NP-40, 0.2% deoxycholate, 0.15 M NaCl, 50 mM Tris, pH 7.8, and a protease inhibitor cocktail (Roche)], triturated and centrifuged at 12 000*g* for 20 min at 4°C. Cell lysates (10 μg) were separated by electrophoresis on 7% SDS–polyacrylamide gel (Invitrogen) and transferred to a nitrocellulose membrane. Signals were revealed with anti-LAMP1 (1:1000, SouthernBiotech), anti-GM130 (1:200, IgG1, clone 35, BD Biosciences) and anti-actin (1:2000, Sigma) antibodies followed by appropriate horseradish peroxydase-coupled secondary antibodies (1:10 000, Amersham) and enhanced chemiluminescence (Pierce). Signal intensities were measured with the LAS-1000CH Luminescent photofilm LTD system, piloted by the IR-LAS-Pro software (Fuji).

Flow cytometry analysis and apoptosis

Cells were fixed in 2% PFA and incubated for 1 h either with an anti-GM130 antibody (1:100) or with an isotypic mAb as a negative control in PBS containing 1% fetal calf serum. Secondary antibody used was an Alexa488 anti-mouse IgG1 (Invitrogen). Apoptosis was analyzed with the Vybrant Apoptosis Assay Kit (Invitrogen) according to the manufacturer's protocol.

GAG dosage

Neurospheres were collected by centrifugation and overnight lysed in acetate buffer (100 mM sodium acetate, pH 5, containing 5 mM cystein, 5 mM EDTA) supplemented with papain 3% (Sigma) at 65°C. After centrifugation, sulfated GAGs were quantified in supernatants with the Blyscan Sulfated Glycosaminoglycan Assay (Biocolor) according to the manufacturer's protocol.

Electron microscopy

Cells were fixed with 2.5% glutaraldehyde in 0.1 M cacodylate buffer and post-fixed with 1% osmium tetroxide for 1 h. Cells were then dehydrated through increasing ethanol baths, and embedded in Epon 812. Ultra-thin sections (70 nm) were prepared using a Reichert Ultracut S Wild M3z microtome (Leica) and contrasted with uranyl acetate and lead citrate. Ultra-structural analyses were performed on a JEOL 1200EXII transmission electron microscope (JEOL) equipped with an Eloise Megaview camera controlled by the Analysis Pro 3.1 software (Eloise).

MPSIIIB genotyping and karyotyping

Genotyping of MPSIIIB mutations was performed by PCR amplification and sequencing of genomic DNA (Supplementary Material, Table S3). Karyotyping was performed by Pasteur-Cerba (Cergy-Pontoise, France). Analyses were performed on the following clones: C2 (passage 8), C3 (passage 21), P1.1 (passage 10), P1.3 (passage 16), P2.2 (passage 16), P2.3 (passage 8).

RT-PCR and qRT-PCR

Total RNA was extracted using TRIzol (Invitrogen) and treated with TurboDNAse (Applied Biosystems). One microgram of total RNA was used to synthesize cDNA with hexanucleotide random primers pdN6 and MMLV reverse transcriptase (Superscript II, Invitrogen). RT-PCR was performed in a thermocycler (Eppendorf) with 50 ng of cDNA

with 'RT-PCR' primers (Supplementary Material, Table S3). qRT-PCR was performed in a Model 7300 Sequence Detector (Applied Biosystems, Foster City, CA, USA) with 100 ng of cDNA and the TaqMan PCR Master Mix (according to Applied Biosystems procedures). Design of qRT-PCR primers (Supplementary Material, Table S3) was done using the Primer Express software.

Bisulfite sequencing

Genomic DNA was treated with EpiTech Bisulfite according to the manufacturer's recommendations (Qiagen). The promoter region of the human OCT4 gene was amplified by PCR. The PCR products were subcloned into pCR2-TOPO (Invitrogen). Ten clones of each sample were verified by sequencing (Eurofins MWG Operon). Primers' 'bisulfite sequencing' are listed in Supplementary Material, Table S3.

Teratoma formation

Approximately 2×10^6 dissociated iPSc were injected intramuscularly in Rag γC $^{-/-}$ mice. Six weeks after injection, teratomas were dissected, fixed in 10% formalin and embedded in paraffin. Sections were stained with hematoxylin and eosin.

Affymetrix exon array hybridization and data analysis

Fibroblasts from patient 2 were exposed to lentivirus vectors coding for GFP (HS+), or to two vectors coding for GFP and NAGLU, respectively (HS−). GFP expression and NAGLU activity were verified in three independent cultures of each type, from which 100 ng of total RNA was isolated, providing three independent samples for each condition. After amplification and labeling with Affymetrix reagents, targets were hybridized to Affymetrix Human Genome U-133 Plus 2.0 chips (47 000 transcripts, 38 500 genes). For neural stem cells, 100 ng of total RNA from C1, C3, P1.1, P1.3 and P2.3 neurospheres were amplified, labeled with Affymetrix reagents and hybridized to Affymetrix-GeneChip Human Exon 1.0 ST arrays. Affymetrix Exon Array data analyses were performed using EASANA from GenoSplice (GenoSplice Technology) (57). For analyses, a third synthetic sample (C1−3) was generated from the two control arrays C1 and C3 to artificially increase the number of reference samples and in order to increase statistical power of results (58). Unpaired statistical analyses were performed using Student's *t*-test as previously described (59). Taking into account probe expression level and probe quality such as cross-hybridization, repeat region and number of GC-rich regions, 11 505 genes were analyzed. Results were considered statistically significant for $P \leq 0.05$ and fold changes ≥ 1.2.

Statistical analyses

Statistics were performed using the SPSS software (SPSS).

SUPPLEMENTARY MATERIAL

Supplementary Material is available at *HMG* online.

ACKNOWLEDGEMENTS

We thank Dr M. Huerre for teratoma analyses, Dr J. Di Santo for providing us the Rag γC mice and Dr S. Yamanaka for plasmid DNA. We thank D. Gentien, C. Hego, C. Reyes for microarray experiments on neurospheres and P. De La Grange from Genosplice. We also thank N. Desmaris, B. Régnault and G. Soubigou for microarray experiments on fibroblasts. We are grateful to Professor M. Yaniv for advices in the redaction of the manuscript.

Conflict of Interest statement. None declared.

FUNDING

This work was supported by the Agence Nationale de la recherche (grant ANR-08-NEUR-005-02) in the frame of ERA-NET NEURON, the Association pour la Recherche sur la Sclérose Latérale Amyotrophique (ARSLA) and the Conny-Maeva Foundation.

REFERENCES

1. Lachmann, R.H., te Vruchte, D., Lloyd-Evans, E., Reinkensmeier, G., Sillence, D.J., Fernandez-Guillen, L., Dwek, R.A., Butters, T.D., Cox, T.M. and Platt, F.M. (2004) Treatment with miglustat reverses the lipid-trafficking defect in Niemann–Pick disease type C. *Neurobiol. Dis.*, **16**, 654–658.
2. Zhang, M., Dwyer, N.K., Love, D.C., Cooney, A., Comly, M., Neufeld, E., Pentchev, P.G., Blanchette-Mackie, E.J. and Hanover, J.A. (2001) Cessation of rapid late endosomal tubulovesicular trafficking in Niemann–Pick type C1 disease. *Proc. Natl Acad. Sci. USA*, **98**, 4466–4471.
3. Ballabio, A. and Gieselmann, V. (2009) Lysosomal disorders: from storage to cellular damage. *Biochim. Biophys. Acta*, **1793**, 684–696.
4. Ginzburg, L. and Futerman, A.H. (2005) Defective calcium homeostasis in the cerebellum in a mouse model of Niemann–Pick A disease. *J. Neurochem.*, **95**, 1619–1628.
5. Pelled, D., Lloyd-Evans, E., Riebeling, C., Jeyakumar, M., Platt, F.M. and Futerman, A.H. (2003) Inhibition of calcium uptake via the sarco/endoplasmic reticulum Ca^{2+}-ATPase in a mouse model of Sandhoff disease and prevention by treatment with *N*-butyldeoxynojirimycin. *J. Biol. Chem.*, **278**, 29496–29501.
6. Kiselyov, K. and Muallem, S. (2008) Mitochondrial Ca^{2+} homeostasis in lysosomal storage diseases. *Cell Calcium*, **44**, 103–111.
7. Sano, R., Annunziata, I., Patterson, A., Moshiach, S., Gomero, E., Opferman, J., Forte, M. and d'Azzo, A. (2009) GM1-ganglioside accumulation at the mitochondria-associated ER membranes links ER stress to Ca(2+)-dependent mitochondrial apoptosis. *Mol. Cell*, **36**, 500–511.
8. Wei, H., Kim, S.J., Zhang, Z., Tsai, P.C., Wisniewski, K.E. and Mukherjee, A.B. (2008) ER and oxidative stresses are common mediators of apoptosis in both neurodegenerative and non-neurodegenerative lysosomal storage disorders and are alleviated by chemical chaperones. *Hum. Mol. Genet.*, **17**, 469–477.
9. Bodennec, J., Pelled, D., Riebeling, C., Trajkovic, S. and Futerman, A.H. (2002) Phosphatidylcholine synthesis is elevated in neuronal models of Gaucher disease due to direct activation of CTP:phosphocholine cytidylyltransferase by glucosylceramide. *FASEB J.*, **16**, 1814–1816.
10. Walkley, S.U. (2004) Secondary accumulation of gangliosides in lysosomal storage disorders. *Semin. Cell Dev. Biol.*, **15**, 433–444.
11. Hocquemiller, M., Vitry, S., Bigou, S., Bruyere, J., Ausseil, J. and Heard, J.M. (2010) GAP43 overexpression and enhanced neurite outgrowth in mucopolysaccharidosis type IIIB cortical neuron cultures. *J. Neurosci. Res.*, **88**, 202–213.
12. Li, H.H., Zhao, H.Z., Neufeld, E.F., Cai, Y. and Gomez-Pinilla, F. (2002) Attenuated plasticity in neurons and astrocytes in the mouse model of Sanfilippo syndrome type B. *J. Neurosci. Res.*, **69**, 30–38.

13. Ausseil, J., Desmaris, N., Bigou, S., Attali, R., Corbineau, S., Vitry, S., Parent, M., Cheillan, D., Fuller, M., Maire, I. *et al.* (2008) Early neurodegeneration progresses independently of microglial activation by heparan sulfate in the brain of mucopolysaccharidosis IIIB mice. *PLoS One*, **3**, e2296.
14. Neufeld, E.F. and Muenzer, J. (2001) The Mucopolysaccharidoses. In Scriver, C.R., Beaudet, A.L., Sly, W.S. and Valle, D. (eds), *The Metabolic and Molecular Basis of Inherited Disease*. McGraw-Hill, New York, pp. 3421–3452.
15. Ferrer, I., Cusi, V., Pineda, M., Galofre, E. and Vila, J. (1988) Focal dendritic swellings in Purkinje cells in mucopolysaccharidoses types I, II and III. A Golgi and ultrastructural study. *Neuropathol. Appl. Neurobiol.*, **14**, 315–323.
16. Hadfield, M.G., Ghatak, N.R., Nakoneczna, I., Lippman, H.R., Myer, E.C., Constantopoulos, G. and Bradley, R.M. (1980) Pathologic findings in mucopolysaccharidosis type IIIB (Sanfilippo's syndrome B). *Arch. Neurol.*, **37**, 645–650.
17. Tamagawa, K., Morimatsu, Y., Fujisawa, K., Hara, A. and Taketomi, T. (1985) Neuropathological study and chemico-pathological correlation in sibling cases of Sanfilippo syndrome type B. *Brain Dev.*, **7**, 599–609.
18. Cressant, A., Desmaris, N., Verot, L., Brejot, T., Froissart, R., Vanier, M.T., Maire, I. and Heard, J.M. (2004) Improved behavior and neuropathology in the mouse model of Sanfilippo type IIIB disease after adeno-associated virus-mediated gene transfer in the striatum. *J. Neurosci.*, **24**, 10229–10239.
19. Li, H.H., Yu, W.H., Rozengurt, N., Zhao, H.Z., Lyons, K.M., Anagnostaras, S., Fanselow, M.S., Suzuki, K., Vanier, M.T. and Neufeld, E.F. (1999) Mouse model of Sanfilippo syndrome type B produced by targeted disruption of the gene encoding alpha-*N*-acetylglucosaminidase. *Proc. Natl Acad. Sci. USA*, **96**, 14505–14510.
20. Vitry, S., Bruyere, J., Hocquemiller, M., Bigou, S., Ausseil, J., Colle, M.A., Prevost, M.C. and Heard, J.M. (2010) Storage vesicles in neurons are related to Golgi complex alterations in mucopolysaccharidosis IIIB. *Am. J. Pathol.*, **177**, 2984–2999.
21. Nakamura, N. (2010) Emerging new roles of GM130, a cis-Golgi matrix protein, in higher order cell functions. *J. Pharmacol. Sci.*, **112**, 255–264.
22. Bunge, S., Knigge, A., Steglich, C., Kleijer, W.J., van Diggelen, O.P., Beck, M. and Gal, A. (1999) Mucopolysaccharidosis type IIIB (Sanfilippo B): identification of 18 novel alpha-*N*-acetylglucosaminidase gene mutations. *J. Med. Genet.*, **36**, 28–31.
23. Harmer, N.J. (2006) Insights into the role of heparan sulphate in fibroblast growth factor signalling. *Biochem. Soc. Trans.*, **34**, 442–445.
24. Natowicz, M.R., Chi, M.M.Y., Lowry, O.H. and Sly, W.S. (1979) Enzymatic identification of mannose 6-phosphate on the recognition marker for receptor-mediated pinocytosis of b-glucuronidase by human fibroblasts. *Proc. Natl Acad. Sci. USA*, **76**, 4322–4326.
25. Van Hoof, F. and Hers, H.G. (1968) The abnormalities of lysosomal enzymes in mucopolysaccharidoses. *Eur. J. Biochem.*, **7**, 34–44.
26. Lubke, T., Lobel, P. and Sleat, D.E. (2009) Proteomics of the lysosome. *Biochim. Biophys. Acta*, **1793**, 625–635.
27. Wraith, J.E. (2009) Enzyme replacement therapy for the management of the mucopolysaccharidoses. *Int. J. Clin. Pharmacol. Ther.*, **47** (Suppl. 1), S63–S65.
28. Pye, D.A., Vives, R.R., Hyde, P. and Gallagher, J.T. (2000) Regulation of FGF-1 mitogenic activity by heparan sulfate oligosaccharides is dependent on specific structural features: differential requirements for the modulation of FGF-1 and FGF-2. *Glycobiology*, **10**, 1183–1192.
29. Pan, C., Nelson, M.S., Reyes, M., Koodie, L., Brazil, J.J., Stephenson, E.J., Zhao, R.C., Peters, C., Selleck, S.B., Stringer, S.E. *et al.* (2005) Functional abnormalities of heparan sulfate in mucopolysaccharidosis-I are associated with defective biologic activity of FGF-2 on human multipotent progenitor cells. *Blood*, **106**, 1956–1964.
30. Lanner, F. and Rossant, J. (2010) The role of FGF/Erk signaling in pluripotent cells. *Development*, **137**, 3351–3360.
31. Ebert, A.D., Yu, J., Rose, F.F. Jr, Mattis, V.B., Lorson, C.L., Thomson, J.A. and Svendsen, C.N. (2009) Induced pluripotent stem cells from a spinal muscular atrophy patient. *Nature*, **457**, 277–280.
32. Lee, G., Papapetrou, E.P., Kim, H., Chambers, S.M., Tomishima, M.J., Fasano, C.A., Ganat, Y.M., Menon, J., Shimizu, F., Viale, A. *et al.* (2009) Modelling pathogenesis and treatment of familial dysautonomia using patient-specific iPSCs. *Nature*, **461**, 402–406.
33. Marchetto, M.C., Carromeu, C., Acab, A., Yu, D., Yeo, G.W., Mu, Y., Chen, G., Gage, F.H. and Muotri, A.R. (2010) A model for neural development and treatment of Rett syndrome using human induced pluripotent stem cells. *Cell*, **143**, 527–539.
34. Brennand, K.J., Simone, A., Jou, J., Gelboin-Burkhart, C., Tran, N., Sangar, S., Li, Y., Mu, Y., Chen, G., Yu, D. *et al.* (2011) Modelling schizophrenia using human induced pluripotent stem cells. *Nature*, **473**, 221–225.
35. Marra, P., Salvatore, L., Mironov, A. Jr, Di Campli, A., Di Tullio, G., Trucco, A., Beznoussenko, G., Mironov, A. and De Matteis, M.A. (2007) The biogenesis of the Golgi ribbon: the roles of membrane input from the ER and of GM130. *Mol. Biol .Cell*, **18**, 1595–1608.
36. Puthenveedu, M.A., Bachert, C., Puri, S., Lanni, F. and Linstedt, A.D. (2006) GM130 and GRASP65-dependent lateral cisternal fusion allows uniform Golgi-enzyme distribution. *Nat. Cell Biol.*, **8**, 238–248.
37. de Graffenried, C.L. and Bertozzi, C.R. (2004) The roles of enzyme localisation and complex formation in glycan assembly within the Golgi apparatus. *Curr. Opin. Cell Biol.*, **16**, 356–363.
38. Rivero, S., Cardenas, J., Bornens, M. and Rios, R.M. (2009) Microtubule nucleation at the cis-side of the Golgi apparatus requires AKAP450 and GM130. *EMBO J.*, **28**, 1016–1028.
39. Kodani, A., Kristensen, I., Huang, L. and Sutterlin, C. (2009) GM130-dependent control of Cdc42 activity at the Golgi regulates centrosome organization. *Mol. Biol. Cell*, **20**, 1192–1200.
40. Kodani, A. and Sutterlin, C. (2008) The Golgi protein GM130 regulates centrosome morphology and function. *Mol. Biol. Cell*, **19**, 745–753.
41. Bulow, H.E. and Hobert, O. (2004) Differential sulfations and epimerization define heparan sulfate specificity in nervous system development. *Neuron*, **41**, 723–736.
42. Gorsi, B. and Stringer, S.E. (2007) Tinkering with heparan sulfate sulfation to steer development. *Trends Cell Biol.*, **17**, 173–177.
43. Berzat, A. and Hall, A. (2010) Cellular responses to extracellular guidance cues. *EMBO J.*, **29**, 2734–2745.
44. Lin, X. (2004) Functions of heparan sulfate proteoglycans in cell signaling during development. *Development*, **131**, 6009–6021.
45. Van Vactor, D., Wall, D.P. and Johnson, K.G. (2006) Heparan sulfate proteoglycans and the emergence of neuronal connectivity. *Curr. Opin. Neurobiol.*, **16**, 40–51.
46. Wei, J.H. and Seemann, J. (2009) Remodeling of the Golgi structure by ERK signaling. *Commun. Integr. Biol.*, **2**, 35–36.
47. Ohmi, K., Kudo, L.C., Ryazantsev, S., Zhao, H.Z., Karsten, S.L. and Neufeld, E.F. (2009) Sanfilippo syndrome type B, a lysosomal storage disease, is also a tauopathy. *Proc. Natl Acad. Sci. USA*, **106**, 8332–8337.
48. Villani, G.R., Di Domenico, C., Musella, A., Cecere, F., Di Napoli, D. and Di Natale, P. (2009) Mucopolysaccharidosis IIIB: oxidative damage and cytotoxic cell involvement in the neuronal pathogenesis. *Brain Res.*, **1279**, 99–108.
49. Villani, G.R., Gargiulo, N., Faraonio, R., Castaldo, S., Gonzalez, Y.R.E. and Di Natale, P. (2007) Cytokines, neurotrophins, and oxidative stress in brain disease from mucopolysaccharidosis IIIB. *J .Neurosci. Res.*, **85**, 612–622.
50. Sardiello, M., Palmieri, M., di Ronza, A., Medina, D.L., Valenza, M., Gennarino, V.A., Di Malta, C., Donaudy, F., Embrione, V., Polishchuk, R.S. *et al.* (2009) A gene network regulating lysosomal biogenesis and function. *Science*, **325**, 473–477.
51. Greenwood, R.S., Hillman, R.E., Alcala, H. and Sly, W.S. (1978) Sanfilippo A syndrome in the fetus. *Clin. Genet.*, **13**, 241–250.
52. Minelli, A., Danesino, C., Lo Curto, F., Tenti, P., Zampatti, C., Simoni, G., Rossella, F. and Fois, A. (1988) First trimester prenatal diagnosis of Sanfilippo disease (MPSIII) type B. *Prenat. Diagn.*, **8**, 47–52.
53. Ellinwood, N.M., Wang, P., Skeen, T., Sharp, N.J., Cesta, M., Decker, S., Edwards, N.J., Bublot, I., Thompson, J.N., Bush, W. *et al.* (2003) A model of mucopolysaccharidosis IIIB (Sanfilippo syndrome type IIIB): *N*-acetyl-alpha-D-glucosmaminidase deficiency in Schipperke dogs. *J. Inherit. Metab. Dis.*, **26**, 489–504.
54. Urayama, A., Grubb, J.H., Sly, W.S. and Banks, W.A. (2004) Developmentally regulated mannose 6-phosphate receptor-mediated transport of a lysosomal enzyme across the blood–brain barrier. *Proc. Natl Acad. Sci. USA*, **101**, 12658–12663.
55. Park, I.H., Lerou, P.H., Zhao, R., Huo, H. and Daley, G.Q. (2008) Generation of human-induced pluripotent stem cells. *Nat. Protoc.*, **3**, 1180–1186.
56. Yu, J., Vodyanik, M.A., Smuga-Otto, K., Antosiewicz-Bourget, J., Frane, J.L., Tian, S., Nie, J., Jonsdottir, G.A., Ruotti, V., Stewart, R. *et al.* (2007)

Induced pluripotent stem cell lines derived from human somatic cells. *Science*, **318**, 1917–1920.
57. de la Grange, P., Dutertre, M., Martin, N. and Auboeuf, D. (2005) FAST DB: a website resource for the study of the expression regulation of human gene products. *Nucleic Acids Res.*, **33**, 4276–4284.
58. Troyanskaya, O., Cantor, M., Sherlock, G., Brown, P., Hastie, T., Tibshirani, R., Botstein, D. and Altman, R.B. (2001) Missing value estimation methods for DNA microarrays. *Bioinformatics*, **17**, 520–525.
59. de la Grange, P., Gratadou, L., Delord, M., Dutertre, M. and Auboeuf, D. (2010) Splicing factor and exon profiling across human tissues. *Nucleic Acids Res.*, **38**, 2825–2838.
60. Takahashi, K., Tanabe, K., Ohnuki, M., Narita, M., Ichisaka, T., Tomoda, K. and Yamanaka, S. (2007) Induction of pluripotent stem cells from adult human fibroblasts by defined factors. *Cell*, **131**, 861–872.
61. Huangfu, D., Maehr, R., Guo, W., Eijkelenboom, A., Snitow, M., Chen, A.E. and Melton, D.A. (2008) Induction of pluripotent stem cells by defined factors is greatly improved by small-molecule compounds. *Nat. Biotechnol.*, **26**, 795–797.

ARTICLE 2

GM130 gain-of-function induces cell pathology in a model of lysosomal storage disease

Human Molecular Genetics (2011) [Epub ahead of print]

HMG Advance Access published December 30, 2011

Human Molecular Genetics, 2011 **1–15**
doi:10.1093/hmg/ddr584

GM130 gain-of-function induces cell pathology in a model of lysosomal storage disease

Elise Roy, Julie Bruyère, Patricia Flamant, Stéphanie Bigou, Jérôme Ausseil, Sandrine Vitry and Jean Michel Heard*

Unité Rétrovirus et Transfert Génétique, INSERM U622, Department of Neuroscience, Institut Pasteur, 28 rue du Dr Roux, 75724 Paris, France

Received October 11, 2011; Revised and Accepted December 6, 2011

Cell pathology in lysosomal storage diseases is characterized by the formation of distended vacuoles with characteristics of lysosomes. Our previous studies in mucopolysaccharidosis type IIIB (MPSIIIB), a disease in which a genetic defect induces the accumulation of undigested heparan sulfate (HS) fragments, led to the hypothesis that abnormal lysosome formation was related to events occurring at the Golgi level. We reproduced the enzyme defect of MPSIIIB in HeLa cells using tetracycline-inducible expression of shRNAs directed against α-N-acetylglucosaminidase (NAGLU) and addressed this hypothesis. HeLa cells deprived of NAGLU accumulated abnormal lysosomes. The Golgi matrix protein GM130 was over-expressed. The cis- and medial-Golgi compartments were distended, elongated and formed circularized ribbons. The Golgi microtubule network was enlarged with increased amounts of AKAP450, a partner of GM130 controlling this network. GM130 down-regulation prevented pathology in HeLa cells deprived of NAGLU, whereas GM130 over-expression in control HeLa cells mimicked the pathology of deprived cells. We concluded that abnormal lysosomes forming in cells accumulating HS fragments were the consequence of GM130 gain-of-function and subsequent alterations of the Golgi ribbon architecture. These results indicate that GM130 functions are modulated by HS glycosaminoglycans and therefore possibly controlled by extracellular cues.

INTRODUCTION

Lysosomal storage diseases (LSDs) are genetic defects affecting the catalytic activity of lysosomal hydrolases, or co-factors necessary for the function of these enzymes, or lysosomal membrane transporters. They result in the accumulation of incompletely digested macromolecule fragments in cells and their environment. A hallmark of LSDs is the formation of vacuoles that accumulate in the cytosol, the nature of which is unclear. Mucopolysaccharidosis type IIIB (MPSIIIB) is an LSD in which the deficiency of α-N-acetylglucosaminidase (NAGLU) results in the accumulation of undigested heparan sulfate (HS) glycosaminoglycans (1). Affected children suffer progressive and severe mental retardation and die prematurely (1). Vacuoles present in MPSIIIB-affected cells are acidic and possess characteristics of lysosomes, like the presence of the lysosomal-associated membrane protein 1 (LAMP1) in the limiting membrane and the presence of lysosomal hydrolases in the lumen (2). However, according to their size, deficient mobility and highly heterogeneous content, these vacuoles are not normal lysosomes. In MPSIIIB mouse cortical neurons, vacuoles are not connected to the endocytic or macroautophagy pathways, which are normally efficient in these cells, and do not possess markers of late endosomes or autophagosomes (2). In contrast to normal lysosomes, the cis–Golgi matrix protein GM130 is present in vacuoles membranes. Abnormal lysosomes are associated with enlarged and disorganized Golgi apparatus, and increased GM130 levels (2). Similar observations were made in affected neurons derived from MPSIIIB patient induced pluripotent stem cells (iPSc) (3). These features are consistent with the hypothesis that abnormal lysosomes accumulating in MPSIIIB cells are caused by events affecting early stages of lysosome biogenesis.

GM130 is a cytosolic coiled-coil protein anchored to Golgi membranes (4). Interactions of GM130 with various partner proteins mediate multiple functions with cardinal roles in cell biology (5). In combination with p115 and GRASP65, GM130 functions as a tethering factor for pre-Golgi carriers

*To whom correspondence should be addressed at: Unité Rétrovirus et Transfert Génétique, INSERM U622, Département de Neuroscience, Institut Pasteur, 28 rue du Dr Roux, 75015 Paris, France. Tel: +33 145688246; Fax: +33 145688940; Email: jmheard@pasteur.fr

undergoing fusion with cis–Golgi cisternae and regulates the fusion of Golgi cisternae into elongated Golgi ribbons (6–8). Binding of GM130 to the A-kinase anchoring protein AKAP450 participates in the regulation of microtubule nucleation on cis-Golgi membranes and to the formation of Golgi-derived microtubule network (9). Interaction of GM130 with Stk25 (also named YSK1), a protein important for neuron polarization, controls the morphology and subcellular distribution of the Golgi apparatus (10). GM130 also controls Golgi disassembly and re-assembly during mitosis, and the organization of the centrosome through binding to Tuba, a guanine exchange factor for Cdc42 (11,12). These various functions converge to confer important roles to GM130 in the control of Golgi size and morphology and in the control of cell polarity and oriented migration.

We investigated the determinants of vacuoles formation and Golgi defects associated with MPSIIIB using HeLa cells in which the inducible expression of specific shRNAs directed against NAGLU induced complete depletion of this enzyme and subsequently the accumulation of undigested HS glycosaminoglycans. NAGLU-depleted HeLa cells faithfully recapitulated defects associated with MPSIIIB, as previously observed in patient iPSc and in mouse or human affected neurons. NAGLU-depleted HeLa cells and non-depleted controls could be conveniently manipulated to inducing GM130 overexpression or down-regulation. These experiments provided evidence for an implication of GM130 in Golgi alterations and vacuole formation associated with NAGLU depletion. They indicate that HS glycosaminoglycans affect regulatory pathways controlling GM130 functions.

RESULTS

Acute NAGLU depletion rapidly induces storage and cell vacuolation

Typical cell features associated with MPSIIIB consist of the storage of partially digested HS glycosaminoglycans, secondary accumulation of glycosphingolipids (13) and formation of intracellular vacuoles expressing lysosomal markers. We examined the installation of these disorders in HeLa cells acutely depleted of the lysosomal enzyme NAGLU, the missing enzyme in MPSIIIB. Five siRNAs were investigated that all induced transient down-regulation of NAGLU in HeLa cells. One sequence was selected for the construction of a tetracycline-inducible shRNA expression plasmid. Plasmid DNA was stably introduced in HeLa cells. Figure 1A and B shows drastic reduction in NAGLU mRNA levels (80–90%) and complete depletion of NAGLU catalytic activity in three independent cell clones upon tetracycline treatment. Down-regulation was maximal 7 days after induction and persisted for 1 week, after which revertant cells having recovered NAGLU activity overgrew the cultures. This result indicates that NAGLU expression conferred a selective advantage over NAGLU-depleted cells.

The consequences of NAGLU depletion were examined in one cell clone ($HeLa^{shNAGLU}$ cells) 7 days after tetracycline induction. Control cells producing normal NAGLU levels consisted of parental HeLa cells, $HeLa^{shNAGLU}$ cells not exposed to tetracycline and HeLa cells stably expressing a scrambled shRNA ($HeLa^{scrambled}$ cells) upon tetracycline treatment. Control cells gave similar results and are thereafter referred to as non-depleted cells.

Glycosaminoglycan levels were measured in extracts of non-depleted and NAGLU-depleted cells using metabolic labeling with [^{3}H]-glucosamine. NAGLU-depleted cells contained higher amounts of glycosaminoglycans than non-depleted cells (5.3-fold, Fig. 1C), indicating accumulation of NAGLU substrate molecules. Consistently, immuno-staining with anti-HS antibodies revealed more abundant and larger intracellular vesicles loaded with HS in NAGLU-depleted than in non-depleted cells (31 ± 1.5 versus 18 ± 0.5 vesicles per cell; 8.6 versus 3.4% of vesicles larger than 0.2 μm^2; Fig. 1D). HS signal at the cell surface and immediate environment was increased in NAGLU-depleted cells (Fig. 1E), suggesting increased levels in the extra-cellular matrix. NAGLU-depleted cells also stored glycosphingolipids, as shown by immuno-staining for the ganglioside GM3 (Fig. 1F). They over-expressed LAMP1 (Fig. 1G) and contained numerous large intracellular vacuoles positive for LAMP1 (Fig. 1D and F). Vacuoles were acidic and contained the lysosomal hydrolase α-L-iduronidase fused to a fluorescent tag (GFP-IDUA, Fig. 2A and B, NAGLU-depleted). Vacuoles did not express the late endosome marker mannose-6-phosphate (M6P) receptor, or the early endosome antigen 1 (EEA1) protein (Fig. 2C and D, NAGLU-depleted). Lipidated LC3 protein (LC3-II), a marker of activated macro-autophagy, was not detected in NAGLU-depleted cells (Fig. 2E, NAGLU-depleted). Cell vacuolation was visible by phase-contrast light microscopy (Fig. 1H). Electron microscopy revealed highly heterogeneous vacuole contents, including clear material, internal debris, electro-dense aggregates and membrane stacks (Fig. 1H). These aspects were highly reminiscent of storage lesions observed in MPSIIIB human (3) or mouse (2) brain cells. In NAGLU-depleted HeLa cells, GM130 staining was more intense than in non-depleted cells (Fig. 1F). LAMP1-positive vesicles co-expressed markers of the pre-Golgi and cis-Golgi compartments, including sec23 (a COPII component), GM130 or GRASP65 (Fig. 1F and Supplementary Material, Fig. S1A). Immuno-gold electron microscopy confirmed that GM130 and LAMP1 were co-localized in storage vesicle limiting membranes (Supplementary Material, Fig. S1B) and showed that doubly stained vesicles were more abundant in NAGLU-depleted cells than in non-depleted cells (4.5 ± 0.5 versus 0.8 ± 0.2 doubly stained vesicle per cell, $n = 20$ cells, $P < 0.001$, Student's t-test). Thus, HeLa cells acutely depleted of the lysosomal enzyme NAGLU rapidly accumulated primary and secondary storage products and developed cellular lesions fully recapitulating the pathology previously described in chronically deficient MPSIIIB neurons (2,3).

Co-labeling of NAGLU-depleted cells showed very limited co-localization of LAMP1, HS and GM3 signals (Fig. 1D and F), suggesting storage in different organelles, as reported in other cell types (14). In contrast, GM130 and GM3 signals mostly overlapped in large vesicular structures (71% of GM3-positive vesicles larger than 1 μm^2 were also positive for GM130 and co-localized signals represented 29% of the vesicle surface, Fig. 1F). This result suggested that GM3, which is synthesized in the cis-Golgi (15–17), accumulated in structures related to this compartment.

NAGLU depletion is associated with alteration of the Golgi complex

We previously observed alterations of the Golgi ribbon architecture in MPSIIIB mouse cortical neurons (2) and in human MPSIIIB patient iPSc and iPSc-derived neurons (3). Immunolabeling of NAGLU-depleted HeLa cells showed high expression of the Golgi-specific GM130 protein indicating expansion of Golgi structures, when compared with non-depleted cells (Fig. 3A). Consistently, western blot showed a higher expression of GM130 in NAGLU-depleted than in non-depleted cells (1.5-fold, $P < 0.05$, Fig. 3B). GM130 mRNA levels were also increased, as determined by quantitative reverse transcription-polymerase chain reaction (RT–PCR) (Fig. 3C). To study further Golgi alterations, the cis-Golgi marker GM130 (4) was used in combination with markers of other Golgi compartments, including giantin—a cis/medial-Golgi marker (18), mannosidase II—a medial-Golgi marker (19), and golgin97 and p230—two markers of the trans-Golgi network (20,21). Immuno-labeling revealed increased expression of all markers analyzed, consistently with increased Golgi size (Fig. 3D). An area of overlap was observed between GM130 and each marker examined, which presumably represents partial co-localization of the proteins. The possibility that the region of overlap might also represent the failure to resolve close, but distinct fluorescent signals cannot be excluded. This observation is in line with previous immunofluorescence microscopy studies showing that although GM130 predominantly localizes to the cis-Golgi, it partially overlaps with medial and trans-Golgi markers (4). GM130 co-localized extensively with giantin and mannosidase II, but showed limited overlap with golgin97 or p230, consistent with the known locations of the proteins that were analyzed. In each case, quantification of co-localized signals showed increased values in NAGLU-depleted cells, when compared with non-depleted cells (data not shown). When protein-specific signals were quantified after excluding the area of overlap, compartment-specific differences were observed (Fig. 3D, see graphs). Whereas giantin and mannosidase II-specific signals were increased in NAGLU-depleted cells, when compared with non-depleted cells, golgin97 and p230-specific signals were unchanged. These results indicate that at least part of the trans-Golgi compartment was not affected, and suggest selective expansion of the cis- and medial-Golgi compartments. Brefeldin A inhibits anterograde transport from the endoplasmic reticulum to the Golgi and induces collapse of normal Golgi stacks (22,23). In NAGLU-depleted cells, the partial resistance of giantin-labeled structures to brefeldin A was reminiscent of observations previously made in MPSIIIB mouse neurons (2), and supported the hypothesis of altered Golgi dynamics (Supplementary Material, Fig. S2).

Examination of Golgi structures in non-depleted cells by electron microscopy showed linear ribbons formed with regular and thin cisternae stacks (Fig. 3Ea). In contrast, Golgi structures in NAGLU-depleted cells consisted of irregular and incorrectly aligned stacks of abnormally elongated Golgi ribbons (Fig. 3Eb). Quantification of ribbon length revealed significant increase when compared with non-depleted cells (1.22 ± 0.07 versus 0.72 ± 0.03 μm, $P < 0.001$) (Fig. 3Eh). Elongated abnormal ribbons exhibited marked tendency to bending, occasionally forming horseshoe-like structures (Fig. 3Ee,f), or even circular structures resembling vesicles with internal membrane stacks (Fig. 3Eg). Quantification of curvature confirmed abnormal ribbon morphology (125.6 ± 3.9 versus 159.8 ± 1.7 degree angle, $P < 0.001$) (Fig. 3Eh). Cisternae were also frequently distended (Fig. 3Ec). Clear storage vesicles apposed to abnormal Golgi structures (Fig. 3Ed) suggested that cisternal distensions could give rise to distended vesicles.

As GM130 is involved in lengthening and maintenance of the Golgi ribbon (8,24), these results suggest that increased GM130 levels induced expansion and disorganization of Golgi structures in NAGLU-depleted HeLa cells.

Golgi expansion in NAGLU-depleted HeLa cells is related to GM130

To determine whether Golgi defects associated with NAGLU depletion were related to GM130, we performed GM130 gain-of-function and loss-of-function experiments in both non-depleted controls and NAGLU-depleted cells.

Golgi size was measured using giantin immuno-staining in cells transiently transfected with either FLAG-tagged GM130 expression plasmid to increase GM130 levels (11), or specific siRNAs aimed at down-regulating GM130 expression (8). DNA transfection was performed after 4 days of treatment with tetracycline, before the occurrence of cell defects. Cells were examined at day 7 and compared with untransfected cells present on the same cover slip (Fig. 4A). In non-depleted cells, giantin staining was reduced in GM130-negative cells when compared with untransfected cells, consistently with previous observations of Golgi fragmentation in the absence of GM130 (8,24). Non-depleted cells expressing FLAG-tagged GM130 showed increased giantin staining indicating Golgi expansion. In NAGLU-depleted cells, GM130 depletion decreased giantin staining, indicating efficient Golgi fragmentation, and FLAG-tagged GM130 expression increased giantin staining, suggesting further Golgi expansion.

Golgi morphology was examined by electron microscopy in cells stably expressing FLAG-tagged GM130 (Fig. 4B). In non-depleted cells, FLAG-tagged GM130 expression was associated with elongation and bending of Golgi ribbons, resulting in aspects very similar to those observed in NAGLU-depleted cells (Figs 3E and 4B). Quantification of Golgi length and curvature showed significantly modified values, when compared with non-depleted cells transfected with control DNA (Fig. 4B). In NAGLU-depleted cells, FLAG-tagged GM130 expression aggravated further Golgi alterations, when compared with NAGLU-depleted cells transfected with control DNA (Fig. 4B). These results show that GM130 over-expression induced Golgi expansion and disorganization in normal cells and therefore strongly suggest that Golgi defects observed in NAGLU-depleted cells were related to increased GM130 levels.

NAGLU depletion is associated with expansion of Golgi microtubule network

Golgi ribbon formation requires Golgi-derived microtubules (25). Microtubule nucleation on Golgi membranes is facilitated by the recruitment of γ-tubulin and γ-TuRC complex to the cis-Golgi via the interaction of GM130 with

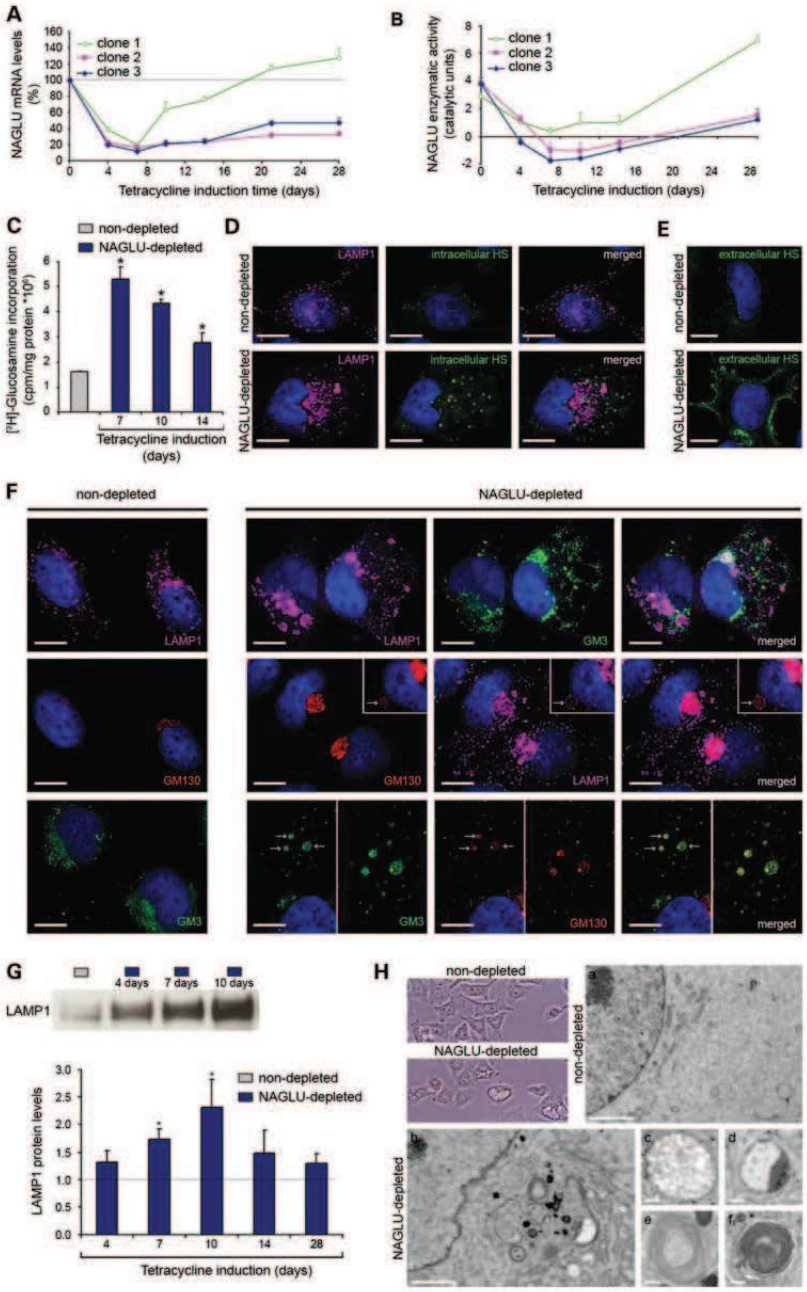

Figure 1. NAGLU-depleted HeLa cells provide an accurate model of MPSIIIB. (**A**) NAGLU mRNA levels normalized to ARPO mRNA (59) were determined by quantitative RT PCR and expressed as percentage versus non-depleted cells (depicted as 100%, grey line). (**B**) NAGLU enzymatic activity was determined by fluorimetric assays. Clone 3 (most robust NAGLU inhibition) was used for subsequent analyses. (**C**) Glycosaminoglycan content was measured by metabolic labeling with [^{3}H]-Glucosamine. (**D**) Cells were immuno-labeled with the HepSS-1 anti-HS antibodies (55) (green), in combination with anti-LAMP1 antibodies (purple). (**E**) Cells were immuno-labeled with the 10E4 anti-HS antibodies (55,60) (green). (**F**) Cells were immuno-labeled with anti-GM3 ganglioside (green), anti-LAMP1 (purple) and anti-GM130 (red) antibodies. (D, E, F) Nuclei were counterstained in blue. Scale bars, 10 μm. Apotome views are shown. NAGLU-depleted cells showed more abundant and distended LAMP1-positive vesicles, larger and more numerous intracellular HS-positive dots, more intense extracellular HS staining and larger and more intense GM3-positive vesicles when compared with non-depleted cells. HS and GM3 showed little co-localization with

AKAP450 (9,26,27). Golgi-nucleated microtubules are highly acetylated and stable (28). Immuno-staining revealed a larger and denser network of acetylated microtubules in NAGLU-depleted cells, when compared with non-depleted cells (Fig. 5A). Increased amount of acetylated microtubules was confirmed by western blot (Fig. 5B). This microtubule subset extended from the giantin-positive Golgi area toward the cell edge, indicating more active microtubule nucleation at the Golgi (Fig. 5C). Consistently, expansion of Golgi-derived microtubules in NAGLU-depleted cells was associated with larger and more intense AKAP450 signal (Fig. 5D). AKAP450 localizes both at the Golgi and at the centrosome (29,30). Whereas the AKAP450-positive area essentially co-localized with the centrosome marker pericentrin in non-depleted cells (Fig. 5D), it was wider in NAGLU-depleted cells, extending over the entire giantin-positive Golgi region (Fig. 5E). These results are consistent with enhanced microtubule nucleation at the cis-Golgi in NAGLU-depleted cells, a phenomenon that can be promoted by increased amounts of GM130–AKAP450 complexes.

Cell vacuolation is mediated by GM130

We next examined whether accumulation of LAMP1-positive vesicles, increased levels of LAMP1 and cell vacuolation in NAGLU-depleted cells were related to GM130.

As described above, GM130 was either transiently depleted with specific siRNAs, or transiently over-expressed using a FLAG-tagged GM130 expression plasmid. LAMP1 signals were quantified by immuno-staining in transfected cells and compared with untransfected cells present on the same cover slip (Fig. 6A). In non-depleted cells, LAMP1 staining was reduced when GM130 expression was abrogated, and increased when FLAG-tagged GM130 was expressed. In NAGLU-depleted cells, FLAG-tagged GM130 expression did not increase LAMP1 signal further. NAGLU-depleted cells in which GM130 was down-regulated showed a drastic reduction in LAMP1 staining, albeit still higher than in normal cells.

Cells stably expressing a lentiviral vector encoding shRNAs directed against GM130, the FLAG-tagged GM130 expression plasmid or control DNA were used to examine the consequences of permanent down-regulation, or over-expression of GM130. Western blot analysis confirmed GM130 down-regulation or over-expression and provided evidence for a link between GM130 and LAMP1 expression levels (Fig. 6B). Indeed, LAMP1 protein levels dropped down below normal levels in both non-depleted and NAGLU-depleted HeLa cells when GM130 expression was down-regulated. When FLAG-tagged GM130 was expressed, LAMP1 levels slightly increased in non-depleted cells, but did not increase further in NAGLU-depleted cells.

These cells were further examined for the presence of vacuoles. Non-depleted cells over-expressing GM130 accumulated distended intracellular vacuoles with typical characteristics of abnormal lysosomes. As observed in NAGLU-depleted cells, these vacuoles were positive for LAMP1, contained the lysosomal enzyme IDUA-GFP and were acidic, but did not express the M6P receptor or EEA1, and cell extracts did not contain LC3-II (Fig. 2, non-depleted+GM130-FLAG). Ultrastructural examination revealed vacuoles resembling those accumulating in NAGLU-depleted cells (Figs 1H and 6C). In some cases, their aspect was highly evocative of Golgi-derived structures (Fig. 6Cd). GM130 down-regulation in NAGLU-depleted cells was associated with an almost total absence of vacuoles (Fig. 6Cc), whereas abundant vacuoles were observed in NAGLU-depleted cells expressing control DNA (data not shown). Vacuoles accumulating in NAGLU-depleted cells over-expressing GM130 presented the same characteristics and morphology as those accumulating in NAGLU-depleted cells expressing control DNA (data not shown).

Taken together, these results indicate that the formation of distended LAMP1-positive intracellular vacuoles, as observed in NAGLU-depleted cells, was mediated by the augmentation of GM130 levels.

DISCUSSION

Induction of the expression of shRNA directed against NAGLU mRNAs by tetracycline resulted in an abrupt deprivation of this enzyme in HeLa cells. After 7 days, NAGLU-depleted cells expressed disorders recapitulating cell alterations associated with MPSIIIB in mice (2) or humans (3). These disorders included the primary storage of HS glycosaminoglycans, the substrate of the missing enzyme, the secondary accumulation of GM3 gangliosides and the formation of distended intracellular vacuoles decorated with the lysosomal marker LAMP1. Rapid installation of cell disorders contrasted with slow neurological deterioration in affected individuals and animal models, indicating that cell damages precede clinical expression of the disease. They suggest acute toxic effects of undigested HS glycosaminoglycans fragments on cardinal cell functions. Consistently, our results showed that they affect GM130 functions, a molecule with multiple biological roles, including intracellular trafficking, Golgi dynamics, cell polarity and oriented cell migration (5).

Observations in NAGLU-depleted HeLa cells are relevant to MPSIIIB cell pathology

Three independent NAGLU-depleted HeLa cell clones exhibited phenotypic changes, when compared with non-depleted control cells. Controls consisted of HeLa cells containing

LAMP1. LAMP1 and GM130 signals co-localized in areas distant from the Golgi apparatus (arrow in F, middle panel). Large GM3-positive vesicles frequently co-localized with GM130 (arrows in F, lower panel). (G) Western blot was used to measure LAMP1 protein levels (110 kDa band) normalized to actin protein levels (data not shown), and expressed as ratios versus non-depleted cells (grey line). (H) Phase-contrast images (upper panel, left) revealed vacuoles in NAGLU-depleted cells which were not seen in non-depleted cells. Electron microscopy: low magnification images showed the absence of vacuoles in non-depleted cells (a) and polymorphic distended vesicles in NAGLU-depleted cells (b); high magnifications revealed clear (c and d) or electron-dense material consisting of membrane stacks (e and f) in vacuole lumen. Scale bars: (a and b) 2 μm; (c, d, f) 0.1 μm; (e) 0.2 μm. (C and G) Graph values are means ± SEM from three independent experiments; $^{*}P < 0.05$, Mann–Whitney test.

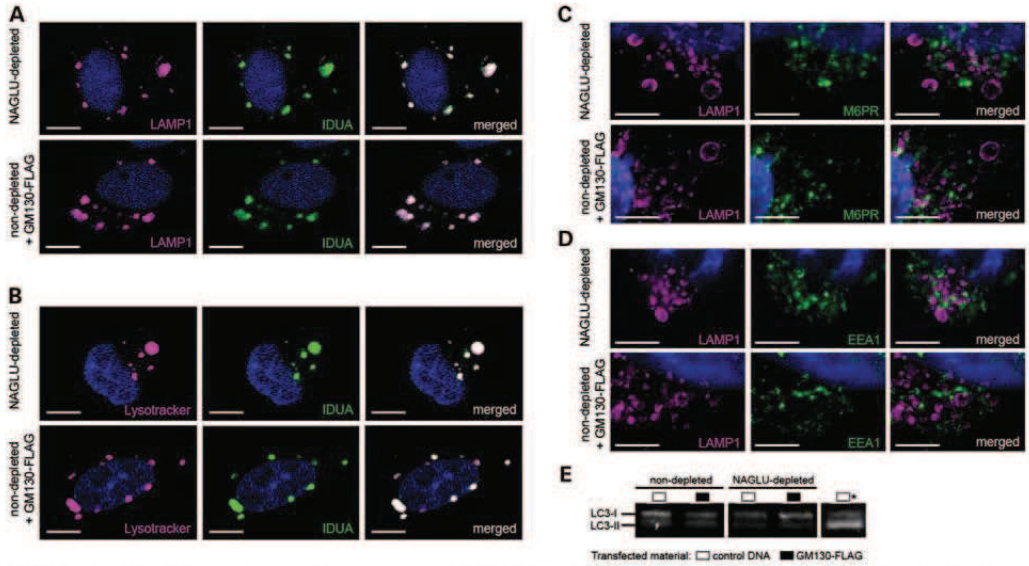

Figure 2. Vesicles with characteristics of abnormal lysosomes are not related to the endocytosis or autophagy pathways. (**A**–**D**) The identity of vesicles accumulating in NAGLU-depleted cells stably expressing control DNA (upper panel), and in non-depleted cells stably over-expressing FLAG-tagged GM130 (lower panel) was analyzed. (A) Cells were transduced with organelle lights lysosome-RFP, which targets LAMP1 (purple) and with HIV-IDUA-GFP (green). Nuclei were counterstained in blue. Merged confocal images revealed co-localization of the two markers in the same vesicles. Scale bars, 10 μm. (B) Cells transduced with HIV-IDUA-GFP (green) were stained with LysoTracker (purple). Nuclei were counterstained in blue. Merged confocal images revealed that vesicles expressing IDUA were acidic. Scale bars, 10 μm. (C) Cells were immuno-labeled with anti-LAMP1 antibodies (purple) and anti-M6P receptor antibodies (green). Nuclei were counterstained in blue. Merged apotome images show that LAMP1 signals did not colocalize with the late endosome marker M6P receptor. Scale bars, 5 μm. (D) Cells were immuno-labeled with anti-LAMP1 antibodies (purple) and anti-EEA1 antibodies (green). Nuclei were counterstained in blue. Merged apotome images show that LAMP1 signals did not colocalize with the early endosomal vesicle marker EEA1. Scale bars, 5 μm. (**E**) LC3-I (16 kDa band) to LC3-II (14 kDa band) conversion was analyzed by western blot on total protein extracts from NAGLU-depleted cells stably expressing control DNA and non-depleted cells stably expressing FLAG-tagged GM130. LC3-II was barely elevated in all experimental conditions, in contrast to a positive control (asterisk) provided by normal cells treated with rapamycin (250 nmol/l) and leupeptin (50 μmol/l).

NAGLU-specific shRNA sequences, which did not receive tetracycline, or HeLa cells containing non-specific scrambled shRNA, which were exposed to tetracycline. These cells were undistinguishable from parental HeLa cells. Phenotypic changes in NAGLU-depleted cells were therefore unlikely due to clonal selection, shRNA insertion in host cell DNA, tetracycline treatment or non-specific effects on mRNA processing.

Phenotypic changes in NAGLU-depleted HeLa cells faithfully reproduced typical MPSIIIB cell disorders. HS glycosaminoglycan and GM3 ganglioside storages are invariably observed in humans (1), mice (31) or dogs (32,33) with MPSIIIB. LAMP1-positive intracellular vacuoles are present in various tissues of the MPSIIIB mouse, including in neurons of the entorhinal (34) and rostral cortex (2). Ultrastructural examination of mouse brain sections (31,35), as well as post-mortem studies of human brain samples (36–38), revealed typical features also present in cultured MPSIIIB mouse cortical neurons (2), MPSIIIB patient-derived iPSc and neurons differentiated from these iPSc (3). These features include the co-existence in the same cell of vacuoles with light granular content and vacuoles with electron dense, often multi-lamellar materials. Alterations of Golgi morphology were initially described in MPSIIIB mouse cortical neurons (2) and also found in neurons derived from MSPIIIB patient iPSc (3). The increased expression of GM130 and the presence of GM130 immuno-reactivity in vacuole limiting membranes were initially observed in MPSIIIB mouse neurons (2). The presence of all these defects in NAGLU-depleted HeLa cells suggests that these cells recruited pathogenic mechanisms related to MPSIIIB.

Phenotypic alterations in NAGLU-depleted HeLa cells are related to GM130 over-expression

A characteristic feature of NAGLU-depleted HeLa cells was the increased size of the Golgi. Enlarged Golgi apparatus expanding into neurites was observed in mouse and human MPSIIIB neurons (2,3). Experimental GM130 over-expression increased Golgi size in control HeLa cells. Since GM130 is over-expressed in MPSIIIB neurons, we concluded that Golgi expansion in these cells was related to GM130 over-expression. This conclusion is in line with previous reports, indicating that GM130 controls Golgi extension. In neurons, the balance between two opposite signaling pathways, one involving Reelin and the other one involving GM130 interaction with YSK1, regulates Golgi dispersion into dendrites (10). In IdlG cells, a chinese hamster ovary mutant cell line that lacks GM130, the length of Golgi cisternae increased

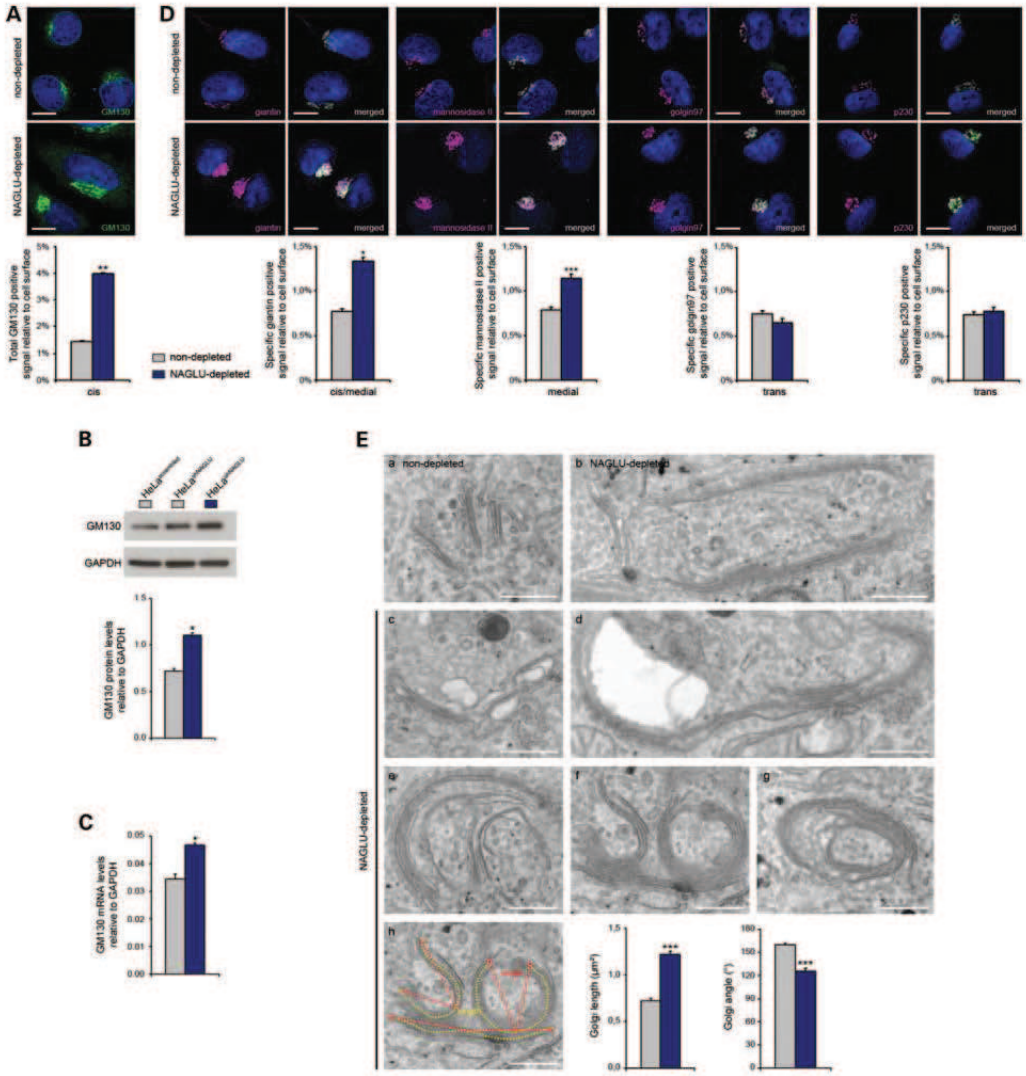

Figure 3. Golgi complex alterations are associated with GM130 over-expression in NAGLU-depleted HeLa cells. (**A**) Cells were immuno-labeled with anti-GM130 (green) antibodies. Nuclei were counterstained in blue. Confocal views revealed expansion of Golgi signal in NAGLU-depleted cells. Scale bars, 10 µm. Total GM130-positive signal was quantified in at least 150 cells in three independent experiments (graph). Values are means ± SEM; $^{**}P < 0.01$, Student's *t*-test. (**B**) Western blot was used to measure GM130 protein levels (130 kDa band) relative to GAPDH protein levels (36 kDa band). (**C**) Amounts of GM130 mRNAs were measured by quantitative RT PCR, normalized to GAPDH mRNA. (B and C) Graph values are means ± SEM from three independent experiments; $^{*}P < 0.05$, Mann Whitney test. (**D**) Cells were immuno-labeled with anti-GM130 antibodies (green), in combination with anti-giantin, anti-mannosidase II, anti-golgin97 or anti-p230 antibodies (purple). Nuclei were counterstained in blue. Merged apotome views revealed co-localization between GM130 and the different markers analyzed (in white). Giantin and mannosidase II co-localized extensively with GM130, whereas golgin97 and p230 showed minimum overlap with GM130. Scale bars, 10 µm. For each marker, specific signal (purple area) was quantified by excluding the co-localized signal (white area). Signals were quantified in at least 100 cells in three independent experiments (graph). Values are means ± SEM; $^{**}P < 0.01$, Student's *t*-test. (**E**) Golgi complex morphology was analyzed by electron microscopy. A typical Golgi complex in non-depleted cells is shown in (a). Pictures in NAGLU-depleted cells show elongation of the Golgi ribbons (b and d), cisternae distensions (c), marked ribbon bending forming horseshoe-like structures (e and f) and closed circular Golgi structures (g). A large clear vesicle apposed to the Golgi is shown in (d). Scale bars, 0.2 µm. Methods used for quantifications of the Golgi length and angle are indicated in (h). Graph: values are means ± SEM from quantifications in at least 50 individual Golgi apparatus; $^{***}P < 0.001$, Student's *t*-test.

upon GM130 over-expression (24). GM130-mediated Golgi expansion may result from increased cisternal membrane fusion triggered by GM130 GRASP65 complexes (8). It may also result from the expansion of tangential Golgi-derived microtubules bound to cis-Golgi membranes triggered by AKAP450-GM130 complexes (9,25).

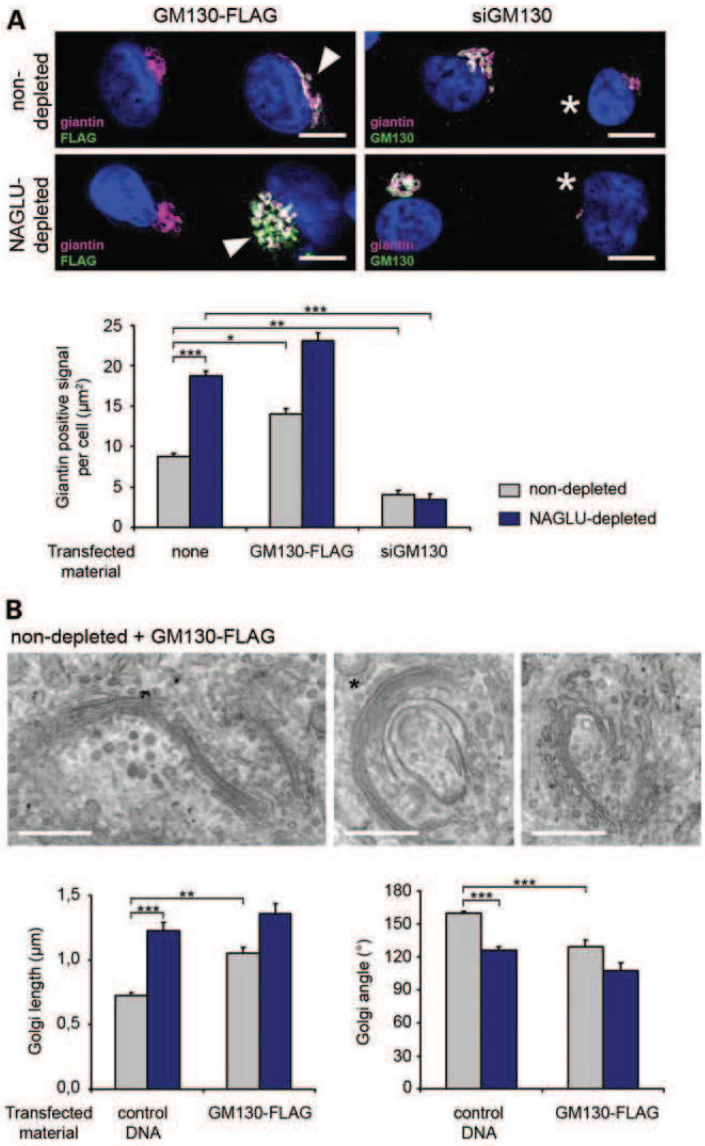

Figure 4. GM130 over-expression induces Golgi complex alterations in non-depleted HeLa cells. (**A**) Cultures transiently transfected with FLAG-tagged GM130 DNA construct (left panel), or siRNAs directed against GM130 (right panel) were immuno-labeled with anti-giantin (purple) antibodies. Anti-FLAG (green) antibodies identified cells over-expressing GM130. Anti-GM130 (green) antibodies identified GM130-expressing and GM130-depleted cells. Nuclei were counterstained in blue. When compared with non-transfected cells visible on the same field, merged apotome views showed higher giantin staining in cells positive for FLAG tag (arrowheads), and lower giantin staining in cells negative for GM130 (asterisks). For single labeling, see Supplementary Material, Figure S3. Scale bars, 10 µm. Giantin signal was quantified in at least 100 cells in three independent experiments (graph). Values are means ± SEM; $^{*}P < 0.05$, $^{**}P < 0.01$, $^{***}P < 0.001$, Student's *t*-test. (**B**) Golgi complex morphology was analyzed by electron microscopy in normal cells stably over-expressing FLAG-tagged GM130. Pictures show elongated Golgi ribbons (left panel), marked Golgi bending (middle panel) and horseshoe-like Golgi structures (right panel). Scale bars, 0.2 µm. Quantification of Golgi length and bending was performed in comparison with cultures receiving control DNA (graphs). Values are means ± SEM from quantifications in at least 40 individual Golgi apparatus; $^{**}P < 0.01$, $^{***}P < 0.001$, Student's *t*-test.

The proliferation and swelling of vacuoles with characteristics of abnormal lysosomes is a hallmark of LSDs (39). It is prominent in various cell types in the MPSIIIB mouse model (31,35) and in MPSIIIB patient neurons. Vacuoles are characterized by their large size, the expression of the lysosomal marker LAMP1 in the limiting membranes and their heterogeneous contents. Vacuoles typical of LSD were observed in NAGLU-depleted HeLa cells. We provided

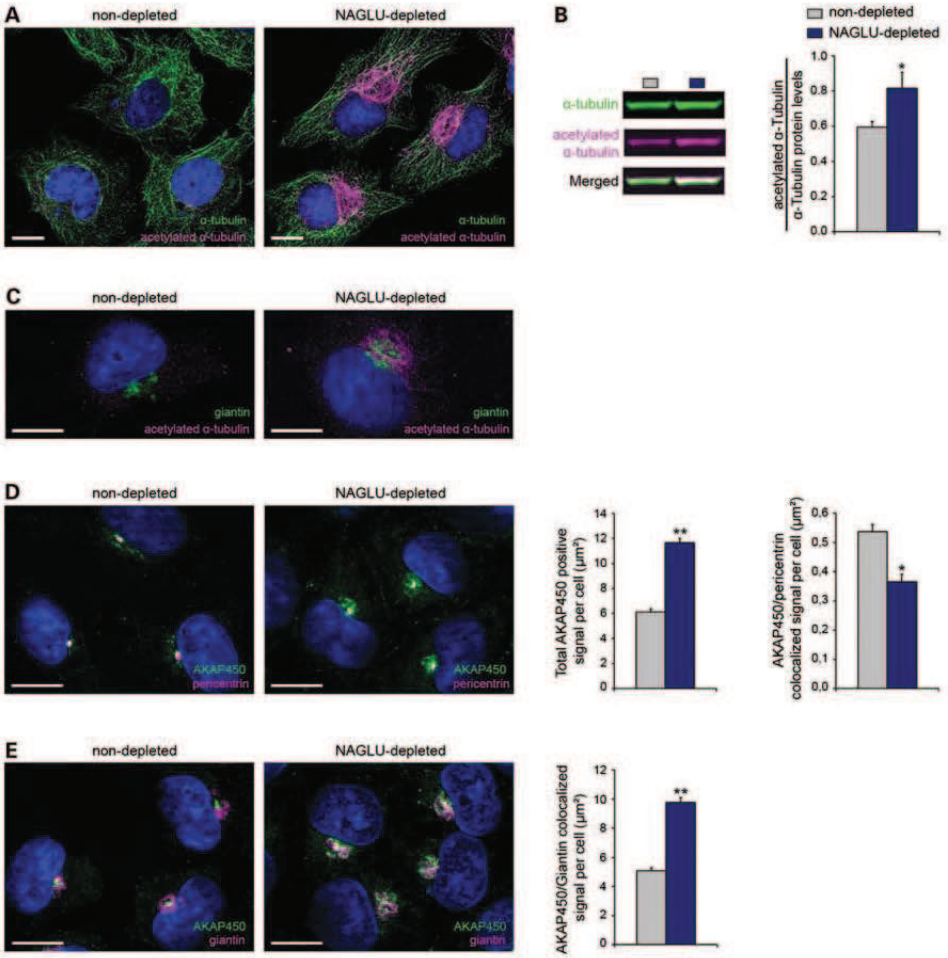

Figure 5. NAGLU depletion was associated with increased cytoskeletal GM130 levels and increased microtubule nucleation at the Golgi. (**A**) Cells were immuno-labeled with anti-α-tubulin (green) and anti-acetylated α-tubulin (purple) antibodies. Merged confocal views of NAGLU-depleted cells showed increased acetylated α-tubulin staining, with normal aspect of the microtubule cytoskeleton. (**B**) Infrared fluorescent western blot was used to measure α-tubulin (in green, 55 kDa band) and acetylated α-tubulin (in purple, 55 kDa band) protein levels. Relative ratios of acetylated versus total α-tubulin levels are shown (graph). Values are means ± SEM from three independent experiments; $^{*}P < 0.05$, Mann Whitney test. (**C**) Cells were immuno-labeled with anti-giantin (green) and anti-acetylated α-tubulin (purple) antibodies. Merged apotome views revealed expansion of acetylated microtubules in the Golgi region of NAGLU-depleted cells. (**D**) Cells were immuno-labeled with anti-AKAP450 (green) and anti-pericentrin (purple) antibodies. Merged apotome views revealed AKAP450 over-expression in NAGLU-depleted cells. Total AKAP450 signal and AKAP450 signal co-localizing with pericentrin were quantified (graphs). (**E**) Cells were immuno-labeled with anti-AKAP450 (green) and anti-giantin (purple) antibodies. AKAP450 over-expression in NAGLU-depleted cells was essentially associated with giantin-positive structures. AKAP450 signal co-localizing with giantin was quantified (graph). (A, C, D, E) Nuclei were counterstained in blue. Scale bars, 10 µm. (D and E) Graph values are means ± SEM from signals quantified in at least 150 cells in three independent experiments; $^{*}P < 0.05$; $^{**}P < 0.01$, Student's *t*-test. For single labeling, see Supplementary Material, Figure S4.

evidence that their formation resulted from GM130 over-expression: they were cleared from NAGLU-depleted HeLa cells when GM130 expression was down-regulated; they were formed in control HeLa cells when GM130 was over-expressed. Ultrastructural aspects let us consider the possibility that at least some of these vacuoles directly emanated from abnormal Golgi structures. Evocative images consisted of dense vacuoles apparently resulting from bent Golgi ribbons forming horseshoe-like structures that subsequently circularized and closed up with stacks of compacted membranes entrapped in the lumen.

GM130 over-expression causes sorting defects in the cis–medial-Golgi compartments

Golgi alterations in NAGLU-depleted cells prevailed in early Golgi compartments but did not affect the trans-Golgi. A well-established role for microtubules and motor proteins moving

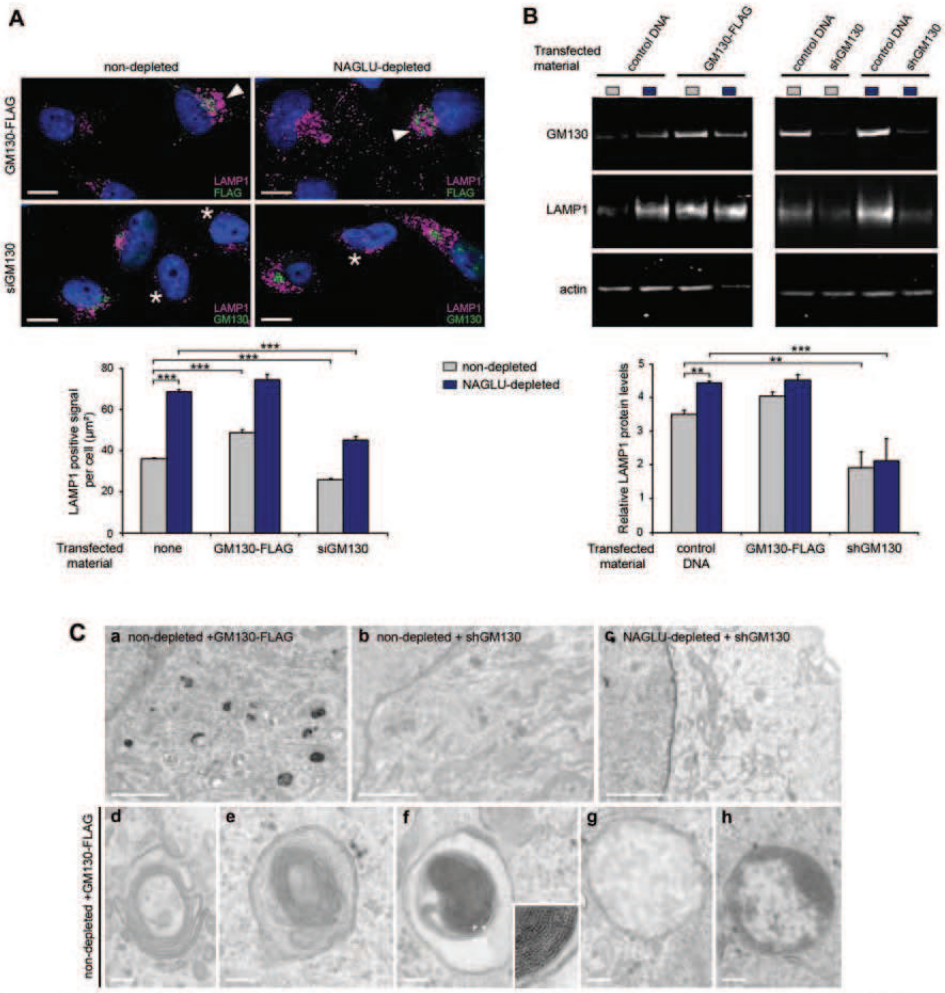

Figure 6. Cell vacuolation is mediated by GM130 expression levels. (**A**) Cultures transiently transfected with FLAG-tagged GM130 DNA construct (upper panels), or siRNAs directed against GM130 (lower panels) were immuno-labeled with anti-LAMP1 (purple) antibodies. Anti-FLAG (green) antibodies identified cells over-expressing GM130. Anti-GM130 (green) antibodies identified GM130-expressing and GM130-depleted cells. Nuclei were counterstained in blue. When compared with untransfected cells visible on the same field, merged apotome views showed higher LAMP1 staining in cells positive for FLAG tag (arrowheads, upper panels), and lower LAMP1 staining in cells negative for GM130 (asterisks, lower panels). For single labeling, see Supplementary Material, Figure S5. Scale bars, 10 µm. LAMP1 signal was quantified (graph). Values are means ± SEM from signals quantified in at least 150 cells in three independent experiments; $***P < 0.001$, Student's *t*-test. (**B**) Total proteins were extracted from cells stably over-expressing control DNA, FLAG-tagged GM130 DNA (left panel) or shRNA against GM130 (right panel) and analyzed by western blot for GM130 (130 kDa band), LAMP1 (110 kDa band) and actin (42 kDa band) expression levels. LAMP1 levels were expressed relative to actin (graph). Values are means ± SEM from three independent experiments; $**P < 0.01$, $***P < 0.001$, Mann Whitney test. (**C**) Cells were processed for electron microscopy. Low magnification images (upper row) showed extensive vacuolation in non-depleted cells over-expressing GM130 (a). In contrast, vacuoles were observed neither in non-depleted (b) nor in NAGLU-depleted (c) cells when GM130 was down-regulated. High magnifications of vacuolar structures observed in non-depleted cells over-expressing GM130 (bottom row) showed numerous vesicles with internal membranes. Morphology was evocative of circular Golgi-like structures (d), typical multi-lamellar vesicles (e) or dark electron-dense fingerprints formed by tightly compacted membranes (f, see insert). Other vesicles were clear (g), or contained heterogeneous granular or fibrillar material (h). Scale bars (a c) 2 µm; (d h) 0.1 µm.

on these tracks is to provide tensile forces required for membrane curvature and fission, which participate to vesicle sorting in the Golgi (40 42). Exacerbated microtubule anchoring and nucleation on Golgi membranes in NAGLU-depleted HeLa cells may enhance membrane deformation in the cis- and medial compartments and contribute to generate abnormal Golgi-derived vesicles. The presence of vesicles positive for the lysosomal marker LAMP1 and for early Golgi markers suggests that the phenomenon principally affected compartments destined to lysosome biogenesis.

The absence of M6P receptor indicates that abnormally formed vesicles were misrouted before they reached the trans-Golgi network. They therefore presumably lacked components necessary for fusion with the endo-lysosomal system, such as clathrin adaptor proteins. This defect can generate a dead-end compartment. Altered response to brefeldin A in NAGLU-depleted HeLa cells and in mouse cortical neurons (2) is consistent with abnormal sorting in proximal Golgi apparatus (43). The accumulation of vesicles positive for GM130, negative for LAMP1 and loaded with GM3 gangliosides may also be a consequence of sorting defects in proximal Golgi compartments, where glycosphingolipid synthesis is initiated. Whereas GM3 ganglioside synthesis principally takes place in proximal Golgi compartments, GM2 ganglioside synthesis is carried out in distal Golgi compartments (15–17). The accumulation of GM3-positive vesicles in NAGLU-depleted HeLa cells, and the predominant overload of GM3 in MPSIIIB mouse (35), dog (32) and children (44) brains, when compared with GM2, may therefore arise as a consequence of sorting defects in proximal Golgi compartments. Our previous observations of normal glycosylation pattern of the lysosomal hydrolase α-L-iduronidase and normal trafficking of ts045VSV-G in MPSIIIB mouse neurons suggested that Golgi defects were nevertheless compatible with unaltered trafficking along the secretory pathway.

GM130 over-expression is a consequence of deficient HS degradation

In MPSIIIB model animals (35) or cultured cells (2,45,46), correction of NAGLU deficiency through genetic trans-complementation indicated that the unique primary cause of cell defects associated with the disease is the defective clearance of undigested HS glycosaminoglycans. Our results show that GM130 is a target of HS glycosaminoglycan pathogenicity.

How do HS affect GM130 functions? HS proteoglycans present at the cell surface and in the extracellular matrix (ECM) bind fibrillar proteins of the matrix and cell surface receptors, including integrins and fibroblast growth factor receptors (FGF-R) (47–49). Modified levels of mRNAs coding for ECM components, integrins and FGF-R were observed in MPSIIIB patient iPSc-derived neural stem cells (3). Expression of these mRNAs was also modified in NAGLU-depleted HeLa cells (data not shown), suggesting alteration of cell sensing of the environment with possible consequences on cell adhesion, proliferation, polarization and migration (50–52). GM130 is also involved in the control of several of these cardinal cell functions (10,53,54). Although links between integrin or FGF-R signaling and GM130 functions have not been established, our results raise the possibility that GM130 acted as a mediator of activation pathways recruited by extra-cellular cues.

MATERIALS AND METHODS

Antibodies

Antibodies (dilutions for immunofluorescence): mouse mAb IgG1 anti-LAMP1 (clone H4A3, 1:200, SouthernBiotech, Birmingham, AL, USA), mouse mAb IgG1 anti-GM130 (clone 35, 1:200, BD Biosciences, Erembodegem, Belgium), rabbit polyclonal anti-GM130 (1:200, Sigma, Lyon, France), rabbit polyclonal anti-Sec23 (COPII, 1:300, Affinity BioReagents, Golden, CO, USA), rabbit polyclonal anti-GRASP65 (1:500, Novus Biologicals, Cambridge, UK), rabbit polyclonal anti-giantin (1:500, Covance, Emeryville, CA, USA), mouse mAb IgG1 anti-golgin97 (clone CDF4, 1:200, Molecular Probes, Eugene, OR, USA), mouse mAb IgG1 anti-p230 (1:200, BD Biosciences), rabbit polyclonal anti-mannosidase II (1:200, Millipore, Molsheim, France), mouse mAb IgM anti-HS clones HepSS-1 and 10E4, which recognize different epitopes on saccharide chains (55) (1:200, Seikagaku, Tokyo, Japan), mouse mAb IgM anti-GM3 (clone GMR6, 1:100, Seikagaku), mouse mAb IgG2a anti-M6P receptor (1:200, AbCam, Cambridge, UK), rabbit polyclonal anti-EEA1 (1:200, Affinity BioReagents), rabbit polyclonal anti-pericentrin (1:1000, AbCam), rat mAb IgG2a anti-α-tubulin (clone YL1/2, 1:200, AbD Serotec, Düsseldorf, Germany), mouse mAb IgG2b anti-acetylated-α-tubulin (clone 6-11B-1, 1:100, Invitrogen, Cergy-Pontoise, France), mouse mAb IgG1 anti-AKAP450 (1:200, BD Biosciences), rabbit polyclonal anti-FLAG (1:200, Sigma) and mouse mAb IgG1 anti-FLAG (clone M2, 1:500, Sigma). Secondary antibodies conjugated to Alexafluor® or DyLightTM were from Molecular Probes (Invitrogen) and Jackson ImmunoResearch Laboratories (West Grove, PA, USA).

Molecular biology

Five siRNAs targeting the human NAGLU mRNA sequence were assayed on HeLa cells. The two best sequences with respect to NAGLU mRNA depletion were selected for shRNA construction. Two scrambled control sequences with similar nucleotide compositions were designed. Selected sequences were introduced in the BLOCK-iT™ Inducible pENTRTM/H1/TO Entry Vector (Invitrogen), according to the manufacturer's instructions. Selected clones expressed the following NAGLU-specific target sequence: 5′-GCCA GAACGAAGTGGTCTA**TTCAAGAGA**TAGACCACTTCG TTCTGGC-3′. The corresponding scrambled sequence was 5′-GGCACGCAAGCGAGTTATA**TTCAAGAGA**TATAAC TCGCTTGCGTGCC-3′. The loop sequence is indicated in bold. GM130 RNA interference (RNAi) was done using previously described siRNA oligos, and a scrambled siRNA duplex as a negative control (8). All DNA and RNA oligos were purchased from Eurogentec. The pFLAG-GM130 plasmid was a kind gift from Dr C. Sutterlin, University of California, Irvine, CA, USA. Control plasmid consisted in the empty pCMV-Tag2 backbone. GM130 shRNA lentiviral particles and control shRNA lentiviral particles were from Santa Cruz (Heidelberg, Germany).

Cell culture and transfections

The cell line, cell culture reagents, media and Dulbecco's phosphate buffered saline (DPBS) were obtained from Invitrogen. Fetal bovine serum (FBS) was from Sigma. The HeLa T-Rex cell line expressing a tetracycline repressor was maintained in MEM medium complemented with 10% FBS, 2 mM

L-glutamine, 100 μg/ml penicillin/streptomycin, 5 μg/ml blasticidin and non-essential amino acids. We used FuGENE® 6 (Roche, Meylan, France) for plasmid transfections, and Lipofectamine™ RNAiMAX (Invitrogen) for siRNA transfections, according to the manufacturer's instructions.

To generate stable cell lines in which the expression of NAGLU can be turned off using tetracycline-inducible shRNA expression, HeLa T-Rex cells were plated in six-well plates and transfected with the inducible pENTRTM/H1/TO plasmids. Forty-eight hours after transfection, the dishes were split, diluted 1:100, 1:500, 1:2000 in 10 cm dishes and zeocin was added to the medium at a concentration of 200 μg/ml. Following a 14-day selection period, zeocin-resistant isolated colonies were picked and propagated. To induce NAGLU depletion, tetracycline was added into the culture medium at a concentration of 1 μg/ml. Negative controls consisted in non-induced cells, providing an internal control for each clone, and tetracycline-induced scrambled controls.

In transient transfection experiments, transfections were performed at day 4 after initiation of tetracycline treatment and cells were grown for 3 days after transfection before analysis. To generate stable cell populations expressing the FLAG-tagged GM130 plasmid construct, cell transfection was followed by G418 selection for 10 days. Negative control consisted of G418-resistant populations transfected with the empty plasmid backbone. Control shRNA and GM130 shRNA lentiviral particle transduction was performed following the manufacturer's recommendations. Following transduction, stable populations were selected via puromycin dihydrochloride selection. Selected cells were treated with tetracycline for 7 days.

Quantitative RT–PCR

Total RNA was extracted with Trizol (Invitrogen) at different time points after tetracycline induction according to the manufacturer's instructions. One microgram of RNA was reverse transcribed as previously described (56). Reverse transcription of the RNAs was followed by Q-PCR performed on a 7300 Real Time PCR System (Applied Biosystems, Foster city, CA, USA) with 100 ng of cDNA. For the amplification of NAGLU and ARPO (endogenous control) cDNAs, reaction mixtures were prepared containing 300 nM of each forward and reverse primers and the SYBR Green PCR Master Mix (according to Applied Biosystems procedures). The following primers were used: for hNAGLU, forward 5′-TTGCATC AGTACCCCATTCTATCA-3′, reverse 5′-GGTGTAATCCG TCTCCACAGACA-3′, and for hARPO forward 5′-CGAGA GCTGATGAAAGAGTTTGG-3′, reverse 5′-CCTCAGTATC CACTGCAGTCATG-3′. For the amplification of GM130 and GAPDH (endogenous control) cDNAs, the primers and TaqMan probes were designed by Applied Biosystems. Reaction mixtures containing the primers, the TaqMan probe and the TaqMan Universal PCR Master Mix were prepared according to Applied Biosystems procedures. Universal cycling conditions (2 min at 50°C, 10 min at 95°C, 40 cycles of 15 s at 95°C and 1 min at 60°C) were used. Each sample was analyzed in triplicate. Negative controls included omission of reverse transcriptase at the cDNA synthesis step and omission of the template at the PCR step. cDNA amounts were expressed as 2exp(Ct1-Ct2), in which Ct1 is a reference Ct measured for the amplification of the endogenous control cDNAs, and Ct2 is the Ct measured for the amplification of the examined cDNA.

Enzyme assays

To determine NAGLU enzymatic activity, cell pellets collected at different time points after tetracycline induction were suspended in water, submitted to 10 freeze thaw cycles and clarified by centrifugation. Samples were diluted to a total protein concentration (determined with a BCA protein assay kit, Pierce, Rockford, IL, USA) of 2 mg/ml, and the enzyme assay for NAGLU was carried out as previously described (57) using 4-methylumbelliferyl-N-acetyl-α-D-glucosaminide (4MU) (Merck, Nottingham, UK) as fluorogenic substrate. Hydrolysis of 1 nmol of substrate per hour per milligram of protein was defined as one catalytic unit.

Glycosaminoglycan analysis

For metabolic labeling, cells treated with tetracycline for 4, 7 or 11 days were further incubated for 3 days with 10 μCi/ml [^{3}H]-glucosamine (Perkin Elmer, Waltham, MA, USA) in medium containing 2% FBS before harvesting, washed with DPBS, suspended in water and lysed using freeze thaw cycles. An aliquot was taken out for determination of the protein concentration using a BCA protein assay kit. Lipids were extracted by the addition of chloroform and methanol (chloroform-methanol-water 4:8:3, v/v/v). After a 10 min incubation at room temperature, extracts were recovered by centrifugation (1000g for 10 min), washed with acetone, dried and subjected to proteolysis overnight at 65°C with 1 mg/ml papain (Sigma) in 100 mM sodium acetate buffer containing 5 mM ethylene diamine tetra-acetic acid and 5 mM cysteine (pH 5.5). The incorporation of [^{3}H]-glucosamine was measured by liquid scintillation counting, and normalized against protein concentration determined with a BCA protein assay kit.

Immunofluorescence microscopy

Cells grown in 10% FBS were processed at day 7. Live-cell staining was performed using LysoTracker® (Invitrogen), a marker of acidic vesicles, Organelle Lights™ Lysosome-RFP (Invitrogen), a baculovirus inducing the production of fluorescent LAMP1, and a lentivirus vector coding for the fluorescent lysosomal hydrolase IDUA-GFP. LysoTracker and Organelle Lights Lysosome-RFP were used according to the manufacturer's instructions. HIV-IDUA-GFP was produced and used as previously described (58).

All other staining was performed on fixed cells. For immunocytochemistry of cytoskeletal elements, cells were fixed for 10 min with ice-cold methanol at −20°C. In other cases, cells were fixed for 15 min with warm 4% paraformaldehyde and permeabilized with saponin (0.01%). Cells were then processed as previously described (2).

Cells were imaged either with an Axioplan 2 imaging optic microscope equipped with Apotome and AxioCam TR camera controlled by the AxioVision software (Zeiss, Le Pecq, France), or with a SP5 confocal system (Leica,

Rueil-Malmaison, France). Time exposure was kept constant for all analyses in the same experiment. For quantification of immuno-labeling, fluorescent signal was binarized, keeping threshold constant for all acquisitions in the same experiment. High threshold allowed recording of specific signals produced by anti-GM130, anti-golgin97, anti-giantin, anti-pericentrin or anti-LAMP1 antibody stainings. Low threshold produced background signal on the entire cell surface, which was used to manually outline the cells, and normalize specific signal to the cell surface. For AKAP450 localization studies, a high threshold was used to restrict analysis to the most intense pixels, mostly localized at the centrosome. A lower threshold was used to bring out Golgi-localized AKAP450 pixels. Signal pixel numbers (specific signal, background signal or co-localized signal) were measured by using the AxioVision co-localization module.

Electron microscopy

Samples and ultrathin sections were prepared at day 7 as previously described (2). Analyses were performed on a JEOL 1200EXII transmission electron microscope (JEOL, Croissy-sur-Seine, France) equipped with an Eloise Megaview camera controlled by analysis Pro 3.1 software (Eloise, Roissy-CDG, France). Quantifications were performed using the interactive measurements module of the AxioVision software.

Western blot analysis

To obtain total protein extracts, cell monolayers were washed with DPBS at day 7 and lysed on ice for 2 min in radio-immunoprecipitation assay buffer (Sigma) containing a protease inhibitor cocktail and a phosphatase inhibitor cocktail (Roche). 1 U/μl of a Benzonase nuclease (Merck) was added to the cell lysate, followed by a 20 min incubation at 37°C. Protein samples (10 μg) were resolved by sodium dodecyl sulfate (SDS) polyacrylamide gel electrophoresis (SDS–PAGE) using 7% Tris-acetate gels (Invitrogen). For GM130 and LAMP1 detection, chemiluminescent western blots were used, as previously described (46). For double detection of total α-tubulin, and acetylated-α-tubulin, infrared fluorescent western blots were used. Gels were blotted onto Immoblion-FL polyvinylidene difluoride membranes (Millipore), which were blocked with Odyssey blocking buffer (Li-Cor Biosciences, Lincoln, NE, USA). The primary antibodies diluted in blocking buffer containing 0.1% (v/v) Tween 20 were added to the membrane and incubated overnight at 4°C. Membranes were then washed with PBST (PBS plus 0.1% (v/v) Tween 20), and revealed with anti-mouse Ig AF680 (Invitrogen) or anti-rat Ig IRDye800 (Li-Cor Biosciences) secondary antibodies, diluted at 1:5000 in Odyssey blocking buffer containing 0.01% (v/v) SDS and 0.1% (v/v) Tween 20. The membrane was washed three times with PBST and visualized using the Odyssey imaging system (Li-Cor Biosciences).

The following antibody dilutions were used: mouse mAb IgG1 anti-LAMP1 (1:500), mouse mAb IgG1 anti-GM130 (1:200), rabbit polyclonal anti-LC3B (1:200, Novus Biologicals), mouse mAb IgG2a anti-actin (1:2000, Sigma), rabbit polyclonal anti-GAPDH (1:5000, Sigma), rat mAb IgG2a anti-α-tubulin (1:1000) and mouse mAb IgG2b anti-acetylated-α-tubulin (1:500).

Statistical analysis

Statistics were performed using the SPSS software (SPSS).

SUPPLEMENTARY MATERIAL

Supplementary Material is available at *HMG* online.

ACKNOWLEDGEMENTS

We thank Dr C. Sutterlin and Dr A. de Matteis for providing us GM130 DNA plasmids. We are grateful to Marie-Christine Prévost at the Plateforme de microscopie ultrastructurale de l'Institut Pasteur for her help with immunogold electron microscopy. We also thank F. Thouron for her help in the isolation of the HeLa cell model, and Dr S. Etienne-Manneville for precious advice.

Conflict of Interest statement. None declared.

FUNDING

This work was supported by the Agence Nationale de la recherche (grant ANR-08-NEUR-005-02), and by the Association Française contre les Myopathies (PhD fellowship to E.R.).

REFERENCES

1. Neufeld, E.F. and Muenzer, J. (2001) The Mucopolysaccharidoses. In Scriver, C.R., Beaudet, A.L., Sly, W.S. and Valle, D. (eds), *The Metabolic and Molecular Basis of Inherited Disease*. McGraw-Hill, New York, pp. 3421–3452.
2. Vitry, S., Bruyere, J., Hocquemiller, M., Bigou, S., Ausseil, J., Colle, M.A., Prevost, M.C. and Heard, J.M. (2010) Storage vesicles in neurons are related to Golgi complex alterations in mucopolysaccharidosis IIIB. *Am. J. Pathol.*, **177**, 2984–2999.
3. Lemonnier, T., Blanchard, S., Toli, D., Roy, E., Bigou, S., Froissart, R., Rouvet, I., Vitry, S., Heard, J.M. and Bohl, D. (2011) Modeling neuronal defects associated with a lysosomal disorder using patient-derived induced pluripotent stem cells. *Hum. Mol. Genet.*, **20**, 3653–3666.
4. Nakamura, N., Rabouille, C., Watson, R., Nilsson, T., Hui, N., Slusarewicz, P., Kreis, T.E. and Warren, G. (1995) Characterization of a cis-Golgi matrix protein, GM130. *J. Cell Biol.*, **131**, 1715–1726.
5. Nakamura, N. (2010) Emerging new roles of GM130, a cis-Golgi matrix protein, in higher order cell functions. *J. Pharmacol. Sci.*, **112**, 255–264.
6. Alvarez, C., Garcia-Mata, R., Hauri, H.P. and Sztul, E. (2001) The p115-interactive proteins GM130 and giantin participate in endoplasmic reticulum-Golgi traffic. *J. Biol. Chem.*, **276**, 2693–2700.
7. Marra, P., Maffucci, T., Daniele, T., Tullio, G.D., Ikehara, Y., Chan, E.K., Luini, A., Beznoussenko, G., Mironov, A. and De Matteis, M.A. (2001) The GM130 and GRASP65 Golgi proteins cycle through and define a subdomain of the intermediate compartment. *Nat. Cell Biol.*, **3**, 1101–1113.
8. Puthenveedu, M.A., Bachert, C., Puri, S., Lanni, F. and Linstedt, A.D. (2006) GM130 and GRASP65-dependent lateral cisternal fusion allows uniform Golgi-enzyme distribution. *Nat. Cell Biol.*, **8**, 238–248.
9. Rivero, S., Cardenas, J., Bornens, M. and Rios, R.M. (2009) Microtubule nucleation at the cis-side of the Golgi apparatus requires AKAP450 and GM130. *EMBO J.*, **28**, 1016–1028.
10. Matsuki, T., Matthews, R.T., Cooper, J.A., van der Brug, M.P., Cookson, M.R., Hardy, J.A., Olson, E.C. and Howell, B.W. (2010) Reelin and stk25

have opposing roles in neuronal polarization and dendritic Golgi deployment. *Cell*, **143**, 826–836.
11. Kodani, A., Kristensen, I., Huang, L. and Sutterlin, C. (2009) GM130-dependent control of Cdc42 activity at the Golgi regulates centrosome organization. *Mol. Biol. Cell*, **20**, 1192–1200.
12. Lowe, M., Gonatas, N.K. and Warren, G. (2000) The mitotic phosphorylation cycle of the cis-Golgi matrix protein GM130. *J. Cell Biol.*, **149**, 341–356.
13. Walkley, S.U. (2004) Secondary accumulation of gangliosides in lysosomal storage disorders. *Semin. Cell Dev. Biol.*, **15**, 433–444.
14. McGlynn, R., Dobrenis, K. and Walkley, S.U. (2004) Differential subcellular localization of cholesterol, gangliosides, and glycosaminoglycans in murine models of mucopolysaccharide storage disorders. *J. Comp. Neurol.*, **480**, 415–426.
15. Iber, H., van Echten, G. and Sandhoff, K. (1992) Fractionation of primary cultured cerebellar neurons: distribution of sialyltransferases involved in ganglioside biosynthesis. *J. Neurochem.*, **58**, 1533–1537.
16. van Echten, G., Iber, H., Stotz, H., Takatsuki, A. and Sandhoff, K. (1990) Uncoupling of ganglioside biosynthesis by Brefeldin A. *Eur. J. Cell Biol.*, **51**, 135–139.
17. Young, W.W. Jr, Lutz, M.S., Mills, S.E. and Lechler-Osborn, S. (1990) Use of brefeldin A to define sites of glycosphingolipid synthesis: GA2/GM2/GD2 synthase is trans to the brefeldin A block. *Proc. Natl Acad. Sci. USA*, **87**, 6838–6842.
18. Linstedt, A.D., Foguet, M., Renz, M., Seelig, H.P., Glick, B.S. and Hauri, H.P. (1995) A C-terminally-anchored Golgi protein is inserted into the endoplasmic reticulum and then transported to the Golgi apparatus. *Proc. Natl Acad. Sci. USA*, **92**, 5102–5105.
19. Novikoff, P.M., Tulsiani, D.R., Touster, O., Yam, A. and Novikoff, A.B. (1983) Immunocytochemical localization of alpha-D-mannosidase II in the Golgi apparatus of rat liver. *Proc. Natl Acad. Sci. USA*, **80**, 4364–4368.
20. Gleeson, P.A., Anderson, T.J., Stow, J.L., Griffiths, G., Toh, B.H. and Matheson, F. (1996) p230 is associated with vesicles budding from the trans-Golgi network. *J. Cell Sci.*, **109**, 2811–2821.
21. Lu, L., Tai, G. and Hong, W. (2004) Autoantigen Golgin-97, an effector of Arl1 GTPase, participates in traffic from the endosome to the trans-golgi network. *Mol. Biol. Cell*, **15**, 4426–4443.
22. Altan-Bonnet, N., Sougrat, R. and Lippincott-Schwartz, J. (2004) Molecular basis for Golgi maintenance and biogenesis. *Curr. Opin. Cell Biol.*, **16**, 364–372.
23. Ward, T.H., Polishchuk, R.S., Caplan, S., Hirschberg, K. and Lippincott-Schwartz, J. (2001) Maintenance of Golgi structure and function depends on the integrity of ER export. *J. Cell Biol.*, **155**, 557–570.
24. Marra, P., Salvatore, L., Mironov, A. Jr, Di Campli, A., Di Tullio, G., Trucco, A., Beznoussenko, G., Mironov, A. and De Matteis, M.A. (2007) The biogenesis of the Golgi ribbon: the roles of membrane input from the ER and of GM130. *Mol. Biol. Cell*, **18**, 1595–1608.
25. Miller, P.M., Folkmann, A.W., Maia, A.R., Efimova, N., Efimov, A. and Kaverina, I. (2009) Golgi-derived CLASP-dependent microtubules control Golgi organization and polarized trafficking in motile cells. *Nat. Cell Biol.*, **11**, 1069–1080.
26. Hurtado, L., Caballero, C., Gavilan, M.P., Cardenas, J., Bornens, M. and Rios, R.M. (2011) Disconnecting the Golgi ribbon from the centrosome prevents directional cell migration and ciliogenesis. *J. Cell Biol.*, **193**, 917–933.
27. Rios, R.M., Sanchis, A., Tassin, A.M., Fedriani, C. and Bornens, M. (2004) GMAP-210 recruits gamma-tubulin complexes to cis-Golgi membranes and is required for Golgi ribbon formation. *Cell*, **118**, 323–335.
28. Chabin-Brion, K., Marceiller, J., Perez, F., Settegrana, C., Drechou, A., Durand, G. and Pous, C. (2001) The Golgi complex is a microtubule-organizing organelle. *Mol. Biol. Cell*, **12**, 2047–2060.
29. Takahashi, M., Shibata, H., Shimakawa, M., Miyamoto, M., Mukai, H. and Ono, Y. (1999) Characterization of a novel giant scaffolding protein, CG-NAP, that anchors multiple signaling enzymes to centrosome and the golgi apparatus. *J. Biol. Chem.*, **274**, 17267–17274.
30. Witczak, O., Skalhegg, B.S., Keryer, G., Bornens, M., Tasken, K., Jahnsen, T. and Orstavik, S. (1999) Cloning and characterization of a cDNA encoding an A-kinase anchoring protein located in the centrosome, AKAP450. *EMBO J.*, **18**, 1858–1868.
31. Li, H.H., Yu, W.H., Rozengurt, N., Zhao, H.Z., Lyons, K.M., Anagnostaras, S., Fanselow, M.S., Suzuki, K., Vanier, M.T. and Neufeld, E.F. (1999) Mouse model of Sanfilippo syndrome type B produced by targeted disruption of the gene encoding alpha-N-acetylglucosaminidase. *Proc. Natl Acad. Sci. USA*, **96**, 14505–14510.
32. Ellinwood, N.M., Ausseil, J., Desmaris, N., Bigou, S., Liu, S., Jens, J.K., Snella, E.M., Mohammed, E.E., Thomson, C.B., Raoul, S. *et al.* (2011) Safe, efficient, and reproducible gene therapy of the brain in the dog models of Sanfilippo and Hurler syndromes. *Mol. Ther.*, **19**, 251–259.
33. Ellinwood, N.M., Wang, P., Skeen, T., Sharp, N.J., Cesta, M., Decker, S., Edwards, N.J., Bublot, I., Thompson, J.N., Bush, W. *et al.* (2003) A model of mucopolysaccharidosis IIIB (Sanfilippo syndrome type IIIB): N-acetyl-alpha-D-glucosaminidase deficiency in Schipperke dogs. *J. Inherit. Metab. Dis.*, **26**, 489–504.
34. Ryazantsev, S., Yu, W.H., Zhao, H.Z., Neufeld, E.F. and Ohmi, K. (2007) Lysosomal accumulation of SCMAS (subunit c of mitochondrial ATP synthase) in neurons of the mouse model of mucopolysaccharidosis III B. *Mol. Genet. Metab.*, **90**, 393–401.
35. Cressant, A., Desmaris, N., Verot, L., Brejot, T., Froissart, R., Vanier, M.T., Maire, I. and Heard, J.M. (2004) Improved behavior and neuropathology in the mouse model of Sanfilippo type IIIB disease after adeno-associated virus-mediated gene transfer in the striatum. *J. Neurosci.*, **24**, 10229–10239.
36. Ferrer, I., Cusi, V., Pineda, M., Galofre, E. and Vila, J. (1988) Focal dendritic swellings in Purkinje cells in mucopolysaccharidoses types I, II and III. A Golgi and ultrastructural study. *Neuropathol. Appl. Neurobiol.*, **14**, 315–323.
37. Hadfield, M.G., Ghatak, N.R., Nakoneczna, I., Lippman, H.R., Myer, E.C., Constantopoulos, G. and Bradley, R.M. (1980) Pathologic findings in mucopolysaccharidosis type IIIB (Sanfilippo's sydnrome B). *Arch. Neurol.*, **37**, 645–650.
38. Tamagawa, K., Morimatsu, Y., Fujisawa, K., Hara, A. and Taketomi, T. (1985) Neuropathological study and chemico-pathological correlation in sibling cases of Sanfilippo syndrome type B. *Brain Dev.*, **7**, 599–609.
39. Heard, J.M., Bruyere, J., Roy, E., Bigou, S., Ausseil, J. and Vitry, S. (2010) Storage problems in lysosomal diseases. *Biochem. Soc. Trans.*, **38**, 1442–1447.
40. Anitei, M. and Hoflack, B. (2011) Exit from the trans-Golgi network: from molecules to mechanisms. *Curr. Opin. Cell Biol.*, **23**, 443–451.
41. Hirschberg, K., Miller, C.M., Ellenberg, J., Presley, J.F., Siggia, E.D., Phair, R.D. and Lippincott-Schwartz, J. (1998) Kinetic analysis of secretory protein traffic and characterization of golgi to plasma membrane transport intermediates in living cells. *J. Cell Biol.*, **143**, 1485–1503.
42. Polishchuk, E.V., Di Pentima, A., Luini, A. and Polishchuk, R.S. (2003) Mechanism of constitutive export from the golgi: bulk flow via the formation, protrusion, and en bloc cleavage of large trans-golgi network tubular domains. *Mol. Biol. Cell*, **14**, 4470–4485.
43. Lippincott-Schwartz, J., Yuan, L.C., Bonifacino, J.S. and Klausner, R.D. (1989) Rapid redistribution of Golgi proteins into the ER in cells treated with brefeldin A: evidence for membrane cycling from Golgi to ER. *Cell*, **56**, 801–813.
44. Hara, A., Kitazawa, N. and Taketomi, T. (1984) Abnormalities of glycosphingolipids in mucopolysaccharidosis type III B. *J. Lipid Res.*, **25**, 175–184.
45. Hocquemiller, M., Vitry, S., Bigou, S., Bruyere, J., Ausseil, J. and Heard, J.M. (2010) GAP43 overexpression and enhanced neurite outgrowth in mucopolysaccharidosis type IIIB cortical neuron cultures. *J. Neurosci. Res.*, **88**, 202–213.
46. Vitry, S., Ausseil, J., Hocquemiller, M., Bigou, S., Dos Santos Coura, R. and Heard, J.M. (2009) Enhanced degradation of synaptophysin by the proteasome in mucopolysaccharidosis type IIIB. *Mol. Cell Neurosci.*, **41**, 8–18.
47. Faye, C., Moreau, C., Chautard, E., Jetne, R., Fukai, N., Ruggiero, F., Humphries, M.J., Olsen, B.R. and Ricard-Blum, S. (2009) Molecular interplay between endostatin, integrins, and heparan sulfate. *J. Biol. Chem.*, **284**, 22029–22040.
48. Harmer, N.J. (2006) Insights into the role of heparan sulphate in fibroblast growth factor signalling. *Biochem. Soc. Trans.*, **34**, 442–445.
49. Lopes, C.C., Dietrich, C.P. and Nader, H.B. (2006) Specific structural features of syndecans and heparan sulfate chains are needed for cell signaling. *Braz. J. Med. Biol. Res.*, **39**, 157–167.

50. Etienne-Manneville, S. and Hall, A. (2001) Integrin-mediated activation of Cdc42 controls cell polarity in migrating astrocytes through PKCzeta. *Cell*, **106**, 489–498.
51. Gupta, S.K., Meiri, K.F., Mahfooz, K., Bharti, U. and Mani, S. (2010) Coordination between extrinsic extracellular matrix cues and intrinsic responses to orient the centrosome in polarizing cerebellar granule neurons. *J. Neurosci.*, **30**, 2755–2766.
52. Shattil, S.J., Kim, C. and Ginsberg, M.H. (2010) The final steps of integrin activation: the end game. *Nat. Rev. Mol. Cell Biol.*, **11**, 288–300.
53. Kodani, A. and Sutterlin, C. (2008) The Golgi protein GM130 regulates centrosome morphology and function. *Mol. Biol. Cell*, **19**, 745–753.
54. Preisinger, C., Short, B., De Corte, V., Bruyneel, E., Haas, A., Kopajtich, R., Gettemans, J. and Barr, F.A. (2004) YSK1 is activated by the Golgi matrix protein GM130 and plays a role in cell migration through its substrate 14-3-3zeta. *J. Cell Biol.*, **164**, 1009–1020.
55. van den Born, J., Salmivirta, K., Henttinen, T., Ostman, N., Ishimaru, T., Miyaura, S., Yoshida, K. and Salmivirta, M. (2005) Novel heparan sulfate structures revealed by monoclonal antibodies. *J. Biol. Chem.*, **280**, 20516–20523.
56. Ausseil, J., Desmaris, N., Bigou, S., Attali, R., Corbineau, S., Vitry, S., Parent, M., Cheillan, D., Fuller, M., Maire, I. *et al.* (2008) Early neurodegeneration progresses independently of microglial activation by heparan sulfate in the brain of mucopolysaccharidosis IIIB mice. *PLoS ONE*, **3**, e2296.
57. Marsh, J. and Fensom, A.H. (1985) 4-Methylumbelliferyl alpha-N-acetylglucosaminidase activity for diagnosis of Sanfilippo B disease. *Clin. Genet.*, **27**, 258–262.
58. Chen, F., Vitry, S., Hocquemiller, M., Desmaris, N., Ausseil, J. and Heard, J.M. (2006) Alpha-L-Iduronidase transport in neurites. *Mol. Genet. Metab.*, **87**, 349–358.
59. Simpson, D.A., Feeney, S., Boyle, C. and Stitt, A.W. (2000) Retinal VEGF mRNA measured by SYBR green I fluorescence: a versatile approach to quantitative PCR. *Mol. Vis.*, **6**, 178–183.
60. David, G., Bai, X.M., Van der Schueren, B., Cassiman, J.J. and Van den Berghe, H. (1992) Developmental changes in heparan sulfate expression: in situ detection with mAbs. *J. Cell Biol.*, **119**, 961–975.

UNPUBLISHED RESULTS

GM130 dysfunction induces centrosome defects in a HeLa cell model of Mucopolysaccharidosis type IIIB

Introduction

Mucopolysaccharidosis IIIB (MPSIIIB) is a lysosomal storage disease (LSD) caused by the deficiency of the lysosomal enzyme N-acetylglucosaminidase (NAGLU) and the subsequent accumulation of heparan sulfate oligosaccharides (HSO). It results in severe central nervous system involvement. The mechanisms involved are poorly understood. To study the link between the accumulation of HS fragments and downstream cell pathology, we previously created a HeLa cell model of the disease, in which NAGLU can be depleted in an inducible manner through the expression of specific shRNAs (Roy et al. 2011). Studies performed in this cell model provided evidence for an implication of GM130, a Golgi matrix protein associated with cis-Golgi membranes, and involved in multiple cell functions through interactions with various partner proteins (Nakamura 2010).

Interactions of GM130 with p115 form a tethering complex mediating the incorporation of pre-Golgi carriers into cis-Golgi cisternae. Interactions with GRASP65 on Golgi membranes are required for lateral fusion of Golgi cisternae and formation of elongated Golgi ribbons (Puthenveedu et al. 2006). Binding of GM130 to the A-kinase anchoring protein AKAP450 participates in the regulation of microtubule nucleation on cis-Golgi membranes and to the formation of Golgi-derived microtubule network (Rivero et al. 2009; Hurtado et al. 2011). This microtubule network is indispensable for Golgi complex assembly and maintenance (Miller et al. 2009). Through these different functions, GM130 therefore appears essential for proper organization and maintenance of the Golgi. Loss of GM130 results in shortening and fragmentation of the Golgi stacks (Puthenveedu et al. 2006; Marra et al. 2007). In addition, GM130 controls the organization of the centrosome by interacting with Tuba, a Guanine Exchange Factor (GEF) for Cdc42 (Kodani and Sutterlin 2008; Kodani et al. 2009). Depletion of GM130 blocks cell cycle progression as a consequence of centrosome multiplication (Kodani and Sutterlin 2008). Finally, through its action on the Golgi and the centrosome, and through

binding to YSK1, GM130 is needed for normal cell polarization and cell migration (Presinger et al. 2004; Matsuki et al. 2010).

In NAGLU-depleted HeLa cells, we showed that Golgi defects consisting of elongated ribbons with marked tendency to bending and important distensions were the consequence of high GM130 levels (Roy et al. 2011). Golgi alterations were associated with increased expression of AKAP450 and expansion of Golgi-derived microtubules. Morphological data suggested that abnormal lysosomes, a hallmark of LSDs were directly derived from abnormal Golgi structures as a consequence of GM130 over-expression. A possible interpretation is that GM130 interactions with AKAP450 and/or GRASP65 are increased when HSO accumulate, leading to cell defects which predominate at the Golgi and affect lysosome biogenesis, giving rise to abnormal lysosomes which are misrouted and accumulate.

The goal of this study was to determine whether other cell functions controlled by GM130 were also affected by HSO accumulation. We documented GM130-mediated control of cell cycle progression and centrosome organization following acute depletion of NAGLU in HeLa cells.

Results

To test the possibility that HSO accumulation impairs cell proliferation and mitotic activity, we monitored the growth behavior of non-depleted and NAGLU-depleted cells over a period of 28 days after tetracycline treatment (Figure 1A and B). The proliferation of HeLa cells rapidly stopped upon NAGLU-depletion. A non-proliferative state was maintained until day 21, after which augmentation of the proliferative rate coincided with selection of revertant cells recovering normal NAGLU levels. Analysis of the DNA profile of PI-labeled cells by flow cytometry showed an increased proportion of cells in the G2 peak with 4N DNA content in NAGLU-depleted cells (26 % versus 19 % in non-depleted cells, Figure 1C). Proliferation arrest

and delay at the G2-M transition were associated with an increased proportion of apoptotic cells (Figure 1D). These results suggested that NAGLU-depleted cells were unable to progress further in the cell cycle and died.

We next investigated whether alterations of cell division in NAGLU-depleted cells could have resulted from aberrant centrosomes. To address this issue, we examined centrosome morphology in mononucleated cells during interphase, using immuno-staining for the pericentriolar marker pericentrin. NAGLU-depleted cells showed supernumerary pericentrin-positive foci, as compared to non-depleted cells that contained the normal set of two to four centrioles (Figure 2A). The proportions of cells containing multiple centrosomes reached 22 % in NAGLU-depleted cells versus 7 % in non-depleted cells ($p<0.01$). Multiple centrioles were also observed by electron microscopy, indicating that alteration was not restricted to the pericentriolar matrix.

We next examined whether modifications of GM130 levels affected this phenotype. GM130 was either transiently depleted with specific siRNAs (Puthenveedu et al. 2006), or transiently over-expressed using a FLAG-tagged GM130 expression plasmid (Kodani et al. 2009). These treatments were performed 4 days after the initiation of tetracycline treatment (i.e. before the occurrence of centrosome defects) and pericentrin-positive foci were scored three days later in mononucleated cells (Figure 2B). Non-transfected cells present on the same coverslip were compared to cells that received siRNAs and did not express GM130, or to cells positive for the FLAG-tagged GM130 construct. In non-depleted cells, siRNA treatment resulted in supernumerary centrosomes (44% of GM130-negative cells versus 7% of GM130-positive cells), in agreement with previous observations (Kodani and Sütterlin, 2008). FLAG-tagged GM130 expression did not affect centrosome number and morphology. In NAGLU-depleted cells, GM130 depletion further increased the proportion of cells with multiple centrosomes (46% of GM130-negative cells versus 22% of GM130-positive cells). NAGLU-depleted cells expressing FLAG-tagged GM130 showed normal centrosome number and morphology, indicating that GM130 over-expression prevented centrosome multiplication.

As centrosome organization is known to be regulated by the interaction of GM130 with Tuba and downstream Cdc42 activation (Kodani et al. 2009), we examined the centrosome phenotype in cells expressing FLAG-tagged GM130Δ690, a truncated version of GM130 that is unable to interact with Tuba. Expression of FLAG-tagged GM130Δ690 did not prevent centrosome multiplication in NAGLU-depleted cells.

These results indicate that Tuba-mediated GM130 functions controlling centrosome organization and cell cycle progression were defective in NAGLU-depleted HeLa cells.

Discussion

Characteristic features of MPSIIIB consist in Golgi defects and accumulation of abnormal lysosomes. They were observed in different MPSIIIB cell models including MPSIIIB mouse neurons, induced pluripotent stem cells (iPSc) derived from patient fibroblasts and NAGLU-depleted HeLa cells (Vitry et al. 2010; Lemmonier et al. 2011; Roy et al. 2011). We previously showed in NAGLU-depleted HeLa cells that these phenotypic alterations were related to GM130 gain-of-function. Here, we report that other cell functions controlled by GM130 were impaired in NAGLU-depleted HeLa cells, namely organization of the centrosome and cell cycle progression. Over-expression of GM130, but not GM130 deleted of Tuba binding sites, corrected these defects, indicating that they were caused by GM130 loss-of-function. These results point to a contrasted situation between GM130 gain-of-function and loss-of-function phenotypes, possibly due to increased GM130 interactions with certain protein partners and defective interactions with others.

Interactions of GM130 with its partners

Elongation of the Golgi ribbon, as observed in NAGLU-depleted cells was highly evocative of increased GM130 interaction with GRASP65 and/or AKAP450. In these cells, GRASP65 and GM130 were expressed in storage vesicles, which presumably emanated from abnormal

Golgi structures. AKAP450 amounts were increased and Golgi-nucleated microtubules expanded, consistent with enhanced formation of GM130-AKAP450 complexes. We therefore consider a model in which increased GM130 interaction with GRASP65 on Golgi membranes and/or AKAP450 at the Golgi-microtubule interface could result in Golgi alterations and subsequent accumulation of abnormal lysosomes. This could lead to reduced amounts of GM130 available for binding Tuba, affecting GM130-mediated control of centrosome organization. A likely hypothesis is that HSO accumulating in the extracellular environment cause aberrant signaling from the cell surface, triggering GM130 mislocalization and modulating GM130 interactions with its partners.

Acute versus chronic NAGLU depletion

Cell cycle defects and centrosome multiplication have not been previously reported in chronically deficient cells such as MPSIIIB mouse neurons. Correction of centrosome defects by over-expressing GM130 in NAGLU-depleted cells indicated that alike defects shared with chronically deficient cells they were related to dysfunction of this protein and therefore not artefacts. Deficient p53 function may account for the expression of cell cycle defects in HeLa cells, which are silent in p53-positive neurons. It is also plausible that compensatory mechanisms existed in chronically deficient neurons to cope with defective GM130/Tuba interaction. For example, compensatory mechanisms could recruit other GEF(s) to activate cdc42. Adaptive mechanisms were previously observed in MPSIIIB patient iPSc in order to circumvent the blockade of fibroblasts growth factor signaling by accumulating HS (Lemonnier et al. 2011). Having in our hands a model of acute NAGLU depletion thus offers a unique opportunity to study specific pathological events triggered by HSO accumulation.

Experimental procedures

Cell culture and transfections

A stable HeLa cell line in which the expression of NAGLU can be turned off using tetracycline-inducible shRNA expression was obtained and cultured as previously described (Roy et al. 2011). We used FuGENE® 6 (Roche) for plasmid transfections, and Lipofectamine™ RNAiMAX (Invitrogen) for siRNA transfections, according to the manufacturer's instructions. All transfections were performed at day 4. GM130 RNA interference (RNAi) was done using previously described siRNA oligos, and a scrambled siRNA duplex as a negative control (Puthenveedu et al. 2006). All DNA and RNA oligos were purchased from Eurogentec. To mediate GM130 over-expression, pFLAG-GM130 and pFLAG-GM130Δ690 plasmids (kind gift from Dr. C. Sutterlin, University of California, Irvine, CA) were used. Control plasmid consisted in the empty pCMV-Tag2 backbone.

Fluorescence labeling and imaging

Cells were fixed at day 7 for 15 min with warm 4% paraformaldehyde (PFA). After blocking with DPBS, 0.01% saponin, 1% BSA, 2% NGS, cells were incubated overnight at 4°C with primary antibodies diluted in blocking buffer. Bound antibodies were revealed after one-hour incubation at room temperature with fluorescent secondary antibodies. Coverslips were mounted in FluoromountG® (SouthernBiotech). Antibodies (dilutions for immunofluorescence): rabbit polyclonal anti-pericentrin (1:1000, AbCam), rabbit polyclonal anti-FLAG (1:200, Sigma), mouse mAb IgG1 anti-FLAG (clone M2, 1:500, Sigma). Secondary antibodies conjugated to Alexafluor® 488, 555 or 647 were from Molecular Probes (Invitrogen) and Jackson ImmunoResearch Laboratories. Cells were imaged with an Axioplan 2 imaging optic microscope equipped with Apotome and AxioCam TR camera controlled by the AxioVision software (Zeiss).

Electron microscopy

Electron microscopy on ultrathin sections was performed as described (Roy et al. 2011). Samples were analyzed on a JEOL 1200EXII transmission electron microscope (JEOL) equipped with an Eloise Megaview camera controlled by analysis Pro 3.1 software (Eloise).

Cell proliferation

Cells were plated in six-well plates at 5000 per well, and cell growth was monitored over time using cell counting methods with a hemacytometer. Rates of cell proliferation were also measured using the CellTiter 96® AQueous One Solution Cell Proliferation Assay (MTS tetrazolium assay, Promega), according to the manufacturer's instructions.

Fluorescence-activated cell sorting analysis

For fluorescence-activated cell sorting (FACS) analysis of apoptosis, a Vybrant® Apoptosis Assay Kit (Molecular Probes, Invitrogen) was used according to the manufacturer's instructions. For cell cycle analysis, 1.10^6 cells were collected, washed twice in DPBS, filtered using cell strainers with 100 µm nylon mesh and fixed in 70% ethanol overnight. After centrifugation (1500 rpm for 10 min), the cell pellets were washed with DPBS, resuspended in 1 ml DPBS containing 40 µg/ml propidium iodide (PI, Invitrogen) and 100 µg/ml RNase (Roche), and incubated at room temperature for 1 h. Cells were collected on a FACSCalibur flow cytometer (BD Biosciences), using CellQuest Pro for collection and FlowJo for analysis.

Statistical Analysis

Statistics were performed using the SPSS software (SPSS).

Figures

Figure 1

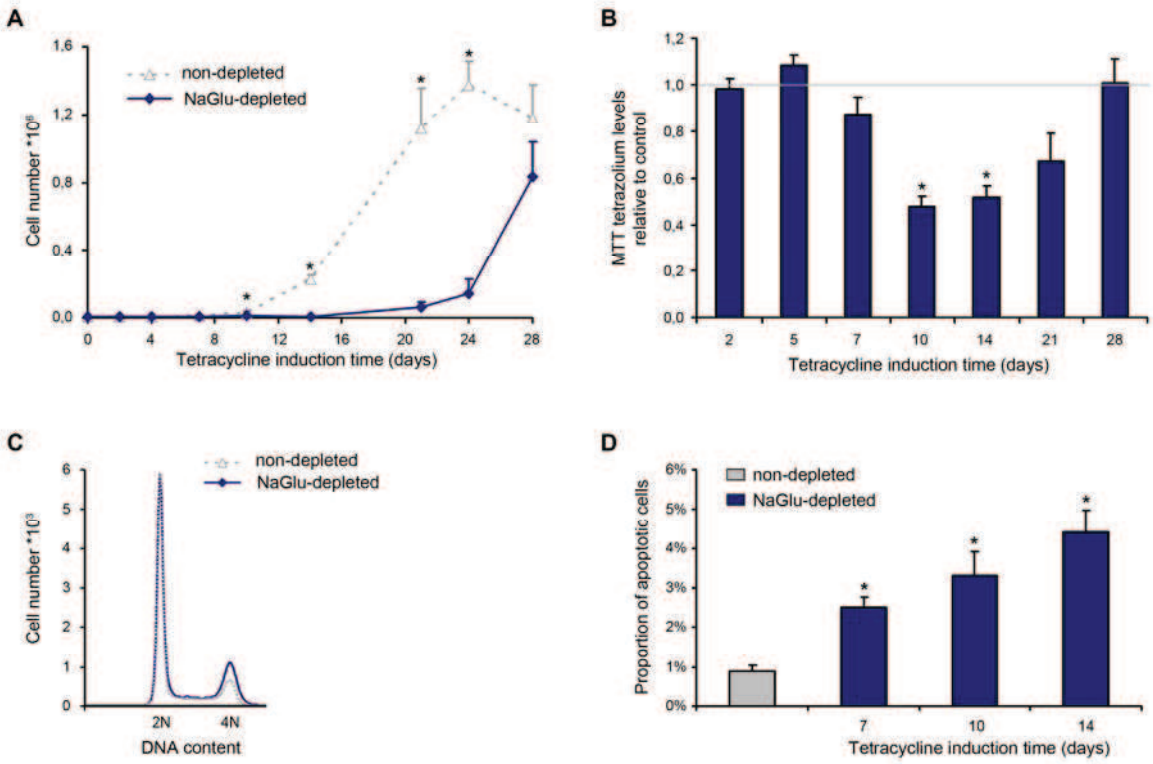

Figure 2

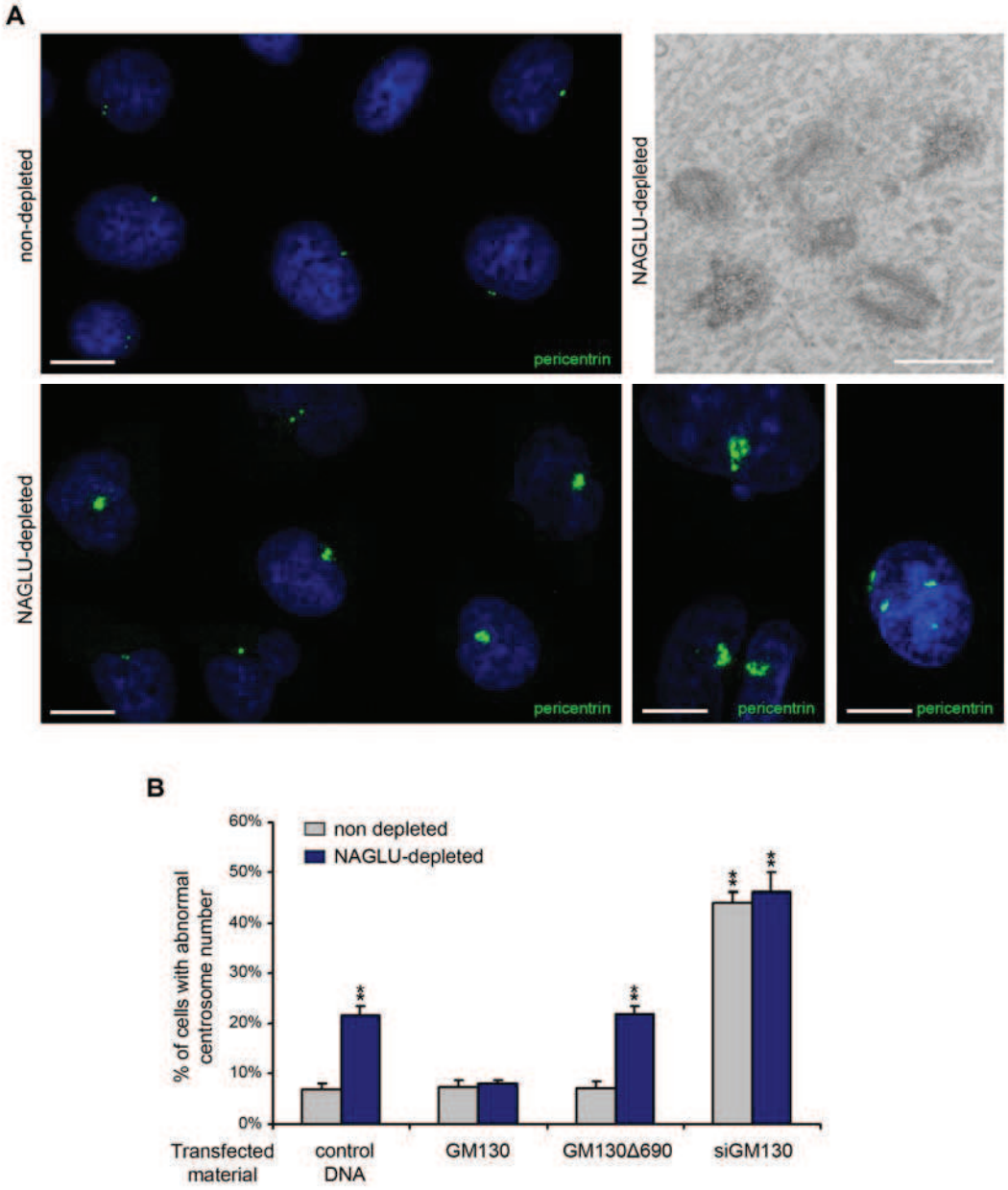
A
non-depleted
pericentrin
NAGLU-depleted
NAGLU-depleted
pericentrin
pericentrin
pericentrin
B
non depleted
NAGLU-depleted
% of cells with abnormal centrosome number
60%
50%
40%
30%
20%
10%
0%
**
**
**
**
Transfected material
control DNA
GM130
GM130Δ690
siGM130

Legends to figures

Figure 1. NAGLU-depleted HeLa cells have a centrosome phenotype that is corrected by GM130 over-expression.

(A) Non-depleted or NAGLU-depleted cells fixed at day 7 were stained with antibodies specific to the pericentriolar protein pericentrin (green). Nuclei were counterstained in blue. Confocal views of NAGLU-depleted cells (lower panel, left) showed abnormal organization and position of the centrosome, as well as multiplication of the centrosome (lower panels, middle and right). Scale bars, 10 μm. These supernumerary centrosomes were further characterized by electron microscopy on ultrathin sections (upper panel, right). Scale bar, 0.5 μm.

(B) The percentage of mononucleated cells with more than 4 pericentrin-positive foci was quantified in non-depleted and NAGLU-depleted cells at day 7. Similar quantifications were performed following expression of a FLAG-tagged GM130 DNA construct, or a FLAG-tagged truncated form of GM130 unable to interact with Tuba (GM130Δ690) DNA construct, or following GM130 depletion by specific siRNAs. Expression of FLAG-tagged DNA constructs was verified by immuno-labeling using anti-FLAG antibodies, and only cells showing a Golgi localization of the FLAG tag were scored (not shown). Loss of GM130 expression by siRNAs was verified by immuno-labeling using anti-GM130 antibodies and only cells negative for GM130 were scored (not shown). Graph values are means ± SEM from at least 150 cells scored in 3 independent experiments; **$p<0.01$ between NAGLU-depleted and non-depleted cells (Chi-square test).

Figure 2. NAGLU-depletion leads to an overall reduction in cell growth and cell cycle delay at the G2-M transition.

(A) The growth of non-depleted and NAGLU-depleted HeLa cells was monitored over a period of 28 days by cell counting methods.

(B) The kinetics of cell growth in NAGLU-depleted cells was measured using a tetrazolium-based colorimetric proliferation assay for cellular viability and metabolic activity. Results are expressed as ratios of NAGLU-depleted *versus* non-depleted cells. The baseline level in non-depleted cells is depicted by the grey line.

(C) Non-synchronized populations of control and NAGLU-depleted HeLa cells were labeled at day 7 with PI and their DNA content was analyzed by flow cytometry. A representative profile from three independent experiments is shown (>30,000 cells per profile).

(D) The rate of apoptosis in non-depleted and NAGLU-depleted cells at different time points was determined using an apoptosis assay kit based on Annexin V detection of apoptotic cells.

Values for all graphs are means ± SEM from 3 independent experiments; *$p<0.05$ between NAGLU-depleted and non-depleted cells (Mann&Whitney test).

References

Alvarez, C., Garcia-Mata, R., et al. (2001) The p115-interactive proteins GM130 and giantin participate in endoplasmic reticulum-Golgi traffic. J Biol Chem, 276, 2693-2700.

Hurtado, L., Caballero, C., et al. (2011) Disconnecting the Golgi ribbon from the centrosome prevents directional cell migration and ciliogenesis. J Cell Biol, 193, 917-933.

Kodani, A., Kristensen, I., et al. (2009) GM130-dependent control of Cdc42 activity at the Golgi regulates centrosome organization. Mol Biol Cell, 20, 1192-1200.

Kodani, A. and Sutterlin, C. (2008) The Golgi protein GM130 regulates centrosome morphology and function. Mol Biol Cell, 19, 745-753.

Lemonnier, T., Blanchard, S., et al. (2011) Modeling neuronal defects associated with a lysosomal disorder using patient-derived induced pluripotent stem cells. Hum Mol Genet.

Lowe, M., Gonatas, N.K., et al. (2000) The mitotic phosphorylation cycle of the cis-Golgi matrix protein GM130. J Cell Biol, 149, 341-356.

Marra, P., Salvatore, L., et al. (2007) The biogenesis of the Golgi ribbon: the roles of membrane input from the ER and of GM130. Mol Biol Cell, 18, 1595-1608.

Matsuki, T., Matthews, R.T., et al. (2010) Reelin and stk25 have opposing roles in neuronal polarization and dendritic Golgi deployment. Cell, 143, 826-836.

Miller, P.M., Folkmann, A.W., et al. (2009) Golgi-derived CLASP-dependent microtubules control Golgi organization and polarized trafficking in motile cells. Nat Cell Biol, 11, 1069-1080.

Nakamura, N. (2010) Emerging new roles of GM130, a cis-Golgi matrix protein, in higher order cell functions. J Pharmacol Sci, 112, 255-264.

Preisinger, C., Short, B., et al. (2004) YSK1 is activated by the Golgi matrix protein GM130 and plays a role in cell migration through its substrate 14-3-3zeta. J Cell Biol, 164, 1009-1020.

Puthenveedu, M.A., Bachert, C., et al. (2006) GM130 and GRASP65-dependent lateral cisternal fusion allows uniform Golgi-enzyme distribution. Nat Cell Biol, 8, 238-248.

Rivero, S., Cardenas, J., et al. (2009) Microtubule nucleation at the cis-side of the Golgi apparatus requires AKAP450 and GM130. EMBO J, 28, 1016-1028.

Roy, E., Buyère, J., et al (2011) GM130 gain-of-function induces cell pathology in a model of lysosomal storage disease. Submitted.

Vitry, S., Bruyere, J., et al. (2010) Storage vesicles in neurons are related to Golgi complex alterations in mucopolysaccharidosis IIIB. Am J Pathol, 177, 2984-2999.

DISCUSSION

DISCUSSION

1. RELEVANCE OF NEW MPSIIIB CELL MODELS

New human cell models of MPSIIIB have been isolated during the course of my PhD thesis training. They greatly facilitated experimentations aimed at addressing questions relevant to cell biology alterations triggered by HSO accumulation in MPSIIIB, which result in progressive mental retardation, neurodegeneration and premature death in children. These new models are based on undifferentiated iPSc derived from patient skin fibroblasts, on neural precursors and differentiated neurons derived from iPSc (Lemonnier et al., 2011), and on HeLa cells that can be deprived of NAGLU, the defective enzyme in MPSIIIB, when treated with tetracycline (Roy et al., 2011).

Success in the isolation of these different models was pointed out by the presence of cardinal features of MPSIIIB cell pathology previously observed in MPSIIIB mouse neurons (Vitry et al., 2010). These features include the primary storage of HSO, the natural substrate of NAGLU, the secondary accumulation of GM3 gangliosides, and the formation of distended intracellular vesicles decorated with the lysosomal marker LAMP1. These vesicles exhibited the typical morphology of storage vesicles accumulating in other LSDs, comprising a population of vacuoles with clear or light granular or fibrillar content, and another population containing electron dense material reminiscent of multi-lamellar inclusions, zebra bodies, or fingerprint-like patterns. Co-existence of the lysosomal marker LAMP1 and the cis-Golgi marker GM130 was detected in a fraction of intracellular storage vesicles, as previously seen in MPSIIIB mouse neurons. In MPSIIIB mouse neurons and in NAGLU-depleted cells, 15% and 18% of LAMP1-positive vesicles expressed GM130, respectively (Vitry et al., 2010; and unpublished data). The presence of GM130 in the limiting membrane of storage vesicles was accompanied by increased expression of GM130, and by alterations of the Golgi morphology evocative of GM130 dysfunction.

All these features without exception were consistently found in MPSIIIB mouse neurons, in undifferentiated patient iPSc, in their neuronal progeny, and in NAGLU-depleted HeLa cells, highlighting the relevance of these models to study MPSIIIB cell

pathology. Despite these common characteristics, our newly isolated models present cell-specific features, making them invaluable tools for investigating LSD cell pathology, as discussed below.

Previously investigated patient skin fibroblasts, or MPSIIIB mouse neurons were chronically deficient cells. These cells reveal features combining primary effects of storage product toxicity, and compensatory mechanisms activated for the protection of affected cells. Adaptive mechanisms can mask phenotypes triggered by HSO accumulation. NAGLU-depleted cells, on the contrary, represent an acute model of MPSIIIB. At early time points after induction of NAGLU inhibition, their study directly reveals toxic effects of HSO accumulation. Therefore, this cell model can allow distinction between direct consequences of HSO accumulation and compensatory mechanisms. Acute models of NPC (Schweitzer et al., 2009) or mucolipidosis IV (Miedel et al., 2008) have recently been produced in HeLa cells. Observations performed shortly after the induction of lysosomal disorders will probably shed new light on intricate cascades of pathogenic events that characterize LSDs.

An additional challenge to study neurological disorders such as LSDs is the simple fact that, for most purposes, biopsy of diseased human tissues is not an option. Studying human brain development in such disorders would require analysis of embryos, which raises ethical concerns. The emerging of iPSc provides a new approach to study both early development and disease pathology in human neurodegenerative diseases. The ESC-like properties of iPSc permit the investigation of early embryogenesis events in a culture system. Their differentiation capacity offers the opportunity to study neural and neuronal differentiation processes. Finally, the directed differentiation of iPSc can provide a source of human neurons, which can be used for electrophysiology studies or neuritogenesis assays, for example. Several groups have generated disease-specific iPSc lines form patients with neurological diseases such as Down's syndrome, Alzheimer's disease, Parkinson's disease, Huntington's disease or Amyotrophic Lateral Sclerosis (for review, see Cundiff and Anderson, 2011). Such experiments often served as a proof-of-concept of the feasibility of establishing iPSc lines. More recently, studies aimed at investigating disease-related phenotypes have started to emerge. For example, neurons derived from Rett syndrome iPSc, an X-linked autism-spectrum neurodevelopmental disorder, showed reduced spine density and altered calcium

signaling (Marchetto et al., 2010). In the group of LSDs, iPSc from mouse origin have been generated to model MPSVII (Meng et al., 2010). Interestingly, it has been shown that iPSc retain 'epigenetic memory' of the donor tissue from which they were derived at early passage (Sullivan et al., 2010). Epigenetic memory is however removed with extended passaging. Epigenetic modifications of genes do not involve change of DNA sequence, but include histone modifications, DNA methylation, and chromatin remodeling. These changes are mitotically and meiotically heritable. This information can be of special interest, since epigenetic factors have been proposed to influence phenotypic variation in LSDs (discussed in the introduction, section 2.3). Combining the iPSc technology with epigenomic profiling might provide an important tool for uncovering the role of non-coding mutations in LSDs.

2. EVIDENCE FOR ACUTE HSO TOXICITY

Examination of HeLa cells at early time-points after NAGLU depletion revealed for the first time acute toxic effects of HSO accumulation. The best evidence for acute HSO toxicity came from increased apoptosis, and rapid selection of revertant cells recovering normal NAGLU levels, which appeared as early as 14 days after tetracycline induction. Whereas chronically deficient cells such as patient fibroblasts proliferate actively, NAGLU-depleted HeLa cells stopped proliferating. Thus, compensatory mechanisms may exist to overcome growth arrest in chronically deficient cells.

The reason for growth arrest induced by acute HSO accumulation was elucidated in HeLa cells. NAGLU-depleted HeLa cells showed centrosome multiplication due to defective GM130 function and as a consequence they underwent cell death. Defective interaction of GM130 with the GEF Tuba at the centrosome, and inefficient Cdc42 activation downstream of GM130-Tuba interaction accounted for this phenotype. Only cells with normal NAGLU levels could proliferate and progressively overgrew the culture, explaining the emergence of revertant cell cultures.

Proliferation defects were also observed in newly established iPSc grown in the absence of NAGLU, suggesting that genetic reprogramming of patient fibroblasts induced by the pluripotency factors Oct4, Klf4, Sox2 and c-Myc erased the activation of compensatory mechanisms. Isolation of iPSc clones therefore encountered major

difficulties that were circumvented by the supply of exogenous NAGLU in order to eliminate HSO.

Once established and over passages, NAGLU-deficient iPSc acquired proliferation capacities when grown in the absence of exogenous NAGLU, showing that cells can rapidly develop adaptive mechanisms allowing survival and permanent growth in response to HSO accumulation. Hypothetical compensatory mechanisms could involve other GEFs recruited by GM130-independent mechanisms to activate Cdc42.

Another element that must be taken into account regarding proliferation deficits in iPSc is that the protocol for iPSc generation uses FGF2, a known ligand of HS. It is well described that HSO accumulation in the MPSIIIB mouse brain leads to impaired FGF2 signaling. Inefficient proliferation of MPSIIIB patient iPSc in response to FGF2, and restored responsiveness to FGF2 upon clearance of HSO through exogenous NAGLU supply strengthened that HSO accumulation severely impairs FGF signaling. The differentiation protocol of iPSc into neuronal progeny also makes use of FGF2. In the absence of NAGLU, differentiation of iPSc was not impaired, indicating proper responsiveness to FGF2. This result provides a second evidence for the emergence of compensatory mechanisms to cope with HSO accumulation.

Taken together, these results strongly reinforce the hypothesis that modified biological functions identified in chronically deficient MPSIIIB cells can result from adaptive processes turned on to survive HSO accumulation. Performing kinetic studies in NAGLU-depleted HeLa cells represents a means to distinguish acute toxicity from secondary compensatory events. Gene expression profiling studies were performed in these cells at an early time point after tetracycline induction, and at a late time point (unpublished results). NAGLU deficiency was associated with the modification of only 134 mRNAs (among 29 000 transcripts) at day 7 following tetracycline induction. Identified genes did not belong to networks of genes converging to the same biological pathways, which rendered interpretation difficult. We believe that a transcriptomic approach is not very meaningful at early stages of acute HSO accumulation. Whereas phenotypic changes are visible, transcriptional responses have probably not been turned on yet. Proteomic studies would possibly be more informative at this stage. In the same line, we showed that FGFR1, and FGFR2 mRNA levels, which are known to be affected in MPSIIIB (Li et al., 2002), were only slightly increased at day 7, but significantly elevated at day 14 (unpublished data). When performed after installation of cell disorders, at day 28 after tetracycline induction, gene expression profiling revealed

network of genes that are coordinately changed in expression levels. Disrupted pathways were related to cell perception to the environment, cell adhesion, regulation of developmental processes, or innate immune responses (Table 4, and discussed later in paragraph 8). Interestingly, these pathways were also disrupted in chronically deficient patient fibroblasts, and in NSCs derived from patient iPSc (Lemonnier et al., 2011), strengthening the relevance of NAGLU-depleted HeLa cells as a model of MPSIIIB.

Although cells treated with tetracycline for 28 days recovered about 25% of NAGLU activity relative to normal cells, they exhibited abnormal cell morphology (data not shown). Together with the observation of altered gene expression profiling, these data suggest that these cells are imprinted with the consequences of compensatory mechanisms developed throughout the duration of HSO accumulation. Investigating regulation of transcriptional activities in these cells may shed light on responses related to compensatory mechanisms.

Gene name		Fold change	Gene function
VCL	vinculin	-1,58	cell adhesion
CADM1	cell adhesion molecule 1	-2,12	cell adhesion
ITGA5	integrin, alpha 5	-2,74	cell adhesion
PRKCA	protein kinase C, alpha	-1,57	cell adhesion
AMIGO2	adhesion molecule with Ig-like domain 2	-2,18	cell adhesion
PXN	paxillin	-1,51	cell adhesion
PRKCA	protein kinase C, alpha	-1,57	cell adhesion
FLRT3	fibronectin leucine rich transmembrane protein 3	-2,73	ECM component
COL5A1	collagen, type V, alpha 1	-2,31	ECM component
LAMA4	laminin, alpha 4	+1,52	ECM component
C1QL1	complement component 1, q subcomponent-like 1	+1,54	innate immune response
C3	complement component 3	+3,57	innate immune response
CFD	complement factor D	+1,71	innate immune response

Table 4: Modification of gene expression profiles. Examples of genes with modified expression levels in NAGLU-depleted HeLa cells versus normal cells at day 28 are shown. Only genes belonging to networks also affected in MPSIIIB patient fibroblasts and NSCs are shown.

3. GOLGI PHENOTYPE

In MPSIIIB mouse neurons, patient iPSc clones, patient neurons, and NAGLU-depleted HeLa cells, increased GM130 immunostaining as compared to normal cells suggested increased Golgi size. In neurons from either human or mouse origin, GM130 staining frequently extended in neurites, reminiscent of the picture observed when the balance between the LKB1-YSK1-GM130 and the Reelin-Dab1 pathways was disturbed (Matsuki et al., 2010). Consistently with this aspect, ultrastructural analysis of

the Golgi morphology in NAGLU-depleted HeLa cells showed elongation of the Golgi ribbons. It was previously shown that GM130 depletion results in disconnection and fragmentation of the Golgi ribbons (Kodani and Sutterlin, 2008), whereas GM130 overexpression leads to increased length of Golgi ribbons (Marra et al., 2007). This picture suggested that GM130 gain-of-function was responsible for the Golgi phenotype.

Further ultrastructural studies in all four cell types revealed disorganization of the Golgi architecture at different levels. Disorganized morphology was characterized by loss of linearity between adjacent stacks forming the ribbon, wider cisterna forming internal bulbs and giving rise to dilated saccules, and accumulation of numerous storage vesicles in proximity, or even connected to the Golgi. These abnormalities sometimes resulted in a vesicular, fragmented aspect of the Golgi apparatus.

Contrary to neurons and NAGLU-depleted HeLa cells, Golgi expansion was not seen in iPSc. In iPSc, the predominant feature was abundant short and not well-aligned stacks with an increased density of vesicles near the ribbons. The wording "fragmentation" was used to describe Golgi phenotype in iPSc, although it clearly differs from Golgi fragmentation as it occurs during apoptosis, or in certain neurodegenerative diseases, or upon GM130 depletion. This fragmented aspect resulted from Golgi disorganization rather than from loss of lateral fusion between neighbouring cisternae. The reason for morphological differences between undifferentiated iPSc and other cell types is unclear, although it is conceivable that different cell types do not show identical phenotypes and that cell specificity is especially marked for recently re-programmed pluripotent stem cells. Contrary to neurons or NAGLU-depleted HeLa cells, iPSc proliferate widely. This proliferative state can possibly impact the Golgi phenotype, since Golgi fragmentation occurs during cell division. Continuing Golgi fragmentation may be incompatible with the formation of elongated ribbons. Amongst all tissues and cell types analyzed, the most striking Golgi defects emerged in MPSIIIB mouse brains, consistent with a link between the presence or absence of cell division and phenotype severity.

Experiments performed in the HeLa cell model confirmed that, as predicted, GM130 gain-of-function was responsible for at least part of the Golgi defects observed upon

NAGLU depletion. Abnormalities consisting in Golgi elongation, failure of stacks to align properly with respect to each other, and apposition of storage vesicles were indeed reproduced by overexpressing GM130 in normal HeLa cells. It remains unclear at this point whether GM130 overexpression is also responsible for the appearance of distended cisternae. The possibility that GM130-independent mechanisms account for this latter defect can not be ruled out.

Evaluation of the kinetics of events occurring at the Golgi level in NAGLU-depleted HeLa cells suggested that early Golgi defects consisted in elongation of Golgi ribbons and distensions of Golgi stacks. Probably due to spatial constraints, elongated Golgi ribbons ultimately exhibited marked tendency to bending, occasionally forming horseshoe-like structures, or even circular vesicular structures filled with Golgi membranes. Important distensions eventually detached from the Golgi apparatus, giving rise to clear vesicular structures. These kinetic studies suggest discrepancies between acutely versus chronically deficient cells. Elongated linear ribbons were prominent in cells depleted of NAGLU at early time points, while predominant features at later time points consisted in loss of linearity between adjacent stacks forming elongated ribbons and vesiculation of the Golgi apparatus, or of Golgi-derived elements. Although immunofluorescence microscopy clearly showed Golgi extension in neurons, electron microscopy did not reveal elongation of Golgi ribbons in these cells, perhaps due to sectioning artifact. Having all the stacks constituting the ribbon on the same section plan might be particularly difficult in conditions of complete Golgi disorganization.

Quantification of the size of the different Golgi compartments in NAGLU-depleted cells showed that the cis- and medial-Golgi were increased, in contrast to the trans-Golgi. Therefore, abnormally elongated Golgi structures and/or abnormally swollen Golgi structures such as Golgi distensions were restricted to early Golgi compartments. Consistently, structural defects in the cis- and medial-Golgi were associated with transport defects in these compartments. When COPI vesicle formation was blocked by BFA, Golgi disassembly and re-localization to ER structures was slightly delayed in MPSIIIB mouse neurons and in NAGLU-depleted HeLa cells. As disruption of Golgi stacks by BFA treatment results in the re-distribution of cis/medial-Golgi, but not trans-Gogi markers into the ER (Lippincott-Schwartz et al., 1989), this result suggests altered retrograde traffic in the cis/medial Golgi and from the Golgi to the ER. However,

abnormal organization of the Golgi did not affect overall transport in the secretory pathway. Investigations of VSV-G trafficking showed that this protein successfully exited the ER to reach the Golgi and the cell surface in cultured MPSIIIB mouse neurons, with no kinetic differences as compared to wild-type neurons (Vitry et al., 2010). In agreement with this observation, several studies showed that Golgi ribbon integrity is not critical for global protein secretion (see 7.3). In these experiments, Golgi proteins such as GM130 (Puthenveedu et al., 2006), GRASP65 (Sutterlin et al., 2005), GMAP210, or golgin160 (Yadav et al., 2009) were depleted, resulting in normal, or only slightly delayed, VSV-G trafficking.

4. ACCUMULATION OF ABNORMAL LYSOSOMES

Since co-localization between LAMP1 and GM130 was extensively and consistently found amongst different MPSIIIB cell models, and since vesicles were frequently found to surround the Golgi apparatus, we postulated that storage vesicles accumulating in MPSIIIB might have a Golgi origin. The HeLa cell model was used to address the relationship between Golgi defects induced by HSO accumulation and the emergence of LAMP1-positive storage vesicles.

The identity of LAMP1-positive storage vesicles accumulating in NAGLU-depleted HeLa cells was first defined (Roy et al., 2011). As previously observed for vesicles accumulating in MPSIIIB mouse neurons (Vitry et al., 2010), these vesicles were identified as abnormal lysosomes. They displayed markers of lysosomes, including LAMP1 in the limiting membrane and the lysosomal hydrolase IDUA in the acidic lumen, but they differed from lysosomes with respect to large size and heterogeneous content. These abnormal lysosomes were formed in the absence of autophagy defects, and they did not express markers of early or late endosomes. In particular, they did not acquire M6PR, which is expressed in late endosomes.

Ultrastructural studies on NAGLU-depleted cells led to the introduction of new mechanistic models for the formation of abnormal lysosomes. As mentioned above, they revealed Golgi defects with prominent vesiculation of the Golgi apparatus, or of Golgi-derived elements. Whereas vesicles emanating from Golgi circularization contained densely packed stacks of membranes and were reminiscent of multi-lamellar inclusions, zebra bodies, or fingerprint-like patterns, vesicles emanating from Golgi

distensions were reminiscent of vacuoles with clear content. Therefore, it can be postulated from a morphological point of view that the two populations of vesicles typically observed in MPSIIIB are derived from the Golgi compartment.

Interestingly, enhanced genesis of storage vesicles with characteristics of abnormal lysosomes could be reproduced by overexpressing GM130 in normal HeLa cells, indicating that this phenomenon was a consequence of GM130 overexpression in NAGLU-depleted cells. Depleting GM130 prevented the genesis of these vesicles.

In agreement with the notion that storage vesicles originate from abnormal Golgi structures, which are derived from early Golgi compartments, we showed in MPSIIIB mouse neurons and/or in NAGLU-depleted HeLa cells that LAMP1-positive vesicles expressed pre-Golgi and cis-Golgi markers including COPII, GM130 and GRASP65 but did not express the trans-Golgi marker golgin97 (Roy et al., 2011; Vitry et al., 2010). Consistently, absence of endosomal markers indicated that abnormally formed vesicles did not transit through the trans-Golgi. Storage vesicles were therefore identified as pre-lysosomes, defined as cis- and medial-Golgi domains enriched in lysosomal proteins and destined to lysosome biogenesis, which were misrouted before they reach the trans-Golgi. Possible consequences on protein sorting and glycosylation are discussed below.

It can be postulated that proteins contained in misrouted pre-lysosomes were almost fully glycosylated by cis- and medial-Golgi resident enzymes, but missed late modifications such as sialylation, which take place in the trans-Golgi (Harduin-Lepers et al., 2005). In agreement with this assumption, it was shown that, as in wild-type neurons, oligosaccharide chains born on IDUA molecules produced in MPSIIIB mouse neurons underwent trimming by the medial Golgi resident Mannosidase II (Vitry et al.,2010). Sialylation was not tested.

Because the TGN is a crucial sorting station, inability of lysosomal proteins to reach the TGN could have important consequences. For instance, the targeting signal of the YXXΦ type contained in the cytosolic tail of LAMP1 could not be recognized normally by AP adaptors and packed in clathrin-coated vesicles at TGN exit sites (van Meel and Klumperman, 2008). Similarly, IDUA tagged with GFP could not properly interact with M6PR located at the membrane of clathrin-coated vesicles budding from the TGN (Ghosh et al., 2003). As lysosomal proteins presumably missed cell machinery components directing their targeting and fusion with the endo-lysosomal system, they

accumulated in vesicular structures representing a dead-end storage compartment that cells are unable to eliminate.

Thus, the HeLa cell model of acute HSO depletion shed light on the mechanisms responsible for the generation of storage vesicles. As these mechanisms rely on early events occurring at the Golgi level, they could not be studied in chronically deficient cells. The utility of the HeLa cell model was further justified by the need to perform transfection experiments for GM130 overexpression or depletion.

The mechanistic model raised here may somehow appear paradoxical. How such widespread Golgi alterations could have effects which are mainly limited to lysosome progenitors? We focused our investigations on lysosomal markers, and therefore observed defects associated with lysosomogenesis. This approach obviously introduced a methodological bias. A search for distended vesicles that would not express lysosomal markers was not performed. Indeed, all Golgi markers used in our studies were components of the Golgi matrix. A systematic examination of Golgi transmembrane proteins could reveal distensions devoid of lysosomal markers. The Golgi membrane protein 1 (GOLM1), a transmembrane protein residing in the cis and medial-Golgi cisternae, represents a good candidate marker for such investigations (Hu et al., 2011). Expression of GOLM1 mRNAs was indeed found upregulated in fibroblasts and NSCs from MPSIIIB patients (Lemonnier et al., 2011). If the hypothesis of global sorting defects is true, such experiments will detect populations of swollen vesicles in MPSIIIB cells, which are derived from the Golgi, and which are LAMP1-negative. These vesicles could contain different classes of glycoproteins and glycolipids which escaped the Golgi before terminal glycosylation steps. Terminal sialic acids have an outstanding impact on the stability of glycoproteins. They ensure longer half-life, and they influence parameters such as thermal stability or resistance to proteolytic degradation (Bork et al., 2009). Augmenting sialylation represents an approach to improve efficacy of therapeutic recombinant glycoproteins such as erythropoietin or blood coagulation factors. It is therefore conceivable that accentuated clearance of synaptophysin, as seen in MPSIIIB mouse brains (Vitry et al., 2009), is a result of deficient sialylation. The impact of defective glycosylation on physiological functions and developmental processes is undeniable. Human disorders linked to defects in Golgi glycosylation have been identified. They belong to the rare genetic disease family called congenital disorders of glycosylation (CDGs) (Ungar, 2009). Amongst them, CDG type IId is

caused by mutations in β-1,4-galactosyltransferase, a trans-Golgi resident enzyme (Nilsson et al., 1991). It results in loss of terminal galactose and sialic acid residues (Hansske et al., 2002). Key clinical phenotypes manifest as severe neurological disorders, hydrocephalus, myopathy and blood clotting defects. Considering the importance of full glycoprotein and glycolipid maturation through the Golgi, it should certainly be examined whether late glycosylation steps are impeded in MPSIIIB cells.

5. LIPID ACCUMULATION

In MPSIIIB mouse neurons and in NAGLU-depleted HeLa cells, LAMP1-positive storage vesicles rarely co-localized with HS or GM3. However, LAMP1-positive vesicles on the one hand, and GM3-positive vesicles on the other hand consistently co-localized with GM130. In NAGLU-depleted cells, large GM3-positive vesicles often sequestered GM130, suggesting that GM3 accumulation was due to defects in the ganglioside biosynthetic pathway. As GM3 is the first ganglioside produced in the cis- and medial-Golgi (Maccioni, 2007; Tettamanti, 2004; van Echten et al., 1990), vesicles enriched in GM3 could be misrouted due to defects in early Golgi compartments and stored. Vesicles enriched in GM3 and vesicles with clusters of lysosomal enzymes are expected to be generated at spatially distinct sites of the Golgi, as shown by the spatial association of enzymes cooperating in the ganglioside biosynthetic pathway (de Graffenried and Bertozzi, 2004). This would explain that albeit they formed through similar mechanisms, LAMP1-positive vesicles and GM3-positive vesicles are distinct from one another.

GM2 is mainly produced in a Golgi compartment which is presumably not altered in MPSIIIB, the trans-Golgi (Young et al., 1990). The hypothesis that ganglioside accumulation in MPSIIIB arises as a consequence of sorting defects in early Golgi compartments is therefore in agreement with the observation that GM2 overload is minimal, as compared to marked GM3 overload. In MPSIIIB mouse brains, GM3 levels were 4-fold higher, compared to normal brains, whereas GM2 levels increased only 2-fold (Cressant et al., 2004). In MPSIIIB dog brains, GM3 and GM2 levels increased 4-fold and 3-fold, respectively (Ellinwood et al., 2011). Although synthesis of GM3 from LacCer peaks in the proximal Golgi, whereas synthesis of GM2 from GM3 precursors

peaks in the distal Golgi, co-localization was observed between the two enzymes catalizing these steps (Maxzud et al., 1995). This suggests that GM2 synthesis is not restricted to distal Golgi compartment, but can also occur in more proximal Golgi compartments. This point explains how sorting defects in early Golgi compartments could also affect GM2 gangliosides.

Defect in GM2 degradation rather than defect in the GM2 biosynthetic pathway represents another possibility, and would explain that GM2 and GM3 accumulate in separate populations of vesicles (McGlynn et al., 2004). Potential mechanisms that may account for deficient GM2 degradation remain to be identified. The possibility that GAGs accumulating within the lysosome could inhibit the lysosomal enzyme involved in GM2 degradation, namely β-hexosaminidase, is unlikely. Indeed, previous reports showed that commercial GAGs do not inhibit this enzyme (Kint and Huys, 1973).

Cholesterol represents another class of lipids which accumulate in MPSIIIB. The strong regional correlation observed between cholesterol and GM3 storage in brains of mice with MPSIIIB (McGlynn et al., 2004) suggests that the mechanisms causing accumulation of these substrates are related. Intracellular distributions of cholesterol and sphingolipids are tightly linked. Both classes of lipids are associated within membrane lipid rafts, which are first assembled in the Golgi (Brown and London, 1998). It was shown that sphingolipids display a high affinity for cholesterol, which results from the structure and the molecular properties of these two lipids (Boggs, 1987). Whereas sphingolipids are synthesized on the luminal surface of the Golgi, cholesterol biosynthesis occurs on the ER. From the preferential interaction between cholesterol and sphingolipids, it was speculated that sphingolipid synthesis in the Golgi acts as a sink for ER-synthesized cholesterol (Holthuis et al., 2001). Sorting of sphingolipids could be the driving force for sorting of cholesterol in the Golgi and further out along the exocytic pathway. According to this view, it is not surprising that sorting defects in the Golgi affect gangliosides and cholesterol at the same time.

6. STORAGE PROBLEMS

According to the hypothesis of global lysosome malfunctioning, storage lesions in LSDs are traditionally viewed as deficient hybrid vesicles, resulting from the fusion of

lysosomes with late endosome, amphisomes or autophagosomes (Fares and Greenwald, 2001; Luzio et al., 2003). Hybrid vesicles are loaded with materials meant for degradation. In LSDs, these vesicles swell, accumulate and proliferate because they are unable to recycle materials contained in their lumen. Storage products are entrapped in storage vesicles, and start to accumulate outside storage vesicles and outside cells. This view appears to be insufficient with regard to our current knowledge of the formation of storage lesions in MPSIIIB (see review in Appendix). We now provided strong evidence that although they contain lysosomal proteins, storage lesions are not lysosomes. As a matter of fact, storage lesions are not connected to the endocytosis or autophagy pathways, but they are likely derived from the Golgi (Vitry et al., 2010; Roy et al., 2011). These results inspire a more open and heterodox vision of LSDs. Are lysosomal diseases Golgi diseases? Such a model should not only be considered in the case of MPSIIIB, but may be extended to other LSDs and offers interesting options for future investigations in the field of LSDs.

In addition, it comes out from these studies that the relationship between storage products and storage lesions, the two main characteristics of LSDs, is not that simple. Primary and secondary storage products, i.e. HS on the one hand, and GM3 gangliosides, scMAS or ubiquitin on the other hand, were not associated with storage vesicles in MPSIIIB mouse neurons, and in NAGLU-depleted cells. Again, the hypothesis of global lysosome malfunctioning could not account for this observation. Further investigations will be required to provide links between storage products and storage lesions. We obtained some indications in fibroblasts or NSCs from MPSIIIB patients that extracellular accumulation of primary storage products may trigger aberrant signaling cascades inside cells, which might be at the origin of Golgi defects and accumulation of storage vesicles (discussed later in paragraphs 8 and 9).

According to our new model, it appears that the term “storage vesicles” is inappropriate to designate vesicles which do not accumulate storage products. The term “abnormal lysosome” would be more accurate to designate vesicles which contain lysosomal proteins, but which differ from normal lysosomes.

Dynamic exploration of endocytosis and macroautophagy in MPSIIIB mouse neurons revealed that these pathways were not affected (Vitry et al., 2010). Material

internalization via non-specific fluid phase endocytosis on the one hand, and turnover of long-lived proteins on the other hand, were not impaired. These observations suggest that endosomes and autophagosomes are able to fuse normally with lysosomes. Abnormal lysosomes likely co-exist with functional lysosomes which maturated normally. These normal lysosomes are able to fuse with endosomes and autophagosomes and to carry out degradative functions, contrary to abnormal lysosomes. Consistently, electron microscopy studies revealed the presence of lysosomes presenting normal ultrastructural features in various MPSIIIB cell models and in MPSIIIB mouse brains (unpublished data).

Whereas pools of abnormal lysosomes do not accumulate HSO, pools of functional lysosomes most probably accumulate HSO. It is possible that cells developed mechanisms allowing them to eliminate these lysosomes loaded with undegraded or partially degraded HSO. Indeed, we observed increased lysosomal exocytosis in NAGLU-depleted HeLa cells, as compared with non-depleted cells, characterized by redistribution of LAMP1 to the plasma membrane (unpublished data). Because abnormal lysosomes are immobile (Vitry et al., 2010), we assume that normal lysosomes only can undergo lysosomal exocytosis, as they do in non-affected cells (Rodriguez et al., 1997). This mechanism might represent a compensatory mechanism more actively recruited than in normal cells in order to promote cellular HSO clearance. It would result in increased HSO amounts delivered in the cell environment. Such regulatory mechanisms could involve the transcription factor EB (TFEB). Previous studies showed that TFEB signaling pathway, which regulates lysosome biogenesis, is activated in a number of LSDs (Sardiello et al., 2009). Further studies also showed that TFEB does not only regulate lysosomal biogenesis, but also lysosomal exocytosis (Medina et al., 2011). In pathological conditions, in which the lysosomal degradative capacity of cells is compromised such as LSDs, TFEB activation could serve degradation needs by enhancing lysosomal proliferation, and it could increase cellular clearance of lysosomal substrates by enhancing lysosomal exocytosis. Such activation could be part of compensatory responses, which are activated to protect the cell from the accumulation of lysosomal substrates. However, albeit a therapeutic strategy based on TFEB overexpression would allow cellular clearance of primary storage products by enhancing exocytosis of normal lysosomes, it is unlikely that abnormal lysosomes, which are immobile, would be eliminated from MPSIIIB cells using such strategy.

7. IMPAIRED GM130 FUNCTIONS

Considering the extent of Golgi alterations, many Golgi matrix proteins are probably affected in MPSIIIB cells. We however focused our investigations on a target matrix protein, GM130, because this protein has been widely analyzed in the literature and plays a central role in the control of Golgi organization (Marra et al., 2007; Puthenveedu et al., 2006). It is the only Golgi protein described so far with such multiple and complex functions, some of which are crucial to neuronal function. Defect in GM130-mediated control of polarity and directed migration, for instance, would be relevant to the neurological manifestations characterizing MPSIIIB. In addition, detection of GM130 in storage vesicles accumulating in various MPSIIIB cell models point to this protein as a possible molecular target for HSO toxicity. GM130 controls Golgi structure, cytoskeleton organization and centrosome organization through interactions with different partner proteins including GRASP65, p115, AKAP450 and Tuba (Nakamura, 2010). These functions were assessed in NAGLU-depleted HeLa cells. They were all affected. Whereas centrosome multiplication and cell cycle arrest were reminiscent of GM130 loss-of-function (Kodani and Sutterlin, 2008), Golgi extension and enhanced nucleation of Golgi-derived microtubules were evocative of GM130 gain-of-function (Puthenveedu et al., 2006; Rivero et al., 2009). Enhanced recruitment of GM130 on Golgi membranes and increased interaction with GRASP65 or p115 at this location, and/or enhanced recruitment of GM130 and increased interaction with AKAP450 at the Golgi-microtubule interface may result in decreased pools of GM130 available at the centrosome for interaction with Tuba. Subcellular analysis of GM130 abundance and localization revealed that GM130 levels might be increased in the cytoskeleton, although this result is still preliminary (data not shown). The levels of Golgi-localized AKAP450 were found up-regulated. Consistently, acetylated, Golgi-nucleated microtubules were expanded. These results suggest increased GM130 interaction with AKAP450 and increased microtubule nucleation at the cis-Golgi through GM130-AKAP450 complexes. As a result, expansion of both the tangential microtubule network linking Golgi stacks, and of the asymmetric microtubule network extending toward the cell leading edge presumably occurs (Kodani and Sutterlin, 2009). Expansion of the former microtubule subset would account for the Golgi phenotype consisting of increased Golgi size and Golgi extension into neuron prolongations. Expansion of the latter microtubule subset would disturb cytoskeletal dynamics.

However, directionality of post-Golgi trafficking would apparently be unaffected, since Golgi-nucleated microtubules still extend in a single direction toward cell edge in NAGLU-depleted cells. Directional post-Golgi trafficking driven by Golgi-derived microtubules is indispensable for polarized cell motility. Removal of Golgi-derived microtubules results in randomized migration patterns (Miller et al., 2009). In such context of elevated levels of Golgi-nucleated microtubules, cell migration may be delayed, but directionality is likely preserved. Although prelimirary, our recent results are consistent with this view.

Other cell defects induced by GM130 dysfunction can potentially be at the origin of cell polarization defects, subsequently leading to migration defects. In NAGLU-depleted cells, the Golgi was less dynamic, as indicated by increased resistance to BFA-induced fragmentation, and the centrosome number and positioning was impaired. As proper alignment of the centrosome and Golgi, remodeling of the Golgi complex, and potential integrity of the Golgi ribbon are essential for cell polarity, this process was likely impeded (Bisel et al., 2008; Hurtado et al., 2011; Yadav et al., 2009). As a consequence, cell migration may be blocked, or delayed. MPSIIIB mouse astrocytes and NSCs derived from the MPSIIIB mouse model, or from iPSc, are more appropriate than HeLa cells to investigate such defects.

This context of defective proliferation, polarization and migration may have consequences on behavior of NSCs and neuritogenesis, possibly relevant to the loss of brain plasticity observed in MPSIIIB. Neurogenesis requires NSC proliferation and motility, neuron specification, and migration of new neurons to become incorporated into the functional circuitry of the brain (Ming and Song, 2005). Neuritogenesis, the first step of neuronal differentiation, takes place soon after mitosis, as the first neurite emerges opposite from the plane of the last mitotic division. This process requires centrosome and Golgi polarization close to the area where the first neurite develops (de Anda et al., 2005). The axon consistently arises from this neurite. Neuritogenesis follows with the elaboration of multiple neurites that subsequently become dendrites, neurite elongation and retraction. Elaboration of the dendritic tree necessitates Golgi extension into dendrites (Ye et al., 2007). Neurogenesis and neuritogenesis are crucial in developing organisms for the establishment of neuronal connections in the CNS, but also later in life, enabling remodeling of neuronal circuits in order to adapt to environmental changes (Duffau, 2006; Ming and Song, 2011). Ongoing neurogenesis

and neuritogenesis underlie neuronal plasticity, influencing learning and memory throughout life.

Problems related to neurogenesis and neuritogenesis were indeed observed in the MPSIIIB mouse model. Neurogenesis defects consisted in reduced capacity of NSCs to proliferate in MPSIIIB mouse brains (Li et al., 2002). Neuritogenesis defects in MPSIIIB mouse neurons consisted in more frequent neurite elongation and branching and less frequent neurite retraction, resulting in a relative overgrowth of neuritic trees (Hocquemiller et al., 2010). Evidence for a direct link between GM130 dysfunction on the one hand, and defective neurogenesis and neuritogenesis on the other hand, remains to be established.

8. IDENTIFICATION OF NEW MOLECULAR TARGETS

Gene expression profiling studies comparing fibroblasts or NSCs from patients and non-affected individuals revealed new molecular targets for future investigations (Lemonnier et al., 2011). Genes with modified expression overlapped between the two cell types. They pointed to modifications of ECM constituents such as laminin, fibronectin or collagen, surface receptors involved in cell adhesion to the ECM such as integrins and FGFRs, growth factors (e.g. FGFs), morphogens (e.g. components of the wnt pathway), and molecules involved in cell sensing of environmental cues (e.g. Slit, Semaphorins and Ephrins). Many of the cell surface proteins pointed by transcriptome analysis are known HS ligands. This suggests that HSO accumulating in MPSIIIB cells are excreted in the cell environment where they interact with ECM constituents and ECM-bound ligands, modifying the bioavailability of multiple signaling molecules, and inducing regulatory mechanisms with consequences on expression levels of ECM proteins. Direct evidence for a biological effect of extracellular HSO had already been obtained in an experimental setting where HSO purified from MPSIIIB samples added onto microglial cell cultures were able to activate these cells (Ausseil et al., 2008).

Pathways responsible for transducing signals inside the cell downstream of the identified cell surface proteins were also affected. For example downstream effectors in the FGF/FGFR activation pathways including several MAPK were down-regulated, in agreement with MAPK dysregulation reported at the early stage of MPSIIIB brain disease (Cecere et al., 2011). Actors of the cascade responsible for focal adhesion

formation and Rho GTPases activation downstream of integrin signaling were also affected. They include proteins that directly interact with the integrin cytoplasmic tail like calpain or protein kinase C-beta, the focal adhesion constituents tensin and parvin, and proteins recruited at focal adhesions such as Rho-GAPs, Rho-GEFs and Cdc42 effector proteins. Defects in these two signal transduction pathways can have consequences on cell-matrix interaction, cell adhesion, cell polarization, cell migration, cell growth or cell differentiation (Hotchin and Hall, 1996; Rubinfeld and Seger, 2005; and see introduction, paragraph 6.7).

Gene expression profiles did not only reveal the consequences of HSO accumulation in the extracellular environment. They also indicated that excreted HSO may have modified sulfation patterns. Three sulfotransferases modulating the density and type of sulfation within HS chains were indeed down-regulated (2-*O*; 6-*O* and 3-*O* sulfotransferases), suggesting modified profiles of ligand sensitivities. In addition to altered sulfation of saccharide chains, the synthesis and degradation of proteoglycans may be affected, as shown by reduced expression of genes coding for glypicans and hyaluronans, and increased levels of chondroitin sulfate proteoglycan mRNAs.

Taken together, these data indicate that accumulation of HSO in the extracellular environment and modifications of the 'saccharide code' carried by their oligosaccharide chains may modify cell perception of environmental cues. Modifications of the ECM environment, either ECM-bound ligands or ECM constituents themselves, may modify cell-matrix interactions. In the CNS, downstream cascades of pathological consequences can manifest as defects in NSC proliferation and migration, neuron polarization, neurite outgrowth and the growth and guidance of axons. Considering the importance of these functions in the control of CNS development and plasticity, important damages may occur in the brain of MPSIIIB children. Interestingly, milder expression of the Golgi phenotype and the rare presence of storage vacuoles in floating MPSIIIB neurospheres may result from less stringent dependence of non-adherent cells on matrix-bound cues, compared with adherent iPSc or differentiating neural cells (Lemonnier et al., 2011).

Perturbations in the different pathways highlighted here were also found in NAGLU-depleted cells analyzed at a late time point, presumably after compensatory

mechanisms have emerged (see section 2). It can be suggested that actors in these pathways are regulated in response to chronic HSO accumulation, whereas they remain unaffected at early stage after acute enzyme depletion.

9. LINK BETWEEN HSO ACCUMULATION AND CELL PATHOLOGY

Two hypotheses can be considered to account for HSO-induced cellular alterations in MPSIIIB, including Golgi alterations, GM130 dysfunction, defective lysosome biogenesis and ganglioside accumulation.

1) Enormous increase of HSO local concentration in intracellular compartments and especially in the Golgi may impair protein and lipid sorting in this organelle. Lectin transporters, defined as non-enzymatic, sugar binding proteins, are essential players in this process (Hauri et al., 2000). One example is the M6PR which interacts with mannose-rich oligosaccharide chains on lysosomal hydrolases (Dahms and Hancock, 2002). A plausible hypothesis would be that HSO accumulating in the Golgi lumen competed for glycoprotein-lectin or glycolipid-lectin interaction. However in our experimental conditions, we did not find evidence for HSO accumulation in the Golgi, but in intracellular structures distinct from the Golgi. The epitope specificity of the antibody used for these experiments may not allow exhaustive detection of all HSO species generated in MPSIIIB. Indeed, monoclonal anti-HS antibodies recognize distinct HS species and show different patterns of immunoreactivity (van den Born et al., 2005). The sensitivity of the antibody could also be too low to detect HS accumulation in Golgi.

2) Development of cell pathology in MPSIIIB may be triggered by HSO secreted in the extracellular environment. This hypothesis is supported by immunostaining with anti-HS antibodies in NAGLU-depleted cells and in iPSc, showing increased reactivity at the cell-substratum interface. Data from gene expression studies in patient fibroblasts or NSCs reinforce the importance of extracellular HSO accumulation. Augmentation of GM130 mRNA levels in NAGLU-depleted cells strongly suggests regulation of GM130 gene expression by extracellular signals. Further investigations will be required to elucidate molecular mechanisms recruited by HSO accumulating in the ECM, which affect GM130 and Golgi functions. These mechanisms could involve the ERK pathway,

which receives inputs from both soluble growth factors and extracellular matrix proteins through specific cell surface receptors, and which is also involved in Golgi remodeling.

10. IMPLICATIONS FOR TREATMENTS

In the embryo, the neural plate forms the neural tube which subsequently becomes the CNS. Neurons are initially produced along the central canal in the neural tube. These neurons then migrate from their birthplace to their final destination, where they differentiate and integrate into the brain circuitry. Two general modes of migration are distinguished during brain development: radial migration, and tangential migration (Marin and Rubenstein, 2003). In radial migration, neurons migrate from the progenitor zone toward the surface of the brain following the radial disposition of the neural tube. Radial migration establishes the general cytoarchitectonical framework of the different brain subdivisions. In the cerebral cortex, it is responsible for assembly into six layers with distinct patterns of connectivity (Rakic, 1988). In tangential migration, cells migrate orthogonal to the direction of radial migration. Tangential migration increases the cellular complexity of brain circuits by allowing the dispersion of multiple neuronal types. Neurons that eventually become pyramidal or glutamatergic neurons tend to migrate radially, whereas GABA (γ-aminobutyric acid)-containing interneurons migrate tangentially (Ghashghaei et al., 2007). Appropriate migration of neurons during development is therefore essential to achieve proper brain architecture, and to build functional synaptic circuitry in the brain.

In children suffering MPSIIIB pre-natal development is presumably normal. Some reports are indicative of BBB permeability to M6P-bearing molecules until birth in mice (Urayama et al., 2004). This suggests that NAGLU can cross both the materno-fetal placental barrier and the BBB, and can be supplied to the fetus by the mother. Consistently, examination of MPSIIIB mouse brains showed normal development of cortical layers and absence of cortical atrophy (Vitry et al., 2009). This result suggests that neurogenesis, neuronal proliferation, and radial migration of neurons might occur normally before birth. However, the possibility can not be ruled out that more subtle defects in tangential migration occurred, with consequences on functionality of the brain circuitry. In a teratoma formation assay, patient iPSc were able to differentiate normally and form the three embryonic germ layers upon NAGLU complementation by recipient

mice (Lemonnier et al., 2011). What happens in absence of NAGLU supply? Formation of embryoid bodies, and subsequent differentiation into the three germ layers was not impaired, neither was differentiation of iPSc into neural progenitors and neurons. The accuracy of these in vitro investigations is however obviously insufficient to detect subtle deviations from normal differentiation pattern, as they may occur during development in vivo.

Although the bulk of neuronal migration occurs during the embryonic period, neurons can also migrate to some extent during early post-natal periods (Ghashghaei et al., 2007). This phenomenon principally concerns tangential migration rather than radial migration (Luskin, 1993; Menezes et al., 2002). Other post-natal developmental processes include synaptogenesis, synaptic pruning, changes in neurotransmitter sensitivity, and dendritic and axonal growth (Webb et al., 2001). Persistence of developmental processes is essential for completition of the functional circuitry of the brain. It underlies important functions including cognitive functions. Disturbances in post-natal cortical development may be relevant to neuropsychiatric disorders such as autism and schizophrenia (Adriani and Laviola, 2004; Lewis et al., 2004).

Our studies in newly isolated MPSIIIB cell models including HeLa cells, iPSc and iPSc-derived neurons showed immediate onset of cell pathology in the absence of NAGLU. These observations suggest that in MPSIIIB children, cellular damages might appear soon after birth, affecting functions such as cell migration that are crucial for CNS development. Even though MPSIIIB is generally not considered a developmental disease, these results, as well as observations made in MPSIIIB patients or animal models, are indicative of early post-natal developmental defects. Reduced neurogenesis started as early as 1 month of age in MPSIIIB mouse brains (Li et al., 2002). In MPSIII children, skill acquisition was impaired at early stages of the disease. Evaluation of the acquisition of early language showed that only 43% acquired the capacity of associating two words before the age of 3 years (Heron et al., 2011). In normal children, changes in neuronal circuitry become increasingly intricate with age to support acquisition of complex skills. Onset of clinical symptoms in MPSIII children, around the age of 2 to 6 years (Neufeld and Muenzer, 2001), coincides with acquisition of complex skills. In addition, HSO levels in affected patients are believed to increase progressively with age, aggravating disease clinical expression.

In MPSIIIB children, a several-years period of progressively aggravating behavioral and cognitive disorders is followed by neurodegeneration, which is a late-onset event (after the age of 7-9 years). When administered at the age of diagnosis, around the age of 4 years, gene therapy treatments will likely halt the neurodegenerative process, as indicated by the normalization of biochemical and histological markers of the disease in the brain of treated animals (Cressant et al., 2004: Ellinwood et al., 2011). However, efficacy with regards to mental retardation may be of concern if developmental damages occur in the early post-natal period, and pre-exist treatment. Plasticity of the brain is maximal in the first two years of life, and continues at reduced rates throughout life (Mundkur, 2005). When administered after the critical period of 2 years, gene therapy treatment will likely stop disease progression, but it will hardly reverse pre-existing developmental damage. Reduction of HS burden very early in life, by the age of 2 years, is presumably the best situation for clinical success. Therefore, the efficacy of gene therapy strategies may rely upon early detection and treatment, prior to symptom onset. Although pre-symptomatic diagnosis raises a number of ethical, economical and technical issues, consideration should be given to expanding newborn screening to include MPSIII once therapy is clinically available (Meikle et al., 2004).

CONCLUSIONS AND PERSPECTIVES

CONCLUSIONS AND PERSPECTIVES

1. CURRENT MODEL

From the data obtained in the present studies, it can be assumed that the development of neuropathology in MPSIIIB is triggered by HSO bound to the ECM, which modifies cell perception of environmental cues (Figure 29). Activation of integrins, responses to growth factors and morphogens, as well as the integration of multiple extracellular signals can be subsequently altered, leading to modified gene expression. Modified expression of genes involved in ECM constitution, in addition to HSO binding to abnormally constituted ECM, would induce a vicious circle perpetuating abnormal cell sensing of the environment. Alterations of cell responses to extracellular signals can have multiple deleterious consequences including on cell adhesion, cell polarization, cell migration, cell growth or cell differentiation.

Our studies shed light on intracellular events occurring in MPSIIIB cells. Defective control of GM130 functions appears as a central event in these cells. A likely hypothesis is that this protein is mislocalized and unable to properly interact with its multiple partners. We showed that GM130 dysfunction is responsible for the biogenesis of abnormal lysosomes and the accumulation of GM3 gangliosides, two fundamental features of MPSIIIB cell pathology. It is at the origin of alterations of the Golgi, centrosome and cytoskeleton, with possible consequences on cell division, polarization, differentiation or migration.

Although the intracellular consequences of GM130 dysfunction have been unraveled, and the importance of aberrant signaling from the cell surface uncovered, the relationship between extracellular and intracellular modifications remain to be determined. Such investigations are rendered difficult by the fact that molecular mechanisms controlling GM130 localization, interactions with partners and functions in normal cells are currently unknown.

Interestingly, pathways controlled by ECM-bound HSO on the one hand, and by GM130 on the other hand converge to the same cellular functions, suggesting that they are tightly linked. In the CNS, alteration of these functions may cause abnormal neurogenesis, defective neurite retraction, and ectopic dendritogenesis, leading to mental retardation and neurodegeneration.

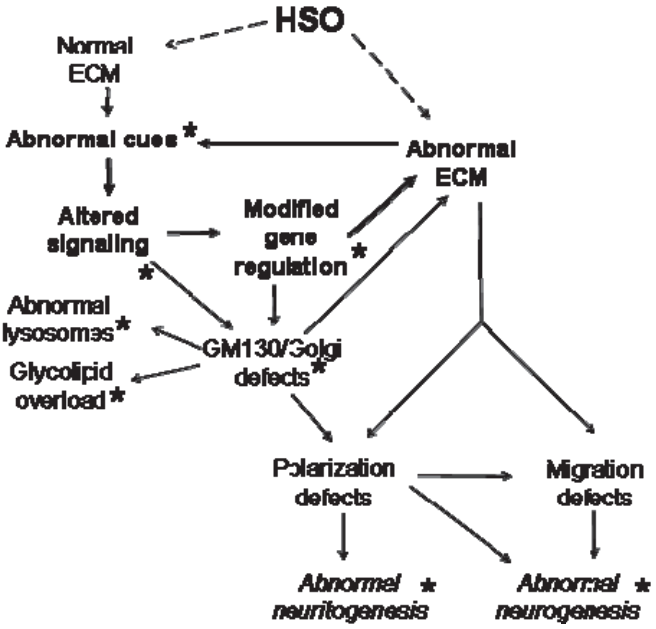

Figure 29: Current view of the pathophysiological cascades in MPSIIIB. Dashed arrows indicate HSO binding to the ECM. Arrows indicate possible downstream effects. A vicious circle perpetuating abnormal cell sensing of the environment is shown in bold. Asterisks indicate experimental observations supporting the effect. Other effects are hypothetical.

2. WORKING HYPOTHESIS

Integrin signaling is highly coordinated with growth factor signaling. General mechanisms underlying cross-talk between integrins and growth factor signaling have been widely analyzed in the literature (Alam et al., 2007; Kim et al., 2011). First, integrins may enhance the activation and autophosphorylation of tyrosine kinase receptors, and they can recruit adaptor proteins to the plasma membrane, which regulate growth factor receptor signaling. Second, focal adhesions can assemble in response to growth factors. Integrins present at focal adhesions can associate with growth factor receptors, modifying the localization of growth factor receptors to become associated with focal adhesions. Last, the interaction between integrins and growth factor receptors can enhance the efficiency of downstream pathways, such as the Ras-MAPK pathway. It has been shown that signals from integrins-Src-FAK complex can be integrated with that of growth factors and be transmitted through the same Ras-MAPK pathway.

In the particular case of the FGF pathway, it has been shown that FGFR activity can be augmented by activation of integrins, and that FGF-1 and FGF-2 can simultaneously

bind FGFR and integrin αvβ3 (Mori et al., 2008; Rusnati et al., 1997). Such cross-talk can be strongly influenced by HS, which is not only able to bind FGFs, but also integrin αvβ3 (Faye et al., 2009).

We consider the hypothesis that extracellular accumulation of HSO in MPSIIIB impacts cross-talk between the FGF and integrin pathways, with downstream consequences on the formation of focal adhesions, the regulation of the cytoskeleton by Rho GTPases, and the activation of the MAPK/ERK signaling pathway. These different events are temporally regulated. One of the first events leading to cell polarization is the formation of new cell contacts with the ECM at the future front of the cells. Inhibition of integrin engagement impairs polarity establishment, characterized by process extension and centrosome-Golgi reorientation (Etienne-Manneville and Hall, 2001). Nascent adhesions mature into large focal adhesions where proteins such as FAK, paxillin or vinculin are recruited, followed by reorganization of the cytoskeleton induced by Rho GTPases activation (Kim et al., 2011). Cytoskeleton reorganization induces the formation of a protrusion in the direction of migration in cells such as astrocytes (Etienne-Manneville and Hall, 2001), and it induces the development of axons and dendrites in neurons (Barnes and Polleux, 2009). This phenomenon is accompanied by reorientation of the Golgi and the centrosome which involves ERK (Bisel et al., 2008). Once cell polarization is established, cell migration can follow.

Deregulated cross-talk between the integrin and FGF pathways would lead to impaired cell adhesion, polarization and migration. It would be relevant to neuritogenesis defects observed in MPSIIIB mouse neurons (Hocquemiller et al., 2010), considering the crucial importance of the actin cytoskeleton in neuritogenesis (da Silva and Dotti, 2002).

Interestingly, some actors of the MAPK and Rho GTPases pathways controlled by activation of integrins and FGFRs, and found to be affected in response to extracellular HS fragments are not only present at the plasma membrane, but also at the Golgi (see paragraph 6.7). Growth factor-induced activation of the MAPK pathway at the Golgi results in GRASP65 phosphorylation by ERK and subsequent remodeling of the Golgi architecture (Bisel et al., 2008). One possibility is that GRASP65-GM130 interactions are controlled by the MAPK/ERK pathway. Although only hypothetical, pools of Rho GTPases present at the Golgi may be involved in cytoskeleton remodeling in response to an adhesion stimulus induced by integrin signaling. This hypothesis is supported by

the observation that 14-3-3ζ has been found associated with integrin complexes, where it acts as an adaptor protein recruiting and activating Rho GTPases to sites of newly attached integrins (Bialkowska et al., 2003; Deakin et al., 2009; O'Toole et al., 2011). As 14-3-3ζ and its specific kinase YSK1 can be targeted at the Golgi by GM130, it can be speculated that 14-3-3ζ can also activate Golgi-localized Rho GTPases in response to integrin activation.

These various hypotheses place GRASP65-GM130 complexes and GM130-YSK1-14-3-3ζ complexes at the interplay between cell surface signaling and Golgi signaling.

This model points to the MAPK/ERK pathway as a potential target for therapeutic intervention. Inhibitors of the MAPK/ERK pathway already exist and have demonstrated remarkable clinical activity for anticancer therapies (Wong et al., 2009). When considering the complexity of cascades of events which account for clinical expression of MPSIIIB, it is unlikely that such inhibitors will have widespread benefits. MAPK/ERK inhibitors may nevertheless provide tools to address questions on cell physiopathology. For example, they might be useful to examine whether Golgi defects or accumulation of abnormal lysosomes are regulated by the MAPK/ERK pathway.

3. FUTURE DIRECTIONS

Preliminary studies performed in the laboratory, and in which I was involved in collaboration with Julie Bruyère and Sandrine Vitry, confirmed that as predicted, MPSIIIB cells exhibit adhesion and polarization defects. They showed that recruitment and activation of focal adhesion proteins were exacerbated under basal conditions in primary astrocytes cultures derived from MPSIIIB mice. Following activation of migration in these cells, recruitment of focal adhesion proteins at the leading edge was delayed. In NAGLU-depleted cells, HS co-localized with β1 and αv integrins at the cell-matrix interface, a feature which was not observed in normal cells. These integrin subunits were overexpressed. These studies will be completed by measuring expression levels of different integrin subunits in MPSIIIB cells. In addition, these preliminary studies suggest that the polarization of astrocytes does not proceed normally in vitro, as measured by the cell capacity to reorient their Golgi and centrosome in front of the nucleus in the migration direction using a wound-healing assay (Etienne-Manneville,

2006). NSCs purified from the MPSIIIB mouse model also exhibited reduced polarization, as compared with controls. Correction of polarization defects in MPSIIIB cells by supplying NAGLU through gene transfer indicated that they were caused by HSO accumulation.

We purified HSO from MPSIIIB patient urines with the aim to assess whether the addition of HSO to the extracellular space of unaffected cells reproduced adhesion and polarization defects seen in MPSIIIB cells. Preliminary experiments using the adhesion phenotype as an endpoint confirmed the crucial impact of extracellular HSO. Alternatively, cell-matrix interaction studies will determine the impact of ECM modifications on cell phenotypes. This question will be addressed by examining the phenotype of normal cells cultivated in an ECM environment produced by MPSIIIB cells.

We will also investigate whether altered signals from integrins and FGFR affect downstream pathways, the cross-talks between these pathways, and if these changes affect GM130 functions. Activation of ERK and Rho GTPases such as Cdc42 will be examined in MPSIIIB cells *versus* normal cells, as well as in normal cells treated with HSO *versus* untreated cells. Intracellular molecular events will be documented, with special emphasis on the control and modulation of GM130 interaction with its multiple protein partners. The hypothesis that GM130 binding to Tuba is decreased, whereas GM130 binding to AKAP450 and/or GRASP65 is increased in response to the accumulation of extracellular HSO will be explored through co-immunoprecipitation experiments. In addition, the implication of the GRASP65-GM130 and GM130-YSK1 complexes in inducing cell polarization and migration defects should be investigated. Since GM130 domains which bind GRASP65 and YSK1 are known, truncated forms of GM130 unable to interact with GRASP65 or YSK1 will represent useful tools.

BIBLIOGRAPHY

BIBLIOGRAPHY

A

Aasen T., Raya A., Barrero M. J., Garreta E., Consiglio A., Gonzalez F., Vassena R., Bilic J., Pekarik V., Tiscornia G., Edel M., Boue S. and Izpisua Belmonte J. C. (2008) Efficient and rapid generation of induced pluripotent stem cells from human keratinocytes. *Nat Biotechnol* 26, 1276-84.

Adriani W. and Laviola G. (2004) Windows of vulnerability to psychopathology and therapeutic strategy in the adolescent rodent model. *Behav Pharmacol* 15, 341-52.

Aerts J. M., Hollak C. E., van Breemen M., Maas M., Groener J. E. and Boot R. G. (2005) Identification and use of biomarkers in Gaucher disease and other lysosomal storage diseases. *Acta Paediatr Suppl* 94, 43-6; discussion 37-8.

Aiuti A., Cattaneo F., Galimberti S., Benninghoff U., Cassani B., Callegaro L., Scaramuzza S., Andolfi G., Mirolo M., Brigida I., Tabucchi A., Carlucci F., Eibl M., Aker M., Slavin S., Al-Mousa H., Al Ghonaium A., Ferster A., Duppenthaler A., Notarangelo L., Wintergerst U., Buckley R. H., Bregni M., Marktel S., Valsecchi M. G., Rossi P., Ciceri F., Miniero R., Bordignon C. and Roncarolo M. G. (2009) Gene therapy for immunodeficiency due to adenosine deaminase deficiency. *N Engl J Med* 360, 447-58.

Alam N., Goel H. L., Zarif M. J., Butterfield J. E., Perkins H. M., Sansoucy B. G., Sawyer T. K. and Languino L. R. (2007) The integrin-growth factor receptor duet. *J Cell Physiol* 213, 649-53.

Allan B. B., Moyer B. D. and Balch W. E. (2000) Rab1 recruitment of p115 into a cis-SNARE complex: programming budding COPII vesicles for fusion. *Science* 289, 444-8.

Allende M. L., Li J., Darling D. S., Worth C. A. and Young W. W., Jr. (2000) Evidence supporting a late Golgi location for lactosylceramide to ganglioside GM3 conversion. *Glycobiology* 10, 1025-32.

Alvarez C., Fujita H., Hubbard A. and Sztul E. (1999) ER to Golgi transport: Requirement for p115 at a pre-Golgi VTC stage. *J Cell Biol* 147, 1205-22.

Alvarez C., Garcia-Mata R., Hauri H. P. and Sztul E. (2001) The p115-interactive proteins GM130 and giantin participate in endoplasmic reticulum-Golgi traffic. *J Biol Chem* 276, 2693-700.

Amaral O., Fortuna A. M., Lacerda L., Pinto R. and Sa Miranda M. C. (1994) Molecular characterisation of type 1 Gaucher disease families and patients: intrafamilial heterogeneity at the clinical level. *J Med Genet* 31, 401-4.

Amsterdam Molecular Therapeutics. (2010) AMT submits its lead product Glybera® application for marketing authorisation to EMA. *[online]* http://www.amtbiopharma.com/ uploads/011110e pdf_44.pdf

Anitei M. and Hoflack B. (2011) Exit from the trans-Golgi network: from molecules to mechanisms. *Curr Opin Cell Biol*.

Arantes R. M. and Andrews N. W. (2006) A role for synaptotagmin VII-regulated exocytosis of lysosomes in neurite outgrowth from primary sympathetic neurons. *J Neurosci* 26, 4630-7.

Arfi A., Richard M., Gandolphe C., Bonnefont-Rousselot D., Therond P. and Scherman D. (2011) Neuroinflammatory and oxidative stress phenomena in MPS IIIA mouse model: the positive effect of long-term aspirin treatment. *Mol Genet Metab* 103, 18-25.

Arfi A., Richard M., Gandolphe C. and Scherman D. (2010) Storage correction in cells of patients suffering from mucopolysaccharidoses types IIIA and VII after treatment with genistein and other isoflavones. *J Inherit Metab Dis* 33, 61-7.

Ariga T., Kobayashi K., Hasegawa A., Kiso M., Ishida H. and Miyatake T. (2001) Characterization of high-affinity binding between gangliosides and amyloid beta-protein. *Arch Biochem Biophys* 388, 225-30.

Aronovich E. L., Johnston J. M., Wang P., Giger U. and Whitley C. B. (2001) Molecular basis of mucopolysaccharidosis type IIIB in emu (Dromaius novaehollandiae): an avian model of Sanfilippo syndrome type B. *Genomics* 74, 299-305.

Ausseil J., Desmaris N., Bigou S., Attali R., Corbineau S., Vitry S., Parent M., Cheillan D., Fuller M., Maire I., Vanier M. T. and Heard J. M. (2008) Early neurodegeneration progresses independently of microglial activation by heparan sulfate in the brain of mucopolysaccharidosis IIIB mice. *PLoS One* 3, e2296.

Avila J. L. and Convit J. (1975) Inhibition of leucocytic lysosomal enzymes by glycosaminoglycans in vitro. *Biochem J* 152, 57-64.

B

Bach G., Zeigler M. and Zlotogora J. (2007) Prevention of lysosomal storage disorders in Israel. *Mol Genet Metab* 90, 353-7.

Bachert C. and Linstedt A. D. (2010) Dual anchoring of the GRASP membrane tether promotes trans pairing. *J Biol Chem* 285, 16294-301.

Bagshaw R. D., Mahuran D. J. and Callahan J. W. (2005) Lysosomal membrane proteomics and biogenesis of lysosomes. *Mol Neurobiol* 32, 27-41.

Bahr B. A., Abai B., Gall C. M., Vanderklish P. W., Hoffman K. B. and Lynch G. (1994) Induction of beta-amyloid-containing polypeptides in hippocampus: evidence for a concomitant loss of synaptic proteins and interactions with an excitotoxin. *Exp Neurol* 129, 81-94.

Bainbridge J. W., Smith A. J., Barker S. S., Robbie S., Henderson R., Balaggan K., Viswanathan A., Holder G. E., Stockman A., Tyler N., Petersen-Jones S., Bhattacharya S. S., Thrasher A. J., Fitzke F. W., Carter B. J., Rubin G. S., Moore A. T. and Ali R. R. (2008) Effect of gene therapy on visual function in Leber's congenital amaurosis. *N Engl J Med* 358, 2231-9.

Ballabio A. and Gieselmann V. (2009) Lysosomal disorders: from storage to cellular damage. *Biochim Biophys Acta* 1793, 684-96.

Banikazemi M., Bultas J., Waldek S., Wilcox W. R., Whitley C. B., McDonald M., Finkel R., Packman S., Bichet D. G., Warnock D. G. and Desnick R. J. (2007) Agalsidase-beta therapy for advanced Fabry disease: a randomized trial. *Ann Intern Med* 146, 77-86.

Barnes A. P. and Polleux F. (2009) Establishment of axon-dendrite polarity in developing neurons. *Annu Rev Neurosci* 32, 347-81.

Barr F. A., Nakamura N. and Warren G. (1998) Mapping the interaction between GRASP65 and GM130, components of a protein complex involved in the stacking of Golgi cisternae. *EMBO J* 17, 3258-68.

Barton N. W., Brady R. O., Dambrosia J. M., Di Bisceglie A. M., Doppelt S. H., Hill S. C., Mankin H. J., Murray G. J., Parker R. I., Argoff C. E. and et al. (1991) Replacement therapy for inherited enzyme deficiency--macrophage-targeted glucocerebrosidase for Gaucher's disease. *N Engl J Med* 324, 1464-70.

Baumkotter J. and Cantz M. (1983) Decreased ganglioside neuraminidase activity in fibroblasts from mucopolysaccharidosis patients. Inhibition of the activity in vitro by sulfated glycosaminoglycans and other compounds. *Biochim Biophys Acta* 761, 163-70.

Beesley C. E., Jackson M., Young E. P., Vellodi A. and Winchester B. G. (2005) Molecular defects in Sanfilippo syndrome type B (mucopolysaccharidosis IIIB). *J Inherit Metab Dis* 28, 759-67.

Bellettato C. M. and Scarpa M. (2010) Pathophysiology of neuropathic lysosomal storage disorders. *J Inherit Metab Dis* 33, 347-62.

Besancon F. and Ankel H. (1974) Binding of interferon to gangliosides. *Nature* 252, 478-80.

Bialkowska K., Zaffran Y., Meyer S. C. and Fox J. E. (2003) 14-3-3 zeta mediates integrin-induced activation of Cdc42 and Rac. Platelet glycoprotein Ib-IX regulates integrin-induced signaling by sequestering 14-3-3 zeta. *J Biol Chem* 278, 33342-50.

Biffi A., Capotondo A., Fasano S., del Carro U., Marchesini S., Azuma H., Malaguti M. C., Amadio S., Brambilla R., Grompe M., Bordignon C., Quattrini A. and Naldini L. (2006) Gene therapy of metachromatic leukodystrophy reverses neurological damage and deficits in mice. *J Clin Invest* 116, 3070-82.

Biffi A., De Palma M., Quattrini A., Del Carro U., Amadio S., Visigalli I., Sessa M., Fasano S., Brambilla R., Marchesini S., Bordignon C. and Naldini L. (2004) Correction of metachromatic leukodystrophy in the mouse model by transplantation of genetically modified hematopoietic stem cells. *J Clin Invest* 113, 1118-29.

Bisel B., Wang Y., Wei J. H., Xiang Y., Tang D., Miron-Mendoza M., Yoshimura S., Nakamura N. and Seemann J. (2008) ERK regulates Golgi and centrosome orientation towards the leading edge through GRASP65. *J Cell Biol* 182, 837-43.

Bivona T. G., Perez De Castro I., Ahearn I. M., Grana T. M., Chiu V. K., Lockyer P. J., Cullen P. J., Pellicer A., Cox A. D. and Philips M. R. (2003) Phospholipase Cgamma activates Ras on the Golgi apparatus by means of RasGRP1. *Nature* 424, 694-8.

Blomgran R., Zheng L. and Stendahl O. (2007) Cathepsin-cleaved Bid promotes apoptosis in human neutrophils via oxidative stress-induced lysosomal membrane permeabilization. *J Leukoc Biol* 81, 1213-23.

Bodennec J., Pelled D., Riebeling C., Trajkovic S. and Futerman A. H. (2002) Phosphatidylcholine synthesis is elevated in neuronal models of Gaucher disease due to direct activation of CTP:phosphocholine cytidylyltransferase by glucosylceramide. *FASEB J* 16, 1814-6.

Boggs J. M. (1987) Lipid intermolecular hydrogen bonding: influence on structural organization and membrane function. Biochim Biophys Acta 906, 353-404.

Boland B., Smith D. A., Mooney D., Jung S. S., Walsh D. M. and Platt F. M. (2010) Macroautophagy is not directly involved in the metabolism of amyloid precursor protein. *J Biol Chem* 285, 37415-26.

Bork K., Horstkorte R. and Weidemann W. (2009) Increasing the sialylation of therapeutic glycoproteins: the potential of the sialic acid biosynthetic pathway. *J Pharm Sci* 98, 3499-508.

Bovolenta P. and Fernaud-Espinosa I. (2000) Nervous system proteoglycans as modulators of neurite outgrowth. *Prog Neurobiol* 61, 113-32.

Braulke T. and Bonifacino J. S. (2009) Sorting of lysosomal proteins. *Biochim Biophys Acta* 1793, 605-14.

Bremer E. G. and Hakomori S. (1982) GM3 ganglioside induces hamster fibroblast growth inhibition in chemically-defined medium: ganglioside may regulate growth factor receptor function. *Biochem Biophys Res Commun* 106, 711-8.

Bretscher M. S. and Munro S. (1993) Cholesterol and the Golgi apparatus. *Science* 261, 1280-1.

Bright N. A., Gratian M. J. and Luzio J. P. (2005) Endocytic delivery to lysosomes mediated by concurrent fusion and kissing events in living cells. *Curr Biol* 15, 360-5.

Brooks A. I., Stein C. S., Hughes S. M., Heth J., McCray P. M., Jr., Sauter S. L., Johnston J. C., Cory-Slechta D. A., Federoff H. J. and Davidson B. L. (2002) Functional correction of established central nervous system deficits in an animal model of lysosomal storage disease with feline immunodeficiency virus-based vectors. *Proc Natl Acad Sci U S A* 99, 6216-21.

Brooks D. A., King B. M., Crawley A. C., Byers S. and Hopwood J. J. (1997) Enzyme replacement therapy in Mucopolysaccharidosis VI: evidence for immune responses and altered efficacy of treatment in animal models. *Biochim Biophys Acta* 1361, 203-16.

Brooks D. A., Muller V. J. and Hopwood J. J. (2006) Stop-codon read-through for patients affected by a lysosomal storage disorder. *Trends Mol Med* 12, 367-73.

Brown D. A. and London E. (1998) Functions of lipid rafts in biological membranes. Annu Rev Cell Dev Biol 14, 111-36.

Burkhardt J. K. (1998) The role of microtubule-based motor proteins in maintaining the structure and function of the Golgi complex. *Biochim Biophys Acta* 1404, 113-26.

Byers S., Rozaklis T., Brumfield L. K., Ranieri E. and Hopwood J. J. (1998) Glycosaminoglycan accumulation and excretion in the mucopolysaccharidoses: characterization and basis of a diagnostic test for MPS. *Mol Genet Metab* 65, 282-90.

C

Cachon-Gonzalez M. B., Wang S. Z., Lynch A., Ziegler R., Cheng S. H. and Cox T. M. (2006) Effective gene therapy in an authentic model of Tay-Sachs-related diseases. *Proc Natl Acad Sci U S A* 103, 10373-8.

Cai H., Reinisch K. and Ferro-Novick S. (2007) Coats, tethers, Rabs, and SNAREs work together to mediate the intracellular destination of a transport vesicle. *Dev Cell* 12, 671-82.

Canuel M., Libin Y. and Morales C. R. (2009) The interactomics of sortilin: an ancient lysosomal receptor evolving new functions. *Histol Histopathol* 24, 481-92.

Cao X., Ballew N. and Barlowe C. (1998) Initial docking of ER-derived vesicles requires Uso1p and Ypt1p but is independent of SNARE proteins. *EMBO J* 17, 2156-65.

Cardone M., Polito V. A., Pepe S., Mann L., D'Azzo A., Auricchio A., Ballabio A. and Cosma M. P. (2006) Correction of Hunter syndrome in the MPSII mouse model by AAV2/8-mediated gene delivery. *Hum Mol Genet* 15, 1225-36.

Caroni P. (2001) New EMBO members' review: actin cytoskeleton regulation through modulation of PI(4,5)P(2) rafts. *EMBO J* 20, 4332-6.

Cartier N., Hacein-Bey-Abina S., Bartholomae C. C., Veres G., Schmidt M., Kutschera I., Vidaud M., Abel U., Dal-Cortivo L., Caccavelli L., Mahlaoui N., Kiermer V., Mittelstaedt D., Bellesme C., Lahlou N., Lefrere F., Blanche S., Audit M., Payen E., Leboulch P., l'Homme B., Bougneres P., Von Kalle C., Fischer A., Cavazzana-Calvo M. and Aubourg P. (2009) Hematopoietic stem cell gene therapy with a lentiviral vector in X-linked adrenoleukodystrophy. *Science* 326, 818-23.

Cataldo A. M., Barnett J. L., Mann D. M. and Nixon R. A. (1996) Colocalization of lysosomal hydrolase and beta-amyloid in diffuse plaques of the cerebellum and striatum in Alzheimer's disease and Down's syndrome. *J Neuropathol Exp Neurol* 55, 704-15.

Cearley C. N. and Wolfe J. H. (2007) A single injection of an adeno-associated virus vector into nuclei with divergent connections results in widespread vector distribution in the brain and global correction of a neurogenetic disease. *J Neurosci* 27, 9928-40.

Cecere F., Di Domenico C., Di Napoli D., Boscia F. and Di Natale P. (2011) Activation of stress kinases in the brain of mucopolysaccharidosis IIIB mice. *J Neurosci Res* 89, 1431-8.

Chabin-Brion K., Marceiller J., Perez F., Settegrana C., Drechou A., Durand G. and Pous C. (2001) The Golgi complex is a microtubule-organizing organelle. *Mol Biol Cell* 12, 2047-60.

Chapman H. A. (1998) Endosomal proteolysis and MHC class II function. *Curr Opin Immunol* 10, 93-102.

Chattopadhyay S., Roberts P. M. and Pearce D. A. (2003) The yeast model for Batten disease: a role for Btn2p in the trafficking of the Golgi-associated vesicular targeting protein, Yif1p. *Biochem Biophys Res Commun* 302, 534-8.

Chen Y. H., Chang M. and Davidson B. L. (2009) Molecular signatures of disease brain endothelia provide new sites for CNS-directed enzyme therapy. *Nat Med* 15, 1215-8.

Chien Y. H., Chiang S. C., Zhang X. K., Keutzer J., Lee N. C., Huang A. C., Chen C. A., Wu M. H., Huang P. H., Tsai F. J., Chen Y. T. and Hwu W. L. (2008) Early detection of Pompe disease by newborn screening is feasible: results from the Taiwan screening program. *Pediatrics* 122, e39-45.

Chiu V. K., Bivona T., Hach A., Sajous J. B., Silletti J., Wiener H., Johnson R. L., 2nd, Cox A. D. and Philips M. R. (2002) Ras signalling on the endoplasmic reticulum and the Golgi. *Nat Cell Biol* 4, 343-50.

Choudhury A., Dominguez M., Puri V., Sharma D. K., Narita K., Wheatley C. L., Marks D. L. and Pagano R. E. (2002) Rab proteins mediate Golgi transport of

caveola-internalized glycosphingolipids and correct lipid trafficking in Niemann-Pick C cells. *J Clin Invest* 109, 1541-50.

Chu J. W. and Sharom F. J. (1990) Interleukin-2 binds to gangliosides in micelles and lipid bilayers. *Biochim Biophys Acta* 1028, 205-14.

Cleary M. A. and Wraith J. E. (1993) Management of mucopolysaccharidosis type III. *Arch Dis Child* 69, 403-6.

Cole N. B., Sciaky N., Marotta A., Song J. and Lippincott-Schwartz J. (1996) Golgi dispersal during microtubule disruption: regeneration of Golgi stacks at peripheral endoplasmic reticulum exit sites. *Mol Biol Cell* 7, 631-50.

Conus S., Perozzo R., Reinheckel T., Peters C., Scapozza L., Yousefi S. and Simon H. U. (2008) Caspase-8 is activated by cathepsin D initiating neutrophil apoptosis during the resolution of inflammation. *J Exp Med* 205, 685-98.

Conus S. and Simon H. U. (2010) Cathepsins and their involvement in immune responses. *Swiss Med Wkly* 140, w13042.

Corthesy-Theulaz I., Pauloin A. and Pfeffer S. R. (1992) Cytoplasmic dynein participates in the centrosomal localization of the Golgi complex. *J Cell Biol* 118, 1333-45.

Cressant A., Desmaris N., Verot L., Brejot T., Froissart R., Vanier M. T., Maire I. and Heard J. M. (2004) Improved behavior and neuropathology in the mouse model of Sanfilippo type IIIB disease after adeno-associated virus-mediated gene transfer in the striatum. *J Neurosci* 24, 10229-39.

Cundiff P. E. and Anderson S. A. (2011) Impact of induced pluripotent stem cells on the study of central nervous system disease. *Curr Opin Genet Dev* 21, 354-61.

D

d'Azzo A., Proia R. L., Kolodny E. H., Kaback M. M. and Neufeld E. F. (1984) Faulty association of alpha- and beta-subunits in some forms of beta-hexosaminidase A deficiency. *J Biol Chem* 259, 11070-4.

Dahms N. M. and Hancock M. K. (2002) P-type lectins. *Biochim Biophys Acta* 1572, 317-40.

Daly T. M., Ohlemiller K. K., Roberts M. S., Vogler C. A. and Sands M. S. (2001) Prevention of systemic clinical disease in MPS VII mice following AAV-mediated neonatal gene transfer. *Gene Ther* 8, 1291-8.

de Anda F. C., Meletis K., Ge X., Rei D. and Tsai L. H. (2010) Centrosome motility is essential for initial axon formation in the neocortex. *J Neurosci* 30, 10391-406.

de Anda F. C., Pollarolo G., Da Silva J. S., Camoletto P. G., Feiguin F. and Dotti C. G. (2005) Centrosome localization determines neuronal polarity. *Nature* 436, 704-8.

De Carvalho Bittencourt M., Herren S., Graber P., Vilbois F., Pasquali C., Berney C., Plitz T., Nicoletti F. and Kosco-Vilbois M. H. (2005) Extracellular lysosome-associated membrane protein-1 (LAMP-1) mediates autoimmune disease progression in the NOD model of type 1 diabetes. *Eur J Immunol* 35, 1501-9.

de Graffenried C. L. and Bertozzi C. R. (2004) The roles of enzyme localisation and complex formation in glycan assembly within the Golgi apparatus. *Curr Opin Cell Biol* 16, 356-63.

Deakin N. O., Bass M. D., Warwood S., Schoelermann J., Mostafavi-Pour Z., Knight D., Ballestrem C. and Humphries M. J. (2009) An integrin-alpha4-14-3-3zeta-paxillin ternary complex mediates localised Cdc42 activity and accelerates cell migration. *J Cell Sci* 122, 1654-64.

Deganuto M., Pittis M. G., Pines A., Dominissini S., Kelley M. R., Garcia R., Quadrifoglio F., Bembi B. and Tell G. (2007) Altered intracellular redox status in Gaucher disease fibroblasts and impairment of adaptive response against oxidative stress. *J Cell Physiol* 212, 223-35.

Degroote S., Wolthoorn J. and van Meer G. (2004) The cell biology of glycosphingolipids. *Semin Cell Dev Biol* 15, 375-87.

Delacour D., Greb C., Koch A., Salomonsson E., Leffler H., Le Bivic A. and Jacob R. (2007) Apical sorting by galectin-3-dependent glycoprotein clustering. *Traffic* 8, 379-88.

Dell'Angelica E. C., Shotelersuk V., Aguilar R. C., Gahl W. A. and Bonifacino J. S. (1999) Altered trafficking of lysosomal proteins in Hermansky-Pudlak syndrome due to mutations in the beta 3A subunit of the AP-3 adaptor. *Mol Cell* 3, 11-21.

Desmaris N., Verot L., Puech J. P., Caillaud C., Vanier M. T. and Heard J. M. (2004) Prevention of neuropathology in the mouse model of Hurler syndrome. *Ann Neurol* 56, 68-76.

Desnick R. J. and Schuchman E. H. (2002) Enzyme replacement and enhancement therapies: lessons from lysosomal disorders. *Nat Rev Genet* 3, 954-66.

Diao A., Frost L., Morohashi Y. and Lowe M. (2008) Coordination of golgin tethering and SNARE assembly: GM130 binds syntaxin 5 in a p115-regulated manner. *J Biol Chem* 283, 6957-67.

Diao A., Rahman D., Pappin D. J., Lucocq J. and Lowe M. (2003) The coiled-coil membrane protein golgin-84 is a novel rab effector required for Golgi ribbon formation. *J Cell Biol* 160, 201-12.

Dice J. F. (2007) Chaperone-mediated autophagy. *Autophagy* 3, 295-9.

Dickson P., Peinovich M., McEntee M., Lester T., Le S., Krieger A., Manuel H., Jabagat C., Passage M. and Kakkis E. D. (2008) Immune tolerance improves the efficacy of enzyme replacement therapy in canine mucopolysaccharidosis I. *J Clin Invest* 118, 2868-76.

Dimos J. T., Rodolfa K. T., Niakan K. K., Weisenthal L. M., Mitsumoto H., Chung W., Croft G. F., Saphier G., Leibel R., Goland R., Wichterle H., Henderson C. E. and Eggan K. (2008) Induced pluripotent stem cells generated from patients with ALS can be differentiated into motor neurons. *Science* 321, 1218-21.

Dirac-Svejstrup A. B., Shorter J., Waters M. G. and Warren G. (2000) Phosphorylation of the vesicle-tethering protein p115 by a casein kinase II-like enzyme is required for Golgi reassembly from isolated mitotic fragments. *J Cell Biol* 150, 475-88.

Dittmer F., Ulbrich E. J., Hafner A., Schmahl W., Meister T., Pohlmann R. and von Figura K. (1999) Alternative mechanisms for trafficking of lysosomal enzymes in mannose 6-phosphate receptor-deficient mice are cell type-specific. *J Cell Sci* 112 (Pt 10), 1591-7.

Dodge J. C., Clarke J., Song A., Bu J., Yang W., Taksir T. V., Griffiths D., Zhao M. A., Schuchman E. H., Cheng S. H., O'Riordan C. R., Shihabuddin L. S., Passini M. A. and Stewart G. R. (2005) Gene transfer of human acid sphingomyelinase corrects neuropathology and motor deficits in a mouse model of Niemann-Pick type A disease. *Proc Natl Acad Sci U S A* 102, 17822-7.

Donaldson J. G. and Lippincott-Schwartz J. (2000) Sorting and signaling at the Golgi complex. *Cell* 101, 693-6.

Driessen C., Bryant R. A., Lennon-Dumenil A. M., Villadangos J. A., Bryant P. W., Shi G. P., Chapman H. A. and Ploegh H. L. (1999) Cathepsin S controls the trafficking and maturation of MHC class II molecules in dendritic cells. *J Cell Biol* 147, 775-90.

Droge W. (2002) Free radicals in the physiological control of cell function. *Physiol Rev* 82, 47-95.

Duffau H. (2006) Brain plasticity: from pathophysiological mechanisms to therapeutic applications. *J Clin Neurosci* 13, 885-97.

Duffner P. K., Barczykowski A., Jalal K., Yan L., Kay D. M. and Carter R. L. Early infantile Krabbe disease: results of the World-Wide Krabbe Registry. *Pediatr Neurol* 45, 141-8.

Duffner P. K., Caggana M., Orsini J. J., Wenger D. A., Patterson M. C., Crosley C. J., Kurtzberg J., Arnold G. L., Escolar M. L., Adams D. J., Andriola M. R., Aron A. M., Ciafaloni E., Djukic A., Erbe R. W., Galvin-Parton P., Helton L. E., Kolodny E. H., Kosofsky B. E., Kronn D. F., Kwon J. M., Levy P. A., Miller-Horn J., Naidich T. P., Pellegrino J. E., Provenzale J. M., Rothman S. J. and Wasserstein M. P. (2009) Newborn screening for Krabbe disease: the New York State model. *Pediatr Neurol* 40, 245-52; discussion 253-5.

Dunbar C. E., Kohn D. B., Schiffmann R., Barton N. W., Nolta J. A., Esplin J. A., Pensiero M., Long Z., Lockey C., Emmons R. V., Csik S., Leitman S., Krebs C. B., Carter C., Brady R. O. and Karlsson S. (1998) Retroviral transfer of the glucocerebrosidase gene into CD34+ cells from patients with Gaucher disease: in vivo detection of transduced cells without myeloablation. *Hum Gene Ther* 9, 2629-40.

Dunn W. A., Jr., Raizada M. K., Vogt E. S. and Brown E. A. (1994) Growth factor-induced neurite growth in primary neuronal cultures of dogs with neuronal ceroid lipofuscinosis. *Int J Dev Neurosci* 12, 185-96.

E

Ebert A. D., Yu J., Rose F. F., Jr., Mattis V. B., Lorson C. L., Thomson J. A. and Svendsen C. N. (2009) Induced pluripotent stem cells from a spinal muscular atrophy patient. *Nature* 457, 277-80.

Efimov A., Kharitonov A., Efimova N., Loncarek J., Miller P. M., Andreyeva N., Gleeson P., Galjart N., Maia A. R., McLeod I. X., Yates J. R., 3rd, Maiato H., Khodjakov A., Akhmanova A. and Kaverina I. (2007) Asymmetric CLASP-dependent nucleation of noncentrosomal microtubules at the trans-Golgi network. *Dev Cell* 12, 917-30.

Ellinwood N. M., Ausseil J., Desmaris N., Bigou S., Liu S., Jens J. K., Snella E. M., Mohammed E. E., Thomson C. B., Raoul S., Joussemet B., Roux F., Cherel Y., Lajat Y., Piraud M., Benchaouir R., Hermening S., Petry H., Froissart R., Tardieu M., Ciron C., Moullier P., Parkes J., Kline K. L., Maire I., Vanier M. T., Heard J. M. and Colle M. A. (2011) Safe, efficient, and reproducible gene therapy of the brain in the dog models of Sanfilippo and Hurler syndromes. *Mol Ther* 19, 251-9.

Ellinwood N. M., Wang P., Skeen T., Sharp N. J., Cesta M., Decker S., Edwards N. J., Bublot I., Thompson J. N., Bush W., Hardam E., Haskins M. E. and Giger U. (2003) A model of mucopolysaccharidosis IIIB (Sanfilippo syndrome type IIIB): N-acetyl-alpha-D-glucosaminidase deficiency in Schipperke dogs. *J Inherit Metab Dis* 26, 489-504.

Escolar M. L., Poe M. D., Provenzale J. M., Richards K. C., Allison J., Wood S., Wenger D. A., Pietryga D., Wall D., Champagne M., Morse R., Krivit W. and Kurtzberg J. (2005) Transplantation of umbilical-cord blood in babies with infantile Krabbe's disease. *N Engl J Med* 352, 2069-81.

Eskelinen E. L. (2005) Maturation of autophagic vacuoles in Mammalian cells. *Autophagy* 1, 1-10.

Esko J. D. and Selleck S. B. (2002) Order out of chaos: assembly of ligand binding sites in heparan sulfate. *Annu Rev Biochem* 71, 435-71.

Etienne-Manneville S. (2006) In vitro assay of primary astrocyte migration as a tool to study Rho GTPase function in cell polarization. *Methods Enzymol* 406, 565-78.

Etienne-Manneville S. and Hall A. (2001) Integrin-mediated activation of Cdc42 controls cell polarity in migrating astrocytes through PKCzeta. *Cell* 106, 489-98.

Ezaki J., Wolfe L. S. and Kominami E. (1993) Molecular basis of lysosomal accumulation of subunit c of mitochondrial ATP synthase in neuronal ceroid-lipofuscinosis. *J Inherit Metab Dis* 16, 296-8.

F

Fantl W. J., Muslin A. J., Kikuchi A., Martin J. A., MacNicol A. M., Gross R. W. and Williams L. T. (1994) Activation of Raf-1 by 14-3-3 proteins. *Nature* 371, 612-4.

Fares H. and Greenwald I. (2001) Regulation of endocytosis by CUP-5, the Caenorhabditis elegans mucolipin-1 homolog. *Nat Genet* 28, 64-8.

Farfel-Becker T., Vitner E., Dekel H., Leshem N., Enquist I. B., Karlsson S. and Futerman A. H. (2009) No evidence for activation of the unfolded protein response in neuronopathic models of Gaucher disease. *Hum Mol Genet* 18, 1482-8.

Faye C., Moreau C., Chautard E., Jetne R., Fukai N., Ruggiero F., Humphries M. J., Olsen B. R. and Ricard-Blum S. (2009) Molecular interplay between endostatin, integrins, and heparan sulfate. *J Biol Chem* 284, 22029-40.

Fehrenbacher N. and Jaattela M. (2005) Lysosomes as targets for cancer therapy. *Cancer Res* 65, 2993-5.

Feinstein T. N. and Linstedt A. D. (2008) GRASP55 regulates Golgi ribbon formation. *Mol Biol Cell* 19, 2696-707.

Filippon L., Vanzin C. S., Biancini G. B., Pereira I. N., Manfredini V., Sitta A., Peralba Mdo C., Schwartz I. V., Giugliani R. and Vargas C. R. (2011) Oxidative stress in patients with mucopolysaccharidosis type II before and during enzyme replacement therapy. *Mol Genet Metab* 103, 121-7.

Foust K. D., Nurre E., Montgomery C. L., Hernandez A., Chan C. M. and Kaspar B. K. (2009) Intravascular AAV9 preferentially targets neonatal neurons and adult astrocytes. *Nat Biotechnol* 27, 59-65.

Freed E., Symons M., Macdonald S. G., McCormick F. and Ruggieri R. (1994) Binding of 14-3-3 proteins to the protein kinase Raf and effects on its activation. *Science* 265, 1713-6.

Friso A., Tomanin R., Salvalaio M. and Scarpa M. (2010) Genistein reduces glycosaminoglycan levels in a mouse model of mucopolysaccharidosis type II. *Br J Pharmacol* 159, 1082-91.

Frustaci A., Chimenti C., Ricci R., Natale L., Russo M. A., Pieroni M., Eng C. M. and Desnick R. J. (2001) Improvement in cardiac function in the cardiac variant of Fabry's disease with galactose-infusion therapy. *N Engl J Med* 345, 25-32.

Fu H., Samulski R. J., McCown T. J., Picornell Y. J., Fletcher D. and Muenzer J. (2002) Neurological correction of lysosomal storage in a mucopolysaccharidosis IIIB mouse model by adeno-associated virus-mediated gene delivery. *Mol Ther* 5, 42-9.

Fu R., Yanjanin N. M., Bianconi S., Pavan W. J. and Porter F. D. (2010) Oxidative stress in Niemann-Pick disease, type C. *Mol Genet Metab* 101, 214-8.

Fukuda M. (1991) Lysosomal membrane glycoproteins. Structure, biosynthesis, and intracellular trafficking. *J Biol Chem* 266, 21327-30.

Fuller M., Rozaklis T., Ramsay S. L., Hopwood J. J. and Meikle P. J. (2004) Disease-specific markers for the mucopolysaccharidoses. *Pediatr Res* 56, 733-8.

Futerman A. H. and Pagano R. E. (1991) Determination of the intracellular sites and topology of glucosylceramide synthesis in rat liver. *Biochem J* 280 (Pt 2), 295-302.

Futerman A. H. and van Meer G. (2004) The cell biology of lysosomal storage disorders. *Nat Rev Mol Cell Biol* 5, 554-65.

G

Ganley I. G., Espinosa E. and Pfeffer S. R. (2008) A syntaxin 10-SNARE complex distinguishes two distinct transport routes from endosomes to the trans-Golgi in human cells. *J Cell Biol* 180, 159-72.

Gaudet D., de Wal J., Tremblay K., Dery S., van Deventer S., Freidig A., Brisson D. and Methot J. (2010) Review of the clinical development of alipogene tiparvovec gene therapy for lipoprotein lipase deficiency. *Atheroscler Suppl* 11, 55-60.

Gerber S. A., Scott C. R., Turecek F. and Gelb M. H. (2001) Direct profiling of multiple enzyme activities in human cell lysates by affinity chromatography/electrospray ionization mass spectrometry: application to clinical enzymology. *Anal Chem* 73, 1651-7.

Ghashghaei H. T., Lai C. and Anton E. S. (2007) Neuronal migration in the adult brain: are we there yet? *Nat Rev Neurosci* 8, 141-51.

Ghosh P., Dahms N. M. and Kornfeld S. (2003) Mannose 6-phosphate receptors: new twists in the tale. *Nat Rev Mol Cell Biol* 4, 202-12.

Gieselmann V. (2005) What can cell biology tell us about heterogeneity in lysosomal storage diseases? *Acta Paediatr Suppl* 94, 80-6; discussion 79.

Ginsberg S. D., Galvin J. E., Lee V. M., Rorke L. B., Dickson D. W., Wolfe J. H., Jones M. Z. and Trojanowski J. Q. (1999) Accumulation of intracellular amyloid-beta peptide (A beta 1-40) in mucopolysaccharidosis brains. *J Neuropathol Exp Neurol* 58, 815-24.

Ginzburg L., Kacher Y. and Futerman A. H. (2004) The pathogenesis of glycosphingolipid storage disorders. *Semin Cell Dev Biol* 15, 417-31.

Giugliani R., Carvalho C. G., Herber S. and de Camargo Pinto L. L. (2011) Recent Advances in Treatment Approaches of Mucopolysaccharidosis VI. *Curr Pharm Biotechnol* 12, 956-62.

Glick B. S. (2000) Organization of the Golgi apparatus. *Curr Opin Cell Biol* 12, 450-6.

Goedert M., Jakes R., Spillantini M. G., Hasegawa M., Smith M. J. and Crowther R. A. (1996) Assembly of microtubule-associated protein tau into Alzheimer-like filaments induced by sulphated glycosaminoglycans. *Nature* 383, 550-3.

Gossen M. and Bujard H. (1992) Tight control of gene expression in mammalian cells by tetracycline-responsive promoters. *Proc Natl Acad Sci U S A* 89, 5547-51.

Grabowski G. A., Barton N. W., Pastores G., Dambrosia J. M., Banerjee T. K., McKee M. A., Parker C., Schiffmann R., Hill S. C. and Brady R. O. (1995) Enzyme therapy in type 1 Gaucher disease: comparative efficacy of mannose-terminated glucocerebrosidase from natural and recombinant sources. *Ann Intern Med* 122, 33-9.

H

Hacein-Bey-Abina S., Garrigue A., Wang G. P., Soulier J., Lim A., Morillon E., Clappier E., Caccavelli L., Delabesse E., Beldjord K., Asnafi V., MacIntyre E., Dal Cortivo L., Radford I., Brousse N., Sigaux F., Moshous D., Hauer J., Borkhardt A., Belohradsky B. H., Wintergerst U., Velez M. C., Leiva L., Sorensen R., Wulffraat N., Blanche S., Bushman F. D., Fischer A. and Cavazzana-Calvo M. (2008) Insertional oncogenesis in 4 patients after retrovirus-mediated gene therapy of SCID-X1. *J Clin Invest* 118, 3132-42.

Hadfield M. G., Ghatak N. R., Nakoneczna I., Lippman H. R., Myer E. C., Constantopoulos G. and Bradley R. M. (1980) Pathologic findings in mucopolysaccharidosis type IIIB (Sanfilippo's sydnrome B). *Arch Neurol* 37, 645-50.

Hall N. A., Lake B. D., Dewji N. N. and Patrick A. D. (1991) Lysosomal storage of subunit c of mitochondrial ATP synthase in Batten's disease (ceroid-lipofuscinosis). *Biochem J* 275 (Pt 1), 269-72.

Hamano T., Gendron T. F., Causevic E., Yen S. H., Lin W. L., Isidoro C., Deture M. and Ko L. W. (2008) Autophagic-lysosomal perturbation enhances tau aggregation in transfectants with induced wild-type tau expression. *Eur J Neurosci* 27, 1119-30.

Hansske B., Thiel C., Lubke T., Hasilik M., Honing S., Peters V., Heidemann P. H., Hoffmann G. F., Berger E. G., von Figura K. and Korner C. (2002) Deficiency of UDP-galactose:N-acetylglucosamine beta-1,4-galactosyltransferase I causes the congenital disorder of glycosylation type IId. *J Clin Invest* 109, 725-33.

Harduin-Lepers A., Mollicone R., Delannoy P. and Oriol R. (2005) The animal sialyltransferases and sialyltransferase-related genes: a phylogenetic approach. Glycobiology 15, 805-17.

Harmatz P., Giugliani R., Schwartz I., Guffon N., Teles E. L., Miranda M. C., Wraith J. E., Beck M., Arash L., Scarpa M., Yu Z. F., Wittes J., Berger K. I., Newman M. S., Lowe A. M., Kakkis E. and Swiedler S. J. (2006) Enzyme

replacement therapy for mucopolysaccharidosis VI: a phase 3, randomized, double-blind, placebo-controlled, multinational study of recombinant human N-acetylgalactosamine 4-sulfatase (recombinant human arylsulfatase B or rhASB) and follow-on, open-label extension study. *J Pediatr* 148, 533-539.

Hauri H., Appenzeller C., Kuhn F. and Nufer O. (2000) Lectins and traffic in the secretory pathway. *FEBS Lett* 476, 32-7.

Heine C., Tyynela J., Cooper J. D., Palmer D. N., Elleder M., Kohlschutter A. and Braulke T. (2003) Enhanced expression of manganese-dependent superoxide dismutase in human and sheep CLN6 tissues. *Biochem J* 376, 369-76.

Helenius A. and Aebi M. (2001) Intracellular functions of N-linked glycans. *Science* 291, 2364-9.

Heron B., Mikaeloff Y., Froissart R., Caridade G., Maire I., Caillaud C., Levade T., Chabrol B., Feillet F., Ogier H., Valayannopoulos V., Michelakakis H., Zafeiriou D., Lavery L., Wraith E., Danos O., Heard J. M. and Tardieu M. (2011) Incidence and natural history of mucopolysaccharidosis type III in France and comparison with United Kingdom and Greece. *Am J Med Genet A* 155A, 58-68.

Hirschberg K., Miller C. M., Ellenberg J., Presley J. F., Siggia E. D., Phair R. D. and Lippincott-Schwartz J. (1998) Kinetic analysis of secretory protein traffic and characterization of golgi to plasma membrane transport intermediates in living cells. *J Cell Biol* 143, 1485-503.

Hirst J., Lui W. W., Bright N. A., Totty N., Seaman M. N. and Robinson M. S. (2000) A family of proteins with gamma-adaptin and VHS domains that facilitate trafficking between the trans-Golgi network and the vacuole/lysosome. *J Cell Biol* 149, 67-80.

Hochuli M., Wuthrich K. and Steinmann B. (2003) Two-dimensional NMR spectroscopy of urinary glycosaminoglycans from patients with different mucopolysaccharidoses. *NMR Biomed* 16, 224-36.

Hocquemiller M., Vitry S., Bigou S., Bruyere J., Ausseil J. and Heard J. M. (2010) GAP43 overexpression and enhanced neurite outgrowth in mucopolysaccharidosis type IIIB cortical neuron cultures. *J Neurosci Res* 88, 202-13.

Holthuis J. C., Pomorski T., Raggers R. J., Sprong H. and Van Meer G. (2001) The organizing potential of sphingolipids in intracellular membrane transport. Physiol Rev 81, 1689-723.

Hoogerbrugge P. M., Brouwer O. F., Bordigoni P., Ringden O., Kapaun P., Ortega J. J., O'Meara A., Cornu G., Souillet G., Frappaz D. and et al. (1995) Allogeneic bone marrow transplantation for lysosomal storage diseases. The European Group for Bone Marrow Transplantation. *Lancet* 345, 1398-402.

Hopwood J. J. and Morris C. P. (1990) The mucopolysaccharidoses. Diagnosis, molecular genetics and treatment. *Mol Biol Med* 7, 381-404.

Horton A. C., Racz B., Monson E. E., Lin A. L., Weinberg R. J. and Ehlers M. D. (2005) Polarized secretory trafficking directs cargo for asymmetric dendrite growth and morphogenesis. *Neuron* 48, 757-71.

Hotchin N. A. and Hall A. (1996) Regulation of the actin cytoskeleton, integrins and cell growth by the Rho family of small GTPases. *Cancer Surv* 27, 311-22.

Hu L., Li L., Xie H., Gu Y. and Peng T. (2011) The Golgi Localization of GOLPH2 (GP73/GOLM1) Is Determined by the Transmembrane and Cytoplamic Sequences. *PLoS One* 6, e28207.

Hurtado L., Caballero C., Gavilan M. P., Cardenas J., Bornens M. and Rios R. M. (2011) Disconnecting the Golgi ribbon from the centrosome prevents directional cell migration and ciliogenesis. *J Cell Biol* 193, 917-33.

Hwu W. L., Chien Y. H., Lee N. C., Chiang S. C., Dobrovolny R., Huang A. C., Yeh H. Y., Chao M. C., Lin S. J., Kitagawa T., Desnick R. J. and Hsu L. W. (2009) Newborn screening for Fabry disease in Taiwan reveals a high incidence of the later-onset GLA mutation c.936+919G>A (IVS4+919G>A). *Hum Mutat* 30, 1397-405.

Hynds D. L., Burry R. W. and Yates A. J. (1997) Gangliosides inhibit growth factor-stimulated neurite outgrowth in SH-SY5Y human neuroblastoma cells. *J Neurosci Res* 47, 617-25.

I

Inder K., Harding A., Plowman S. J., Philips M. R., Parton R. G. and Hancock J. F. (2008) Activation of the MAPK module from different spatial locations generates distinct system outputs. *Mol Biol Cell* 19, 4776-84.

J

Jarvela I., Lehtovirta M., Tikkanen R., Kyttala A. and Jalanko A. (1999) Defective intracellular transport of CLN3 is the molecular basis of Batten disease (JNCL). *Hum Mol Genet* 8, 1091-8.

Jeyakumar M., Dwek R. A., Butters T. D. and Platt F. M. (2005) Storage solutions: treating lysosomal disorders of the brain. *Nat Rev Neurosci* 6, 713-25.

Jeyakumar M., Smith D. A., Williams I. M., Borja M. C., Neville D. C., Butters T. D., Dwek R. A. and Platt F. M. (2004) NSAIDs increase survival in the Sandhoff disease mouse: synergy with N-butyldeoxynojirimycin. *Ann Neurol* 56, 642-9.

Journet A., Chapel A., Kieffer S., Roux F. and Garin J. (2002) Proteomic analysis of human lysosomes: application to monocytic and breast cancer cells. *Proteomics* 2, 1026-40.

Juhasz G. and Neufeld T. P. (2006) Autophagy: a forty-year search for a missing membrane source. *PLoS Biol* 4, e36.

Jung S. C., Han I. P., Limaye A., Xu R., Gelderman M. P., Zerfas P., Tirumalai K., Murray G. J., During M. J., Brady R. O. and Qasba P. (2001) Adeno-associated viral vector-mediated gene transfer results in long-term enzymatic and functional correction in multiple organs of Fabry mice. *Proc Natl Acad Sci U S A* 98, 2676-81.

K

Kakavanos R., Turner C. T., Hopwood J. J., Kakkis E. D. and Brooks D. A. (2003) Immune tolerance after long-term enzyme-replacement therapy among patients who have mucopolysaccharidosis I. *Lancet* 361, 1608-13.

Kao S., Jaiswal R. K., Kolch W. and Landreth G. E. (2001) Identification of the mechanisms regulating the differential activation of the mapk cascade by epidermal growth factor and nerve growth factor in PC12 cells. *J Biol Chem* 276, 18169-77.

Kawashima N., Yoon S. J., Itoh K. and Nakayama K. (2009) Tyrosine kinase activity of epidermal growth factor receptor is regulated by GM3 binding through carbohydrate to carbohydrate interactions. *J Biol Chem* 284, 6147-55.

Keeling K. M., Brooks D. A., Hopwood J. J., Li P., Thompson J. N. and Bedwell D. M. (2001) Gentamicin-mediated suppression of Hurler syndrome stop mutations restores a low level of alpha-L-iduronidase activity and reduces lysosomal glycosaminoglycan accumulation. *Hum Mol Genet* 10, 291-9.

Khanna R., Soska R., Lun Y., Feng J., Frascella M., Young B., Brignol N., Pellegrino L., Sitaraman S. A., Desnick R. J., Benjamin E. R., Lockhart D. J. and Valenzano K. J. (2010) The pharmacological chaperone 1-deoxygalactonojirimycin reduces tissue globotriaosylceramide levels in a mouse model of Fabry disease. *Mol Ther* 18, 23-33.

Kim S. H., Turnbull J. and Guimond S. (2011) Extracellular matrix and cell signalling: the dynamic cooperation of integrin, proteoglycan and growth factor receptor. *J Endocrinol* 209, 139-51.

Kim S. J., Zhang Z., Hitomi E., Lee Y. C. and Mukherjee A. B. (2006) Endoplasmic reticulum stress-induced caspase-4 activation mediates apoptosis and neurodegeneration in INCL. *Hum Mol Genet* 15, 1826-34.

King B., Savas P., Fuller M., Hopwood J. and Hemsley K. (2006) Validation of a heparan sulfate-derived disaccharide as a marker of accumulation in murine mucopolysaccharidosis type IIIA. *Mol Genet Metab* 87, 107-12.

Kint J. A., Dacremont G., Carton D., Orye E. and Hooft C. (1973) Mucopolysaccharidosis: secondarily induced abnormal distribution of lysosomal isoenzymes. *Science* 181, 352-4.

Kint J. A. and Huys A. (1973) Interactions between acid hydrolases of human liver and mucopolysaccharides. *Arch Int Physiol Biochim* 81, 375-6.

Kishnani P. S., Corzo D., Nicolino M., Byrne B., Mandel H., Hwu W. L., Leslie N., Levine J., Spencer C., McDonald M., Li J., Dumontier J., Halberthal M., Chien Y. H., Hopkin R., Vijayaraghavan S., Gruskin D., Bartholomew D., van der Ploeg A., Clancy J. P., Parini R., Morin G., Beck M., De la Gastine G. S., Jokic M., Thurberg B., Richards S., Bali D., Davison M., Worden M. A., Chen Y. T. and Wraith J. E. (2007) Recombinant human acid [alpha]-glucosidase: major clinical benefits in infantile-onset Pompe disease. *Neurology* 68, 99-109.

Klionsky D. J. (2005) The molecular machinery of autophagy: unanswered questions. *J Cell Sci* 118, 7-18.

Kodani A., Kristensen I., Huang L. and Sutterlin C. (2009) GM130-dependent control of Cdc42 activity at the Golgi regulates centrosome organization. *Mol Biol Cell* 20, 1192-200.

Kodani A. and Sutterlin C. (2008) The Golgi protein GM130 regulates centrosome morphology and function. *Mol Biol Cell* 19, 745-53.

Kodani A. and Sutterlin C. (2009) A new function for an old organelle: microtubule nucleation at the Golgi apparatus. *EMBO J* 28, 995-6.

Kreuger J., Spillmann D., Li J. P. and Lindahl U. (2006) Interactions between heparan sulfate and proteins: the concept of specificity. *J Cell Biol* 174, 323-7.

L

Lachmann R. H. (2006) Miglustat: substrate reduction therapy for glycosphingolipid lysosomal storage disorders. *Drugs Today (Barc)* 42, 29-38.

Lachmann R. H., Grant I. R., Halsall D. and Cox T. M. (2004a) Twin pairs showing discordance of phenotype in adult Gaucher's disease. *QJM* 97, 199-204.

Lachmann R. H., te Vruchte D., Lloyd-Evans E., Reinkensmeier G., Sillence D. J., Fernandez-Guillen L., Dwek R. A., Butters T. D., Cox T. M. and Platt F. M. (2004b) Treatment with miglustat reverses the lipid-trafficking defect in Niemann-Pick disease type C. *Neurobiol Dis* 16, 654-8.

Ladinsky M. S., Wu C. C., McIntosh S., McIntosh J. R. and Howell K. E. (2002) Structure of the Golgi and distribution of reporter molecules at 20 degrees C reveals the complexity of the exit compartments. *Mol Biol Cell* 13, 2810-25.

Larocca M. C., Shanks R. A., Tian L., Nelson D. L., Stewart D. M. and Goldenring J. R. (2004) AKAP350 interaction with cdc42 interacting protein 4 at the Golgi apparatus. *Mol Biol Cell* 15, 2771-81.

Larsson C. (2006) Protein kinase C and the regulation of the actin cytoskeleton. *Cell Signal* 18, 276-84.

Le Borgne R., Alconada A., Bauer U. and Hoflack B. (1998) The mammalian AP-3 adaptor-like complex mediates the intracellular transport of lysosomal membrane glycoproteins. *J Biol Chem* 273, 29451-61.

Lemonnier T., Blanchard S., Toli D., Roy E., Bigou S., Froissart R., Rouvet I., Vitry S., Heard J. M. and Bohl D. (2011) Modeling neuronal defects associated with a lysosomal disorder using patient-derived induced pluripotent stem cells. *Hum Mol Genet*.

Levy H., Or A., Eyal N., Wilder S., Widgerson M., Kolodny E. H., Zimran A. and Horowitz M. (1991) Molecular aspects of Gaucher disease. *Dev Neurosci* 13, 352-62.

Lewis D. A., Cruz D., Eggan S. and Erickson S. (2004) Postnatal development of prefrontal inhibitory circuits and the pathophysiology of cognitive dysfunction in schizophrenia. *Ann N Y Acad Sci* 1021, 64-76.

Li H., Malani N., Hamilton S. R., Schlachterman A., Bussadori G., Edmonson S. E., Shah R., Arruda V. R., Mingozzi F., Wright J. F., Bushman F. D. and High K. A. (2011) Assessing the potential for AAV vector genotoxicity in a murine model. *Blood* 117, 3311-9.

Li H. H., Yu W. H., Rozengurt N., Zhao H. Z., Lyons K. M., Anagnostaras S., Fanselow M. S., Suzuki K., Vanier M. T. and Neufeld E. F. (1999) Mouse model of Sanfilippo syndrome type B produced by targeted disruption of the gene encoding alpha-N-acetylglucosaminidase. *Proc Natl Acad Sci U S A* 96, 14505-10.

Li H. H., Zhao H. Z., Neufeld E. F., Cai Y. and Gomez-Pinilla F. (2002) Attenuated plasticity in neurons and astrocytes in the mouse model of Sanfilippo syndrome type B. *J Neurosci Res* 69, 30-8.

Li Y., Scott C. R., Chamoles N. A., Ghavami A., Pinto B. M., Turecek F. and Gelb M. H. (2004) Direct multiplex assay of lysosomal enzymes in dried blood spots for newborn screening. *Clin Chem* 50, 1785-96.

Lin H. Y., Chong K. W., Hsu J. H., Yu H. C., Shih C. C., Huang C. H., Lin S. J., Chen C. H., Chiang C. C., Ho H. J., Lee P. C., Kao C. H., Cheng K. H., Hsueh C. and Niu D. M. (2009) High incidence of the cardiac variant of Fabry disease revealed by newborn screening in the Taiwan Chinese population. *Circ Cardiovasc Genet* 2, 450-6.

Linstedt A. D., Jesch S. A., Mehta A., Lee T. H., Garcia-Mata R., Nelson D. S. and Sztul E. (2000) Binding relationships of membrane tethering components. The giantin N terminus and the GM130 N terminus compete for binding to the p115 C terminus. *J Biol Chem* 275, 10196-201.

Litvak V., Argov R., Dahan N., Ramachandran S., Amarilio R., Shainskaya A. and Lev S. (2004) Mitotic phosphorylation of the peripheral Golgi protein Nir2 by Cdk1 provides a docking mechanism for Plk1 and affects cytokinesis completion. *Mol Cell* 14, 319-30.

Liu J., Prunuske A. J., Fager A. M. and Ullman K. S. (2003) The COPI complex functions in nuclear envelope breakdown and is recruited by the nucleoporin Nup153. *Dev Cell* 5, 487-98.

Lloyd-Evans E., Morgan A. J., He X., Smith D. A., Elliot-Smith E., Sillence D. J., Churchill G. C., Schuchman E. H., Galione A. and Platt F. M. (2008) Niemann-Pick disease type C1 is a sphingosine storage disease that causes deregulation of lysosomal calcium. *Nat Med* 14, 1247-55.

Lopes C. C., Dietrich C. P. and Nader H. B. (2006) Specific structural features of syndecans and heparan sulfate chains are needed for cell signaling. *Braz J Med Biol Res* 39, 157-67.

Lowe M., Rabouille C., Nakamura N., Watson R., Jackman M., Jamsa E., Rahman D., Pappin D. J. and Warren G. (1998) Cdc2 kinase directly phosphorylates the cis-Golgi matrix protein GM130 and is required for Golgi fragmentation in mitosis. *Cell* 94, 783-93.

Lowe M. (2011) Structural organization of the Golgi apparatus. *Curr Opin Cell Biol* 23, 85-93.

Luiro K., Kopra O., Blom T., Gentile M., Mitchison H. M., Hovatta I., Tornquist K. and Jalanko A. (2006) Batten disease (JNCL) is linked to disturbances in mitochondrial, cytoskeletal, and synaptic compartments. *J Neurosci Res* 84, 1124-38.

Luskin M. B. (1993) Restricted proliferation and migration of postnatally generated neurons derived from the forebrain subventricular zone. *Neuron* 11, 173-89.

Luzi P., Abraham R. M., Rafi M. A., Curtis M., Hooper D. C. and Wenger D. A. (2009) Effects of treatments on inflammatory and apoptotic markers in the CNS of mice with globoid cell leukodystrophy. *Brain Res* 1300, 146-58.

Luzio J. P., Parkinson M. D., Gray S. R. and Bright N. A. (2009) The delivery of endocytosed cargo to lysosomes. *Biochem Soc Trans* 37, 1019-21.

Luzio J. P., Poupon V., Lindsay M. R., Mullock B. M., Piper R. C. and Pryor P. R. (2003) Membrane dynamics and the biogenesis of lysosomes. *Mol Membr Biol* 20, 141-54.

Luzio J. P., Pryor P. R. and Bright N. A. (2007) Lysosomes: fusion and function. *Nat Rev Mol Cell Biol* 8, 622-32.

M

Ma P., Beck S. L., Raab R. W., McKown R. L., Coffman G. L., Utani A., Chirico W. J., Rapraeger A. C. and Laurie G. W. (2006) Heparanase deglycanation of syndecan-1 is required for binding of the epithelial-restricted prosecretory mitogen lacritin. *J Cell Biol* 174, 1097-106.

Maccioni H. J. (2007) Glycosylation of glycolipids in the Golgi complex. *J Neurochem* 103 Suppl 1, 81-90.

Maegawa G. H., Stockley T., Tropak M., Banwell B., Blaser S., Kok F., Giugliani R., Mahuran D. and Clarke J. T. (2006) The natural history of juvenile or subacute GM2 gangliosidosis: 21 new cases and literature review of 134 previously reported. *Pediatrics* 118, e1550-62.

Maegawa G. H., van Giersbergen P. L., Yang S., Banwell B., Morgan C. P., Dingemanse J., Tifft C. J. and Clarke J. T. (2009) Pharmacokinetics, safety and tolerability of miglustat in the treatment of pediatric patients with GM2 gangliosidosis. *Mol Genet Metab* 97, 284-91.

Maguire A. M., High K. A., Auricchio A., Wright J. F., Pierce E. A., Testa F., Mingozzi F., Bennicelli J. L., Ying G. S., Rossi S., Fulton A., Marshall K. A., Banfi S., Chung D. C., Morgan J. I., Hauck B., Zelenaia O., Zhu X., Raffini L., Coppieters F., De Baere E., Shindler K. S., Volpe N. J., Surace E. M., Acerra C., Lyubarsky A., Redmond T. M., Stone E., Sun J., McDonnell J. W., Leroy B. P., Simonelli F. and Bennett J. (2009) Age-dependent effects of RPE65 gene therapy for Leber's congenital amaurosis: a phase 1 dose-escalation trial. *Lancet* 374, 1597-605.

Maguire A. M., Simonelli F., Pierce E. A., Pugh E. N., Jr., Mingozzi F., Bennicelli J., Banfi S., Marshall K. A., Testa F., Surace E. M., Rossi S., Lyubarsky A., Arruda V. R., Konkle B., Stone E., Sun J., Jacobs J., Dell'Osso L., Hertle R., Ma J. X., Redmond T. M., Zhu X., Hauck B., Zelenaia O., Shindler K. S., Maguire M. G., Wright J. F., Volpe N. J., McDonnell J. W., Auricchio A., High K. A. and Bennett J. (2008) Safety and efficacy of gene transfer for Leber's congenital amaurosis. *N Engl J Med* 358, 2240-8.

Malik V., Rodino-Klapac L. R., Viollet L., Wall C., King W., Al-Dahhak R., Lewis S., Shilling C. J., Kota J., Serrano-Munuera C., Hayes J., Mahan J. D., Campbell K. J., Banwell B., Dasouki M., Watts V., Sivakumar K., Bien-Willner R., Flanigan K. M., Sahenk Z., Barohn R. J., Walker C. M. and Mendell J. R. (2010) Gentamicin-induced readthrough of stop codons in Duchenne muscular dystrophy. *Ann Neurol* 67, 771-80.

Malinowska M., Wilkinson F. L., Bennett W., Langford-Smith K. J., O'Leary H. A., Jakobkiewicz-Banecka J., Wynn R., Wraith J. E., Wegrzyn G. and Bigger B. W. (2009) Genistein reduces lysosomal storage in peripheral tissues of mucopolysaccharide IIIB mice. *Mol Genet Metab* 98, 235-42.

Manno C. S., Pierce G. F., Arruda V. R., Glader B., Ragni M., Rasko J. J., Ozelo M. C., Hoots K., Blatt P., Konkle B., Dake M., Kaye R., Razavi M., Zajko A., Zehnder J., Rustagi P. K., Nakai H., Chew A., Leonard D., Wright J. F., Lessard R. R., Sommer J. M., Tigges M., Sabatino D., Luk A., Jiang H., Mingozzi F., Couto L., Ertl H. C., High K. A. and Kay M. A. (2006) Successful transduction of liver in hemophilia by AAV-Factor IX and limitations imposed by the host immune response. *Nat Med* 12, 342-7.

Marchetto M. C., Carromeu C., Acab A., Yu D., Yeo G. W., Mu Y., Chen G., Gage F. H. and Muotri A. R. (2010) A model for neural development and treatment of Rett syndrome using human induced pluripotent stem cells. *Cell* 143, 527-39.

Marin O. and Rubenstein J. L. (2003) Cell migration in the forebrain. *Annu Rev Neurosci* 26, 441-83.

Markoulaki S., Hanna J., Beard C., Carey B. W., Cheng A. W., Lengner C. J., Dausman J. A., Fu D., Gao Q., Wu S., Cassady J. P. and Jaenisch R. (2009) Transgenic mice with defined combinations of drug-inducible reprogramming factors. *Nat Biotechnol* 27, 169-71.

Marks D. L. and Pagano R. E. (2002) Endocytosis and sorting of glycosphingolipids in sphingolipid storage disease. *Trends Cell Biol* 12, 605-13.

Marks W. J., Jr., Bartus R. T., Siffert J., Davis C. S., Lozano A., Boulis N., Vitek J., Stacy M., Turner D., Verhagen L., Bakay R., Watts R., Guthrie B., Jankovic J., Simpson R., Tagliati M., Alterman R., Stern M., Baltuch G., Starr P. A., Larson P. S., Ostrem J. L., Nutt J., Kieburtz K., Kordower J. H. and Olanow C. W. Gene delivery of AAV2-neurturin for Parkinson's disease: a double-blind, randomised, controlled trial. *Lancet Neurol* 9, 1164-72.

Marra P., Maffucci T., Daniele T., Tullio G. D., Ikehara Y., Chan E. K., Luini A., Beznoussenko G., Mironov A. and De Matteis M. A. (2001) The GM130 and GRASP65 Golgi proteins cycle through and define a subdomain of the intermediate compartment. *Nat Cell Biol* 3, 1101-13.

Marra P., Salvatore L., Mironov A., Jr., Di Campli A., Di Tullio G., Trucco A., Beznoussenko G., Mironov A. and De Matteis M. A. (2007) The biogenesis of the Golgi ribbon: the roles of membrane input from the ER and of GM130. *Mol Biol Cell* 18, 1595-608.

Martinez-Vicente M. and Cuervo A. M. (2007) Autophagy and neurodegeneration: when the cleaning crew goes on strike. *Lancet Neurol* 6, 352-61.

Matallanas D., Sanz-Moreno V., Arozarena I., Calvo F., Agudo-Ibanez L., Santos E., Berciano M. T. and Crespo P. (2006) Distinct utilization of effectors and biological outcomes resulting from site-specific Ras activation: Ras functions in lipid rafts and Golgi complex are dispensable for proliferation and transformation. *Mol Cell Biol* 26, 100-16.

Matas O. B., Martinez-Menarguez J. A. and Egea G. (2004) Association of Cdc42/N-WASP/Arp2/3 signaling pathway with Golgi membranes. *Traffic* 5, 838-46.

Matsuda J., Suzuki O., Oshima A., Yamamoto Y., Noguchi A., Takimoto K., Itoh M., Matsuzaki Y., Yasuda Y., Ogawa S., Sakata Y., Nanba E., Higaki K., Ogawa Y., Tominaga L., Ohno K., Iwasaki H., Watanabe H., Brady R. O. and Suzuki Y. (2003) Chemical chaperone therapy for brain pathology in G(M1)-gangliosidosis. *Proc Natl Acad Sci U S A* 100, 15912-7.

Matsuda J., Vanier M. T., Saito Y. and Suzuki K. (2001) Dramatic phenotypic improvement during pregnancy in a genetic leukodystrophy: estrogen appears to be a critical factor. *Hum Mol Genet* 10, 2709-15.

Matsuki T., Matthews R. T., Cooper J. A., van der Brug M. P., Cookson M. R., Hardy J. A., Olson E. C. and Howell B. W. (2010) Reelin and stk25 have opposing roles in neuronal polarization and dendritic Golgi deployment. *Cell* 143, 826-36.

Maxzud M. K., Daniotti J. L. and Maccioni H. J. (1995) Functional coupling of glycosyl transfer steps for synthesis of gangliosides in Golgi membranes from neural retina cells. *J Biol Chem* 270, 20207-14.

Mayinger P. (2011) Signaling at the Golgi. *Cold Spring Harb Perspect Biol* 3.

McAllister A. K. (2001) Neurotrophins and neuronal differentiation in the central nervous system. *Cell Mol Life Sci* 58, 1054-60.

McEachern K. A., Nietupski J. B., Chuang W. L., Armentano D., Johnson J., Hutto E., Grabowski G. A., Cheng S. H. and Marshall J. (2006) AAV8-mediated expression of glucocerebrosidase ameliorates the storage pathology in the visceral organs of a mouse model of Gaucher disease. *J Gene Med* 8, 719-29.

McGlynn R., Dobrenis K. and Walkley S. U. (2004) Differential subcellular localization of cholesterol, gangliosides, and glycosaminoglycans in murine models of mucopolysaccharide storage disorders. *J Comp Neurol* 480, 415-26.

McInnes B., Potier M., Wakamatsu N., Melancon S. B., Klavins M. H., Tsuji S. and Mahuran D. J. (1992) An unusual splicing mutation in the HEXB gene is associated with dramatically different phenotypes in patients from different racial backgrounds. *J Clin Invest* 90, 306-14.

McPhee S. W., Janson C. G., Li C., Samulski R. J., Camp A. S., Francis J., Shera D., Lioutermann L., Feely M., Freese A. and Leone P. (2006) Immune responses to AAV in a phase I study for Canavan disease. *J Gene Med* 8, 577-88.

Medina D. L., Fraldi A., Bouche V., Annunziata F., Mansueto G., Spampanato C., Puri C., Pignata A., Martina J. A., Sardiello M., Palmieri M., Polishchuk R., Puertollano R. and Ballabio A. (2011) Transcriptional activation of lysosomal exocytosis promotes cellular clearance. *Dev Cell* 21, 421-30.

Meier E. M., Schwarzmann G., Furst W. and Sandhoff K. (1991) The human GM2 activator protein. A substrate specific cofactor of beta-hexosaminidase A. *J Biol Chem* 266, 1879-87.

Meikle P. J., Fietz M. J. and Hopwood J. J. (2004) Diagnosis of lysosomal storage disorders: current techniques and future directions. *Expert Rev Mol Diagn* 4, 677-91.

Meikle P. J., Hopwood J. J., Clague A. E. and Carey W. F. (1999) Prevalence of lysosomal storage disorders. *JAMA* 281, 249-54.

Mellman I. (1996) Endocytosis and molecular sorting. *Annu Rev Cell Dev Biol* 12, 575-625.

Mendell J. R., Campbell K., Rodino-Klapac L., Sahenk Z., Shilling C., Lewis S., Bowles D., Gray S., Li C., Galloway G., Malik V., Coley B., Clark K. R., Li J., Xiao X., Samulski J., McPhee S. W., Samulski R. J. and Walker C. M. (2010) Dystrophin immunity in Duchenne's muscular dystrophy. *N Engl J Med* 363, 1429-37.

Menezes J. R., Marins M., Alves J. A., Froes M. M. and Hedin-Pereira C. (2002) Cell migration in the postnatal subventricular zone. *Braz J Med Biol Res* 35, 1411-21.

Meng X. L., Shen J. S., Kawagoe S., Ohashi T., Brady R. O. and Eto Y. (2010) Induced pluripotent stem cells derived from mouse models of lysosomal storage disorders. *Proc Natl Acad Sci U S A* 107, 7886-91.

Meuillet E., Cremel G., Dreyfus H. and Hicks D. (1996) Differential modulation of basic fibroblast and epidermal growth factor receptor activation by ganglioside GM3 in cultured retinal Muller glia. *Glia* 17, 206-16.

Miaczynska M., Pelkmans L. and Zerial M. (2004) Not just a sink: endosomes in control of signal transduction. *Curr Opin Cell Biol* 16, 400-6.

Miedel M. T., Rbaibi Y., Guerriero C. J., Colletti G., Weixel K. M., Weisz O. A. and Kiselyov K. (2008) Membrane traffic and turnover in TRP-ML1-deficient

cells: a revised model for mucolipidosis type IV pathogenesis. *J Exp Med* 205, 1477-90.

Miljan E. A., Meuillet E. J., Mania-Farnell B., George D., Yamamoto H., Simon H. G. and Bremer E. G. (2002) Interaction of the extracellular domain of the epidermal growth factor receptor with gangliosides. *J Biol Chem* 277, 10108-13.

Miller P. M., Folkmann A. W., Maia A. R., Efimova N., Efimov A. and Kaverina I. (2009) Golgi-derived CLASP-dependent microtubules control Golgi organization and polarized trafficking in motile cells. *Nat Cell Biol* 11, 1069-80.

Ming G. L. and Song H. (2005) Adult neurogenesis in the mammalian central nervous system. *Annu Rev Neurosci* 28, 223-50.

Ming G. L. and Song H. (2011) Adult neurogenesis in the mammalian brain: significant answers and significant questions. *Neuron* 70, 687-702.

Mingozzi F., Hasbrouck N. C., Basner-Tschakarjan E., Edmonson S. A., Hui D. J., Sabatino D. E., Zhou S., Wright J. F., Jiang H., Pierce G. F., Arruda V. R. and High K. A. (2007) Modulation of tolerance to the transgene product in a nonhuman primate model of AAV-mediated gene transfer to liver. *Blood* 110, 2334-41.

Miura K., Jacques K. M., Stauffer S., Kubosaki A., Zhu K., Hirsch D. S., Resau J., Zheng Y. and Randazzo P. A. (2002) ARAP1: a point of convergence for Arf and Rho signaling. *Mol Cell* 9, 109-19.

Modlich U., Bohne J., Schmidt M., von Kalle C., Knoss S., Schambach A. and Baum C. (2006) Cell-culture assays reveal the importance of retroviral vector design for insertional genotoxicity. *Blood* 108, 2545-53.

Montini E., Cesana D., Schmidt M., Sanvito F., Ponzoni M., Bartholomae C., Sergi Sergi L., Benedicenti F., Ambrosi A., Di Serio C., Doglioni C., von Kalle C. and Naldini L. (2006) Hematopoietic stem cell gene transfer in a tumor-prone mouse model uncovers low genotoxicity of lentiviral vector integration. *Nat Biotechnol* 24, 687-96.

Moran D., Galperin E. and Horowitz M. (1997) Identification of factors regulating the expression of the human glucocerebrosidase gene. *Gene* 194, 201-13.

Mori S., Wu C. Y., Yamaji S., Saegusa J., Shi B., Ma Z., Kuwabara Y., Lam K. S., Isseroff R. R., Takada Y. K. and Takada Y. (2008) Direct binding of integrin alphavbeta3 to FGF1 plays a role in FGF1 signaling. *J Biol Chem* 283, 18066-75.

Moyer B. D., Allan B. B. and Balch W. E. (2001) Rab1 interaction with a GM130 effector complex regulates COPII vesicle cis--Golgi tethering. *Traffic* 2, 268-76.

Muenzer J., Wraith J. E., Beck M., Giugliani R., Harmatz P., Eng C. M., Vellodi A., Martin R., Ramaswami U., Gucsavas-Calikoglu M., Vijayaraghavan S., Wendt S., Puga A. C., Ulbrich B., Shinawi M., Cleary M., Piper D., Conway A. M. and Kimura A. (2006) A phase II/III clinical study of enzyme replacement therapy with idursulfase in mucopolysaccharidosis II (Hunter syndrome). *Genet Med* 8, 465-73.

Mundkur N. (2005) Neuroplasticity in children. *Indian J Pediatr* 72, 855-7.

Murrey H. E. and Hsieh-Wilson L. C. (2008) The chemical neurobiology of carbohydrates. *Chem Rev* 108, 1708-31.

N

Nakagawa M., Koyanagi M., Tanabe K., Takahashi K., Ichisaka T., Aoi T., Okita K., Mochiduki Y., Takizawa N. and Yamanaka S. (2008) Generation of induced pluripotent stem cells without Myc from mouse and human fibroblasts. *Nat Biotechnol* 26, 101-6.

Nakagawa T., Setou M., Seog D., Ogasawara K., Dohmae N., Takio K. and Hirokawa N. (2000) A novel motor, KIF13A, transports mannose-6-phosphate receptor to plasma membrane through direct interaction with AP-1 complex. *Cell* 103, 569-81.

Nakai H., Montini E., Fuess S., Storm T. A., Grompe M. and Kay M. A. (2003) AAV serotype 2 vectors preferentially integrate into active genes in mice. *Nat Genet* 34, 297-302.

Nakajima H., Hirata A., Ogawa Y., Yonehara T., Yoda K. and Yamasaki M. (1991) A cytoskeleton-related gene, uso1, is required for intracellular protein transport in Saccharomyces cerevisiae. *J Cell Biol* 113, 245-60.

Nakamura N., Lowe M., Levine T. P., Rabouille C. and Warren G. (1997) The vesicle docking protein p115 binds GM130, a cis-Golgi matrix protein, in a mitotically regulated manner. *Cell* 89, 445-55.

Nakamura N. (2010) Emerging new roles of GM130, a cis-Golgi matrix protein, in higher order cell functions. *J Pharmacol Sci* 112, 255-64.

Nakato H. and Kimata K. (2002) Heparan sulfate fine structure and specificity of proteoglycan functions. *Biochim Biophys Acta* 1573, 312-8.

Nathwani A. C., Tuddenham E. G., Rangarajan S., Rosales C., McIntosh J., Linch D. C., Chowdary P., Riddell A., Pie A. J., Harrington C., O'Beirne J., Smith K., Pasi J., Glader B., Rustagi P., Ng C. Y., Kay M. A., Zhou J., Spence Y., Morton C. L., Allay J., Coleman J., Sleep S., Cunningham J. M., Srivastava D., Basner-Tschakarjan E., Mingozzi F., High K. A., Gray J. T., Reiss U. M., Nienhuis A. W. and Davidoff A. M. (2011) Adenovirus-Associated Virus Vector-Mediated Gene Transfer in Hemophilia B. *N Engl J Med*.

Neudorfer O., Pastores G. M., Zeng B. J., Gianutsos J., Zaroff C. M. and Kolodny E. H. (2005) Late-onset Tay-Sachs disease: phenotypic characterization and genotypic correlations in 21 affected patients. *Genet Med* 7, 119-23.

Neufeld E. F. and Muenzer J. (2001) The mucopolysaccharidoses. In: The Metabolic and Molecular Basis of Inherited Disease. *8th ed. Edition (C.R. Scriver ALB, W.S. Sly, D. Valle, ed), pp 3421-3452. New York: McGraw-Hill*.

Ni X. and Morales C. R. (2006) The lysosomal trafficking of acid sphingomyelinase is mediated by sortilin and mannose 6-phosphate receptor. *Traffic* 7, 889-902.

Nilsson T., Lucocq J. M., Mackay D. and Warren G. (1991) The membrane spanning domain of beta-1,4-galactosyltransferase specifies trans Golgi localization. *EMBO J* 10, 3567-75.

Nishimura T., Takahashi M., Kim H. S., Mukai H. and Ono Y. (2005) Centrosome-targeting region of CG-NAP causes centrosome amplification by recruiting cyclin E-cdk2 complex. *Genes Cells* 10, 75-86.

Nixon R. A. and Cataldo A. M. (2006) Lysosomal system pathways: genes to neurodegeneration in Alzheimer's disease. *J Alzheimers Dis* 9, 277-89.

Nixon R. A., Wegiel J., Kumar A., Yu W. H., Peterhoff C., Cataldo A. and Cuervo A. M. (2005) Extensive involvement of autophagy in Alzheimer disease: an immuno-electron microscopy study. *J Neuropathol Exp Neurol* 64, 113-22.

Nixon R. A., Yang D. S. and Lee J. H. (2008) Neurodegenerative lysosomal disorders: a continuum from development to late age. *Autophagy* 4, 590-9.
Noda T., Fujita N. and Yoshimori T. (2009) The late stages of autophagy: how does the end begin? *Cell Death Differ* 16, 984-90.

O

O'Toole T. E., Bialkowska K., Li X. and Fox J. E. (2011) Tiam1 is recruited to beta1-integrin complexes by 14-3-3zeta where it mediates integrin-induced rac1 activation and motility. *J Cell Physiol*.
Ohmi K., Kudo L. C., Ryazantsev S., Zhao H. Z., Karsten S. L. and Neufeld E. F. (2009) Sanfilippo syndrome type B, a lysosomal storage disease, is also a tauopathy. *Proc Natl Acad Sci U S A* 106, 8332-7.
Ohno K., Saito S., Sugawara K. and Sakuraba H. (2008) Structural consequences of amino acid substitutions causing Tay-Sachs disease. *Mol Genet Metab* 94, 462-8.
Onken B., Wiener H., Philips M. R. and Chang E. C. (2006) Compartmentalized signaling of Ras in fission yeast. *Proc Natl Acad Sci U S A* 103, 9045-50.
Owada M. and Neufeld E. F. (1982) Is there a mechanism for introducing acid hydrolases into liver lysosomes that is independent of mannose 6-phosphate recognition? Evidence from I-cell disease. *Biochem Biophys Res Commun* 105, 814-20.

P

Palmer K. J., Hughes H. and Stephens D. J. (2009) Specificity of cytoplasmic dynein subunits in discrete membrane-trafficking steps. *Mol Biol Cell* 20, 2885-99.
Pan C., Nelson M. S., Reyes M., Koodie L., Brazil J. J., Stephenson E. J., Zhao R. C., Peters C., Selleck S. B., Stringer S. E. and Gupta P. (2005) Functional abnormalities of heparan sulfate in mucopolysaccharidosis-I are associated with defective biologic activity of FGF-2 on human multipotent progenitor cells. *Blood* 106, 1956-64.
Park I. H., Arora N., Huo H., Maherali N., Ahfeldt T., Shimamura A., Lensch M. W., Cowan C., Hochedlinger K. and Daley G. Q. (2008a) Disease-specific induced pluripotent stem cells. *Cell* 134, 877-86.
Park I. H., Lerou P. H., Zhao R., Huo H. and Daley G. Q. (2008b) Generation of human-induced pluripotent stem cells. *Nat Protoc* 3, 1180-6.
Park I. H., Zhao R., West J. A., Yabuuchi A., Huo H., Ince T. A., Lerou P. H., Lensch M. W. and Daley G. Q. (2008c) Reprogramming of human somatic cells to pluripotency with defined factors. *Nature* 451, 141-6.
Parkinson-Lawrence E. J., Shandala T., Prodoehl M., Plew R., Borlace G. N. and Brooks D. A. (2010) Lysosomal storage disease: revealing lysosomal function and physiology. *Physiology (Bethesda)* 25, 102-15.
Passafaro M., Nakagawa T., Sala C. and Sheng M. (2003) Induction of dendritic spines by an extracellular domain of AMPA receptor subunit GluR2. *Nature* 424, 677-81.

Passini M. A., Dodge J. C., Bu J., Yang W., Zhao Q., Sondhi D., Hackett N. R., Kaminsky S. M., Mao Q., Shihabuddin L. S., Cheng S. H., Sleat D. E., Stewart G. R., Davidson B. L., Lobel P. and Crystal R. G. (2006) Intracranial delivery of CLN2 reduces brain pathology in a mouse model of classical late infantile neuronal ceroid lipofuscinosis. *J Neurosci* 26, 1334-42.

Pastores G. M., Barnett N. L. and Kolodny E. H. (2005) An open-label, noncomparative study of miglustat in type I Gaucher disease: efficacy and tolerability over 24 months of treatment. *Clin Ther* 27, 1215-27.

Patterson G. H., Hirschberg K., Polishchuk R. S., Gerlich D., Phair R. D. and Lippincott-Schwartz J. (2008) Transport through the Golgi apparatus by rapid partitioning within a two-phase membrane system. *Cell* 133, 1055-67.

Patterson M. C., Vecchio D., Prady H., Abel L. and Wraith J. E. (2007) Miglustat for treatment of Niemann-Pick C disease: a randomised controlled study. *Lancet Neurol* 6, 765-72.

Pattingre S., Espert L., Biard-Piechaczyk M. and Codogno P. (2008) Regulation of macroautophagy by mTOR and Beclin 1 complexes. *Biochimie* 90, 313-23.

Pelham H. R. (2001) Traffic through the Golgi apparatus. *J Cell Biol* 155, 1099-101.

Pelled D., Riebeling C., van Echten-Deckert G., Sandhoff K. and Futerman A. H. (2003) Reduced rates of axonal and dendritic growth in embryonic hippocampal neurones cultured from a mouse model of Sandhoff disease. *Neuropathol Appl Neurobiol* 29, 341-9.

Persico A., Cervigni R. I., Barretta M. L. and Colanzi A. (2009) Mitotic inheritance of the Golgi complex. *FEBS Lett* 583, 3857-62.

Peters C. and Steward C. G. (2003) Hematopoietic cell transplantation for inherited metabolic diseases: an overview of outcomes and practice guidelines. *Bone Marrow Transplant* 31, 229-39.

Peterson S. B. and Liu J. (2010) Unraveling the specificity of heparanase utilizing synthetic substrates. *J Biol Chem* 285, 14504-13.

Platt F. M. and Walkley S. U. (2004) Lysosomal Disorders of the Brain. *Oxford press*.

Polishchuk E. V., Di Pentima A., Luini A. and Polishchuk R. S. (2003) Mechanism of constitutive export from the golgi: bulk flow via the formation, protrusion, and en bloc cleavage of large trans-golgi network tubular domains. *Mol Biol Cell* 14, 4470-85.

Poorthuis B. J., Wevers R. A., Kleijer W. J., Groener J. E., de Jong J. G., van Weely S., Niezen-Koning K. E. and van Diggelen O. P. (1999) The frequency of lysosomal storage diseases in The Netherlands. *Hum Genet* 105, 151-6.

Preisinger C., Short B., De Corte V., Bruyneel E., Haas A., Kopajtich R., Gettemans J. and Barr F. A. (2004) YSK1 is activated by the Golgi matrix protein GM130 and plays a role in cell migration through its substrate 14-3-3zeta. *J Cell Biol* 164, 1009-20.

Pryor P. R. and Luzio J. P. (2009) Delivery of endocytosed membrane proteins to the lysosome. *Biochim Biophys Acta* 1793, 615-24.

Pulvirenti T., Giannotta M., Capestrano M., Capitani M., Pisanu A., Polishchuk R. S., San Pietro E., Beznoussenko G. V., Mironov A. A., Turacchio G., Hsu V. W., Sallese M. and Luini A. (2008) A traffic-activated Golgi-based signalling circuit coordinates the secretory pathway. *Nat Cell Biol* 10, 912-22.

Puri V., Watanabe R., Dominguez M., Sun X., Wheatley C. L., Marks D. L. and Pagano R. E. (1999) Cholesterol modulates membrane traffic along the endocytic pathway in sphingolipid-storage diseases. *Nat Cell Biol* 1, 386-8.

Puthenveedu M. A., Bachert C., Puri S., Lanni F. and Linstedt A. D. (2006) GM130 and GRASP65-dependent lateral cisternal fusion allows uniform Golgi-enzyme distribution. *Nat Cell Biol* 8, 238-48.

Puthenveedu M. A. and Linstedt A. D. (2001) Evidence that Golgi structure depends on a p115 activity that is independent of the vesicle tether components giantin and GM130. *J Cell Biol* 155, 227-38.

R

Rakic P. (1988) Specification of cerebral cortical areas. *Science* 241, 170-6.

Ramaswami U., Wendt S., Pintos-Morell G., Parini R., Whybra C., Leon Leal J. A., Santus F. and Beck M. (2007) Enzyme replacement therapy with agalsidase alfa in children with Fabry disease. *Acta Paediatr* 96, 122-7.

Ramirez I. B. and Lowe M. (2009) Golgins and GRASPs: holding the Golgi together. *Semin Cell Dev Biol* 20, 770-9.

Raper S. E., Chirmule N., Lee F. S., Wivel N. A., Bagg A., Gao G. P., Wilson J. M. and Batshaw M. L. (2003) Fatal systemic inflammatory response syndrome in a ornithine transcarbamylase deficient patient following adenoviral gene transfer. *Mol Genet Metab* 80, 148-58.

Raposo G., Marks M. S. and Cutler D. F. (2007) Lysosome-related organelles: driving post-Golgi compartments into specialisation. *Curr Opin Cell Biol* 19, 394-401.

Reczek D., Schwake M., Schroder J., Hughes H., Blanz J., Jin X., Brondyk W., Van Patten S., Edmunds T. and Saftig P. (2007) LIMP-2 is a receptor for lysosomal mannose-6-phosphate-independent targeting of beta-glucocerebrosidase. *Cell* 131, 770-83.

Reddy A., Caler E. V. and Andrews N. W. (2001) Plasma membrane repair is mediated by Ca(2+)-regulated exocytosis of lysosomes. *Cell* 106, 157-69.

Rehling P., Darsow T., Katzmann D. J. and Emr S. D. (1999) Formation of AP-3 transport intermediates requires Vps41 function. *Nat Cell Biol* 1, 346-53.

Reolon G. K., Reinke A., de Oliveira M. R., Braga L. M., Camassola M., Andrades M. E., Moreira J. C., Nardi N. B., Roesler R. and Dal-Pizzol F. (2009) Alterations in oxidative markers in the cerebellum and peripheral organs in MPS I mice. *Cell Mol Neurobiol* 29, 443-8.

Reuser A. J., Kroos M. A., Hermans M. M., Bijvoet A. G., Verbeet M. P., Van Diggelen O. P., Kleijer W. J. and Van der Ploeg A. T. (1995) Glycogenosis type II (acid maltase deficiency). *Muscle Nerve* 3, S61-9.

Rink J., Ghigo E., Kalaidzidis Y. and Zerial M. (2005) Rab conversion as a mechanism of progression from early to late endosomes. *Cell* 122, 735-49.

Rios R. M., Sanchis A., Tassin A. M., Fedriani C. and Bornens M. (2004) GMAP-210 recruits gamma-tubulin complexes to cis-Golgi membranes and is required for Golgi ribbon formation. *Cell* 118, 323-35.

Rivero S., Cardenas J., Bornens M. and Rios R. M. (2009) Microtubule nucleation at the cis-side of the Golgi apparatus requires AKAP450 and GM130. *EMBO J* 28, 1016-28.

Rocha V., Cornish J., Sievers E. L., Filipovich A., Locatelli F., Peters C., Remberger M., Michel G., Arcese W., Dallorso S., Tiedemann K., Busca A., Chan K. W., Kato S., Ortega J., Vowels M., Zander A., Souillet G., Oakill A., Woolfrey A., Pay A. L., Green A., Garnier F., Ionescu I., Wernet P.,

Sirchia G., Rubinstein P., Chevret S. and Gluckman E. (2001) Comparison of outcomes of unrelated bone marrow and umbilical cord blood transplants in children with acute leukemia. *Blood* 97, 2962-71.

Rodriguez-Boulan E. and Musch A. (2005) Protein sorting in the Golgi complex: shifting paradigms. *Biochim Biophys Acta* 1744, 455-64.

Rodriguez A., Webster P., Ortego J. and Andrews N. W. (1997) Lysosomes behave as Ca2+-regulated exocytic vesicles in fibroblasts and epithelial cells. *J Cell Biol* 137, 93-104.

Rops A. L., van der Vlag J., Lensen J. F., Wijnhoven T. J., van den Heuvel L. P., van Kuppevelt T. H. and Berden J. H. (2004) Heparan sulfate proteoglycans in glomerular inflammation. *Kidney Int* 65, 768-85.

Roy E., Bruyere J., Flamant P., Bigou S., Ausseil J., Vitry S. and Heard J. M. (2011) GM130 gain-of-function induces cell pathology in a model of lysosomal storage disease. *Hum Mol Genet*.

Royle S. J., Bright N. A. and Lagnado L. (2005) Clathrin is required for the function of the mitotic spindle. *Nature* 434, 1152-7.

Rubinfeld H. and Seger R. (2005) The ERK cascade: a prototype of MAPK signaling. *Mol Biotechnol* 31, 151-74.

Rusnati M., Tanghetti E., Dell'Era P., Gualandris A. and Presta M. (1997) alphavbeta3 integrin mediates the cell-adhesive capacity and biological activity of basic fibroblast growth factor (FGF-2) in cultured endothelial cells. *Mol Biol Cell* 8, 2449-61.

Ryazantsev S., Yu W. H., Zhao H. Z., Neufeld E. F. and Ohmi K. (2007) Lysosomal accumulation of SCMAS (subunit c of mitochondrial ATP synthase) in neurons of the mouse model of mucopolysaccharidosis III B. *Mol Genet Metab* 90, 393-401.

S

Saftig P. and Klumperman J. (2009) Lysosome biogenesis and lysosomal membrane proteins: trafficking meets function. *Nat Rev Mol Cell Biol* 10, 623-35.

Salminen-Mankonen H. J., Morko J. and Vuorio E. (2007) Role of cathepsin K in normal joints and in the development of arthritis. *Curr Drug Targets* 8, 315-23.

Salmivirta M., Lidholt K. and Lindahl U. (1996) Heparan sulfate: a piece of information. *FASEB J* 10, 1270-9.

Sango K., Takano M., Ajiki K., Tokashiki A., Arai N., Kawano H., Horie H. and Yamanaka S. (2005) Impaired neurite outgrowth in the retina of a murine model of Sandhoff disease. *Invest Ophthalmol Vis Sci* 46, 3420-5.

Sano R., Annunziata I., Patterson A., Moshiach S., Gomero E., Opferman J., Forte M. and d'Azzo A. (2009) GM1-ganglioside accumulation at the mitochondria-associated ER membranes links ER stress to Ca(2+)-dependent mitochondrial apoptosis. *Mol Cell* 36, 500-11.

Sapperstein S. K., Lupashin V. V., Schmitt H. D. and Waters M. G. (1996) Assembly of the ER to Golgi SNARE complex requires Uso1p. *J Cell Biol* 132, 755-67.

Sardiello M., Palmieri M., di Ronza A., Medina D. L., Valenza M., Gennarino V. A., Di Malta C., Donaudy F., Embrione V., Polishchuk R. S., Banfi S.,

Parenti G., Cattaneo E. and Ballabio A. (2009) A gene network regulating lysosomal biogenesis and function. *Science* 325, 473-7.

Sawkar A. R., Cheng W. C., Beutler E., Wong C. H., Balch W. E. and Kelly J. W. (2002) Chemical chaperones increase the cellular activity of N370S beta -glucosidase: a therapeutic strategy for Gaucher disease. *Proc Natl Acad Sci U S A* 99, 15428-33.

Scales S. J., Pepperkok R. and Kreis T. E. (1997) Visualization of ER-to-Golgi transport in living cells reveals a sequential mode of action for COPII and COPI. *Cell* 90, 1137-48.

Schiffmann R., Fitzgibbon E. J., Harris C., DeVile C., Davies E. H., Abel L., van Schaik I. N., Benko W., Timmons M., Ries M. and Vellodi A. (2008) Randomized, controlled trial of miglustat in Gaucher's disease type 3. *Ann Neurol* 64, 514-22.

Schlessinger J., Plotnikov A. N., Ibrahimi O. A., Eliseenkova A. V., Yeh B. K., Yayon A., Linhardt R. J. and Mohammadi M. (2000) Crystal structure of a ternary FGF-FGFR-heparin complex reveals a dual role for heparin in FGFR binding and dimerization. *Mol Cell* 6, 743-50.

Schuck S. and Simons K. (2004) Polarized sorting in epithelial cells: raft clustering and the biogenesis of the apical membrane. *J Cell Sci* 117, 5955-64.

Schulze H., Kolter T. and Sandhoff K. (2009) Principles of lysosomal membrane degradation: Cellular topology and biochemistry of lysosomal lipid degradation. *Biochim Biophys Acta* 1793, 674-83.

Schweitzer J. K., Pietrini S. D. and D'Souza-Schorey C. (2009) ARF6-mediated endosome recycling reverses lipid accumulation defects in Niemann-Pick Type C disease. *PLoS One* 4, e5193.

Seemann J., Jokitalo E. J. and Warren G. (2000) The role of the tethering proteins p115 and GM130 in transport through the Golgi apparatus in vivo. *Mol Biol Cell* 11, 635-45.

Shapiro B. E., Pastores G. M., Gianutsos J., Luzy C. and Kolodny E. H. (2009) Miglustat in late-onset Tay-Sachs disease: a 12-month, randomized, controlled clinical study with 24 months of extended treatment. *Genet Med* 11, 425-33.

Sharma D. K., Choudhury A., Singh R. D., Wheatley C. L., Marks D. L. and Pagano R. E. (2003) Glycosphingolipids internalized via caveolar-related endocytosis rapidly merge with the clathrin pathway in early endosomes and form microdomains for recycling. *J Biol Chem* 278, 7564-72.

Shen J. S., Meng X. L., Moore D. F., Quirk J. M., Shayman J. A., Schiffmann R. and Kaneski C. R. (2008) Globotriaosylceramide induces oxidative stress and up-regulates cell adhesion molecule expression in Fabry disease endothelial cells. *Mol Genet Metab* 95, 163-8.

Shihabuddin L. S. and Aubert I. (2010) Stem cell transplantation for neurometabolic and neurodegenerative diseases. *Neuropharmacology* 58, 845-54.

Shorter J., Beard M. B., Seemann J., Dirac-Svejstrup A. B. and Warren G. (2002) Sequential tethering of Golgins and catalysis of SNAREpin assembly by the vesicle-tethering protein p115. *J Cell Biol* 157, 45-62.

Shorter J. and Warren G. (1999) A role for the vesicle tethering protein, p115, in the post-mitotic stacking of reassembling Golgi cisternae in a cell-free system. *J Cell Biol* 146, 57-70.

Siegel D. A. and Walkley S. U. (1994) Growth of ectopic dendrites on cortical pyramidal neurons in neuronal storage diseases correlates with abnormal accumulation of GM2 ganglioside. *J Neurochem* 62, 1852-62.

Sillibourne J. E., Milne D. M., Takahashi M., Ono Y. and Meek D. W. (2002) Centrosomal anchoring of the protein kinase CK1delta mediated by attachment to the large, coiled-coil scaffolding protein CG-NAP/AKAP450. *J Mol Biol* 322, 785-97.

Simonaro C. M., D'Angelo M., He X., Eliyahu E., Shtraizent N., Haskins M. E. and Schuchman E. H. (2008) Mechanism of glycosaminoglycan-mediated bone and joint disease: implications for the mucopolysaccharidoses and other connective tissue diseases. *Am J Pathol* 172, 112-22.

Simons K. and Gruenberg J. (2000) Jamming the endosomal system: lipid rafts and lysosomal storage diseases. *Trends Cell Biol* 10, 459-62.

Smith D., Wallom K. L., Williams I. M., Jeyakumar M. and Platt F. M. (2009) Beneficial effects of anti-inflammatory therapy in a mouse model of Niemann-Pick disease type C1. *Neurobiol Dis* 36, 242-51.

Smith R. S. (1980) The short term accumulation of axonally transported organelles in the region of localized lesions of single myelinated axons. *J Neurocytol* 9, 39-65.

Sonnichsen B., Lowe M., Levine T., Jamsa E., Dirac-Svejstrup B. and Warren G. (1998) A role for giantin in docking COPI vesicles to Golgi membranes. *J Cell Biol* 140, 1013-21.

Spada M., Pagliardini S., Yasuda M., Tukel T., Thiagarajan G., Sakuraba H., Ponzone A. and Desnick R. J. (2006) High incidence of later-onset fabry disease revealed by newborn screening. *Am J Hum Genet* 79, 31-40.

Sridharan R., Tchieu J., Mason M. J., Yachechko R., Kuoy E., Horvath S., Zhou Q. and Plath K. (2009) Role of the murine reprogramming factors in the induction of pluripotency. *Cell* 136, 364-77.

Stringer S. E. and Gallagher J. T. (1997) Heparan sulphate. *Int J Biochem Cell Biol* **29**, 709-14.

Stroes E. S., Nierman M. C., Meulenberg J. J., Franssen R., Twisk J., Henny C. P., Maas M. M., Zwinderman A. H., Ross C., Aronica E., High K. A., Levi M. M., Hayden M. R., Kastelein J. J. and Kuivenhoven J. A. (2008) Intramuscular administration of AAV1-lipoprotein lipase S447X lowers triglycerides in lipoprotein lipase-deficient patients. *Arterioscler Thromb Vasc Biol* 28, 2303-4.

Sullivan G. J., Bai Y., Fletcher J. and Wilmut I. (2010) Induced pluripotent stem cells: epigenetic memories and practical implications. *Mol Hum Reprod* 16, 880-5.

Sutterlin C., Hsu P., Mallabiabarrena A. and Malhotra V. (2002) Fragmentation and dispersal of the pericentriolar Golgi complex is required for entry into mitosis in mammalian cells. *Cell* 109, 359-69.

Sutterlin C., Polishchuk R., Pecot M. and Malhotra V. (2005) The Golgi-associated protein GRASP65 regulates spindle dynamics and is essential for cell division. *Mol Biol Cell* 16, 3211-22.

Suzuki K. and Ohsumi Y. (2007) Molecular machinery of autophagosome formation in yeast, Saccharomyces cerevisiae. *FEBS Lett* 581, 2156-61.

Suzuki M., Sugimoto Y., Ohsaki Y., Ueno M., Kato S., Kitamura Y., Hosokawa H., Davies J. P., Ioannou Y. A., Vanier M. T., Ohno K. and Ninomiya H. (2007) Endosomal accumulation of Toll-like receptor 4 causes constitutive secretion of cytokines and activation of signal transducers and activators of transcription in Niemann-Pick disease type C (NPC) fibroblasts: a potential basis for glial cell activation in the NPC brain. *J Neurosci* 27, 1879-91.

T

Tai A. W., Chuang J. Z., Bode C., Wolfrum U. and Sung C. H. (1999) Rhodopsin's carboxy-terminal cytoplasmic tail acts as a membrane receptor for cytoplasmic dynein by binding to the dynein light chain Tctex-1. *Cell* 97, 877-87.

Takahashi K., Okita K., Nakagawa M. and Yamanaka S. (2007a) Induction of pluripotent stem cells from fibroblast cultures. *Nat Protoc* 2, 3081-9.

Takahashi K., Tanabe K., Ohnuki M., Narita M., Ichisaka T., Tomoda K. and Yamanaka S. (2007b) Induction of pluripotent stem cells from adult human fibroblasts by defined factors. *Cell* 131, 861-72.

Takahashi K. and Yamanaka S. (2006) Induction of pluripotent stem cells from mouse embryonic and adult fibroblast cultures by defined factors. *Cell* 126, 663-76.

Takahashi M., Shibata H., Shimakawa M., Miyamoto M., Mukai H. and Ono Y. (1999) Characterization of a novel giant scaffolding protein, CG-NAP, that anchors multiple signaling enzymes to centrosome and the golgi apparatus. *J Biol Chem* 274, 17267-74.

Takahashi M., Yamagiwa A., Nishimura T., Mukai H. and Ono Y. (2002) Centrosomal proteins CG-NAP and kendrin provide microtubule nucleation sites by anchoring gamma-tubulin ring complex. *Mol Biol Cell* 13, 3235-45.

Tang D., Yuan H. and Wang Y. (2010) The role of GRASP65 in Golgi cisternal stacking and cell cycle progression. *Traffic* 11, 827-42.

Tasken K. A., Collas P., Kemmner W. A., Witczak O., Conti M. and Tasken K. (2001) Phosphodiesterase 4D and protein kinase a type II constitute a signaling unit in the centrosomal area. *J Biol Chem* 276, 21999-2002.

Tessitore A., del P. M. M., Sano R., Ma Y., Mann L., Ingrassia A., Laywell E. D., Steindler D. A., Hendershot L. M. and d'Azzo A. (2004) GM1-ganglioside-mediated activation of the unfolded protein response causes neuronal death in a neurodegenerative gangliosidosis. *Mol Cell* 15, 753-66.

Tettamanti G. (2004) Ganglioside/glycosphingolipid turnover: new concepts. *Glycoconj J* 20, 301-17.

Toledo M. S., Suzuki E., Handa K. and Hakomori S. (2005) Effect of ganglioside and tetraspanins in microdomains on interaction of integrins with fibroblast growth factor receptor. *J Biol Chem* 280, 16227-34.

Tropak M. B., Reid S. P., Guiral M., Withers S. G. and Mahuran D. (2004) Pharmacological enhancement of beta-hexosaminidase activity in fibroblasts from adult Tay-Sachs and Sandhoff Patients. *J Biol Chem* 279, 13478-87.

Tsukita S. and Ishikawa H. (1980) The movement of membranous organelles in axons. Electron microscopic identification of anterogradely and retrogradely transported organelles. *J Cell Biol* 84, 513-30.

Turnbull J., Powell A. and Guimond S. (2001) Heparan sulfate: decoding a dynamic multifunctional cell regulator. *Trends Cell Biol* 11, 75-82.

Turner J. R. and Tartakoff A. M. (1989) The response of the Golgi complex to microtubule alterations: the roles of metabolic energy and membrane traffic in Golgi complex organization. *J Cell Biol* 109, 2081-8.

U

Ungar D. (2009) Golgi linked protein glycosylation and associated diseases. *Semin Cell Dev Biol* 20, 762-9.

Urayama A., Grubb J. H., Sly W. S. and Banks W. A. (2004) Developmentally regulated mannose 6-phosphate receptor-mediated transport of a lysosomal enzyme across the blood-brain barrier. *Proc Natl Acad Sci U S A* 101, 12658-63.

Uttenweiler A. and Mayer A. (2008) Microautophagy in the yeast Saccharomyces cerevisiae. *Methods Mol Biol* 445, 245-59.

V

van den Born J., Salmivirta K., Henttinen T., Ostman N., Ishimaru T., Miyaura S., Yoshida K. and Salmivirta M. (2005) Novel heparan sulfate structures revealed by monoclonal antibodies. *J Biol Chem* 280, 20516-23.

van Echten G., Iber H., Stotz H., Takatsuki A. and Sandhoff K. (1990) Uncoupling of ganglioside biosynthesis by Brefeldin A. *Eur J Cell Biol* 51, 135-9.

van Meel E. and Klumperman J. (2008) Imaging and imagination: understanding the endo-lysosomal system. *Histochem Cell Biol* 129, 253-66.

Vergarajauregui S., Connelly P. S., Daniels M. P. and Puertollano R. (2008) Autophagic dysfunction in mucolipidosis type IV patients. *Hum Mol Genet* 17, 2723-37.

Villani G. R., Di Domenico C., Musella A., Cecere F., Di Napoli D. and Di Natale P. (2009) Mucopolysaccharidosis IIIB: oxidative damage and cytotoxic cell involvement in the neuronal pathogenesis. *Brain Res* 1279, 99-108.

Visigalli I., Delai S., Politi L. S., Di Domenico C., Cerri F., Mrak E., D'Isa R., Ungaro D., Stok M., Sanvito F., Mariani E., Staszewsky L., Godi C., Russo I., Cecere F., Del Carro U., Rubinacci A., Brambilla R., Quattrini A., Di Natale P., Ponder K., Naldini L. and Biffi A. (2010) Gene therapy augments the efficacy of hematopoietic cell transplantation and fully corrects mucopolysaccharidosis type I phenotype in the mouse model. *Blood* 116, 5130-9.

Vitner E. B., Platt F. M. and Futerman A. H. (2010) Common and uncommon pathogenic cascades in lysosomal storage diseases. *J Biol Chem* 285, 20423-7.

Vitry S., Ausseil J., Hocquemiller M., Bigou S., Dos Santos Coura R. and Heard J. M. (2009) Enhanced degradation of synaptophysin by the proteasome in mucopolysaccharidosis type IIIB. *Mol Cell Neurosci* 41, 8-18.

Vitry S., Bruyere J., Hocquemiller M., Bigou S., Ausseil J., Colle M. A., Prevost M. C. and Heard J. M. (2010) Storage vesicles in neurons are related to Golgi complex alterations in mucopolysaccharidosis IIIB. *Am J Pathol* 177, 2984-99.

Vladutiu G. D. and Rattazzi M. C. (1979) Excretion-reuptake route of beta-hexosaminidase in normal and I-cell disease cultured fibroblasts. *J Clin Invest* 63, 595-601.

W

Walkley S. U., Baker H. J., Rattazzi M. C., Haskins M. E. and Wu J. Y. (1991) Neuroaxonal dystrophy in neuronal storage disorders: evidence for major GABAergic neuron involvement. *J Neurol Sci* 104, 1-8.

Walkley S. U. (1995) Pyramidal neurons with ectopic dendrites in storage diseases exhibit increased GM2 ganglioside immunoreactivity. *Neuroscience* 68, 1027-35.

Walkley S. U. (1998) Cellular pathology of lysosomal storage disorders. *Brain Pathol* 8, 175-93.

Walkley S. U. and Vanier M. T. (2009) Secondary lipid accumulation in lysosomal disease. *Biochim Biophys Acta* 1793, 726-36.

Walkley S. U., Wurzelmann S. and Siegel D. A. (1987) Ectopic axon hillock-associated neurite growth is maintained in metabolically reversed swainsonine-induced neuronal storage disease. *Brain Res* 410, 89-96.

Wang X. Q., Sun P. and Paller A. S. (2003a) Ganglioside GM3 blocks the activation of epidermal growth factor receptor induced by integrin at specific tyrosine sites. *J Biol Chem* 278, 48770-8.

Wang Y., Satoh A. and Warren G. (2005) Mapping the functional domains of the Golgi stacking factor GRASP65. *J Biol Chem* 280, 4921-8.

Wang Y., Seemann J., Pypaert M., Shorter J. and Warren G. (2003b) A direct role for GRASP65 as a mitotically regulated Golgi stacking factor. *EMBO J* 22, 3279-90.

Watson G., Bastacky J., Belichenko P., Buddhikot M., Jungles S., Vellard M., Mobley W. C. and Kakkis E. (2006) Intrathecal administration of AAV vectors for the treatment of lysosomal storage in the brains of MPS I mice. *Gene Ther* 13, 917-25.

Webb S. J., Monk C. S. and Nelson C. A. (2001) Mechanisms of postnatal neurobiological development: implications for human development. *Dev Neuropsychol* 19, 147-71.

Wegrzyn G., Jakobkiewicz-Banecka J., Narajczyk M., Wisniewski A., Piotrowska E., Gabig-Ciminska M., Kloska A., Slominska-Wojewodzka M., Korzon-Burakowska A. and Wegrzyn A. (2010) Why are behaviors of children suffering from various neuronopathic types of mucopolysaccharidoses different? *Med Hypotheses* 75, 605-9.

Wei H., Kim S. J., Zhang Z., Tsai P. C., Wisniewski K. E. and Mukherjee A. B. (2008) ER and oxidative stresses are common mediators of apoptosis in both neurodegenerative and non-neurodegenerative lysosomal storage disorders and are alleviated by chemical chaperones. *Hum Mol Genet* 17, 469-77.

Wei J. H. and Seemann J. (2009a) Mitotic division of the mammalian Golgi apparatus. *Semin Cell Dev Biol* 20, 810-6.

Wei J. H. and Seemann J. (2009b) Remodeling of the Golgi structure by ERK signaling. *Commun Integr Biol* 2, 35-6.

Whitelock J. M. and Iozzo R. V. (2005) Heparan sulfate: a complex polymer charged with biological activity. *Chem Rev* 105, 2745-64.

Wilcox W. R. (2004) Lysosomal storage disorders: the need for better pediatric recognition and comprehensive care. *J Pediatr* 144, S3-14.

Wilson C., Venditti R., Rega L. R., Colanzi A., D'Angelo G. and De Matteis M. A. (2011) The Golgi apparatus: an organelle with multiple complex functions. *Biochem J* 433, 1-9.

Witczak O., Skalhegg B. S., Keryer G., Bornens M., Tasken K., Jahnsen T. and Orstavik S. (1999) Cloning and characterization of a cDNA encoding an A-kinase anchoring protein located in the centrosome, AKAP450. *EMBO J* 18, 1858-68.

Wong E. S., Fong C. W., Lim J., Yusoff P., Low B. C., Langdon W. Y. and Guy G. R. (2002) Sprouty2 attenuates epidermal growth factor receptor ubiquitylation and endocytosis, and consequently enhances Ras/ERK signalling. *EMBO J* 21, 4796-808.

Wong K. K. (2009) Recent developments in anti-cancer agents targeting the Ras/Raf/MEK/ERK pathway. *Recent Pat Anticancer Drug Discov* 4, 28-35.

Worgall S., Sondhi D., Hackett N. R., Kosofsky B., Kekatpure M. V., Neyzi N., Dyke J. P., Ballon D., Heier L., Greenwald B. M., Christos P., Mazumdar M., Souweidane M. M., Kaplitt M. G. and Crystal R. G. (2008) Treatment of late infantile neuronal ceroid lipofuscinosis by CNS administration of a serotype 2 adeno-associated virus expressing CLN2 cDNA. *Hum Gene Ther* 19, 463-74.

Wraith J. E., Clarke L. A., Beck M., Kolodny E. H., Pastores G. M., Muenzer J., Rapoport D. M., Berger K. I., Swiedler S. J., Kakkis E. D., Braakman T., Chadbourne E., Walton-Bowen K. and Cox G. F. (2004) Enzyme replacement therapy for mucopolysaccharidosis I: a randomized, double-blinded, placebo-controlled, multinational study of recombinant human alpha-L-iduronidase (laronidase). *J Pediatr* 144, 581-8.

Wu W. J., Erickson J. W., Lin R. and Cerione R. A. (2000) The gamma-subunit of the coatomer complex binds Cdc42 to mediate transformation. *Nature* 405, 800-4.

X

Xiang Y. and Wang Y. (2010) GRASP55 and GRASP65 play complementary and essential roles in Golgi cisternal stacking. *J Cell Biol* 188, 237-51.

Y

Yadav S., Puri S. and Linstedt A. D. (2009) A primary role for Golgi positioning in directed secretion, cell polarity, and wound healing. *Mol Biol Cell* 20, 1728-36.

Yam G. H., Zuber C. and Roth J. (2005) A synthetic chaperone corrects the trafficking defect and disease phenotype in a protein misfolding disorder. *FASEB J* 19, 12-8.

Yamada S., Taketomi T. and Yoshimura A. (2004) Model analysis of difference between EGF pathway and FGF pathway. *Biochem Biophys Res Commun* 314, 1113-20.

Yamamoto N., Hirabayashi Y., Amari M., Yamaguchi H., Romanov G., Van Nostrand W. E. and Yanagisawa K. (2005) Assembly of hereditary amyloid

beta-protein variants in the presence of favorable gangliosides. *FEBS Lett* 579, 2185-90.

Ye B., Zhang Y., Song W., Younger S. H., Jan L. Y. and Jan Y. N. (2007) Growing dendrites and axons differ in their reliance on the secretory pathway. *Cell* 130, 717-29.

Yoshimura S., Yoshioka K., Barr F. A., Lowe M., Nakayama K., Ohkuma S. and Nakamura N. (2005) Convergence of cell cycle regulation and growth factor signals on GRASP65. *J Biol Chem* 280, 23048-56.

Yoshimura S. I., Nakamura N., Barr F. A., Misumi Y., Ikehara Y., Ohno H., Sakaguchi M. and Mihara K. (2001) Direct targeting of cis-Golgi matrix proteins to the Golgi apparatus. *J Cell Sci* 114, 4105-15.

Young W. W., Jr., Lutz M. S., Mills S. E. and Lechler-Osborn S. (1990) Use of brefeldin A to define sites of glycosphingolipid synthesis: GA2/GM2/GD2 synthase is trans to the brefeldin A block. *Proc Natl Acad Sci U S A* 87, 6838-42.

Yu R. K., Bieberich E., Xia T. and Zeng G. (2004) Regulation of ganglioside biosynthesis in the nervous system. *J Lipid Res* 45, 783-93.

Yu J., Vodyanik M. A., Smuga-Otto K., Antosiewicz-Bourget J., Frane J. L., Tian S., Nie J., Jonsdottir G. A., Ruotti V., Stewart R., Slukvin, II and Thomson J. A. (2007) Induced pluripotent stem cell lines derived from human somatic cells. *Science* 318, 1917-20.

Z

Zafeiriou D. I., Savvopoulou-Augoustidou P. A., Sewell A., Papadopoulou F., Badouraki M., Vargiami E., Gombakis N. P. and Katzos G. S. (2001) Serial magnetic resonance imaging findings in mucopolysaccharidosis IIIB (Sanfilippo's syndrome B). *Brain Dev* 23, 385-9.

Zheng Y., Rozengurt N., Ryazantsev S., Kohn D. B., Satake N. and Neufeld E. F. (2003) Treatment of the mouse model of mucopolysaccharidosis I with retrovirally transduced bone marrow. *Mol Genet Metab* 79, 233-44.

Zschenker O., Illies T. and Ameis D. (2006) Overexpression of lysosomal acid lipase and other proteins in atherosclerosis. *J Biochem* 140, 23-38.

APPENDIX

APPENDIX

During my PhD thesis, I signed a review article discussing relationships between storage products and storage lesions in lysosomal diseases. This review is presented is this Annex.

Before starting my PhD, I also participated in other research studies aimed at assessing the efficacy and safety of novel gene transfer approaches for hemophilia. This work was conducted in the laboratory of Dr K.A. High, and initiated during a training required for the obtention of the diploma of Engineer in Biotechnology (equivalent to Master of Science). I pursued this work afterwards, and I signed three research articles, also found in this Annex.

Biochemical Society Transactions www.biochemsoctrans.org

Storage problems in lysosomal diseases

Jean Michel Heard[1], Julie Bruyère, Elise Roy, Stéphanie Bigou, Jérôme Ausseil and Sandrine Vitry

Retrovirus and Genetic Transfer Unit, Department of Neuroscience, Institut Pasteur, 28 rue du Dr Roux, 75015 Paris, France, and INSERM U622, Institut Pasteur, Paris, France

Abstract

Biochemical disorders in lysosomal storage diseases consist of the interruption of metabolic pathways involved in the recycling of the degradation products of one or several types of macromolecules. The progressive accumulation of these primary storage products is the direct consequence of the genetic defect and represents the initial pathogenic event. Downstream consequences for the affected cells include the accumulation of secondary storage products and the formation of histological storage lesions, which appear as intracellular vacuoles that represent the pathological hallmark of lysosomal storage diseases. Relationships between storage products and storage lesions are not simple and are still largely not understood. Primary storage products induce malfunction of the organelles where they accumulate, these being primarily, but not only, lysosomes. Consequences for cell metabolism and intracellular trafficking combine the effects of primary storage product toxicity and the compensatory mechanisms activated to protect the cell. Induced disorders extend far beyond the primarily interrupted metabolic pathway.

Introduction

LSDs (lysosomal storage diseases) form a group of rare inherited genetic defects of the metabolism, which is at the same time well defined and extremely heterogeneous. More than 50 disorders are recognized as LSDs. This number is constantly increasing, and it is expected that more diseases, on which knowledge is currently limited, will be considered to be LSDs when better documented. Beyond genetic inheritance and alteration of a metabolic pathway, criteria leading to the identification of a disease as LSD rely on the combination of defined biochemical and histological features.

Biochemical disorders in LSDs consist of the interruption of metabolic pathways involved in the recycling of degradation products of one or several types of macromolecules. As a consequence of inefficient recycling, imperfectly degraded substances accumulate in cells with cascades of deleterious repercussions. Substances accumulating as the direct consequence of the genetic defect are the primary storage products. They represent the initial pathogenic event, which may result in both cell-autonomous defects and environmental reactions, e.g. inflammation [1]. Downstream consequences include the secondary accumulation of other substances, the secondary storage products, which have not always been molecularly identified. The histological hallmark of LSDs is cell vacuolation (Figure 1A). With time, cells in most severely affected tissues become progressively clogged with cytoplasmic inclusions. Since inclusions contain materials that cells are apparently unable to eliminate, and cell vacuolation is clearly related to the storage process, inclusions are often referred to as storage lesions.

Although storage products and storage lesions are the two main characteristics of LSDs, the nature of their relationship is not simple and is still largely not understood. In the present review, we examine their complex links.

A problem of content

Almost every metabolic pathway aimed at recycling substances produced by macromolecule degradation in lysosomes has been involved in LSDs. Indeed, the most convivial classification of LSDs relies on the nature of affected macromolecules [2], and therefore, in most cases, refers to specific storage products. These products may be precisely identified, as, for example, in lipidoses or MPSs (mucopolysaccharidoses), or poorly characterized, as in neuronal ceroid lipofuscinoses.

Despite the fact that the metabolic defect concerns all cells in the organism, depending on the affected pathway and the specific metabolic activity of deficient cells, storage products are preferentially generated in certain tissues, where they predominantly accumulate and cause disorders. The geographies of the accumulation of storage products and that of the installation of storage lesions are largely superimposed. Subsequently, the condition of the most affected organs results in the clinical manifestations that specify the disease type. For example, skeletal muscles are the most diseased organs in Pompe disease, which affects glycogen degradation; bone and joint development is impaired in MPS type VI because of the interruption of dermatan sulfate catabolism; and demyelination in metachromatic leukodystrophy is associated with the accumulation of long-chain fatty acids in the central nervous system.

Key words: autophagy, Golgi matrix protein 130 (GM130), lysosomal storage disease (LSD), lysosome-associated membrane protein (LAMP), lysosome biogenesis, Rab GTPase.

Abbreviations used: GM130, Golgi matrix protein 130; LAMP1, lysosome-associated membrane protein 1; LSD, lysosomal storage disease; MPS, mucopolysaccharidosis.

[1]To whom correspondence should be addressed (email jmheard@pasteur.fr).

Figure 1| Storage lesions in the MPSIIIB mouse brain

Cortical fragments of a 9-month-old MPSIIIB mouse were processed for electron microscopy (**A**), immunofluorescence (**B**), immunogold (**C**), Western blotting (**D**) or immunostaining (**E**). (**A**) Ultrastructural analysis show polymorphic distended vesicles in neurons (two left-hand columns), microglial cells (third column) and astrocytes (right-hand column). Low (top row) and high (bottom row) magnifications of the same fields are shown. Extreme left- and right-hand panels of the bottom row show zebra bodies. Scale bars, 1 μm. (**B**) Parasagittal cortical sections immunolabelled for the lysosomal marker LAMP1 (in purple) and the neuronal marker NeuN (left, in green), the microglial marker CD11b (middle, in green) and the astrocyte marker GFAP (glial fibrillary acidic protein) (right, in green) show comparable LAMP1 accumulation, notwithstanding marked differences in the aspect of storage lesions in these three cell types. Images are confocal fluorescence micrographs. Scale bars, 10 μm. (**C**) Ultrathin cryosection stained with anti-LAMP1 antibodies coupled to 10-nm-diameter gold particles reveal LAMP1 in the limiting membranes of two storage lesions with different aspects (dark vesicle in the upper left corner and clear vesicle in the middle). Scale bar, 0.5 μm. (**D**) Western blot analysis of brain protein extracts with anti-LAMP1 antibodies show increased signal in the brain of MPSIIIB mice, as compared with wild-type mice. The LAMP1 signal was normalized when the expression of the missing lysosomal enzyme α-N-acetylglucosaminidase was induced through adeno-associated vector-mediated gene therapy directed to the brain (MPSIIIB+AAV-NaGlu). Molecular masses of LAMP1 signals are indicated in kDa on the left. (**E**) LAMP1 overexpresion and correction after gene therapy were similarly observed after immunostaining of MPSIIIB mouse cortical sections. Scale bars, 100 μm.

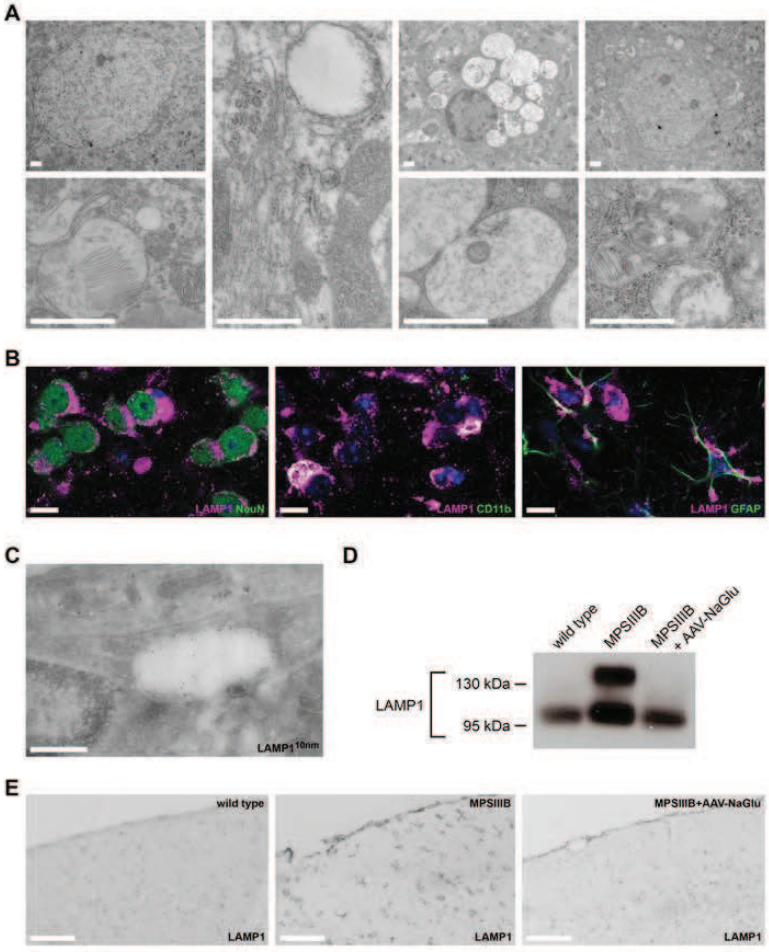

Coincidence of storage products and storage lesions in the same organs led to the notion that disease expression results from cell disorders that are induced by cytoplasmic inclusions, which are themselves caused by the accumulation of storage products in the lysosomes, the organelles in which these products are generated. This simple view appears to be insufficient with regard to our current knowledge of LSDs. Indeed, the accumulation of the primary storage products is associated with more or less severe malfunctioning of the organelles in which they are produced and stored, inducing pathological consequences beyond the primarily affected metabolic pathway.

A problem of container

Examination of storage lesions by electron microscopy confirmed the high heterogeneity of storage lesions, which is already visible on standard pathology sections. Cell inclusions are large structures with different types of content, ranging from clear amorphous material, internal debris, internal vesicles, membrane fragments, dense aggregates and multilamellar structures occasionally forming zebra bodies (Figure 1A). Ultrastructural studies not only showed that storage lesions differed depending on the affected cell type, but also provided evidence that multiple types of inclusions coexisted in the same cell. Thus a given type of primary storage product can be associated with multiple types of storage lesions. Contrasting with their polymorphism in individual disease, inclusions show similar features in different LSDs. For example, zebra bodies were observed in many LSDs. Thus different types of primary storage products can be associated with similar storage lesions.

The relationship between the primary storage products and the storage lesions is therefore not a binary one. It involves additional players, the secondary storage products. Assuming that secondary storage products participate in storage lesions accounts for the observation of different types of lesions in different types of cell, since secondary storage products probably differ depending on the cell type. On the other hand, if cascades of events triggered in different diseases converge to common biochemical alterations and to the accumulation of common secondary storage products in different LSDs, it is then understandable that similar lesions are observed in different diseases. According to this view, storage is not solely a problem of content, the accumulating primary products, but also a problem of container, the organelles that become unable to degrade and recycle certain substances as a secondary consequence of primary storage. Malfunctioning of the container leading to the secondary storage of a variety of materials appears a common feature that specifies LSDs.

The most likely problematic container is obviously the lysosome. Consistently, lysosomal markers are associated with storage lesions. Overexpression of the lysosomal marker LAMP1 (lysosome-associated membrane protein 1) is associated with many LSDs [3]. The association of LAMP1 with intracellular inclusions was detected in various cell types, notwithstanding the fact that these inclusions showed very different aspects. For example, in the brain of MPSIIIB mice, both inclusions in microglial cells, which appear as clusters of rounded white drops, and inclusions in neurons and astrocytes, which are frequently dark and spread over the cell surface, were stained with anti-LAMP1 antibodies (Figure 1B). The ultrastructural detection of LAMP1 immunoreactivity in the limiting membranes of intracellular inclusions indicated that storage lesions are related to lysosomes (Figure 1C).

Experimental evidence has actually been provided in some LSDs that lysosomal functions were altered beyond the metabolic pathway directly affected by the missing protein. Early studies of MPSs documented the inhibition of the catalytic activities of several lysosomal enzymes by glycosaminoglycans, the primary storage products in these diseases [4]. Cholesterol accumulation in Niemann–Pick type C and other LSDs causes inhibition of lysosomal sphingomyelinase [5] and lysosomal glucosylceramidase [6]. In mucolipidosis IV, inhibition of the degradation of lysosomal ABC (ATP-binding cassette) transporters increases undegraded substrate overload [7]. Since the fusion of lysosomes with late endosomes, phagosomes or amphisomes is the terminal step of endocytosis, phagocytosis and macro-autophagy respectively, a global deficiency of lysosomal functions affects these pathways. Consistently, alteration of fluid-phase endocytosis was reported in Niemann–Pick type C disease [8], alteration of phagocytosis in monocytes increases susceptibility to infection in patients with Gaucher disease [9] or α-mannosidosis [10], alteration of macro-autophagy was reported in several LSDs [11,12]. Depending on the disease, macro-autophagy appears to be activated, as in Niemann–Pick C disease [13], neuronal ceroid lipofuscinosis [14] or G_{M1} gangliosidosis [15], or deficient as in mucolipidosis IV [16] or multiple sulfatase deficiency [17]. In many cases, macro-autophagy is both activated and deficient, as shown in the skeletal and cardiac muscles of mice and patients with Pompe disease [18], and to a lesser extent as a consequence of relative starvation in the liver of the mouse models of MPSI and MPSVII [19]. In contrast, our studies of brain tissues in the mouse models of MPSI, MPSIIIA and MPSIIIB did not find any evidence of increased formation or accumulation of autophagolysosomes, and dynamic studies of macro-autophagy in MPSIIIB cultured neurons indicated that this pathway was normally efficient.

According to the hypothesis of global lysosome malfunctioning, storage lesions in LSDs consist in deficient hybrid vesicles, as documented in the *Caenorhabditis elegans* model of mucolipidosis IV [20]. Hybrid vesicles result from the fusion of lysosomes with late endosome, amphisomes or autophagosomes that are loaded with materials meant for degradation [21]. In LSDs, these vesicles swell, accumulate and proliferate because they are unable to recycle materials contained in their lumen. Lysosome biogenesis is regulated through a gene network controlled by TFEB (transcription

Figure 2 | Altered expression of GM130 and disorganization of the Golgi architecture in MSPIIIB mouse neurons

(**A**) Cortical fragments from a wild-type mouse (left-hand panel), or a 9-month-old MPSIIIB mouse (right-hand panel) were processed for immunofluorescence to simultaneously reveal the neuronal marker Map2 (in purple) and the *cis*-Golgi protein GM130 (in green). Increased and more tubular GM130 signals are visible in MPSIIIB mouse neurons. Images are confocal fluorescence micrographs. Scale bars, 10 μm. (**B**) MPSIIIB cortical neuron cultures (day 10) were stained for LAMP1 (in purple) and GM130 (in green). Storage vesicles located in neurites appear doubly positive. Images are confocal fluorescence micrographs. Scale bars, 10 μm. (**C**) Ultrathin cryosections from 9-month-old MPSIIIB mouse cortex were co-stained with gold-coupled anti-GM130 (10-nm-diameter particles arrows) and anti-LAMP1 (15-nm-diameter particles, arrowheads) antibodies. GM130 antibodies stained Golgi stacks (G) and a LAMP1-positive storage vesicle (StV). Scale bar, 0.2 μm. (**D**) Ultrathin sections of cortical fragments from a 9-month-old MPSIIIB mouse show disorganized Golgi (G) adjacent to storage vesicles (StV) in a neuron (left-hand panel) and an astrocyte (right-hand panel). Continuity between altered Golgi saccules and storage vesicles is visible. ER, endoplasmic reticulum; m, mitochondrion. Scale bars, 0.5 μm.

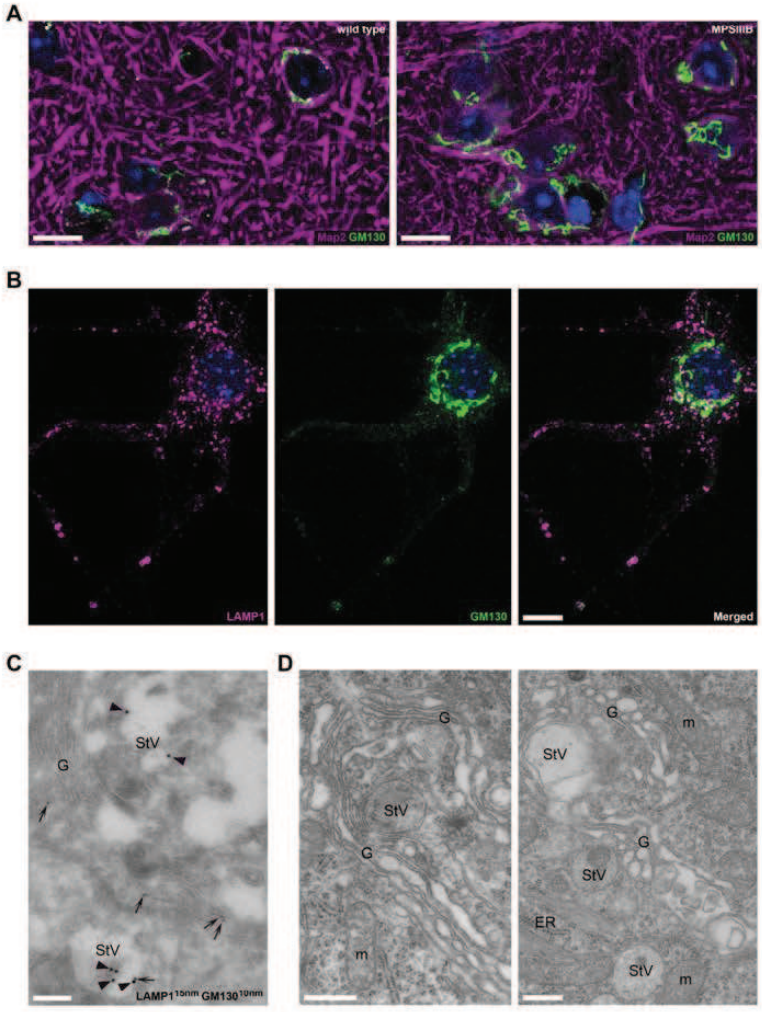

factor EB). In response to storage, this factor co-ordinates the transcriptional activation of lysosomal genes, leading to the multiplication of engorged lysosomes and/or hybrid vesicles [22].

A problem of delivery

Alteration of macro-autophagy was particularly well documented in Niemann–Pick type C disease, showing overexpression of beclin1, an early inducer of macro-autophagy

[13]. Interestingly, studies of Niemann–Pick type C disease also emphasized the possible role of membrane trafficking defects in LSDs [23]. In Niemann–Pick type C cells, as well as in glycosphingolipid disorders, the transport of cholesterol and glycosphingolipids from the late endosomes to various destinations, including the plasma membrane, is defective [24]. Endocytic vesicles are immobile due to increased amounts of the small GTPase Rab7 bound to membranes [25,26] and to the inhibition of Rab4 [27]. Impaired cholesterol delivery is reversed by overexpressing various small GTPases of the Rab family [28] or the ADP-ribosylation factor Arf6 [29]. Cholesterol efflux out of the endosomal recycling compartment is accompanied with Golgi retargeting of glycosphinglolipids. Defects in membrane traffic and lipid metabolism are also associated with mucolipidosis type IV, in which mucolipin-1, a lysosomal non-specific cation channel, is deficient [30]. In MPSs, cholesterol and glycosphingolipids accumulate in structures that are distinct from glycosaminoglycan storage sites, suggesting intracellular trafficking defects in addition to lysosome disability [31]. These observations support the notion that a number of LSDs are related to defects that have an impact on lysosome biogenesis in addition to lysosome functioning.

Our recent findings in the cortical neurons of the MPSIIIB mouse model suggest trafficking defects at a pre-Golgi, or *cis*-Golgi, step of lysosome biogenesis. GM130 (Golgi matrix protein 130) is a tethering protein which controls vesicle trafficking in pre- and *cis*-Golgi compartments. It is also a Golgi matrix component that forms molecular complexes with vesicle coat proteins and cargo transporters, and which plays essential roles in Golgi morphogenesis and nucleation of microtubules at the Golgi surface [32–34]. We detected GM130 in storage lesion membranes, which were also stained for LAMP1 (Figures 2A–2C). These vesicles were immobile, abundant in proximal and distal neurites, and resistant to brefeldin A, a drug that induces Golgi collapse into the endoplasmic reticulum. They were frequently associated with disorganized Golgi ribbon structures (Figure 2D). Our results suggest that storage lesions in MPSIIIB neurons are related to aberrant Golgi saccules, which appear to be unable to interact with adjacent intra-Golgi, downstream or upstream compartments, and form a dead-end pathway that gives rise to accumulating storage vesicles [35].

According to the trafficking defect models, it is not so much the amounts of undigested products to be stored that raise a problem, but rather the toxicity of these products for basic cell biological functions, which results in aberrant delivery systems. Permanent residues left inside inappropriate delivery containers progressively increase the amounts of stored material and form storage lesions.

Perspectives

LSDs are progressive diseases in which the inefficient recycling of macromolecules degradation products in lysosomes is tolerated for long periods of time before disorders compromise cell functions and survival. Tolerance to cell disorders is presumably made possible through the activation of compensatory mechanisms. Acute models of LSDs, in which distinction can be made between the consequences of primary storage product toxicity and compensatory mechanisms, will presumably shed new light on the relationship of storage products with storage lesions. Acute models of Niemann–Pick type C [29] or mucolipidosis IV [36] have recently been produced for this purpose in HeLa cells. Observations performed shortly after the induction of lysosomal disorders will probably help to decipher the complexity of the intricate cascades of pathogenic events that characterize LSDs.

Funding

This work was supported by the Agence National de la Recherche [grant number ANR-08-MNP-023].

References

1 Ausseil, J., Desmaris, N., Bigou, S., Attali, R., Corbineau, S., Vitry, S., Parent, M., Cheillan, D., Fuller, M., Maire, I. et al. (2008) Early neurodegeneration progresses independently of microglial activation by heparan sulfate in the brain of mucopolysaccharidosis IIIB mice. PLoS ONE **3**, e2296
2 Ballabio, A. and Gieselmann, V. (2009) Lysosomal disorders: from storage to cellular damage. Biochim. Biophys. Acta **1793**, 684–696
3 Meikle, P.J., Brooks, D.A., Ravenscroft, E.M., Yan, M., Williams, R.E., Jaunzems, A.E., Chataway, T.K., Karageorgos, L.E., Davey, R.C., Boulter, C.D. et al. (1997) Diagnosis of lysosomal storage disorders: evaluation of lysosome-associated membrane protein LAMP-1 as a diagnostic marker. Clin. Chem. **43**, 1325–1335
4 Avila, J.L. and Convit, J. (1975) Inhibition of leucocytic lysosomal enzymes by glycosaminoglycans *in vitro*. Biochem J. **152**, 57–64
5 Reagan, Jr, J.W., Hubbert, M.L. and Shelness, G.S. (2000) Posttranslational regulation of acid sphingomyelinase in Niemann–Pick type C1 fibroblasts and free cholesterol-enriched chinese hamster ovary cells. J. Biol. Chem. **275**, 38104–38110
6 Salvioli, R., Scarpa, S., Ciaffoni, F., Tatti, M., Ramoni, C., Vanier, M.T. and Vaccaro, A.M. (2004) Glucosylceramidase mass and subcellular localization are modulated by cholesterol in Niemann–Pick disease type C. J. Biol. Chem. **279**, 17674–17680
7 Schaheen, L., Patton, G. and Fares, H. (2006) Suppression of the cup-5 mucolipidosis type IV-related lysosomal dysfunction by the inactivation of an ABC transporter in *C. elegans*. Development **133**, 3939–3948
8 Lachmann, R.H., te Vruchte, D., Lloyd-Evans, E., Reinkensmeier, G., Sillence, D.J., Fernandez-Guillen, L., Dwek, R.A., Butters, T.D., Cox, T.M. and Platt, F.M. (2004) Treatment with miglustat reverses the lipid-trafficking defect in Niemann–Pick disease type C. Neurobiol. Dis. **16**, 654–658
9 Marodi, L., Kaposzta, R., Toth, J. and Laszlo, A. (1995) Impaired microbicidal capacity of mononuclear phagocytes from patients with type I Gaucher disease: partial correction by enzyme replacement therapy. Blood **86**, 4645–4649
10 Malm, D., Halvorsen, D.S., Tranebjaerg, L. and Sjursen, H. (2000) Immunodeficiency in α-mannosidosis: a matched case-control study on immunoglobulins, complement factors, receptor density, phagocytosis and intracellular killing in leucocytes. Eur. J. Pediatr. **159**, 699–703
11 Kiselyov, K., Jennigs, Jr, J.J., Rbaibi, Y. and Chu, C.T. (2007) Autophagy, mitochondria and cell death in lysosomal storage diseases. Autophagy **3**, 259–262
12 Settembre, C., Fraldi, A., Rubinsztein, D.C. and Ballabio, A. (2008) Lysosomal storage diseases as disorders of autophagy. Autophagy **4**, 113–114
13 Pacheco, C.D. and Lieberman, A.P. (2008) The pathogenesis of Niemann–Pick type C disease: a role for autophagy? Expert Rev. Mol. Med. **10**, e26

14 Cao, Y., Espinola, J.A., Fossale, E., Massey, A.C., Cuervo, A.M., MacDonald, M.E. and Cotman, S.L. (2006) Autophagy is disrupted in a knock-in mouse model of juvenile neuronal ceroid lipofuscinosis. J. Biol. Chem. **281**, 20483–20493
15 Takamura, A., Higaki, K., Kajimaki, K., Otsuka, S., Ninomiya, H., Matsuda, J., Ohno, K., Suzuki, Y. and Nanba, E. (2008) Enhanced autophagy and mitochondrial aberrations in murine G_{M1}-gangliosidosis. Biochem. Biophys. Res. Commun. **367**, 616–622
16 Jennings, Jr, J.J., Zhu, J.H., Rbaibi, Y., Luo, X., Chu, C.T. and Kiselyov, K. (2006) Mitochondrial aberrations in mucolipidosis type IV. J. Biol. Chem. **281**, 39041–39050
17 Settembre, C., Fraldi, A., Jahreiss, L., Spampanato, C., Venturi, C., Medina, D., de Pablo, R., Tacchetti, C., Rubinsztein, D.C. and Ballabio, A. (2008) A block of autophagy in lysosomal storage disorders. Hum. Mol. Genet. **17**, 119–129
18 Raben, N., Baum, R., Schreiner, C., Takikita, S., Mizushima, N., Ralston, E. and Plotz, P. (2009) When more is less: excess and deficiency of autophagy coexist in skeletal muscle in Pompe disease. Autophagy **5**, 111–113
19 Woloszynek, J.C., Coleman, T., Semenkovich, C.F. and Sands, M.S. (2007) Lysosomal dysfunction results in altered energy balance. J. Biol. Chem. **282**, 35765–35771
20 Fares, H. and Greenwald, I. (2001) Regulation of endocytosis by CUP-5, the *Caenorhabditis elegans* mucolipin-1 homolog. Nat. Genet. **28**, 64–68
21 Luzio, J.P., Poupon, V., Lindsay, M.R., Mullock, B.M., Piper, R.C. and Pryor, P.R. (2003) Membrane dynamics and the biogenesis of lysosomes. Mol. Membr. Biol. **20**, 141–154
22 Sardiello, M., Palmieri, M., di Ronza, A., Medina, D.L., Valenza, M., Gennarino, V.A., Di Malta, C., Donaudy, F., Embrione, V., Polishchuk, R.S. et al. (2009) A gene network regulating lysosomal biogenesis and function. Science **325**, 473–477
23 Pagano, R.E. (2003) Endocytic trafficking of glycosphingolipids in sphingolipid storage diseases. Philos. Trans. R. Soc. London Ser. **B 358**, 885–891
24 Chang, T.Y., Reid, P.C., Sugii, S., Ohgami, N., Cruz, J.C. and Chang, C.C. (2005) Niemann-Pick type C disease and intracellular cholesterol trafficking. J. Biol. Chem. **280**, 20917–20920
25 Zhang, M., Dwyer, N.K., Love, D.C., Cooney, A., Comly, M., Neufeld, E., Pentchev, P.G., Blanchette-Mackie, E.J. and Hanover, J.A. (2001) Cessation of rapid late endosomal tubulovesicular trafficking in Niemann-Pick type C1 disease. Proc. Natl. Acad. Sci. U.S.A. **98**, 4466–4471
26 Lebrand, C., Corti, M., Goodson, H., Cosson, P., Cavalli, V., Mayran, N., Faure, J. and Gruenberg, J. (2002) Late endosome motility depends on lipids via the small GTPase Rab7. EMBO J. **21**, 1289–300
27 Choudhury, A., Sharma, D.K., Marks, D.L. and Pagano, R.E. (2004) Elevated endosomal cholesterol levels in Niemann-Pick cells inhibit rab4 and perturb membrane recycling. Mol. Biol. Cell **15**, 4500–4511
28 Kaptzan, T., West, S.A., Holicky, E.L., Wheatley, C.L., Marks, D.L., Wang, T., Peake, K.B., Vance, J., Walkley, S.U. and Pagano, R.E. (2009) Development of a Rab9 transgenic mouse and its ability to increase the lifespan of a murine model of Niemann-Pick type C disease. Am. J. Pathol. **174**, 14–20
29 Schweitzer, J.K., Pietrini, S.D. and D'Souza-Schorey, C. (2009) ARF6-mediated endosome recycling reverses lipid accumulation defects in Niemann-Pick type C disease. PLoS ONE **4**, e5193
30 Luzio, J.P., Bright, N.A. and Pryor, P.R. (2007) The role of calcium and other ions in sorting and delivery in the late endocytic pathway. Biochem. Soc. Trans. **35**, 1088–1091
31 McGlynn, R., Dobrenis, K. and Walkley, S.U. (2004) Differential subcellular localization of cholesterol, gangliosides, and glycosaminoglycans in murine models of mucopolysaccharide storage disorders. J. Comp. Neurol. **480**, 415–426
32 Marra, P., Salvatore, L., Mironov, Jr, A., Di Campli, A., Di Tullio, G., Trucco, A., Beznoussenko, G., Mironov, A. and De Matteis, M.A. (2007) The biogenesis of the Golgi ribbon: the roles of membrane input from the ER and of GM130. Mol. Biol. Cell **18**, 1595–608
33 Puthenveedu, M.A., Bachert, C., Puri, S., Lanni, F. and Linstedt, A.D. (2006) GM130 and GRASP65-dependent lateral cisternal fusion allows uniform Golgi-enzyme distribution. Nat. Cell Biol. **8**, 238–248
34 Rivero, S., Cardenas, J., Bornens, M. and Rios, R.M. (2009) Microtubule nucleation at the *cis*-side of the Golgi apparatus requires AKAP450 and GM130. EMBO J. **28**, 1016–1028
35 Vitry, S., Bruyère, J., Hocquemiller, M., Bigou, S., Ausseil, J., Colle, M.A., Prevost, M.C. and Heard, J.M. (2010) Storage vesicles in neurons are related to Golgi complex altertions in mucopolysaccharidesis IIIB. Am. J. Pathol., doi:10.2353/ajpath.2010.100447
36 Miedel, M.T., Rbaibi, Y., Guerriero, C.J., Colletti, G., Weixel, K.M., Weisz, O.A. and Kiselyov, K. (2008) Membrane traffic and turnover in TRP-ML1-deficient cells: a revised model for mucolipidosis type IV pathogenesis. J. Exp. Med. **205**, 1477–1490

Received 26 April 2010
doi:10.1042/BST0381442

blood

2011 117: 3974-3982
Prepublished online February 16, 2011;
doi:10.1182/blood-2010-09-309732

Catalytic domain modification and viral gene delivery of activated factor VII confers hemostasis at reduced expression levels and vector doses in vivo

Paris Margaritis, Elise Roy, Armida Faella, Harre D. Downey, Lacramioara Ivanciu, Giulia Pavani, Shangzhen Zhou, Ralph M. Bunte and Katherine A. High

Blood (print ISSN 0006-4971, online ISSN 1528-0020), is published weekly by the American Society of Hematology, 2021 L St, NW, Suite 900, Washington DC 20036.

Catalytic domain modification and viral gene delivery of activated factor VII confers hemostasis at reduced expression levels and vector doses in vivo

Paris Margaritis,[1-3] Elise Roy,[1,2] Armida Faella,[1,2] Harre D. Downey,[1,2] Lacramioara Ivanciu,[1,2] Giulia Pavani,[1,2] Shangzhen Zhou,[2] Ralph M. Bunte,[4] and Katherine A. High[1-3,5]

[1]Division of Hematology and [2]Center for Cellular and Molecular Therapeutics, The Children's Hospital of Philadelphia, Philadelphia, PA; [3]Department of Pediatrics, University of Pennsylvania School of Medicine, Philadelphia, PA; [4]University Laboratory Animal Resources, University of Pennsylvania, Philadelphia, PA; and [5]Howard Hughes Medical Institute, The Children's Hospital of Philadelphia, Philadelphia, PA

Catalytic domain variants of activated factor VII (FVIIa) with enhanced hemostatic properties are highly attractive for the treatment of bleeding disorders via gene-based therapy. To explore this in a hemophilic mouse model, we characterized 2 variants of murine activated FVII (mFVIIa-VEAY and mFVIIa-DVQ) with modified catalytic domains, based on recombinant human FVIIa (rhFVIIa) variants. Using purified recombinant proteins, we showed that murine FVIIa (mFVIIa) and variants had comparable binding to human and murine tissue factor (TF) and exhibited similar extrinsic coagulant activity. In vitro in the absence of TF, the variants showed a 6- to 17-fold enhanced proteolytic and coagulant activity relative to mFVIIa, but increased inactivation by antithrombin. Gene delivery of mFVIIa-VEAY resulted in long-term, effective hemostasis at 5-fold lower expression levels relative to mFVIIa in hemophilia A mice or in hemophilia B mice with inhibitors to factor IX. However, expression of mFVIIa-VEAY at 14-fold higher than therapeutic levels resulted in a progressive mortality to 70% within 6 weeks after gene delivery. These results are the first demonstration of the hemostatic efficacy of continuous expression, in the presence or absence of inhibitors, of a high-activity gene-based FVIIa variant in an animal model of hemophilia. (*Blood*. 2011;117(15):3974-3982)

Introduction

Over the past 3 decades, discoveries in multiple disciplines have been instrumental in the molecular dissection of hemophilia. These resulted in the development of novel therapies for the disease, including more effective treatment for the most serious complication in factor replacement, the development of inhibitory antibodies to factor VIII (FVIII) or IX (FIX). In particular, rhFVIIa (commercially known as NovoSeven [Novo Nordisk]) has a proven record of successful treatment for hemophilia patients with inhibitors, by providing localized hemostasis when administered at supraphysiologic doses of 90-110 μg/kg.[1] However, its short plasma half-life (2.7 hours) necessitates frequent infusions, resulting in high treatment costs[2] and preventing its use as a universal hemostatic agent.

For pharmacologic intervention, efforts to enhance the procoagulant activity of rhFVIIa have focused on chemical modification/formulation[3,4] or the rational design of novel, high-specific activity variants of rhFVIIa. This has been achieved by enhancing the phospholipid binding or increasing the catalytic activity of rhFVIIa.[5-8] Although data from human subjects suggest that a single-dose of a rhFVIIa variant (rhFVIIa-DVQ, also known as NN1731) with enhanced, TF-independent activity is safe,[9] efficacy and long-term safety data in hemophilic patients are limited. Moreover, the majority of its in vivo efficacy data have been derived using nonhomologous animal models in short-term studies, where potential species incompatibilities between human FVIIa and endogenous (animal) TF[10] may affect the hemostatic outcomes.[11,12]

As an alternative to rhFVIIa infusion, we have demonstrated in animal models the efficacy of gene-based FVIIa therapy for inherited bleeding disorders. In a pilot study, we generated a murine factor VII (mFVII) transgene (mFVII-2RKR) that can be secreted in its active form (mFVIIa) and, after continuous expression via viral vector–mediated gene delivery, effect hemostasis in vivo in hemophilic mice.[13,14] Moreover, in a multiyear study, we confirmed our approach in hemophilic dogs using canine FVII-2RKR (cFVIIa) as a transgene and demonstrated the complete elimination of spontaneous bleeds, a characteristic disease feature of these animals, without any evidence of thrombosis.[15] Although the adeno-associated virus (AAV) serotype 8 (AAV8) vector used in that study was the most efficient choice for expression,[16] the relatively high viral vector doses used compared with similar approaches with canine FVIII (1.2- to 12.5-fold[17,18]) or FIX (12- to 24-fold[19]) impose a technical barrier for further development of a FVIIa gene-based approach that needs to be addressed.

An avenue to overcome this limitation is to use transgene variants of FVIIa with enhanced activity that can potentially lower minimum required expression levels and translate to lower viral vector dose requirements. Here, we explore this possibility by a comprehensive characterization of 2 murine FVIIa (mFVIIa) variants with amino acid substitutions in their catalytic domains, based on rhFVIIa variants. We demonstrate that (1) mFVIIa variants exhibit increased TF-independent coagulant activity relative to mFVIIa; (2) gene transfer of a high-activity mFVIIa variant

Submitted September 24, 2010; accepted January 7, 2011. Prepublished online as *Blood* First Edition paper, February 16, 2011; DOI 10.1182/blood-2010-09-309732.

The online version of this article contains a data supplement.

The publication costs of this article were defrayed in part by page charge payment. Therefore, and solely to indicate this fact, this article is hereby marked "advertisement" in accordance with 18 USC section 1734.

can achieve long-term hemostasis at a substantially lower expression level (and lower viral vector doses) compared with mFVIIa; (3) the presence of inhibitors to human factor IX does not alter or reduce hemostatic efficacy in hemophilic mice expressing the mFVIIa variant; and (4) high-level continuous expression of this mFVIIa variant leads to rapid mortality. These results are the first to demonstrate the improved hemostatic efficacy of gene-based FVIIa variants for the treatment of hemophilia but also indicate what are likely to be the major safety considerations for gene-based strategies using enhanced activity coagulation factor(s).

Methods

Plasmid construction and AAV vector production

The plasmid vectors for mFVII, mFVIIa, and the liver-specific, adeno-associated virus (AAV) vector plasmid backbone have been previously described.[14] The mFVIIa-DVQ and VEAY variants were constructed by PCR mutagenesis and helper-free, recombinant AAV virus vector production was performed as previously described.[14] Vector genome (vg) titering for each construct was performed side-by-side in duplicate and confirmed by slot blot as well as silver staining.

Recombinant proteins and purification

Stable cell lines expressing mFVII, mFVIIa, mFVIIa-DVQ or mFVIIa-VEAY containing a C-terminal epitope tag were established as previously described.[14] All murine proteins (except mFVII) contained the Arg-Lys-Arg-Arg-Lys-Arg (RKRRKR [2RKR]) sequence inserted at Arg152-Ile153 of the mature protein. Recombinant proteins were purified using an antibody column, as previously described.[14] Human soluble TF (hsTF) and murine soluble TF (msTF) were kind gifts from Dr S. Krishnaswamy (Children's Hospital of Philadelphia) and Dr Mirella Ezban (Måløv, Novo Nordisk, Denmark), respectively. Human FX (hFX) and activated hFX (hFXa) were kind gifts from Dr R. M. Camire (Children's Hospital of Philadelphia).

Peptidyl substrate cleavage and TF binding

Proteins (100nM) were incubated in reaction buffer (20mM HEPES, 150mM NaCl pH 7.4 [HBS], 5mM $CaCl_2$ and 0.1% [wt/vol] PEG 8000 [HBS-PEG-$CaCl_2$]) at 25°C in the presence or absence of soluble TF and 400μM phosphatidylcholine/phosphatidylserine (75%/25%, PCPS). Binding to human or murine soluble TF was performed using a range of concentrations (0-2μM [hsTF] or 0-150nM [msTF]). Spectrozyme FVIIa (American Diagnostica) was added at 375nM immediately before monitoring the A_{405nm} as a function of time using a VMax plate reader (Molecular Devices). Dissociation constant (K_d) determination was performed from the fitted data obtained, essentially as previously described.[20] Although we cannot exclude the possibility of phospholipids influencing the FVII/FVIIa interaction with soluble TF (hence the amidolytic activity and K_d), we do not believe that it is likely, based on previous reports with human FVII.[20,21]

Macromolecular substrate cleavage

Proteins (200nM) were incubated in reaction buffer at 25°C with 100μM PCPS. The reaction was initiated by the addition of 100nM hFX and aliquots of the reaction were quenched at several time points up to 3.5 minutes in HBS with 0.1% [wt/vol] PEG 8000 and 50mM EDTA (HBS-PEG-EDTA). The hFXa chromogenic substrate (Spectrozyme FXa, American Diagnostica) was added at a final concentration of 100μM. Human FXa activity was monitored by measuring the A_{405nm} as a function of time at 25°C. The concentration of hFXa/min (nM hFXa/min) was determined by interpolation from the linear dependence of the initial rate of Spectrozyme FXa hydrolysis on known concentrations of hFXa that were determined separately. The initial steady-state rate of hFXa formation was determined from the slope of plots that documented the linear appearance of hFXa with time, expressed as nM hFXa/min.

Coagulation assays

Prothrombin time (PT) and activated partial thromboplastin time (aPTT) assays on plasma, cell culture supernatants, and purified proteins were determined as previously described,[14] using human factor deficient plasmas (George King Bio-Medical, Inc). Clotting activity was determined by performing clotting assays on serial dilutions of samples (in Tris-buffered saline [TBS]-bovine serum albumin [BSA, 0.01%]), using a standard curve with rhFVIIa. Briefly, for PT assays, 25 μL of sample were incubated with 25 μL of human FVII deficient plasma for 1 minute and 100 μL of Innovin (CSL-Behring) were added before measuring the time to clot using a Start4 instrument (Diagnostica Stago). For aPTT assays, 25 μL of sample were incubated with an equal volume of aPTT reagent (Trinity Biotech) and 25 μL of human FVIII or FIX deficient plasma for 3 minutes at 37°C and, after the addition of 25 μL of 25mM $CaCl_2$, time to clot formation was measured using a Start4 instrument. Baseline values for PT assays were: 32.2 ± 1.9 seconds (wild-type C57BL/6 mice); 28.2 ± 4.8 seconds (hemophilia A [HA] mice); 34.1 ± 3.0 (hemophilia B, [HB] mice). Baseline values for aPTT assays were: 32.1 ± 2.4 seconds (wild-type C57BL/6 using human FIX–deficient plasma); 37.9 ± 1.6 seconds (wild-type C57BL/6 using human FVIII–deficient plasma); 57.7 ± 9.7 seconds (HA); 58.8 ± 3.9 seconds (HB). Baseline values were obtained from at least 10 mice.

Animal experiments, in vivo hemostatic challenge assays and histologic analysis

All experimental procedures were reviewed and approved by the Institutional Animal Care and Use Committee (IACUC) at The Children's Hospital of Philadelphia. Eight- to 12-week-old hemophilia A[22] or B[23] mice on a C57BL/6 background were used for all animal experiments. Recombinant AAV delivery and collection of mouse plasma samples were performed as previously described.[15] The tail-clip and $FeCl_3$ assay were performed at or after 7 weeks after AAV administration, as previously described.[13] Histologic analysis was performed on tissues fixed in 10% formalin overnight at 4°C, as previously described.[24] Staining for fibrin(ogen) on paraffin sections was performed as previously described.[13] For immunofluorescence staining, paraffin sections were hydrated through xylene and graded alcohol and equilibrated in deionized water. Nonspecific binding was blocked with 3% BSA. They were then incubated with rat anti–mouse CD31 monoclonal antibody (10 μg/mL; catalog no. 558738, BD Pharmingen), and FITC-conjugated anti–Fibrin(ogen) polyclonal antibody (10 μg/mL; catalog no. F0111, Dako) overnight at 4°C; developed with Cy3-conjugated donkey anti–rat IgG (10 μg/mL; catalog no. 712-165-150, Jackson ImmunoResearch Laboratories) and mounted with VectaShield DAPI mounting medium (Vector Laboratories). The sections were analyzed using a Leica TCS-SP2 AOBS confocal laser scanning microscope on a Leica DM-IRE2 inverted microscope stand.

ELISA for mFVIIa

Detection of free mFVIIa in the mouse plasma was performed using an enzyme-linked immunosorbent assay (ELISA), as previously described[13] with some modifications. Briefly, samples were diluted 20- or 80-fold in blocking buffer (1% skim milk in phosphate-buffered saline [PBS]) and incubation with the biotinylated Phe-Pro-Arg-chloromethylketone (Biotin-FPR-CMK, 77 μg/mL final concentration; Haematologic Technologies) was performed overnight at 4°C on an orbital shaker (300 rpm). Murine FVII/mFVIIa in the samples was captured using a custom rat anti-mFVII/a monoclonal antibody (Green Mountain Antibodies) coated at 10 μg/mL in 50mM $NaHCO_3$, pH 9.6. This antibody was raised against purified recombinant mFVIIa and maps on the heavy chain of mFVII/mFVIIa (P.M., E.R., unpublished observations, May 2008). Detection of the biotin moiety on the FPR-CMK in the active site of mFVIIa (not mFVII) was by incubation with horseradish peroxidase (HRP) labeled streptavidin (catalog no. 554066, BD Pharmingen) and visualized by addition of *o*-phenylenediamine dihydrochloride (1 mg/mL in 0.01M sodium citrate, pH 4.5). For quantification, a standard curve mFVIIa or mFVIIa-VEAY in 1:20 or 1:80 diluted untreated HA or HB plasma (in blocking buffer) was used. Because this method essentially detects active site occupancy by the biotinylated FPR-CMK, it

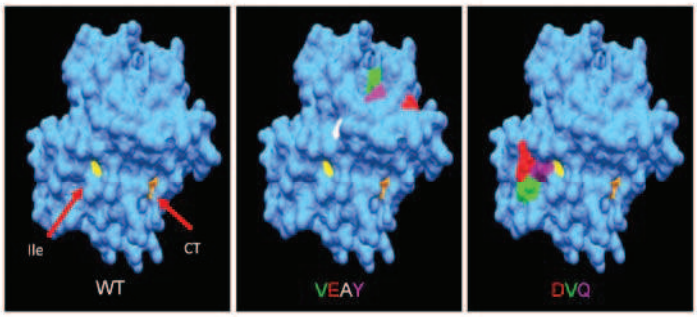

Figure 1. Spatial localization of the mutations in mFVIIa-VEAY (VEAY) and mFVIIa-DVQ (DVQ) on the heavy chain compared with mFVII wild-type (WT). The crystal structure of the heavy chain of human FVIIa (1DAN[31]) was used as a template for homology modeling (see "Statistical analysis and protein percentage identity calculation and homology-based modeling"). The catalytic triad (CT, orange [His193, Asp242, Ser194]) and the location of the newly formed N-terminus of the heavy chain of the activated form are shown (Ile153, yellow). The VEAY mutations are: Leu305Val (green); Ala314Glu (red); Lys337Ala (white); Ile374Tyr (magenta). The DVQ mutations are: Val158Asp (red); Glu296Val (green); Met298Gln (purple). Amino acid numbering refers to the mature secreted mFVII.

detects mFVIIa and not mFVII. Baseline values for mFVIIa in mouse plasma were ~ 150 ng/mL and were subtracted from the presented data.

Generation of inhibitors to hFIX

Baseline mouse plasma samples were obtained after tail bleeding several days before the start of the experiment. Mice were subsequently injected subcutaneously with 200 μL of an emulsion consisting of complete Freund adjuvant (CFA; Sigma-Aldrich) and 20 μg of human FIX (hFIX; Mononine, CSL-Behring). Four dorsal sites were used, 50 μL per site. Three weeks later, the procedure was repeated substituting CFA with incomplete Freund adjuvant (IFA; Sigma-Aldrich) but injecting 4 different dorsal sites. Plasma samples were obtained after tail bleeding for determination of antibody level (total anti-hFIX IgG) and inhibitor titer (Bethesda assay), performed as previously described.[25] Application of this protocol in HA mice or by weekly (for 8 weeks) intravenous administration of 2.5 U recombinant human FVIII (Refacto [Pfizer Inc] or Kogenate [Bayer Healthcare]) did not result in inhibitory antibody formation for reasons that are unclear.

Statistical analysis and protein percentage identity calculation and homology-based modeling

Data were analyzed using a Mann-Whitney (nonparametric) test. Survival data analysis was performed using the log-rank (Mantel-Cox) test in the Prism Version 5.0 software package (GraphPad Software). In all tests, differences were considered significant at $P < .05$. Percentage identity for human, mouse and canine proteins was calculated from the linear protein sequence alignment, using the ClustalW function of the MegAlign software (part of the Lasergene software package, DNAStar Inc). Homology-based modeling of the heavy chains of murine FVII and variants VEAY and DVQ was performed with the SWISS-MODEL homology-modeling server from the ExPASys web site (http://swissmodel.expasy.org/workspace/).[26-29]

Results

Purification, amidolytic and proteolytic activity of mFVIIa, mFVIIa-DVQ and mFVIIa-VEAY

Previous reports have identified key residues in the catalytic domain of the human FVII sequence that can be modified to enhance its catalytic activity, specifically at positions 158 (V = > D), 296 (E = > V) and 298 (M = > Q; mutant DVQ[30]) as well as 305 (L = > V), 314 (S = > E), 337 (K = > A) and 374 (F = > Y; mutant VEAY[7]). Because murine FVII exhibits extensive sequence identity to human FVII (70%), we introduced these mutations in the mFVIIa backbone (containing the RKRRKR PACE/furin cleavage site[14]) and generated mFVIIa-DVQ and mFVIIa-VEAY (Figure 1). Purified recombinant proteins exhibited the expected fragment sizes (Figure 2A). Zymogen mFVII purified under identical conditions was in the single-chain form, indicating that there was no autoactivation during the purification process. Murine FVIIa as well as

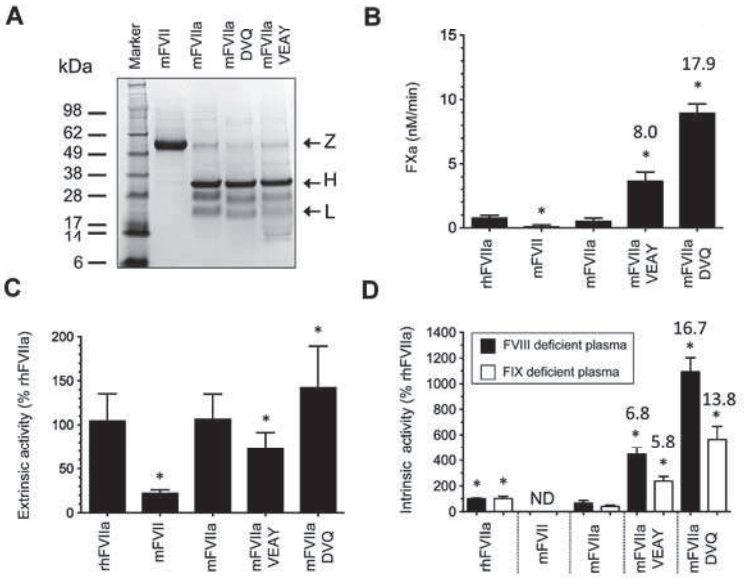

Figure 2. Characterization of recombinant proteins. (A) Approximately 4 μg of purified protein (mFVII, mFVIIa, mFVIIa-DVQ and mFVIIa-VEAY) was electrophoresed under reducing conditions and stained with Coomassie blue. The molecular sizes of the marker are shown on the left. Arrows indicate the zymogen form (Z), heavy (H) and light (L) chains. The lower-molecular-weight bands (10-16 kDa) are most likely degradation products, as have been previously observed in human recombinant FVIIa preparations.[30,33] The differential staining of light and heavy chains with Coomassie blue is commonly found in human[32,33] as well as murine FVIIa preparations.[10,14] (B) Proteolytic activity of proteins using human FX as a macromolecular substrate in the absence of tissue factor expressed as nM FXa/min. Data were derived from at least 3 independent experiments. *$P < .04$ compared with mFVIIa. Fold increase is indicated relative to mFVIIa. (C) Extrinsic coagulant activity of recombinant proteins (% of rhFVIIa) in human FVII–deficient plasma. (D) Intrinsic coagulant activity of recombinant proteins (% of rhFVIIa) in human FVIII or FIX deficient plasma. Data for panels C and D were derived from at least 4 experimental points. *$P < .03$ compared with mFVIIa. ND indicates not detectable. Fold increase in activity in panels C and D is indicated relative to mFVIIa. All data are shown as average ± 1 SD.

Table 1. Binding of recombinant proteins to human or murine soluble TF derived from at least 2 independent experiments

	Protein				
Cofactor	mFVII	mFVIIa	mFVIIa-DVQ	mFVIIa-VEAY	rhFVIIa
hsTF	ND	86.7 ± 22.8	42.4 ± 20.7	71.7 ± 22.2	12.1 ± 6.0
msTF	ND	2.0 ± 0.5	2.9 ± 0.8	3.2 ± 1.9	ND

Values, stated as K_d (nM) were derived from amidolytic activity assays.
ND indicates not determined (data fitting was not possible).

both mFVIIa variants were present in almost 100% active form (Figure 2A).

We subsequently investigated the binding of recombinant proteins to msTF or hsTF indirectly by measuring cleavage of a small peptidyl substrate (amidolytic activity of the FVIIa-TF complex). Murine FVIIa and its variants were stimulated in the presence of increasing concentrations of msTF or hsTF and showed similar binding compared with each other (Table 1), although binding to hsTF was not as tight as previously reported using surface plasmon resonance.[10] Zymogen mFVII showed negligible amidolytic activity. Because the rhFVIIa-DVQ and rhFVIIa-VEAY exhibit enhanced intrinsic activity toward peptidyl and macromolecular substrates,[7] we determined the activity of the recombinant mFVII/FVIIa proteins toward macromolecular substrate (FX), in the absence of TF (Figure 2B). Human FX was used as a substitute for murine FX because the latter was not commercially available. Under those experimental conditions, compared with mFVIIa, both mFVIIa-VEAY and mFVIIa-DVQ exhibited enhanced rates of activated hFX (hFXa) generation ($P < .03$) that ranged from 8-fold (mFVIIa-VEAY) to 17.9-fold (mFVIIa-DVQ). In contrast, rhFVIIa exhibited a rate of hFXa generation similar to mFVIIa ($P = .11$) and zymogen mFVII showed substantially reduced proteolytic activity ($P < .04$ vs mFVIIa). Together, these data demonstrate that the specific modifications present in the catalytic site of the mFVIIa variants do not alter binding to TF but substantially enhance their proteolytic activity, compared with mFVIIa.

mFVIIa variants exhibit enhanced in vitro coagulant activity

Next, we examined the coagulant activity of recombinant proteins using extrinsic (PT) and intrinsic (aPTT) coagulation pathway assays, compared with rhFVIIa (100%). As expected,[14] mFVIIa had similar extrinsic activity to rhFVIIa (91%), whereas mFVII had approximately 22% extrinsic activity (Figure 2C). Compared with mFVIIa, the mFVIIa-VEAY and mFVIIa-DVQ variants exhibited modestly reduced ($P = .01$) and elevated ($P = .03$) extrinsic activity, respectively (Figure 2C). However, in the intrinsic (TF-independent) clotting assay using human FVIII or FIX deficient plasmas, both mFVIIa variants showed increased activity in both plasmas ($P < .002$ vs mFVIIa; Figure 2D). The fold enhancement was not statistically different between FVIII and FIX deficient plasma ($P > .07$). Zymogen mFVII had minimal activity (< 1%) and none of the recombinant proteins exhibited appreciable coagulant activity in hFX-deficient plasma (data not shown). Similar results were obtained using mouse HA or HB plasma (data not shown). Both variants displayed enhanced inactivation in HA or HB mouse plasma in the order of mFVIIa-VEAY ≫ mFVIIa-DVQ > mFVIIa, that was antithrombin-dependent (supplemental Figure 1, available on the *Blood* Web site; see the Supplemental Materials link at the top of the online article), similar to previous observations with their human counterparts.[7] These data confirm the observed enhancement in proteolytic activity (see "Purification, amidolytic and proteolytic activity of mFVIIa, mFVIIa-DVQ and mFVIIa-VEAY") and indicate that mFVIIa-VEAY and mFVIIa-DVQ had essentially unaltered TF-dependent but substantially enhanced TF-independent coagulant activity compared with mFVIIa.

mFVIIa-VEAY normalizes the hemophilia A phenotype at greatly reduced AAV vector doses and expression levels

The inactivation profiles of the mFVIIa variants suggest that their improved hemostatic properties in vitro may not necessarily translate to enhanced hemostatic efficacy in vivo in a gene transfer setting. This is particularly relevant for mFVIIa-VEAY, which exhibited the fastest inactivation. We chose the mFVIIa-VEAY variant to demonstrate whether improved hemostatic effects can be observed with enhanced activity FVIIa variants even with unfavorable inactivation profiles.

We constructed an AAV serotype 8 vector carrying either the mFVIIa or mFVIIa-VEAY transgene under the control of a liver-specific promoter/enhancer, as previously described.[14] Preliminary dose-escalation studies in HA mice demonstrated that normalization of the hemophilic aPTT was achieved using tail vein administration of 1.2×10^{12} vector genomes (vg)/mouse for mFVIIa ($P = .31$ vs wild-type) and a substantially lower dose (40- to 100-fold) for AAV-mFVIIa-VEAY (mFVIIa-VEAY [L], $P = .08$ vs wild-type; Figure 3A). A dose of AAV-mFVIIa-VEAY comparable to AAV-mFVIIa resulted in superphysiologic reduction of the aPTT (mFVIIa-VEAY [H], $P = .007$ vs wild-type; Figure 3A). We thus determined the long-term efficacy (in vitro and in vivo) using AAV in 2 cohorts of HA mice, as follows: mice treated with AAV-mFVIIa (1.2×10^{12} vg/mouse) and mice treated with 40- to 100-fold lower doses of AAV-mFVIIa-VEAY ($1.2\text{-}3 \times 10^{10}$ vg/mouse, AAV-mFVIIa-VEAY [L]).

Both cohorts exhibited long-term normalization of the hemophilic aPTT (Figure 3B; $P > .05$ for AAV-mFVIIa-VEAY [L] vs AAV-mFVIIa at all timepoints). However, this was achieved at ~ 5-fold lower circulating protein levels for mFVIIa-VEAY compared with mFVIIa (0.6 ± 0.25 μg/mL vs 3.0 ± 0.75 μg/mL at the expression plateau [4 weeks after AAV administration], respectively; $P < .002$). To further confirm this observation, we determined relative mRNA levels in the transduced mouse livers for each cohort (harvested after 14 weeks after AAV administration). Both cohorts exhibited increased mFVII/mFVIIa transcript levels compared with untreated mice but AAV-mFVIIa-VEAY (L) treated

Table 2. $FeCl_3$ vessel occlusion within 5 minutes of $FeCl_3$ application in AAV-mFVIIa, AAV-mFVIIa-VEAY or untreated HA mice

Mouse group	Mice with full occlusion (%) within 5 minutes	Mice with no occlusion (%)
AAV-mFVIIa* (n = 9)	3 (33%)	4 (45%)
AAV-mFVIIa-VEAY (n = 9)	3 (33%)	6 (67%)
HA, untreated (n = 11)	0 (0%)	11 (100%)

Number of mice (n) is indicated for each group.
*Two mice showed partial occlusion at 5-6 minutes after $FeCl_3$ application.

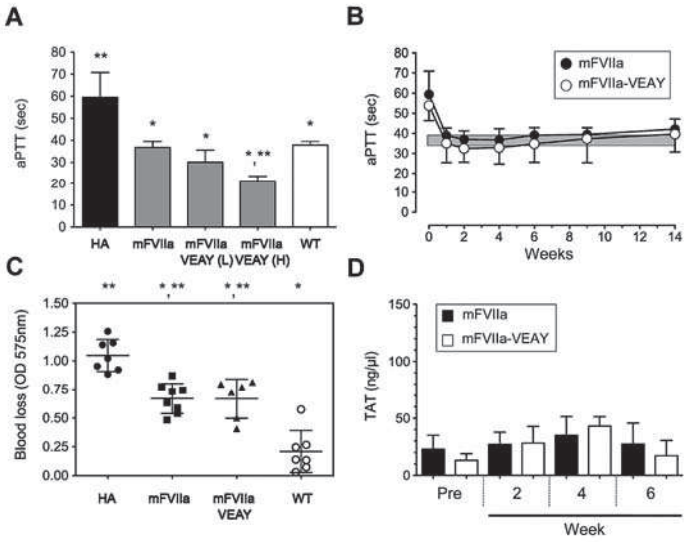

Figure 3. Hemostatic efficacy of mFVIIa-VEAY after gene transfer in hemophilia A mice. (A) Dose escalation study in HA mice receiving 1.2×10^{12} vg of AAV-mFVIIa, $1.2\text{-}3 \times 10^{10}$ vg of AAV-mFVIIa-VEAY (low dose, mFVIIa-VEAY [L]) or $0.6\text{-}0.3 \times 10^{12}$ vg of AAV-mFVIIa-VEAY (high dose, mFVIIa-VEAY [H]). Activated partial thromboplastin time (aPTT) values are shown for samples assayed at 6 weeks post AAV administration. Wild-type (WT) and HA aPTTs are also shown. Each cohort consisted of at least 3 mice. $^*P < .009$ vs HA; $^{**}P < .007$ vs WT. All AAV vectors were of serotype 8. (B) aPTT in HA mice after delivery of AAV-mFVIIa (1.2×10^{12} vg/mouse) or AAV-mFVIIa-VEAY ($1.2\text{-}3 \times 10^{10}$ vg/mouse). Each cohort consisted of 10 mice. The gray box indicates the range of aPTT values using human FVIII deficient plasma in hemostatically normal mice (37.9 ± 1.6 seconds, n = 10). (C) Blood loss after a tail clip injury in AAV-treated HA mice compared with wild-type (WT) and HA controls. $^*P < .002$ compared with HA; $^{**}P < .001$ vs WT. (D) TAT levels compared with baseline (Pre) in HA mice after gene transfer. All data are shown as average ± 1 SD.

mice had ~ 10-fold lower levels than the AAV-mFVIIa treated mice (supplemental Figure 2).

We subsequently investigated whether hemostatic efficacy with mFVIIa-VEAY can be achieved at these greatly reduced vector doses/expression levels compared with mFVIIa, using 2 in vivo hemostatic challenges. In the tail clip assay, both AAV-mFVIIa and AAV-mFVIIa-VEAY (L) mice exhibited a similar ($P = .98$) reduction in blood loss compared with untreated HA mice ($P < .002$ for either cohorts vs HA) although not at levels seen with hemostatically normal mice (Figure 3C), similar to our previous observations.[13,14] In another hemostatic challenge ($FeCl_3$ carotid artery injury), both AAV-mFVIIa and AAV-mFVIIa-VEAY (L) mice exhibited stable vessel occlusion within 5 minutes in 33% of the cases after $FeCl_3$ application, although partial occlusion was also observed in 2 of 9 AAV-mFVIIa treated mice (Table 2). In terms of safety, we did not observe any difference in levels of thrombin-antithrombin (TAT) complex for either cohort (Figure 3D).

To further investigate hemostatic efficacy of mFVIIa-VEAY in a setting of hemophilic inhibitors, we used a protocol (Figure 4A) to generate inhibitors to human FIX (hFIX) in HB mice. This resulted in induction of neutralizing antibodies as measured by a Bethesda assay (range, 6-26 Bethesda units [BU], Figure 4B) as well as total anti-hFIX IgG (Figure 4C, timepoints A-C). We subsequently administered low-dose AAV-mFVIIa-VEAY (3×10^{10} vg/mouse), similar to those administered in HA mice (see "mFVIIa-VEAY normalizes the hemophilia A phenotype at greatly reduced AAV vector doses and expression levels"). Because the expressed mFVIIa-VEAY transgene product would result in erroneous Bethesda titer (because it is a clotting-based assay), we measured total anti-hFIX IgG after gene transfer as a surrogate test. We found that this was similar to pre-AAV infusion levels (weeks 4 and 9 vs timepoint C, $P \geq .2$; Figure 4C). This indicates that the immune response to hFIX remained stable over the course of the experiment, after AAV administration. More importantly,

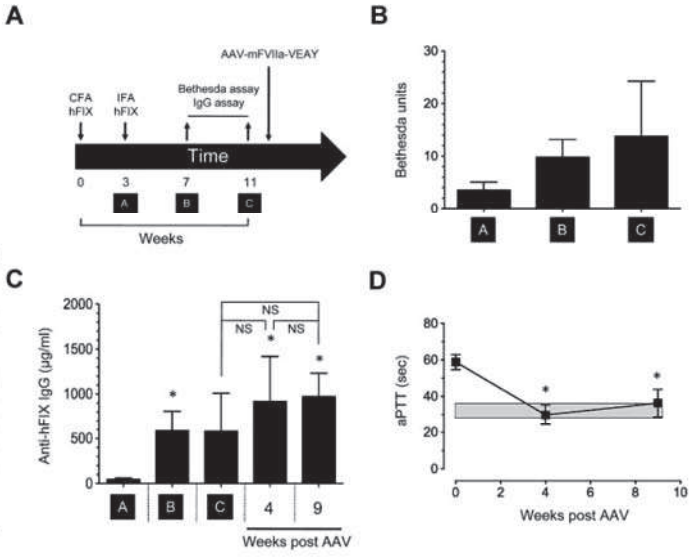

Figure 4. Continuous expression of mFVIIa-VEAY in hemophilia B mice with inhibitors. (A) Scheme for generating anti–human FIX inhibitory antibodies in HB mice. Downward arrows indicate injection of complete or incomplete Freund adjuvant (CFA and IFA, respectively) complexed with 20 µg of hFIX or administration of AAV-expressing mFVIIa-VEAY. Upwards arrows indicate collection of tail blood to assay Bethesda titer and total anti-hFIX IgG. Timepoints A-C are indicated. (B) Bethesda titers of HB mice before administration of AAV-mFVIIa-VEAY. (C) Total anti-hFIX IgG in HB mice prior (timepoints A-C) and after administration of AAV-mFVIIa-VEAY. $^*P < .05$ vs timepoint A. Nonsignificant (NS) differences are indicated. (D) aPTT in HB mice with inhibitors to hFIX after administration of AAV-mFVIIa-VEAY. $^*P < .05$ vs baseline (week 0). A gray box indicates the range in hemostatically normal mice using human FIX–deficient plasma (32.1 ± 2.4 seconds, n = 10). All data shown as average ± 1 SD.

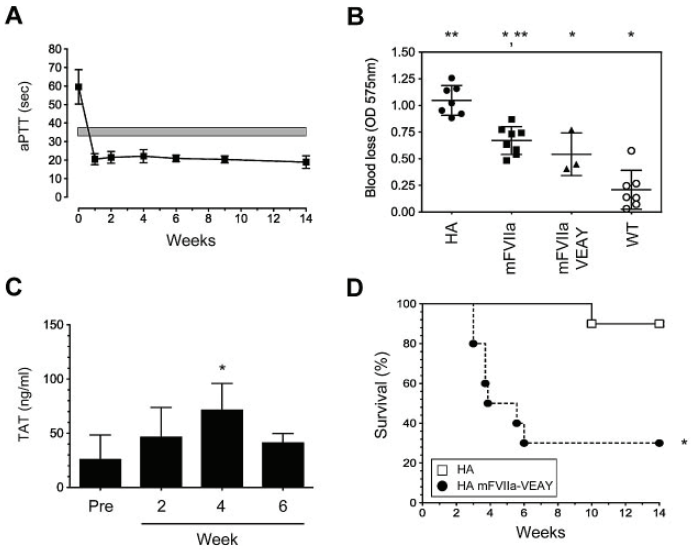

Figure 5. Hemostatic efficacy of mFVIIa-VEAY after high-dose gene transfer in hemophilia A mice. (A) aPTT in HA mice after delivery of AAV-mFVIIa-VEAY (1.2×10^{12} vg/mouse). The initial cohort consisted of 10 mice. The gray box indicates the range of aPTT values using human FVIII-deficient plasma in hemostatically normal mice (37.9 ± 1.6 seconds, n = 10). (B) Blood loss after a tail clip assay, compared with AAV-mFVIIa–treated HA mice, or untreated HA and wild-type (WT) mice, whose data are depicted in Figure 3C and are repeated here for comparison. $^{*}P < .02$ vs HA; $^{**}P < .002$ vs WT. (C) TAT levels in AAV-mFVIIa-VEAY–treated mice as a function of time. $^{*}P < .03$ vs baseline (Pre). (D) Survival of HA mice treated with high-dose AAV-mFVIIa-VEAY (AAV-mFVIIa-VEAY [H], ●), relative to untreated HA controls (□). All cohorts initially consisted of 10 mice. $^{*}P < .004$ between HA-mFVIIa-VEAY (H) survival compared with untreated HA. All data (except in panel D) shown as average ± 1 SD.

AAV-mFVIIa-VEAY administration resulted in expression of mFVIIa-VEAY at ~ 1 μg/mL (assayed at 4 or 9 weeks after AAV administration) and near normalization of the aPTT as seen in HA mice (compare Figure 4D with Figure 3B). This suggests that the presence of inhibitory antibodies does not change the hemostatic effects of mFVIIa-VEAY. This was also observed using AAV-mFVIIa injected at 1.2×10^{12} vg/mouse (P.M., A.F., unpublished observations, July 2009).

Together, these data suggest that, in agreement with the in vitro enhancement of intrinsic activity seen for mFVIIa-VEAY, in vivo hemostatic efficacy similar to mFVIIa can be achieved by lower level of expression of mFVIIa-VEAY and reduced AAV vector doses.

Overexpression of mFVIIa-VEAY in hemophilic mice results in rapid and increased mortality

Our previous observations of enhanced mortality in hemophilic mice overexpressing mFVIIa[13] set a precedence for investigating the safety profile of FVIIa gene therapy. To establish this for mFVIIa-VEAY, we treated a cohort of HA mice with AAV-mFVIIa-VEAY at an identical (high) vector dose to AAV-mFVIIa (1.2×10^{12} vg/mouse, AAV-mFVIIa-VEAY [H]). In agreement with its enhanced intrinsic activity, the AAV-mFVIIa-VEAY (H) mice exhibited a sustained, supraphysiologic reduction of the aPTT (~ 20 seconds; Figure 5A), well below levels observed for the other 2 cohorts ($P < .001$, compare to Figure 3B). Steady-state expression of mFVIIa-VEAY in this cohort was ~ 8 μg/mL (at 4 weeks after AAV) and reduction in blood loss after a tail clip assay was similar to the mFVIIa cohort (Figure 5B, $P = .28$). Compared with hemostatically normal mice, the observed blood loss was not statistically different (Figure 5B, $P = .07$). However, we observed a time-dependent increase in TAT complex formation (Figure 5C), and a rapid decrease in survival to 30% within the first 6 weeks after vector administration. This was in contrast to untreated HA mice (Figure 5D, $P < .004$) or the other cohorts (AAV-mFVIIa and AAV-mFVIIa-VEAY [L]) that showed nearly 100% survival (data not shown) within the same experimental time period.

Histopathologic examination was used to further investigate the cause of death in 6 mice in the AAV-mFVIIa-VEAY (H) cohort. Necropsy revealed no gross abnormalities and histologic analyses in the spleen, liver or kidneys were normal compared with 6 untreated HA mice (data not shown). Major pathologic findings were confined to the heart and lungs. We observed visible thrombi in the heart (6 of 6 mice; Figure 6A-B), predominantly in the atria, as well as fibrosis (4 of 6 mice) and occasional inflammatory cell infiltrates in the myocardium (2 of 6 mice; data not shown). In the lungs, we observed hemorrhage (5 of 6 mice) as well as fibrin deposition that extended into the lung parenchyma (Figure 6C-E), that was absent in untreated HA controls (Figure 6E). These findings are similar to those observed previously in transgenic mice overexpressing mFVIIa[13] and, together with the elevated levels of TAT, pulmonary hemorrhage and fibrin deposition, are indicative of ongoing clot formation in the microcirculation as the most likely cause of death in these mice.

Discussion

The development of inhibitory antibodies against FVIII or FIX remains the most serious and most common complication of the current treatment of hemophilia by protein replacement.[34] Although treatment of inhibitor patients with bolus infusion of rhFVIIa is effective, frequent and high dose administration is necessary. As an alternative to bolus dosing, we have previously used gene delivery to continuously express an engineered activated FVII transgene and shown efficacy in small (murine) and large (canine) hemophilic models.[14,15] In particular, multiyear expression of gene-based cFVIIa in hemophilic dogs was safe and resulted in elimination of spontaneous bleeds[15] that are characteristic in that model.[35] However, that study also underscored that improvements aimed to lower the hemostatically effective viral vector dose will be necessary before a human application.

We hypothesized that enhancement of the catalytic function of our FVIIa transgene would confer hemostatic efficacy at lower

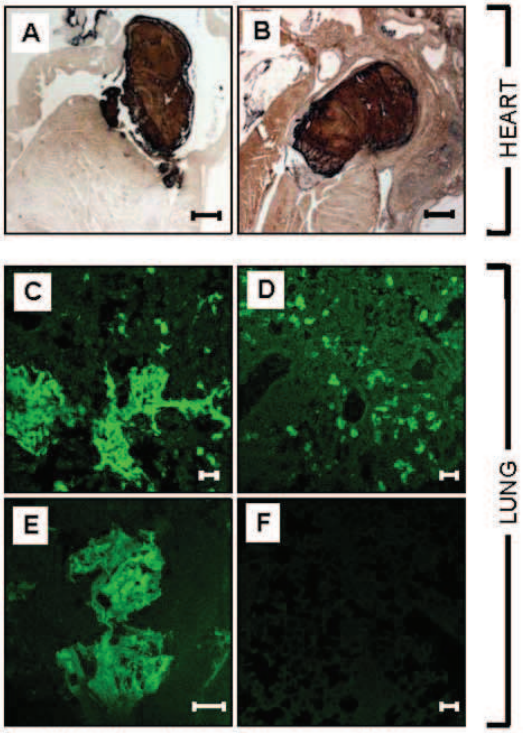

Figure 6. Histologic analysis of hearts and lungs of HA mice overexpressing mFVIIa-VEAY. Fibrin(ogen) immunohistochemical staining in the heart (A-B) showing visible thrombi in the atria. (C-F) Immunofluorescent staining for fibrin(ogen) in the lungs of AAV-mFVIIa-VEAY HA–treated mice (C-E) showing fibrin(ogen) deposition in the lung parenchyma in contrast to untreated HA control mice (F). Scale bars, 500 μm (A-B) and 50 μm (C-F).

expression levels, and hence, reduce the vector dose. The hemophilia mouse model, having well-established in vivo hemostatic endpoints, offers a convenient platform to systematically test this hypothesis. Here, we generated and characterized 2 murine FVIIa variants with enhanced intrinsic activity, that harbored corresponding mutations from enhanced activity human FVIIa variants with catalytic domain modifications.[7] A series of in vitro assays using purified recombinant proteins demonstrated that the murine FVIIa variants model their human counterparts in terms of enhanced activity as well as faster inhibition kinetics compared with the parent mFVIIa molecule. Although these opposing attributes may limit efficacy in a protein infusion setting, continuous expression of such FVIIa variants via gene delivery results in more favorable pharmacokinetic parameters. In the latter setting, hemostatic efficacy will be governed by the balance of expression level, rate of inhibition/secretion, clearance and extravascular dissemination of the expressed transgene. Our in vivo data using mFVIIa-VEAY clearly demonstrate that continuous expression can overcome its relatively unfavorable inactivation profile, and result in long-term hemostatic efficacy at lower expression levels and vector doses relative to the parent mFVIIa transgene. This was evident using 2 in vivo hemostatic challenge assays that demonstrated similar responses between HA mice expressing mFVIIa (~ 3 μg/mL) or mFVIIa-VEAY (~ 0.6 μg/mL). In addition, our data show that the presence of inhibitors to FIX did not appear to change the hemostatic effect of mFVIIa-VEAY. This is the first report for liver-directed FVIIa gene transfer in a hemophilia in vivo model complicated by inhibitors and lends further support for the therapeutic application of this approach. Clearly, the use of mFVIIa-DVQ or other variants with substantially enhanced activity would be expected to have more pronounced effects than mFVIIa-VEAY shown here.

We have previously shown that expression of mFVIIa in the range of 3-4 μg/mL in hemophilia B mice transgenic for mFVIIa results in mortality within months from birth that was positively associated with FX activity levels.[13] Here, expression of ~ 8 μg/mL of mFVIIa-VEAY in hemophilia A mice, nearly 14-fold higher than therapeutic for this variant (~ 0.6 μg/mL), resulted in increased mortality but at a substantially shorter timeframe than previously seen (weeks vs months[13]). This observation thus identifies the enzymatic activity of the mFVIIa transgene as a risk factor, in addition to expression levels. In contrast, hemophilia A mice expressing ~ 0.6 μg/mL (mFVIIa-VEAY) did not show evidence of a prothrombotic phenotype within the duration of this study, suggestive of a relatively wide therapeutic window of effecting hemostasis with this enhanced variant of mFVIIa.

Earlier clinical studies demonstrated an upper limit to doses of AAV serotype 2 vector that could be infused systemically into humans without triggering an immune response that destroyed the transduced cells.[36,37] Thus the ability to achieve hemostasis at lower vector doses is a key step in successful translation to clinical studies for AAV-mediated gene transfer. The data presented here suggest a possible strategy to attain this goal with gene-based FVIIa therapy. Clearly, the issue of safety is of prime importance when using enhanced activity FVIIa variants in this setting. However, there are 2 experimental observations that limit the potential for thrombotic complications: (1) reduced-level expression of mFVIIa-VEAY (~ 0.6 μg/mL vs ~ 3 μg/mL for mFVIIa) in hemophilia A mice is hemostatically effective without thrombotic manifestations, as shown here; (2) long-term expression of cFVIIa at levels of ~ 2 μg/mL is efficacious and not associated with thrombosis in hemophilic dogs, a large animal model of hemophilia.[15] Based on these preclinical data, it seems unlikely that high expression levels of high-activity FVIIa transgene(s) will be necessary for hemostatic efficacy, thus minimizing the overall thrombotic risk. Using inducible expression cassettes under the control of exogenously supplied activator drugs can further reduce this. Because of the high conservation between canine and human FVII (75% identity), our results also suggest that variants of cFVIIa with properties analogous to those described here can be generated. Further gene-transfer experiments in hemophilic dogs with such variants will address the issue of improvements in hemostatic efficacy as well as safety in a clinically relevant animal model of hemophilia.

In addition to on-demand therapy, daily treatment of inhibitor patients prophylactically with rhFVIIa at pharmacologic doses for 3 months has been shown to reduce the number of bleeds, an effect that surprisingly extended in the 3-month follow-up.[38] The precise mechanism behind these extended hemostatic effects in the absence of administered rhFVIIa is unclear; it may involve the presence of rhFVIIa in the extravascular space[39] as has been shown in mice.[40,41] Remarkably, we have previously shown that portal vein administration of AAV-cFVIIa at a subtherapeutic vector dose in a hemophilia B dog resulted in elimination of spontaneous bleeding episodes.[15] Although more confirmatory experiments are necessary, this suggests that continuous, low-level expression of FVIIa, as facilitated by gene transfer, may have long-term clinical benefits similar to a prophylactic rhFVIIa regimen. Within this context, the ability of enhanced activity FVIIa variants to effect hemostasis at reduced AAV vector doses, represents an additional

improvement for this application that can be tested further in hemophilic dogs.

In conclusion, we have applied modifications in the catalytic domain of mFVIIa that resulted in mFVIIa variants with increased, TF-independent activity in vitro. After gene transfer in a mouse model of hemophilia, our data using the mFVIIa-VEAY variant underscore the following: (1) low-level expression of mFVIIa-VEAY (~ 0.6 μg/mL) is safe and hemostatically effective even in the presence of inhibitors, having a 5-fold advantage compared with mFVIIa; and (2) expression of this variant at ~ 14-fold higher (~ 8 μg/mL) levels in hemophilic mice results in rapid mortality. The data are thus suggestive of a relatively wide therapeutic window for this approach that can overcome the limitation of the high AAV-FVIIa vector doses previously shown as necessary for hemostatic efficacy in hemophilic dogs.[15] However, as variants of other coagulation factors (eg, FIX-Padua[42] or FIX-K5A/V10K and FIX-R338A[43]) may offer improved hemostatic properties in gene transfer settings for hemophilia, the data presented here also indicate that careful consideration should be given along the axis of hemostasis (efficacy) and thrombosis (safety) using such variants.

Acknowledgments

The authors thank Drs R. M. Camire, R. Toso, V. R. Arruda, U. Hedner, M. Ezban, and E. Persson for helpful discussions; Drs S. Krishnaswamy and M. Ezban for the preparation of human and murine soluble TF, respectively; Dr R. M. Camire for the preparation of human FX/FXa, and Daniel Martinez at the Children's Hospital of Philadelphia Pathology Core Facility.

The authors also thank the Howard Hughes Medical Institute and the Pennsylvania Department of Health for financial support. The Pennsylvania Department of Health specifically disclaims responsibility for any analysis, interpretations, or conclusions.

Authorship

Contribution: P.M. designed and performed research, analyzed data and wrote the manuscript; E.R. designed and performed research and analyzed data; A.F, H.D.D., L.I., and G.P. performed research; S.Z. provided the AAV vector; R.M.B. performed histopathologic analysis; and K.A.H. designed research, analyzed data, and wrote the manuscript.

Conflict-of-interest disclosure: The authors declare no competing financial interests.

Correspondence: Dr Paris Margaritis, 3501 Civic Center Blvd, 5000 Colket Translational Research Bldg, The Children's Hospital of Philadelphia, Philadelphia, PA 19104; e-mail: margaritis@email.chop.edu.

References

1. Hedner U. Recombinant factor VIIa: its background, development and clinical use. *Curr Opin Hematol*. 2007;14(3):225-229.
2. Hedner U. Recombinant factor VIIa (Novoseven) as a hemostatic agent. *Semin Hematol*. 2001; 38(4 Suppl 12):43-47.
3. Weimer T, Wormsbacher W, Kronthaler U, Lang W, Liebing U, Schulte S. Prolonged in-vivo half-life of factor VIIa by fusion to albumin. *Thromb Haemost*. 2008;99(4):659-667.
4. Yatuv R, Dayan I, Carmel-Goren L, et al. Enhancement of factor VIIa haemostatic efficacy by formulation with PEGylated liposomes. *Haemophilia*. 2008.
5. Harvey SB, Stone MD, Martinez MB, Nelsestuen GL. Mutagenesis of the gamma-carboxyglutamic acid domain of human factor VII to generate maximum enhancement of the membrane contact site. *J Biol Chem*. 2003;278(10):8363-8369.
6. Nelsestuen GL, Stone M, Martinez MB, Harvey SB, Foster D, Kisiel W. Elevated function of blood clotting factor VIIa mutants that have enhanced affinity for membranes. Behavior in a diffusion-limited reaction. *J Biol Chem*. 2001;276(43): 39825-39831.
7. Persson E, Bak H, Ostergaard A, Olsen OH. Augmented intrinsic activity of Factor VIIa by replacement of residues 305, 314, 337 and 374: evidence of two unique mutational mechanisms of activity enhancement. *Biochem J*. 2004;379(Pt 2):497-503.
8. Persson E, Kjalke M, Olsen OH. Rational design of coagulation factor VIIa variants with substantially increased intrinsic activity. *Proc Natl Acad Sci U S A*. 2001;98(24):13583-13588.
9. Moss J, Scharling B, Ezban M, Sorensen TM. Evaluation of the safety and pharmacokinetics of a fast-acting recombinant FVIIa analogue, NN1731, in healthy male subjects. *J Thromb Haemost*. 2008.
10. Petersen LC, Norby PL, Branner S, et al. Characterization of recombinant murine factor VIIa and recombinant murine tissue factor: a human-murine species compatibility study. *Thromb Res*. 2005;116(1):75-85.
11. Lauritzen B, Tranholm M, Ezban M. rFVIIa and a new enhanced rFVIIa-analogue, NN1731, reduce bleeding in clopidogrel-treated and in thrombocytopenic rats. *J Thromb Haemost*. 2009.
12. Tranholm M, Kristensen K, Kristensen AT, Pyke C, Rojkjaer R, Persson E. Improved hemostasis with superactive analogs of factor VIIa in a mouse model of hemophilia A. *Blood*. 2003;102(10): 3615-3620.
13. Aljamali MN, Margaritis P, Schlachterman A, et al. Long-term expression of murine activated factor VII is safe, but elevated levels cause premature mortality. *J Clin Invest*. 2008;118(5):1825-1834.
14. Margaritis P, Arruda VR, Aljamali M, Camire RM, Schlachterman A, High KA. Novel therapeutic approach for hemophilia using gene delivery of an engineered secreted activated Factor VII. *J Clin Invest*. 2004;113(7):1025-1031.
15. Margaritis P, Roy E, Aljamali MN, et al. Successful treatment of canine hemophilia by continuous expression of canine FVIIa. *Blood*. 2009;113(16): 3682-3689.
16. Wang L, Wang H, Bell P, et al. Systematic evaluation of AAV vectors for liver directed gene transfer in murine models. *Mol Ther*. 2010;18(1):118-125.
17. Jiang H, Lillicrap D, Patarroyo-White S, et al. Multiyear therapeutic benefit of AAV serotypes 2, 6, and 8 delivering factor VIII to hemophilia A mice and dogs. *Blood*. 2006;108(1):107-115.
18. Sabatino DE, Lange AM, Altynova ES, et al. Efficacy and safety of long-term prophylaxis in severe hemophilia A dogs following liver gene therapy using AAV vectors. *Mol Ther*. 2011;19(3): 442-449.
19. Wang L, Calcedo R, Nichols TC, et al. Sustained correction of disease in naive and AAV2-pretreated hemophilia B dogs: AAV2/8-mediated, liver-directed gene therapy. *Blood*. 2005;105(8):3079-3086.
20. Toso R, Bernardi F, Tidd T, et al. Factor VII mutant V154G models a zymogen-like form of factor VIIa. *Biochem J*. 2003;369(Pt 3):563-571.
21. Ruf W, Rehemtulla A, Morrissey JH, Edgington TS. Phospholipid-independent and -dependent interactions required for tissue factor receptor and cofactor function. *J Biol Chem*. 1991;266(4): 2158-2166.
22. Bi L, Lawler AM, Antonarakis SE, High KA, Gearhart JD, Kazazian HH Jr. Targeted disruption of the mouse factor VIII gene produces a model of haemophilia A. *Nat Genet*. 1995;10(1):119-121.
23. Lin HF, Maeda N, Smithies O, Straight DL, Stafford DW. A coagulation factor IX-deficient mouse model for human hemophilia B. *Blood*. 1997;90(10):3962-3966.
24. Tai SJ, Herzog RW, Margaritis P, et al. A viable mouse model of factor X deficiency provides evidence for maternal transfer of factor X. *J Thromb Haemost*. 2008;6(2):339-345.
25. Fields PA, Arruda VR, Armstrong E, et al. Risk and prevention of anti-factor IX formation in AAV-mediated gene transfer in the context of a large deletion of F9. *Mol Ther*. 2001;4(3):201-210.
26. Arnold K, Bordoli L, Kopp J, Schwede T. The SWISS-MODEL workspace: a web-based environment for protein structure homology modelling. *Bioinformatics*. 2006;22(2):195-201.
27. Kiefer F, Arnold K, Kunzli M, Bordoli L, Schwede T. The SWISS-MODEL Repository and associated resources. *Nucleic Acids Res*. 2009;37:D387-392.
28. Schwede T, Kopp J, Guex N, Peitsch MC. SWISS-MODEL: An automated protein homology-modeling server. *Nucleic Acids Res*. 2003; 31(13):3381-3385.
29. Guex N, Peitsch MC. SWISS-MODEL and the Swiss-PdbViewer: an environment for comparative protein modeling. *Electrophoresis*. 1997; 18(15):2714-2723.
30. Persson E, Olsen OH. Assignment of molecular properties of a superactive coagulation factor VIIa variant to individual amino acid changes. *Eur J Biochem*. 2002;269(23):5950-5955.
31. Banner DW, D'Arcy A, Chene C, et al. The crystal

structure of the complex of blood coagulation factor VIIa with soluble tissue factor. *Nature*. 1996; 380(6569):41-46.

32. Nicolaisen EM, Thim L, Jacobsen JK, et al. FVIIa derivatives obtained by autolytic and controlled cathepsin G mediated cleavage. *FEBS Lett*. 1993;317(3):245-249.

33. Toso R, Pinotti M, High KA, Pollak ES, Bernardi F. A frequent human coagulation Factor VII mutation (A294V, c152) in loop 140s affects the interaction with activators, tissue factor and substrates. *Biochem J*. 2002;363(Pt 2):411-416.

34. Hedner U. History of rFVIIa therapy. *Thromb Res*. 2010;125(Suppl 1):S4-S6.

35. Russell KE, Olsen EH, Raymer RA, et al. Reduced bleeding events with subcutaneous administration of recombinant human factor IX in immune-tolerant hemophilia B dogs. *Blood*. 2003; 102(13):4393-4398.

36. Manno CS, Pierce GF, Arruda VR, et al. Successful transduction of liver in hemophilia by AAV-Factor IX and limitations imposed by the host immune response. *Nat Med*. 2006;12(3):342-347.

37. Mingozzi F, Maus MV, Hui DJ, et al. CD8(+) T-cell responses to adeno-associated virus capsid in humans. *Nat Med*. 2007;13(4):419-422.

38. Konkle BA, Ebbesen LS, Erhardtsen E, et al. Randomized, prospective clinical trial of recombinant factor VIIa for secondary prophylaxis in hemophilia patients with inhibitors. *J Thromb Haemost*. 2007;5(9):1904-1913.

39. Hedner U, Lee CA. First 20 years with recombinant FVIIa (NovoSeven). *Haemophilia*. 2011; 17(1):e172-e182. doi: 10.1111/j.1365-2516.2010.02352.x.

40. Gopalakrishnan R, Hedner U, Ghosh S, et al. Biodistribution of pharmacologically administered recombinant factor VIIa (rFVIIa). *J Thromb Haemost*. 2010;8(2):301-310.

41. Hoffman M, Colina CM, McDonald AG, Arepally GM, Pedersen L, Monroe DM. Tissue factor around dermal vessels has bound factor VII in the absence of injury. *J Thromb Haemost*. 2007;5(7): 1403-1408.

42. Simioni P, Tormene D, Tognin G, et al. X-linked thrombophilia with a mutant factor IX (factor IX Padua). *N Engl J Med*. 2009;361(17):1671-1675.

43. Schuettrumpf J, Herzog RW, Schlachterman A, Kaufhold A, Stafford DW, Arruda VR. Factor IX variants improve gene therapy efficacy for hemophilia B. *Blood*. 2005;105(6):2316-2323.

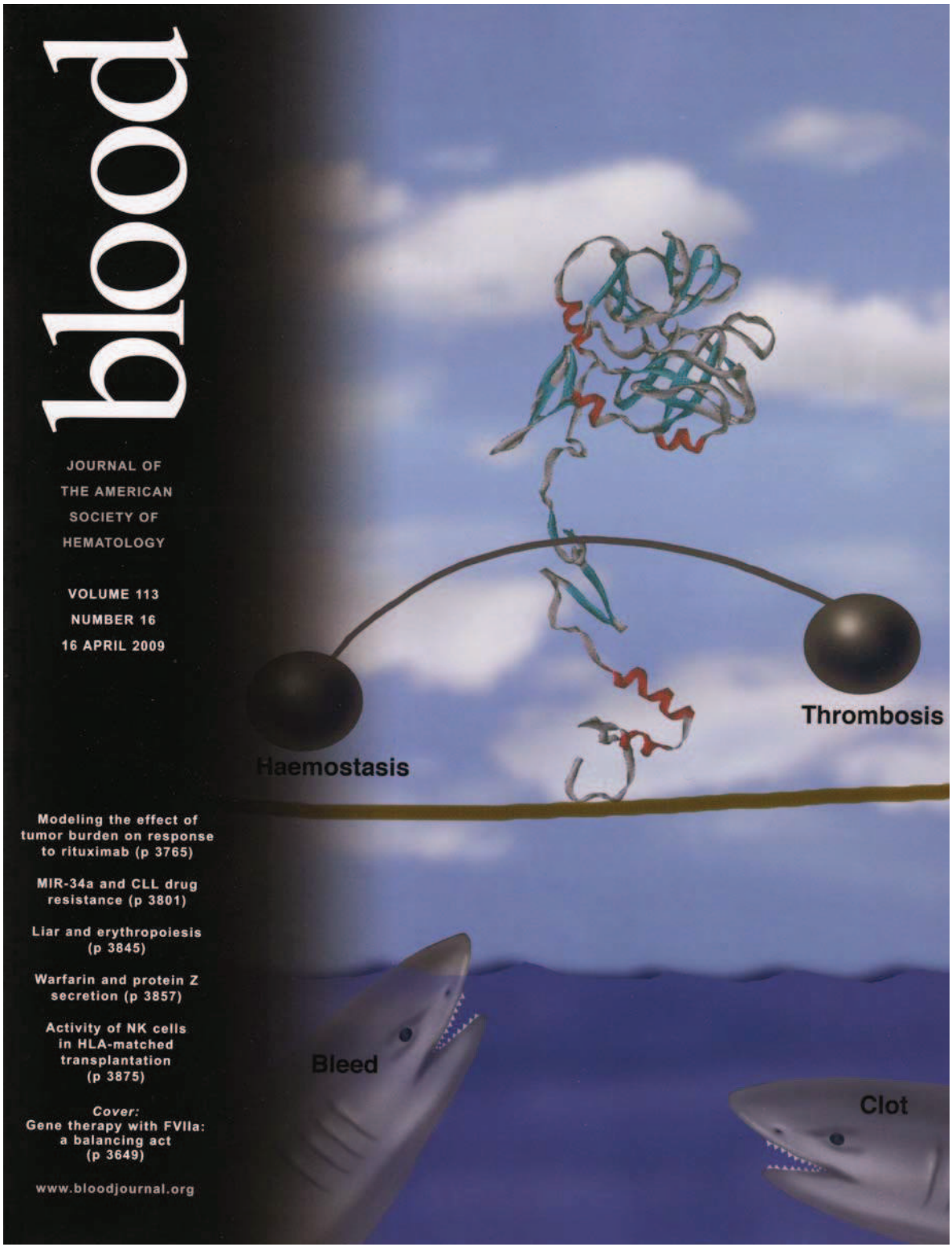
blood
JOURNAL OF
THE AMERICAN
SOCIETY OF
HEMATOLOGY
VOLUME 113
NUMBER 16
16 APRIL 2009
Modeling the effect of tumor burden on response to rituximab (p 3765)
MIR-34a and CLL drug resistance (p 3801)
Liar and erythropoiesis (p 3845)
Warfarin and protein Z secretion (p 3857)
Activity of NK cells in HLA-matched transplantation (p 3875)
Cover:
Gene therapy with FVIIa: a balancing act (p 3649)
www.bloodjournal.org
Haemostasis
Thrombosis
Bleed
Clot

blood

2009 113: 3682-3689
Prepublished online December 23, 2008;
doi:10.1182/blood-2008-07-168377

Successful treatment of canine hemophilia by continuous expression of canine FVIIa

Paris Margaritis, Elise Roy, Majed N. Aljamali, Harre D. Downey, Urs Giger, Shangzhen Zhou, Elizabeth Merricks, Aaron Dillow, Mirella Ezban, Timothy C. Nichols and Katherine A. High

Blood (print ISSN 0006-4971, online ISSN 1528-0020), is published weekly by the American Society of Hematology, 2021 L St, NW, Suite 900, Washington DC 20036.

Successful treatment of canine hemophilia by continuous expression of canine FVIIa

Paris Margaritis,[1] Elise Roy,[1] Majed N. Aljamali,[1] Harre D. Downey,[1] Urs Giger,[2] Shangzhen Zhou,[1] Elizabeth Merricks,[3] Aaron Dillow,[3] Mirella Ezban,[4] Timothy C. Nichols,[3] and Katherine A. High[1,5]

[1]Division of Hematology, Children's Hospital of Philadelphia, PA; [2]Section of Medical Genetics, School of Veterinary Medicine, University of Pennsylvania, Philadelphia; [3]Department of Pathology and Laboratory Medicine, University of North Carolina, Chapel Hill; [4]Biopharmaceutical Research Unit, Novo Nordisk A/S, Måløv, Denmark; and [5]Howard Hughes Medical Institute, Children's Hospital of Philadelphia, PA

Continuous expression of activated factor VII (FVIIa) via gene transfer is a potential therapeutic approach for hemophilia patients with or without inhibitory antibodies to human factor VIII (FVIII) or IX (FIX). Here, we investigate whether gene transfer of an engineered canine FVIIa (cFVIIa) transgene can affect hemostasis in a canine model of hemophilia, a good predictor of efficacy of hemophilia treatments. Purified recombinant cFVIIa exhibited 12-fold higher tissue factor–dependent activity than purified recombinant zymogen cFVII. Subsequently, we generated a serotype 8 recombinant adeno-associated viral vector expressing cFVIIa from a liver-specific promoter. Vector delivery via the portal vein in hemophilia A and B dogs was well tolerated, and long-term expression of cFVIIa resulted in a shortening of the prothrombin time, partial correction of the whole blood clotting time and thromboelastography parameters, and a complete absence of spontaneous bleeding episodes. No evidence of hepatotoxicity, thrombotic complications, or inhibitory immune response was found. These data provide the first evidence for in vivo efficacy and safety of continuously expressed FVIIa as a FVIII/FIX-bypassing agent in a large animal model of hemophilia, avoiding the risk of inhibitor formation associated with bolus FVIII or FIX infusion. (Blood. 2009;113:3682-3689)

Introduction

Despite the availability of plasma-derived and recombinant human factor VIII (rhFVIII) or factor IX (rhFIX) as therapeutics for hemophilia, inhibitor formation (20%-30% in severe hemophilia A; ~ 5% in severe hemophilia B[1,2]) remains a serious complication in a substantial fraction of these patients. Pharmacologic doses of activated recombinant human factor VII (rhFVIIa) administered in multiple doses[3] or a single high dose[4] has been successful in effecting hemostasis in such patients as well as in patients with platelet disorders[5] and FVII deficiency.[6,7] Dosing of rhFVIIa has also demonstrated efficacy in short-term secondary prophylaxis.[8] However, the need for repeated injections (daily dosing) because of the short plasma half-life may limit its convenience for prolonged periods of prophylaxis.

In an effort to bypass these drawbacks, we have previously demonstrated that a factor VII transgene engineered to be secreted in its activated form (FVIIa) can correct the hemostatic parameters in mouse models of hemophilia A (HA) and B (HB), after either adeno-associated viral (AAV) vector delivery[9] or in transgenic animals.[10] However, a necessary step preceding human application is the demonstration of safety and efficacy in a large animal (canine) model. This important hemophilia model closely resembles the human disorder in terms of size, physiology, and the genetic determinants of immune response because it is outbred instead of inbred.[11] In addition, it has been a good predictor of efficacy in hemophilia treatments.[12-15] Viral-mediated gene transfer of factor VIII (FVIII) or factor IX (FIX) in this model demonstrated that the antigenicity of the transgene product remains a concern[16,17] because these animals may not be fully tolerant to wild-type FVIII or FIX. On the other hand, continuous expression of murine FVIIa in immunocompetent hemophilic mice after gene transfer did not result in a transgene-specific immune response, as evidenced by the long-term expression.[9] Therefore, FVIIa gene transfer may not only effect hemostasis and bypass an inhibitor (functional advantage), but, at the same time, evade a transgene-specific immune response resulting from tolerance to the introduced transgene (immunologic advantage).

To demonstrate whether this advantage carried through to an outbred large animal, we used the canine hemophilia model and evaluated gene-based, AAV-mediated continuous expression of canine factor VIIa (cFVIIa) as a treatment for hemophilia. We show long-term efficacy with a marked improvement in the bleeding diathesis with no evidence of hepatotoxicity, thrombotic complications, or an inhibitory immune response to cFVIIa. Thus, our results provide the first evidence for efficacy and safety of the gene-based FVIII/FIX bypassing agent FVIIa for the treatment of hemophilia in a large animal model. This strategy can also be applied in platelet disorders, FVII deficiency or for prophylaxis in congenital hemophilia complicated by inhibitor development.

Methods

Plasmid construction, protein purification, and AAV production

A pcDNA3-based (Invitrogen, Carlsbad, CA) plasmid vector containing the canine factor VII (cFVII) cDNA[18] was used to generate cFVIIa by polymerase chain reaction mutagenesis (by insertion of the Arg-Lys-Arg-Arg-Lys-Arg [RKRRKR] sequence at position 152 in the mature cFVII

Submitted July 14, 2008; accepted December 4, 2008. Prepublished online as *Blood* First Edition paper, December 23, 2008; DOI 10.1182/blood-2008-07-168377.

An Inside *Blood* analysis of this article appears at the front of this issue.

The publication costs of this article were defrayed in part by page charge payment. Therefore, and solely to indicate this fact, this article is hereby marked "advertisement" in accordance with 18 USC section 1734.

sequence), as previously described.[9] To purify cFVII or cFVIIa, a C-terminal epitope tag (HPC4) was added to the translated peptide sequence, as previously described,[9] thus generating cFVII-HPC4 and cFVIIa-HPC4. Stable cell lines based on human embryonic kidney cells (HEK-293) were generated by transfection and selection in G418, and proteins were purified from vitamin K–supplemented conditioned medium using a 1-step immunoaffinity column (against the HPC4 epitope), as previously described.[9] Protein concentration was determined spectrophotometrically using a molecular weight of 50 000 and an extinction coefficient ($E_{280}^{0.1\%}$) of 1.39. The AAV plasmid used for vector production-directed expression of cFVIIa (without the HPC4 tag) from a liver-specific promoter (human α_1 antitrypsin [hAAT]) and enhancer (4 copies of the apolipoprotein E [apoE] enhancer), as previously described.[9] Production of serotype 8 AAV vector was performed by triple transfection, essentially as previously described.[9]

Clotting assays for purified proteins

Prothrombin time (PT) assays using purified recombinant protein were performed in duplicate using a fibrometer (STart Instrument; Diagnostica Stago, Parsippany, NJ) by recording the clot time of recombinant protein (25 μL in Tris-buffered saline [TBS]; 50 mM Tris, 150 mM NaCl, 0.1% bovine serum albumin, pH 7.5; TBS–bovine serum albumin [BSA]) using equal volumes of canine FVII-deficient plasma[18] and, after incubation at 37°C, 100 μL of relipidated recombinant human tissue factor (TF; Innovin; Dade Behring, Deerfield, IL) as a source of TF. Activated partial thromboplastin time (aPTT) assays of recombinant proteins were performed in duplicate by diluting recombinant protein in a total of 25 μL of canine factor VIII– or canine factor IX–deficient plasma and adding 1-in-4 dilution of aPTT reagent (25 μL total volume in imidazole buffer; Biomerieux, Durham, NC). After incubation at 37°C for 3 minutes, 25 μL of 25 mM $CaCl_2$ was added and time to clot was recorded. For both PT and aPTT, purified recombinant proteins were compared using a reference standard curve of rhFVIIa. In these experimental assay systems, normalization of canine FVII-deficient plasma PT was observed using approximately 70 ng/mL cFVIIa and approximately 200 ng/mL rhFVIIa. Normalization of the HA and HB aPTT was observed at 20 μg/mL of either cFVIIa or rhFVIIa.

Clotting assays for mouse and dog experiments

PT assays for mouse or canine plasma samples were performed by recording the time to clot after mixing 25 μL of sample (diluted 40-fold [canine] or 160-fold [mouse] in TBS-BSA), 25 μL of human FVII-deficient plasma and, after incubation at 37°C, addition of 100 μL Innovin. aPTT assays for mouse plasma samples were performed as described above (see "Clotting assays for purified proteins"), but using undiluted aPTT reagent. Whole blood clotting time (WBCT) was performed essentially as previously described.[16] Thromboelastography was performed as previously described[19] using freshly drawn blood and initiating coagulation using 1 in 200 000 dilution of Innovin. Comparison in thromboelastography parameters between the AAV-treated dogs and normal or untreated HA/HB dogs was performed using data points from at least 1 week after the last normal canine plasma infusion, after gene transfer.

cFVIIa antigen determination

The concentration of the expressed cFVIIa in canine plasma was determined from clotting activity using the STAclot kit (Diagnostica Stago), as previously described for rhFVIIa.[20] Briefly, a standard curve of increasing cFVIIa concentration (50 μL sample) in dilution buffer (50 mM 1,4-piperazinediethanesulfonic acid, 100 mM NaCl, 2 mM ethylenediaminetetraacetic acid, 0.1% BSA, pH 7.2) was generated using 50 μL of human FVII-deficient plasma and 50 μL of recombinant soluble human TF/phospholipid mixture. After a 3-minute incubation at 37°C, 50 μL of 25 mM $CaCl_2$ was added and the time to clot was recorded. A typical standard curve had a correlation coefficient (r^2) of more than 0.97 ($\log_{10}$ [concentration] vs $\log_{10}$ [clot time]). In this assay, zymogen cFVII exhibited negligible activity (~ 3% relative to cFVIIa). Citrated plasma samples from treated, untreated HA or HB, or control (normal) dogs were diluted 10- or 50-fold in dilution buffer, and clot time was determined. Concentration of cFVIIa in those samples was derived from the obtained standard curve. Canine FVIIa levels in normal, untreated HA or HB dogs were determined using at least 4 individual samples (in the case of HA or HB) or using a pooled sample from at least 4 dogs (in the case of normal dogs).

D-dimer, fibrinogen, and thrombin-antithrombin assays

D-dimer determination was performed in duplicate on citrated plasma dog samples using the enzyme-linked immunosorbent assay-based Asserachrom D-Di kit (Diagnostica Stago).[21] Fibrinogen levels in citrated dog plasma samples were determined in duplicate using a clotting-based assay (Clauss method; Dade Behring) that used a human plasma standard as a reference.[21] Assays were performed according to the manufacturer's instructions but using half the volume of each reagent. Thrombin-antithrombin (TAT) assays were performed in duplicate on citrated plasma using the Enzygnost TAT micro kit (Dade Behring). D-dimer, fibrinogen, and TAT levels in normal, untreated HA or HB dogs were determined using at least 4 individual samples (in HA or HB) or using a pooled sample from at least 4 dogs (in the case of normal dogs).

AAV vector administration in hemophilia mice and dogs

All animal experiments were approved by the Institutional Animal Care and Use Committee at the Children's Hospital of Philadelphia and the University of North Carolina at Chapel Hill. Administration of vector in HA mice was performed in 200 μL volume (vector in phosphate-buffered saline–5% sorbitol) via the tail vein. Plasma samples were collected in 3.8% citrate via sectioning of the tail. Liver-directed, portal vein vector infusion in 3 HA (HA-1-J55, HA-2-J57, and HA-3-E66) and 1 HB (HB-1-J10) dogs of the University of North Carolina at Chapel Hill colony was performed as previously described.[22] Antibodies against AAV8 or cFVIIa were detected by enzyme-linked immunosorbent assay using either AAV8 or recombinant cFVIIa-coated plates, essentially as previously described.[16] Canine serum chemistries (gamma-glutamyltranspeptidase, aspartate aminotransferase, alanine aminotransferase, creatine phosphokinase, alkaline phosphatase, serum glutamic pyruvic transaminase, serum glutamic oxaloacetic transaminase, total bilirubin, and platelet counts) were analyzed in an automated clinical pathology laboratory. Normal range of values for each test was derived from 18 clinically healthy dogs on a mixed genetic background. Monitoring was done every 2 days for the first 1 to 2 weeks after AAV-cFVIIa administration, then every 1 to 3 months thereafter.

Statistical analysis

An unpaired 2-tailed Student *t* test or a 2-sided Fisher exact test (for analysis of bleeding episodes) was used for statistical analysis, with *P* less than .05 indicating statistical significance.

Results

Purification of recombinant zymogen cFVII and cFVIIa

Initially, we generated HEK-293–based stable cell lines expressing zymogen cFVII or cFVIIa, both proteins containing a C-terminal epitope tag (HPC4) for immunoaffinity purification (Figure 1A).[9] Recombinant zymogen cFVII and cFVIIa were successfully purified from vitamin K–supplemented conditioned medium. In contrast to zymogen cFVII, which was purified in a single-chain form (indicating lack of autoactivation during purification), cFVIIa was purified almost exclusively in the 2-chain, fully activated form (Figure 1B). The lower molecular weight bands observed at 10 to 16 kDa are probably degradation products, as have been previously observed in human recombinant FVIIa preparations.[23,24] Although the heavy and light chains of cFVIIa exhibited differential staining with Coomassie blue, this is commonly found in human[23,24] as well as murine FVIIa preparations.[9,25]

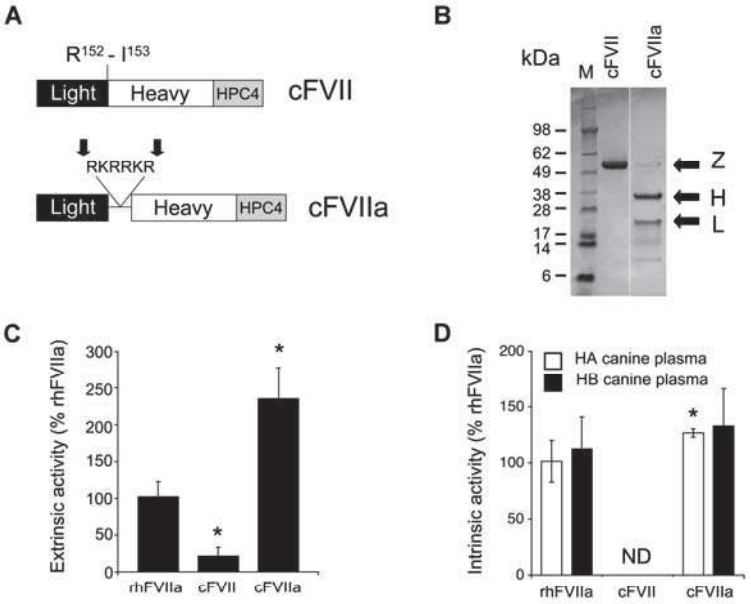

Figure 1. Construction and in vitro characterization of canine FVII and canine FVIIa. (A) The canine FVII and FVIIa constructs contained a C-terminal epitope tag (HPC4) for immunoaffinity purification. To generate canine FVIIa, we introduced a short amino acid sequence (RKRRKR) at the normal site of cleavage of canine FVII (Arg^{152}-Ile^{153}, indicated), which is recognized by an intracellular protease of the PACE/furin type. Cleavage at this sequence (indicated by ↓) results in the secretion of a 2-chain, activated molecule. (B) Polyacrylamide gel electrophoresis of zymogen (Z) cFVII and cFVIIa under reducing conditions. The molecular size marker (M) bands in kDa are indicated as well as the heavy (~35 kDa, H) and light (~20 kDa, L) chains. (C) TF-dependent activity of cFVII and cFVIIa in a PT-based clotting assay using canine FVII-deficient plasma relative to rhFVIIa (100%). $^*P < .05$ versus rhFVIIa. (D) TF-independent activity of cFVII and cFVIIa in an aPTT-based clotting assay using either canine hemophilia A (HA) or B (HB) plasma, relative to rhFVIIa (100%). ND indicates nondetectable activity.

In vitro activity of zymogen cFVII and cFVIIa

Subsequently, we investigated the proteolytic activity of zymogen cFVII and cFVIIa, using rhFVIIa as a reference standard. Using pooled canine plasma from FVII-deficient dogs,[18] we determined the TF-dependent activity of cFVIIa using relipidated recombinant human TF (Innovin). In this system, zymogen cFVII exhibited very low activity (~ 20% of rhFVIIa, $P < .001$ vs rhFVIIa; Figure 1C) in contrast to cFVIIa, which exhibited approximately 240% of rhFVIIa ($P < .001$ vs rhFVIIa; Figure 1C), approximately 12-fold higher activity than zymogen cFVII. In a TF-independent aPTT-based assay using HA or HB canine plasma, cFVIIa exhibited a slightly increased (HA, $P = .044$) or comparable (HB, $P = .44$) activity relative to rhFVIIa (Figure 1D). In that assay, zymogen cFVII had negligible activity (Figure 1D). It is possible that the disparity in extrinsic and intrinsic activity of cFVIIa relative to rhFVIIa is the result of the use of human relipidated TF. Collectively, these data demonstrate that cFVII can be engineered so that it is secreted in a 2-chain, biologically active form.

Efficacy of AAV-mediated cFVIIa gene transfer in hemophilic mice and dogs

We generated a serotype 8 AAV vector (AAV8-cFVIIa, Figure 2A) directing expression of cFVIIa via a liver-specific promoter, similar to our previous studies in mice.[9,10] The cFVIIa transgene in this AAV vector did not contain the C-terminal epitope tag (HPC4). In preliminary experiments designed to test the functionality of the AAV vector, we performed tail vein vector administration in hemophilic mice at a dose of 0.3 to 1.2E12 vector genomes/mouse (1.2-4.8E13 vector genomes/kg). After gene transfer, expression of cFVIIa resulted in long-term, cross-species, sustained hemostatic functionality (Figure 2B), as demonstrated by normalization of the hemophilic aPTT ($P > .06$ vs normal mice, except for day 42 [$P = .01$]) and concurrent supraphysiologic shortening in the PT ($P < .001$ vs normal mice). These experiments thus confirmed the functionality of the vector subsequently used in the dog experiments and suggested that cFVIIa expression in HA but otherwise immunocompetent mice did not induce an inhibitory immune response.

Because the AAV8-cFVIIa vector dose that would result in hemostatic efficacy in hemophilic dogs was unknown, we initially infused an HB male dog (HB-1-J10) with 2.06E13 vector genomes/kg via the portal vein (Table 1). This dose only resulted in a modest reduction in WBCT and no change in the PT, a finding that was not the result of an immune response to cFVIIa (Figure 2C,D; and data not shown). These observations were similar throughout the observation period of this animal (beyond day 527 depicted, up to 34 months, ongoing). Based on this result, we infused progressively higher doses of AAV8-cFVIIa (3- or 6-fold) in HA dogs (Table 1). Both HA and HB dogs respond similarly to infusions of rhFVIIa (Brinkhous et al[12]; T.C.N., personal communication, August 2008) and thus were expected to perform similarly after AAV8-cFVIIa gene transfer. The AAV8-cFVIIa–treated HA dogs exhibited an initial reduction in WBCT and PT because of prophylactic normal canine plasma infusions (daily for the first 4-5 days after vector administration, Figure 2C and D, respectively). Subsequently, we observed a long-term, stable reduction, well below preinfusion times for both WBCT and PT (Figure 2C and D, respectively). This was a result of sustained cFVIIa gene expression that ranged between 1.3 and 2.6 μg/mL ($P < .03$ vs normal or untreated HA dogs; Figure 2E). As expected, the treated HB-1-J10 dog that did not exhibit a measurable reduction in the PT did not exhibit a change in cFVIIa antigen levels (Figure 2E).

To further demonstrate efficacy, we performed thromboelastography analysis of whole blood from the treated HA dogs. We observed a greatly improved clot dynamics profile (data not shown) and a sustained, near-normalization of the reaction time (time to initial fibrin formation[26]; $P = .03$ [HA-1-J55], $P = .08$ [HA-2-J57], $P = .004$ [HA-3-E66] vs normal dogs; Figure 2F), well below HA values ($P < .001$ vs HA). The treated HA dogs also exhibited near-normalization of the maximum clot amplitude (data not shown). Corroborating its WBCT, PT, and cFVIIa antigen levels, the treated HB-1-J10 dog showed a modest improvement in these

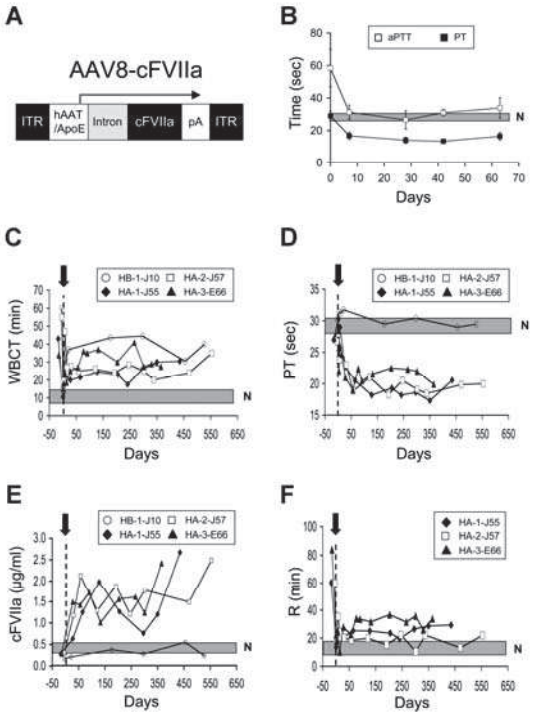

Figure 2. In vivo efficacy of AAV-mediated gene transfer of cFVIIa in hemophilia A and B dogs. (A) AAV8 vector used for infusion in hemophilia mice and dogs. Inverted terminal repeats (ITRs) flank the expression cassette composed of an hAAT/apoE promoter/enhancer, a synthetic intron, the cFVIIa cDNA (with 5′ UTR and absence of the HPC4 tag) and a polyadenylation signal (pA) from bovine growth hormone. (B) PT and aPTT in HA mice (n = 6) after tail vein administration of AAV8-cFVIIa. A shaded box represents the range of values for aPTT in normal (N) mice, determined from at least 4 mice. (C) WBCT after portal vein AAV8-cFVIIa vector administration (↓) in HA and HB dogs. A shaded box represents the range of values for normal dogs. A vertical dotted line represents day 0. Prophylactic plasma treatment was administered on days 2 to 4 (HA-1-J55, HA-2-J57), 2 to 5 (HA-3-E66), and 1 to 5 as well as for 2 days after nonspontaneous bleeding episodes in the HB dog (occurring on days 11, 159, and 228 after AAV administration). (D) PT after portal vein AAV8-cFVIIa vector administration (↓) in HA and HB dogs. A shaded box represents the range of values for normal dogs. A vertical dotted line represents day 0. (E) cFVIIa expression after portal vein AAV8-cFVIIa vector administration (↓) in HA and HB dogs. A shaded box represents the range of values for normal, HA, and HB dogs. (F) Reaction time (time to initial fibrin formation) in thromboelastography analysis of whole blood in the treated HA dogs after AAV8-cFVIIa vector infusion (↓). A shaded box represents the range of values for normal dogs.

thromboelastography parameters compared with untreated HB controls (data not shown).

AAV-cFVIIa–treated hemophilic dogs do not exhibit spontaneous bleeding episodes

Because dogs with hemophilia exhibit approximately 5 or 6 spontaneous bleeding episodes per year,[27,28] we used the number of spontaneous bleeds as a clinically relevant efficacy endpoint. Control untreated HA and HB dogs that were observed concurrently within this study exhibited 12 and 21 spontaneous bleeds in 36 and 60 cumulative months of observation, respectively (Table 2). In a cumulative 34 months (HB) and 45 months (HA) of observation, the AAV8-cFVIIa treated dogs did not exhibit any spontaneous bleeding episodes, in contrast to the expected 15 (HB) and 21 (HA) episodes ($P < .002$ vs historical data in this dog colony[27,28] or the paired concurrent controls; Table 2). The lowest dosed HB dog exhibited 3 nonspontaneous bleeds within the first 8 months after AAV vector administration and each after a hemostatic challenge (the initial surgery for vector delivery, a liver biopsy performed to study cFVIIa expression, and dog fighting; normal canine plasma was administered daily for each episode for up to 3 days). Remarkably, despite the lack of appreciable changes in WBCT, PT, or cFVIIa expression in this dog (up to 34 months of observation, ongoing), AAV8-cFVIIa administered at vector doses that did not raise the circulating levels of cFVIIa resulted in a measurable phenotypic impact.

Safety of long-term cFVIIa expression in the AAV-treated hemophilic dogs

Serum chemistries for liver and kidney functions before and after gene transfer were closely monitored throughout the study. Values of serum creatine phosphokinase, AP, total bilirubin, aspartate aminotransferase, alanine aminotransferase, serum glutamyl pyruvic transaminase, serum glutamyl oxaloacetic transaminase, and gamma glutamyl transpeptidase were determined and found to be within the normal range in all dogs (Table 3). AP levels for the HB-1-J10 dog were marginally elevated for the first 2 weeks, but this dog also had slightly raised AP levels even before AAV infusion (Table 3). Platelet counts were within the normal range throughout the study (Figure 3A). Because mice continuously expressing mFVIIa at levels more than 2 μg/mL exhibited premature mortality,[10] to further address the safety of this gene transfer approach, we used 3 different assays: levels of TAT complex, D-dimer levels (elevated levels of which are indicators of thromboembolic disease and disseminated intravascular coagulation [DIC] in dogs[29,30]), and fibrinogen levels, elevated levels of which are associated with cardiovascular disease.[31] We did not detect any significant changes in TAT or D-dimer levels relative to pre-AAV administration ($P > .2$) in any of the vector doses used in AAV-treated dogs throughout the observation period (Figure 3B and C, respectively). Fibrinogen levels displayed some variability with time and 2 of 4 dogs (HB-1-J10 and HA-1-J55) exhibited a transient (~ 1 week in duration) elevation, possibly because of a postoperative response to the administered analgesia before and after surgery, as previously described.[32] In any case, analysis of postoperative samples starting 1 week after the last prophylactic normal canine plasma infusion revealed fibrinogen levels that were within the normal range for HA and HB dogs ($P > .05$ vs untreated HB for the HB dog; $P > .12$ vs untreated HA for the HA-1-J55,

Table 1. Hemophilia dogs used in this study

Dog	Phenotype	Sex	Age at vector infusion	Weight at vector infusion, kg	Vector dose, vector genomes/kg	Total vector, vector genomes
HB-1-J10	HB	Male	3 mo	8.1	2.06E13	1.67E14
HA-1-J55	HA	Male	11 mo	19.3	6.25E13	1.25E15
HA-2-J57	HA	Female	1.2 y	21.1	1.25E14	2.6E15
HA-3-E66	HA	Male	6.5 y	20.0	1.25E14	2.5E15

Table 2. Spontaneous bleeding episodes in the hemophilia-treated dogs and untreated HA and HB controls recorded concurrently with this study

Dog	Vector, vector genomes/kg	Spontaneous bleeds, observed/expected	Months observed	Untreated HA, bleeds/observation period (mo)	Untreated HB, bleeds/observation period (mo)
HB-1-J10	2.06E13	0/15*	34	Dog 1 (8/24)	Dog 1 (4/12)
HA-1-J55	6.25E13	0/8	18	Dog 2 (4/12)	Dog 2 (9/24)
HA-2-J57	1.25E14	0/7	15		Dog 3 (8/24)
HA-3-E66	1.25E14	0/6	12		
Cumulative spontaneous bleeds				12 in 36 mo	21 in 60 mo
HB		0 in 34 mo			
HA		0 in 45 mo			
Expected spontaneous bleeds					
HB		15 in 34 mo			
HA		21 in 45 mo			

*The HB (male) dog exhibited 3 nonspontaneous bleeding episodes within the first 8 months of observation.

HA-2-J57, and HA-3-E66 dogs; Figure 3D). This was in agreement with the lack of significant changes in D-dimer levels observed (Figure 3C). Lastly, as expected, all AAV-treated dogs exhibited sustained anti-AAV8 antibodies, which developed within the first 4 weeks after vector infusion that were predominantly IgG2 (data not shown). It is noted that there is an initial drop in the WBCT and after AAV administration; however, this is probably the result of prophylaxis with normal plasma that is administered at the time of vector infusion. Only one dog (HA-3-E66) exhibited a transient rise in anti-cFVIIa IgG above background at day 7 after AAV infusion, returning to baseline at day 28 (data not shown). This antibody was not inhibitory because the WBCT was still below its baseline throughout that period even though the dog was no longer receiving normal canine plasma prophylaxis. Collectively, these findings further corroborate the long-term hemostatic and phenotypic effects observed after AAV8-cFVIIa gene transfer and indicate that continuous cFVIIa expression has an excellent safety profile throughout the duration of this study (34 months for the HB dog; 18 months for HA dogs [longest individual observation]).

Discussion

Gene therapy has focused on targeting monogenic disorders in which the relationship between gene transfer and phenotypic improvement is straightforward. In particular, hemophilia has been

Table 3. Serum chemistries in the AAV-treated hemophilia dogs

Day	CPK 59-895 U/L	AP 5-131 U/L	SGPT 12-118 U/L	SGOT 15-66 U/L	Total bilirubin 0.1-0.3 mg/dL	GGTP 1.0-12 U/L
HB-1-J10 dog						
Baseline	340	134	37	33	0.1	< 5
3	344	163	101	27	0.1	< 5
14	283	136	32	27	0.1	< 5
108	253	67	46	25	0.1	< 5
297	145	45	45	23	0.2	< 5
358	87	25	40	24	0.1	< 5
527	104	32	36	19	0.3	< 5
HB-1-J10 dog						
Baseline	13	79	28	32	0.1	< 5
3	207	81	65	37	0.2	< 5
93	133	48	72	41	0.2	< 5
296	80	44	41	31	0.2	< 5
435	100	29	71	31	0.2	< 5
HA-2-J57 dog						
Baseline	100	46	34	35	0.2	< 5
3	103	91	46	22	0.2	< 5
86	116	41	47	44	0.2	< 5
275	80	22	31	24	0.2	< 5
470	107	41	47	27	0.3	< 5
554	131	33	87	35	0.2	< 5
HA-3-E66 dog						
Baseline	152	20	73	45	0.1	< 5
3	243	47	98	49	0.1	< 5
6	177	41	68	36	0.1	< 5
105	131	15	55	33	0.1	< 5
301	153	15	44	32	0.1	< 5
365	93	16	53	34	0.1	< 5

The normal range (derived from 18 clinically healthy dogs) is stated for each test. CPK indicates creatine phosphokinase; AP, alkaline phosphatase; SGPT, serum glutamic pyruvic transaminase; SGOT, serum glutamic oxaloacetic transaminase; and GGPT, gamma glutamyl transpeptidase.

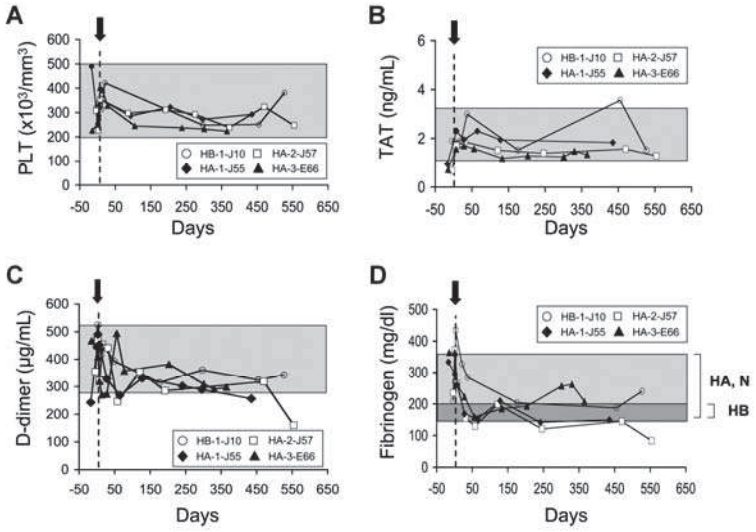

Figure 3. Safety of continuous expression of cFVIIa. Platelet counts (PLT) (A), levels of TAT (B), D-dimer (C), and fibrinogen (D) are shown as a function of time, after AAV8-cFVIIa administration (arrow). Day 0 is indicated by a dotted line. A shaded box represents the range of values for normal (N), HA, or HB dogs (except in panel D where it is indicated for HA, N, and HB separately).

very well characterized, both biochemically and molecularly, and extensive knowledge exists in terms of therapeutic interventions. However, despite several gene transfer clinical trials using a variety of vectors and routes of administration,[15] none has yet addressed the possibility of such an approach in patients with inhibitors, where preexisting immunity would diminish the human FVIII or FIX therapeutic expression from a delivery vector. To address this, we have previously demonstrated that gene transfer of a FVII transgene engineered for secretion in an activated form can normalize the hemophilic phenotype in mice.[9] Such an approach would be particularly beneficial in hemophilia patients with inhibitors because patients would be tolerant to the introduced transgene (FVIIa). Therefore, continuous expression of FVIIa would afford functional and immunologic advantages, effecting hemostasis in both HA and HB with or without inhibitors as well as other coagulation disorders, as observed with bolus dosing of rhFVIIa.

Here, we provide proof-of-concept for this gene transfer approach using continuous expression of canine FVIIa in hemophilic dogs. This large animal model has been a good predictor for efficacy in hemophilia using a range of products.[12-15] However, because FVIIa is a protease (in contrast to previous gene transfer approaches using zymogen FVIII or FIX), the issue of safety, especially with respect to thrombosis, is pertinent. Hence, our study focused on demonstrating both efficacy and safety, and we report 3 major findings in hemophilic dogs: (1) canine FVII can be engineered for secretion in a biologically active, 2-chain form; (2) continuous expression of FVIIa at levels of approximately 2 µg/mL (~40 nM) can result in a marked, long-term improvement in the bleeding diathesis, despite only partial correction of in vitro hemostatic parameters; and (3) at these expression levels and administered AAV8 vector doses, we observed no hepatotoxicity or increased risk of thrombosis.

With respect to levels of expression necessary for efficacy, our results are similar to those obtained in hemophilic mice transgenic for murine FVIIa (mFVIIa) or after AAV-mFVIIa-mediated gene transfer.[9,10] An administered dose in the range of 6.25 to 12.5E13 vector genomes/kg led to sustained cFVIIa expression of 1.5 to 2.5 µg/mL, resulting in supraphysiologic reduction in the PT (as expected) and a partial or near-correction of the WBCT and thromboelastography parameters, respectively. This suggests that, in both animal models of hemophilia, hemostatic efficacy can be achieved at levels comparable with bolus rhFVIIa infusion in humans. However, the effective vector dose in hemophilic dogs was 2- to 5-fold higher than doses required in mice, resembling similar findings with cFVIII or cFIX.[33,34] This observation thus justifies the use of this large animal model in preclinical gene transfer studies using FVIIa, as a predictor of efficacy in humans; it is worth noting that dogs, in contrast to mice, predicted the correct dosing in a human liver trial using an AAV-human FIX vector.[35] Moreover, the lack of clinically relevant endpoints in mouse studies, such as the spontaneous bleeding episodes observed in hemophilic dogs, further underlines the value of the canine model of hemophilia. Indeed, we observed a complete lack of spontaneous bleeds in the AAV-treated hemophilic dogs throughout this study, a clear improvement in the bleeding diathesis. Comparable results would be expected after AAV-mediated gene transfer of cFVIIa in hemophilic dogs with inhibitors,[36] similar to the phenotypic improvement demonstrated in hemophilic mice with hFVIII inhibitors, after transplantation of genetically modified platelets expressing mFVIIa.[37]

The evident improvement in the bleeding diathesis has particular clinical importance with respect to a human application of this gene transfer approach. The major morbidity in hemophilia patients results from repeated bleeds into the joints.[38] If these result from damage in the joint microenvironment, it is conceivable that continuous expression of FVIIa may result in a reduced number of joint bleeds. We have previously shown that continuous expression of mFVIIa at levels of 0.5 to 1.5 µg/mL in hemophilic mice resulted in restoration of hemostasis after a hemostatic challenge in the microcirculation, but not a challenge in the large vessels.[10] Hence, a potential explanation for the absence of spontaneous bleeds (including joint bleeds) in this study may be that continuous expression of FVIIa offers a "protective" and localized hemostatic effect, particularly in the microcirculation. Surprisingly, despite the lack of appreciable changes in the hemostatic parameters and cFVIIa levels in the treated HB dog after low-dose AAV8-cFVIIa infusion, we only observed 3 nonspontaneous bleeds within the first 8 months after vector administration in an observation period of 34 months. Similar results in HA dogs receiving a low vector

dose would be expected given the similarity of these 2 hemophilia models in response to rhFVIIa infusions.[12] The fact that AAV-mediated, low vector dose FVIIa gene transfer may offer some clinical benefit certainly warrants further investigation in the dog model because it will be safe and may have potential application in prophylaxis. Such experiments in dogs, which are currently underway, will help define the lowest expression levels that result in a measurable clinical improvement.

An important observation in hemophilic mice transgenic for mFVIIa was the premature mortality of mice continuously expressing mFVIIa at levels more than 2 μg/mL.[10] Because the dog model of hemophilia has been a good predictor of efficacy of hemophilia treatments, it was therefore pertinent in this study, where FVIIa is continuously expressed, to carefully examine the potential for thromboembolic disease, DIC, and hepatotoxicity. Levels of TAT and D-dimer throughout the study were within the normal range of HA/HB dogs, even in dogs that received the highest vector dose (HA-2-J57, HA-3-E66), suggesting that continuous expression of FVIIa at the levels reported here does not result in a procoagulant state. This was in good agreement with the partial correction of their in vitro hemostatic parameters. The possibility of systemic consumptive coagulation was evaluated using platelet counts, D-dimer and fibrinogen levels, biomarkers used for the diagnosis of DIC,[39] all of which were negative. Lastly, monitoring liver enzymes did not reveal any evidence of hepatotoxicity and demonstrated, for the first time, that AAV8 vector doses up to 2.6 E15 vector genomes are well tolerated in hemophilic dogs.

An important observation of the current study is that the level of expression required for efficacy is higher in comparison to similar AAV-based, liver-directed approaches for hemophilia using cFVIII or cFIX, where phenotypic improvement was observed with as little as 4% to 9% of cFVIII (4-20 ng/mL.,[33,40] assuming 100-200 ng/mL is 100%) or 5% of cFIX (~ 250 ng/mL.,[22] assuming 5 μg/mL is 100%). Consequently, the AAV8 vector doses used here were higher than used for AAV8-cFVIII (1E13 vector genomes/kg[40]) or AAV8-cFIX (5.25E13 vector genomes/kg[41]). However, this is not surprising; recombinant FVIIa has a substantially shorter half-life (~ 2.5 hours[42]) than either recombinant FVIII (~12 hours[43]) or FIX (~ 19 hours[44]) and pharmacologic levels required for hemostatic efficacy are higher (as shown by bolus dosing of rhFVIIa compared with recombinant FVIII or FIX). Clearly, a strategy to reduce the effective vector dose may be desirable and is currently underway, using a combination of improved AAV vectors[45] as well as optimization of guanine-cytosine content, cis-regulatory elements, and codon usage.[46] Moreover, complementary to improvements on the DNA level, changes on the protein level may also be implemented using high-activity variants of FVIIa.[47,48]

In conclusion, our data demonstrate that liver-directed, AAV8-mediated gene transfer of cFVIIa in HA and HB dogs is safe in the short and medium term and results in a marked and sustained phenotypic improvement. Although conventional gene transfer for hemophilia is based on delivery of FVIII or FIX for therapeutic expression, this is the first proof-of-concept delivery of a gene-based FVIII/FIX bypassing agent in a large animal model of hemophilia. This approach has potential applications not only for hemophilia gene therapy but also for platelet disorders, FVII deficiency, or prophylaxis in congenital hemophilia complicated by inhibitors, as has been reported for rhFVIIa.[8]

Acknowledgments

The authors thank Dr Ulla Hedner (Novo Nordisk), Dr Sriram Krishnaswamy, and Dr Rodney M. Camire at the Children's Hospital of Philadelphia for helpful discussions.

This work was supported by the Howard Hughes Medical Institute (K.A.H.) and the National Institutes of Health (NIH, Bethesda, MD; grants U01 HL66948 and P01 HL074124, K.A.H.; HL063098, T.C.N.; and RR02512, U.G.).

Authorship

Contribution: P.M. designed and performed research, analyzed data, and wrote the paper; E.R. performed research and analyzed data; M.N.A. and H.D.D. performed research; U.G. has worked on FVII-deficient dogs and provided the canine FVII-deficient plasma; S.Z. provided the AAV vector preparation; E.M. and A.D. performed research; M.E. provided reagents and assisted in the development of the cFVIIa antigen assay; T.C.N. performed research and analyzed data; and K.A.H. designed research and wrote the paper.

Conflict-of-interest disclosure: M.E. is an employee of Novo Nordisk A/S. The remaining authors declare no competing financial interests.

Correspondence: Katherine A. High, William H. Bennett Professor of Pediatrics, Investigator, Howard Hughes Medical Institute, Children's Hospital of Philadelphia, 3615 Civic Center Blvd, 302 Abramson Research Center, Philadelphia, PA 19104; e-mail: high@email.chop.edu.

References

1. DiMichele D. Inhibitor development in haemophilia B: an orphan disease in need of attention. Br J Haematol. 2007;138:305-315.
2. Leissinger CA. Inhibitor development in patients with hemophilia: an overview. Semin Hematol. 2006;43[suppl]:S1-S2.
3. Hedner U. Recombinant factor VIIa: its background, development and clinical use. Curr Opin Hematol. 2007;14:225-229.
4. Kenet G, Martinowitz U. Single-dose recombinant activated factor VII therapy in hemophilia patients with inhibitors. Semin Hematol. 2008;45[suppl]: S38-S41.
5. White GC 2nd. Congenital and acquired platelet disorders: current dilemmas and treatment strategies. Semin Hematol. 2006;43[suppl]:S37-S41.
6. Brenner B, Wiis J. Experience with recombinant-activated factor VII in 30 patients with congenital factor VII deficiency. Hematology. 2007;12:55-62.
7. Mariani G, Konkle BA, Ingerslev J. Congenital factor VII deficiency: therapy with recombinant activated factor VII—a critical appraisal. Haemophilia. 2006;12:19-27.
8. Konkle BA, Ebbesen LS, Erhardtsen E, et al. Randomized, prospective clinical trial of recombinant factor VIIa for secondary prophylaxis in hemophilia patients with inhibitors. J Thromb Haemost. 2007;5:1904-1913.
9. Margaritis P, Arruda VR, Aljamali M, Camire RM, Schlachterman A, High KA. Novel therapeutic approach for hemophilia using gene delivery of an engineered secreted activated Factor VII. J Clin Invest. 2004;113:1025-1031.
10. Aljamali MN, Margaritis P, Schlachterman A, et al. Long-term expression of murine activated factor VII is safe, but elevated levels cause premature mortality. J Clin Invest. 2008;118:1825-1834.
11. High K. Gene transfer for hemophilia: can therapeutic efficacy in large animals be safely translated to patients? J Thromb Haemost. 2005;3: 1682-1691.
12. Brinkhous KM, Hedner U, Garris JB, Diness V, Read MS. Effect of recombinant factor VIIa on the hemostatic defect in dogs with hemophilia A, hemophilia B, and von Willebrand disease. Proc Natl Acad Sci U S A. 1989;86:1382-1386.
13. Brinkhous KM, Sandberg H, Garris JB, et al. Purified human factor VIII procoagulant protein: comparative hemostatic response after infusions into hemophilic and von Willebrand disease dogs. Proc Natl Acad Sci U S A. 1985;82:8752-8756.
14. Brinkhous KM, Sigman JL, Read MS, et al. Recombinant human factor IX: replacement therapy, prophylaxis, and pharmacokinetics in canine hemophilia B. Blood. 1996;88:2603-2610.
15. Murphy SL, High KA. Gene therapy for haemophilia. Br J Haematol. 2008;140:479-487.

16. Herzog RW, Fields PA, Arruda VR, et al. Influence of vector dose on factor IX-specific T and B cell responses in muscle-directed gene therapy. Hum Gene Ther. 2002;13:1281-1291.
17. Ponder KP. Gene therapy for hemophilia. Curr Opin Hematol. 2006;13:301-307.
18. Callan MB, Aljamali MN, Margaritis P, et al. A novel missense mutation responsible for factor VII deficiency in research Beagle colonies. J Thromb Haemost. 2006;4:2616-2622.
19. Viuff D, Ezban M, Lind V, et al. Effect of rFVIIa and NN1731 (rFVIIa analogue) on thromboelastography (TEG) in whole blood obtained from haemophilia A dogs. 21st Congress of the International Society on Thrombosis and Haemostasis. Geneva, Switzerland, 2007.
20. Scharling B, Nielsen GG, Klitgaard T, et al. Comparison of coagulant activity of factor VII and activated factor VII activity assays when used for determination of recombinant activated factor VII levels in plasma. Blood Coagul Fibrinolysis. 2007; 18:677-684.
21. Raife T, Friedman KD, Fenwick B. Lepirudin prevents lethal effects of Shiga toxin in a canine model. Thromb Haemost. 2004;92:387-393.
22. Mount JD, Herzog RW, Tillson DM, et al. Sustained phenotypic correction of hemophilia B dogs with a factor IX null mutation by liver-directed gene therapy. Blood. 2002;99:2670-2676.
23. Nicolaisen EM, Thim L, Jacobsen JK, et al. FVIIa derivatives obtained by autolytic and controlled cathepsin G mediated cleavage. FEBS Lett. 1993;317:245-249.
24. Toso R, Pinotti M, High KA, Pollak ES, Bernardi F. A frequent human coagulation Factor VII mutation (A294V, c152) in loop 140s affects the interaction with activators, tissue factor and substrates. Biochem J. 2002;363:411-416.
25. Petersen LC, Norby PL, Branner S, et al. Characterization of recombinant murine factor VIIa and recombinant murine tissue factor: a human-murine species compatibility study. Thromb Res. 2005;116:75-85.
26. Wiinberg B, Jensen AL, Rojkjaer R, Johansson P, Kjelgaard-Hansen M, Kristensen AT. Validation of human recombinant tissue factor-activated thromboelastography on citrated whole blood from clinically healthy dogs. Vet Clin Pathol. 2005;34:389-393.
27. McCormack WM Jr, Seiler MP, Bertin TK, et al. Helper-dependent adenoviral gene therapy mediates long-term correction of the clotting defect in the canine hemophilia A model. J Thromb Haemost. 2006;4:1218-1225.
28. Russell KE, Olsen EH, Raymer RA, et al. Reduced bleeding events with subcutaneous administration of recombinant human factor IX in immune-tolerant hemophilia B dogs. Blood. 2003; 102:4393-4398.
29. Dewhurst E, Cue S, Crawford E, Papasouliotis K. A retrospective study of canine D-dimer concentrations measured using an immunometric "point-of-care" test. J Small Anim Pract. 2008;49:344-348.
30. Nelson OL. Use of the D-dimer assay for diagnosing thromboembolic disease in the dog. J Am Anim Hosp Assoc. 2005;41:145-149.
31. Koenig W. Fibrin(ogen) in cardiovascular disease: an update. Thromb Haemost. 2003;89:601-609.
32. Bosmans T, Gasthuys F, Duchateau L, de Bruin T, Verhoeven G, Polis I. A comparison of tepoxalin-buprenorphine combination and buprenorphine for postoperative analgesia in dogs: a clinical study. J Vet Med A Physiol Pathol Clin Med. 2007; 54:364-369.
33. Sarkar R, Mucci M, Addya S, et al. Long-term efficacy of adeno-associated virus serotypes 8 and 9 in hemophilia a dogs and mice. Hum Gene Ther. 2006;17:427-439.
34. Wang L, Nichols TC, Read MS, Bellinger DA, Verma IM. Sustained expression of therapeutic level of factor IX in hemophilia B dogs by AAV-mediated gene therapy in liver. Mol Ther. 2000;1: 154-158.
35. Manno CS, Pierce GF, Arruda VR, et al. Successful transduction of liver in hemophilia by AAV-Factor IX and limitations imposed by the host immune response. Nat Med. 2006;12:342-347.
36. Tinlin S, Webster S, Giles AR. The development of homologous (canine/anti-canine) antibodies in dogs with haemophilia A (factor VIII deficiency): a ten-year longitudinal study. Thromb Haemost. 1993;69:21-24.
37. Ohmori T, Ishiwata A, Kashiwakura Y, et al. Phenotypic correction of hemophilia A by ectopic expression of activated factor VII in platelets. Mol Ther. 2008;16:1359-1365.
38. Dunn AL. Management and prevention of recurrent hemarthrosis in patients with hemophilia. Curr Opin Hematol. 2005;12:390-394.
39. Levi M. Disseminated intravascular coagulation. Crit Care Med. 2007;35:2191-2195.
40. Jiang H, Lillicrap D, Patarroyo-White S, et al. Multiyear therapeutic benefit of AAV serotypes 2, 6, and 8 delivering factor VIII to hemophilia A mice and dogs. Blood. 2006;108:107-115.
41. Wang L, Calcedo R, Nichols TC, et al. Sustained correction of disease in naive and AAV2-pretreated hemophilia B dogs: AAV2/8-mediated, liver-directed gene therapy. Blood. 2005;105: 3079-3086.
42. Klitgaard T, Nielsen TG. Overview of the human pharmacokinetics of recombinant activated factor VII. Br J Clin Pharmacol. 2008;65:3-11.
43. Powell JS, Nugent DJ, Harrison JA, et al. Safety and pharmacokinetics of a recombinant factor VIII with pegylated liposomes in severe hemophilia A. J Thromb Haemost. 2008;6:277-283.
44. Roth DA, Kessler CM, Pasi KJ, Rup B, Courter SG, Tubridy KL. Human recombinant factor IX: safety and efficacy studies in hemophilia B patients previously treated with plasma-derived factor IX concentrates. Blood. 2001;98:3600-3606.
45. Nathwani AC, Gray JT, Ng CY, et al. Self-complementary adeno-associated virus vectors containing a novel liver-specific human factor IX expression cassette enable highly efficient transduction of murine and nonhuman primate liver. Blood. 2006;107:2653-2661.
46. Wu Z, Sun J, Zhang T, et al. Optimization of self-complementary AAV vectors for liver-directed expression results in sustained correction of hemophilia B at low vector dose. Mol Ther. 2008;16: 280-289.
47. Sommer C, Norbert Jorgensen P, Salanti Z, Clausen JT, Jensen LB. Immunogenicity of novel recombinant human activated factor VII analogues on factor VII neonatally tolerized rats. Thromb Haemost. 2007;98:721-725.
48. Tranholm M, Kristensen K, Kristensen AT, Pyke C, Rojkjaer R, Persson E. Improved hemostasis with superactive analogs of factor VIIa in a mouse model of hemophilia A. Blood. 2003;102:3615-3620.

Research article

Long-term expression of murine activated factor VII is safe, but elevated levels cause premature mortality

Majed N. Aljamali,[1] Paris Margaritis,[1] Alexander Schlachterman,[1] Shing Jen Tai,[1] Elise Roy,[1] Ralph Bunte,[2] Rodney M. Camire,[1] and Katherine A. High[1,3]

[1]Division of Hematology, The Children's Hospital of Philadelphia, Philadelphia, Pennsylvania, USA.
[2]Department of Pathology, School of Veterinary Medicine, University of Pennsylvania, Philadelphia, Pennsylvania, USA.
[3]Howard Hughes Medical Institute, The Children's Hospital of Philadelphia, Philadelphia, Pennsylvania, USA.

Intravenous infusion of recombinant human activated Factor VII (FVIIa) has been used for over a decade in the successful management of bleeding episodes in patients with inhibitory antibodies to Factor VIII or Factor IX. Previously, we showed that expression of murine FVIIa (mFVIIa) from an adeno-associated viral (AAV) vector corrected abnormal hemostatic parameters in hemophilia B mice. To pursue this as a therapeutic approach, we sought to define safe and effective levels of FVIIa for continuous expression. In mice transgenic for mFVIIa or injected with AAV-mFVIIa, we analyzed survival, expression levels, in vitro and in vivo coagulation tests, and histopathology for up to 16 months after birth/mFVIIa expression. We found that continuous expression of mFVIIa at levels at or below 1.5 μg/ml was safe, effective, and compatible with a normal lifespan. However, expression levels of 2 μg/ml or higher were associated with thrombosis and early mortality, with pathologic findings in the heart and lungs that were rescued in a low–factor X (low-FX) mouse background, suggesting a FX-mediated effect. The findings from these mouse models of continuous FVIIa expression have implications for the development of a safe gene transfer approach for hemophilia and are consistent with the possibility of thromboembolic risk of continuously elevated FVIIa levels.

Introduction

Hemophilia results from mutations in either of 2 genes, *F8* or *F9*, which encode proteins in the intrinsic pathway of coagulation. The current approach to therapy is intravenous infusion of the missing or defective coagulation factor, but work by Hedner and colleagues has established that infusion of recombinant human activated Factor VII (rhFVIIa; NovoSeven), a critical protein in the extrinsic pathway, can restore hemostasis through rhFVIIa-catalyzed generation of thrombin in patients with antibodies to Factor VIII (FVIII) or Factor IX (FIX) (1–3). Based on the current understanding of the coagulation cascade, all patients with hemophilia could conceivably be treated with rhFVIIa, a protein to which all such patients have immunological tolerance. This would simplify hemophilia management to a single product, but the high cost, short half-life, and ongoing concerns about risk of thrombosis with rhFVIIa (4) have limited this approach.

In previous studies in hemophilic mice, we showed that a gene transfer approach could circumvent the issue of short half-life, because activated FVII can be continuously expressed from a donated gene introduced into the liver via an adeno-associated viral (AAV) vector (5). The engineered FVII construct contained a nucleotide sequence encoding RKRRKR (referred to herein as 2RKR) inserted between Arg152 and Ile153 — the normal site of cleavage — to allow secretion of activated FVII. Expression of such an engineered FVIIa improved hemostasis in hemophilia B (HB) mice following AAV-mediated gene transfer. To further pursue vector-mediated expression of FVIIa as a possible therapeutic approach, we sought to define the range of FVIIa levels that restore hemostasis and are safe when expressed continuously. As an experimental approach, we generated transgenic mice expressing a range of levels of murine FVIIa (mFVIIa), detected using an assay specific for mFVIIa that shows minimal cross-reactivity to mFVII. We categorized mice from different transgenic lines as low and high expressers based on plasma levels of mFVIIa and crossed them to HB mice. We carried out similar analyses of mice injected with an AAV vector expressing mFVIIa. We found that when mFVIIa was continuously expressed in transgenic mice, even low levels were sufficient to improve hemostasis in a mouse model of hemophilia; moreover, continuous expression of mFVIIa at levels up to 1,500 ng/ml (30 nM) was compatible with a normal lifespan in mice. Identical findings were observed in mice injected with doses of AAV-mFVIIa adequate to generate circulating mFVIIa levels of 300–800 ng/ml (6–16 nM), and overexpression of mFVIIa at levels greater than 2,000 ng/ml (40 nM) caused early mortality in both normal and hemophilic mice, with pathology predominantly in heart and lungs. We also demonstrated that crossing mFVIIa-overexpressing mice into a newly generated low-factor X (low-FX) mouse model (6) resulted in restoration of normal longevity and decreased thrombin generation, which indicates that the shortened lifespan of the high expressers is mediated through the coagulation cascade rather than another mFVIIa-mediated signaling event. These results establish ranges for hemostatic efficacy of continuously expressed mFVIIa in a mouse model and also define upper limits for safety for continuously expressed mFVIIa. They also demonstrate an association between continuously elevated levels of FVIIa and premature mortality.

Nonstandard abbreviations used: -a, activated; AAV, adeno-associated viral (virus); aPTT, activated partial thromboplastin time; FIX, Factor IX; FVII, Factor VII; FVIII, Factor VIII; FX, Factor X; h-, human; HB, hemophilia B; m-, murine; p-, plasmid; PT, prothrombin time; rh-, recombinant human; TAT, thrombin-antithrombin; TF, tissue factor; TTR, transthyretin.

Conflict of interest: R.M. Camire receives research support from Novo Nordisk.

Citation for this article: *J. Clin. Invest.* **118**:1825–1834 (2008). doi:10.1172/JCI32878.

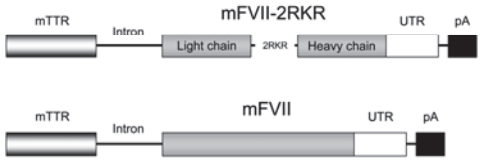

Figure 1
Transgenic construct for mFVIIa (mFVII-2RKR) and mFVII zymogen mice. The mFVIIa/mFVII cDNA is under control of the mTTR promoter separated by a synthetic intron. A polyadenylation signal (pA) from bovine growth hormone follows the 3′ untranslated region (UTR) for both cDNAs.

Results

Generation of transgenic mice expressing mFVIIa at a range of levels. Our initial studies using AAV vector–mediated FVIIa gene transfer demonstrated the efficacy of continuously expressed mFVIIa in effecting hemostasis in a murine model of hemophilia (5). As a next step, we sought to determine the minimum levels of mFVIIa required for efficacy and the maximum levels that would be safely tolerated. We chose to analyze the safety and efficacy of a range of circulating mFVIIa levels using both transgenic and AAV-injected mice; compared with vector-treated mice, transgenic animals offer the advantages of decreased intragroup variation in mFVIIa levels among littermates, maintenance of similar levels of mFVIIa from one generation to the next, and no requirement for vector preparation and injection. For construction of the transgene, we used the mFVII cDNA (7) in order to ensure optimal interaction with murine tissue factor (TF), and we engineered the mFVII construct to allow secretion of activated mFVIIa by insertion of a nucleotide sequence encoding 2RKR between Arg152 and Ile153, as previously described (5). A cDNA coding for a WT mFVII was also used to generate control animals expressing WT (zymogen) mFVII (Figure 1). In both constructs, expression was under the control of the murine transthyretin (TTR) promoter as previously described (8). Founders (14 of 160 [8.7%] microinjected fertilized eggs for the mFVIIa constructs, 5 of 55 [9%] for the mFVII zymogen constructs) were identified both by genotyping and, in the case of the mFVIIa transgenic mice, by shortening of the prothrombin time (PT), with 100% concordance between the 2 assays in the mFVIIa mice. We analyzed a total of 12 independent founder lines carrying the mFVIIa transgene and 5 lines carrying the mFVII (zymogen) transgene. Founder lines are referred to herein as F0; subsequent generations of offspring from crosses into C57BL/6 pure background are denoted N1–N4. As expected from the transgene positional effects, the transgenic founder lines expressed a range of mFVII or mFVIIa levels from 500 to 5,500 ng/ml, as measured by total antigen ELISA and by PT (Table 1). However, mFVIIa levels were approximately equivalent from one generation to the next (F0, 3,730 ± 715 ng/ml; N1, 3,540 ± 1,300 ng/ml; N2, 3,110 ± 955 ng/ml; $P = 0.232$). An active site inhibitor-based ELISA was also developed to determine levels of mFVIIa in the transgenic founder lines; this showed minimal crossreactivity to mFVII zymogen (Table 1) and was used for the remainder of the study. Although overexpression of a procoagulant factor most likely results in some degree of inactivation by circulating serpins, the antigen assay used here with an active site inhibitor enabled us to define the levels and the effect of free, uninhibited mFVIIa. For additional analyses, mFVIIa transgenic animals were grouped arbitrarily into low expressers (500–1,500 ng/ml mFVIIa as assessed by active site inhibitor ELISA) or high expressers (2,000–5,500 ng/ml mFVIIa). For both groups, transgenic mice were born in expected proportions (50% in cross with C57BL/6 WT or HB), and nontransgenic littermates were used as controls in all assays.

Hemostasis is improved in mice with hemophilia A or HB after crossing to mFVIIa transgenic mice or administering AAV-mFVIIa. To assess the efficacy of continuously expressed mFVIIa in restoring hemostasis in hemophilic mice, we crossed carrier hemophilic (both A and B) C57BL/6 female mice to mFVIIa transgenic male mice and assessed mFVIIa levels, PT, activated partial thromboplastin time (aPTT), and thrombin-antithrombin (TAT) complex levels and performed assays of in vivo clot formation (blood loss after tail clip, real-time clot formation in cremaster muscle arterioles after laser injury, and occlusion of carotid artery after $FeCl_3$ injury) in transgenic and nontransgenic littermates. As expected, the nontransgenic littermates, both WT and hemophilic, showed baseline levels of mFVIIa in the circulation (~150 ng/ml), while average mFVIIa levels in the HB–low-mFVIIa transgenic mice were approximately 1,000 ng/ml and in the HB–high-mFVIIa transgenic mice about 3,000 ng/ml (Figure 2A). PT progressively shortened as circulating mFVIIa levels increased (Figure 2B). The aPTT was restored to the WT range in hemophilic mice expressing low-range mFVIIa ($P = 0.6$ versus WT) and was reduced to shorter than normal values for the high expressers ($P < 0.0001$ versus WT; Figure 2C). As a surrogate measure of thrombin generation, we measured the levels of TAT. HB mice expressing low and high levels of mFVIIa showed a dose-dependent increase in TAT levels ($P < 0.05$, HB–low-mFVIIa versus HB–high-mFVIIa; Figure 2D). These data were further confirmed by shortening of clot formation times and increase in alpha angles on rotational thromboelastometry in citrated blood from HB mice with the mFVIIa transgene compared with nontransgenic HB littermates (data not shown). Similar results for in vitro clotting assays were obtained when mFVIIa transgenic mice were crossed with hemophilia A mice (data not shown). In contrast to HB-mFVIIa transgenic animals, HB mice transgenic for mFVII zymogen (expressing about 1,700 ng/ml total antigen and approximately 150 ng/ml mFVIIa) showed a modest reduction in PT, no improvement in aPTT, and no increase in TAT levels (Figure 2). For comparison, another cohort of HB mice ($n = 8$) were injected via the portal vein with an AAV2 vector at a range of doses (3×10^{11}–1.2×10^{12} vector genomes/mouse). This resulted in

Table 1
mFVII and mFVIIa levels in transgenic founders or WT controls

Group	*n*	mFVII/FVIIa total antigen (ng/ml)	mFVIIa antigen, biotinylated inhibitor ELISA (ng/ml)	PT (s)
High-mFVIIa Tg	6	4,250 ± 1,100	3,150 ± 800	11.9 ± 0.9
Low-mFVIIa Tg	6	2,000 ± 350	1,150 ± 600	15.2 ± 1.2
WT[A]	30	900 ± 450	150 ± 100	21.9 ± 1.0
mFVII Tg	5	2,050 ± 550	150 ± 50	20.8 ± 1.3
WT[B]	4	800 ± 300	100 ± 100	22.4 ± 0.7

Values are mean ± 1 SD. [A]Littermates of mFVIIa transgenic mice. [B]Littermates of mFVII transgenic mice.

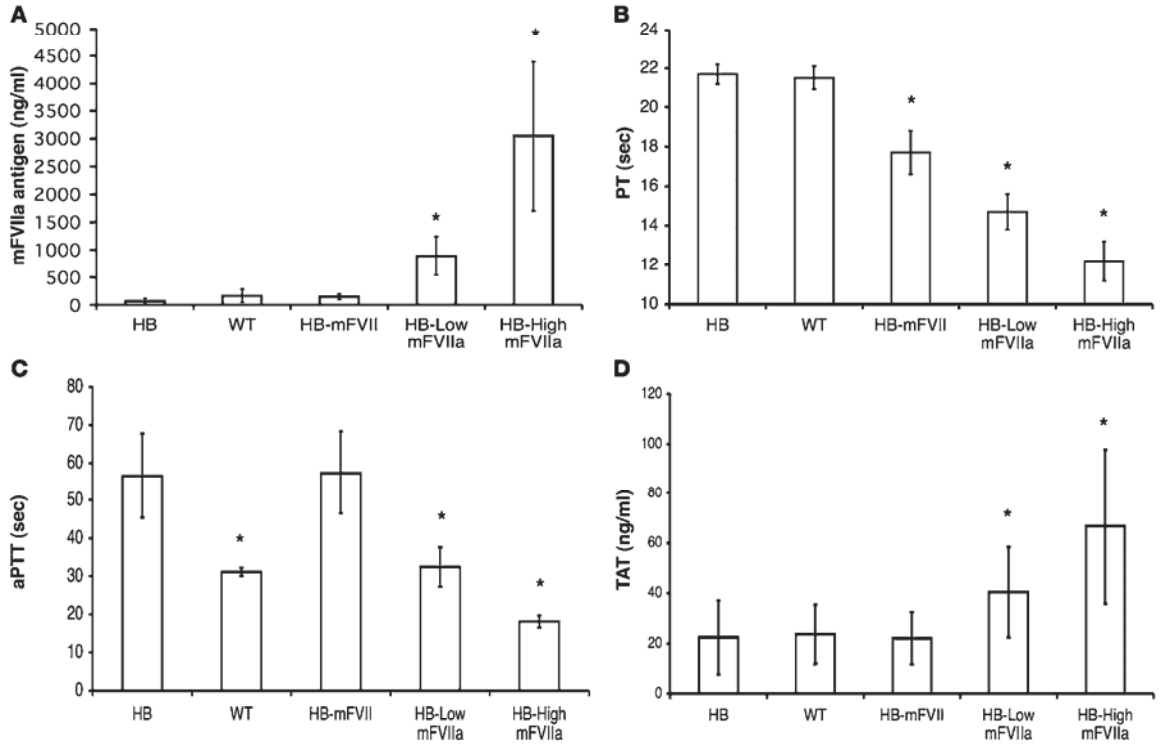

Figure 2
Efficacy of the mFVIIa or the mFVII zymogen transgene in HB mice. (**A**) Plasma mFVIIa levels (mFVII levels were measured by a separate antigen ELISA resulting in ~1,700 ng/ml), (**B**) PT, (**C**) aPTT, and (**D**) TAT levels in littermate HB ($n = 21$), WT ($n = 21$), HB-mFVII ($n = 4$), HB–low-mFVIIa ($n = 10$), and HB–high-mFVIIa ($n = 7$) mice. *$P < 0.05$ versus HB. Values are mean ± 1 SD.

mFVIIa levels of 300–800 ng/ml (mean, 510 ng/ml), which was adequate to reduce aPTT, PT, and blood loss following a tail-clip assay and to dramatically improve long-term survival (Table 2). Thus, the results obtained from the AAV-injected mice closely resemble those obtained from the transgenic mice.

Low levels of mFVIIa improve in vivo clot formation in the microcirculation of hemophilic mice, but not in the macrocirculation of mFVIIa transgenic mice. To further analyze the hemostatic efficacy of varying mFVIIa levels, we used assays that allowed us to assess clot formation in a living mouse. A tail-clip bleeding test, in which the tail was severed at a diameter of 3 mm, was used to determine total blood loss during a 10-minute time period, as measured by $OD_{575\,nm}$ of a saline solution into which the tail was submerged, following red blood cell lysis. Total blood loss and bleeding time were reduced in the HB-mFVIIa transgenic mice compared with hemophilic nontransgenic littermates ($P < 0.05$), although not to the normal levels seen in WT littermates (Figure 3A and data not shown). In contrast to the in vitro coagulation assays (PT and aPTT), there was no difference in bleeding time parameters between HB–low-mFVIIa and HB–high-mFVIIa mice ($P = 0.5$; data not shown). Hemophilic mice transgenic for mFVII zymogen showed no significant improvement in blood loss following tail clip compared with hemophilic nontransgenic littermates (data not shown).

In a second in vivo model, thrombus formation was assessed following a laser injury to a small arteriole (50 μm diameter) in the cremaster muscle by monitoring platelet accumulation at the site of injury (9). By assessing both kinetics of clot formation and the size of the formed thrombus, we determined that untreated HB littermates ($n = 2$, 14 injury sites) failed to form clots even after the extended time period of 10 minutes. In contrast, both HB–low-mFVIIa and HB–high-mFVIIa mice ($n = 3$, 24 sites) displayed kinetics and clot volume indistinguishable from those of WT littermates ($n = 5$, 30 sites; Figure 3B), which suggests that relatively modest levels of mFVIIa (mean ~1,000 ng/ml, or 20 nM, in low expressers) cause improved hemostasis in the microcirculation. This finding of efficacy at low-mFVIIa levels in the cremaster arteriole model is consistent with data we generated using an AAV-mFVIIa vector to correct hemostasis in hemophilic mice (Table 2). Finally, using a third in vivo test of thrombosis, the $FeCl_3$–carotid artery injury model, we found no evidence of clot formation in either the high or the low expressers (Figure 3C).

Continuous expression of mFVIIa at less than 1,500 ng/ml is associated with normal life expectancy, but expression at more than 2,000 ng/ml is associated with premature mortality. To assess the safety of continuous expression of mFVIIa, we determined survival in cohorts of mFVIIa transgenic, nonhemophilic mice as a function of circulat-

Table 2
Efficacy and survival following hepatic administration of AAV2-mFVIIa in HB mice

Group	mFVIIa (μg/ml)	PT (s)	aPTT (s)	$OD_{575\ nm}$[A]	Survival at 19 mo	Clots[B]
AAV2-mFVIIa	0.51 ± 0.19[C,D]	27.9 ± 2.3[C]	49.1 ± 16.3[C]	0.7 ± 0.5[C,D]	85%[E]	68 of 68[C]
	(*n* = 11)	(*n* = 11)	(*n* = 11)	(*n* = 14)	(*n* = 14)	(*n* = 10)
HB	0.16 ± 0.07	31.3 ± 3.5	66.3 ± 9.7[D]	2.6 ± 0.7[D]	45%	0 of 30
	(*n* = 3)	(*n* = 3)	(*n* = 3)	(*n* = 13)	(*n* = 11)	(*n* = 5)
WT	0.13 ± 0.11	29.9 ± 1.6	34.9 ± 2.6	0.3 ± 0.2	100%	45 of 45
	(*n* = 5)	(*n* = 5)	(*n* = 5)	(*n* = 15)	(*n* = 5)	(*n* = 5)

AAV2-mFVIIA was administered at 3×10^{11}–1.2×10^{12} vector genomes/mouse. Untreated HB and WT mice were used as controls. Values for mFVIIa, PT, aPTT, and $OD_{575\ nm}$ are mean ± 1 SD. [A]Hemoglobin content following tail-clip assay. [B]Number of clots in the cremaster muscle following injury. [C]$P < 0.01$ versus HB. [D]$P < 0.01$ versus WT. [E]$P < 0.05$ versus HB.

ing mFVIIa levels (Figure 4). Over a 16-month period of observation, survival in the low mFVIIa expressers was equivalent to that of nontransgenic WT littermates. Longer periods of observation, up to 24 months, showed the same result (data not shown), and these results are consistent with those obtained from AAV-injected mice (Table 2). However, for the high mFVIIa expressers, survival was reduced, with 50% of founders surviving at 16 months ($P < 0.02$ versus WT; Figure 4). Results were similar when the high expressers were crossed to HB mice: FIX levels less than 1% did not protect against premature mortality (data not shown). Backcrossing into C57BL/6 mice further reduced survival, with typically 20% of pups dying in the first 72 h after birth. Even among those surviving the first 72 h, lifespan was shortened compared with nontransgenic littermates, with 50% of N1 mice dead at 3 months ($P < 0.0001$ versus WT) and 50% of N2 mice dead at 1 month ($P < 0.0001$ versus WT; Figure 4). Mortality rates on backcrossing were similar for 3 separate high-mFVIIa founder lines. The cause of the progressively earlier mortality on backcrossing was investigated, but not found:

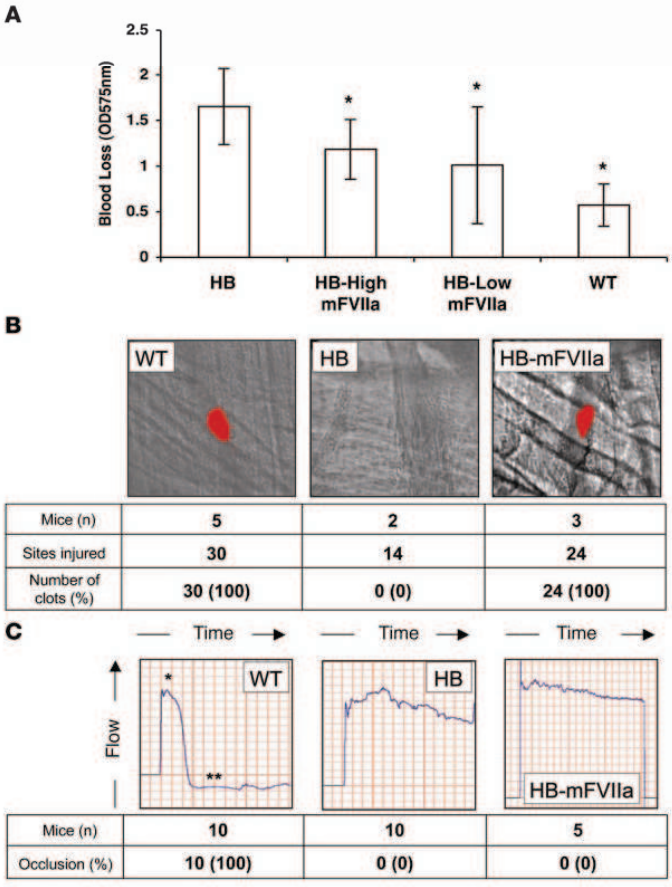

Figure 3
In vivo tests of coagulation. (**A**) Blood loss in mFVIIa transgenic HB mice expressing low (HB-Low mFVIIa, $n = 10$) or high (HB-High mFVIIa, $n = 8$) levels of mFVIIa, compared with HB ($n = 20$) and WT ($n = 10$) littermates. *$P < 0.05$ versus HB. Values are mean ± 1 SD. (**B**) Representative cremaster real-time thrombus formation in WT, HB, or HB-mFVIIa (high and low expresser) mice. (**C**) $FeCl_3$ carotid artery injury in WT, HB, or HB-mFVIIa (high and low expresser) mice. The single asterisk denotes the time at which the $FeCl_3$ patch was applied; the double asterisk denotes vessel occlusion. Results are from 1 indicative mouse per group.

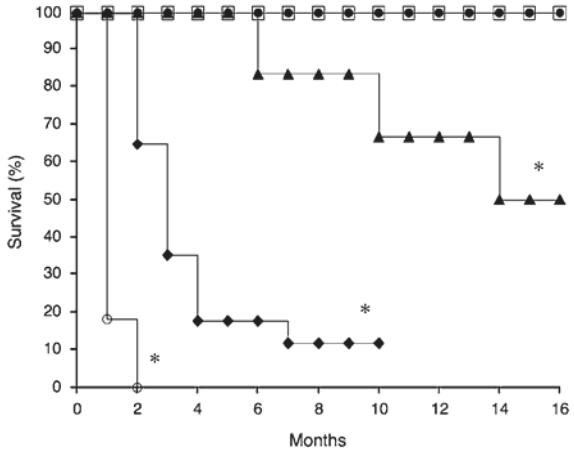

Figure 4
Expression of high mFVIIa levels is associated with increased mortality after crossing the founder C57BL/6–SJL mice into C57BL/6 pure strain background. Kaplan-Meier survival plot of transgenic mFVIIa mice with low or high levels of transgene expression compared with WT littermates. Curves for high mFVIIa expressers exclude animals dying within 72 h of birth. Squares, WT (n = 10); filled circles, low-mFVIIa N1–N4 (n = 25); triangles, high-mFVIIa F0 (n = 6); diamonds, high-mFVIIa N1 (n = 17); open circles, high-mFVIIa N2 (n = 11). *P < 0.05 versus WT.

we did not observe significant differences in platelet counts or TF levels (prepared from pulmonary and cardiac cell lysates) in the N1 and N2 mice (data not shown). Moreover, we did not observe any significant differences in TAT levels, clotting times (PT), or mFVIIa levels (data not shown).

Premature mortality in high FVIIa–expressing mice is associated with pathologic findings in heart and lungs. To investigate the causes of premature mortality, we carried out histopathologic studies of high FVIIa expressers on both normal and HB backgrounds. Results were identical for normal and hemophilic background in high-mFVIIa transgenic mice sacrificed or expiring at time points ranging from 2 to 6 months of age. Necropsy revealed no gross abnormalities. Histopathologic analyses of brain, liver, and kidney were also normal. Major pathologic findings were confined to the lungs and heart (Figure 5). The lungs of 4 of 8 mice examined showed increased fibrin deposition and intimal/smooth muscle proliferation in the pulmonary vasculature. In the hearts of all 8 mice examined, even in these relatively young mice aged less than 6 months, thrombi were present in coronary vessels and in the chambers of the heart. Occasional patchy inflammatory cell infiltrates were also noted. Immunohistochemical staining for fibrin showed increased fibrin deposition in the myocardium in a multifocal pattern. As a follow-up to these observations, we sacrificed 6 low-mFVIIa transgenic mice on a normal background at 18 months of age to search for evidence of pathologic findings in heart or lungs, but these tissues appeared normal even in these older low-mFVIIa transgenic mice (data not shown). None of these findings were observed in the 10 age-matched nontransgenic controls examined (P = 0.02 in lungs; P < 0.0001 in heart) or in the 6 low-mFVIIa transgenic mice examined up to 18 months of age (P = 0.085 in lungs; P < 0.0001 in heart).

Crossing to low-FX mice restores normal survival. Although the mechanism of action of high-dose FVIIa is still controversial, the end product is the generation of FXa. In an effort to rescue the high-expressing mFVIIa transgenic mice, which had repeatedly succumbed at early time points, and to determine whether the premature mortality was mediated through FXa generation, we crossed these mice to mice with low levels of mFX activity. These mice are *F10* knockouts and knockins for a *F10* variant based on a human FX (hFX) mutation (FX^{Friuli}; ref. 10) that results in low FX activity (~5.5%) in homozygous mice without affecting survival (6). The targeted knockin of the murine $F10^{Friuli}$ allele ($F10^{tm2Ccmt}$) allows expression of this variant from the endogenous promoter. To determine whether low mFX activity rescued the early mortality seen in mice overexpressing mFVIIa, we crossed these 2 mouse lines and analyzed littermates with high mFVIIa levels and low, mid-range, or normal mFX activity (about 3%, 50%, and 100%, respectively; Figure 6). The low-mFX mice were on a predominantly C57BL/6 background (backcrossed for 5 generations). Coagulation assays showed comparable levels of mFVIIa in all 3 groups as measured by ELISA (Figure 6A). As expected, mice with low mFX activity had prolonged PT compared with mice with mid-range or WT mFX activity (Figure 6B). TAT levels also varied among the 3 groups of mice, with markedly elevated levels in mFVIIa transgenic mice with 100% mFX activity, lower but still elevated levels in mice with 50% mFX activity, and levels close to those of nontransgenic WT littermates in mice with 3% mFX activity (Figure 6C). The consequences of these altered coagulation parameters are clear in the survival curves for these animals. Among mice expressing high levels of mFVIIa, survival at 11 months was 0% for mice with WT mFX activity (F1 and F2, P < 0.0001 versus WT), 18% for mice with 50% mFX activity (P < 0.0001 versus WT), and 100% for mice with 3% mFX activity (Figure 6D). Histologic analysis of tissues from 4 high-mFVIIa mice with either 100% or 50% mFX showed thrombi similar in distribution to those found in high-mFVIIa mice crossed to hemostatically normal mice (Figure 5 and data not shown).

Discussion

The development of rhFVIIa to effect hemostasis in hemophilic patients with inhibitors was a major advance in the management of what is currently the most common complication of treatment for hemophilia. However, the short half-life and substantial expense of the product remain impediments to more extensive use in the setting of hemophilia. Gene transfer offers the possibility of circumventing the short half-life, because expression from the donated gene is continuous. In addition, as a gene therapy product, FVIIa has the advantage that all hemophilic subjects are fully tolerant to it. Ongoing advances in AAV-mediated gene transfer suggest that successful clinical application will occur for other clotting factors (11, 12). We undertook the studies here in an attempt to define safe and efficacious levels of FVIIa in the setting of continuous expression.

The present study reports 2 major findings: first, that continuously expressed FVIIa demonstrates safety and hemostatic efficacy over a fairly broad range of levels and over the lifespan of the mouse, and second, that high-level continuous expression of FVIIa is associated with early mortality, by a mechanism dependent on FX. Previously, we showed that AAV-mediated gene transfer of an engineered FVIIa construct to the liver resulted

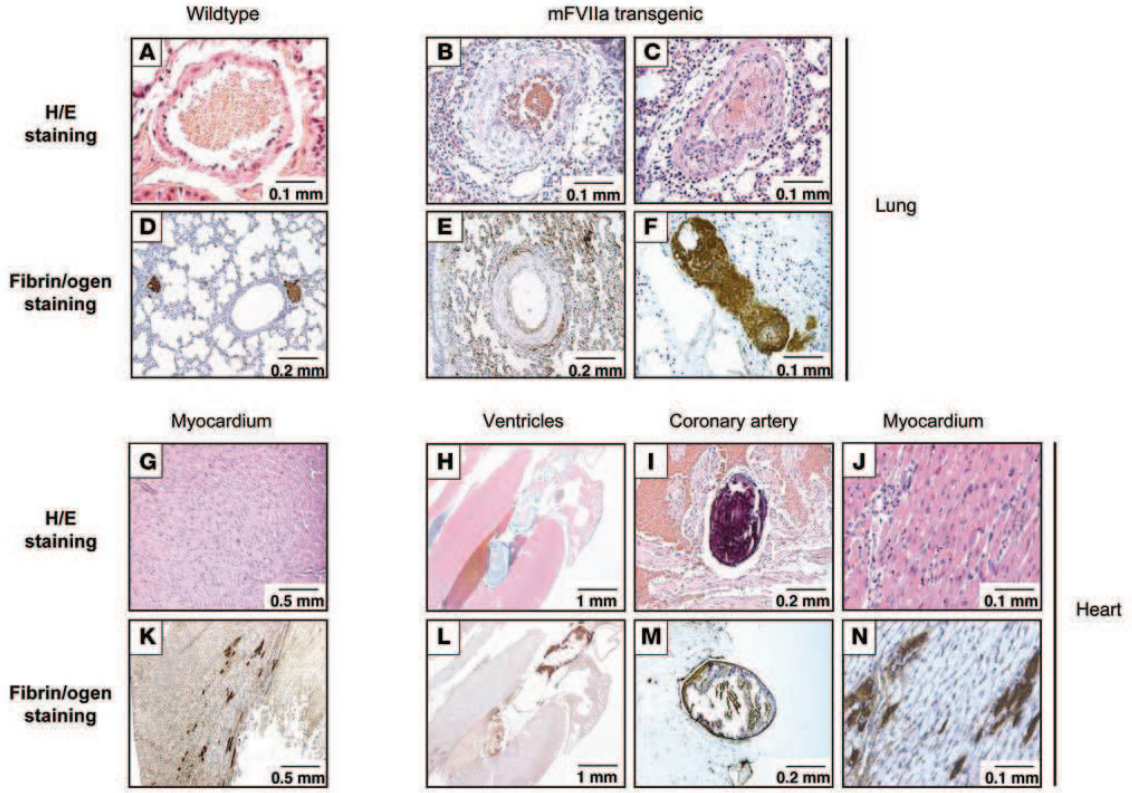

Figure 5

Histological findings in lungs and hearts of high-mFVIIa transgenic mice compared with WT littermates. Intimal/smooth muscle proliferation was observed in the pulmonary veins (**B** and **C**) as well as fibrin deposition in the pulmonary bed (**E** and **F**) of mFVIIa transgenic mice, but neither was seen in WT mice (**A** and **D**). Thrombi were observed in the coronary artery (**I** and **M**) and ventricles (**H** and **L**) as well as inflammatory infiltrates in the myocardium (**J** and **N**) of mFVIIa transgenic mice, but none were observed in WT mice (**G** and **K**). Original magnification, ×20 (**H** and **L**); ×40 (**G** and **K**); ×100 (**D**, **E**, **I**, and **M**); ×200 (**A**–**C**, **F**, **J**, and **N**).

in continuous expression of FVIIa and that hemophilic mice expressing mFVIIa for periods up to 6 months exhibited correction of plasma-based coagulation assays (PT and aPTT) and partial correction of the tail-clip bleeding time after vector infusion (5). We demonstrate that circulating levels of mFVIIa in the range of 500–1,500 ng/ml (10–30 nM) in hemophilic mice shorten the PT, correct the aPTT to the normal range, and modestly increase TAT levels. The levels seen in the low-mFVIIa transgenic mice closely approximated the levels obtained from AAV-mediated transduction, as seen in our previous study (5) and in data presented here (Table 2). These levels are similar to the peak therapeutic levels seen in patients infused with recombinant FVIIa (10–20 nM; ref. 13). Moreover, these mice exhibited a normal lifespan through the 16-month study duration, similar to AAV-treated mice (Table 2), and at necropsy showed no unusual pathology. In terms of efficacy, in vivo tests of coagulation provide a more nuanced view of mFVIIa-supported hemostasis in hemophilic mice than do standard plasma-based assays. Clot formation in the microvasculature, as measured in the cremaster arterioles after a laser injury, appeared indistinguishable from that seen in WT mice, and blood loss on the tail-clip assay was reduced compared with hemophilic nontransgenic littermates, although not to the levels seen in WT littermates. On the other hand, in the $FeCl_3$ injury model of the carotid artery (macrovasculature), there was no clot formation in the transgenic mice, even after a prolonged period of observation.

A possible explanation for these discordant findings of clot formation in the micro- and macrocirculation may be due to differences in multiple factors, including the size of the vessel and/or the mechanism of clot formation in these settings. Chou et al. showed that clot formation in the microcirculation relies primarily on circulating TF, e.g., from microparticles (14). Clot formation in large diameter vessels, on the other hand, depends on exposure of vessel wall (subendothelial) TF (15). Additionally, the difference seen in the 3 injury models used here may be a reflection of the type of injury. For example, thrombus formation in the $FeCl_3$ model appears to rely primarily on the glycoprotein VI–collagen pathway (16), whereas in the laser-induced injury model, initial thrombus formation relies on the TF-mediated pathway of thrombin generation (17). Finally, although we do not have direct evidence, we cannot exclude the possibility that continuous expression results in an increased extravascular pool of mFVIIa

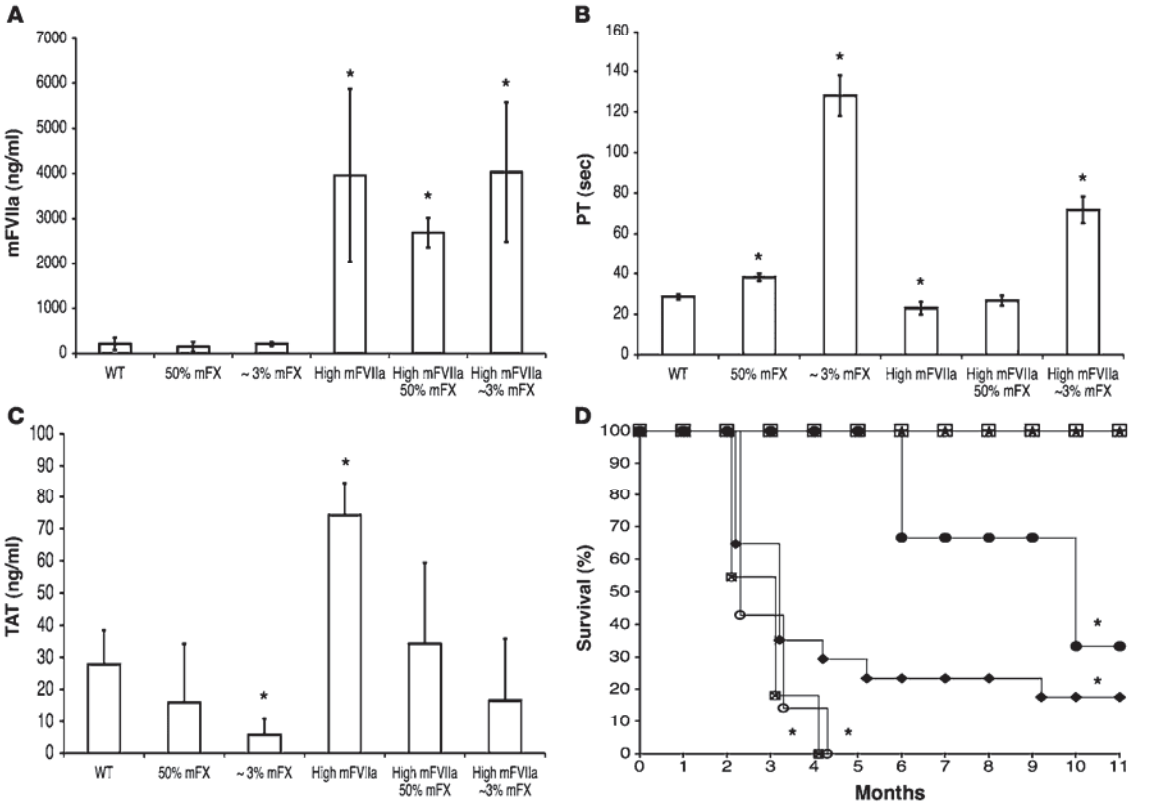

Figure 6

Hemostatic differences in high-mFVIIa transgenic mice. (**A**) mFVIIa antigen; (**B**) PT measurements using hFX-deficient plasma; (**C**) TAT levels; and (**D**) Kaplan-Meier survival plot of high-mFVIIa transgenic mice in a background between ~3% and 100% mFX. (**A–C**) $n = 3$ (~3% mFX and high-mFVIIa ~3% mFX), 4 (high-mFVIIa), 6 (WT), 8 (50% mFX), 12 (high-mFVIIa 50% mFX). (**D**) Open squares, WT ($n = 10$); filled circles, high-mFVIIa F0 ($n = 3$); stars, high-mFVIIa F2 ~3% mFX ($n = 8$); diamonds, high-mFVIIa F2 50% mFX ($n = 17$); crossed-out squares, high-mFVIIa F1 100% mFX ($n = 11$); open circles, high-mFVIIa F2 100% mFX ($n = 7$). $^*P < 0.05$ versus WT. Values are mean ± 1 SD.

that may affect, or at least facilitate, the differences seen in the in vivo injury models described here. Elevated levels of extravascular FVIIa have been proposed as the explanation for the reduced number of bleeds observed in hemophilic patients undergoing daily infusions of rhFVIIa, both during and for 3 months after the infusions (18, 19). Additionally, hFVIIa activity of 34% has been reported in human lymph fluid that bathes the extravascular space (20). More pertinent to this study, the presence of mFVIIa has previously been demonstrated in the perivascular space outside dermal vessels even in the absence of tissue damage (21).

A critical question is the relationship of these findings to the frequency of bleeding in patients with hemophilia. The major morbidity of hemophilia stems from repeated bleeds into the joints that result in synovial hypertrophy, intense neovascularization, and inflammation (22). If indeed most of these bleeds begin as unsealed nicks in the microcirculation, then a normalized response to a hemostatic challenge in the microcirculation, as continuously expressed FVIIa seems to provide, could conceivably result in a reduced number of joint bleeds. A caveat in extrapolating these findings to humans is that mice generally have platelet counts 3- to 4-fold higher than do humans (23), which may result in a better outcome in this model, although the murine mean platelet volume is also smaller (one-half that of human platelets; refs. 24, 25), which compensates for the increased count. If, as has been proposed, most of the blood-borne TF comes from leukocyte-derived microparticles (14), the difference in platelet counts may be of limited concern in interpretation of results. The effect of continuously expressed FVIIa on frequency of joint bleeds will perhaps be better assessed in a canine model of hemophilia, where observation of animals over many years has established a baseline number of readily diagnosed bleeds, including joint bleeds, in untreated animals (26). Improvement of hemostasis in a large-animal model has previously been a strong predictor of efficacy of products in human subjects (27–29).

In addition to defining a range at which continuously expressed FVIIa appears to be safe and improves hemostasis, the other major finding in this study is the early mortality associated with high-level continuous expression of FVIIa. Although mice expressing lower levels of FVIIa exhibited normal lifespan and

absence of pathology (100% of mice alive and free of pathologic changes at 16 months), those expressing FVIIa in the range of 3,000 ng/ml showed early mortality, with 50% of founder mice surviving at 16 months. Several lines of evidence suggest that increased thrombin generation and resultant pathologic thrombus formation account for this finding. The most direct evidence comes from histopathologic studies of the high-FVIIa mice, which exhibited pathologic thrombi and increased fibrin deposition even at young ages. These findings are reminiscent of those described by Ameri et al. in mice transgenic for hFIX, although those animals exhibited altered histopathology and premature mortality with modest increases in FIX levels (30), whereas in our study continuous expression of mFVIIa appeared safe over a broad range of lower levels. Our finding of pathology primarily in the heart and lungs is consistent with the high levels of TF in these organs (31, 32) and supports the concept of TF forming a hemostatic envelope that affords additional hemostatic protection against repetitive mechanical injury for the vasculature of the heart and lungs (33). This observation also demonstrates the power of the transgenic approach used here that afforded extremely high levels of mFVIIa expression. We were not able to attain circulating levels this high using AAV vectors; in practice this may constitute an unexpected safety feature of AAV2-mediated FVIIa expression.

Consistent with the histologic findings, other evidence suggesting increased thrombin generation as the cause of the premature mortality includes the elevated TAT levels in the high expressers and rescue of the high expressers by crossing to low-mFX mice. The normalization of the TAT levels in the high expressers after crossing to the low-mFX mice and the restoration of survival despite being crossed to a predominantly C57BL/6 background lends further support to thrombin generation as the etiology of the early mortality. However, we cannot exclude a role for other genetic factors. The moderate TAT levels in the low expressers, although statistically different from those in WT mice, suggest thrombin levels that are well-tolerated in the organism, while the more marked increase in the high expressers does not suggest this (Figure 2D and Figure 4).

As was the case for the efficacy findings in the murine model (vide supra), the issue for the findings of increased mortality is how they relate to the risk of increased thrombin generation in humans continuously expressing FVIIa (i.e., after gene transfer). There has been ongoing controversy about the risk of thromboembolic events in individuals receiving bolus infusions of rhFVIIa (4, 34). Initial experience with rhFVIIa, mostly in the hemophilia population, established that the risk of myocardial infarction, deep venous thrombosis, and cerebrovascular accidents as a consequence of rhFVIIa infusion was low, less than 1% in retrospective studies, and occurred mostly in older patients with predisposing conditions (34). Conversely, a recent prospective study of 399 patients with stroke caused by intracerebral hemorrhage who received either rhFVIIa or placebo showed a significant increase in arterial thromboembolic events, mainly myocardial or cerebral infarction, in the FVIIa-treated group, although overall this group showed increased survival and less disability compared with the placebo group (35). Clearly, the patients in the cerebral hemorrhage group were older and had predisposing factors for thrombosis compared with the hemophilia patients initially studied. Nevertheless, although our model relies on continuous expression of FVIIa in contrast to bolus infusion, our data are consistent with the finding that thromboembolic events are indeed a potential consequence of elevated FVIIa levels.

In summary, we have established that continuous expression of activated FVII is safe over a range of levels in a mouse model of hemophilia (300–1,500 ng/ml, or 6–30 nM) and that these levels improve hemostasis as judged by in vitro clotting assays and by hemostatic response to a laser injury in the microcirculation. Although a direct comparison between mice and humans is difficult due to the differences in the mode of administration (bolus infusion versus continuous), these levels of expression fall within the clinically defined therapeutic range (10–20 nM peak) and can be achieved by AAV-mediated gene transfer. However, we also show early mortality, characterized by thrombus formation and fibrin deposition in lungs and heart, as a complication of continuous expression at levels greater than 2,000 ng/ml (40 nM). This early mortality was rescued by crossing to mice with low circulating levels of FX. Our data suggest that the margin between the lowest effective dose (6 nM) and the highest safe dose (30 nM) is narrow, but this is characteristic of a number of drugs that alter coagulation.

Enabled by continuing advances in systems biology and by the ability to transfer any gene of interest, novel therapeutic approaches to genetic disorders based on transfer of genes other than those affected by mutations will continue to be explored (36, 37). Based on the FVIIa model, it will be crucial to carefully define the boundaries of safety and efficacy over prolonged periods of time and to scrutinize the effect of continuous transgene expression on disease pathophysiology.

Methods

Generation of FVIIa and FVII transgenic mice. The 2.3-kb fragment containing the mFVII-2RKR transgene (mFVIIa, containing the full mFVII untranslated region) with a synthetic intron from the AAV-hAAT-mFVIIa (5) was partially digested and purified with *Sac*II and *Xba*I. A *Kpn*I linker fragment containing *Sac*II and *Xba*I sites was ligated to a *Kpn*I-digested plasmid containing the liver-specific mTTR promoter (38) driving expression of hFIX (pTTR-hFIX; ref. 8). The intron-mFVIIa fragment was ligated to the pTTR vector. To generate pTTR-mFVII (zymogen), pTTR-mFVIIa and pAAV-hAAT-mFVII (containing the full mFVII untranslated region) were partially digested with *Cla*I/*Xba*I to release mFVIIa and mFVII, respectively, and the *Cla*I/*Xba*I mFVII fragment was ligated into digested pTTR vector. Sequencing was performed to confirm the presence or absence of the 2RKR sequence in mFVII cDNA. Purified plasmid preparations were generated for each construct by standard cesium chloride gradient purification. The fragments for microinjection were released by *Hind*III restriction enzyme digestion, isolated by agarose gel electrophoresis, recovered by ethanol precipitation, and purified with an Elutip-d minicolumn (Sigma-Aldrich) according to the manufacturer's instructions. DNA fragments were dissolved in injection buffer (10 mM Tris and 0.1 mM EDTA, pH 7.5) and adjusted to the appropriate concentration. DNA was injected into a minimum of 150 fertilized eggs at a concentration of 5 ng/μl using standard microinjection techniques (Transgenic and Chimeric Mouse Facility, University of Pennsylvania) (39). Genomic DNA was extracted from tail biopsies or blood using tissue and blood DNA extraction kits (Qiagen). Transgenic pups were identified by a TTR-specific forward primer (5′-GGCAGGGATCAGCAGCCTGG-3′) and a cDNA-specific reverse primer (5′-CCCCACATTCCTCTTCCTCCTCTTCCTTCGGCCTTGG-3′), with a PCR program of 95°C for 2 min, 30 cycles of 94°C for 30 s, 62°C for 1 min, and 72°C for 1.5 min, and a final extension at 72°C for 20 min.

Experimental animals and AAV administration. All procedures and animal care were approved by the IACUC at the Children's Hospital of Philadelphia. The transgenic founders were hybrid F1 generation resulting from a cross between C57BL/6 and SJL mice (The Jackson Laboratory). Transgenic mice were further backcrossed to pure C57BL/6 mice, resulting in early mortality (vide infra); thus all studies were conducted in F0 and N1–N4 mice, using nontransgenic congenic littermates as controls. Murine platelet counts were determined as previously described (40). AAV vector was prepared as previously described (5) and administered via the portal vein as previously described (41).

Tail-clip assay (severe bleeding model). For tail-clip assays, tails were prewarmed at 37°C for 2 min and then cut at a diameter of 3 mm and immersed in prewarmed saline. Time to cessation of bleeding was recorded if less than 10 min; otherwise, the experiment was terminated at 10 min and the tail cauterized to stop bleeding. The blood-containing saline was centrifuged at 520 *g* for 10 min at 4°C. Subsequently, 6 ml lysis buffer (10 mM $KHCO_3$, 150 mM NH_4Cl, and 1 mM EDTA) was added to the red blood cell pellet, and the lysis proceeded for 10 min at room temperature, after which the samples were centrifuged as described above and $OD_{575\ nm}$ of the supernatants was measured. For all assays, nontransgenic littermates served as controls.

$FeCl_3$ carotid artery model. The carotid arteries of adult mice were exposed, a Doppler flow probe (model 0.5VB; Transonic Machinery Systems) was placed on the surface of the exposed artery, and a baseline blood flow measurement was recorded. Subsequently, a 2 mm^2 piece of Whatman No. 1 paper soaked in a 15% solution of $FeCl_3$ was applied to the adventitial surface of the exposed artery for 2 min, after which it was removed and carotid artery blood flow was recorded. Time to carotid artery occlusion was defined as the time from initiation of arterial injury until the onset of stable occlusion (42).

Real-time wide-field intravital microscopy. The cremaster muscles of adult mice were exposed, stretched, and pinned across the intravital microscopy tray. The rat anti-CD41 (murine platelet glycoprotein complex IIb/IIIa) Alexa Fluor 555–labeled antibody (Invitrogen) was infused at a dose of 10 mg/mouse. Immediately after infusion of the antibody, a laser-induced injury was performed on the vessel wall of the cremasteric arterioles (9). The injuries were performed using a pulse-nitrogen dye laser applied through the micropoint laser system (Photonic Instruments). We used an Olympus BX61WI fixed-stage motorized upright fluorescence microscope with a long-distance condenser and ×40 water-immersion objective. Data analysis was carried out using Slidebook 4.0 software (Intelligent Imaging Innovations). Fluorescence data were captured digitally for up to 10 ms per event for 300 frames. The amount of platelet accumulation in the developing thrombi was determined as the sum of all pixel values of the platelet-specific signal and expressed as relative fluorescent units, an arbitrary unit in which the integrated platelet fluorescence intensity is reflected.

Protein expression and purification, antibody production, and development of ELISAs. mFVIIa was purified, and polyclonal antibodies against purified mFVIIa were raised in rabbits as previously described (5). A fraction of the antibody was labeled with HRP according to the manufacturer's instructions (Roche). Total mFVII/mFVIIa protein was measured by a sandwich ELISA using purified mFVII protein as a standard and the rabbit anti-mFVII as capture and detecting (HRP-labeled) antibody. To measure the levels of mFVIIa in mouse plasma, we developed a second ELISA with minimal cross-reactivity to mFVII zymogen. Briefly, diluted murine plasmas were first incubated with an excess of a biotinylated active site probe D-phenylalanyl-L-prolyl-L-arginine chloromethyl ketone (Haematologic Technologies) for 30 min at 4°C, after which the mixture was loaded onto a plate precoated with the rabbit anti-mFVII antibody and incubated at 4°C for 1 hour. The bound fraction of the biotinylated inhibitor was detected after a 30-min incubation at room temperature with HRP-streptavidin (BD Biosciences — Pharmingen). $OD_{450\ nm}$ was measured, and protein concentrations were calculated against a standard curve constructed from serial dilutions of purified mFVIIa protein. As a third method, mFVIIa levels were extrapolated from a standard curve generated by spiking known amounts of purified mFVIIa into normal mouse plasma followed by clotting assay. PTs from diluted plasma samples were plotted, and mFVIIa levels were estimated against the standard curve. Levels of mFVIIa expression determined by PT standard curve and inhibitor-based ELISA were in excellent agreement ($r > 0.93$), whereas the total antigen ELISA reported higher total antigen as a result of endogenous mFVII present in mouse plasma samples or mFVIIa complexed with serpins. TF levels were assayed in cell lysates from pulmonary and cardiac C57BL/6 or SJL tissues by Western blotting using primary antibodies raised in 2 different species, i.e., goat anti-mTF (Santa Cruz Biotechnologies Inc.) and sheep anti-hTF (Haematologic Technologies) (43).

TAT and clotting assays. All reagents were prewarmed to 37°C before use. Mouse plasma for clotting assays was collected into one-tenth volume of 3.8% sodium citrate solution from the tail following a small snip. The first drop was discarded. PTs were measured by adding 50 μl citrated mouse plasma diluted 1:40 to 50 μl hFVII- or hFX-deficient plasma (bioMérieux), and the time to clot formation was recorded with a fibrometer (BBL Fibrosystem; Becton Dickinson) after adding 200 μl rhTF with calcium (Innovin; Dade Behring). aPTTs were measured by adding 50 μl undiluted citrated mouse plasma to 50 μl hFIX-deficient plasma (bioMérieux) and 50 μl aPTT reagent (bioMérieux). The mix was incubated at 37°C for 3 min before 50 μl of 25 mM $CaCl_2$ was added, and time to clotting was recorded with a fibrometer. The TAT complex assay was performed on citrated mouse plasma using the Enzygnost TAT micro kit (Dade Behring) following the manufacturer's protocol. Rotational thromboelastometry was performed using citrated whole blood, as previously described (44).

Histology and immunohistochemistry. Tissues obtained at necropsy were fixed in 10% formalin and paraffin embedded according to standard protocols. Tissues were sectioned and stained with H&E. In addition, immunohistochemistry was performed using fibrin/fibrinogen polyclonal antibody (Dako) following the manufacturer's protocol.

Statistics. A 2-tailed Student's *t* test was used for statistical analysis. Kaplan-Meier plots and analysis were performed using the JMP 6.0 software package (SAS Institute). Statistical analysis on the pathology findings was performed using Fisher's exact test. A *P* value less than 0.05 was considered significant.

Acknowledgments

The authors wish to thank Daniel Martinez at the Children's Hospital of Philadelphia Pathology Core facility as well as Valder R. Arruda for his helpful comments and discussions. K.A. High was supported by the Howard Hughes Medical Institute and by NIH grants U01 HL66948 and P01 HL074124.

Received for publication June 1, 2007, and accepted in revised form February 15, 2008.

Address correspondence to: Katherine A. High, Howard Hughes Medical Institute, The Children's Hospital of Philadelphia, 3615 Civic Center Blvd., 302 Abramson Research Center, Philadelphia, Pennsylvania 19104, USA. Phone: (215) 590-4521; Fax: (215) 590-3660; E-mail: high@email.chop.edu.

Majed N. Aljamali's present address is: Novo Nordisk A/S, Måløv, Denmark.

1. Hedner, U., and Ingerslev, J. 1998. Clinical use of recombinant FVIIa (rFVIIa). *Transfus. Sci.* **19**:163–176.
2. Ingerslev, J., et al. 1996. Major surgery in haemophilic patients with inhibitors using recombinant factor VIIa. *Haemostasis.* **26**(Suppl. 1):118–123.
3. Shapiro, A.D. 2000. Recombinant factor VIIa in the treatment of bleeding in hemophilic children with inhibitors. *Semin. Thromb. Hemost.* **26**:413–419.
4. O'Connell, K.A., Wood, J.J., Wise, R.P., Lozier, J.N., and Braun, M.M. 2006. Thromboembolic adverse events after use of recombinant human coagulation factor VIIa. *JAMA.* **295**:293–298.
5. Margaritis, P., et al. 2004. Novel therapeutic approach for hemophilia using gene delivery of an engineered secreted activated Factor VII. *J. Clin. Invest.* **113**:1025–1031.
6. Tai, S.J., et al. 2007. A viable mouse model for Factor X deficiency provides evidence for maternal transfer of Factor X. *J. Thromb. Haemost.* **6**:339–345.
7. Idusogie, E., et al. 1996. Characterization of a cDNA encoding murine coagulation factor VII. *Thromb. Haemost.* **75**:481–487.
8. Sabatino, D.E., et al. 2004. Novel hemophilia B mouse models exhibiting a range of mutations in the Factor IX gene. *Blood.* **104**:2767–2774.
9. Falati, S., Gross, P., Merrill-Skoloff, G., Furie, B.C., and Furie, B. 2002. Real-time in vivo imaging of platelets, tissue factor and fibrin during arterial thrombus formation in the mouse. *Nat. Med.* **8**:1175–1181.
10. James, H.L., Girolami, A., and Fair, D.S. 1991. Molecular defect in coagulation factor X Friuli results from a substitution of serine for proline at position 343. *Blood.* **77**:317–323.
11. Manno, C.S., et al. 2006. Successful transduction of liver in hemophilia by AAV-Factor IX and limitations imposed by the host immune response. *Nat. Med.* **12**:342–347.
12. Nathwani, A.C., et al. 2007. Safe and efficient transduction of the liver after peripheral vein infusion of self-complementary AAV vector results in stable therapeutic expression of human FIX in nonhuman primates. *Blood.* **109**:1414–1421.
13. Villar, A., et al. 2004. Pharmacokinetics of activated recombinant coagulation factor VII (NovoSeven) in children vs. adults with haemophilia A. *Haemophilia.* **10**:352–359.
14. Chou, J., et al. 2004. Hematopoietic cell-derived microparticle tissue factor contributes to fibrin formation during thrombus propagation. *Blood.* **104**:3190–3197.
15. Day, S.M., et al. 2005. Macrovascular thrombosis is driven by tissue factor derived primarily from the blood vessel wall. *Blood.* **105**:192–198.
16. Dubois, C., Panicot-Dubois, L., Merrill-Skoloff, G., Furie, B., and Furie, B.C. 2006. Glycoprotein VI-dependent and -independent pathways of thrombus formation in vivo. *Blood.* **107**:3902–3906.
17. Dubois, C., Panicot-Dubois, L., Gainor, J.F., Furie, B.C., and Furie, B. 2007. Thrombin-initiated platelet activation in vivo is vWF independent during thrombus formation in a laser injury model. *J. Clin. Invest.* **117**:953–960.
18. Hedner, U. 2006. Potential role of rFVIIa in prophylaxis in severe haemophilia patients with inhibitors. *J. Thromb. Haemost.* **4**:2498–2500.
19. Konkle, B., Friedrich, U., and Abrams, Z. 2006. Secondary prophylactic treatment with rFVIIa in patients with haemophilia A or B and inhibitors with high requirements for on-demand treatment [abstract]. *Haemophilia.* **12**:363.
20. Miller, G.J., et al. 2000. Haemostatic factors in human peripheral afferent lymph. *Thromb. Haemost.* **83**:427–432.
21. Hoffman, M., et al. 2007. Tissue factor around dermal vessels has bound factor VII in the absence of injury. *J. Thromb. Haemost.* **5**:1403–1408.
22. Dunn, A.L. 2005. Management and prevention of recurrent hemarthrosis in patients with hemophilia. *Curr. Opin. Hematol.* **12**:390–394.
23. Peters, L.L., et al. 2005. Quantitative trait loci for baseline white blood cell count, platelet count, and mean platelet volume. *Mamm. Genome.* **16**:749–763.
24. Sachs, U.J., and Nieswandt, B. 2007. In vivo thrombus formation in murine models. *Circ Res* **100**:979–991.
25. Ware, J. 2004. Dysfunctional platelet membrane receptors: from humans to mice. *Thromb. Haemost.* **92**:478–485.
26. Russell, K.E., et al. 2003. Reduced bleeding events with subcutaneous administration of recombinant human factor IX in immune-tolerant hemophilia B dogs. *Blood.* **102**:4393–4398.
27. Brinkhous, K.M., Hedner, U., Garris, J.B., Diness, V., and Read, M.S. 1989. Effect of recombinant factor VIIa on the hemostatic defect in dogs with hemophilia A, hemophilia B, and von Willebrand disease. *Proc. Natl. Acad. Sci. U. S. A.* **86**:1382–1386.
28. Brinkhous, K.M., et al. 1985. Purified human factor VIII procoagulant protein: comparative hemostatic response after infusions into hemophilic and von Willebrand disease dogs. *Proc. Natl. Acad. Sci. U. S. A.* **82**:8752–8756.
29. Brinkhous, K.M., et al. 1996. Recombinant human factor IX: replacement therapy, prophylaxis, and pharmacokinetics in canine hemophilia B. *Blood.* **88**:2603–2610.
30. Ameri, A., Kurachi, S., Sueishi, K., Kuwahara, M., and Kurachi, K. 2003. Myocardial fibrosis in mice with overexpression of human blood coagulation factor IX. *Blood.* **101**:1871–1873.
31. Drake, T.A., Morrissey, J.H., and Edgington, T.S. 1989. Selective cellular expression of tissue factor in human tissues. Implications for disorders of hemostasis and thrombosis. *Am. J. Pathol.* **134**:1087–1097.
32. Fleck, R.A., Rao, L.V., Rapaport, S.I., and Varki, N. 1990. Localization of human tissue factor antigen by immunostaining with monospecific, polyclonal anti-human tissue factor antibody. *Thromb. Res.* **59**:421–437.
33. Mackman, N. 2005. Tissue-specific hemostasis in mice. *Arterioscler. Thromb. Vasc. Biol.* **25**:2273–2281.
34. Roberts, H.R., Monroe, D.M., 3rd, and Hoffman, M. 2004. Safety profile of recombinant factor VIIa. *Semin. Hematol.* **41**:101–108.
35. Mayer, S.A., et al. 2005. Recombinant activated factor VII for acute intracerebral hemorrhage. *N. Engl. J. Med.* **352**:777–785.
36. Deconinck, N., et al. 1997. Expression of truncated utrophin leads to major functional improvements in dystrophin-deficient muscles of mice. *Nat. Med.* **3**:1216–1221.
37. Nelson, R. 2004. Utrophin therapy for Duchenne muscular dystrophy? *Lancet Neurol.* **3**:637.
38. Yan, C., Costa, R.H., Darnell, J.E., Jr., Chen, J.D., and Van Dyke, T.A. 1990. Distinct positive and negative elements control the limited hepatocyte and choroid plexus expression of transthyretin in transgenic mice. *EMBO J.* **9**:869–878.
39. Hogan, B., et al. 1986. *Manipulating the mouse embryo: a laboratory manual.* Cold Spring Harbor Laboratory Press. Cold Spring Harbor, New York, USA. 332 pp.
40. Rauova, L., et al. 2006. Role of platelet surface PF4 antigenic complexes in heparin-induced thrombocytopenia pathogenesis: diagnostic and therapeutic implications. *Blood.* **107**:2346–2353.
41. Nakai, H., et al. 1998. Adeno-associated viral vector-mediated gene transfer of human blood coagulation factor IX into mouse liver. *Blood.* **91**:4600–4607.
42. Farrehi, P.M., Ozaki, C.K., Carmeliet, P., and Fay, W.P. 1998. Regulation of arterial thrombolysis by plasminogen activator inhibitor-1 in mice. *Circulation.* **97**:1002–1008.
43. Szotowski, B., et al. 2005. Alterations in myocardial tissue factor expression and cellular localization in dilated cardiomyopathy. *J. Am. Coll. Cardiol.* **45**:1081–1089.
44. Callan, M.B., et al. 2006. A novel missense mutation responsible for factor VII deficiency in research Beagle colonies. *J. Thromb. Haemost.* **4**:2616–2622.

RESUME - Défauts cellulaires dans les maladies de surcharge lysosomale

La mucopolysaccharidose IIIB (MPSIIIB) est une maladie de surcharge lysosomale (MSL) causée par une accumulation d'oligosaccharides d'héparane sulphate (OHS), induisant chez les enfants atteints un retard mental progressif, une neurodégénérescence et une mort prématurée. Les mécanismes physiopathologiques impliqués sont mal compris. Il est nécessaire d'élucider ces mécanismes, afin d'évaluer l'efficacité d'un traitement par thérapie génique en regard de la perte de la plasticité neuronale, et pour définir les meilleures conditions de traitement. Pour cela, de nouveaux modèles cellulaires de la maladie ont été créés. Des cellules souches pluripotentes induites ont été générées à partir de fibroblastes de patients, lesquelles ont ensuite été différenciées en une lignée neuronale. Un modèle HeLa a également été créé dans lequel l'expression de shRNAs dirigés contre la α-N-acétylglucosaminidase (NAGLU), l'enzyme manquante dans la MPSIIIB, est induite par la tétracycline. Ces modèles ont été isolés avec succès, et présentent les caractéristiques pathologiques fondamentales de la MPSIIIB. L'étude de ces modèles a montré que : I) Les OHS excrétés dans la matrice extracellulaire modifient la perception cellulaire des signaux environnementaux, affectant les voies de signalisation en aval avec des conséquences sur la morphologie du Golgi. II) L'accumulation de vésicules de stockage intracellulaires qui caractérisent les MSLs est due à la surexpression de la protéine cis-golgienne GM130 et aux altérations du Golgi qui en résultent. Ces vésicules sont possiblement des lysosomes anormaux formés dans le Golgi cis et médian qui sont déroutés à une étape précoce de la biogenèse du lysosome, donnant naissance à un compartiment « cul-de-sac ». III) D'autres fonctions cellulaires contrôlées par GM130 sont affectées dont la morphologie du centrosome ou la nucléation des microtubules. Ces données suggèrent de possibles conséquences sur la polarisation et la migration cellulaire, et la neuritogenèse.

Mots-clé : maladie de surcharge lysosomale (MSL) ; Mucopolysaccharidose IIIB (MPSIIIB) ; Héparane sulphate (HS) ; Golgi ; GM130.

ABSTRACT - Cell disorders in lysosomal storage diseases

Mucopolysaccharidosis type IIIB (MPSIIIB) is a lysosomal storage disease (LSD) characterized by accumulation of heparan sulfate oligosaccharides (HSO), which results in progressive mental retardation, neurodegeneration and premature death in children. The underlying mechanisms are poorly understood. Coming to a better understanding of the pathophysiology of MPSIIIB has become a necessity to assess the efficacy of gene therapy treatment regarding loss of neuronal plasticity, and to define the best conditions for treatment. To address the link between HSO accumulation and downstream pathological events, new cell models of MPSIIIB were created. First, induced pluripotent stem cells (iPSc) were generated from fibroblasts of affected children, followed by differentiation of patient-derived iPSc into a neuronal progeny. Second, a HeLa cell model was created in which expression of shRNAs directed against α-N-acetylglucosaminidase (NAGLU), the deficient enzyme in MPSIIIB, is induced by tetracycline. Success in the isolation of these different models was pointed by the presence of cardinal features of MPSIIIB cell pathology. Studies in these models showed that: I) HSO excreted in the extracellular matrix modifies cell perception of environmental cues, affecting downstream signalling pathways with consequences on the Golgi morphology. II) Accumulation of intracellular storage vesicles, a hallmark of LSDs is due to overexpression of the cis-Golgi protein GM130 and subsequent Golgi alterations. It is likely that these vesicles are abnormal lysosomes formed in the cis- and medial-Golgi which are misrouted at an early step of lysosome biogenesis, giving rise to a dead-end compartment. III) Other cell functions controlled by GM130 are affected, including centrosome morphology and microtubule nucleation. These data point to possible consequences on cell polarization, cell migration and neuritogenesis.

Keywords: Lysosomal storage disease (LSD); Mucopolysaccharidosis IIIB (MPSIIIB); heparan sulfate (HS); Golgi; GM130.

LABORATORY: Unité Rétrovirus et Transfert Génétique, INSERM U622
Institut Pasteur, 28 rue du Dr Roux, 75724 Paris Cedex 15